THE UNIVERSITY OF ALBERTA

# STABLE AND UNSTABLE CONVERGING FLOWS OF VISCOELASTIC FLUIDS

by

Ⓒ PETER J. CATANIA

A THESIS

SUBMITTED TO THE FACULTY OF GRADUATE STUDIES AND RESEARCH
IN PARTIAL FULFILMENT OF THE REQUIREMENTS FOR THE DEGREE
OF DOCTOR OF PHILOSOPHY
IN
CHEMICAL ENGINEERING
DEPARTMENT OF CHEMICAL ENGINEERING

EDMONTON, ALBERTA
FALL, 1977

THE UNIVERSITY OF ALBERTA

FACULTY OF GRADUATE STUDIES AND RESEARCH

The undersigned certify that they have read, and recommend to the Faculty of Graduate Studies and Research, for acceptance, a thesis entitled STABLE AND UNSTABLE COVERGING FLOWS OF VISCOELASTIC FLUIDS submitted by PETER J. CATANIA in partial fulfilment of the requirements for the degree of

Doctor of Philosophy
in Chemical Engineering

F.A. Seyer
Supervisor

R.E. Mather

J.B. Hudson

External Examiner

Date Aug. 15, 1977

# ABSTRACT

The objectives of this research were: (a) to measure and correlate axial velocities upstream of an abrupt contraction, (b) to describe the upstream flow field by measuring cone semi-angles and location of eddy centers, (c) to determine the effects of instability on the Bagley plots, the total pressure loss-flow rate curve and contraction losses, and (d) to present a criterion for the onset of fracture based on inlet conditions.

A flow visualization method was used to measure axial and radial velocities. Qualitative observations of the upstream flow field and the jet of fluid issuing from the capillary tube were obtained; pressure traces were measured at a pressure tap upstream of the contraction. The contraction losses and shear stresses for three aqueous sugar solutions, an oil Primol-355 and an 0.20 percent aqueous solution of Separan AP-30 were obtained from Bagley plots. The Newtonian solutions were used to establish the experimental accuracy.

The experimental results and conclusions are: Within region I, (a) a stable wine glass structured flow field was observed, (b) the axial velocities within the central accelerating core are represented by

$$V^{*} = \exp(-(Z^{**})^{1.4})[1.0+0.41\eta^{2}]^{-2.0}$$

(c) the radial velocity component at high flow rates or

small initial cone semi-angles, and for r<D is negligible ($V_r \leq 0.15V_z$), (d) the initial cone semi-angles are represented by

$$\phi_0 = 19\left(\frac{D^3}{\theta_0 Q}\right)^{0.60}$$

(e) as flow rate increases the location of the eddy centers progressively moves farther away from the contraction along a well defined path, (f) comparison of eddy centers at the same flow rate reveal that the eddy centers are located farther upstream in larger sized reservoirs, and (g) the pressure traces and the jet of fluid are smooth.

Within region II, the central core of fluid oscillated to and fro (swirling motion); the intensity and frequency of these oscillations increases with flow rate. There are no measurable changes in the pressure traces and on the jet of fluid.

Within region III, (a) the flow field is "chaotic", (b) the onset and magnitude of measurable pressure fluctuations, independent of L/D ratio, coincide reasonably with the visually observed onset of region III, (c) the jet of fluid oscillates with a frequency approximately equal to the frequency of the pressure fluctuations, (d) the oscillation of the flow field between stable and "chaotic" flows results in two Bagley plots, two values of the contraction losses, and a discontinuity in the total pressure loss-flow rate curve. The flow curve is unaffected by the onset of flow instabilities.

The dependence of contraction losses on capillary tube diameter, reservoir size, and Reynolds number can be explained in terms of the upstream flow field, i.e., stable, swirling, or "chaotic". It is incorrect to correlate contraction losses with Reynolds number when, over the same range of Reynolds numbers, the flow field changes from stable to "chaotic".

Hencky's strain measure, based on inlet conditions, suggests that the onset of flow instabilities (region II) commences at a flow rate given by

$$Q_c = 120.52\left(\frac{n'+1}{3n'+1}\right)^2 \frac{D^3}{\theta_0}$$

At fixed fluid properties, this criterion qualitatively predicts the dependence of tube diameter on the onset of flow instabilities.

# ACKNOWLEDGEMENT

This author acknowledges the financial assistance received from the National Research Council of Canada, and comments and suggestions from members of my advisory committee and external examiner, Dr. John Vlachopoulos. Appreciation is extended to Dr. Frederick A. Seyer, the author's advisor. His stimulating discussions and patience will not be forgotten. The cooperation and considerations received from members of the Faculty of Engineering, University of Regina are appreciated. In addition to the above, gratitude is expressed to the following indivduals:

a. Dr. B. Tinker, Vice-President, University of Regina

b. Dr. E. Bilgen, Department of Mechanical Engineering, Ecole Polytechnique, Montreal, Quebec;

c. Dr. Cliff Shook, Department of Chemistry and Chemical Engineering, University of Saskatchewan, Saskatoon, Saskatchewan.

The technical competence of Mr. Dave Wier of the Audio Visual Department and the excellent typing provided by Mrs. S. Phillips and Ms. L.C. Lockhart is appreciated.

This dissertation would not have been completed without the patience and moral support received from my family.

# TABLE OF CONTENTS

Page

LIST OF TABLES .................................... xii

LIST OF FIGURES ................................... xix

INTRODUCTION ...................................... xxv

I. REVIEW OF LITERATURE ........................... 1

1.1 Contraction Losses ............................ 1
1.1.1 Newtonian Fluids ............................ 1
1.1.2 Purely Viscous non-Newtonian Fluids ......... 7
1.1.3 Viscoelastic Fluids ......................... 12

1.2 Instability ................................... 23
1.2.1 Capillary Initiation ........................ 26
1.2.2 Inlet Initiation ............................ 29
1.2.3 Effects of Entry Geometry and Capillary ..... 33
1.2.4 Empirical Correlations - Prediction of Flow Instabilities ............. 36

II. EXPERIMENTAL EQUIPMENT AND PROCEDURE .......... 48

2.1 Experimental Equipment ........................ 48
2.1.1 Flow System ................................. 48
2.1.2 Entry Region ................................ 48
2.1.3 Capillary Tubes ............................. 50

2.2 Experimental Fluids and Tracer Particles . 53
2.2.1 Experimental Fluids ......................... 53
2.2.2 Tracer Particles ............................ 54

2.3 Photographic Methods .......................... 55
2.3.1 Optical System .............................. 55
2.3.2 Streak Photographs .......................... 59
2.3.3 Analysis of Streak Photographs - Digitizer Method ..................... 62
2.3.4 Analysis of Streak Photographs - Direct Method ........................ 69

2.4 Procedure ..................................... 72
2.4.1 Preparation of Polymer ...................... 72
2.4.2 Data Collection ............................. 73
(i) Pressure ...................................... 73
(ii) Velocity Distributions ....................... 78
(iii) Qualitative Observations ..................... 78

Page

III. RESULTS AND DISCUSSION ........................ 80

3.1 Newtonian Fluids ........................ 80
3.1.1 Friction Factor - Reynolds Number ............................ 80
3.1.2 Contraction Losses ................ 83

3.2 Viscoelastic Fluid ...................... 89
3.2.1 Friction Factor - Reynolds Number ............................ 89
3.2.2 Visual Observations .............. 89
(i) Velocity Field Within Reservoir .................... 91
(ii) Pressure Traces ............ 95
(iii) Jet of Fluid ............. 103
3.2.3 Criteria for Onset of Instability . 105

3.3 Effects of Instability .................. 109
3.3.1 Bagley Plot ...................... 109
3.3.2 Flow Curve ....................... 112
3.3.3 Total Pressure Loss - Flow Rate Curve ............................ 113
3.3.4 Contraction Losses ............... 117

3.4 Velocity Field Upstream of Contraction ... 123
3.4.1 Velocity - Digitizer and Direct Methods .......................... 123
3.4.2 Cone Angles ...................... 135
3.4.3 Eddy Centers ..................... 138
3.4.4 Core Velocities .................. 141
(i) Sink Flow Model ............. 146
(ii) K2 Model .................... 151
(iii) Exponential Decay Model .... 157
(iv) Radial Dependence .......... 181

3.5 Prediction of Instability ............... 199

IV. CONCLUSIONS AND RECOMMENDATIONS ............... 212

4.1 Conclusions ............................. 212

4.2 Recommendations ......................... 218

REFERENCES .................................. 220

## APPENDICES

Page

A. CALIBRATION .................................... 234

A.1 Pressure Transducers ...................... 235
A.2 Thrust Calibration ........................ 236
A.3 Cylinder and Instron Calibration ......... 236
A.4 Normal Force Spring ....................... 237
A.5 Aluminum Dust Particles ................... 237

B. TOTAL PRESSURE LOSS - L/D DATA .................. 251

C. CONTRACTION LOSSES ............................. 283

C.1 Newtonian Fluids .......................... 284
C.2 Viscoelastic Solution ..................... 285

D. PHYSICAL PROPERTIES ............................. 294

D.1 Newtonian Fluids .......................... 295
D.2 Viscoelastic Solution ..................... 296

E. VELOCITY PROFILES ............................... 315

E.1 Axial Velocity Profiles - Direct Method .. 316
E.2 Axial and Radial Velocity Profiles - Digitizer Method ........................ 356
E.3 Mathematical Simplifications ............. 419
E.4 Centerline Axial Velocities .............. 427
E.5 Parameter $r_0$ ........................... 436

F. EDDY CENTERS AND CONE SEMI-ANGLES ............... 441

F.1 Eddy Centers .............................. 442
F.2 Cone Semi-Angles .......................... 450

Page

G. ERROR ANALYSIS .................................... 456

G.1 Digitizer Method Error .................... 457

G.2 Direct Method Error ....................... 466

G.3 Pressure Tranducers and Pressure Tap Error .................................. 466

H. NOMENCLATURE ...................................... 471

## LIST OF TABLES

Page

1.1 Effect of L/D on Onset of Instability ......... 35

1.2 Critical Shear Stress at Onset of Instability . 39

1.3 Recoverable Shear Strain at Onset of Instability .................................. 41

2.1 Internal Reservoir Dimensions ................. 49

2.2 Capillary Tube Length to Diameter Ratios ...... 49

2.3 Time Intervals for Streak Analysis ............ 57

3.1 Estimated Standard Error (e.s.e.) for Newtonian Contraction Losses .................. 86

3.2 Observations Within Regions I, II and III ..... 104

3.3 $\tau_w$ and $S_R$ at Onset of Instability ............. 106

3.4 Flow Rates and Upstream Axial Locations Where Velocities Were Measured ...................... 124

3.5 Critical Extensional Stresses at Onset of Instability ................................ 201

3.6 Comparison of $P_u$ with $\Delta P_c$ at Onset of Flow Instabilities ................................ 203

3.7 Critical Values of S ($S_c$) ................... 208

A.1 Calibration of Transducer 1 .................. 239

A.2 Calibration of Transducer 2 .................. 242

A.3 Calibration of Transducer 3 .................. 244

A.4 Calibration of Transducer 4 .................. 246

A.5 Thrust Calibration ........................... 248

A.6 Calibration For Variable Speed Setting ........ 248

B.1 Total Pressure Loss - L/D Data: Sugar Solution #1, 0.20 cm I.D. Capillary Tube, Small Reservoir 254

B.2 Total Pressure Loss - L/D Data: Sugar Solution #3, 0.20 cm I.D. Capillary Tube, Small Reservoir 255

Page

B.3 Total Pressure Loss - L/D Data: Sugar Solution #4, 0.20 cm I.D. Capillary Tube, Small Reservoir 257

B.4 Total Pressure Loss - L/D Data: Primol-355 Oil, 0.20 cm I.D. Capillary Tube, Small Reservoir .. 258

B.5 Total Pressure Loss - L/D Data: Sugar Solution #1, 0.20 cm I.D. Capillary Tube, Large Reservoir 259

B.6 Total Pressure Loss - L/D Data: Sugar Solution #3, 0.20 cm I.D. Capillary Tube, Large Reservoir 260

B.7 Total Pressure Loss - L/D Data: Sugar Solution #4, 0.20 cm I.D. Capillary Tube, Large Reservoir 261

B.8 Total Pressure Loss - L/D Data: Primol-355 Oil, 0.20 cm I.D. Capillary Tube, Large Reservoir ... 262

B.9 Total Pressure Loss - L/D Data: 0.20% Separan AP-30, 0.10 cm I.D. Capillary Tube, Small Reservoir .................................... 263

B.10 Total Pressure Loss - L/D Data: 0.20% Separan AP-30, 0.20 cm I.D. Capillary Tube, Small Reservoir .................................... 266

B.11 Total Pressure Loss - L/D Data: 0.20% Separan AP-30, 0.30 cm I.D. Capillary Tube, Small Reservoir .................................... 268

B.12 Total Pressure Loss - L/D Data: 0.20% Separan AP-30, 0.10 cm I.D. Capillary Tube, Large Reservoir .................................... 271

B.13 Total Pressure Loss - L/D Data: 0.20% Separan AP-30, 0.20 cm I.D. Capillary Tube, Large Reservoir .................................... 274

B.14 Total Pressure Loss - L/D Data: 0.20% Separan AP-30, 0.30 cm I.D. Capillary Tube, Large Reservoir .................................... 277

C.1 Contraction Losses and Reynolds Numbers for Newtonian Fluids, Small Reservoir ............. 287

C.2 Contraction Losses and Reynolds Numbers for Newtonian Fluids, Large Reservoir ............. 288

C.3 Contraction Losses and Reynolds Numbers for 0.20% Separan AP-30, Small Reservoir .......... 289

Page

C.4 Contraction Losses and Reynolds Numbers for 0.20% Separan AP-30, Large Reservoir .......... 291

D.1 Shear Stress - Shear Rate for Newtonian Solutions .................................... 300

D.2 Viscosity and Density, Newtonian Solutions .... 302

D.3 Physical Properties of 0.20% Separan AP-30; Batch 2 - Small Reservoir ...................... 303

D.4 Physical Properties of 0.20% Separan AP-30; Batch 1 - Large Reservoir ..................... 304

D.5 Normal Force Data ............................. 306

E.1 Axial Velocity Data, 0.10 cm I.D. Capillary, $Q = 0.016\ cm^3/sec$, Small Reservoir ............ 318

E.2 Axial Velocity Data, 0.10 cm I.D. Capillary, $Q = 0.040\ cm^3/sec$, Small Reservoir ............ 320

E.3 Axial Velocity Data, 0.10 cm I.D. Capillary, $Q = 0.119\ cm^3/sec$, Small Reservoir ............ 323

E.4 Axial Velocity Data, 0.20 cm I.D. Capillary, $Q = 0.040\ cm^3/sec$, Small Reservoir ............ 325

E.5 Axial Velocity Data, 0.20 cm I.D. Capillary, $Q = 0.238\ cm^3/sec$, Small Reservoir ............ 327

E.6 Axial Velocity Data, 0.20 cm I.D. Capillary, $Q = 0.318\ cm^3/sec$, Small Reservoir ............ 329

E.7 Axial Velocity Data, 0.30 cm I.D. Capillary, $Q = 0.040\ cm^3/sec$, Small Reservoir ............ 332

E.8 Axial Velocity Data, 0.30 cm I.D. Capillary, $Q = 0.318\ cm^3/sec$, Small Reservoir ............ 333

E.9 Axial Velocity Data, 0.30 cm I.D. Capillary, $Q = 0.635\ cm^3/sec$, Small Reservoir ............ 335

E.10 Axial Velocity Data, 0.20 cm I.D. Capillary, $Q = 0.159\ cm^3/sec$, Large Reservoir ............ 338

Page

E.11 Axial Velocity Data, 0.20 cm I.D. Capillary, $Q = 0.318\ cm^3/sec$, Large Reservoir ............ 340

E.12 Axial Velocity Data, 0.20 cm I.D. Capillary, $Q = 0.794\ cm^3/sec$, Large Reservoir ............ 342

E.13 Axial Velocity Data, 0.20 cm I.D. Capillary, $Q = 1.589\ cm^3/sec$, Large Reservoir ............ 345

E.14 Axial Velocity Data, 0.30 cm I.D. Capillary, $Q = 0.318\ cm^3/sec$, Large Reservoir ............ 348

E.15 Axial Velocity Data, 0.30 cm I.D. Capillary, $Q = 0.635\ cm^3/sec$, Large Reservoir ............ 350

E.16 Axial Velocity Data, 0.30 cm I.D. Capillary, $Q = 1.589\ cm^3/sec$, Large Reservoir ............ 353

E.17 Radial Velocities - Digitizer Method, $Q = 0.016\ cm^3/sec$, 0.10 cm I.D. Capillary Tube, Small Reservoir ............................ 358

E.18 Radial Velocities - Digitizer Method, $Q = 0.040\ cm^3/sec$, 0.10 cm I.D. Capillary Tube, Small Reservoir ............................ 360

E.19 Radial Velocities - Digitizer Method, $Q = 0.119\ cm^3/sec$, 0.10 cm I.D. Capillary Tube, Small Reservoir ............................ 362

E.20 Radial Velocities - Digitizer Method, $Q = 0.040\ cm^3/sec$, 0.20 cm I.D. Capillary Tube, Small Reservoir ............................ 364

E.21 Radial and Axial Velocities - Digitizer Method, $Q = 0.159\ cm^3/sec$, 0.20 cm I.D. Capillary Tube, Small Reservoir ............................ 266

E.22 Radial Velocities - Digitizer Method, $Q = 0.238\ cm^3/sec$, 0.20 cm I.D. Capillary Tube, Small Reservoir ............................ 369

Page

E.23 Radial Velocities - Digitizer Method, $Q = 0.318$ cm$^3$/sec, 0.20 cm I.D. Capillary Tube, Small Reservoir .............................. 371

E.24 Radial Velocities - Digitizer Method, $Q = 0.040$ cm$^3$/sec, 0.30 cm I.D. Capillary Tube, Small Reservoir .............................. 373

E.25 Radial and Axial Velocities - Digitizer Method, $Q = 0.159$ cm$^3$/sec, 0.30 cm I.D. Capillary Tube, Small Reservoir .............................. 373

E.26 Radial Velocities - Digitizer Method, $Q = 0.318$ cm$^3$/sec, 0.30 cm I.D. Capillary Tube, Small Reservoir .............................. 378

E.27 Radial Velocities - Digitizer Method, $Q = 0.635$ cm$^3$/sec, 0.30 cm I.D. Capillary Tube, Small Reservoir .............................. 381

E.28 Radial and Axial Velocities - Digitizer Method, $Q = 1.589$ cm$^3$/sec, 0.20 cm I.D. Capillary Tube, Large Reservoir .............................. 384

E.29 Radial and Axial Velocities - Digitizer Method, $Q = 1.906$ cm$^3$/sec, 0.20 cm I.D. Capillary Tube, Large Reservoir .............................. 385

E.30 Radial and Axial Velocities - Digitizer Method, $Q = 2.383$ cm$^3$/sec, 0.20 cm I.D. Capillary Tube, Large Reservoir .............................. 387

E.31 Radial and Axial Velocities - Digitizer Method, $Q = 2.701$ cm$^3$/sec, 0.20 cm I.D. Capillary Tube, Large Reservoir .............................. 389

E.32 Radial and Axial Velocities - Digitizer Method, $Q = 3.177$ cm$^3$/sec, 0.20 cm I.D. Capillary Tube, Large Reservoir .............................. 392

E.33 Radial and Axial Velocities - Digitizer Method, $Q = 3.812$ cm$^3$/sec, 0.20 cm I.D. Capillary Tube, Large Reservoir .............................. 395

Page

E.34 Radial and Axial Velocities - Digitizer Method, $Q = 4.866\ cm^3/sec$, 0.20 cm I.D. Capillary Tube, Large Reservoir .............................. 398

E.35 Radial and Axial Velocities - Digitizer Method, $Q = 4.866\ cm^3/sec$, 0.30 cm I.D. Capillary Tube, Large Reservoir .............................. 401

E.36 Radial and Axial Velocities - Digitizer Method, $Q = 6.354\ cm^3/sec$, 0.30 cm I.D. Capillary Tube, Large Reservoir .............................. 403

E.37 Radial and Axial Velocities - Digitizer Method, $Q = 7.148\ cm^3/sec$, 0.30 cm I.D. Capillary Tube, Large Reservoir .............................. 405

E.38 Radial and Axial Velocities - Digitizer Method, $Q = 7.943\ cm^3/sec$, 0.30 cm I.D. Capillary Tube, Large Reservoir .............................. 406

E.39 Radial and Axial Velocities - Digitizer Method, $Q = 8.737\ cm^3/sec$, 0.30 cm I.D. Capillary Tube, Large Reservior .............................. 408

E.40 Axial and Radial Velocities - Digitizer Method, $Q = 9.531\ cm^3/sec$, 0.30 cm I.D. Capillary Tube, Large Reservoir .............................. 410

E.41 Axial and Radial Velocities - Digitizer Method, $Q = 10.325\ cm^3/sec$, 0.30 cm I.D. Capillary Tube, Large Reservoir .............................. 413

E.42 Axial and Radial Velocities - Digitizer Method, $Q = 11.120\ cm^3/sec$, 0.30 cm I.D. Capillary Tube, Large Reservoir .............................. 416

E.43 Shear Component of Deformation Rate Tensor .... 423

E.44 Centerline Axial Velocity at Contraction ...... 428

E.45 Variation of Parameter $r_0$ with Reservoir Size, Capillary Tube I.D., Flow Rate, and Dimensionless Axial Position Z** ............. 437

F.1 Eddy Center Location, 0.10 cm I.D. Capillary, L/D = 55.08, Small Reservoir .................. 443

Page

F.2 Eddy Center Location, 0.20 cm I.D. Capillary, L/D = 54.96, Small Reservoir .................. 444

F.3 Eddy Center Location, 0.30 cm I.D. Capillary, L/D = 55.04, Small Reservoir .................. 445

F.4 Eddy Center Location, 0.10 cm I.D. Capillary, L/D = 55.08, Large Reservoir .................. 446

F.5 Eddy Center Location, 0.20 cm I.D. Capillary, L/D = 54.96, Large Reservoir .................. 447

F.6 Eddy Center Location, 0.30 cm I.D. Capillary, L/D = 55.04, Large Reservoir .................. 448

F.7 Cone Semi-Angles, Small Reservoir ............. 451

F.8 Cone Semi-Angles, Large Reservoir ............. 453

G.1 Calibration of Digitizer ...................... 459

## LIST OF FIGURES

Page

1.1 Apparatus and Pressure Profile .............. 2

1.2 Hagenbach Correction Factor vs. Flow Behavior Index .............................. 11

1.3 Couette Correction Factor vs. Flow Behavior Index .............................. 15

1.4 Velocity Flow Field for Viscoelastic Fluid .. 24

1.5 Reservoir Pressure as a Function of Volumetric Flow Rate at Onset of Fracture .............. 28

2.1 Reservoir and Pressure Tap Location ......... 51

2.2 Capillary Holding Device ..................... 52

2.3 Schematic of Optical System ................. 56

2.4 Streak Photograph, 0.20 cm I.D., $Q = 0.318$ cm$^3$/sec .......................... 60

2.5 Streak Photograph, 0.20 cm I.D., $Q = 0.040$ cm$^3$/sec .......................... 61

2.6 Eddy Center Location, 0.30 cm I.D., $Q = 9.531$ cm$^3$/sec .......................... 63

2.7 Schematic of Digitizer ....................... 64

2.8 Schematic of Streak Analysis ................ 66

2.9 Direct Method; Streak Length Along Several Streamlines ......................... 70

2.10 Axial Velocity - Upstream Axial Position Plot .............................. 71

2.11 Transient - Steady State Pressure Displacement Trace for Primol-355 Oil ................... 74

2.12 Transient - Steady State Pressure Displacement Trace for Sugar Solution No. 1 ............. 75

3.1 Bagley Plot- Newtonian Fluid; Low Reynolds Numbers ..................................... 81

Page

3.2 Bagley Plot - Newtonian Fluid ............... 82

3.3 Friction Factor - Reynolds Numbers; Newtonian Solutions ........................... 84

3.4 $\Phi$ versus Reynolds Number for Newtonian Fluids 88

3.5 Friction Factor - Reynolds Number; 0.20% Separan AP-30 ............................. 90

3.6 Regions of Flow Instabilities ............... 94

3.7 Pressure Displacement Traces Within Region III 96

3.8 Pressure Fluctuations; 0.10 cm I.D., Small Reservoir ........................... 99

3.9 Pressure Fluctuations; 0.20 cm I.D., Small Reservoir ........................... 100

3.10 Pressure Fluctuations; 0.30 cm I.D., Small Reservoir ........................... 101

3.11 Bagley Plot - 0.20% Separan AP-30 ........... 110

3.12 Bagley Plot - 0.20% Separan AP-30; Effect of Flow Instability ......................... 111

3.13 Total Pressure Loss - Flow Rate Curve; 0.30 cm I.D. Capillary, Large Reservoir ..... 114

3.14 Total Pressure Loss - Flow Rate Curve; 0.30 cm I.D. Capillary, Small Reservoir ..... 115

3.15 $\Phi_t$ versus $N'_{Re}$ - 0.20% Separan AP-30, Large Reservoir ............................ 118

3.16 $\Phi_t$ versus $N'_{Re}$ - 0.20% Separan AP-30, Small Reservoir ............................ 119

3.17 Axial Velocity Profile - Digitizer Method, Large Reservoir, z/D = 37.59 ................ 127

3.18 Axial Velocity Profile - Digitizer Method, Large Reservoir, z/D = 25.06 ................ 128

3.19 Axial Velocity Profile - Digitizer Method, Large Reservoir, z/D = 12.53 ................ 129

Page

3.20 Axial Velocity Profiles - 0.10 cm I.D., Direct Method, $Q = 0.119\ cm^3/sec$ ............ 131

3.21 Axial Velocity Profiles - 0.20 cm I.D., Direct Method, $Q = 0.318\ cm^3/sec$ ............ 132

3.22 Axial Velocity Profiles - 0.30 cm I.D., Direct Method, $Q = 0.318\ cm^3/sec$ ............ 133

3.23 Initial Cone Semi-Angles .................... 136

3.24 Reservoir Effect on Upstream Cone Angle Development; $Q = 0.318\ cm^3/sec$ .............. 139

3.25 Reservoir Effect on Upstream Cone Angle Development; $Q = 0.238$ and $0.635\ cm^3/sec$ .... 140

3.26 Location of Eddy Centers, 0.30 cm I.D., Small Reservoir ............................ 142

3.27 Centerline Velocity; Sink Flow Model ........ 148

3.28 Centerline Stretch Rate; Sink Flow Model .... 150

3.29 Typical Centerline Axial Velocity; K2 Model; 0.30 cm I.D. Capillary ...................... 153

3.30 Typical Centerline Axial Velocity; K2 Model; 0.10 and 0.30 cm I.D. Capillaries ........... 154

3.31 Typical Centerline Stretch Rate; K2 Model; 0.30 cm I.D. Capillary ...................... 155

3.32 Typical Centerline Stretch Rate; K2 Model; 0.10 and 0.30 cm I.D. Capillaries ........... 156

3.33 Centerline Axial Velocity; Exponential Decay Model .............................. 160

3.34 Axial Centerline Velocity at Contraction versus Flow Rate ........................... 162

3.35 Axial Centerline Velocity at Contraction versus Q/A ................................ 164

3.36 V* versus Z*; 0.10 cm I.D. Capillary, Small Reservoir ........................... 169

Page

3.37 V* versus Z*; 0.20 cm I.D. Capillary, Small Reservoir .............................. 170

3.38 V* versus Z*; 0.30 cm I.D. Capillary, Small Reservoir .............................. 171

3.39 V* versus Z*; 0.20 cm I.D. Capillary, Large Reservoir .............................. 172

3.40 V* versus Z*; 0.30 cm I.D. Capillary, Large Reservoir .............................. 173

3.41 $b_1$ versus $(\theta_0 Q/D^3)$ ......................... 174

3.42 Axial Velocity (V*) versus Dimensionless Axial Position (Z**) ......................... 177

3.43 Typical Centerline Stretch Rates; Exponential Decay Model; 0.30 cm I.D. Capillary ......... 179

3.44 Typical Centerline Stretch Rates; Exponential Decay Model; 0.10 cm I.D. Capillary ......... 180

3.45 Typical Example of Constant Stretch Rate; 0.30 cm I.D., Q = 0.318 $cm^3$/sec ............. 182

3.46 Effect of Reservoir Size and Axial Position on $r_0$; 0.30 cm I.D. Capillary, Q = 0.318 $cm^3$/sec .......................... 184

3.47 Effect of Reservoir Size and Axial Position on $r_0$; 0.20 cm I.D. Capillary Q = 0.318 $cm^3$/sec .......................... 185

3.48 Radial Dependence of Axial Velocity; 0.10 cm I.D. Capillary (L/D = 55.08), Small Reservoir 187

3.49 Radial Depemdence of Axial Velocity; 0.20 cm I.D. Capillary (L/D = 54.96), Small Reservoir 188

3.50 Radial Dependence of Axial Velocity, 0.30 cm I.D. Capillary (L/D = 55.04), Small Reservoir 189

3.51 Radial Dependence of Axial Velocity; 0.20 cm I.D. Capillary (L/D = 54.96), Large Reservoir 190

3.52 Radial Dependence of Axial Velocity, 0.30 cm I.D. Capillary (L/D = 55.04), Large Reservoir 191

Page

3.53 Radial Dependence of Axial Velocity ......... 194

3.54 Comparison of Axial Velocities for 0.20 cm I.D. Capillary, $Q = 0.318\ cm^3/sec$, Small Reservoir ............................ 195

3.55 Comparison of Axial Velocities for 0.30 cm I.D. Capillary, $Q = 1.589\ cm^3/sec$, Large Reservoir ............................ 197

3.56 Sensitivity of Flow Rate at Onset of Instability, $S_c$ Criterion .................. 210

A-1 Normal Force Spring Calibration ............. 249

A-2 Size Distribution of Aluminum Dust Particles ...................................... 250

B-1 Pressure Fluctuations; 0.10 cm I.D. Capillary, Large Reservoir .................. 280

B-2 Pressure Fluctuations; 0.20 cm I.D. Capillary, Large Reservoir .................. 281

B-3 Pressure Fluctuations; 0.30 cm I.D. Capillary, Large Reservoir .................. 282

C-1 Pressure Profile and Bagley Plot ............ 293

D-1 Newtonian Viscosities ....................... 308

D-2 Flow Curve - 0.20% Separan AP-30; High Apparent Shear Rates ....................... 309

D-3 Flow Curve - 0.20% Separan AP-30; Low Apparent Shear Rates ....................... 310

D-4 Apparent Viscosity - 0.20% Separan AP-30 .... 311

D-5 Inertial Contribution to Normal Force (Rheogoniometer) ........................... 312

D-6 Normal Stress ............................... 313

D-7 Relaxation Time ............................. 314

E-1 Maximum Ratio $(V_r/V_z)_M$ 0.10 cm I.D. Small Reservoir ............................ 424

Page

E-2 Maximum Ratio $(V_r/V_z)_M$, 0.20 cm I.D. Small Reservoir .............................. 425

E-3 Maximum Ratio $(V_r/V_z)_M$, 0.30 cm I.D. Small Reservoir .............................. 426

E-4 Axial Centerline Velocity; 0.10 cm I.D. (L/D = 55.08), Small Reservoir .............. 429

E-5 Axial Centerline Velocity; 0.20 cm I.D. (L/D = 54.96), Small Reservoir .............. 430

E-6 Axial Centerline Velocity; 0.30 cm I.D. (L/D = 55.04), Small Reservoir .............. 431

E-7 Axial Centerline Velocity; 0.20 cm I.D. (L/D = 54.96), Large Reservoir (High Flow Rates) ........................... 432

E-8 Axial Centerline Velocity; 0.20 cm I.D. (L/D = 54.96), Large Reservoir (Low Flow Rates) ............................ 433

E-9 Axial Centerline Velocity; 0.30 cm I.D. (L/D = 55.04), Large Reservoir (High Flow Rates) ........................... 434

E-10 Axial Centerline Velocity; 0.30 cm I.D. (L/D = 55.04), Large Reservoir (Low Flow Rates) ............................ 435

F-1 Eddy Center Location ............................ 449

G-1 Flow Behavior at Pressure Tap ............... 470

# INTRODUCTION

The character of velocity fields of polymer melts and solutions is of considerable rheological importance and technological interest. Much time and effort have been spent by rheologists on developing experimental techniques to determine normal stresses of polymer melts and solutions, e.g., the rotational viscometer and capillary rheometer. The rotational viscometer is limited to low shear rates, whereas the latter is suitable for measuring normal stresses at high shear rates. Among the possible geometries for a capillary rheometer, the flow from a reservoir or pipe to a tube of small diameter has received considerable attention during the past decades. The flow at the entrance of a capillary, which is the main focus of this dissertation, is described as a converging accelerative flow. This converging accelerative flow is a particularly important one because of the wealth of data and experience derived from the use of capillary rheometers. Many industrially important processes such as the flow of a polymer melt into a die or spinneret, the drawing-down of a molten polymer fibre, sheet or tube are examples of this kind of flow.

The polymer process industry has long realized that the rate of production is limited by distortions in the extrudate (melt fracture) which is related to flow and stress fields in the entry region. Several onset criteria have been suggested. These criteria, based on correlations of melt fracture with rheologically relevant dimensionless or dimensional parameters, seem justified only on empirical grounds since the actual upstream flow field is complex. These correlations, if successful, do not constitute an explanation for the onset of fracture. It has been conjectured that the onset of these flow instabilities may be initiated either in the entry region ahead of the capillary tube or within the tube itself. It is not possible to state unequivocally that the initiation site is either one or the other. There is general agreement (27, 52, 132, 184) that: (a) the initiation site for melts exemplified by low density polythylene (LDPE) melts and for several polymer solutions occurs within the entry region, and (b) the onset of melt fracture results in the breakdown of the characteristics "wine glass" flow field within the entry region. With high density polyethylene (HDPE) melts, the initiation site is believed to occur within the capillary tube (27, 130, 183). Explanations for melt fracture based on inlet conditions (59) have not been tested severely since details of the upstream velocity field are not well known.

In order that the design of processes involving polymer melts or solutions proceed on a sound engineering basis, a quantitative understanding of entrance flow is urgently needed. Based upon the aforementioned, the objectives of this research are:

1. To measure and correlate the velocity field within the accelerating region of flow upstream of a capillary entrance.

2. To determine the onset of flow instability as observed in the upstream velocity field, the pressure traces, and the jet of fluid.

3. To evaluate onset criteria based on inlet conditions and on steady laminar shear flow (SLSF) in the capillary tube.

4. To determine the effects of reservoir size and capillary tube length to diameter ratio on the onset of flow instabilities.

5. To determine the effects of instability on the contraction losses.

# CHAPTER I

# REVIEW OF LITERATURE

## 1.1 CONTRACTION LOSSES

The review deals with: (a) the analyses which have been developed to predict contraction losses, and (b) the comparison of contraction losses predicted through these analyses with experimental data for SLSF. The types of fluids considered are Newtonian and non-Newtonian. Non-Newtonian fluids, those whose shear stress is not linearly dependent upon the shear rate, can be classified into purely viscous and viscoelastic. With purely viscous non-Newtonian fluids the shear stress is a function only of the shear rate, whereas with the viscoelastic fluids there is a partial recovery of deformation upon the removal of the deforming stresses (131).

### 1.1.1 NEWTONIAN FLUIDS

When a fluid flows from a reservoir into a capillary tube the velocity distribution undergoes a change from some initial profile at the inlet of the capillary tube to a fully developed velocity distribution downstream. With reference to Figure 1.1, if fully developed flow existed from Section 2 up to the inlet, referred to as Section 1, the corresponding pressure loss, $P_1^* - P_2$, over the length, L, is given by the Hagen-Poiseuille law (20). This law

FIGURE 1.1

APPARATUS AND PRESSURE PROFILE

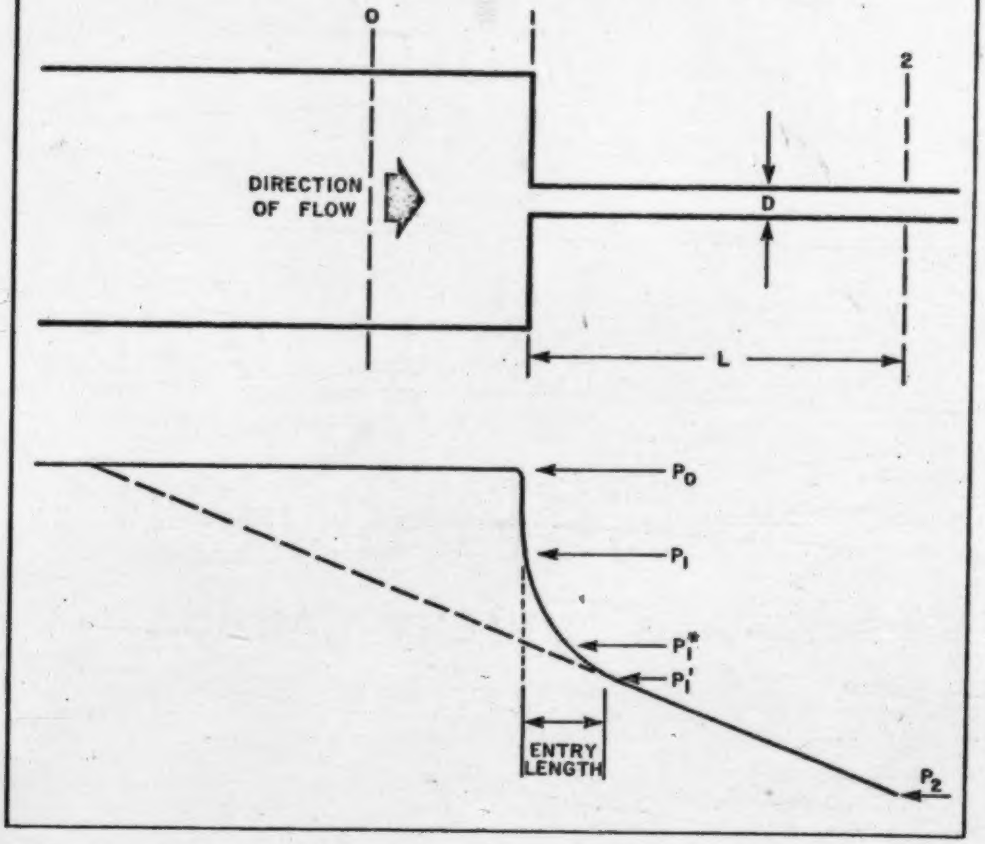
0
2
DIRECTION OF FLOW
D
L
$P_0$
$P_1$
$P_1^*$
$P_1'$
ENTRY LENGTH
$P_2$

states that

$$\frac{P_1^* - P_2}{\rho\ V^2/2} = \frac{64}{N_{Re}}\ \frac{L}{D} \qquad 1.1$$

where V is the average velocity in the capillary tube, D is the capillary tube internal diameter, $N_{Re}$ is the capillary tube Reynolds number, and $\rho$ is the fluid density.

The contraction losses, defined as $P_0 - P_1^*$, are comprised of: (a) the pressure loss due to frictional dissipation upstream of the contraction (assumed to be negligible), (b) the pressure loss due to the restriction in the cross-sectional area $(P_0 - P_1)$, and (c) the pressure loss arising from the development of the velocity profile in the entry length of the capillary tube $(P_1 - P_1')$.

Inertial Contribution

Consider flows with significant inertial effects, i.e., capillary tube Reynolds numbers greater than 1000 but less than 2100 (161). By assuming: (a) negligible frictional dissipation upstream of the contraction (69), (b) an infinite reservoir, and (c) a flat velocity profile at Section 1, the macroscopic mechanical energy (ME) balance when applied between Sections 0 and 1 yields the relationship

$$\frac{P_0 - P_1}{\rho\ V^2/2} = 1.0 \qquad 1.2$$

Hagenbach (69) assumed that the remaining pressure loss, $P_1 - P_1'$, was due to the change in kinetic energy arising from the development of a flat velocity profile at Section 1 to a fully developed parabolic profile downstream of the contraction. This results in

$$\frac{P_1 - P_1'}{\rho\, V^2/2} = 1.0 \qquad 1.3$$

Overall, the contraction loss, $\Phi_H$, is

$$\Phi_H = \frac{P_0 - P_1^*}{\rho\, V^2/2} = 2.0 \qquad 1.4$$

Other theoretical analyses leading to predictions of $\Phi_H$ were summarized by Catania (38) and Sylvester (161). Values of $\Phi_H$ are reported to vary from 2.08 to 2.41 (26, 33, 35, 36, 45, 100, 148, 150, 167, 181) depending upon the analysis and the assumptions used. Therefore, contraction losses at high Reynolds numbers can be summarized as

$$\Phi_H = K' \quad 2.00 \leq K' \leq 2.41 \qquad 1.5$$

where K' is the Hagenbach correction factor. If an infinite contraction is not assumed, then the average velocity at Section 0 is not negligible with respect to the average velocity in the capillary tube (Section 2). Based on kinetic energy considerations alone, the macroscopic ME balance, when applied between Sections 0 and 2, yields

$$\Phi_H = 2.0\ (1 - \beta^2) \qquad 1.6$$

where $\beta$ is the ratio of the capillary tube area to the reservoir area (93). Equation 1.6 reduces to Equation 1.4 when $\beta = 0$, i.e., an infinite reservoir. The development of Equation 1.6 assumes fully developed flow at Section 0 and negligible frictional dissipation upstream of the contraction (92). The latter assumption was indicated by observing that pressure gradients upstream of the contraction were negligible, as a first approximation, compared to pressure gradients downstream of the contraction (4).

Kaye and Rosen (93), using a 0.409 inch I.D. capillary tube, experimentally measured the contraction losses through a sharp edged contraction for values of $\beta$ that ranged from 0.026 to 0.636. The data were represented by

$$\Phi_H = (2.32 \pm .05)(1 - \beta^2) \qquad 1.7$$

Over a wide range of values of $\beta$ and for geometries other than a sharp edged contraction, experimental results, with one exception (4), can be summarized as Equation 1.8 (6, 59, 96, 97, 161)

$$\Phi_H = (2.26 \pm .26)(1 - \beta^2) \qquad 1.8$$

Astarita (4) reported a Hagenbach correction factor of 5.48. This large value could be the result of a vena contracta observed in the pressure profiles along the capillary tube which has not been taken into account in Equation 1.7.

This points to a limitation of the preceding analyses - overlooking the existence of a vena contracta and the associated entry losses.

## Viscous Contribution

The equations of motion were solved numerically for flow through a sharp edged contraction and for Reynolds numbers less than 200 (180). The predicted contraction losses are represented by

$$\Phi_c = \frac{K(N_{Re},\beta)}{N_{Re}} \qquad 1.9$$

where $K(N_{Re},\beta)$ is the Couette correction factor. With contraction ratios less than 0.25 (36, 180) and under creeping flow conditions, $N_{Re} << 1.0$, the Couette correction factor is predicted to be constant. The particular value for this constant depends upon the geometry, the assumptions, and the analysis (40, 86, 127, 145, 146, 164, 185), hence, the value may range from 14.52 to 47.9. Experimentally determined Couette correction factors are reported to vary from 24.0 to 37.3 (28, 30, 40, 102) which agree with the theoretical analyses.

At capillary tube Reynolds numbers between 5 and 100, the experimentally measured contraction losses (4, 93, 162) are greater than those obtained from numerical analyses (36, 180). This difference may be the result of larger circulative flow in the corners of the reservoir. Kaye and Rosen (93) suggested that the Couette correction factor may be expressed as

$$\Phi_c = (159 \pm 30)(1 - \beta^2) \qquad 1.10$$

This dependence of the Couette correction factor on the contraction ratio is in agreement with the analysis presented by Vrentas and Duda (180).

Over the complete range of Reynolds numbers, Holmes (84) stated that the results can be cast into the form

$$\Phi = \Phi_H + \Phi_c \qquad 1.11$$

or

$$\Phi = K'(\beta) + \frac{K(N_{Re},\beta)}{N_{Re}} \qquad 1.12$$

The Hagenbach and Couette factors are given by Equations 1.8 and 1.10 respectively. It must be pointed out that Equation 1.12 was not obtained theoretically, i.e., it is not a solution to the equations of motion for laminar flow of a Newtonian fluid through a sharp edged sudden contraction. The merit of Equation 1.12 is that it can correlate experimental data (93, 154, 161) over a wide range of Reynolds numbers.

### 1.1.2 PURELY VISCOUS NON-NEWTONIAN FLUID

A simple viscous model that gives good representation of shear behavior for purely viscous non-Newtonian fluids is the power law represented by Equation 1.13 (113)

$$\tau_w = \frac{D\Delta P}{4L} = K_0\left(\frac{8V}{D}\right)^{n'} \qquad 1.13$$

where $K_0$ and n' are taken as constants. $K_0$ and n' are obtained from capillary viscometer data as

$$n' = d(\log\tau_w)/d(\log(\frac{8V}{D})) \qquad 1.14$$

$$K_0 = \tau_w/(\frac{8V}{D})^{n'} \qquad 1.15$$

Here, $\tau_w$ is the shear stress evaluated at the capillary tube wall under SLSF and 8V/D or $\dot{\gamma}$ is the apparent shear rate. The capillary wall shear rate is obtained from

$$\dot{\gamma}_w \equiv (-\frac{dV_z}{dr})_w = \frac{3n'+1}{4n'} (\frac{8V}{D}) \qquad 1.16$$

The power law model predicts that shear stress has a linear relationship with apparent shear rate when plotted on log-log coordinates. Many fluids approximate this behavior over a range of one decade in apparent shear rate but show significant curvature over wider ranges. Hence, compared with Newtonian fluids, the non-Newtonian fluids cannot be characterized simply by one rheological parameter such as viscosity.

Dimensional analysis (13) suggests that the Hagenbach and Couette correction factors depend upon the flow behavior index. Therefore,

$$\Phi = K'(\beta,n') + \frac{K(N'_{Re},\beta,n')}{N'_{Re}} \qquad 1.17$$

where the Newtonian Reynolds number has been replaced by the generalized Reynolds number, $N'_{Re}$. This was defined by

Metzner and Reed (113) as

$$N'_{Re} = \frac{D^{n'} V^{2-n'} \rho}{K_0 8^{n'-1}} \qquad 1.18$$

and was developed in the following manner: In SLSF through a circular tube, the friction factor, f, is given by Equation 1.19 (20)

$$f = \tau_w / (\rho \; V^2/2) \qquad 1.19$$

The substitution of $\tau_w$ from Equation 1.13 into 1.19 gives

$$f = \frac{16 K_0 8^{n'-1}}{\rho D^{n'} V^{2-n'}} \qquad 1.20$$

For Newtonian fluids in laminar flow the friction factor and Reynolds number are related by

$$f = 16/N_{Re} \qquad 1.21$$

The generalized Reynolds number is obtained by equating Equation 1.20 and 1.21. Therefore, all fluids whose shear behavior is represented by a power law model must follow the usual f versus $N'_{Re}$ relationship in the laminar flow region when use is made of the generalized Reynolds number.

The dependence of the Hagenbach and Couette correction factors on the flow behavior index has been predicted by several authors for an infinite reservoir, assuming a flat velocity profile at the contraction (26, 36, 41, 45, 165).

A comparison between these predictions and experimental data is shown in Figure 1.2 for the Hagenbach correction factor with the flow behavior indices being less than unity. Overall, the Hagenbach correction factor, and hence the contraction losses, are predicted to be less than the value for Newtonian fluids (n' = 1.0). The relatively large differences between predicted and experimental values of K' is partially attributed to the elastic nature of the experimental fluids. The effect of elasticity, as will be explained in the next section, is an increase in contraction losses at a given Reynolds number. The dependence of K' on the flow behavior index proposed by Collins and Schowalter (45) has been experimentally verified for $0.585 \leq n' \leq 1.00$ and $20 \leq N'_{Re} \leq 1942$ in a 2 to 1 contraction (144) and is in reasonable agreement with experimental results reported by Dodge and Metzner (55). For flow behavior indices less than unity, contraction losses can be represented, therefore, by

$$\Phi_H = K'(\beta,n') = f(n')(1 - \beta^2) \qquad 1.22$$

where f(n') is given by Collins and Schowalter (45).

The dependence of the Couette correction factor on the flow behavior index for $N'_{Re} << 1.0$, proposed by Tomita (165), was modified by Boles and Bogue (29) and for infinite contraction ratios is given by Equation 1.23 on page 12.

FIGURE 1.2

HAGENBACH CORRECTION FACTOR VS. FLOW BEHAVIOR INDEX

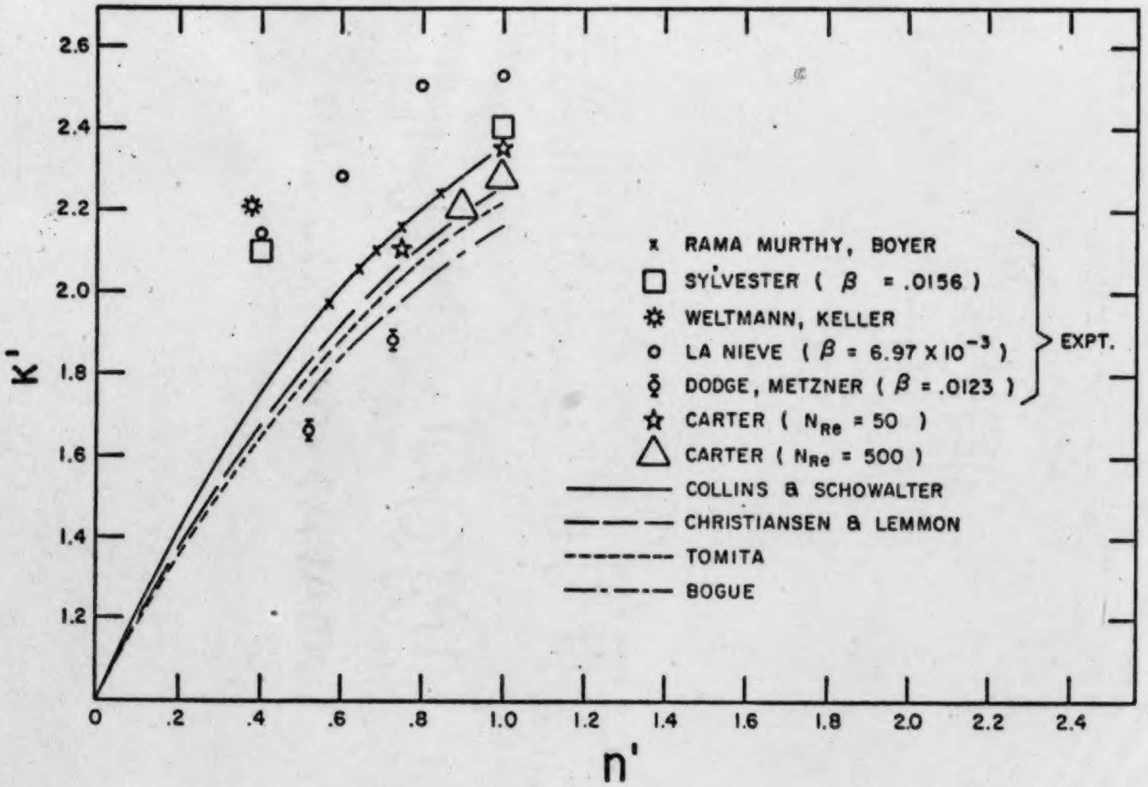

$$\Phi_c = \frac{18.88}{(n')^{0.7} N'_{Re}} \qquad 1.23$$

To account for finite contraction ratios, Equation 1.23 is modified by the multiplication factor $(1 - \beta^2)$, as is the case for Newtonian fluids.

### 1.1.3 VISCOELASTIC FLUIDS

For many polymer melts contraction losses were measured at capillary tube Reynolds numbers less than $10^{-3}$ (22, 30, 73, 102). Contraction losses with polymer solutions, although measured at high Reynolds numbers (5, 144, 154, 161), support the conclusions that can be drawn from data obtained with polymer melts.

A viscoelastic fluid with the same shear stress-shear rate behavior in SLSF but characterized by different elastic properties may result in different values of the contraction losses, $\Delta P_c$. Therefore, the Couette correction may depend upon the elastic nature of the fluid. At a fixed value of $\beta$ ($\beta$ = 0.1616), Astarita, Greco, and Peluso (5) measured contraction losses for several concentrations of Separan ET-597 and Carbopol. For each concentration the flow behavior index, n', was constant over the range of apparent shear rates where contraction losses were measured. Furthermore, log-log plots of $\Phi$ versus $N'_{Re}$ were linearly related with a slope equal to -1.0. They concluded that the Couette correction factor may be a unique function of the flow behavior index. Unfortunately, the data for the highly elastic fluids (Separan ET-597) and for the weakly elastic fluids (Carbopol) overlapped only over a limited range of n' (Figure 1.3). This left open the question of whether elastic effects would result in a family of curves relating the Couette correction factor to the flow behavior index. This question was partially resolved by Sylvester (161) who measured contraction losses at a fixed β (β = 0.0156) and for several concentrations of three different polymers. These polymers were Separan AP-30, Polyox, and CMC and each had a flow behavior index approximately equal to 0.40. The Couette correction factors, plotted in Figure 1.3, ranged from 185 for the weakly elastic Polyox solutions to 490 for the highly elastic Separan AP-30 solutions. The results substantiated the claim that fluids having the same shear stress-shear rate behavior but different elastic properties result in different values of $\Delta P_c$.

Since contraction losses are dependent upon the nature of the flow field in the entry region and since polymer rheology affects the flow field in the entry region, we cannot separate polymer rheology and geometry for viscoelastic fluids as implied by Han (72).

## Prediction and Measurement of Contraction Losses

A method widely used to measure contraction losses is the Philippoff-Gaskins analysis (3, 30, 58, 95, 103, 137).

## LEGEND FOR FIGURE 1.3

| SYMBOL | AUTHOR | POLYMER | $\beta$ |
|---|---|---|---|
| △ | Astarita et al. | ET-597 | .1616 |
| ▽ | Astarita et al. | Carbopol | .1616 |
| ●$_4$ | Han | HDPE | .0069 |
| ●$_3$ | Han | HDPE | .0123 |
| ●$_2$ | Han | HDPE | .0277 |
| ●$_1$ | Han | HDPE | .1111 |
| ▲ | Sylvester | Polyox | .0156 |
| □ | Sylvester | CMC | .0156 |
| ■ | Sylvester | Separan | .0156 |

FIGURE 1.3

# COUETTE CORRECTION FACTOR
# vs.
# FLOW BEHAVIOR INDEX

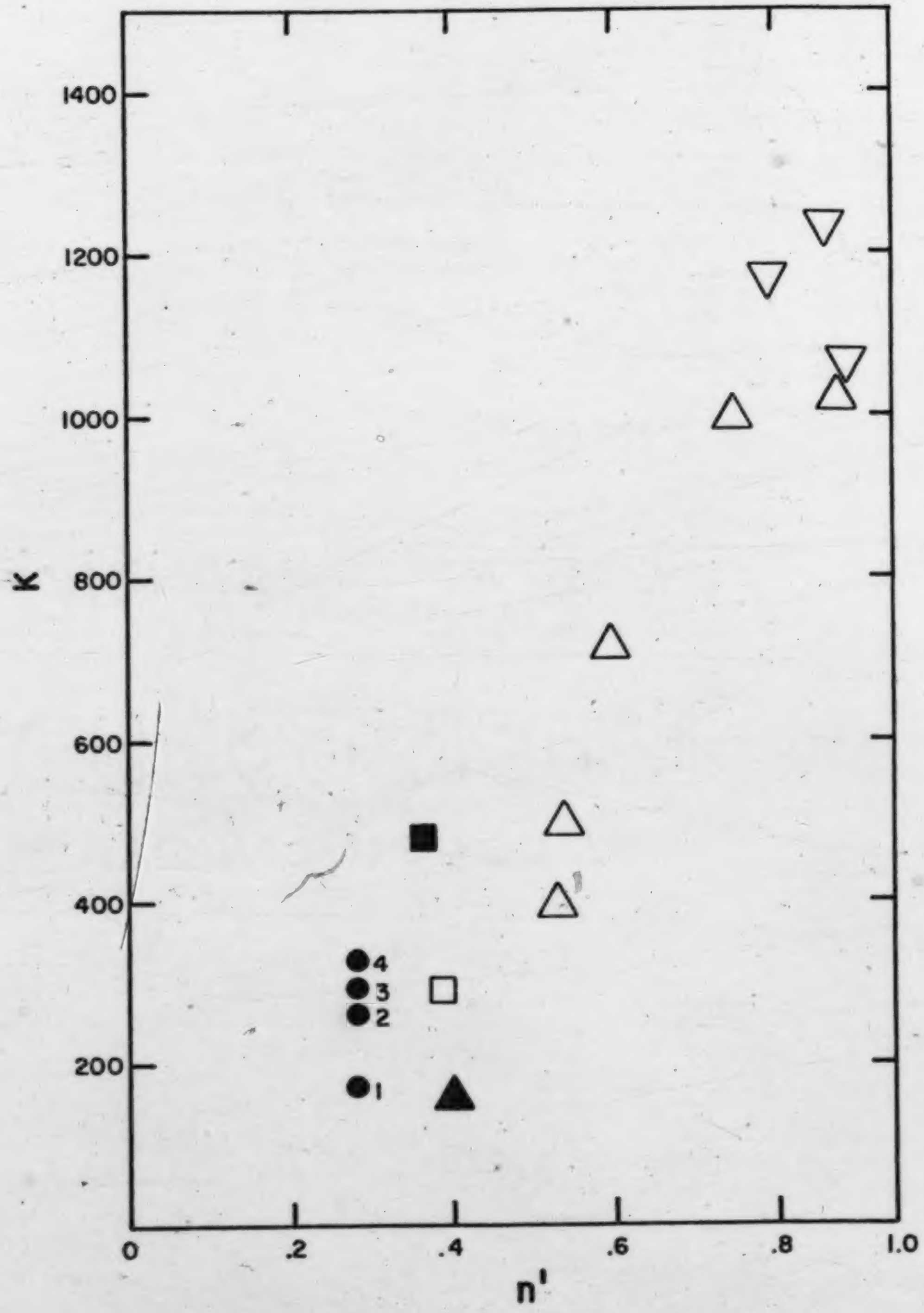

This analysis was modified by Bagley (8) in order to separate the viscous and elastic contribution of the overall contraction losses and shall be referred henceforth as the PGB analysis. The PGB analysis assumes that the contraction losses can be represented as an additional length of the capillary tube in the developed flow regime, $\varepsilon_v D$, where $\varepsilon_v$ is an end correction factor (8). The total pressure loss, $\Delta P_t$, measured from a position upstream of the contraction to the end of the capillary tube is given as

$$\begin{aligned}\Delta P_t &= \Delta P_d + \Delta P_c \\ &= \Delta P_d + \Delta P_v + \Delta P_e \qquad 1.24\end{aligned}$$

where $\Delta P_d$ is the pressure loss under SLSF within the capillary tube, $\Delta P_v$ is the fraction of the contraction loss arising from viscous dissipation, and $\Delta P_e$ is the remaining fraction arising from the elastic nature of the fluid. Exit pressures are assumed to be negligible. Philippoff and Gaskins (137) assumed that

$$\Delta P_e = \tau_w S_R \qquad 1.25$$

where $S_R$ is the recoverable shear strain. The substitution of Equation 1.25 into Equation 1.24 with

$$\Delta P_d = 4\tau_w \, L/D \qquad 1.26$$

and

$$\Delta P_v = 4\tau_w \varepsilon_v \qquad 1.27$$

yields

$$\Delta P_t = 4\tau_w(\frac{L}{D} + \varepsilon_v + S_R/4) \qquad 1.28$$

A plot of $\Delta P_t$ versus L/D at a fixed shear rate (Bagley plot) gives a line with slope equal to $4\tau_w$ and an intercept of

$$\Delta P_c = 4\tau_w(\varepsilon_v + S_R/4) \qquad 1.29$$

Bagley (8) extended this analysis by using Hooke's law (Equation 1.30)

$$\tau_w = G\ S_R \qquad 1.30$$

where G is the elastic modulus. Therefore, for viscoelastic fluids the contraction losses can be represented as

$$\begin{aligned}\Delta P_c &= \Delta P_v + \Delta P_e \\ &= 4\tau_w \varepsilon_v + \tau_w^2/G \qquad 1.31\end{aligned}$$

If a power law model (113) is assumed, Equation 1.31 becomes

$$\Delta P_c = 4\varepsilon_v K_0 \dot{\gamma}^{n'} + (\frac{K_0^2}{G})\dot{\gamma}^{2m} \qquad 1.32$$

where m is assumed to be equal to n' and $\dot{\gamma}$ is the apparent shear rate in the capillary tube in SLSF. The exponent, 2m, appearing in Equation 1.32, is the same as that which appears in the relationship of the normal stresses with apparent shear rate (27)

$$(P_{11}-P_{22})_w = K_1\dot{\gamma}^{2m} \qquad 1.33$$

Variations of either Equation 1.31 or 1.32 have been reported in the literature (72, 102, 161, 169).

The prediction of $\Delta P_e$ using the PGB analysis, Equation 1.31 or 1.32, is questionable since Hooke's law is not valid over a wide range of fluids and shear rates. Hooke's law is valid only when the flow behavior index, n', is equal to the exponent, m, and G is equal to $K_0^2/K_1$. This can be shown by writing Equation 1.30 as

$$\tau_w = GS_R = \frac{G(P_{11}-P_{22})_w}{\tau_w} = \frac{GK_1\gamma^{2m-n'}}{K_0} \qquad 1.34$$

However, the Bagley plots are useful in determining the total contraction losses and is a preferred method whenever capillary tube diameters are small. It is preferred because of experimental difficulty in ensuring that burrs at each pressure tap are removed when small diameter capillary tubes are used to obtain pressure profiles. Furthermore, even if the burrs were removed the presence of a pressure tap alters the velocity field in the immediate vicinity of the tap (73, 79, 126, 163). This gives rise to pressure tap errors as large as 40% of the primary normal stress difference.

An empirical correlation of $\Delta P_e$ with the primary normal stress difference in SLSF in the capillary tube was presented by LaNieve and Bogue (102). After subtracting the viscous contribution, as estimated by Weissberg's analysis (185), they correlated the experimentally measured contraction losses with the primary normal stress difference by Equation 1.35.

$$\Delta P_e = \alpha_3(m,\beta)(P_{11}-P_{22})_w. \qquad 1.35$$

The proportionality constant, $\alpha_3$, is empirically related to the exponent, m, and the contraction ratio, $\beta$. Therefore, LaNieve and Bogue's results can be rewritten as

$$\Delta P_e = \alpha_3(m,\beta)K_1\dot{\gamma}^{2m} \qquad 1.36$$

Equation 1.36 is equivalent to the second term in Equation 1.32 when m=n' and

$$\alpha_3(m,\beta)K_1 = K_0^2/G \qquad 1.37$$

Metzner et al. (116) presented an analysis whereby $\Delta P_e$ was not only predicted independent of Hooke's law but was based on flow conditions within the entry region (prior to the contraction). These authors used a momentum balance to show that the contraction losses, $\Delta P_e$, at high Reynolds numbers are equal to the primary normal stress difference evaluated at the contraction. This primary normal stress difference can be related to measurable physical properties in SLSF in the capillary tube provided the kinematics upstream of the contraction and a constitutive equation are available.

Uebler's (173) analysis of the velocity field within two diameters of the contraction suggested that, as a first approximation, the flow is radially directed towards the origin of a spherical coordinate system. The origin is located downstream within the capillary tube at a point determined by the extrapolation of the streamlines. This gave rise to kinematics referred to as sink flow kinematics (90). By using sink flow kinematics and a convective Maxwell model (116), the primary normal stresses at the contraction are found to be proportional to the shear stresses evaluated at the capillary tube wall under SLSF. Therefore,

$$\Delta P_e = \alpha_1(r_\infty)\tau_w \qquad 1.38$$

where $\alpha_1$ is related to a constant $r_\infty$. This constant enters into the analysis in order to satisfy the boundary condition whereby the primary normal stresses tend to zero at sufficiently large values of r, i.e., $r = r_\infty$. As pointed out by Metzner et al. (116):

> Quantitative assessment of the prediction of the analysis, for elongational flow described by the kinematics ... are hindered by the form of the result ... which contains two parameters that are not known precisely in most cases.

The two parameters referred to above are $\alpha_1$ and $r_\infty$. Experimentally, log-log plots of $\Delta P_e$ versus $\tau_w$ do not result in a linear relationship as suggested by Equation 1.38 (72). In general, the PGB analysis (8, 137), the empirical correlation of $\Delta P_e$ with the primary normal stress difference (102), the analysis of Metzner et al. (116), and experimental results (161, 72) suggest that

$$\Delta P_e = \beta_1 \tau_w + \beta_2 \tau_w^2 + \beta_3 \tau_w^3 + \ldots \qquad 1.39$$

where parameters $\beta_1$, $\beta_2$, $\beta_3$, etc. are evaluated experimentally.

The sink flow kinematics used by Metzner et al. (116) does not allow for the existence of shear within the converging flow region that was observed in the stress-birefringent patterns (30, 63). The use of this kinematics has been made questionable also by the analyses of the photographs of the flow field in the entry region (24, 130, 140, 142). These photographs show that shear exists within the converging region and the streamlines are not radially directed toward the origin of a spherical coordinate system, except for the immediate vicinity of the contraction. Furthermore, Cogswell (46) and Boger and Rama Murthy (24) measured velocities at the edge of the converging stream of the order 10% of the centerline velocity which is not approximately equal to the centerline velocity as measured by Uebler (173). More recently, Nakamura et al. (123) presented experimental evidence which shows clearly that the axial velocities measured within 1.5 diameters upstream and for values of $r \leq 0.275D$ are dependent on radial position. For example, at 0.50 tube diameters upstream the axial velocity at $r = 0.275D$ is equal to 0.55 times the centerline axial velocity. The above experimental evidence does not negate Metzner et al.'s method but points out the need for a better description of the upstream velocity field within the accelerating flow region in order to predict contraction losses independent of Hooke's law.

Basically, two flow patterns have been visually observed in the entry region upstream of the contraction for polymer melts and solutions. These flow patterns are exemplified by considering a high density (linear) polyethylene melt (HDPE) and a low density (branched) polyethylene melt (LDPE). For HDPE (27, 132, 188), polybutadiene (176), and polypropylene (10, 47), the flow field is similar to that observed for Newtonian fluids in creeping flow (43). The fluid converges into the capillary through a 180° solid angle with a small recirculation in the corners of the reservoir. For LDPE (10, 12, 188), polymethyl methacrylate (12, 47), polystyrene (27, 188) and for several dilute polymer solutions (12, 67, 119, 142, 168, 116), the flow field is more complex. Under creeping flow conditions the flow field is similar to HDPE. Increasing the flow rate results in a flow field that is described as being "wine glass shaped" (WGS) (116, 173) and hereinafter is referred to as a stable flow field.

A qualitative description of the stable flow field is shown in Figure 1.4. The fluid entering into the capillary tube is confined to a central core which extends upstream into the reservoir. This distance is dependent upon the contraction ratio, the flow rate, and the capillary tube diameter. The lengths of the arrows within the central core qualitatively represent the axial distances that a particle would traverse over a short time interval. Surrounding the central core are large eddies that extend up to the walls of the reservoir. The velocities within this region are significantly less than those within the central core. As the flow rate increases the location of the eddy centers move farther away from the contraction with the central core extending farther into the reservoir (50, 188). The tangent to the outermost streamline that enters into the capillary tube at the contraction defines an initial cone semi-angle, $\phi_0$. This initial cone semi-angle decreases with increasing shear rate (46, 47, 116, 129, 130) and elasticity (12, 44, 188). This suggests that the primary correlation quantity for $\phi_0$ is $D^3/\theta_0 Q$. White and Kondo (188) have shown that other quantities such as $\frac{1}{2}\frac{(P_{11}-P_{22})_w}{\tau_w}$ and $\frac{\Delta P_c}{\tau_w}$ are derived from this primary correlation quantity.

## 1.2 INSTABILITY

As polymeric materials are extruded from a capillary tube at high flow rates, irregularities are noted in the extrudate. This phenomenon is known as melt fracture

FIGURE 1.4

VELOCITY FLOW FIELD FOR VISCOELASTIC FLUID

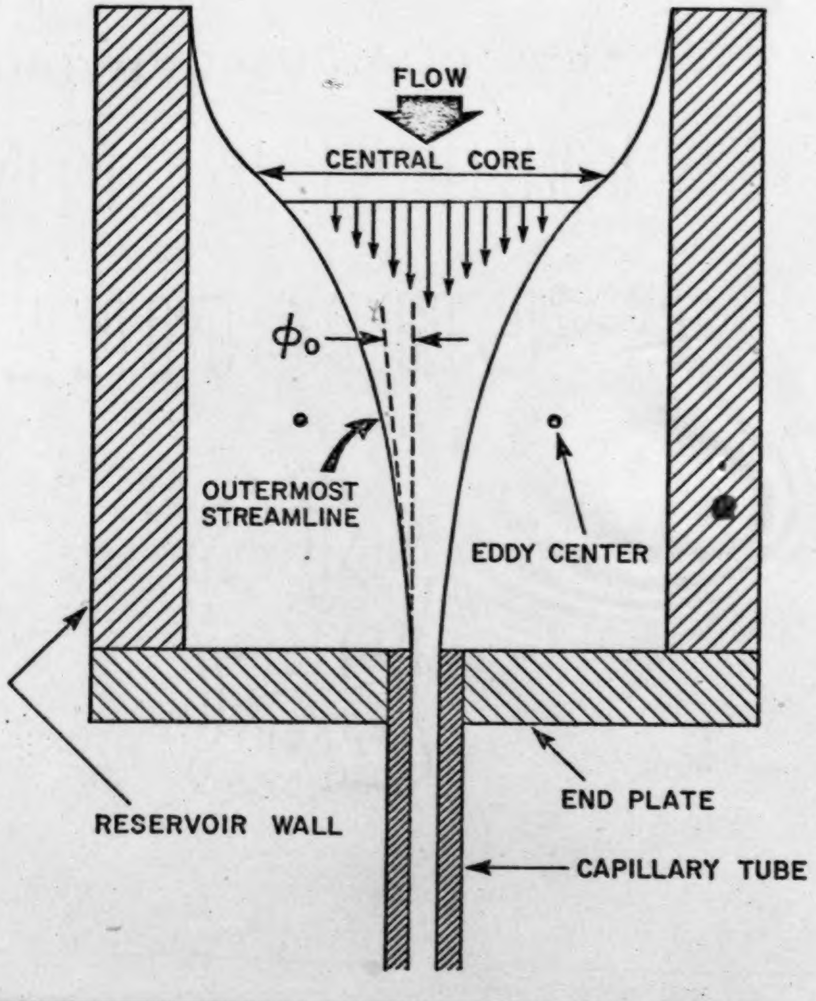
FLOW
CENTRAL CORE
$\phi_0$
OUTERMOST STREAMLINE
EDDY CENTER
RESERVOIR WALL
END PLATE
CAPILLARY TUBE

(27, 177, 188), although it is best described as flow instability (12, 134). Bialas and White (19) extensively reviewed the distorted extrudates of various polymer melts and have categorized them into basically two types:

a. The extrudate has a screw thread-like appearance typical of HDPE.

b. The extrudate has an uneven swell and eventually a very severe distortion at high flow rates. This is typical of LDPE.

The distortions in the extrudate and in the flow field upstream of the contraction observed for polymer solutions (119, 130, 132, 143) are similar to those observed for LDPE melts (12, 188). Therefore, it can be inferred that the initiation site, the mechanisms causing the onset of fracture, and the effects of reservoir geometry and capillary tube length on the onset of melt fracture for LDPE should also be applicable to polymer solutions.

Experimental studies have been directed toward the determination of the initiation site for the onset of flow instabilities and the resulting features of the disturbed flow (12, 24, 53, 63, 130 , 142). In general, the initiation site may occur within the inlet region (inlet type fracture) or within the capillary tube (capillary initiation). As pointed out by Rothenberger (149) and others (27, 134, 136) the initiation site itself may be a variable. Visual observations of changes in the velocity field within the reservoir (12, 24, 130, 132, 142) or within the capillary tube (17, 53, 107) are used in determining the initiation site. Indirect methods such as the total pressure loss-flow rate curve referred to as the apparent shear stress-apparent shear rate curve (52, 53, 105, 120) and the flow curve referred to as true shear stress-apparent shear rate curve (136, 182) have also been used. The flow curve is obtainable from the total pressure loss-flow rate curve once the total pressure losses are corrected for end effects. The end effects are obtainable from Bagley plots or from pressure profiles.

### 1.2.1 CAPILLARY INITIATION

It has been suggested that the initiation site may exist within the capillary tube rather than in the inlet region (19). In HDPE melts, the flow curve indicates, almost without exception, a double value of the shear stress or apparent shear rate at the onset of flow instabilities (23, 53, 105). However, plots for entrance effects, i.e., log-log plots of the total pressure loss versus flow rate, show that at the onset of instabilities no discontinuity is present.

The existence of a double value of the apparent shear rate is revealed by the use of a constant stress rheometer (1, 3, 179, 183). A constant stress rheometer is achieved by maintaining a constant pressure in the reservoir producing a controlled piston force or by direct application of a gas at a controlled pressure. The volumetric flow rate is measured to obtain the apparent shear rate. On the other hand, the existence of a fluctuation of the shear rate (53, 120) and a double value of shear stress is revealed by a constant rate rheometer which is a hydraulic cylinder moving at a constant rate. The shear stress can be evaluated either by the Bagley plot or by pressure profiles. It can be deduced that the double value of the shear stress and fluctuating shear rate can be explained best in terms of the relationship between volumetric flow rate and reservoir pressure as given in the flow curve (105, 134). The flow curve given in Figure 1.5 is divided into three regions: a stable region, an unstable region, and a second stable region. At flow rates less than $Q_A$ the velocity field is stable and viscosity decreases with increasing shear stress. The extrudate is smooth. The cyclic path indicated by the arrows represents the periodic pressure flow rate sequence that would be followed for an imposed mean flow rate lying in the unstable region. The horizontal lines represent essentially discontinuous jumps in the flow rate. If the chosen volumetric flow rate lies in the unstable region, the actual volumetric flow rate alternates between the two limits, $Q_0$ and $Q_1$, and the extrudate surface changes accordingly from smooth to rough. This interpretation implies that the nature of the flow field within the capillary tube is important in setting up the instability. The onset of flow instabilities can be shifted to higher apparent shear rates by broadening the molecular weight distribution (120), by reducing the mole-

FIGURE 1.5

RESERVOIR PRESSURE AS A FUNCTION OF VOLUMETRIC FLOW RATE AT ONSET OF FRACTURE

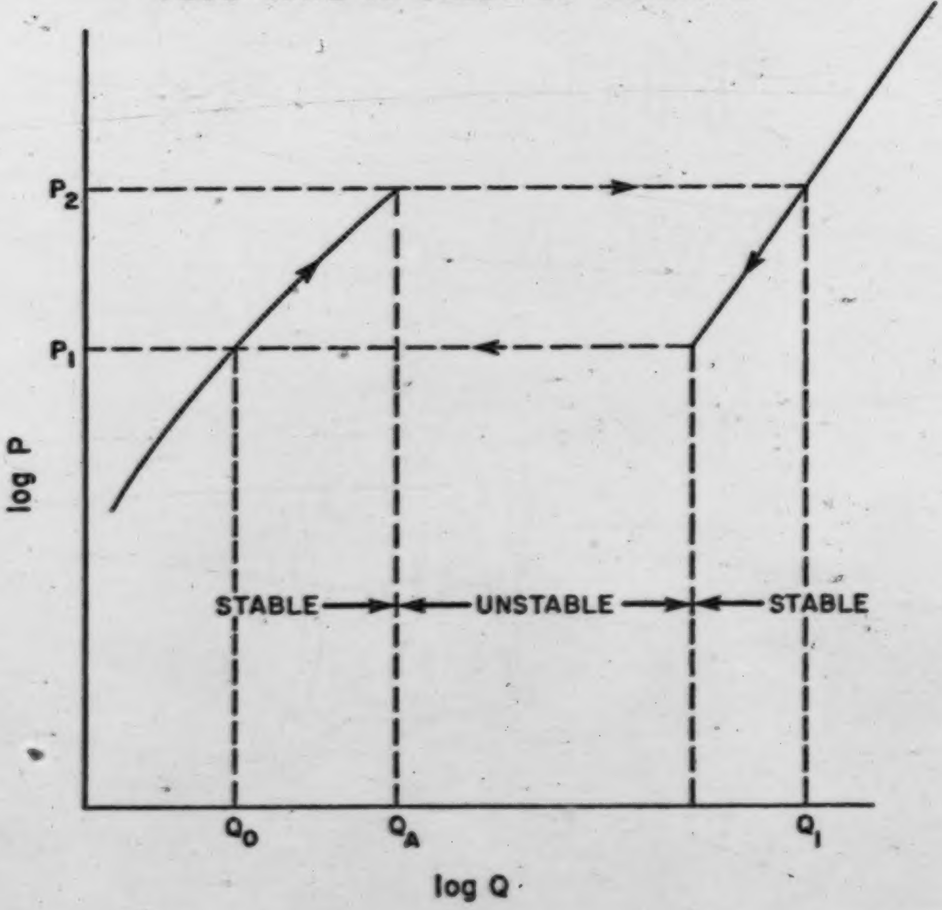

cular weight (179), or by increasing the temperature of the polymer melt (103, 117, 177).

Most authors attribute the cause of melt fracture in HDPE melts to slip at the wall (18, 135, 182) although other mechanisms or explanations have been discussed by Casey (37), Hagler (70), Bogue and White (27), Petrie and Denn (136) and Myerholtz (120). Direct evidence of slip at the wall is limited. Benbow and Lamb (18) presented evidence that this occurred above the onset of melt fracture. Recently, den Otter (54) found slip at the wall in low temperature flows of ethylene-propylene melts. Indirect evidence has been presented by Lupton and Regester (105) and Blyler and Hart (23) by the inclusion of a non-zero velocity at the wall as a boundary condition for flow through a circular tube; the shear rate or the velocity gradient at the tube wall is linear with respect to $D^{-1}$ at a constant $\tau_w$. In the event of slip at the tube wall the slope of this line is positive while for zero slip at the wall the slope is equal to zero. Results for HDPE melts substantiated the mechanism of slip at the wall (23, 105).

Although photographs of the unstable flow field in the entry region are few and not very detailed, Bagley and Birks (10) concluded that the frequency of observed recoiling in the flow field (description given on page 30) are greater than those observed for the flow of LDPE melts.

### 1.2.2 INLET INITIATION

The discontinuity noted in the flow curve of HDPE melts is absent for LDPE melts (16, 23, 105, 179), polystyrene (179), and polymethyl methacrylate (16). The plots of the entrance effects, i.e., log-log plots of the total pressure loss versus flow rate, exhibit a discontinuity at the onset of melt fracture. Hence, for the flow of LDPE melts, polystyrene, and polymethyl methacrylate, the onset of flow instabilities is believed to occur within the inlet region (136, 187, 188). The plotting of the experimental data for LDPE according to the analysis presented by Blyler and Hart (23) confirmed that slip at the wall was nonexistent. In addition, the experimental measurements of velocity within the vicinity of the capillary tube wall (17, 53) showed that the velocity at the capillary tube wall was equal to zero for polybutadiene and LDPE melts. Maxwell and Galt (107) measured velocity profiles but their results are doubtful due to errors in measuring the distance from the wall.

The stable flow field within the inlet region for LDPE melts was described in pages 22-23 wherein the melt enters into the capillary tube through a central accelerating core as it passes from the reservoir into the capillary tube. At the onset of flow instabilities the stable flow field breaks down (12, 188). The fluid normally entering the capillary tube through the WGS core recoils and as the material recoils the fluid enters into the capillary tube from the eddies surrounding the core. This phenomenon is periodic and its frequency increases with flow rate. Correspondingly, the extrudate is distorted. Prior to the recoiling of the fluid, observations of a slight swirling or spiraling motion have been observed (12, 132, 188). The intensity increased with increasing flow rate with a corresponding helical distortion of the extrudate. Fluctuations in the pressure were measured when the spiraling motion became more accentuated (12).

An unstable flow field similar to that reported for LDPE melts has been observed for polymer solutions (30, 119, 130, 142). Recently, Rama Murthy (142) reported visual observations based on the flow field for a 1.49% solution of Separan AP-30 in a 50% by weight glycerol-water mixture. He observed that at low flow rates the flow field was WGS but at a certain flow rate this flow field developed a "spiraling flow" (description given by Rama Murthy) whose intensity increased with flow rate. The flow field failed to exhibit any regularity with further increases in flow rate and was described as being "chaotic" (description given by Rama Murthy). At even higher flow rates this "chaotic" flow field abruptly changed to the stable flow field that is associated with the stable flow of HDPE melts. In all of the above observations no attempt was made to obtain photographs from which the details of the velocity components can be measured. These observations do suggest, however, that failure of the material, as an explanation of melt fracture, need not be involved.

In an attempt to predict the onset of flow instabilities certain theoretical considerations such as linear stability theory (135), the accelerating wave mechanism (37), and the growth and magnitude of the normal forces within the entry region (116, 119, 173) have been considered. The application of such theories requires a tractable constitutive equation and a detailed knowledge of the upstream velocity field. Since the stable flow field is complex and has not been fully described either mathematically or empirically, existing analyses have dealt only with the stability of shearing flows in the capillary tube (147). This was simplified even further to the analysis of the stability of shearing flows between infinite parallel plates (109, 138). Ultman and Denn (174) suggested that when the velocity of propagation of the shear wave is of the same order of magnitude as the frictional velocity, a discontinuity occurs in the slope of the streamline. Although the streamlines were not obtained directly, Boger and Rama Murthy (24) observed that for several aqueous polymer solutions the velocity distribution at the entrance of the capillary tube underwent an abrupt change. This occurred when the ratio of the shear wave velocity to the frictional velocity, evaluated under SLSF in the capillary tube, was equal to unity.

Since there is no detailed empirical description of the stable flow field in the entry region, mechanisms previously mentioned cannot be tested rigorously as to their ability to predict the onset of instabilities in polymers where initiation occurs in the inlet.

### 1.2.3 EFFECTS OF ENTRY GEOMETRY AND CAPILLARY

The effects of entry geometry (48, 70, 114, 152, 170, 188) and capillary length to diameter ratio (12, 13, 70, 85, 134) on the onset of flow instabilities are not firmly established. When the initiation site is inlet initiation, Tordella (170) reported that shear rates at the onset of flow instabilities increased by an order of magnitude as the die entry half-angle was altered from 90 degrees to 20 degrees. Metzner, Carley and Park (114) reported a slight increase in shear rates which was significantly less than the two orders of magnitude increase observed by Cogswell and Lamb (48). On the other hand, Schreiber, Bagley and Birks (152) stated that the entry half-angle had no effect on the delay of flow instabilities. They concluded that for flows in conical shaped entrances the frequency of recoiling of the center flow is higher and the magnitude lower. This reduced the distortion in the extrudate and could cause misjudgement in estimating the flow rate at which instability commences. Finally, Hagler (70) reported critical shear rates (or shear stresses) 30 to 50 percent lower in a 45° entrance than in a 90° entrance. When the initiation site is in the capillary, the effect of the die entry geometry on the onset of flow instabilities was found to be independent of die entry geometry (53). However, Hagler (70) observed that the shear rates at the onset of flow instabilities for HDPE melts decreased two to three times as the die entry half-angle increased from 45 degrees to 90 degrees. This is consistent with results reported by Cogswell and Lamb (48) and Ferrari (62) for polypropylene melts. Cogswell and Lamb (48) used slightly tapered die entry half-angles, half-angles less than 4.5 degress, whereas Ferrari (62) varied the tapered angle from 90 to 3 degrees. A more detailed investigation of the flow field within the entry region would assist in understanding the effects of entry geometry on the onset of flow instabilities.

The effect of the length to diameter ratio on the onset of flow instabilities for several polymer melts is summarized in Table 1.1. With the exception of the results reported by Hagler (70) and Ballenger et al. (13) for HDPE melt and Ferrari (62) for polypropylene, all the cited authors reported that the length to diameter ratio of the capillary tube had an effect on the onset of flow instabilities. The majority of these results indicated that as the length to diameter ratio increased the critical shear stress increased, i.e., higher throughputs could be achieved prior to the extrudate being distorted. It was postulated that fluctuations should decay down the capillary tube so that increasing the length of the capillary tube should tend to stabilize the extrudate (85, 134, 152). Han and Lamonte (80) measured the pressure fluctuations for a LDPE melt along the capillary tube length. They found that the pressure fluctuations decreased along the

## TABLE 1.1

## EFFECT OF L/D ON ONSET OF INSTABILITY

| AUTHOR | POLYMER | CASE 1 | CASE 2 | CASE 3 |
|---|---|---|---|---|
| Ballenger et al. | polystyrene | | x | |
| | LDPE | | x | |
| | HDPE | x | | |
| Bartos, Holomek | polybutadiene | | | x |
| Cogswell, Lamb | polypropylene | | x | |
| Dennison | HDPE | | x | |
| den Otter | LDPE | | x | |
| | HDPE | | | x |
| Ferrari | polyproplylene | x | | |
| Hagler | LDPE | | x | |
| | HDPE | x | | |
| Han, Lamonte | LDPE | | x | |
| Klein, Fusser | polyisobutylene | | x | |
| Myerholtz | HDPE | | | x |
| Rama Murthy | Separan AP-30 Solution | | x | |
| Tomita, Shimbo | polyethylene oxide solution | | x | |
| Westover | HDPE | | x | |

Case 1 - No effect of L/D

Case 2 - As L/D increases the shear stress evaluated at the onset of fracture, $(\tau_w)_c$, increases

Case 3 - As L/D increases the shear stress evaluated at the onset of fracture, $(\tau_w)_c$, decreases capillary tube length and distortions in the extrudate occurred only when the pressure fluctuations existed up to the tube exit. Contrary evidence was presented by den Otter (53). He showed that when LDPE melts were extruded between flat, parallel plates there were no pressure fluctuations downstream of the entry region, even at very high shear stresses when the extrudate was severely distorted. The reason for this contradiction is not resolved, therefore, the results must be considered with caution.

To summarize, in LDPE melt flow, the pressure fluctuations in the entry region arise from velocity fluctuations or from a vortex-induced alternating flow. This points out the need for details on the upstream velocity field and theories which "determine the ability of the system to propagate a disturbance" (136).

### 1.2.4 EMPIRICAL CORRELATIONS - PREDICTION OF FLOW INSTABILITIES

The correlations of melt fracture with rheologically relevant dimensionless parameters seem justified only on empirical grounds since actual flow patterns are complex (134). These correlations, if successful, do not constitute an explanation for the onset of flow instabilities.

It was suggested (134, 136) that the Reynolds number (inertial phenomenon) which successfully correlates the transition from laminar to turbulent flow (20) was relevant because there appeared to be a slight correlation between the Reynolds number and the onset of flow instability. Experimental values of the Reynolds number at the onset of melt fracture varied from $10^{-4}$ (114) to values of the order 100 (142). Consequently, a suitable criterion was not found. The inertial phenomenon would predict: (a) at fixed fluid properties, the critical flow rate would be directly proportional to D, and (b) at a fixed die diameter, the critical flow rate would be directly proportional to the apparent viscosity. However, experimental evidence, as indicated by Tordella's results (171), showed that for fixed fluid properties the critical flow rate is directly proportional to $D^3$, whereas at a fixed die diameter the critical flow rate is inversely proportional to the apparent viscosity.

The experiment of Spencer and Dillon (158) indicated that the onset of melt fracture for several polymer melts and several die diameters occurred at a constant value of V/D or, equivalently, a constant apparent shear rate, 8V/D. With the aid of a flow curve, this implied a constant shear stress. The introduction of a dimensional quantity, having the dimensions of time, allows for the formation of a dimensionless group, $V\theta/D$, which has been used also as a criterion (24). Spencer and Dillon (158) further proposed that melt fracture for polymer melts occurs when the shear stress is of the order $10^6$ dyn/cm$^2$. The dependence of instability on entry geometry and L/D ratios need not imply a simple straightforward critical shear stress or shear rate criterion. The critical shear stress for polymer melts and solutions tabulated in Table 1.2 show a sevenfold variation for polymer melts, a 250-fold variation for polymer solutions and over four orders of magnitude variation between polymer melts and solutions. Therefore, the shear stress criterion proposed for polymer melts, i.e., melt fracture occurs whenever the shear stress is $10^6$ dyn/cm$^2$, is not applicable to polymer solutions.

Bagley (8) attempted to correlate the onset of fracture with a critical value of the recoverable shear strain (equation given below)

$$S_R = (\tau_w)_M/G \qquad 1.40$$

where $(\tau_w)_M$ is the shear stress evaluated at the onset of fracture for polymer melts. By using a Maxwell model, the elastic modulus, G, can be related to the viscosity and the relaxation time of the fluid (147, 190) by

$$G = \mu/\theta \qquad 1.41$$

The substitution of Equation 1.41 into Equation 1.40 with $(\tau_w)_M$ evaluated under SLSF in the capillary tube yields

$$S_R = 8\,\frac{V\theta}{D} \qquad 1.42$$

The Weissenberg number, defined as the ratio of the primary normal stress to the shear stress in SLSF in the capillary

## TABLE 1.2

## CRITICAL SHEAR STRESS AT ONSET OF INSTABILITY

| AUTHOR | POLYMER MELTS | $(\tau_w)_c \times 10^{-6}$ (dyn/cm$^2$) |
|---|---|---|
| Bagley | Polyethylene | 1.28 - 2.26 |
| Bartos | numerous polymers | 0.695 - 4.0 |
| Blyler, Hart | LDPE | 2.0 |
| Hagler | LDPE | 0.586 - 0.863 |
|  | HDPE | 2.04 - 3.21 |
| Lupton, Regester | HDPE | 3.0 |
| Metzner, et al. | Polyethylene | 3.17 |
| Myerholtz | HDPE | 2.9 - 3.3 |
| Oyanagi | HDPE | 1.96 - 3.49 |
| Vlachopoulos, Alam | LDPE | 1.02 - 1.433 |
|  | HDPE | 1.464 - 2.592 |
|  | Polypropylene | 1.062 - 1.41 |
| Vlachopoulos, Lidorikis | Polystyrene | 0.68 - 2.15 |
| Westover | HDPE | 1.65 - 3.78 |
|  | **SOLUTIONS** |  |
| Murch | 0.5% Separan AP-30; 30% glycerine-water mixture | 0.0003 |
| Oliver, Bragg | 0.10% ET-597 | 0.0006 |
| Paul, Southern | Polystyrene-benzene | 0.015 - 0.932 |
| Rama Murthy | 1.49% Separan AP-30; 50% glycerine-water mixture | 0.00006 - 0.00024 |
| Vinogradov, Martin | Aluminum naphthenate | 0.00075 - 0.006 |

tube, has been suggested also as a criterion (134). This is equal to twice the recoverable shear strain as shown by the equation below

$$N_{ws} = \frac{(P_{11}-P_{22})_w}{\tau_w} = 2\gamma\theta = 16\,\frac{V\theta}{D} = 2S_R \qquad 1.43$$

Reported values of the recoverable shear strain at the onset of fracture are given in Table 1.3. $S_R$ varies from 2.2 to 66.81 for both polymer melts and solutions. This variation is due in part to the variation in methods of estimating the elastic modulus, i.e., the pressure loss measurements (Equation 1.31), or the normal stress measurements.

Southern and Paul (157) extended the criterion of a recoverable shear strain by noting that

$$(S_R)_M \simeq (S_R)_S \qquad 1.44$$

The proposed criterion for polymer solutions takes the form of

$$\left(\frac{C}{\rho}\right)^2 (\tau_w)_M \leq (\tau_w)_S \leq \left(\frac{C}{\rho}\right) (\tau_w)_M \qquad 1.45$$

where $\rho$ is the density of the polymer melt, C is the concentration of the polymer solution, $(C/\rho)$ is the polymer volume fraction, and $(\tau_w)_S$ is the shear stress evaluated at the onset of fracture for polymer solutions. The shear stresses at melt fracture predicted by Equation 1.45 for several polymer solutions are in agreement with experimental

## TABLE 1.3

## RECOVERABLE SHEAR STRAIN AT ONSET OF INSTABILITY

| AUTHOR | POLYMER MELTS | $S_R$ |
|---|---|---|
| Bagley | LDPE | 15.0 |
| | HDPE | 6.4 |
| Barnett | Polypropylene | 12.2 - 35.5 |
| Gruver, Kraus | Polybutadiene | 11.0 - 19.6 |
| Han, Lamonte | Polystyrene | 2.2 |
| Howells , Benbow | Polymethyl-methacrylate | 7.2 |
| Huseby | theory | 25.1 |
| Rothenberger | theory | 2.6 |
| McCoy, Denn, Schott | HDPE | 7.42 - 8.08 |
| Spencer, Dillon | Polystyrene | 7.08 - 7.67 |
| Tordella | Polyethylene | 5.0 |
| Vlachopoulos, Alam | Polystyrene | 3.0 - 66.81 |
| | Polypropylene | 13.59 - 28.74 |
| | LDPE | 5.46 - 13.65 |
| | HDPE | 31.08 - 53.87 |
| | SOLUTIONS | |
| Kroesser | Vistanex L100 | 17.0 - 27.0 |
| | B100 | 12.7 - 42.8 |
| Williams | Polyethylene | 11.0 - 28.0 |
| Boger, Rama Murthy | Separan AP-30 | 6.0 |

results (119, 133, 142).

In general, the preceding criteria correlate fracture with measurements in SLSF in the capillary tube. This is not consistent with experimental observations. Experimental observations show that for many polymer melts and solutions, fracture occurs within the inlet region (inlet initiation) and within this region the fluid is subjected to both shear and elongation deformations (12, 24, 47, 63, 77). For these fluids, the mechanisms put forward as the cause of fracture, based on inlet conditions, have not been severely tested since details of the converging velocity field are not well known. If one assumes, as a first approximation, that the coverging velocity field is effectively an extensional flow then a criterion for the onset of fracture should be related to fluid properties in extensional flow (48, 60). den Otter (53) stated that "when the pressure has reached a sufficiently high value, a breakdown of melt fracture takes place." Thus, melt fracture as a consequence of tensile failure in extensional flow may be correlated with the pressure losses in the entry region (70, 88). The concept of a critical pressure loss is also reflected in the apparent shear rate-apparent shear stress curve wherein, at fracture, a discontinuity is observed in the curve (page 27).

Cogswell (46) assumed that the converging flow through an orifice can be analyzed in terms of the extensional and shear components separately. This allowed for derivation of the relationships between volumetric flow rate, pressure drop, and the maximum extensional stress at the die entry. In summary, melt fracture is predicted to occur whenever the extensional stress, $\tau$, exceeds some critical value given by

$$(\tau)_{cr} = \frac{3}{8}\,(3n'+1)P_u \qquad 1.46$$

and $P_u$ is the pressure loss in the upstream entry region given by

$$P_u = \frac{8}{3(n'+1)}\ \frac{\dot{\gamma}\mu_A}{\tan\phi_0} \qquad 1.47$$

where $\mu_A$ is the apparent viscosity evaluated at $\dot{\gamma}$. As $\phi_0$ tends to 90 degrees, the entry pressure losses and the extensional stresses tend to zero. However, as $\phi_0$ tends to zero degrees both $P_u$ and $(\tau)_{cr}$ tend to infinity. This is believed to be highly unlikely. At intermediate values of $\phi_0$, $P_u$ and $(\tau)_{cr}$ are directly proportional to the shear stresses evaluated under SLSF in the capillary. Hürlimann and Knappe (88) also postulated a critical contraction loss. From the PGB analysis, the contraction losses are given by

$$\Delta P_c = 4\tau_w\varepsilon_t \qquad 1.48$$

At melt fracture

$$(\tau_w)_M\,MW = \text{critical value} \qquad 1.49$$

hence, Equations 1.48 and 1.49 imply that whenever $\Delta P_c$ exceeds a critical value, $(\Delta P_c)_{cr}$, fracture will occur. Hagler (70) measured the contraction losses for a LDPE and a HDPE melt for flows in an abrupt contraction and found that at the onset of fracture $(\Delta P_c)_{cr} = .29$ to $.30 \times 10^8$ dyn/cm$^2$ for LDPE and $(\Delta P_c)_{cr} = .72$ to $.76 \times 10^8$ dyn/cm$^2$ for HDPE. These data lend support to a critical value of $\Delta P_c$ at the onset of fracture. The significance of Hürlimann and Knappe's analysis is the correlation of $(\Delta P_c)_{cr}$ with a critical extensional stress level at fracture. They concluded that "melt fracture starts when the extensional stress in the die inlet exceeds a critical value."

Everage and Ballman (60) proposed a critical extensional stress level directly by postulating that fracture is a consequence of tensile failure in extensional deformation. Whenever the material attains a critical value of the stretch rate, $\Gamma_c$, given by the limiting condition

$$2\theta\Gamma_c = 1.0 \qquad 1.50$$

the material is unable to reach steady-state or as stated by Everage and Ballman (60) "... the material is unable to deform with sufficient rapidity to reach a steady-state stress level and fracture may result." From a Maxwell model, the relaxation time of a fluid is

$$\theta = \mu_E/G_E \qquad 1.51$$

where the subscript E refers to extensional deformation and the elastic modulus is given by

$$G_E = \frac{\tau}{\varepsilon_R} = \frac{\mu_E \Gamma}{\varepsilon_R} . \qquad 1.52$$

where $\varepsilon_R$ is the recoverable extensional strain. Combining Equation 1.51 and 1.52 yields

$$\theta\Gamma = \varepsilon_R \qquad 1.53$$

Everage and Ballman's (60) hypothesis implies, therefore, a critical value of the recoverable extensional strain. This hypothesis can be tested quantitatively by determining if the maximum stretch rate is effectively constant at the onset of melt fracture. An approximate calculation of the maximum stretch rate, utilizing the velocity field for the flow of an incompressible Newtonian fluid through a cone (60), yields

$$\Gamma_{max} = \frac{12Q}{\pi D^3 \cot\phi_0^3} \left[\frac{(1-\cos 2\phi_0)}{(1-\cos\ \phi_0)^2 (1+2\cos\phi_0)}\right] \qquad 1.54$$

In terms of the capillary wall shear rate, the maximum stretch rate is

$$\Gamma_{max} = \frac{3\dot{\gamma}_w}{8\cot\phi_0^3} \left[\frac{(1-\cos 2\phi_0)}{(1-\cos\ \phi_0)^2 (1+2\cos\phi_0)}\right] \qquad 1.55$$

Therefore, for a constant initial cone semi-angle, $\phi_0$, a critical volumetric flow rate or a critical capillary tube apparent shear rate criterion is implied from the recoverable extensional strain criterion. By using Equation 1.54 and the data reported by Ferrari (62), Everage and Ballman (60) calculated that $\Gamma_{max}$ at the onset of fracture was reasonably constant ($760\ sec^{-1} \leq \Gamma_{max} \leq 1195\ sec^{-1}$). These results quantitatively support the proposal which states "... that melt fracture is a consequence of tensile failure of the material in elongation deformation" (60). It has been shown in the previous section (Section 1.2.3) that the onset of instabilities within the inlet region varies with the entry geometry, the capillary tube length and the type of polymer. Hence $\Gamma_{max}$ is expected to vary accordingly.

The hypothesis presented by Everage and Ballman (60), which is an extension of the work of Denn and Marrucci (51), is based upon a time dependent stress growth resulting from the converging flow field. Since this converging flow field is affected by the magnitude of the flow rate (see pages 22-23) for a description of the flow field with flow rate), the fluid is subjected to different strain histories. It seems sensible, therefore, to compare all fluids at a constant strain level, S, which takes into account not only the magnitude of the stretch rate but also time, i.e., Hencky's strain measure (70), which is also referred to as the total strain (98). The total strain is defined as

$$S = \int_{t_i}^{t_f} \Gamma\, dt \qquad 1.56$$

Parameter S has been used successfully to correlate velocity data (90) and transient elogational viscosity data (1). Acierno et al. (1) found that the transient elongational viscosity-total strain curves obtained from spinning (where the melt is extruded, solidified, and then drawn up as a filament) and inverse siphon experiments (fluid is drawn vertically into a capillary tube creating a vertical liquid filament) resulted in a single curve. The data obtained from the inverse siphon experiment covered the initial part of the transient curve while the data from the spinning experiment yielded the upper part of the same transient curve. By using the total strain rather than the strain rate in a fibre spinning experiment, the axial stresses, measured at different rates of extrusion, and take-up rates were correlated by a single curve (87). Therefore, an extension of Everage and Ballman's proposal integrated with the work of Acierno et al. (1) suggests the total strain as a criterion for the onset of melt fracture.

# CHAPTER II

# EXPERIMENTAL EQUIPMENT AND PROCEDURE

## 2.1 EXPERIMENTAL EQUIPMENT

The experimental equipment consisted of the flow system (Instron and a stainless steel hydraulic cylinder), the entry region, and the capillary tubes.

### 2.1.1 FLOW SYSTEM

A constant flow rate was maintained by an Instron, Model TM, and two stainless steel hydraulic cylinders which were 15.24 cm I.D. (cylinder 1) and 15.60 cm I.D. (cylinder 2). Cylinder 1 was used in obtaining the data for the Newtonian solutions while cylinder 2 was used for the viscoelastic solution. The calibration of each cylinder, given in Appendix A, revealed that the calculated and measured flow rates were within one half of one percent of each other. Hence, it was concluded that there was no seepage of fluid between the inner cylinder wall and the piston. The cross head speed of the Instron was calibrated as outlined in the Instron manual.

### 2.1.2 ENTRY REGION

The physical dimensions of the two square reservoirs are given in Table 2.1. The internal length of each reservoir assured that the velocity distributions for the Newtonian and viscoelastic solutions were developed at

## TABLE 2.1

## INTERNAL RESERVOIR DIMENSIONS

| RESERVOIR | WIDTH (cm) | LENGTH (cm) |
|---|---|---|
| Small (S) | 2.62 | 25.40 |
| Large (L) | 25.49 | 71.70 |

## TABLE 2.2

## CAPILLARY TUBE LENGTH TO DIAMETER RATIOS

| | L/D RATIOS | | |
|---|---|---|---|
| | CAPILLARY TUBE 1 | CAPILLARY TUBE 2 | CAPILLARY TUBE 3 |
| CAPILLARY NO. | 0.10 cm | 0.20 cm | 0.30 cm |
| A | --- | 31.60 | --- |
| B | 35.03 | 34.99 | 34.97 |
| C | 55.08 | 54.96 | 55.04 |
| D | 71.32 | 71.23 | 71.13 |
| E | 96.45 | 96.38 | 96.36 |
| F | --- | --- | 145.00 |
| G | 148.48 | 148.45 | 148.53 |
| H | --- | 151.00 | --- |
| I | --- | 160.16 | --- |
| J | 222.08 | 222.36 | 213.38 |
| K | 305.08 | 304.95 | 304.83 |
| L | 450.00 | 457.43 | --- |

the location of the pressure taps even under the worst possible condition, i.e., the highest Reynolds number. The pressure taps, schematically shown in Figure 2.1, were located 10.2 cm and 27.9 cm from the entrance in reservoirs S and L respectively where pressures and pressure traces were measured. In reservoir S the fluid entered through a diverging cone having a maximum diameter of 2.54 cm while in reservoir L a diffuser plate was located approximately 5 cm from the inlet end. The sides of each reservoir were constructed of 2.54 cm thick transparent lucite plate to allow for flow visualization. The end plates were of anodized aluminum.

### 2.1.3 CAPILLARY TUBES

The precision bore 0.10, 0.20, and 0.30 cm I.D. borosilicate glass capillary tubes, hereinafter referred to as capillary tubes 1, 2, and 3 respectively, were manufactured by Fischer & Porter Co. The internal diameters of the capillaries had a tolerance of ±.00076 cm. For each diameter, several tube lengths were cut into length to diameter ratios that varied from 31.60 to a maximum of 457.43. The various length to diameter ratios for the three capillary tubes are given in Table 2.2; capillary no. C was used in the measurement of velocities. The capillary tube lengths used in the measurement of pressure losses are given in Appendix B.

Schematically shown in Figure 2.2 is the device for

FIGURE 2.1
RESERVOIR AND PRESSURE TAP LOCATION

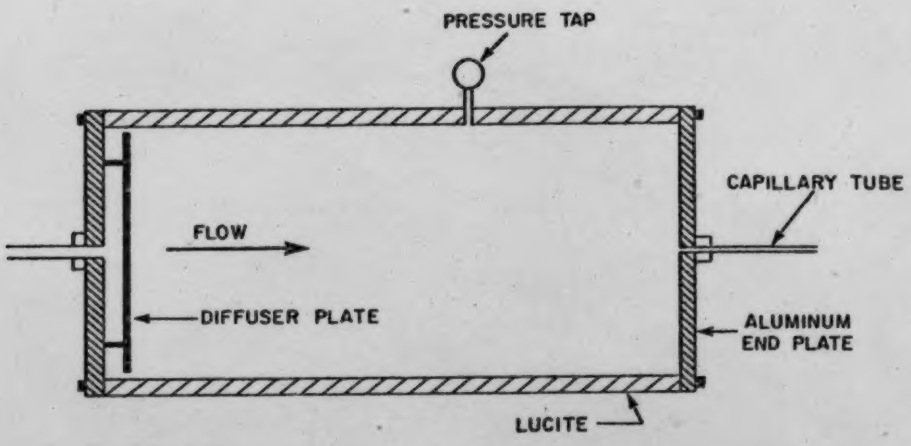
PRESSURE TAP
CAPILLARY TUBE
FLOW
DIFFUSER PLATE
ALUMINUM END PLATE
LUCITE

RESERVOIR L

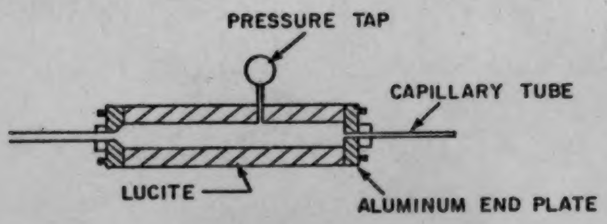
PRESSURE TAP
CAPILLARY TUBE
LUCITE
ALUMINUM END PLATE

RESERVOIR S

FIGURE 2.2

CAPILLARY HOLDING DEVICE

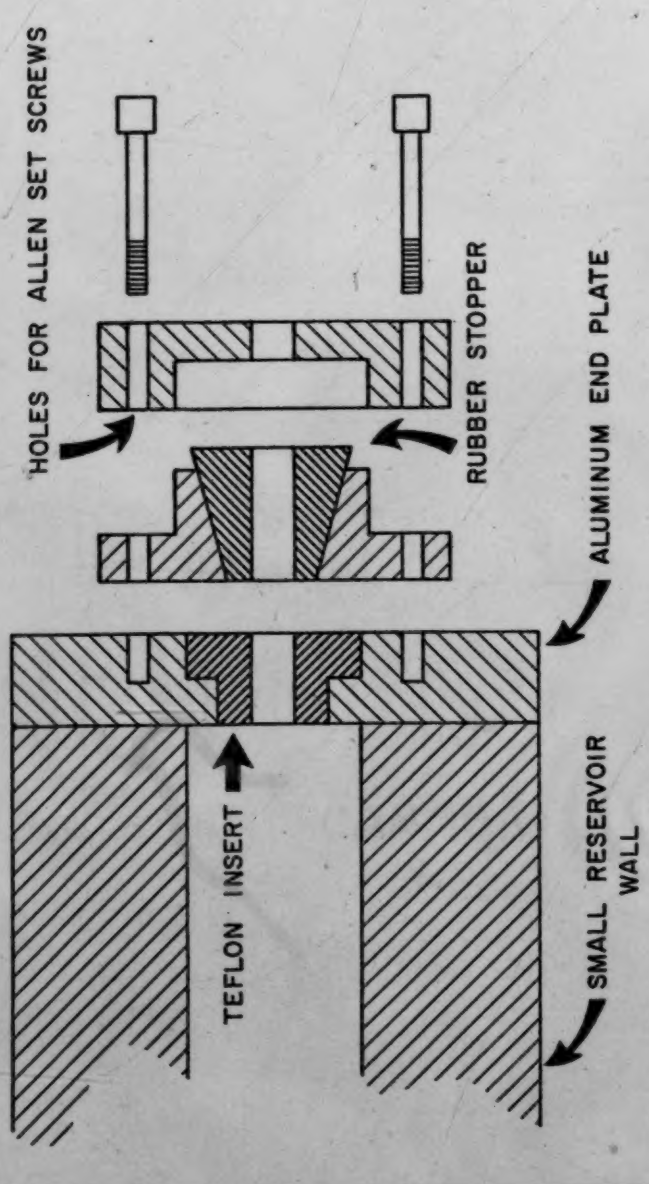
HOLES FOR ALLEN SET SCREWS
RUBBER STOPPER
ALUMINUM END PLATE
TEFLON INSERT
SMALL RESERVOIR WALL

holding the capillary tubes firmly in place flush with the inside surface of the aluminum end plate. This holding device was capable of withstanding maximum pressures of $7 \times 10^6$ and $4 \times 10^6$ dyn/cm$^2$ in reservoirs S and L respectively.

## 2.2 EXPERIMENTAL FLUIDS AND TRACER PARTICLES

Several aqueous sugar solutions, an oil, and one concentration of Separan AP-30 were the experimental fluids while aluminum dust particles were used as tracer particles in the photographic method.

### 2.2.1 EXPERIMENTAL FLUIDS

The Newtonian fluids used were three aqueous sugar solutions of 46%, 53%, and 61% by weight and an oil, Primol-355. The physical properties of these sugar solutions and the oil are tabulated in Appendix D, Section D.1.

The polymer solution was a 0.20% aqueous solution of Separan AP-30 which is a high molecular weight synthetic polymer (molecular weight between 2 and $3 \times 10^6$) manufactured by the Dow Chemical Company. The approximate composition of this polymer is represented by the formula given below:

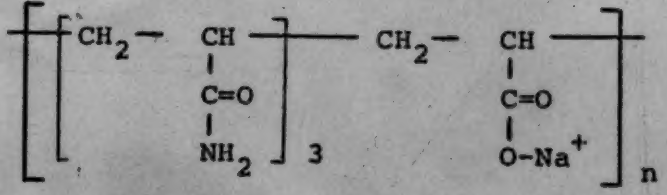

$$\left[ \left[ CH_2 - \underset{\substack{| \\ C=O \\ | \\ NH_2}}{CH} \right]_3 - CH_2 - \underset{\substack{| \\ C=O \\ | \\ O\text{-}Na^+}}{CH} \right]_n$$

The physical properties are given in Appendix D, Section D.2. The solution showed no significant changes in physical properties over a two month interval. Degradation due to bacterial presence was eliminated by the addition of a small amount of sodium benzoate. Furthermore, the solution was used only once to ensure that the physical properties did not change from run to run owing to mechanical degradation.

### 2.2.2 TRACER PARTICLES

The flow visualization method of injecting hydrogen bubbles (approximately .01 cm diameter) into the fluid proved to be impractical. This impracticality resulted from the extremely small velocities in the recirculation region surrounding the central core of fluid that entered into the capillary tube. The hydrogen bubbles accumulated and adhered to the viewing surface of the reservoir distorting the image when viewed through the camera lens. To circumvent this problem aluminum dust particles (manufactured by Baker, lot number 2347) at approximately 0.00075 volume percent were used as the tracer. The measured maximum width of each of these thin, irregularly shaped particles, given in Appendix A, Section A.4, varied from 3 to 34 microns with a mean maximum length of 13 microns. The maximum width was 0.7 times the maximum length with the thickness estimated to be 1 micron. To prevent the particles from adhering to each other in the solution they were dispersed in a small quantity of water (approximately 1 $cm^3$) prior to being mixed with the polymer solution.

## 2.3 PHOTOGRAPHIC METHODS

An optical method of measurement was used to obtain streak photographs of aluminum dust particles in the polymeric solution in order to measure the local axial and radial velocities within the converging flow field.

### 2.3.1 OPTICAL SYSTEM

The optical system, schematically shown in Figure 2.3, consisted of an arc lamp, a converging lens, a chopping disc, a reservoir, and a camera assembly. A Christie transformer with a maximum output of 3300 watts D.C. operated the Christie Xenon arc-lamp. The set of converging mirrors in the lamp-housing, No. BSF 50, were located so that they directed the light beam through the narrow slit located on the reservoir. An adjustable slit placed immediately prior to the converging lens produced a light beam smaller than the slits on the chopping disc.

The 38.1 cm diameter, 0.32 cm thick, chopping disc was divided into an equal number of radial slits and spokes. The variable speed motor driving the chopping disc and the interchangeable pulley sizes allowed the time interval (the time for the slit to cut the beam of light) to vary over the desired range. A stroboscope was used to determine the revolutions per minute (R.P.M.) of the motor. Table 2.3 lists the various combinations of motor R.P.M. and pulley turndown ratios that allowed the time interval to vary from $8.98 \times 10^{-3}$ seconds to 137.92

FIGURE 2.3

SCHEMATIC OF OPTICAL SYSTEM

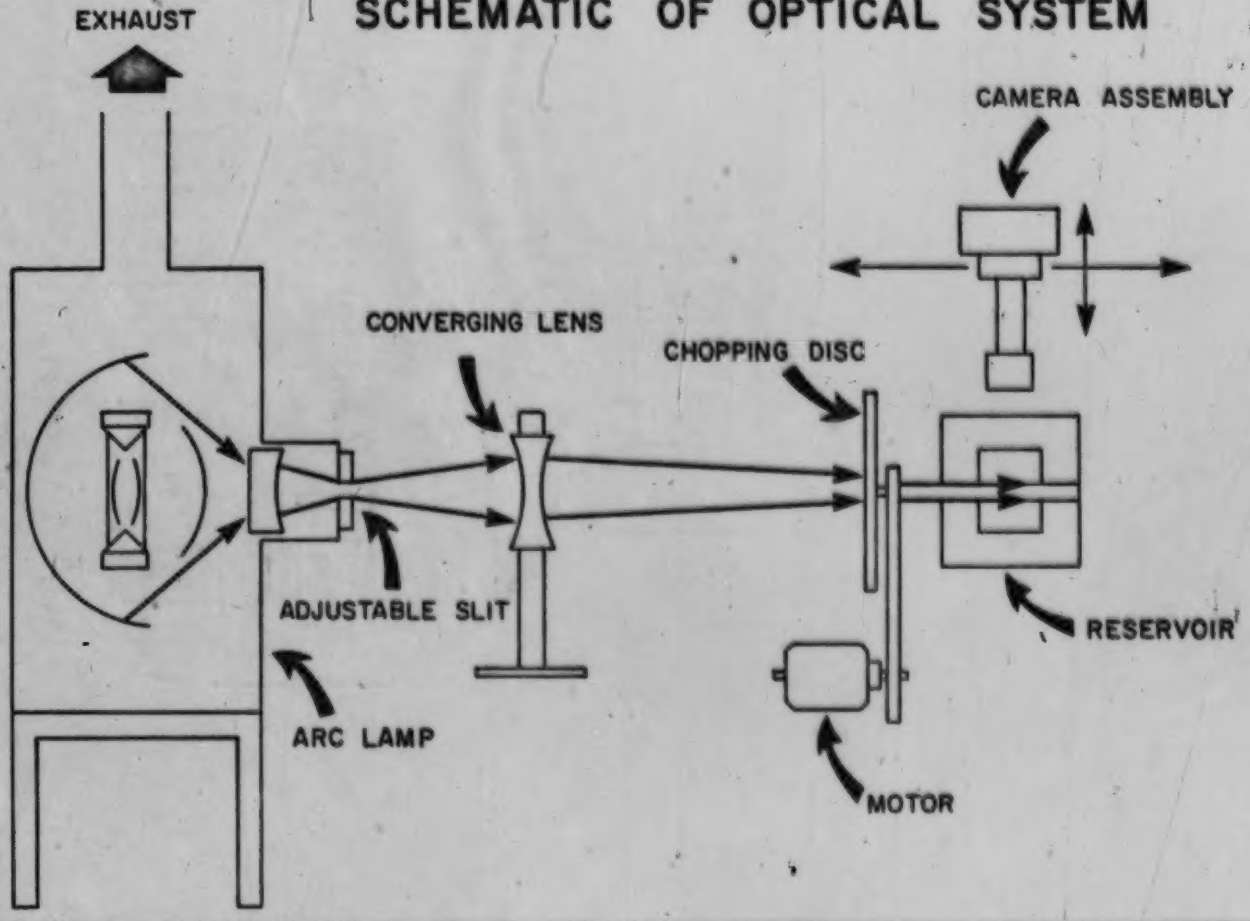
EXHAUST
CAMERA ASSEMBLY
CONVERGING LENS
CHOPPING DISC
ADJUSTABLE SLIT
RESERVOIR
ARC LAMP
MOTOR

## TABLE 2.3

## TIME INTERVALS FOR STREAK ANALYSIS

| PULLEY TURNDOWN RATIO (P.T.R.) | MOTOR R.P.M. | NUMBER SLITS-SPOKES | TIME INTERVAL (sec x $10^{-3}$) |
|---|---|---|---|
| 1.0 | 334 | 20 | 8.98 |
| 1.0 | 259 | 20 | 11.61 |
| 1.0 | 218 | 20 | 13.76 |
| 1.0 | 79 | 20 | 38.10 |
| 1.0 | 75 | 20 | 39.87 |
| 1.0 | 71 | 20 | 42.10 |
| .375 | 141 | 20 | 113.41 |
| .375 | 306 | 30 | 52.28 |
| .375 | 302 | 20 | 26.49 |
| .375 | 97 | 20 | 82.47 |
| .375 | 462 | 20 | 6.50 |
| .375 | 158 | 20 | 17.32 |
| .375 | 82 | 20 | 50.79 |
| .375 | 87 | 20 | 91.95 |
| .375 | 60.5 | 20 | 132.23 |
| .375 | 175 | 20 | 45.72 |
| .375 | 87 | 20 | 91.95 |
| .375 | 137 | 20 | 64.78 |
| .375 | 291 | 20 | 27.49 |
| .375 | 145 | 20 | 55.14 |
| .375 | 330 | 20 | 24.24 |
| .375 | 90 | 20 | 88.85 |
| .375 | 58 | 20 | 137.92 |
| .375 | 73 | 20 | 54.61 |
| .375 | 172.5 | 20 | 46.38 |
| .375 | 63.5 | 20 | 125.98 |
| .375 | 63 | 20 | 126.98 |
| .375 | 177 | 20 | 45.19 |
| .375 | 325 | 20 | 24.61 |

× $10^{-3}$ seconds. The pulley turndown ratio is the ratio of the diameter of the pulley on the chopping disc to the diameter of the pulley attached to the motor. The chopping disc was located perpendicular to the light beam with its center in the plane of the light beam. To minimize reflections, the interior surfaces, with the exception of the light slit on the side of each reservoir and the camera viewing area, were painted black. In addition, the room was in total darkness during the experimental run.

A rod having a diameter equal to the internal diameter of the Teflon insert (shown in Figure 2.2) was tapered to a point at one end so that the camera could focus on the center of the capillary tube. This rod was painted black to minimize reflections. It was pushed through the teflon insert such that only the tapered portion protruded into the reservoir. A Miranda 35 mm camera was located perpendicular to the light beam and was secured to Setco Building Blocks which were equipped with micrometers graduated in 0.001 inch increments in the vertical and horizontal planes. The camera was focused on the tip of the tapered rod. Since the depth of the field of the camera was greater than the thickness of the beam of light, aluminum particles within the beam's thickness were illuminated and recorded on the film. The error in measured velocities associated with the depth of the field of the camera and the thickness of the light beam is discussed in Appendix G.

The projection of a frame onto the digitizer screen using the digitizer method (a detailed description of the method is given in Section 2.3.3 and a schematic representation of the digitizer is shown in Figure 2.7) was used to magnify the photos obtained. The data obtained from reservoir S were magnified using a 1:2.8/105 mm lens and extension tubes. The depth of field of the camera was 0.20 cm and the resulting magnifications were 8.225, 9.063, 18.00, and 24.50. For reservoir L data, a 1:1.9/50 mm lens and an unextended helicoid tube adaptor resulted in the magnification of 2.175; the depth of field of the camera was 0.40 cm. Tri-X film with ASA rating of 400 was used throughout the experiment.

### 2.3.2 STREAK PHOTOGRAPHS

Typical streak photographs are shown in Figures 2.4 and 2.5. The flow field shown in Figure 2.4 was obtained with capillary tube 2 in reservoir S at the maximum flow rate of 0.318 $cm^3$/sec (flow moving from left to right) with the velocities being tabulated in Appendix E, Section E.1. The film exposure time was one second and the time interval for a streak was 55.14 x $10^{-3}$ seconds. Figure 2.4 shows the typical WGS core surrounded by large eddies and the acceleration along several streamlines with the maximum at the center of the core. Velocities were determined by either the digitizer or direct method using several photographs similar to Figure 2.4. Figure 2.5 shows

FIGURE 2.4
STREAK PHOTOGRAPH, 0.20 cm I.D.
Q = 0.318 cm$^3$/sec

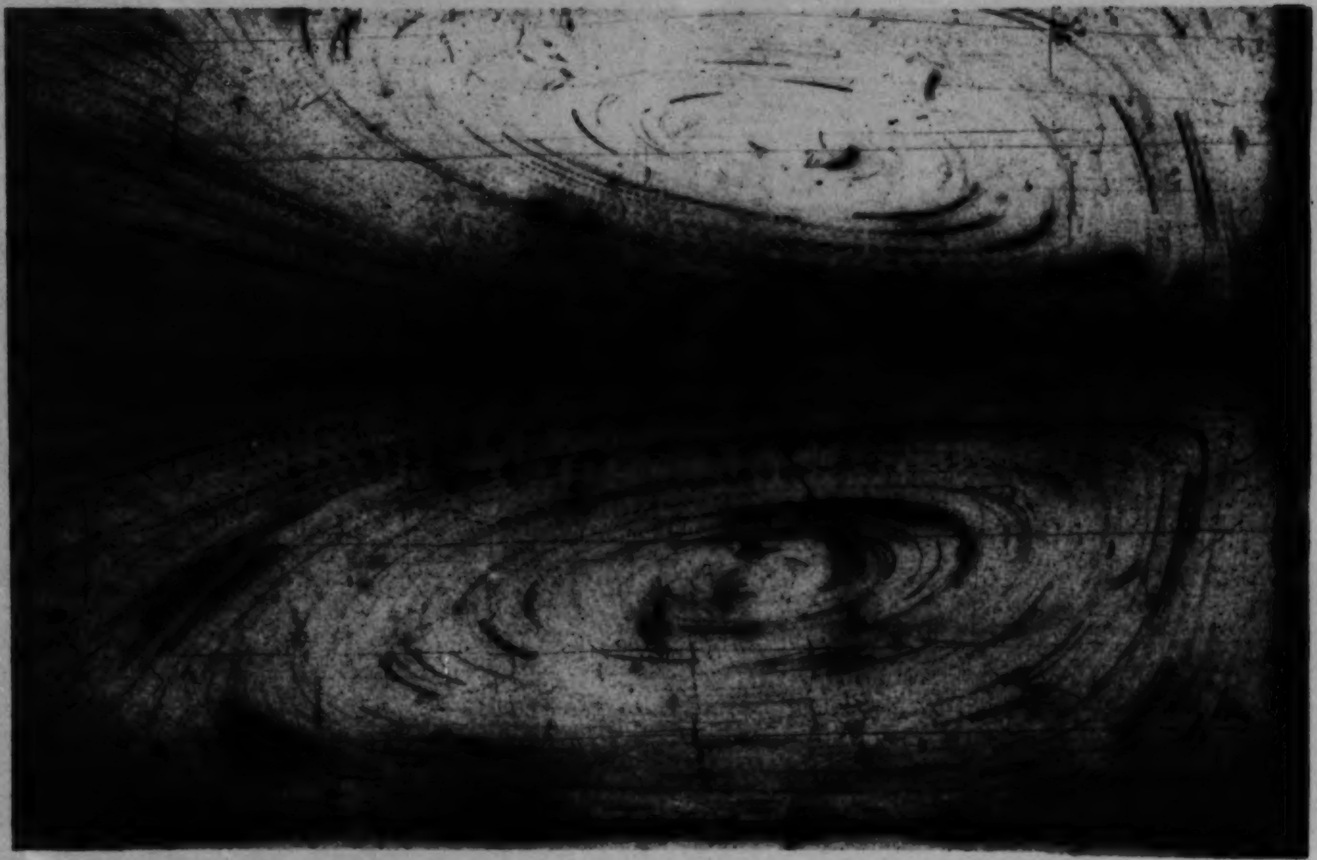

FIGURE 2.5
STREAK PHOTOGRAPH, 0.20 cm I.D.
Q = 0.040 $cm^3/sec$

that even at the lowest flow rate of 0.040 $cm^3$/sec the flow field is still of a central core surrounded by large eddies. However, the eddy centers are significantly nearer to the plane of the capillary entrance than at higher flow rates.

In addition to measuring the velocity development upstream, the location of the eddy centers and cone semi-angles were measured to complete the description of the flow field. Figure 2.6 is a representative photograph used in determining the location of the eddy centers. Photographs similar to this figure were obtained with the film exposure time of 5 seconds and a f stop of f:5.6. Cone semi-angles were measured from photographs similar to those shown in Figures 2.4 and 2.5. The results (cone semi-angles and location of eddy centers) are reported in Appendix F and discussed in Chapter III (pages 135-141).

### 2.3.3 ANALYSIS OF STREAK PHOTOGRAPHS - DIGITIZER METHOD

The digitizer is comprised of a projector and a stand, a mirror, and a frosted glass screen as shown schematically in Figure 2.7. The X-Y frame of the digitizer screen was 58.10 cm by 55.10 cm. The mirror was positioned such that the reflected light was normal to the glass screen. To determine the magnification, a Keuffel and Esser ruler graduated in 0.01 inches as well as a cross hair device graduated in 0.10 mm intervals were photographed, projected onto the digitizer screen, and measured. The

FIGURE 2.6
EDDY CENTER LOCATION, 0.30 cm I.D.
$Q = 9.531\ \mathrm{cm}^3/\mathrm{sec}$

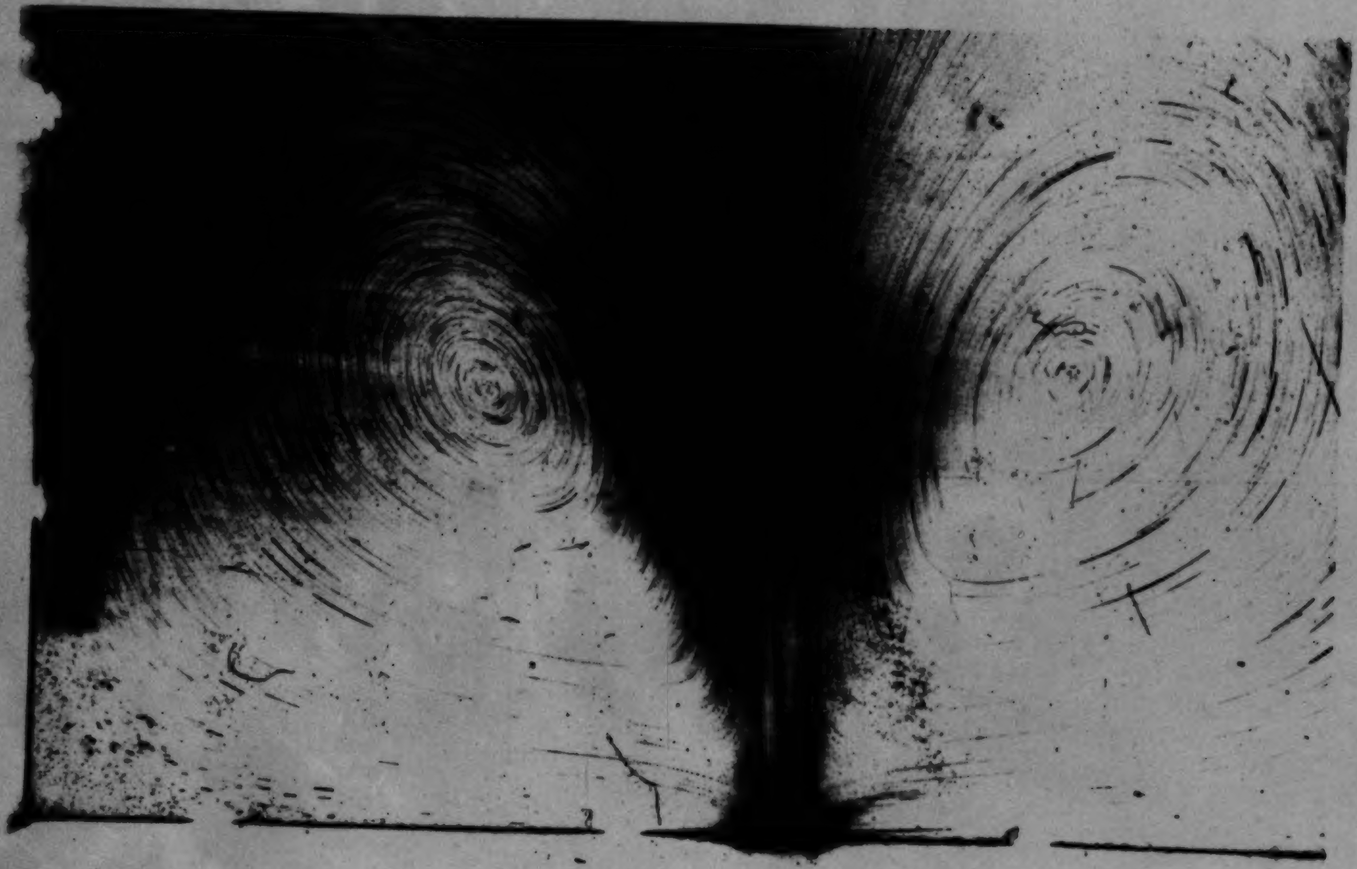

FIGURE 2.7

SCHEMATIC OF DIGITIZER

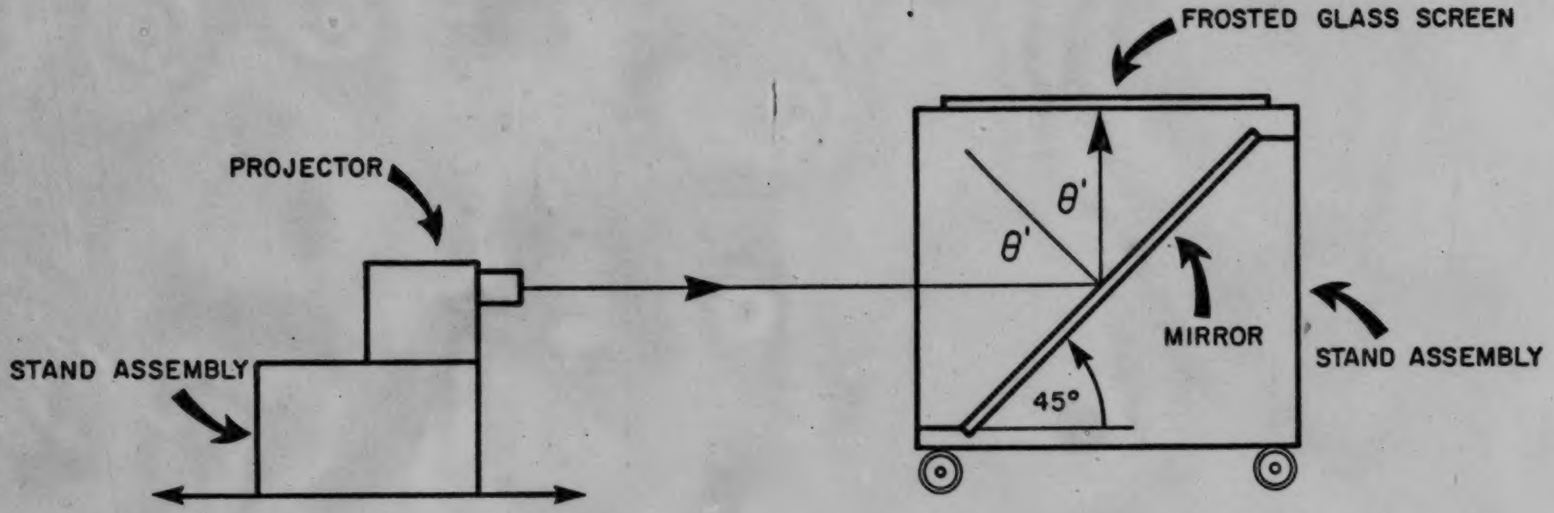
FROSTED GLASS SCREEN
PROJECTOR
θ'
θ'
MIRROR
STAND ASSEMBLY
STAND ASSEMBLY
45°

magnification was altered by moving the projector and the stand either closer to or farther away from the mirror.

The digitizer method consists of projecting a series of frames onto the digitizer screen. The coordinates of the reservoir wall and the streaks coordinates were recorded and stored in an IBM computer. The location of each coordinate was obtained by the use of a cross hair device that was connected to a variable resistor for the X and Y axes of the digitizer screen. The errors associated with the digitizer method are discussed in Appendix G.

Figure 2.8 schematically depicts a projected series of streaks viewed in a plane normal to the camera assembly in an accelerating region of the flow. The arrows represent the streaks and their direction for the time interval required by a slit in the chopping disc to cut the beam of light. The dotted lines represent the axial and radial distances measured relative to the wall of the reservoir. These distances (for a given streak), obtained from the transformation of coordinates from one Cartesian coordinate system to another, are represented by Equations 2.1 and 2.2.

$$\text{axial distance} = \Delta x = \frac{(Y_4 - Y_3)m_1}{(m_1^2 + 1)^{\frac{1}{2}}} + \frac{(X_4 - X_3)}{(m_1^2 + 1)^{\frac{1}{2}}} \qquad 2.1$$

FIGURE 2.8

SCHEMATIC OF STREAK ANALYSIS

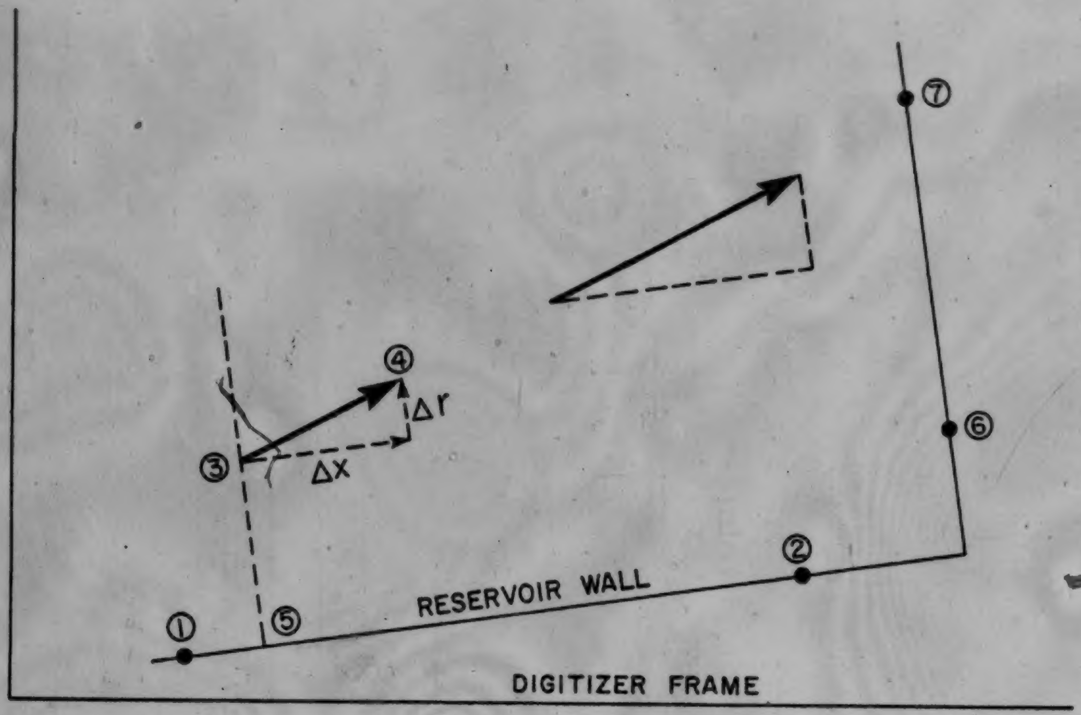
⑦
④
$\Delta r$
③
$\Delta x$
⑥
②
RESERVOIR WALL
①
⑤
DIGITIZER FRAME

$$\text{radial distance} = \Delta r = \frac{(Y_4 - Y_3)}{(m_1^2 + 1)^{1/2}} + \frac{(X_3 - X_4)m_1}{(m_1^2 + 1)^{1/2}} \qquad 2.2$$

where $m_1$ is the slope of the wall of the reservoir relative to the digitizer's X axis. The coordinates $(X_1,Y_1)$ and $(X_2,Y_2)$ were used to determine $m_1$ for reservoir L while $(X_6,Y_6)$ and $(X_7,Y_7)$ were used for reservoir S. Different coordinates were used for reservoir S because at the magnification of 24.50 and with the center of the reservoir coincident with the center of the digitizer frame the reservoir wall was projected beyond the screen. Hence, the slope $m_1$ was calculated by

$$m_1 = - \left[\frac{(Y_7 - Y_6)}{(X_7 - X_6)}\right]^{-1} \qquad 2.3$$

It was necessary, therefore, to record four coordinates relative to the digitizer's X axis in determining the location of a streak and the velocities. In most cases a single streak was used to determine the local velocity. In regions where the flow was slow several streaks were used since single streaks were too short to be measured accurately. The distance from coordinate 3 to the wall of the reservoir (coordinate 5) was determined by

$$r' = [(X_5 - X_3)^2 + (Y_3 - Y_5)^2]^{\frac{1}{2}} \qquad 2.4$$

The location of coordinate 5 was determined by the intersection of a line passing through coordinate 3 and having a slope equal to $-1/m_1$, i.e., perpendicular to the reservoir wall.

With the axial and radial distances, the number of streaks, and the time interval per streak known, the local axial and radial velocities were determined by

$$V_z = \Delta x/tM \qquad 2.5$$

$$V_r = \Delta r/tM \qquad 2.6$$

where

$$t = \frac{60}{WN} \times \frac{1}{P.T.R.} \qquad 2.7$$

M = number of streaks

N = number of slits and spokes on the chopping disc

W = number of revolutions per minute

P.T.R. = pulley turndown ratio.

These velocities, which were measured only at three upstream axial positions, are tabulated in Appendix E, Section E.2. The three axial positions corresponding to 1.5, 1.0, and 0.5 times the axial location of the eddy center are given in Table 3.4 (page 124).

### 2.3.4 ANALYSIS OF STREAK PHOTOGRAPHS - DIRECT METHOD

In the later stages of this work it was found more convenient to project the photographs directly onto graph paper which was graduated in 0.10 inch divisions. The streak lengths were traced directly onto the paper for all frames on the film corresponding to an experimental run. The axial velocities were determined as a continuous function of axial location. Thus, in contrast to the digitizer method, axial velocities were measured for all axial locations upstream of the contraction. A discussion of the error associated with this method is given in Appendix G, Section G.2. Figure 2.9 shows streaks along several streamlines as traced onto the graph paper with capillary tube 3 in reservoir S and at a flow rate of 0.40 $cm^3$/sec. The streak lengths were converted into axial velocities by using Equations 2.1, 2.5, and 2.7. The resulting axial velocities are plotted in Figure 2.10 for streamlines corresponding to those in Figure 2.9. Radial velocities were measured with the digitizer method and are tabulated in Appendix E, Section E.2.

The direct method was used also to measure cone semi-angles within the entry region. These angles are defined as the tangent to the outermost streamline that

FIGURE 2.9

DIRECT METHOD, STREAK LENGTH ALONG SEVERAL STREAMLINES

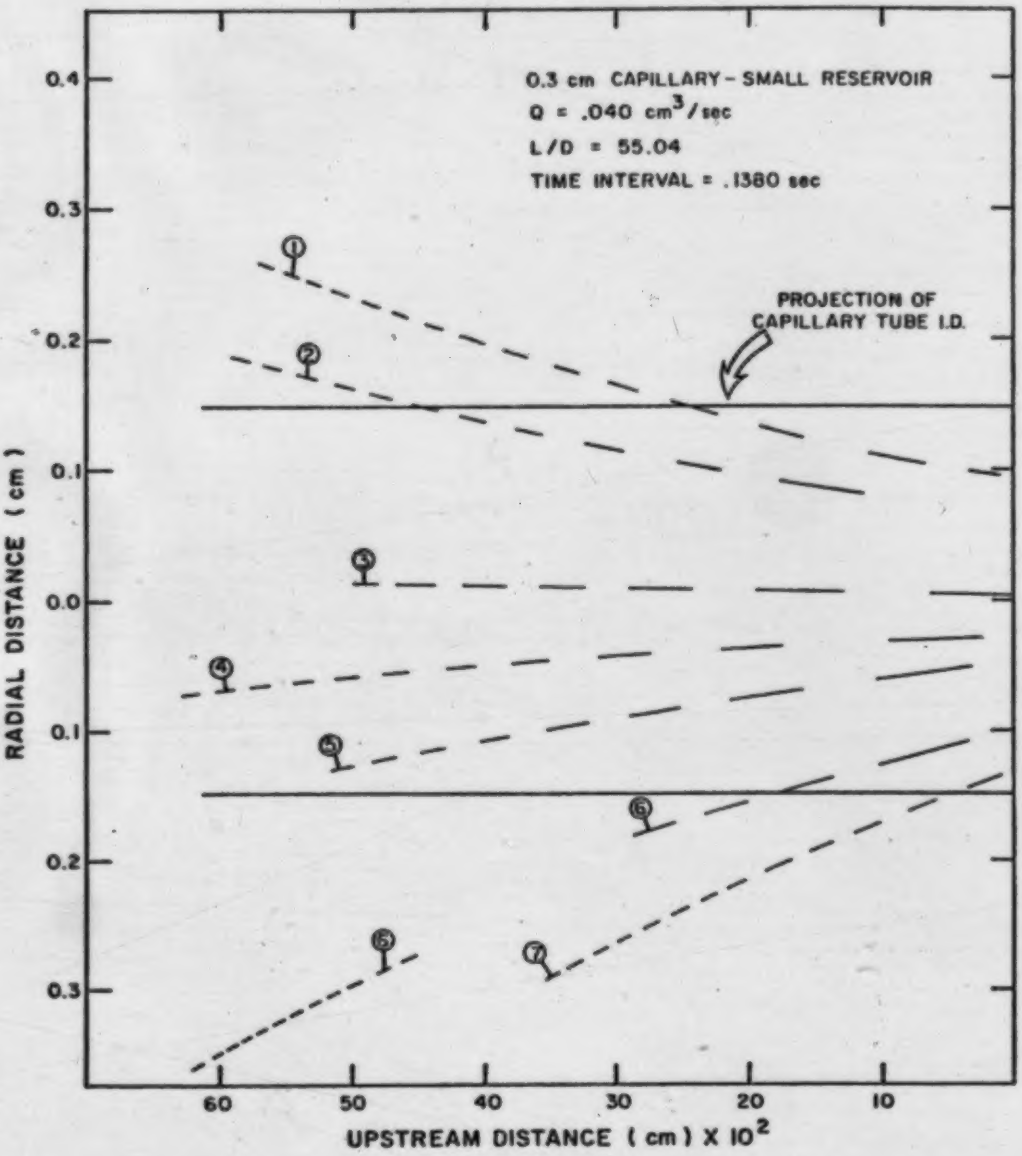

FIGURE 2.10

## AXIAL VELOCITY - UPSTREAM AXIAL POSITION PLOT

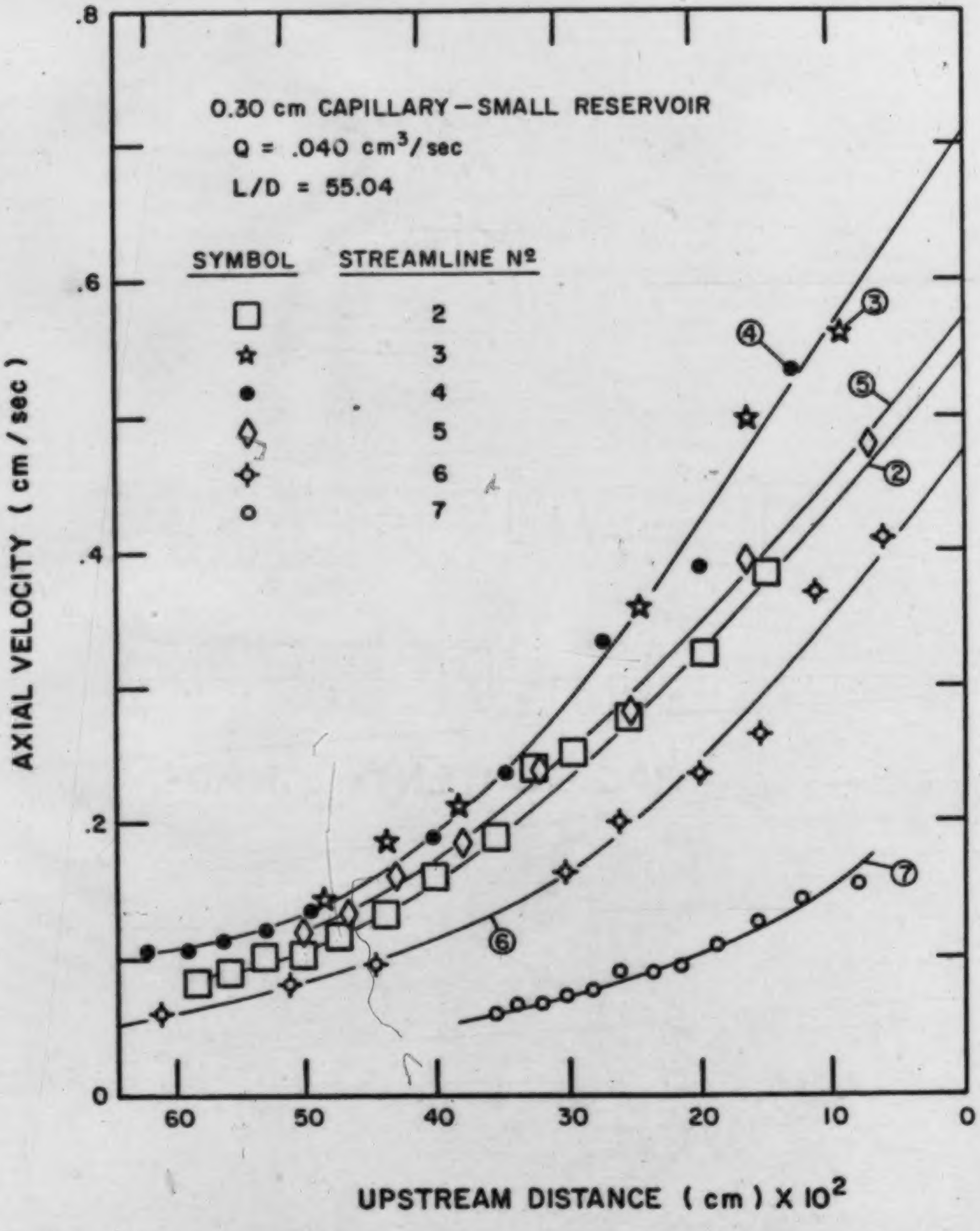

entered into the capillary tube. This streamline, however, was not known precisely for all of the experimental runs. For example, in Figure 2.9 the initial cone semi-angle, i.e., the cone angle at the contraction, and the cone angles upstream of the contraction were estimated by streamline labeled as number 7, which as shown, was not exactly the outermost streamline that entered into the capillary tube. For this example the initial cone semi-angle was equal to 20°. The maximum error in estimating the cone semi-angles was as large as 15 percent.

## 2.4 PROCEDURE

This section describes the procedure used in the preparation of the polymeric solution and the procedures used in obtaining pressure data, velocity data, and observations of the jet of fluid issuing from the capillary tube exit.

### 2.4.1 PREPARATION OF POLYMER

Since two batches of a 0.20% weight solution of Separan AP-30 were used and since it was necessary to ensure that the physical properties were the same, each batch was prepared in an identical manner. The following procedure was adhered to in dissolving the solute: A stainless steel tank, 79 cm I.D., was filled to a height of 91.5 cm with tap water. The solute was added slowly so as to ensure that all particles were wetted without the formation of large lumps. At the same time, a mixer agitated the solution at a moderate speed and continued to do so for a period of 10 hours after the final amount of solute was added to the solution. The solution was left unsheared for a period of 24 hours.

The fluid properties were measured and results are reported in Appendix D, Section D.2. The data indicated no significant differences in the physical properties for the two batches. The first batch was used in obtaining the total pressure losses which in turn were used to construct the Bagley plots. The second batch was used in the measurement of velocity distributions upstream of the contraction. In all experimental runs the temperature of the polymer solution was maintained at 68 ± 0.5°F.

### 2.4.2 DATA COLLECTION

#### (i) PRESSURE

The transducers were balanced and then checked against the calibration curves given in Appendix A, Section A.1 prior to the commencement of every experimental run. The pressure transmission line and transducer were filled with the solution used in the experimental run with one side of the transducer open to the atmosphere. After ensuring that no air pockets were trapped in either the pressure line or in the transducer, pressures were measured with typical transient-steady state pressure displacement traces given in Figures 2.11 and 2.12. The time required to attain steady state at a Reynolds number equal to 10.49

FIGURE 2.11

TRANSIENT-STEADY STATE PRESSURE DISPLACEMENT TRACE FOR PRIMOL - 355 OIL

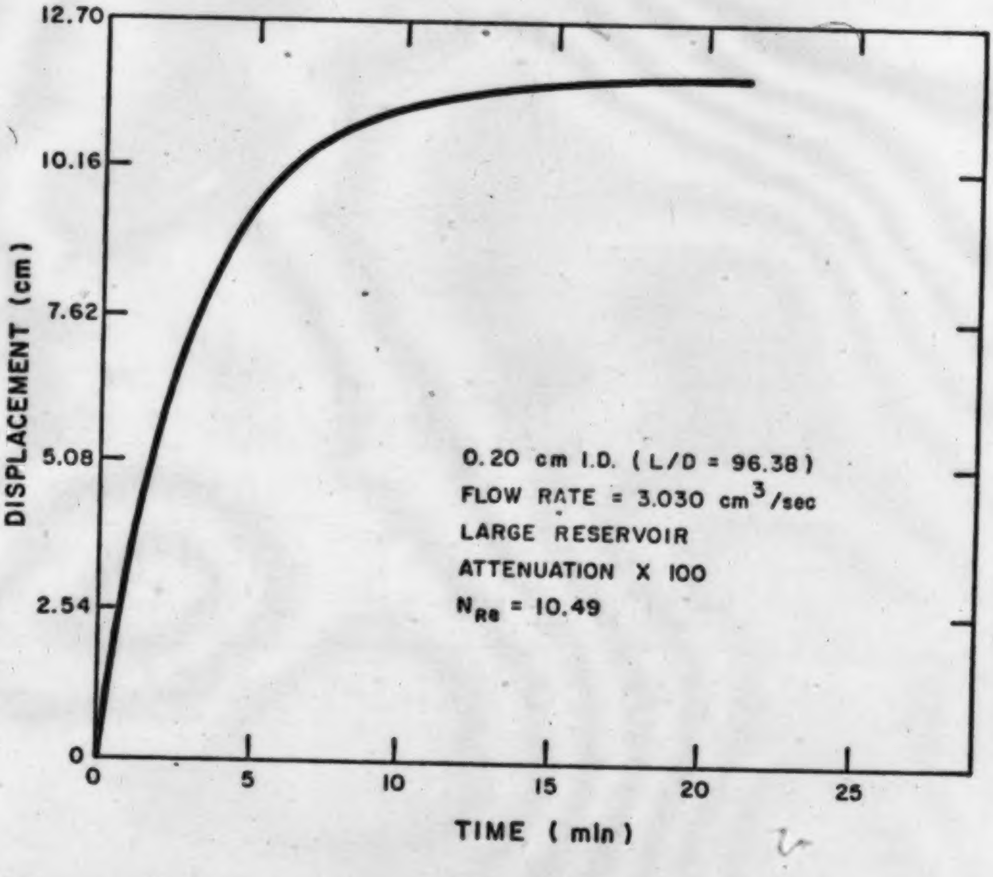

FIGURE 2.12

## TRANSIENT-STEADY STATE PRESSURE DISPLACEMENT TRACE FOR SUGAR SOLUTION Nº I

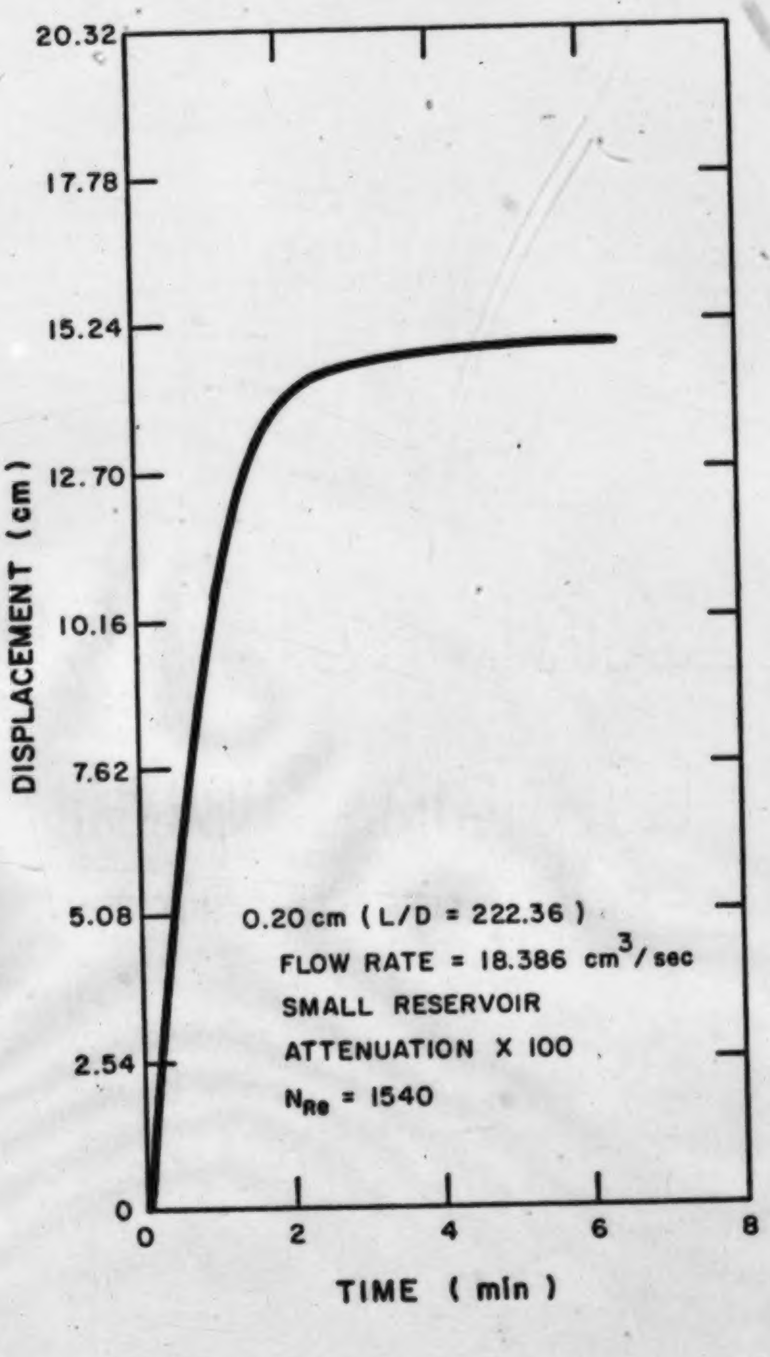

(shown in Figure 2.11) was approximately 18 minutes in comparison to 4 minutes at a Reynolds number of 1540 (shown in Figure 2.12). The steady state values of pressure obtained with several length to diameter ratios are tabulated in Appendix B. These data, as discussed in Appendix C, were used in constructing the Bagley plots. The pressure correction factors given in the tables in Appendix B account for the fact that the centers of the capillary tube and pressure transducer were not in the same horizontal plane. These pressure corrections must be added to the intercept of the Bagley plot to obtain the correct values of the contraction losses. The shear stresses under SLSF in the capillary tube were obtained from the slope of the Bagley plots. These data (contraction losses and shear stresses) are tabulated in Appendices C and D respectively for both Newtonian solutions and the polymer solution.

The time required for the centerline velocity to reach 99% of the fully developed centerline velocity, $t_\infty$, was approximated by considering the reservoir to be an infinitely long, horizontal tube (20): thus,

$$t_\infty \simeq \frac{0.8\rho R^2}{\mu} \qquad 2.8$$

The experimental values of $t_\infty$, $(t_\infty)_e$, for the data in Figure 2.11 and 2.12 were 18 minutes and 4 minutes respectively. These are significantly longer than the 1.2 and 0.3 minutes calculated by the use of Equation 2.8 and are representative of the maximum difference between experimental and calculated values of $t_\infty$. Initially the difference was attributed to the trapped air within the hydraulic cylinder. This was examined by comparing the experimental and calculated values of $t_\infty$ for the remaining runs in both reservoirs (this was possible since the same procedure was used to fill the hydraulic cylinder in all experimental runs). In reservoir S results can be summarized as

$$2t_\infty \lesssim (t_\infty)_e \lesssim 20t_\infty \qquad 2.9$$

whereas in reservoir L summary of results is

$$.01t_\infty \lesssim (t_\infty)_e \lesssim 20t_\infty \qquad 2.10$$

In view of the large discrepancies between experimental and calculated values of $t_\infty$ we cannot conclusively state that trapped air within the hydraulic cylinder resulted in the large values of $(t_\infty)_e$ obtained from the data in Figures 2.11 and 2.12. With polymer solutions in a parallel flat plate viscometer the time to attain steady state increased with elasticity number (128) defined as

$$EL = \frac{4\theta\mu_0}{\rho D^2} \qquad 2.11$$

The elasticity numbers for the polymer solution were equal to 3.2 and 0.03 in reservoirs S and L respectively. This suggests that as a first approximation $(t_\infty)_e$ should be at least equal to or greater than the Newtonian values. However, experimental values of $t_\infty$ were, in a significant number of experimental runs, less than the Newtonian values. It can be concluded that the time to reach steady state seemed to be a result of experimental design.

### (ii) VELOCITY DISTRIBUTIONS

No velocity profiles were measured for the Newtonian solutions. The two methods used to measure velocity profiles for the polymer solution are discussed in Sections 2.3.3 and 2.3.4 of this chapter. The digitizer method was used to measure the axial velocity profiles at high flow rates in the reservoir L; the results are tabulated in Appendix E, Section E.2. The direct method was used with reservoir L at low flow rates and for all flow rates in reservoir S; the results are tabulated in Appendix E, Section E.1. All radial velocities were measured using the digitizer method and the data are tabulated in Appendix E, Section E.2.

### (iii) QUALITATIVE OBSERVATIONS

The qualitative observations are: (a) visual observations of changes in the flow pattern upstream of the contraction, (b) recording pressure traces at the pressure tap located upstream of the contraction, and (c) visual observations of the jet of fluid issuing from the capillary tube. The instabilities affected the observations, the discussion of which can be found in Chapter III.

# CHAPTER III

# RESULTS AND DISCUSSION

## 3.1 NEWTONIAN FLUIDS

The discussion deals with friction factors and contraction losses obtained from Bagley plots for all Newtonian fluids used in this research - three aqueous sugar solutions and an oil, Primol-355.

### 3.1.1 FRICTION FACTOR - REYNOLDS NUMBER

A comparison between the experimental and theoretical values of the friction factor determined under SLSF in the capillary tube was used to establish the accuracy of the experimental technique. Bagley plots were constructed for the four Newtonian fluids by plotting the total pressure losses, measured in both reservoirs and for several lengths of capillary tube 2, against the capillary tube length to diameter ratio. The total pressure loss - L/D data are tabulated in Appendix B. By curve fitting these data to Equation 1.28 using the least squares method, the shear stresses at the capillary tube wall and the contraction losses were obtained from the slope and intercept respectively. The recoverable shear strain, $S_R$, in Equation 1.28 is equal to zero for Newtonian fluids. Typical Bagley plots for the Primol-355 oil and for the sugar solution #1 are shown in Figures 3.1 and 3.2 respectively. Figure 3.1 represents Bagley plots for low

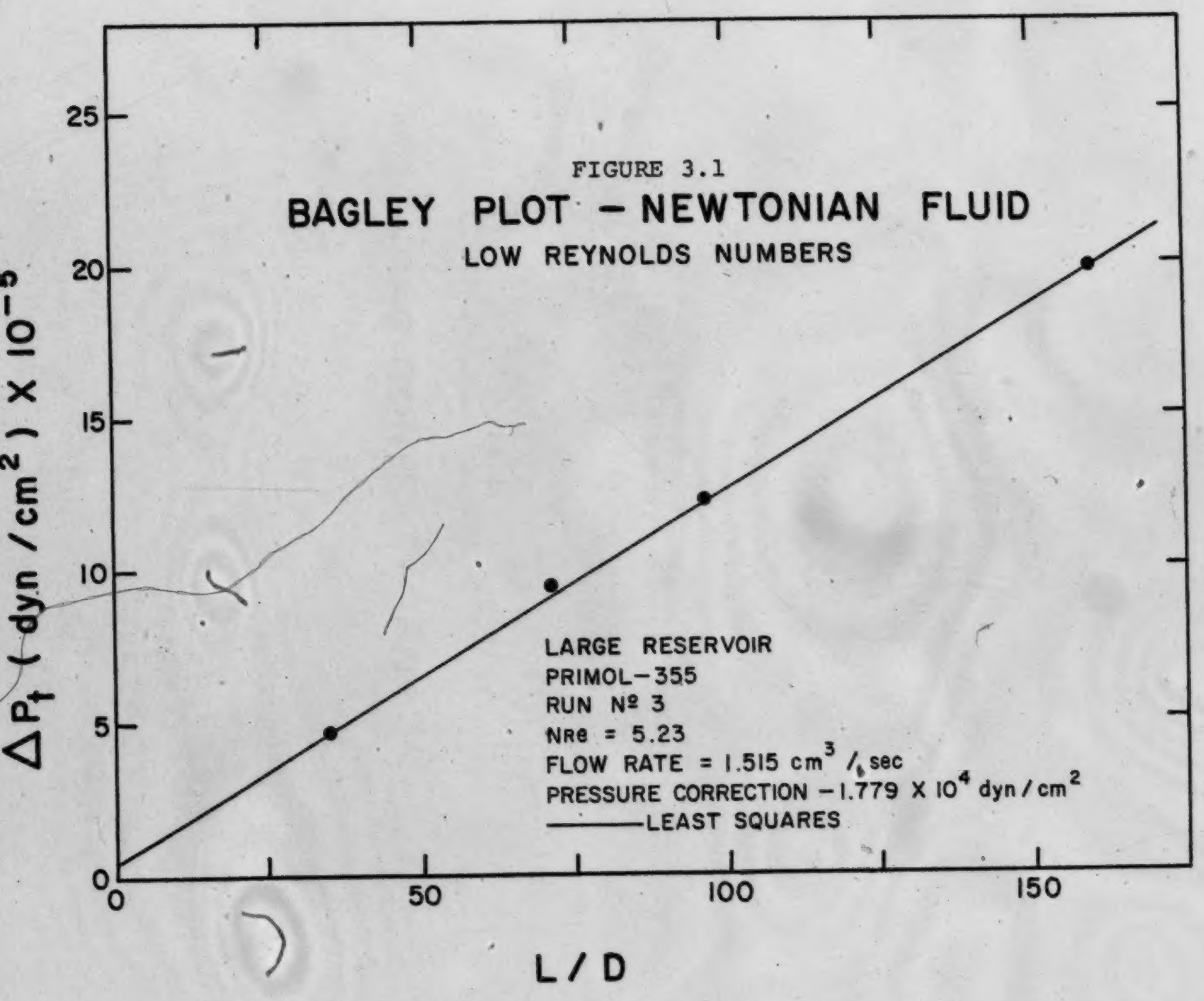

FIGURE 3.1

BAGLEY PLOT – NEWTONIAN FLUID

LOW REYNOLDS NUMBERS

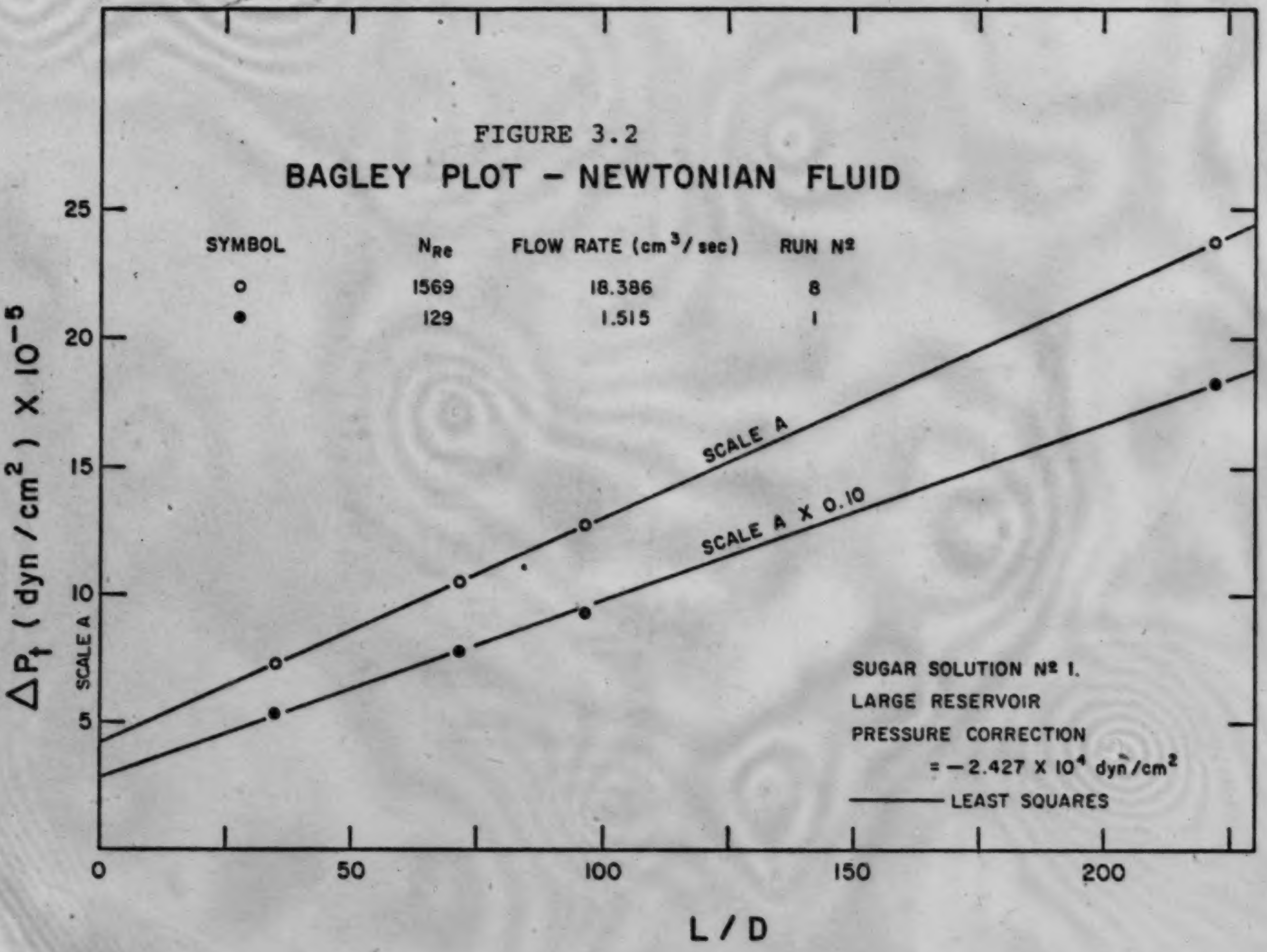

FIGURE 3.2

BAGLEY PLOT - NEWTONIAN FLUID

Reynolds numbers while Figure 3.2 presents those for intermediate and high Reynolds numbers. These and the Bagley plots obtained with the remaining data in Appendix B are linear. The pressure correction referred to in Figures 3.1 and 3.2 arose from the fact that the centers of the capillary tube and the pressure transducers were not in the same horizontal plane. Consequently, the correction factor must be added to the value of the intercept to obtain the true value of the contraction losses.

The friction factors were calculated by using Equation 3.1 and the shear stress data are tabulated in Appendix D. The results are plotted in Figure 3.3.

$$f = \tau_w/(\rho V^2/2) \qquad 3.1$$

For Reynolds numbers that varied from 2.60 to 1569, the average deviation from the theoretical relationship, $f = 16/N_{Re}$, was less than four percent.

### 3.1.2 CONTRACTION LOSSES

The contraction losses, obtained from Bagley plots and tabulated in Appendix C, are plotted against the Reynolds number in Figure 3.4 (page 88). To determine the accuracy in the measurement of the contraction losses, the estimated standard errors (e.s.e.), Equation 3.2 (page 85), were obtained at a low, an intermediate, and at a high Reynolds number for each Newtonian fluid.

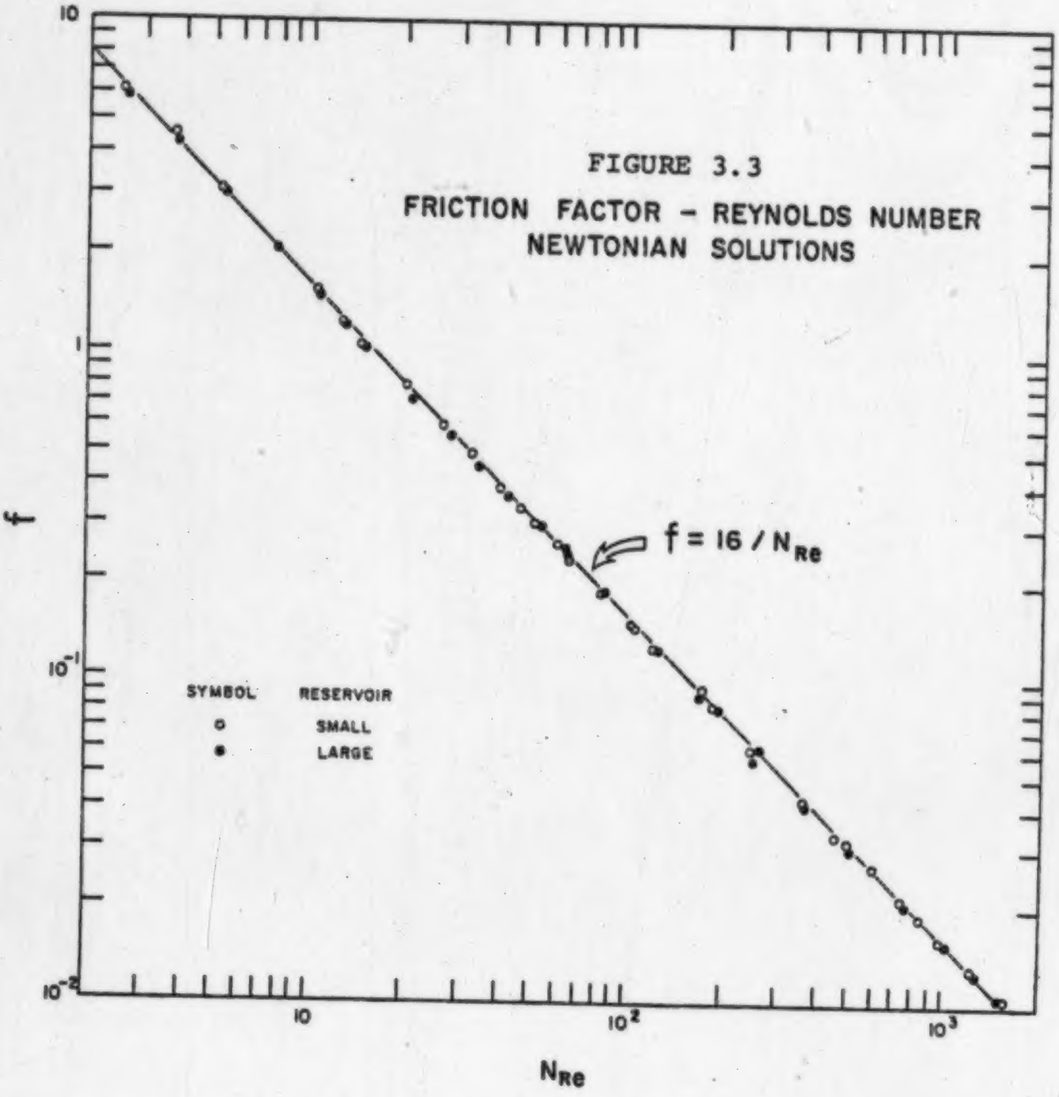

FIGURE 3.3

FRICTION FACTOR - REYNOLDS NUMBER
NEWTONIAN SOLUTIONS

$$\text{e.s.e.} = \frac{s^2 \sum_{i=1}^{n} x_i^2}{n \sum_{i=1}^{n} (x_i - \bar{x})^2} \qquad 3.2$$

where

$$s^2 = \sum_{i=1}^{n} \varepsilon_i^2 / n-2 \qquad 3.3$$

The minimum values of the e.s.e. are given in Table 3.1. For a given fluid, the contraction losses became an increasingly larger fraction of the total pressure losses as the Reynolds number increased. Hence, the percent error, as shown in Table 3.1, decreased with increasing Reynolds number. Consider as an example the data for sugar solution No. 3. Although the e.s.e. increased from 0.09 x $10^4$ dyn/$cm^2$ to 1.55 x $10^4$ dyn/$cm^2$ as the Reynolds number increased from 46.73 to 870.7, the percent error (as determined by Equation 3.4 below) decreased from 16 percent to 3 percent.

$$\%\ \text{error} = \frac{\text{e.s.e.}}{\Delta P_c} \times 100 \qquad 3.4$$

The largest percent error occurred with the Primol-355 oil where the contraction losses were small, hence, difficult to measure accurately. In addition there was substantial scatter in the total pressure loss-L/D data. This scatter was a result of experimental location wherein temperature fluctuations of ±1°F resulted in the viscosity varying by 3.9 percent. (The experimental location was changed when data were taken with the sugar solutions. In

## TABLE 3.1

## ESTIMATED STANDARD ERROR (e.s.e.) FOR NEWTONIAN CONTRACTION LOSSES

| Solution | Run Number | $N_{Re}$ | $\Delta P_c \times 10^{-4}$ ($dyn/cm^2$) | e.s.e. $\times 10^{-4}$ ($dyn/cm^2$) | Percent Error |
|---|---|---|---|---|---|
| Primol - 355 | 1 | 2.60 | 2.77 | 1.12 | 40 |
| | 3 | 5.16 | 4.43 | 2.05 | 46 |
| | 7 | 14.58 | 18.63 | 1.31 | 7 |
| Sugar #4 | 1 | 20.63 | 2.32 | 0.54 | 23 |
| | 3 | 33.22 | 3.39 | 0.09 | 3 |
| | 6 | 62.15 | 7.21 | 1.12 | 16 |
| Sugar #3 | 8 | 46.73 | 0.57 | 0.09 | 16 |
| | 3 | 268.1 | 5.76 | 0.94 | 16 |
| | 7 | 870.7 | 51.75 | 1.55 | 3 |
| Sugar #1 | 1 | 126.9 | 0.57 | 0.12 | 21 |
| | 4 | 509.2 | 4.98 | 0.08 | 2 |
| | 8 | 1539.8 | 44.90 | 1.85 | 4 |

the new location the temperature of the fluids was maintained within ±0.5°F.) This temperature fluctuation resulted in a 1.7 percent change in the viscosity of the sugar solutions, hence, there were smaller percent errors. As a result of the large percent errors in measuring the contraction losses it was not possible to claim significant differences between the contraction losses obtained with either reservoir.

The contraction losses plotted in Figure 3.4 and the data reported by Sylvester (161) as well as those reported by Astarita and Greco (4) can be represented by Equation 1.12. More specifically, for contraction ratios approaching zero, the contraction losses, according to Kaye and Rosen (93), can be represented by Equation 3.5

$$\Phi = (2.26 \pm .26) + \frac{159 \pm 30}{N_{Re}} \qquad 3.5$$

Equation 3.5 is plotted in Figure 3.4 and is indeed representative of the contraction losses measured in this research for contraction ratios approaching zero. At finite contraction ratios, Φ is predicted to decrease as β increases (Equations 1.8 and 1.10). Sylvester (161) and Astarita and Greco (4) reported an increase in Φ as β increased. This contradiction can be explained in terms of the presence of a vena contracta and inaccurate measurements of pressure both of which gave rise to larger values of Φ.

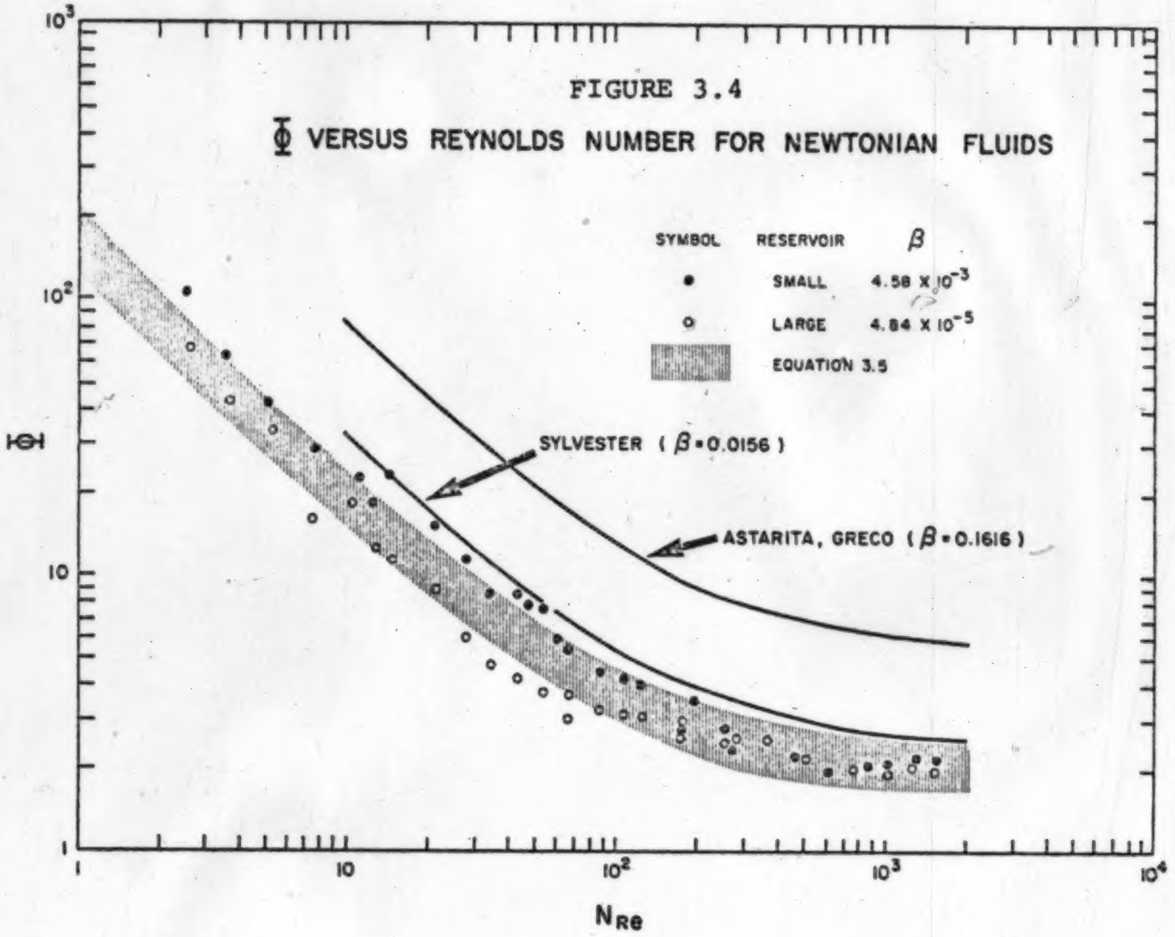

FIGURE 3.4

$\Phi$ VERSUS REYNOLDS NUMBER FOR NEWTONIAN FLUIDS

## 3.2 VISCOELASTIC FLUID

The friction factors and Reynolds numbers obtained from the aqueous 0.20% solution of Separan AP-30 are discussed. In addition, visual observations are given on: (a) velocity field within the reservoir, (b) pressure traces, and (c) jet of fluid. A discussion on criteria for the onset of instability is also included in this section.

### 3.2.1 FRICTION FACTOR - REYNOLDS NUMBERS

The friction factors and Reynolds numbers obtained with the viscoelastic fluid are shown graphically in Figure 3.5. Individual points deviate less than 8 percent from the straight line, $f = 16/N'_{Re}$, for generalized Reynolds numbers from 0.13 to 1866. The shear stresses used in computing the friction factors were estimated from the slopes of the Bagley plots. Measured pressure losses used in constructing the Bagley plots can be found in Appendix B; the resulting shear stresses are tabulated in Appendix D.

### 3.2.2 VISUAL OBSERVATIONS

Three observations used in determining the limits of stability were: (a) visual observations of the flow field within the reservoir, (b) observations of fluctuations in the pressure traces, and (c) visual observations of the jet of fluid issuing from the capillary tube.

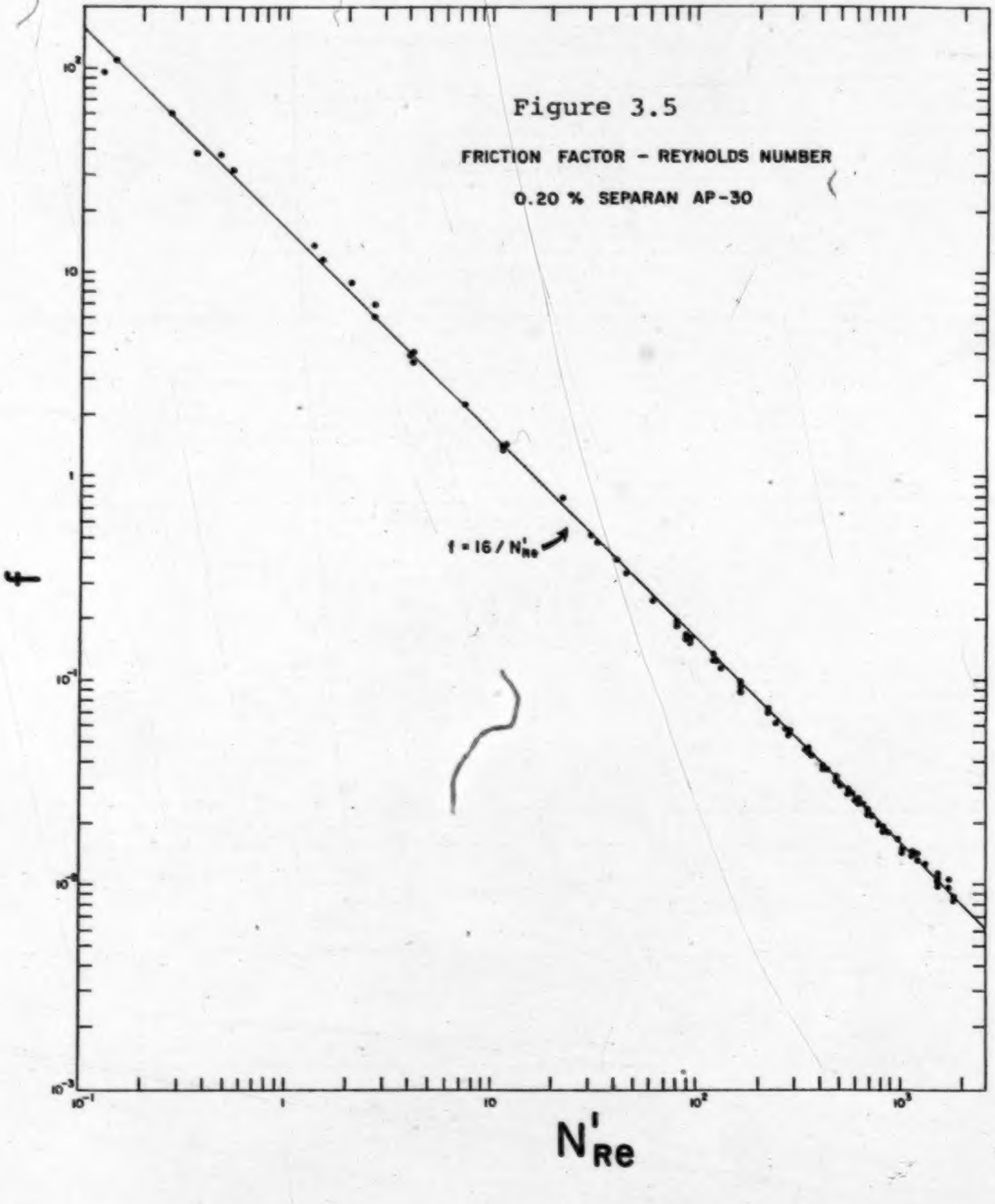

Figure 3.5

FRICTION FACTOR - REYNOLDS NUMBER

0.20 % SEPARAN AP-30

### (i) Velocity Field Within Reservoir

At low flow rates, hereinafter referred to as region I, stable flow fields existed within the reservoir. The qualitative features of the stable flow field discussed in Chapter I, i.e., the cone semi-angles, the center of the eddies, and the velocity distribution within the converging flow field, were measured and will be discussed in the following sections of this chapter. At intermediate flow rates, in what will be termed region II, a departure from the stable flow field was observed; within this region the flow field developed a swirling motion. A further increase in flow rate resulted in a flow field that failed to exhibit any regularity and could best be described as "chaotic." This will be referred to as region III.

A departure from the stable flow field occurred at the onset of region II. In this region the flow field developed a very slow swirling motion. The following description given by Rama Murthy (142) and observed by Ballanger and White (12) and Oyanagi (132) is also representative of the features of the flow field that were observed in this study when the word "reservoir" is substituted for the word "barrel":

> The stream entering into the tube appeared to oscillate to and fro in the barrel like a snake tail when viewed in a single plane. This swirling motion in the barrel swept the fluid in the secondary flow region, continuously dragging it into the tube ... At increased shear rates, the swirling flow became more vigorous ... The overall nature of the flow appeared to remain similar

except for the intensity of swirling.

It was found in this research that if the crosshead speed of the Instron was gradually increased to the desired setting, which amounts to a gradual increase in flow rate, a stable flow field could exist within region II. This procedure did not always guarantee success. The procedure had to be repeated several times before obtaining a sufficient number of photographs from which the velocity profiles could be constructed.

Within region III the flow field failed to exhibit any regularity and it is described as "chaotic." In a few experimental runs the flow field within the reservoir was observed to oscillate between stable and "chaotic" flow fields. This seemed to occur at random and the duration of time that the flow field remained stable or "chaotic" was long enough so that the oscillation could be observed by eye. In a preliminary experimental run a stable flow field was observed over a four minute duration before the flow field abruptly became "chaotic." The seven experimental runs where the oscillating flow field was observed in reservoir L were run number 11 for capillary tube 1, run numbers 8, 9, and 10 for capillary tube 2, and run numbers 10, 12, and 16 for capillary tube 3. In reservoir S, this was observed for run number 9 with capillary tube 1. To the best of the author's knowledge, this is the first time that observations of the flow field oscillating between a stable and a "chaotic" flow regime within the reservoir have been reported. This observation offers an explanation for the behavior in the pressure traces reported by Kizior (94) and in the jet of fluid issuing from the capillary tube reported by Kroesser (98). In both experiments the flow rate was constant.

The flow rates at the visually observed onset of regions II and III are plotted in Figure 3.6 against the capillary tube diameter. Since the velocity profiles were not measured for capillary tube 1 in reservoir L, the flow rate defining the commencement of region II was estimated by extrapolation. Region II, as shown in Figure 3.6, extended over flow rates that ranged from approximately 1.6 $cm^3$/sec to 4.9 $cm^3$/sec for capillary tube 2 and 4.9 $cm^3$/sec to 11.1 $cm^3$/sec for capillary tube 3 in reservoir L. The flow rates covered by region II in reservoir S, although not documented, were observed to be less than 0.01, 0.06 and 0.10 $cm^3$/sec for capillary tubes 1, 2, and 3 respectively. These were smaller than the increments of flow rate used in obtaining the velocity profiles and were within the accuracy of measuring flow rates used to define the onset of region III. Therefore, the onset of region III was considered to be coincident with the onset of region II in reservoir S. A broad classificiation of the flow field into three regions has been reported for other dilute polymer solutions (142) and melts (12, 188). However, the observations of Rama Murthy (142) indicated that beyond region III the flow field abruptly changed to a

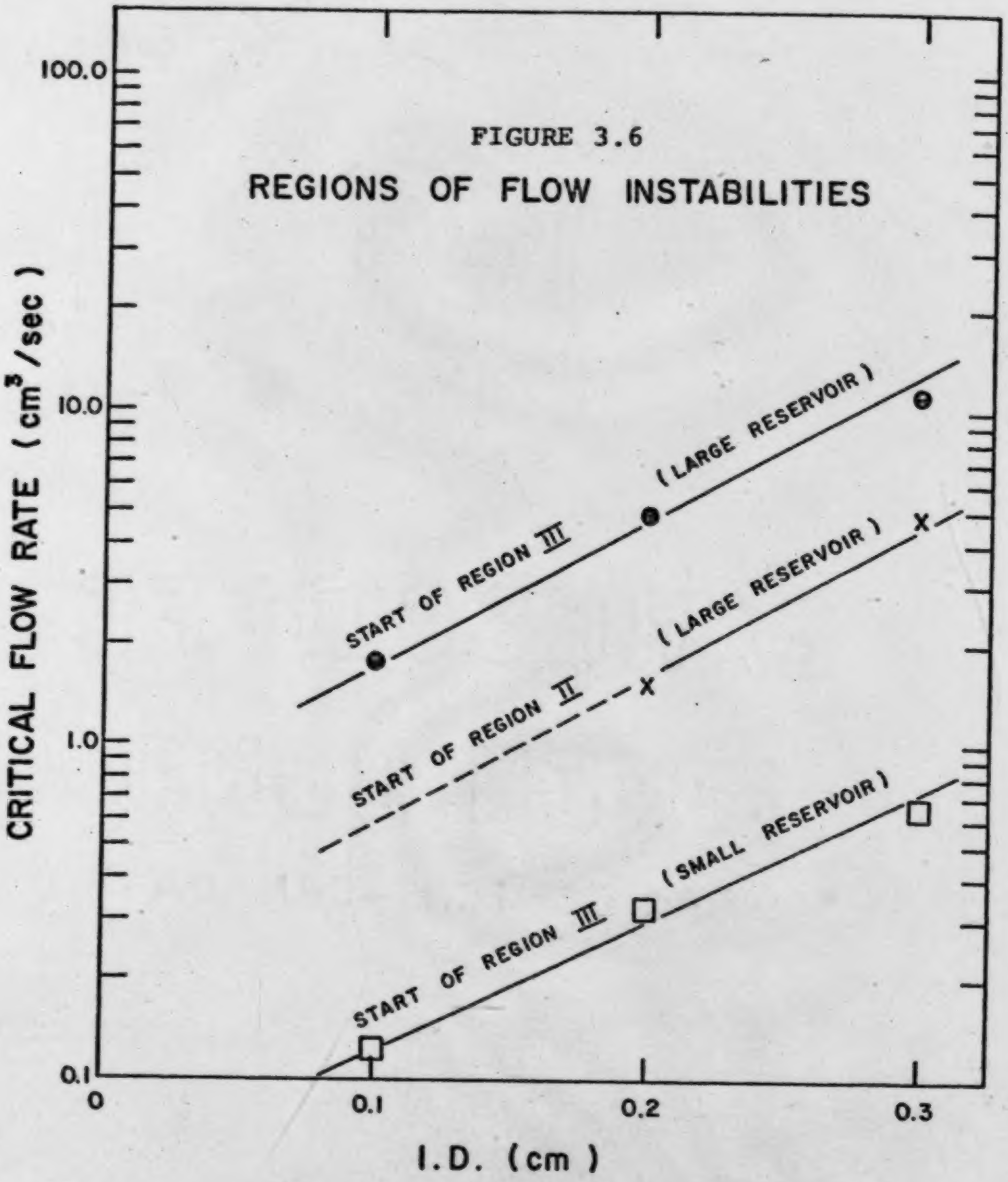

FIGURE 3.6

REGIONS OF FLOW INSTABILITIES

stable flow field that is similar to that observed with the flow of HDPE melts. This was not observed in this research.

(ii) Pressure Traces

All pressure traces were taken at the pressure taps located 10.2 and 27.9 cm upstream of the contraction. Smooth pressure displacement traces, similar to those shown in Figures 2.11 and 2.12 in Chapter II (pages 74 and 75), were obtained with stable flow fields in region I. Within region II the pressure traces remained smooth, i.e., pressure fluctuations, if they existed, were too small to be measured. Pressure fluctuations were measurable only for the flow rates within region III.

Two typical pressure traces within region III are shown in Figure 3.7. When the flow field within the reservoir was observed to oscillate between stable and "chaotic," the resulting pressure traces were similar to trace A. In trace A the difference in pressure between stable and "chaotic" flow fields was most discernible. At higher flow rates, it was difficult to differentiate between the two levels of pressure directly. With reference to trace A, the lowest level of pressure corresponds to the existence of a stable flow field within the reservoir while the upper level corresponds to the existence of a "chaotic" flow field within the reservoir. Pressure traces similar to trace A were reported by Kizior (94); the results of Kizior's research indicated that both the upper and lower

FIGURE 3.7

PRESSURE DISPLACEMENT TRACES WITHIN REGION III

**TRACE A**

0.10 cm I.D., SMALL RESERVOIR
FLOW RATE 1.271 cc / sec

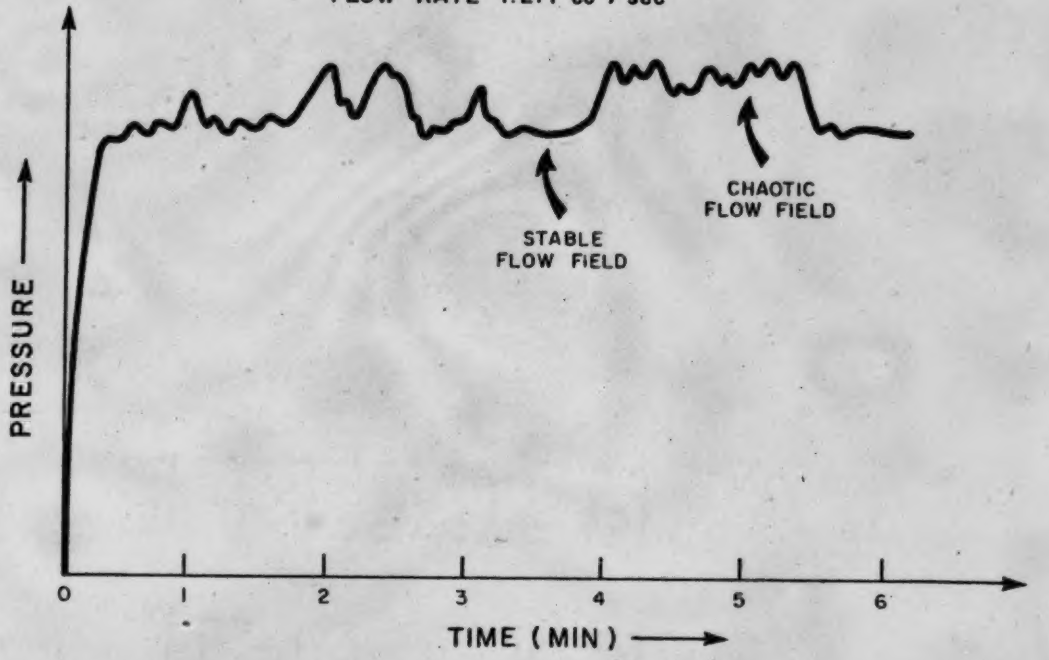

**TRACE B**

0.20 cm I.D., SMALL RESERVOIR
FLOW RATE 2.542cc / sec

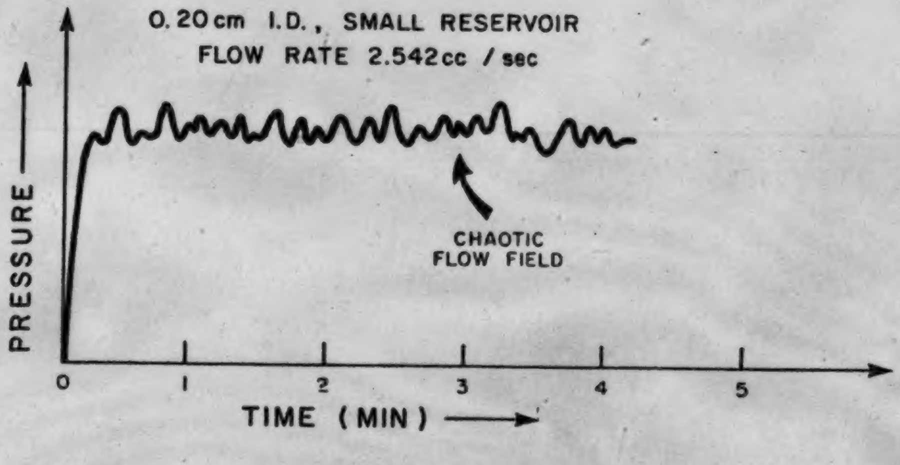

values of pressure remained constant with respect to time. This means that if pressure fluctuations existed they were too small to be measured. Therefore, the upper level of pressure in trace A measured by Kizior (94) corresponded to a flow field which was neither funnel-shaped nor "chaotic." As mentioned previously, the oscillation of the flow field between a stable and a "chaotic" flow was observed only for eight experimental runs in the present work. In the remaining runs within region III where only a "chaotic" flow field was observed, the pressure traces were similar to trace B. With the exception of a time scale, the changes in pressure in traces A and B appear to be the same. However, upon closer examination one may discern that these two pressure traces resulted from differences in the state of the upstream flow field. These results indicate the significance of having both visual observations of the flow field and pressure traces.

With respect to the pressure traces in Figure 3.7, an average value of pressure, calculated after the transient period, was defined as

$$\overline{P} = \frac{P_{max}+P_{min}}{2} \qquad 3.6$$

where $P_{max}$ and $P_{min}$ are the maximum and minimum values of pressure recorded for an experimental run. The pressure fluctuation, P, reported in this work was defined to be equal to the difference between the average value of pressure and the maximum deviation or fluctuation from the average. The resulting pressure fluctuations for the experimental runs in reservoir S are shown graphically in Figures 3.8, 3.9 and 3.10 for capillary tubes 1, 2, and 3 respectively for several length to diameter ratios. Although there is considerable scatter about a single line, the data show that pressure fluctuations are largely independent of the capillary tube length to diameter ratio. This suggests that the onset of flow instability is also independent of the capillary tube length to diameter ratio. The line drawn through the data points in Figures 3.9 and 3.10 intersects the abscissa at flow rates that coincide reasonably with the onset flow rates that were obtained by visual observations of the flow field. The latter flow rates were used to define the onset of region III (Figure 3.6, page 94). Plots similar to those shown in Figures 3.8 to 3.10 were also obtained with reservoir L and can be found in Appendix B. In spite of the subjectivity of visual observations and the limited resolution in measuring pressure fluctuations, the agreement between the two kinds of data is considered good.

The onset of pressure fluctuations did not coincide with the onset of visually observed "chaotic" flow field for capillary tube 1. In this case, the flow rate defining the onset of region III was 0.119 $cm^3$/sec when determined visually and 1.0 $cm^3$/sec from the pressure measurements (Figure 3.8). It is not possible to explain

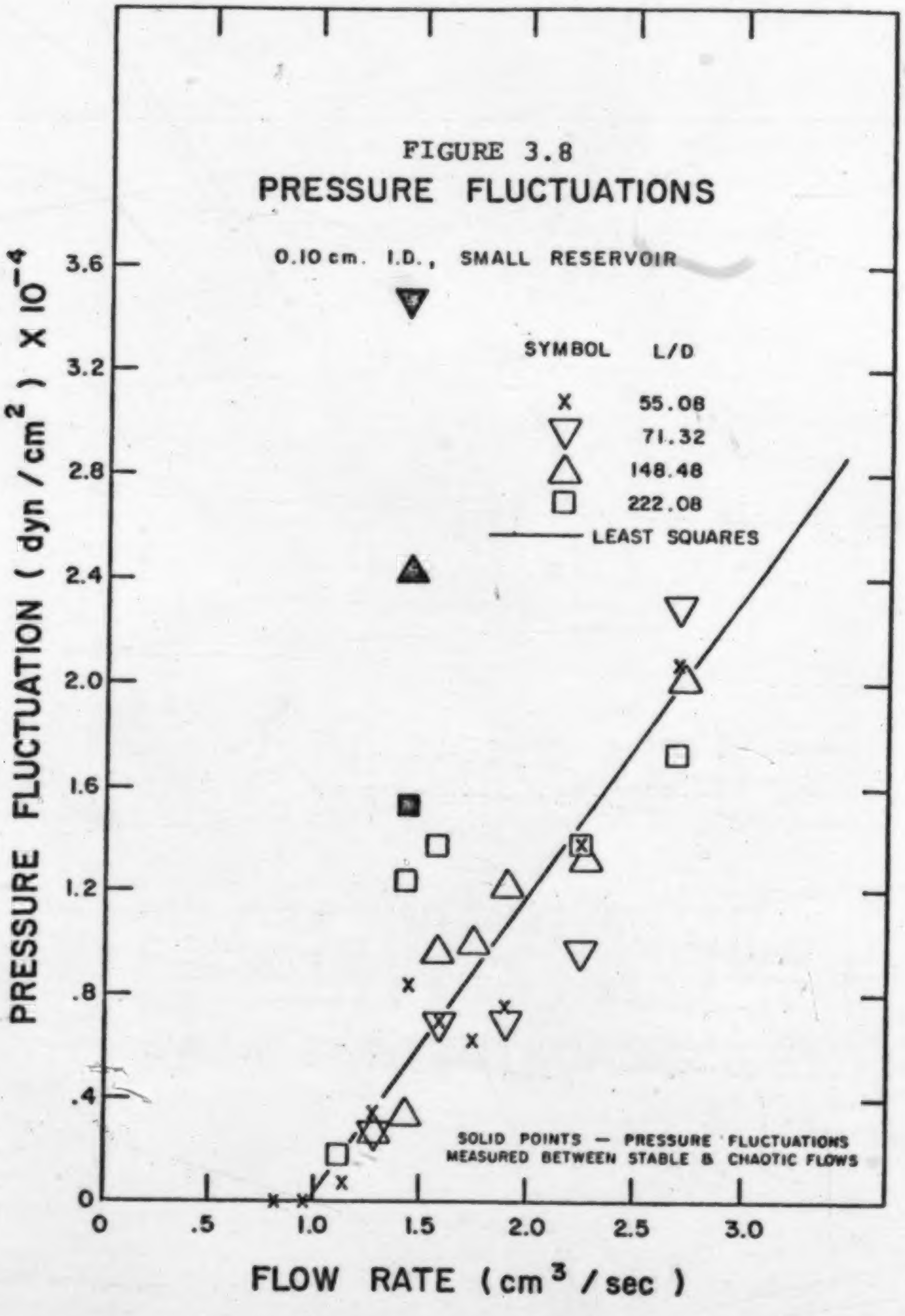

FIGURE 3.8

PRESSURE FLUCTUATIONS

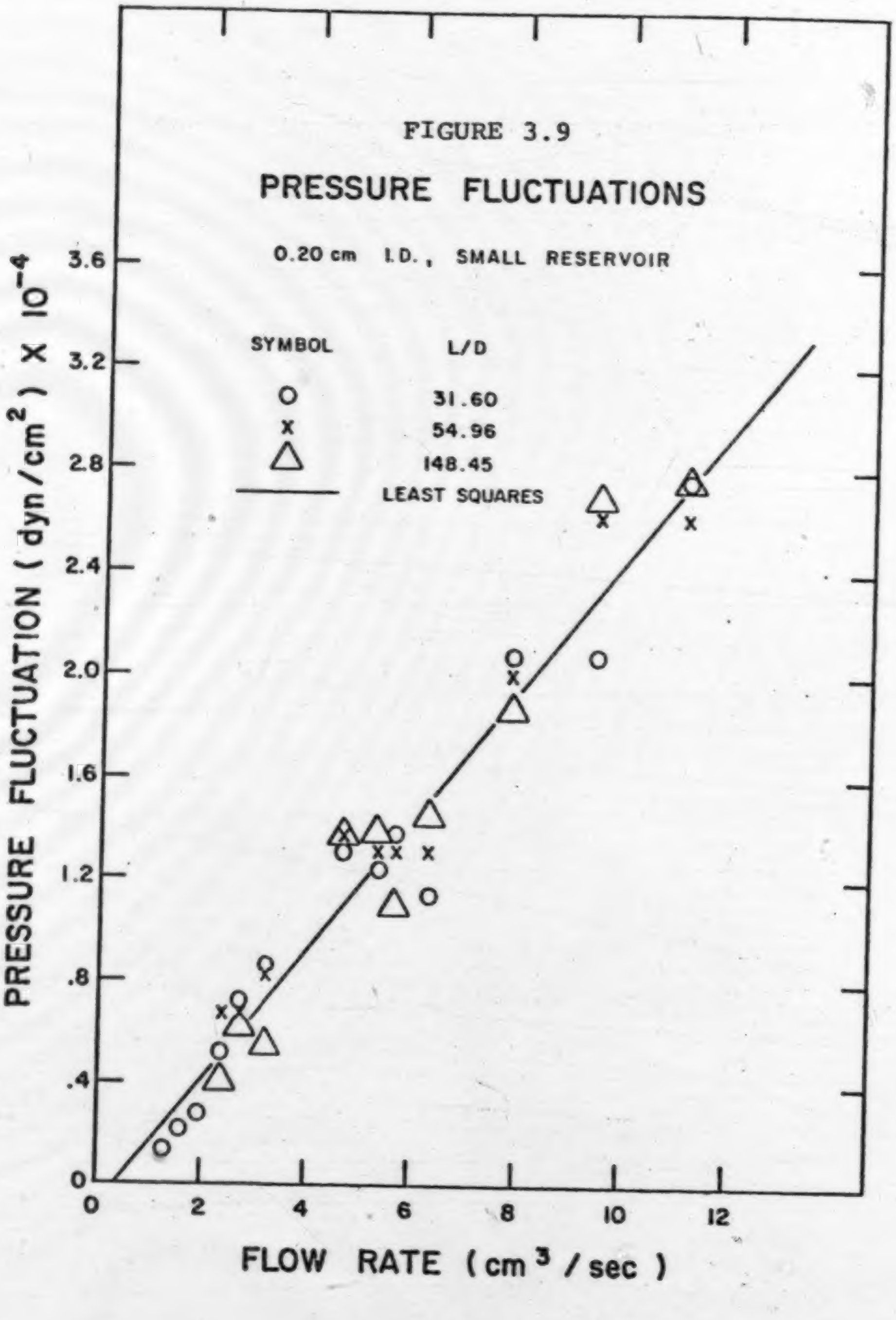

FIGURE 3.9

PRESSURE FLUCTUATIONS

0.20 cm I.D., SMALL RESERVOIR

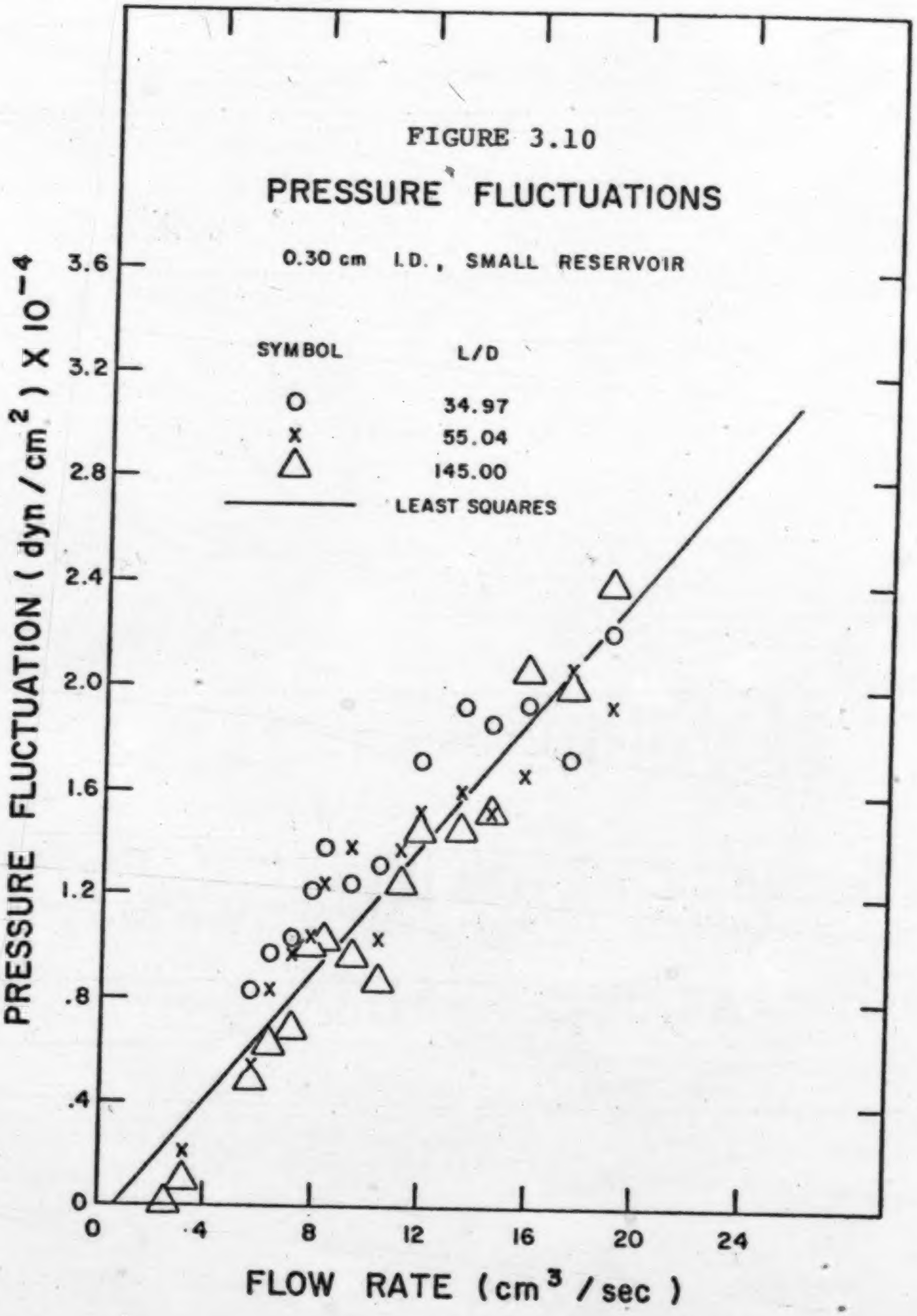

FIGURE 3.10

PRESSURE FLUCTUATIONS

0.30 cm I.D., SMALL RESERVOIR

this discrepancy directly but it may have been caused by air in the system. Experimentally, it was observed that when an air pocket of substantial size was deliberately trapped within the reservoirs it acted as a damping mechanism which delays the onset of a "chaotic" flow field to higher flow rates. These flow rates were at least an order of magnitude larger than the critical flow rates in which no air was trapped in the reservoirs. Hence, the limits of stability can be significantly increased if a gas is trapped in the system. All visible trapped air was removed from the reservoirs in the experimental runs but some air always remained in the hydraulic cylinder. Although care was exercised in reproducing the experimental procedure, there was no guarantee that the quantity of trapped air was constant. In view of the sensitivity of the stability limit to air pockets, an unaccounted for variation in the quantity of trapped air could have caused the noted discrepancy. Another factor which could have caused the discrepancy was the use of two batches of the 0.20% Separan solution. Since the solution was prepared in a limited quantity, it was necessary to have two batches. The first was used in obtaining the pressure traces and the second was used in measuring the velocity profiles and recording visual observations. However, the physical properties of these two batches tabulated in Appendix D are essentially the same over a wide range of apparent shear rates. Therefore, it is unlikely that the discrepancy was a result of the differences between the physical properties of the two batches.

At a flow rate equal to 1.43 $cm^3$/sec, several of the data points in Figure 3.8, given as solid points, are considerably above the straight line. Similar results are shown in Figures B.1 to B.3 in Appendix B (pages 280-282). These large pressure fluctuations are representative of the fluctuations which occurred when the flow field was observed to oscillate between stable and "chaotic" flows. If pressure fluctuations were measured only over the interval of time when the flow field was observed to be "chaotic" the pressure fluctuations are consistent with the remaining data.

In summary, the following generalizations can be made:

(a) The onset of measurable pressure fluctuations coincide reasonably with the visually observed onset of region III.

(b) The onset of region III is independent of the capillary tube length to diameter ratio.

(c) Pressure fluctuations that lie significantly above the remaining data can be explained in terms of the state of the flow field within the reservoir.

### (iii) Jet of Fluid

The third set of observations involved the qualitative features of the jet of fluid issuing from the capillary tube. For flow rates within regions I and II the jet of fluid was observed to be smooth. With the "chaotic" flow field that was observed in region III, the jet of fluid fluctuated with a frequency that was approximately equal to the frequency of the pressure fluctuations. When the flow field within the reservoir was observed to oscillate between stable and "chaotic" the jet of fluid oscillated between two different trajectories. In one trajectory, corresponding to the stable flow field, the jet of fluid was smooth; in the other, corresponding to the "chaotic" flow field, the jet was distorted. This offers an explanation for the "curious phenomenon" reported by Kroesser (98) wherein the jet of fluid, at a constant flow rate, oscillated between the above mentioned two trajectories.

A summary of observations of the flow field within the reservoir, the pressure fluctuations, and the jet of fluid issuing from the capillary tube is given in Table 3.2.

TABLE 3.2

OBSERVATIONS WITHIN REGIONS I, II, AND III

| OBSERVATION | REGION I | REGION II | REGION III |
|---|---|---|---|
| Flow field in reservoir | Stable | Swirling or Stable | Chaotic or Chaotic-Stable |
| Pressure fluctuations | Zero | Not Measurable | Measurable |
| Jet of fluid | Smooth | Smooth | Oscillating |

These observations together with: (a) the visual observations reported by Rama Murthy (142), and others (12, 130, 132), (b) the pressure profiles measured by Han and Lamonte (80), and (c) the fact that the flow curve for this polymer solution is smooth, suggest that for polymer solutions or melts characterized by a WGS upstream flow field, the initiation site may occur within the inlet region rather than within the capillary tube.

### 3.2.3 CRITERIA FOR ONSET OF INSTABILITY

The flow rates defining the onset of regions II and III, Figure 3.6 (page 94), lead to the evaluation of dimensional and dimensionless parameters as a means of correlating the limits of stability. The two most commonly used parameters referred to in the literature, the critical shear stress and the recoverable shear strain, were calculated and are tabulated in Table 3.3. Parameters with no asterisk were evaluated at the onset of region II while those with an asterisk were evaluated at the onset of region III. The flow rate used in evaluating the shear stress and the recoverable shear stain for capillary tube 1 in reservoir L was determined by extrapolating the data in Figure 3.6. The data in Table 3.3 indicate that the shear stress and the recoverable shear stain (which is directly proportional to the shear stress): (a) vary somewhat with capillary tube diameter, (b) vary strongly with reservoir size, and (c) depend upon the type of instability

## TABLE 3.3

### $\tau_w$ and $S_R$ AT ONSET OF INSTABILITY

| RESERVOIR S | I.D. (cm) | | |
|---|---|---|---|
| | 0.10 | 0.20 | 0.30 |
| $Q^*$ (cm$^3$/sec) | 0.119 | 0.318 | 0.635 |
| $\tau_w^*$ (dyn/cm$^2$) | 125.0 | 72.6 | 56.0 |
| $S_R^* = \left(\frac{\tau_w MW}{CR_0T}\right)$ | 7.7 | 4.5 | 3.5 |
| $\tau_w^{***}$ (dyn/cm$^2$) | 167-1667 | 167-1667 | 167-1667 |
| RESERVOIR L | | | |
| $Q^*$ (cm$^3$/sec) | 1.750 | 4.866 | 11.120 |
| $Q$ (cm$^3$/sec) | 0.580** | 1.589 | 4.866 |
| $\tau_w^*$(dyn/cm$^2$) | 630.1 | 305.0 | 240.0 |
| $\tau_w$ (dyn/cm$^2$) | 296.0 | 162.0 | 154.0 |
| $S_R^* = \left(\frac{\tau_w MW}{CR_0T}\right)$ | 38.8 | 18.8 | 14.8 |
| $S_R = \left(\frac{\tau_w MW}{CR_0T}\right)$ | 18.2 | 10.0 | 9.5 |
| $\tau_w^{***}$ (dyn/cm$^2$) | 167-1667 | 167-1667 | 167-1667 |

* Onset of region III

** By extrapolation of data in Figure 3.6

*** Southern and Paul (157) assuming the shear stress at the onset of instability for polymer melts varies from $10^5$ to $10^6$ dyn/cm$^2$ and the density of the melt is 1.20 gm/cm$^3$

(regions II or III).

Variations in $\tau_w$ or $S_R$ with the type of instability and capillary is exemplified by the data in reservoir L. At the onset of region II, $S_R$ increased from 9.5 to 18.2 as the capillary tube diameter decreased from 0.30 to 0.10 cm. On the other hand, at the onset of region III, $S_R$ was almost twice as large, $14.8 \leq S_R \leq 38.8$. These values are within the range reported for other polymer solutions (98, 190) wherein $S_R$ ranged from 6.0 to 42.8 and 2.2 to 66.81 (see Table 1.3, page 41) for polymer melts. With a fixed tube diameter, stable flow fields within the inlet region were observed to exist up to higher flow rates or equivalently higher shear stresses in reservoir L. For example, with capillary tube 3 the shear stress evaluated at the onset of region II was 56 dyn/cm$^2$ in reservoir S, whereas in reservoir L it was 154 dyn/cm$^2$. Although reasons for this behavior are not clear it is postulated that the difference may be due to differences in the upstream velocity field (Section 3.4.4, page 141) with reservoir size.

The range of shear stresses at the onset of flow instabilities (region II or III), although four orders of magnitude less than $10^6$ dyn/cm$^2$ for polymer melts, are in reasonable agreement with shear stresses calculated from the analysis presented by Southern and Paul (157), $167 \leq \tau_w \leq 1667$ dyn/cm$^2$. Furthermore, shear stresses evaluated at the onset of region II or III compare favourably with critical shear stresses obtained by other researchers (98, 119, 130, 142). Murch (119), using a 0.5% solution of Separan AP-30 in a 30 percent by weight glycerine-water mixture and with $\beta = 1.86 \times 10^{-6}$, observed that the stable flow field broke down at shear stresses approximately equal to 500 dyn/cm$^2$. It is not clear, however, whether this breakdown corresponded with the onset of region II or III. In a more concentrated solution, 1.49% Separan AP-30 in a 50 percent by weight glycerol-water mixture and with $\beta = 18.5 \times 10^{-3}$, the estimated shear stress at the onset of regions II and III were 500 and 3000 dyn/cm$^2$ respectively (142). Oliver and Bragg (130) reported inlet flow instabilities for orifice flows and with a 0.10% aqueous solution of ET-597, $\beta$ varying from $92.2 \times 10^{-4}$ to $4.0 \times 10^{-2}$, the estimated shear stress at the onset of region III varied from 225 to 20 dyn/cm$^2$.

In summary, variations in $S_R$ may arise from: (a) the type of instability (region II or III), (b) variations with the reservoir size, and (c) variations with the capillary tube diameter. The recoverable shear strain or shear stress criterion, although simple to evaluate and requiring little, if any, additional experimentation, does not account for the observed dependence on capillary tube diameter and reservoir size. More critically, these criteria, which are based on conditions in SLSF in the capillary tube, are not consistent with experimental observation wherein initiation occurs within the inlet region. Criteria based on inlet conditions have been proposed by Cogswell (46), Everage and Ballman (60), and Hürlimann and Knappe (88). Since these criteria depend upon inlet conditions, i.e., initial cone semi-angle and the velocity field, the discussion of these criteria is delayed to Section 3.5. The features of the flow field, the cone semi-angles, and the velocity field are discussed in Section 3.4.

## 3.3 EFFECTS OF INSTABILITY

The effects of instability are discussed in conjunction with the Bagley plots, the flow curve, the total pressure loss-flow rate curve, and the contraction losses.

### 3.3.1 BAGLEY PLOT

The average values of pressure (Equation 3.6, page 97), measured at the reservoir wall at a location upstream of the contraction, were used in constructing the Bagley plots. A typical Bagley plot is given in Figure 3.11 for a flow rate within region III. The plot is linear and the shear stress, equal to four times the slope, is in good agreement with the extrapolation of the shear stress data obtained with a Weissenberg rheogoniometer (Appendix D). Figure 3.12 shows two Bagley plots for an experimental run where oscillations between a stable and a "chaotic" flow field were observed within the reservoir. In this case the two Bagley plots resulted from pressures measured with a stable flow field (lower plot) and for pressures measured with a "chaotic" flow field (upper plot).

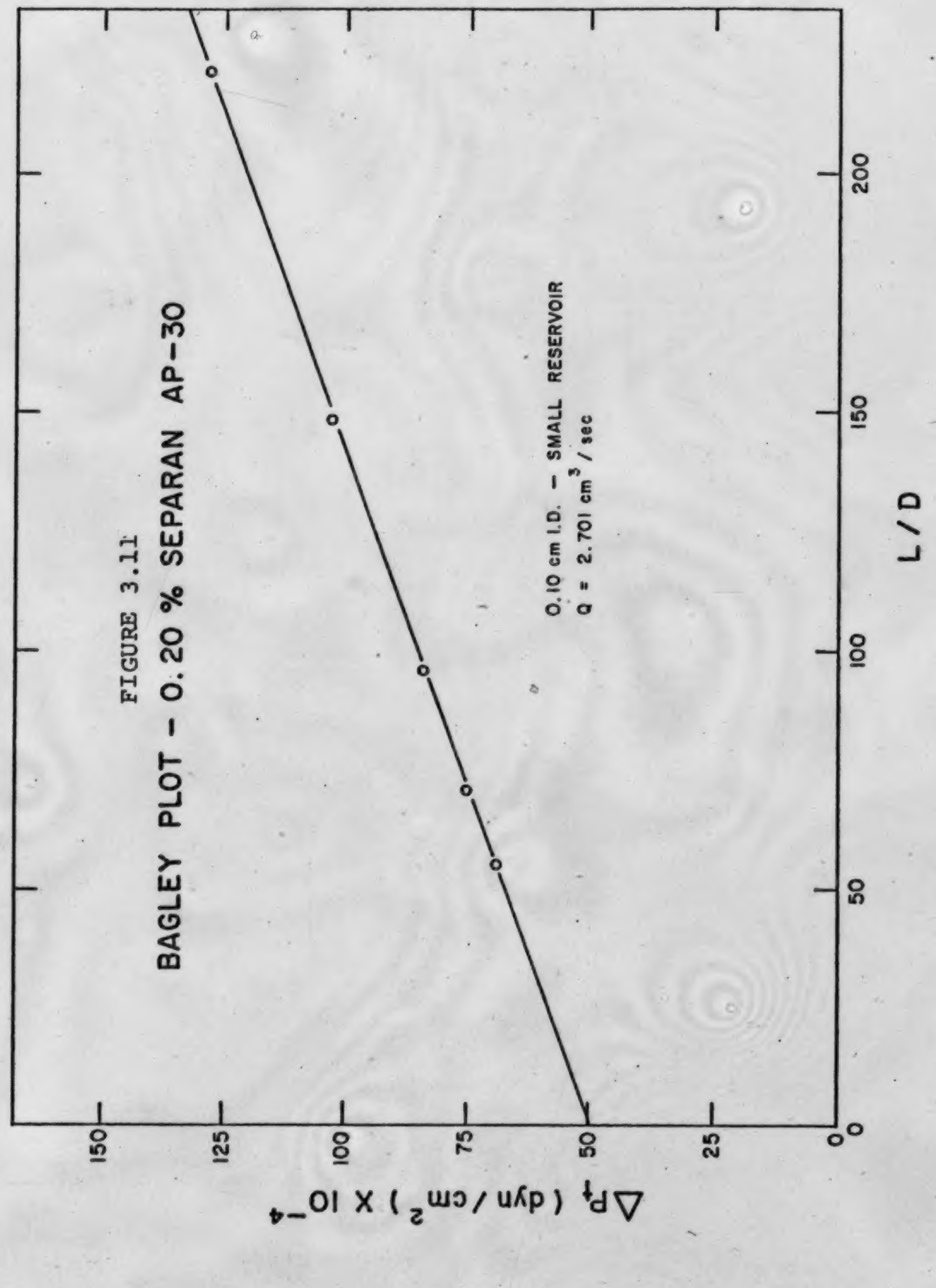

FIGURE 3.11

BAGLEY PLOT - 0.20 % SEPARAN AP-30

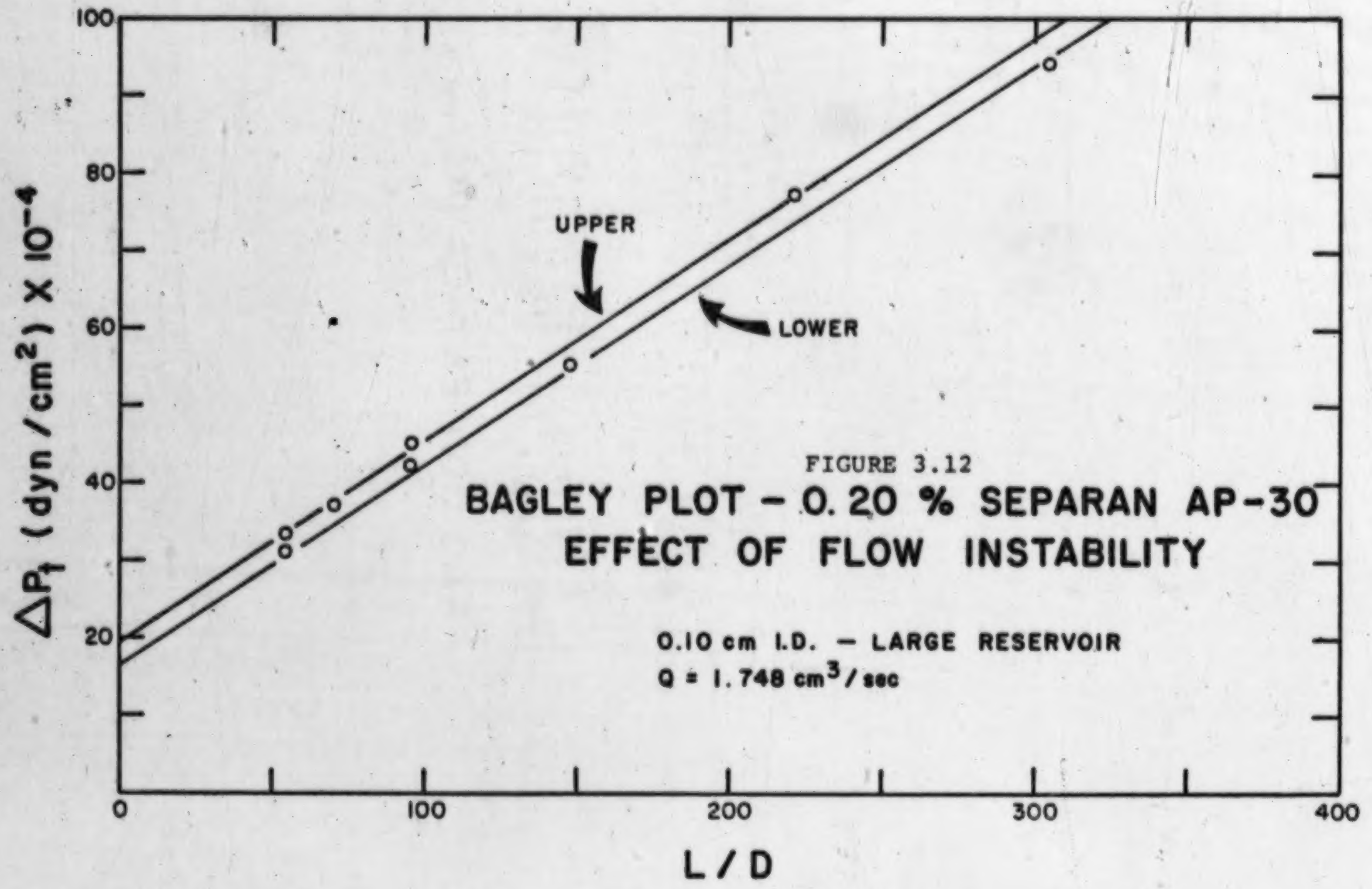

FIGURE 3.12

BAGLEY PLOT – 0.20 % SEPARAN AP-30
EFFECT OF FLOW INSTABILITY

In both cases, the plots are linear and the resulting shear stresses are the same whether evaluated from the upper or lower plot. The intercept of the upper plot is greater than the intercept of the lower plot, hence, instability resulted in an increase in the contraction losses.

At a constant flow rate within region III and for a given capillary tube length to diameter ratio the pressure trace may be either smooth or similar to trace A or B in Figure 3.7. In terms of the flow field within the reservoir it may be stable, may oscillate between a stable and a "chaotic" flow or may be "chaotic". The total pressure losses are related to the state of the flow field. Therefore, in constructing true Bagley plots, i.e., measuring total pressure losses for several capillary tube length to diameter ratios, it is necessary to know the state of the flow field with each capillary tube length to diameter ratio. Furthermore, although stable flow fields are implied from zero pressure fluctuations it is not possible to differentiate between pressure trace A or B without a knowledge of the flow field. The construction of Bagley plots using average values of pressure (Equation 3.6) without a knowledge of the state of the flow field will result in errors in evaluating shear stresses and the contraction losses.

### 3.3.2 FLOW CURVE

The shear stresses used to construct the flow curve, Figure D.2 in Appendix D, were obtained from the Bagley plots for reservoir L. No significant differences in shear stresses were found when reservoir S was used. The flow curve was smooth and continuous over a wide range of apparent shear rates. The onset of flow instability had no effect on the flow curve. This is consistent with results reported for other polymer solutions and melts where instability occurs within the inlet region (inlet initiation).

### 3.3.3 TOTAL PRESSURE LOSS - FLOW RATE CURVE

Typical $\Delta P_t$-Q plots, Figures 3.13 and 3.14, were constructed with the data tabulated in Appendix B. Values of $\Delta P_t$, were averaged over the time interval that the flow field was either "chaotic" or stable. Figure 3.13 shows that the total pressure losses within regions I and II increased with increasing flow rate although the flow field in region I was stable and within region II a swirling motion was observed. No abrupt increase in pressure was measurable. At several flow rates within region III two values of pressures were measured. For the remaining flow rates within region III and for all flow rates within regions I and II only one value of pressure was measured. The sudden increase in $\Delta P_t$ (pressure jump) at the onset of region III can be explained in terms of a change from a stable to "chaotic" flow field within the reservoir. With reference to Figure 3.7 (page 96), at a given flow rate the upper level of pressure corresponds to a "chaotic" flow field and the lower level of pressure corresponds to the existence of a stable flow field. If Equation 3.6

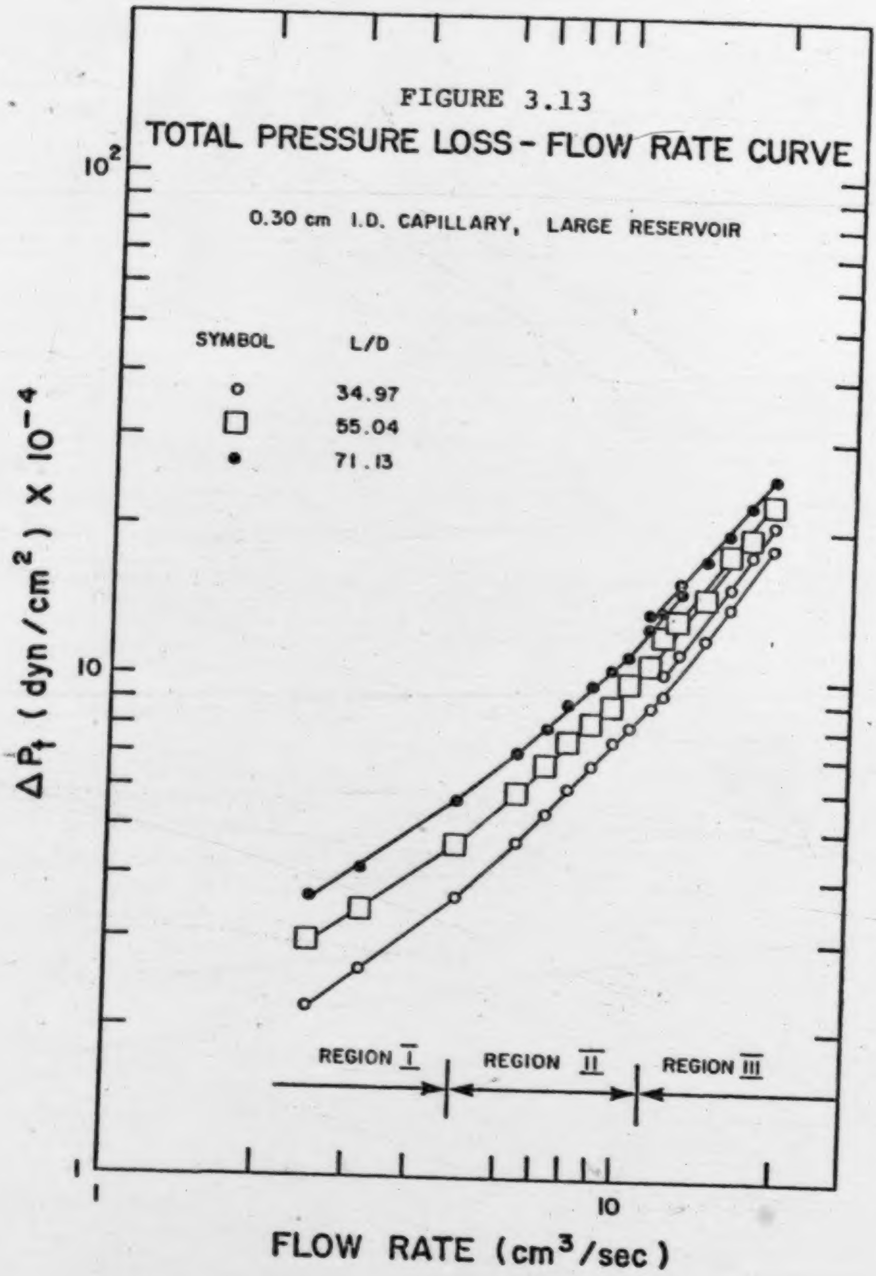

FIGURE 3.13

TOTAL PRESSURE LOSS - FLOW RATE CURVE

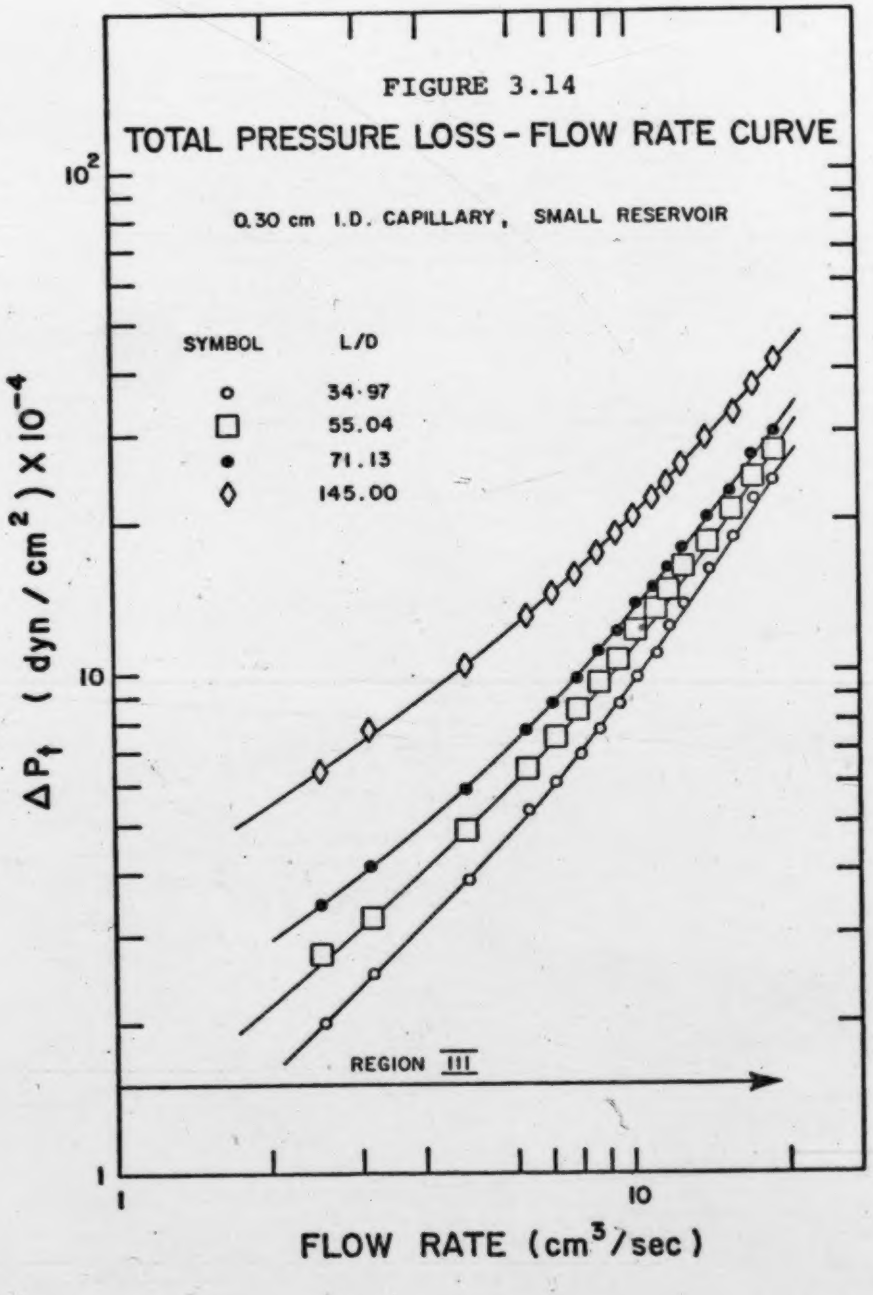

FIGURE 3.14

TOTAL PRESSURE LOSS - FLOW RATE CURVE

0.30 cm I.D. CAPILLARY, SMALL RESERVOIR

were used to determine an average value of $\Delta P_t$, a pressure jump would still exist. The magnitude of the pressure jump would be reduced since the new value of $\Delta P_t$ would now lie midway between the two measured levels of pressure. Therefore, the sudden increase in the $\Delta P_t$-Q curve is not a result of interpretation of the pressure displacement traces.

The data graphically shown in Figure 3.13 indicate that the difference in pressure arising from changes in the state of the flow field within region III was independent of the L/D ratio. As the capillary tube length increased, the ratio of this difference in pressure to the total measured pressure loss, $\Delta P_t$, tended to zero. Therefore, in the limit of very large L/D ratios, the $\Delta P_t$-Q curve would appear to be smooth even at the onset of region III. The curves passing through the data in Figure 3.14 are smooth, although these data were obtained with flow rates well within region III. Visual observations indicated that the flow field became "chaotic" for flow rates exceeding 0.635 $cm^3$/sec (Figure 3.6). The lowest flow rate where the total pressure losses were measured for the data shown in Figure 3.14 was 2.5 $cm^3$/sec.

In summary, sudden increase in pressure observed in the total pressure loss-flow rate curves occurred at the onset of region III and this pressure jump can be explained in terms of the transition between a stable motion to one described as "chaotic." Furthermore, this sudden increase in pressure occurred at a flow rate that was independent of L/D ratios, i.e., the onset of fracture was independent of L/D ratios. It is important to emphasize that these plots, $\Delta P_t$ vs Q, are useful in determining the onset of fracture (region III) only when the pressure jump is of such magnitude that it can be measured.

### 3.3.4 CONTRACTION LOSSES

Contraction losses are shown graphically in Figure 3.15 and 3.16 as a function of the capillary tube generalized Reynolds numbers. Included for comparison purposes are the data for Newtonian fluids that were reported in Section 3.1.2, page 83. The flow rates defining the onset of region III as obtained from the onset of measurable pressure fluctuations and the visually observed onset of a "chaotic" flow field were coincident. The only exception was for capillary tube 1 in reservoir S; hence, contraction losses obtained with the 0.10 cm I.D. capillary are not plotted in Figure 3.16.

Day (50) measured contraction losses and observed the qualitative features of the flow field for the flow of poly (ethylene oxide) solutions through an orifice. The results can be summarized as follows:

(a) Under creeping flow conditions the fluid behaved like a Newtonian fluid, i.e., it entered into the orifice through a 180 degree solid angle and the contraction losses were equal to the Newtonian contraction losses.

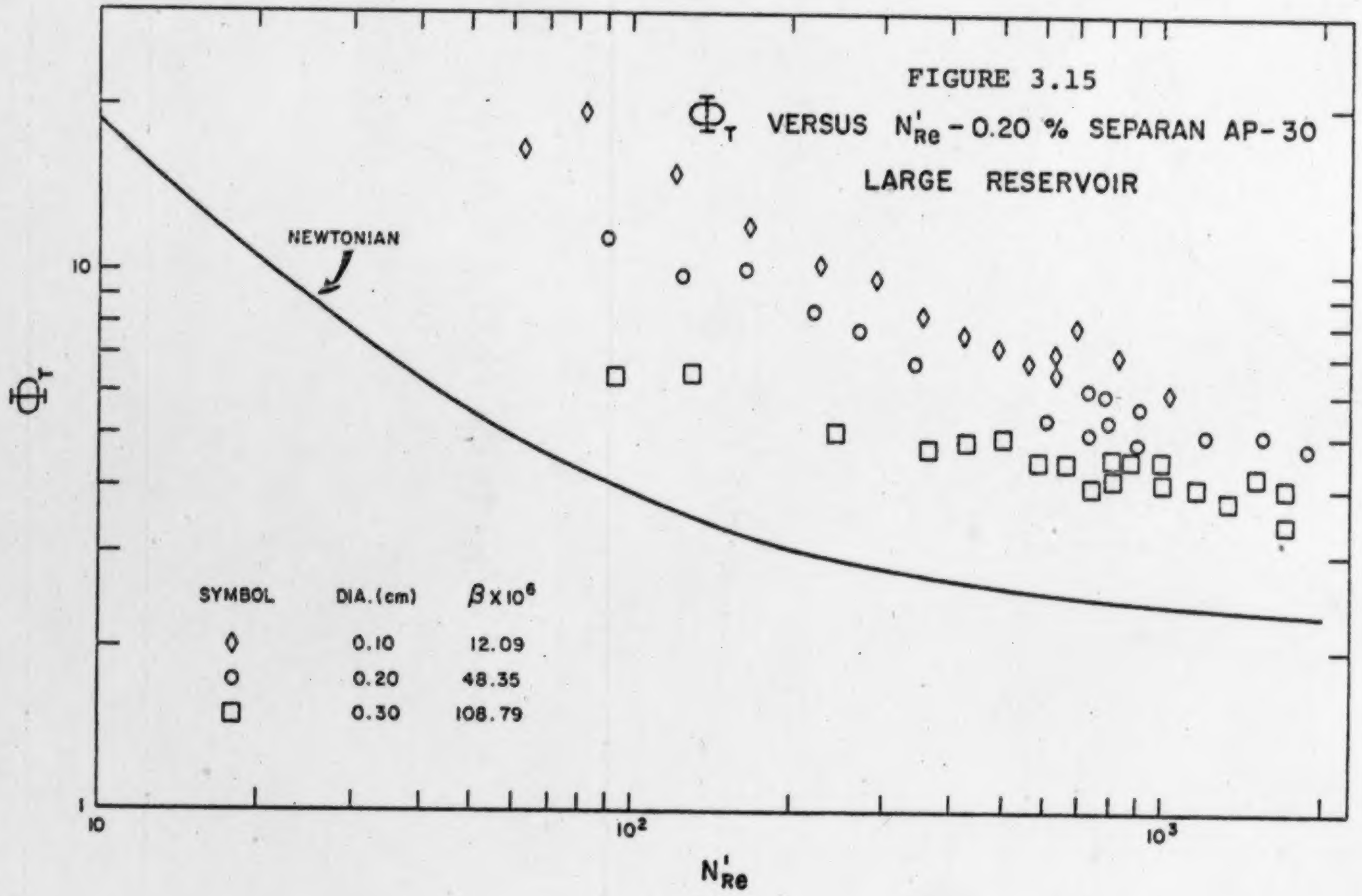

FIGURE 3.15

$\Phi_T$ VERSUS $N'_{Re}$ - 0.20 % SEPARAN AP-30

LARGE RESERVOIR

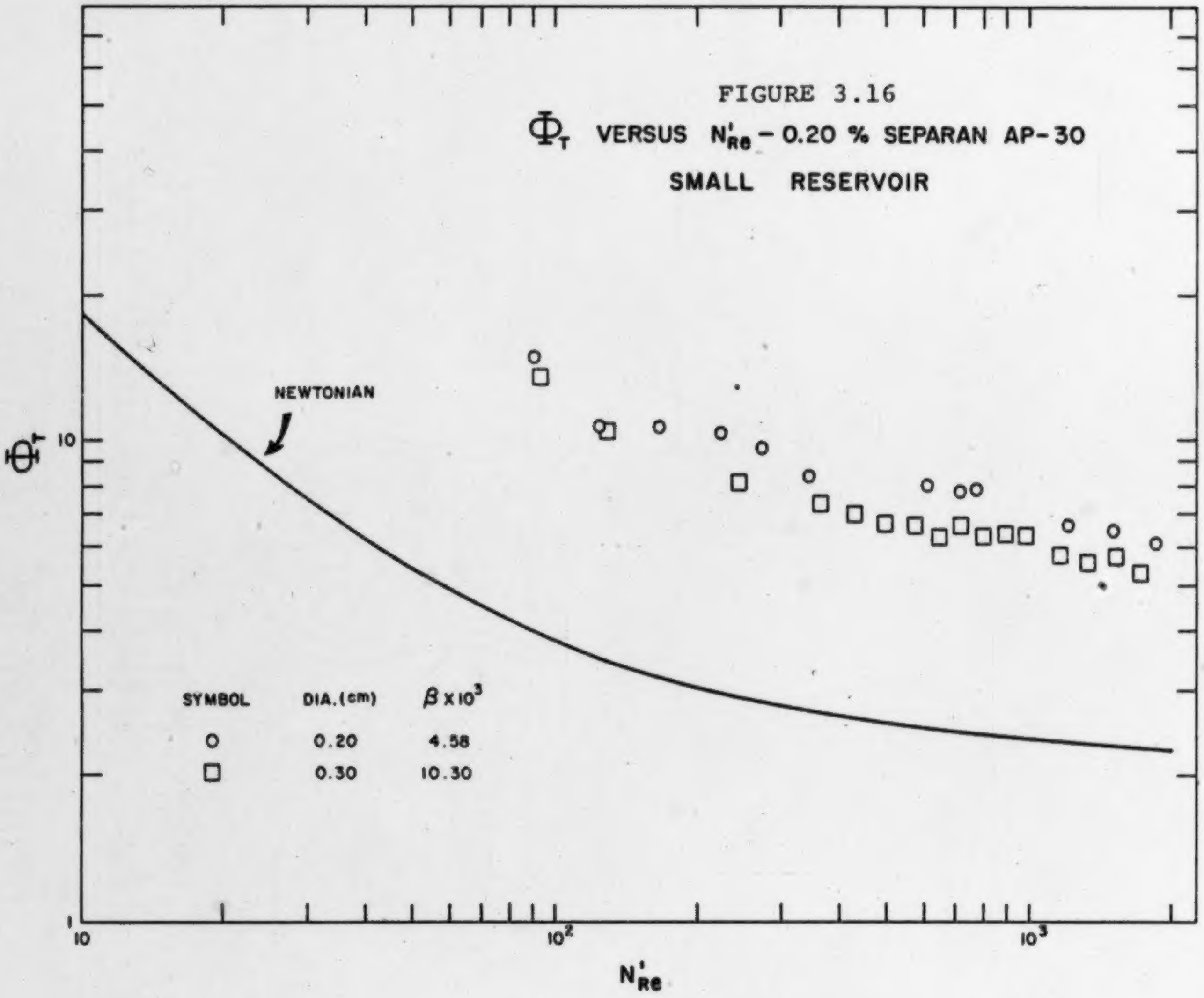

FIGURE 3.16

$\Phi_T$ VERSUS $N'_{Re}$ - 0.20 % SEPARAN AP-30

SMALL RESERVOIR

(b) When a certain Reynolds number was reached the fluid behavior changed abruptly. An extremely small vortex appeared exactly at the edge of the orifice which grew in both width and depth as Reynolds number increased. Correspondingly, the contraction losses increased to the extent that they were greater than Newtonian results at the same Reynolds number. This will be classified as the onset of region I.

In this dissertation contraction losses were measured at Reynolds numbers approaching the upper limit of region I as well as Reynolds numbers within regions I I and III where a swirling motion and a "chaotic" flow field were observed respectively. The effects of these flow fields (stable, swirling, chaotic) on $\Phi_t$ is exemplified by the data plotted in Figure 3.15. At Reynolds numbers evaluated at the onset of region II, 121, 126 and 246 for capillary tubes 1, 2, and 3 respectively, there is insufficient data in Figure 3.15 to show conclusively an effect of the change from a stable to an observed swirling motion on $\Phi_t$. At the onset of region III, however, the data indicated an increase in $\Phi_t$. This occurred at $N'_{Re} = 620$, 721, and 816, for capillary tubes 1, 2, and 3 respectively. Contraction losses measured with reservoir S and plotted in Figure 3.16, were obtained at $N'_{Re} \geq 91$, whereas the onset of region III was observed to occur at $N'_{Re} \simeq 10$. Hence, contraction losses in reservoir S were measured only within region III. At several $N'_{Re}$ within region III two values of $\Phi_t$

are shown in Figure 3.15. For example, with capillary tube 1 and at $N'_{Re}$ = 620, the two values of $\Phi_t$ are 6.46 and 7.08. As the flow field oscillated between stable and "chaotic" the pressure displacement traces were similar to trace A in Figure 3.7. This gave rise to two Bagley plots (Section 3.3.1, page 111), hence, two values of $\Phi_t$.

The effect of tube diameter on contraction losses can be rationalized in terms of the condition of the flow field within the inlet region. With reference to the data plotted in Figure 3.15, flow fields were observed to be stable for all capillary tube I.D.'s at $N'_{Re}$ < 125 but, at $N'_{Re}$ < 125, $\Phi_t$ increased as capillary tube I.D. decreased. At $N'_{Re} \simeq 90$ the initial cone semi-angles for capillary tubes 1, 2, and 3 were 0.5, 0.90, and 1.2 degrees (Figure 3.23, page 136) respectively. Hence, the area occupied by the recirculation region was greatest for capillary tube 1. The effect of the larger recirculation region was a measured increase in contraction losses. At $N'_{Re}$ > 125 the difference in $\Phi_t$ with I.D. arose from differences in the state of the flow field. This is exemplified by comparing contraction losses measured with capillary tubes 1 and 3. At $N'_{Re} \simeq 246$ a stable flow field was observed with capillary tube 3, whereas a swirling motion was observed with capillary tube 1. At a higher Reynolds number, e.g., $N'_{Re} \simeq 730$, a "chaotic" flow field and a swirling motion were observed with capillary tube 1 and 3 respectively. The flow fields were observed to be "chaotic" in both capillary tubes only at $N'_{Re} > 816$.

Comparison of data obtained with both reservoirs revealed that $\Phi_t$ was consistently larger when obtained with reservoir S. This is not surprising since contraction losses measured with reservoir S were obtained only within region III, whereas in reservoir L contraction losses were measured in regions I, II, and III. At Reynolds numbers approaching 2000 the flow field was "chaotic" in both reservoirs. Equation 1.12 in Chapter I suggests that when the flow fields are the same in both reservoirs contraction losses may be correlated with $N'_{Re}$. We have shown that the Hagenbach correction factors are evaluated when a "chaotic" flow field exists and the Couette correction factor, although not measured, would have been obtained when the flow field was stable. Therefore, we conclude that it is not correct to correlate contraction losses over a wide range of Reynolds numbers when over the same range of Reynolds numbers the flow field changes from stable to "chaotic."

In summary, contraction losses depend upon capillary tube diameter and reservoir size. This dependence can be rationalized in terms of the conditions of the flow field within the inlet region. Furthermore, correlation of $\Phi_t$ with $N'_{Re}$ should be based on the same inlet flow field, as with Newtonian fluids. For the polymer solution used in this research and over the range of $N'_{Re}$ where contraction losses were measured, three distinct flow fields were observed in the inlet region. Hence, a correlation of $\Phi_t$

with $N'_{Re}$ is not presented.

## 3.4 VELOCITY FIELD UPSTREAM OF CONTRACTION

Three features of the flow field upstream of the contraction were measured:

(a) the axial and radial velocity components within the central accelerating core measured by the digitizer and direct methods,

(b) the cone semi-angles at and upstream of the contraction, and

(c) the location of the center of the eddies.

The cone semi-angles and the location of the eddy centers are given in order to present a complete description of the flow field within the reservoir.

### 3.4.1 VELOCITY - DIGITIZER AND DIRECT METHODS

Table 3.4 summarizes flow rates and dimensionless upstream axial locations where axial velocity profiles were measured. As indicated in the table, the velocity profiles obtained by the digitizer method were measured only at three upstream axial locations hereinafter referred to as axial locations 1, 2, and 3 respectively. The resulting total of approximately 10,000 individual data points obtained by the digitizer method are tabulated in Appendix E, Section E.2. The digitizer method was used also in measuring radial velocity components with the results tabulated in Appendix E, Section E.2.

As a typical example of the digitizer data, consider

## TABLE 3.4

## FLOW RATES AND UPSTREAM AXIAL LOCATIONS WHERE VELOCITIES WERE MEASURED

| RESERVOIR | CAPILLARY I.D. | Q(cm$^3$/sec) | z/D |
|---|---|---|---|
| S | | | |
| | 0.10 | 0.016 | * |
| | (L/D = 55.08) | 0.040 | * |
| | | 0.119 | * |
| | 0.20 | 0.040 | * |
| | (L/D = 54.96 | 0.159 | 3.29 |
| | | 0.159 | 6.57 |
| | | 0.159 | 9.86 |
| | | 0.238 | * |
| | | 0.318 | * |
| | 0.30 | 0.040 | * |
| | | 0.159 | 1.46 |
| | | 0.159 | 2.92 |
| | | 0.159 | 4.38 |
| | | 0.318 | * |
| | | 0.635 | * |
| L | | | |
| | 0.20 | 0.159 | * |
| | (L/D = 54.96) | 0.318 | * |
| | | 0.794 | * |
| | | 1.589** | 15.34 |
| | | 1.589** | 30.67 |
| | | 1.589** | 46.00 |
| | | 1.906 | 15.60 |
| | | 1.906 | 31.20 |
| | | 1.906 | 46.80 |
| | | 2.383 | 17.33 |
| | | 2.383 | 34.65 |
| | | 2.383 | 51.98 |
| | | 2.701 | 17.71 |
| | | 2.701 | 35.42 |
| | | 2.701 | 53.13 |

* velocities measured by the direct method

## TABLE 3.4 (continued)

| RESERVOIR | CAPILLARY I.D. | Q(cm$^3$/sec) | z/D |
|---|---|---|---|
| | | 3.177 | 18.26 |
| | | 3.177 | 36.52 |
| | | 3.177 | 54.78 |
| | | 3.812 | 19.39 |
| | | 3.812 | 38.78 |
| | | 3.812 | 58.17 |
| | | 4.866 | 19.73 |
| | | 4.866 | 39.45 |
| | | 4.866 | 59.18 |
| | 0.30<br>(L/D = 55.04) | 0.318 | * |
| | | 0.635 | * |
| | | 1.589 | * |
| | | 4.866 | 10.95 |
| | | 4.866 | 21.90 |
| | | 6.354 | 11.56 |
| | | 6.354 | 23.12 |
| | | 7.148 | 11.92 |
| | | 7.148 | 23.12 |
| | | 7.943 | 12.04 |
| | | 7.943 | 24.08 |
| | | 8.737 | 12.45 |
| | | 8.737 | 24.90 |
| | | 9.531 | 12.53 |
| | | 9.531 | 25.06 |
| | | 9.531 | 37.59 |
| | | 10.325 | 12.72 |
| | | 10.325 | 25.44 |
| | | 10.325 | 38.16 |
| | | 11.120 | 12.72 |
| | | 11.120 | 25.44 |
| | | 11.120 | 38.16 |

* velocities measured by the direct method

the axial velocities measured with capillary tube 3 at a flow rate of 9.531 $cm^3$/sec in reservoir L. One may recall from Figure 3.6 (page 94) that flow rates between 4.866 $cm^3$/sec and 11.120 $cm^3$/sec were within region II. Stable flow fields within this region were obtainable only when the crosshead speed of the Instron was gradually increased to the desired setting; this amounted to a gradual increase in flow rate. The velocity profiles shown in Figures 3.17 to 3.19 are for the stable flow field. Forty to 300 individual data points were measured to determine velocity profiles. The velocity profiles shown in Figures 3.17 to 3.19 are axially symmetric with the axial velocity along the centerline being well defined at axial locations 2 and 3. The centerline velocities obtained from Figures 3.17 and 3.18 were 3.4 and 22.0 cm/sec respectively. At axial position 1 the velocity along the centerline was not well defined and was estimated in the following manner: With the data in Figure 3.19, lines were drawn through the individual data points that were close to the centerline. These lines were extrapolated until they intersected. The velocity corresponding to this intersection was used as an estimate of the centerline axial velocity which, for this example, was 93.0 cm/sec.

The flow rates where the velocity profiles were measured by the direct method, as tabulated in Table 3.4, have been denoted by an asterisk. Raw data are tabulated in Appendix E, Section E.1. With these data velocity

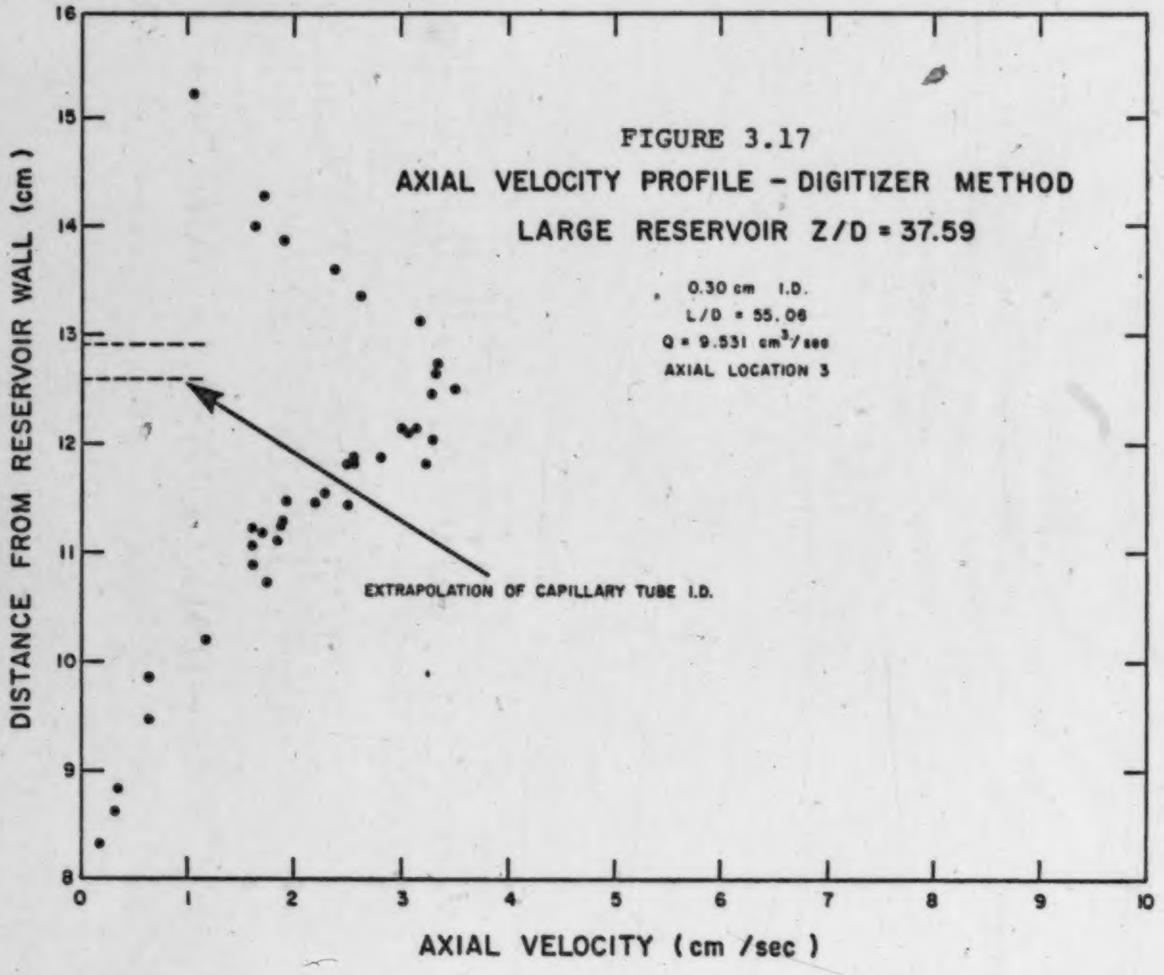

FIGURE 3.17
AXIAL VELOCITY PROFILE - DIGITIZER METHOD
LARGE RESERVOIR Z/D = 37.59

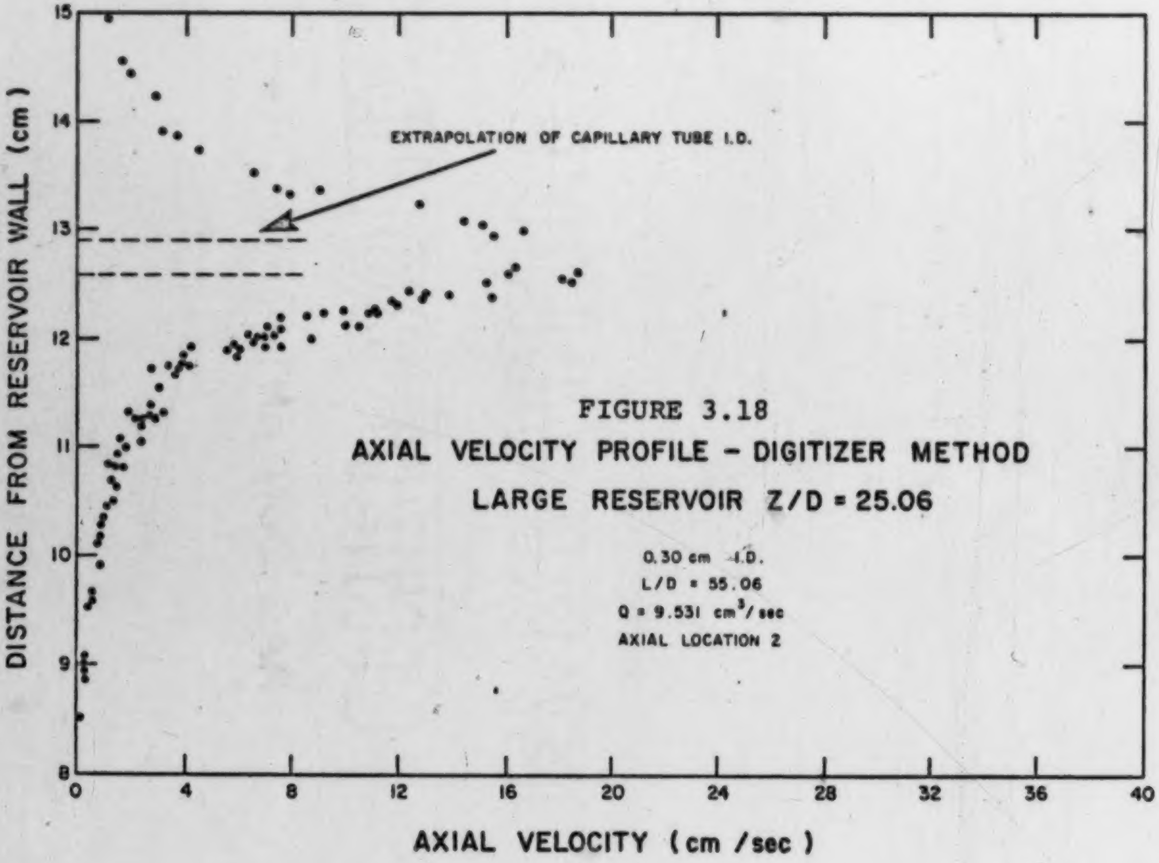

FIGURE 3.18

AXIAL VELOCITY PROFILE - DIGITIZER METHOD

LARGE RESERVOIR Z/D = 25.06

0.30 cm I.D.
L/D = 55.06
Q = 9.531 $cm^3/sec$
AXIAL LOCATION 2

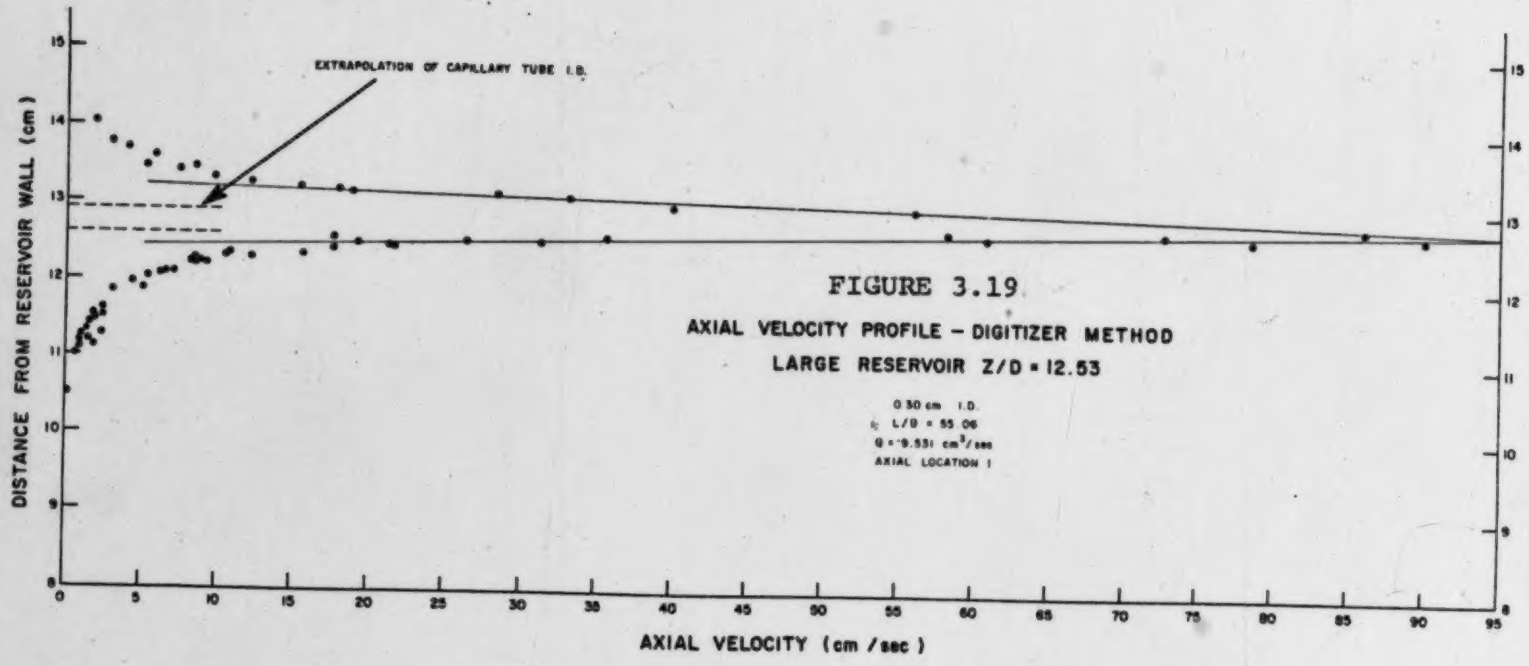

FIGURE 3.19

AXIAL VELOCITY PROFILE – DIGITIZER METHOD

LARGE RESERVOIR Z/D = 12.53

profiles were constructed and are given in Figures 3.20 to 3.22 at several upstream axial locations for the three capillary tubes. The data plotted in Figure 3.22 were obtained with capillary tube 3 in reservoir S and at a flow rate of 0.318 $cm^3$/sec. This flow rate was within region I, i.e., it is less than 0.635 $cm^3$/sec. The axial velocity profiles at the contraction, $z/D = 0.0$, were not measured directly but were obtained in the following manner: From the projected photographs, consecutive streaks along a streamline were measured and the axial velocity was determined as a function of position in the reservoir. This allowed plots of velocity versus axial position to be made which included measured velocities to within one or two streak lengths of the capillary entrance. Between this axial location and the contraction, the axial velocity was estimated by a linear extrapolation of the axial velocity-position plot to the entrance. The location nearest to the contraction where the axial velocity could be measured moved farther away from the contraction as the streak length increased. In all cases the length of extrapolation was less than one tube diameter and in some cases was as small as one sixth of the tube diameter.

Several conclusions can be drawn from the data plotted in Figures 3.17 to 3.22:

(a) The axial velocity profiles are not flat. In Figure 3.22, for example, at one diameter upstream of the contraction the axial velocities at the centerline and at a

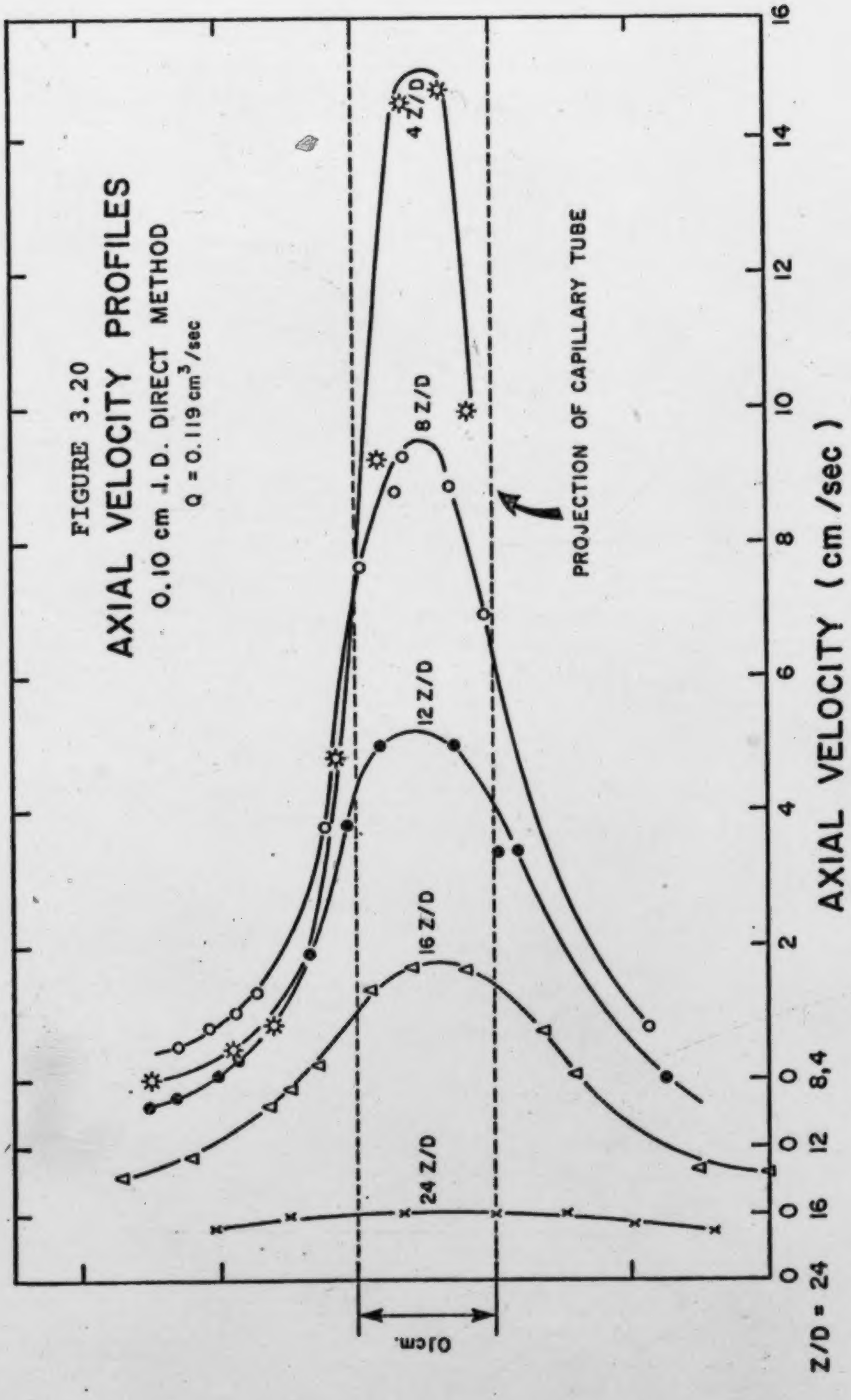

FIGURE 3.20

AXIAL VELOCITY PROFILES

0.10 cm I.D. DIRECT METHOD

$Q = 0.119\ cm^3/sec$

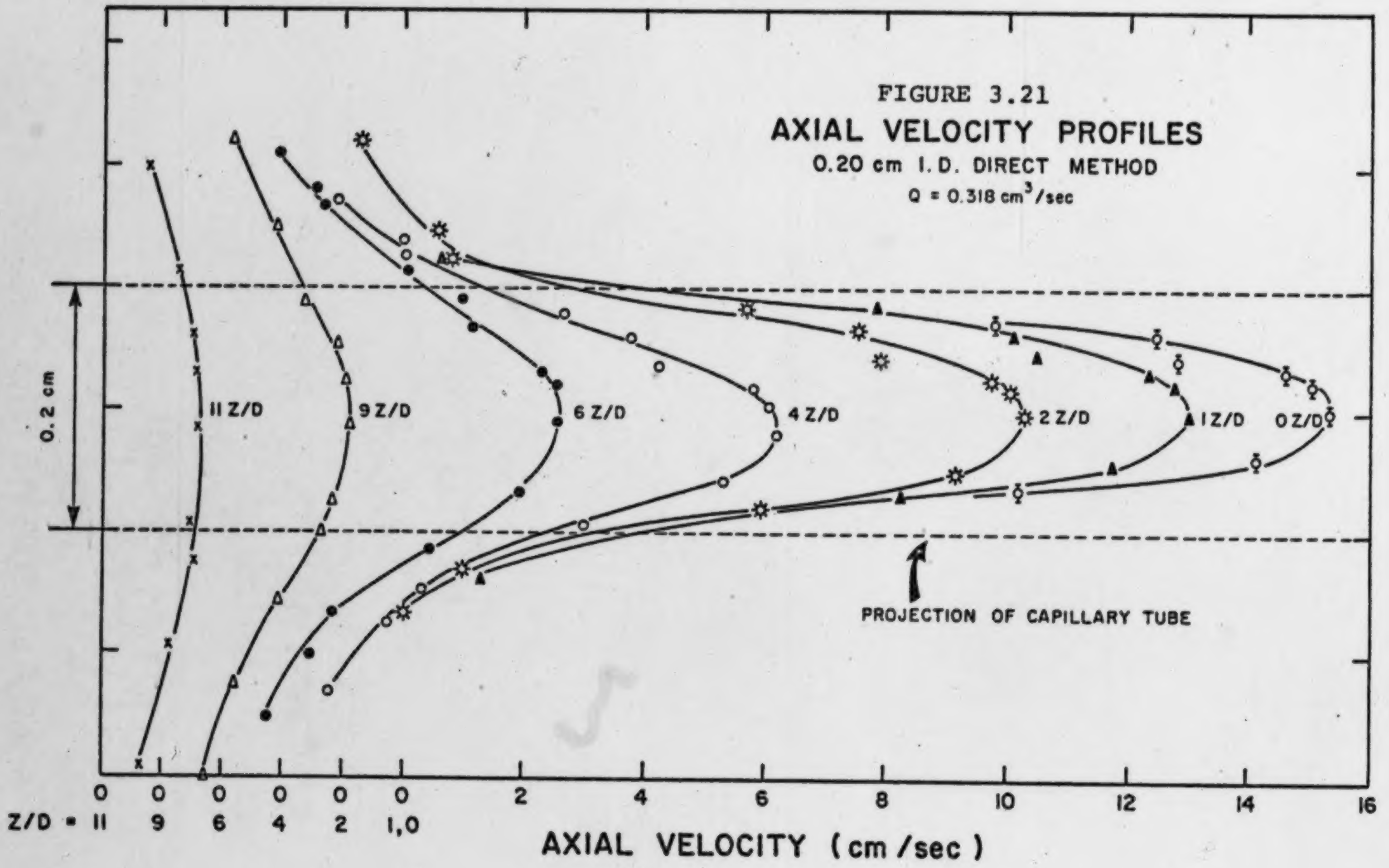

FIGURE 3.21

AXIAL VELOCITY PROFILES

0.20 cm I.D. DIRECT METHOD

Q = 0.318 cm$^3$/sec

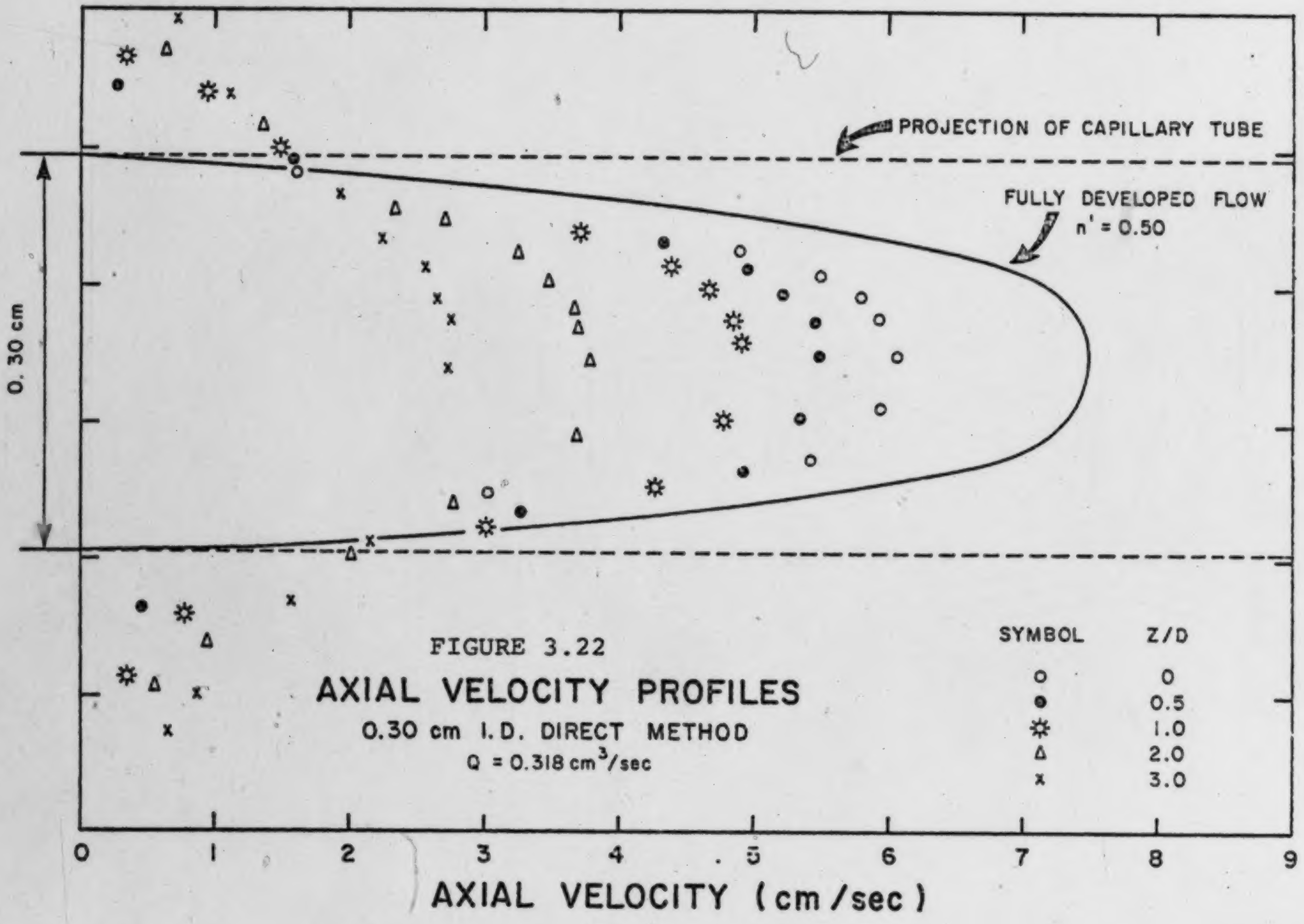

FIGURE 3.22

AXIAL VELOCITY PROFILES

0.30 cm I.D. DIRECT METHOD

$Q = 0.318\ cm^3/sec$

radial position equal to D/2.0 were 4.9 cm/sec and 1.5 cm/sec respectively. At these same coordinates $z/D = 1.0$, $r = 0.0$, and $z/D = 1.0$, $r = D/2.0$, the respective velocities with capillary tube 2 at a flow rate of 0.318 $cm^3/sec$ (Figure 3.21) were 13.0 cm/sec and 4.0 cm/sec. Therefore, any empirical relationship must include axial and radial dependence.

(b) The development of the axial velocity profiles was such that as z/D approached zero the velocity profiles in the reservoir approached the fully developed velocity profile for flow in the capillary. The degree of development at the contraction was estimated from the ratio of the velocity along the centerline at the contraction to the velocity along the centerline for a power law fluid in SLSF in the capillary tube. This ratio, given by Equation 3.7, was approximately 0.75 and it remained constant for all of the data.

$$\frac{V_z\big|_{\mathbb{C}} \text{ @ } z/D = 0}{V_z\big|_{\mathbb{C}} \text{ @ SLSF}} = \frac{V_0}{V\left(\frac{3n'+1}{n'+1}\right)} = 0.75 \qquad 3.7$$

(c) At large upstream axial locations the axial velocity profiles over a radial distance less than D/2.0 approached a flat distribution. This axial location varied with capillary tube diameter and flow rate. In Figure 3.20, the velocity profiles were considered to be reasonably flat at distances approaching 24 diameters upstream. At upstream axial locations beyond the development of the WGS structured flow field, the velocity profiles, although not measured directly, were assumed to be those associated with fully developed flow in the reservoirs.

### 3.4.2 CONE ANGLES

In many experimental runs the visualization of the outermost streamline did not extend up to the contraction. It was necessary in these cases to extrapolate the outermost streamline to the contraction in order to estimate the initial cone semi-angle, $\phi_0$. This resulted in errors as large as 15 percent in $\phi_0$. Initial cone semi-angles less than one half of a degree were too small to be measured with confidence. The measured initial cone semi-angles tabulated in Appendix F are plotted in Figure 3.23 against the parameter, $D^3/\theta_0 Q$. This parameter was suggested indirectly by independent experimental observations of Metzner et al. (116), Cogswell and Lamb (48), and Clegg (44). Metzner et al. (116) suggested that for a given fluid the initial cone semi-angles were proportional to $D^3/Q$; this was also suggested independently by Cogswell and Lamb (48). Clegg (44) observed that at a constant $D^3/Q$ the initial cone semi-angles were inversely proportional to the relaxation time of the fluid. The integration of these experimental observations leads to the formation of the dimensional group, $D^3/\theta_0 Q$ (188).

FIGURE 3.23

INITIAL CONE SEMI-ANGLES

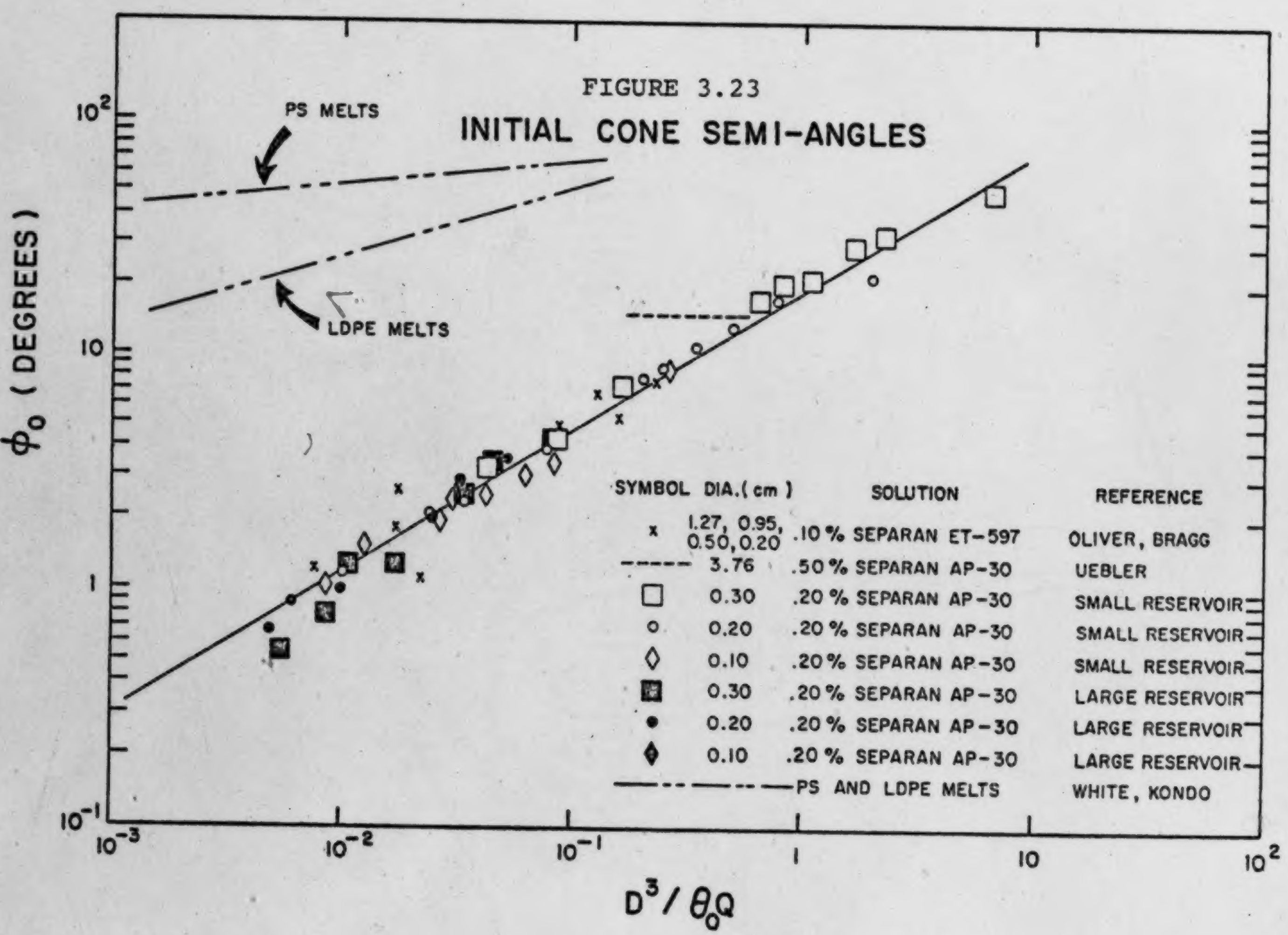

By using the zero shear relaxation time, $\theta_0$, as a characteristic relaxation time, the data in Figure 3.23 can be reasonably represented by Equation 3.8. Equation 3.8 is shown as the solid line in Figure 3.23.

$$\phi_0 = 19\left(\frac{D^3}{\theta_0 Q}\right)^{0.6} \text{ for } 6 \times 10^{-3} < \left(\frac{D^3}{\theta_0 Q}\right) < 10 \qquad 3.8$$

Values of $(D^3/\theta_0 Q)$ less than $6 \times 10^{-3}$ corresponded approximately with the onset of region III, whereas for exceedingly small flow rates, values of $D^3/\theta_0 Q > 10$, the initial cone semi-angles, although not measured, asymptotically approach 90 degrees. The data in Figure 3.23 also indicate that the initial cone semi-angles were the same in both reservoirs for values of $(D^3/\theta_0 Q)$ that overlapped. The initial cone semi-angles measured by Oliver and Bragg (130) for a 0.10% aqueous solution of Separan ET-597 ($\theta_0$ = 1 sec) as well as those reported by Uebler (173) for a 0.50% aqueous solution of Separan AP-30 ($\theta_0$ = 5 sec) are in good agreement with these data as shown in Figure 3.23. Ballenger and White (12) presented a correlation of $\phi$ with $\Delta P_c/\tau_w$. We have found, with the limited data where both $\Delta P_c$ and $\phi$ were measured, a similar correlation, however, there is significant scatter in the data. The initial cone semi-angles measured in this research as well as those measured by others (12, 130, 188) suggest that the exponent and the proportionality constant in Equation 3.8 are dependent upon concentration and and type of polymer.

The cone semi-angles were measured at axial locations other than at the contraction. Like the initial cone semi-angles, these were measured tangent to the outermost streamline. A typical example of the growth of the cone semi-angles at several flow rates for both capillary tubes 2 and 3 is given in Figures 3.24 and 3.25. The remaining data can be found in Appendix F, Section F.2. The cone semi-angles were independent of reservoir size within the accuracy of measurement and over the range of z/D where they were measured. Although $\phi_R$ was not measured directly at axial locations greater than those tabulated in the Appendix, the dependence of the growth of $\phi_R$ with reservoir size was implied from observations of the flow field in both reservoirs. At the maximum values of z/D, where cone semi-angles were measured in reservoir S, the cross-sectional area of the central core of fluid was approximately equal to the reservoir's cross-sectional area. At the same flow rate and within reservoir L, the core area occupied a small fraction of the total cross-sectional area due to the order of magnitude increase in the physical dimensions of reservoir L. Hence, in reservoir L the core extended farther upstream and the cone semi-angles could be measured to larger values of z/D.

### 3.4.3 EDDY CENTERS

A third characteristic of the flow field within the reservoir is the location of the eddies that surround

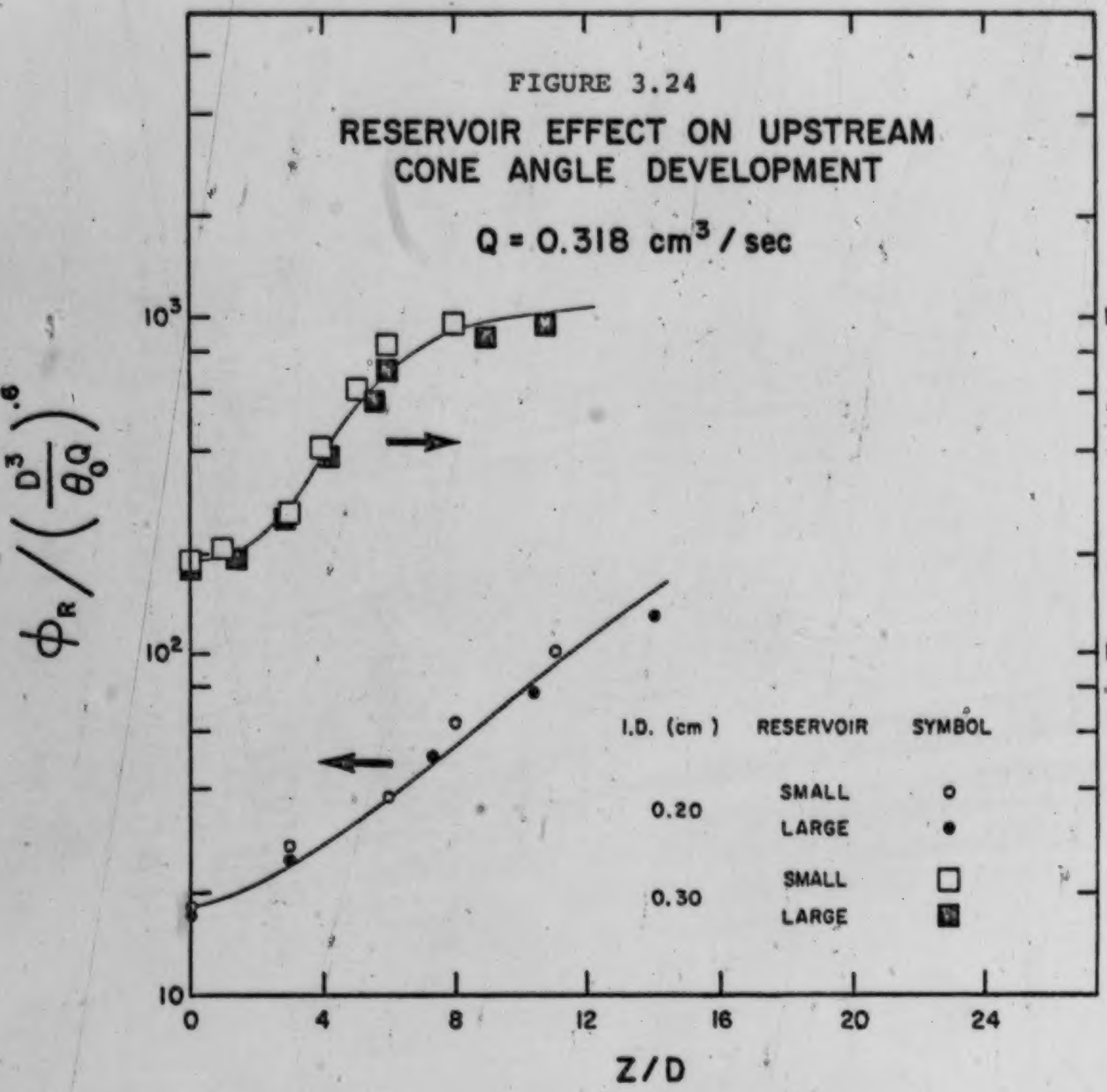

FIGURE 3.24

RESERVOIR EFFECT ON UPSTREAM CONE ANGLE DEVELOPMENT

$Q = 0.318\ cm^3/sec$

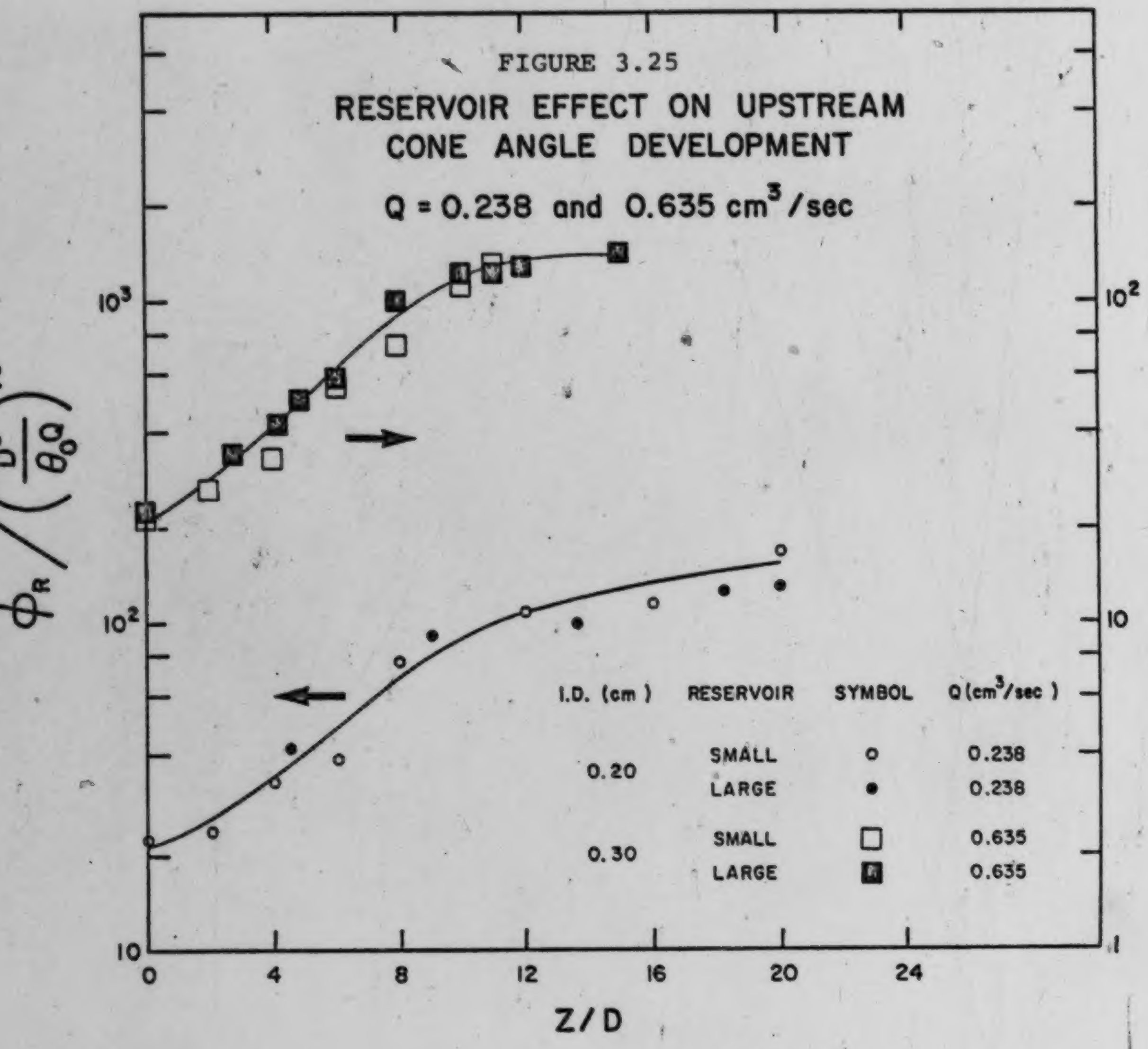

FIGURE 3.25

RESERVOIR EFFECT ON UPSTREAM CONE ANGLE DEVELOPMENT

Q = 0.238 and 0.635 cm$^3$/sec

the central core of the fluid. The relative size and the location of these eddies are reported in terms of the location of the center of the eddies and the data are tabulated in Appendix F. The data for capillary tube 3 in reservoir S are plotted in Figure 3.26. The figure shows that as the flow rate increased, the location of the eddy centers progressively moved farther away from the contraction and along a well defined path. Comparison of eddy centers in both reservoirs at the same flow rate revealed that the location of the eddy center was located farther upstream in reservoir L. This was not surprising since as mentioned in the previous section it was observed that for a given flow rate and capillary tube the accelerating core was observed to extend farther upstream in reservoir L.

### 3.4.4 CORE VELOCITIES

Based on the typical axial velocities plotted in Figures 3.17 to 3.22, empirical correlations must include both axial and radial dependence. To obtain an empirical relationship that would describe the dependence on axial location three models were considered: the sink flow model, the K2 model, and the exponential decay model.

The sink flow model has been used previously to describe the velocity field for the flow of polymer solutions through a sudden contraction (116, 173). Velocity profiles within two diameters upstream of the contraction were measured for a 2 inch I.D. tube protruding 4.05

FIGURE 3.26

LOCATION OF EDDY CENTERS

0.30 cm I.D., SMALL RESERVOIR

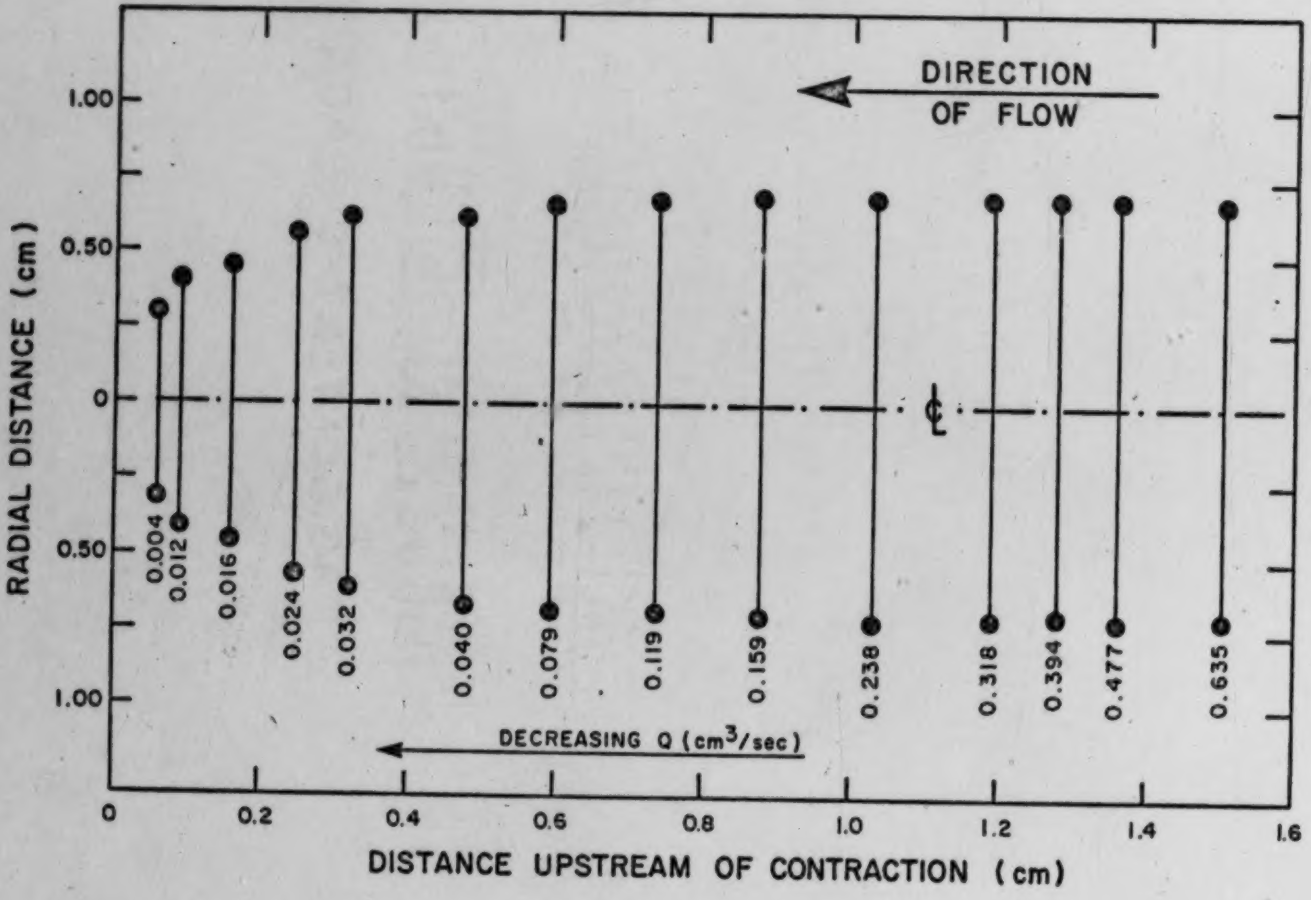

diameters into a 18 inch square reservoir (173). Within the experimental scatter and over the range of available data, the velocity field was adequately represented by the sink flow model. Since the flow field was described as being WGS the streamlines were curved, i.e., the cone semi-angles increased with increasing upstream axial location. The sink flow kinematics assumes that the flow is radially directed toward the origin of a spherical coordinate system, i.e., cone semi-angles are independent of upstream axial location. This results in smaller cross-sectional flow areas farther upstream of the contraction. Therefore, the centerline velocities predicted by the sink flow model are expected to be larger than experimental data at axial locations farther upstream of the contraction.

In an inverse siphon experiment, the fluid is drawn vertically into a capillary tube. This creates a vertical liquid filament which is qualitatively similar to the flow field observed in the inlet region. Hence, the velocity flow field measured in the inverse siphon experiment may approximate the flow field in the inlet region. A description of the velocity field was obtained by photographing the cross sections of the vertical filament, assuming a flat velocity profile at each cross section and equating the integral of velocity over the cross-sectional flow area with the known volumetric flow rate. With this method, Kanel (90) presented an empirical relationship between velocity and axial location that is referred to as the

"K 2 kinematics." However, 83% of his experimental runs and 30% of Weinberger's experimental runs (184), which were reported in Kanel's dissertation, are not represented by the K 2 model. In general, velocity was correlated with axial position by

$$V_z = \frac{4Q}{\pi} (C_1 z + C_2)^{2/p} \qquad 3.9$$

where z is the distance up into the liquid column and $V_z$ is the velocity in the z direction. Parameter p varied from 0.50 to 3.0 (1, 90, 184) and the constants $C_1$ and $C_2$ were evaluated experimentally for each run. With p equal to unity, Equation 3.9 is referred to as the K 2 model. As pointed out by Kanel (90) reasons for the variations in the values of p are not known. More recently, Halmos and Boger (71) measured centerline axial velocities downstream of a sudden expansion for aqueous solutions of Methocel 90HG and Separan AP-30. Centerline velocities were measured by Boger and Rama Murthy (25) in the 2 to 1 contraction using the same experimental apparatus and polymer solutions. Velocities predicted using Equation 3.9, with p equal to a constant, resulted in consistent deviations from the experimentally measured velocities in the sudden expansion or sudden contraction experiment. To be consistent, p must vary with axial position, z/D. This variation in p is brought into focus by comparing predicted and experimental stretch rates. Downstream of the sudden expansion, the experimentally determined stretch rates decreased from values that ranged from 32.3 to 43.3 $\sec^{-1}$ at the expansion to values approaching zero (6 to 20 tube diameters downstream). Between these two limits the stretch rate passed through a maximum value which was 2 to 4 times as large as stretch rates evaluated at the expansion (71). The axial location of the maximum stretch rates varied from 2 to 6 diameters downstream. Similar results were obtained for flow through a sudden contraction (25), i.e., the stretch rates passed through a maximum value as the contraction was approached. Stretch rates derived with Equation 3.9, with p equal to a constant, are not consistent with these experimental data. To be so, p must vary with axial position. In summary, since there have been significant variations from a K 2 model, i.e., p varies from experiment to experiment, and the fact that parameter p varies with axial position, it is purely by chance if the K 2 model is representative of velocity-position data obtained in this research.

The first part of Section 3.4.4 attempted to fit the velocities along the centerline to the sink flow and the K 2 models over a range of upstream axial locations. As a rule of thumb, the maximum axial location was chosen to be approximately equal to an axial distance one and one half times the axial location of the eddy center.

This axial location defined the major portion of the converging flow field. Beyond this, velocities were too small to be measured accurately. This maximum axial location corresponded with an axial position where the product of the derivative of the centerline velocity, $\Gamma$, times the zero shear relaxation time of the fluid, $\theta_0$, was equal to unity. This dimensionless parameter, $\Gamma\theta_0$, employed by Acierno et al. (1) in analyzing the transient elogational behavior of dilute polymer solutions, is also used in the determination of an empirical criterion to predict the onset of flow instabilities (Section 3.5, page 199). The derivative of the centerline velocity (where stretch rates are a maximum) is an integral part of the stability analysis, as will be shown in this section. Therefore, the chosen model should predict derivatives of velocities that are in quantitative agreement with experimental data in addition to being representative of velocity data. The final part of Section 3.4.4 discusses the exponential decay model and the development of an empirical relationship with radial location.

### (i) Sink Flow Model

If it is assumed that the flow upstream of the capillary is radially directed toward the origin of a spherical coordinate system, with the origin determined by the extrapolation of streamlines, the continuity equation for a symmetric flow field (116) reduces to

$$V_1 = \frac{f(\phi_0)}{r^2} \qquad 3.10$$

$$V_2 = V_3 = 0 \qquad 3.11$$

where r is the radial coordinate and $V_1$, $V_2$, and $V_3$ are velocity conponents in the r, $\theta$ and $\phi$ directions. By normalizing the radial velocity with respect to the average velocity in the capillary, V, and radial position with respect to the capillary tube radius, R, Equation 3.10 can be rewritten as

$$\left(\frac{V_1}{V}\right)_{\mathcal{C}\!\!\!\!\mathcal{L}} = \frac{f(\phi_0)}{VR^2}\left(\frac{r}{R}\right)^{-2.0} \qquad 3.12$$

Therefore, in logarithmic coordinates the slope of a plot of dimensionless velocity along the centerline, $\left(\frac{V_1}{V}\right)_{\mathcal{C}\!\!\!\!\mathcal{L}}$, versus $\left(\frac{r}{R}\right)$ should be equal to -2.0 if Equation 3.12 is valid. Consider as a typical example velocity data measured with capillary tube 3. Measured centerline velocities for flow rates that range from 0.040 $cm^3$/sec to 1.589 $cm^3$/sec are plotted in Figure 3.27. The respective upstream axial locations, z /D, are also given for each data point. Plots similar to those in Figure 3.27, although not reported, were obtained with capillary tubes 1 and 2. The solid lines representing Equation 3.12 are in good agreement with experimental data only in the vicinity of the contraction. This was originally suggested by Murch (119) and Kanel (90).

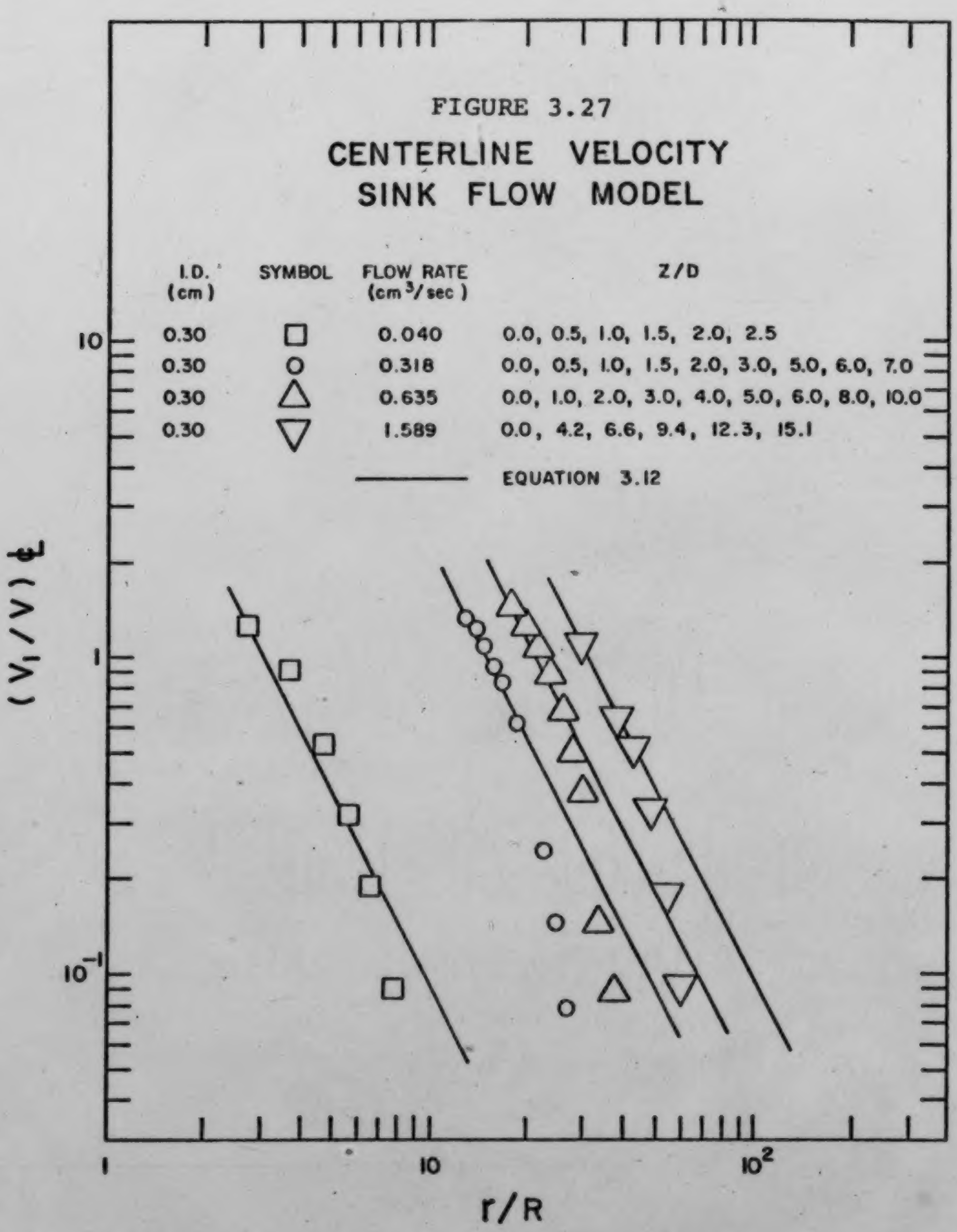

FIGURE 3.27

CENTERLINE VELOCITY
SINK FLOW MODEL

At a flow rate of 0.040 $cm^3$/sec agreement was obtained for upstream axial locations as large as 2.0 diameters upstream, whereas at a flow rate of 1.589 $cm^3$/sec good agreement was obtained at upstream axial locations as large as 6.6 diameters. At axial locations greater than 2.0 or 6.6 diameters the sink flow model predicts velocities that are significantly higher than the experimental data. This discrepancy, as mentioned earlier (page 143 ), arises from the WGS central core wherein the actual cross-sectional flow area is greater than that predicted by the sink flow model.

The derivative of velocity along the centerline obtained by differentiating Equation 3.12 with respect to r/R yields

$$\frac{d(V_1/V)}{d(r/R)} = \frac{-2f(\phi_0)}{VR^3} \left(\frac{r}{R}\right)^{-3.0} \qquad 3.13$$

Equation 3.13 states that on logarithmic coordinates $\frac{d(V_1/V)}{d(r/R)}$ versus $(\frac{r}{R})$ should result in a linear relationship having a slope equal to -3.0. The solid lines in Figure 3.28 represent Equation 3.13. Significant differences exist between the predicted and measured derivatives of velocity. The derivative of experimental velocity along the centerline, as shown in Figure 3.28, remained relatively constant over a wide range of upstream axial locations. The range of upstream axial locations was observed to vary

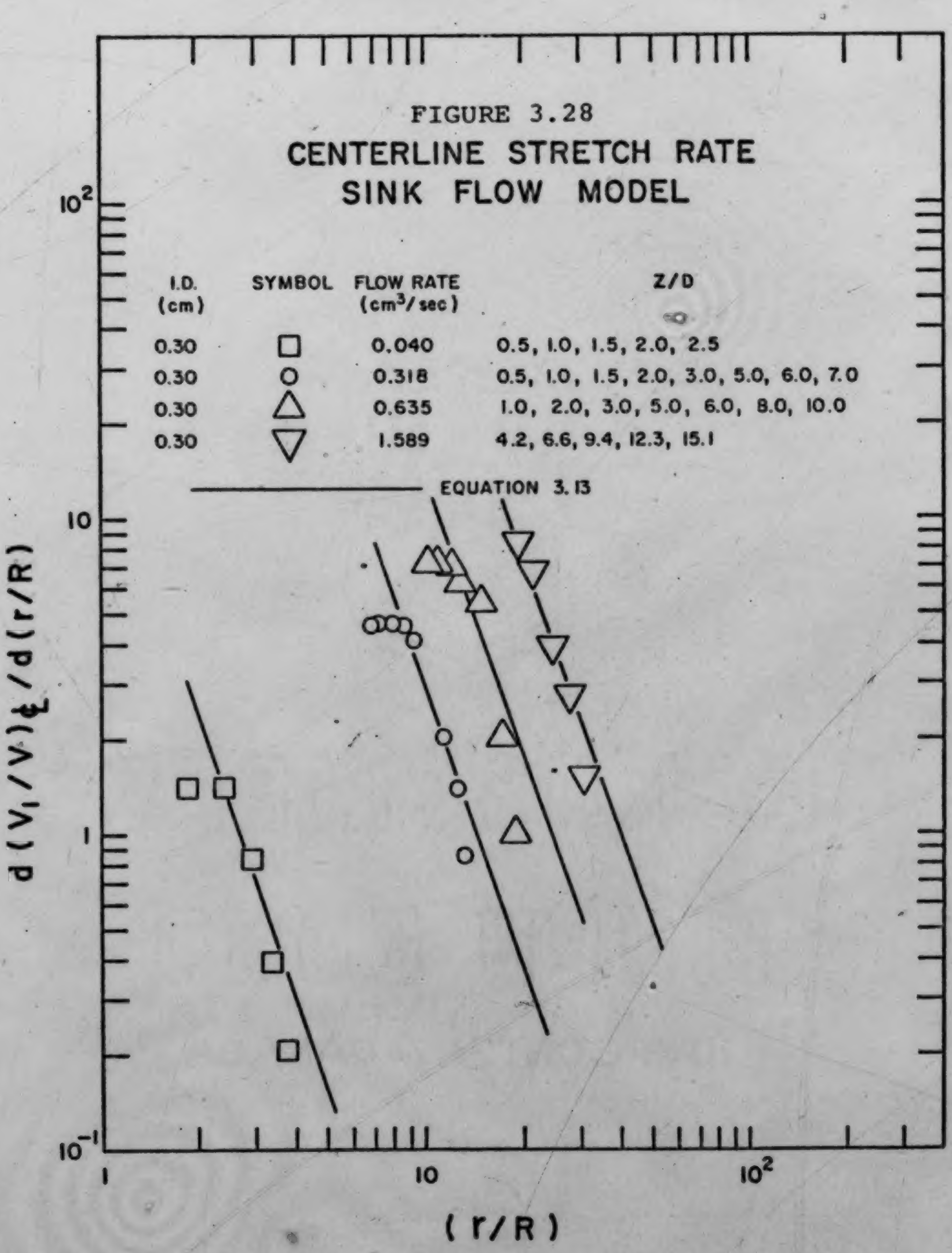

FIGURE 3.28
CENTERLINE STRETCH RATE
SINK FLOW MODEL

with capillary tube and flow rate. For example, the data in Figure 3.28 indicate that at a flow rate of 0.040 $cm^3$/sec the range was from 0.50 to 1.00 diameters upstream, whereas at a flow rate of 0.635 $cm^3$/sec the range was from 1.0 to 3.0 diameters. Derivatives of velocity are not reported for axial locations less than 0.50 diameters upstream since velocities were not measured at these axial locations. At a flow rate of 1.589 $cm^3$/sec, velocity measurements were not available for axial locations less than 4.2 diameters, hence, experimental data are not shown. At axial locations far removed from the contraction poor agreement existed between the predicted and experimental derivatives of velocity; the predicted derivatives of velocity were consistently higher than experimental values.

In summary, the sink flow model is inadequate in representing the relationship between velocity and its derivative along the centerline with upstream axial location. The flow upstream of the capillary entrance is not radially directed toward the origin of a spherical coordinate system.

### (ii) K 2 Model

In a cylindrical coordinate system with its origin at the center of the capillary tube at the contraction, the K 2 model can be rewritten in general as

$$v_z\big|_{\mathfrak{C}} = a + a_1(z/D) + a_2(z/D)^2 \qquad 3.14$$

The values of the three parameters a, $a_1$, and $a_2$ in Equation 3.14 and their dependence on capillary tube diameter and flow rate must be evaluated experimentally. Although deviations from the K 2 model are known to exist (25, 71, 90), it was expected to be a better approximation of the velocity data compared to the sink flow model. Differentiation of Equation 3.14 with respect to z yields

$$v_{z,z}\big|_{℄} = \left(\frac{a_1}{D}\right) + 2\left(\frac{a_2}{D}\right)\left(\frac{z}{D}\right) \tag{3.15}$$

Equation 3.15 predicts that the derivative of velocity is linear with respect to axial location. As pointed out in page 144 this is inconsistent with data obtained by Halmos and Boger (71) and Boger and Rama Murthy (25); the data obtained in the present study are consistent with those reported by these authors.

Typical experimental velocities and derivatives along the centerline are given in Figures 3.29 to 3.32 for capillary tube 3. In addition, results are also shown for capillary tube 1 at a flow rate of 0.119 $cm^3$/sec (Figures 3.30 and 3.32) where the accelerating core extended farthest into reservoir S. The parameters a, $a_1$, and $a_2$ in Equation 3.14 were obtained by the least squares method. The K 2 model is in good agreement with the velocity data but consistent large deviations in the derivatives of velocity were observed for all of the data with typical results shown in Figures 3.31 and 3.32. The derivatives of

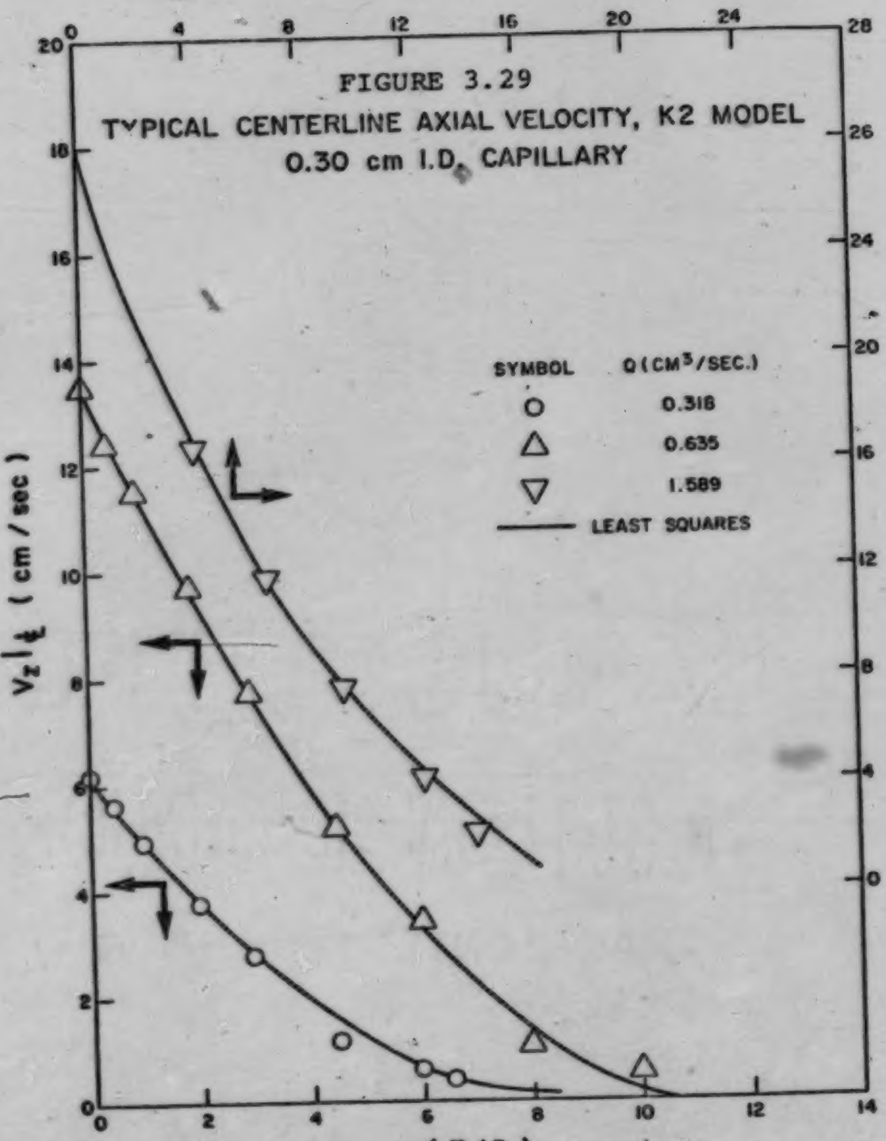

FIGURE 3.29
TYPICAL CENTERLINE AXIAL VELOCITY, K2 MODEL
0.30 cm I.D. CAPILLARY

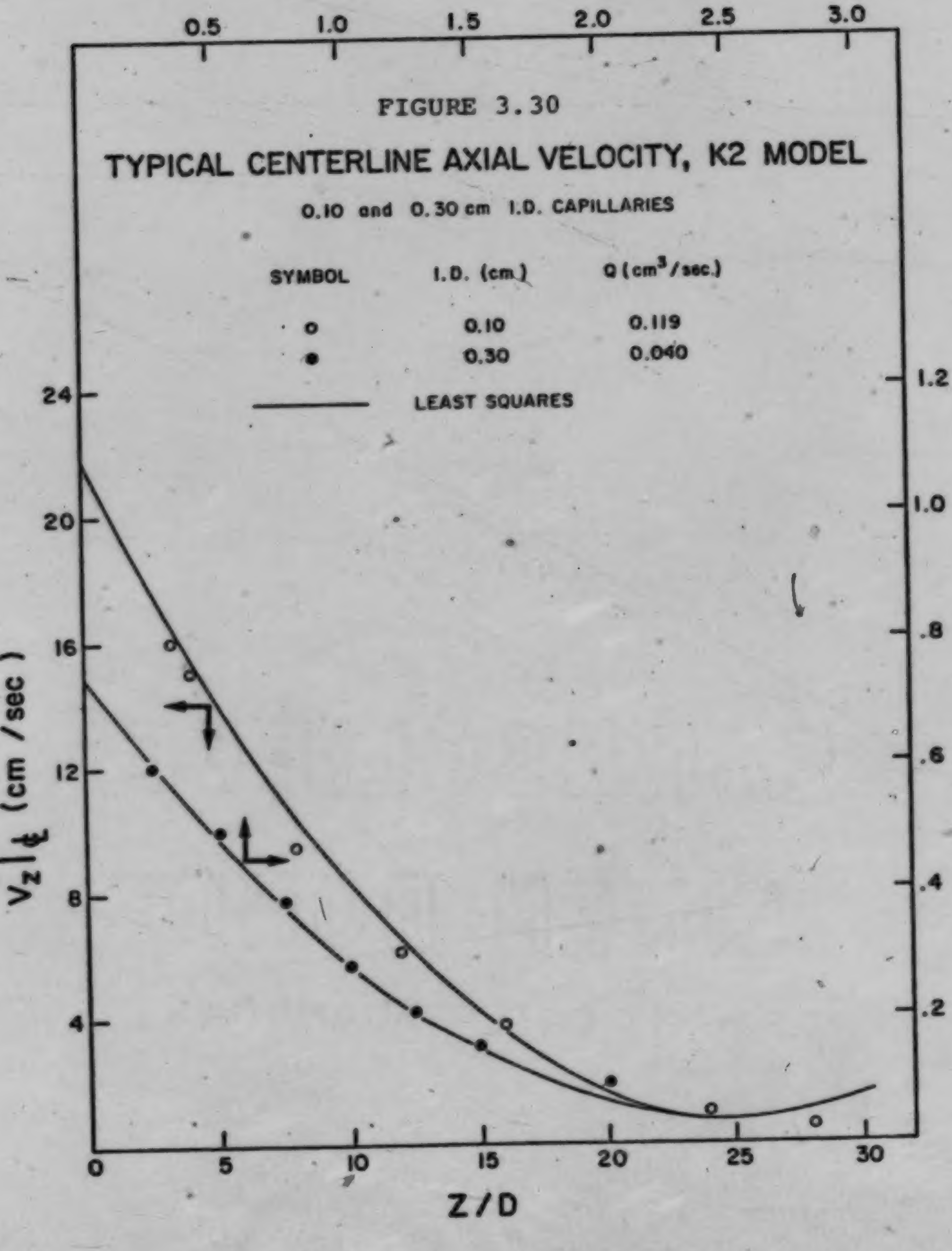

FIGURE 3.30

TYPICAL CENTERLINE AXIAL VELOCITY, K2 MODEL

0.10 and 0.30 cm I.D. CAPILLARIES

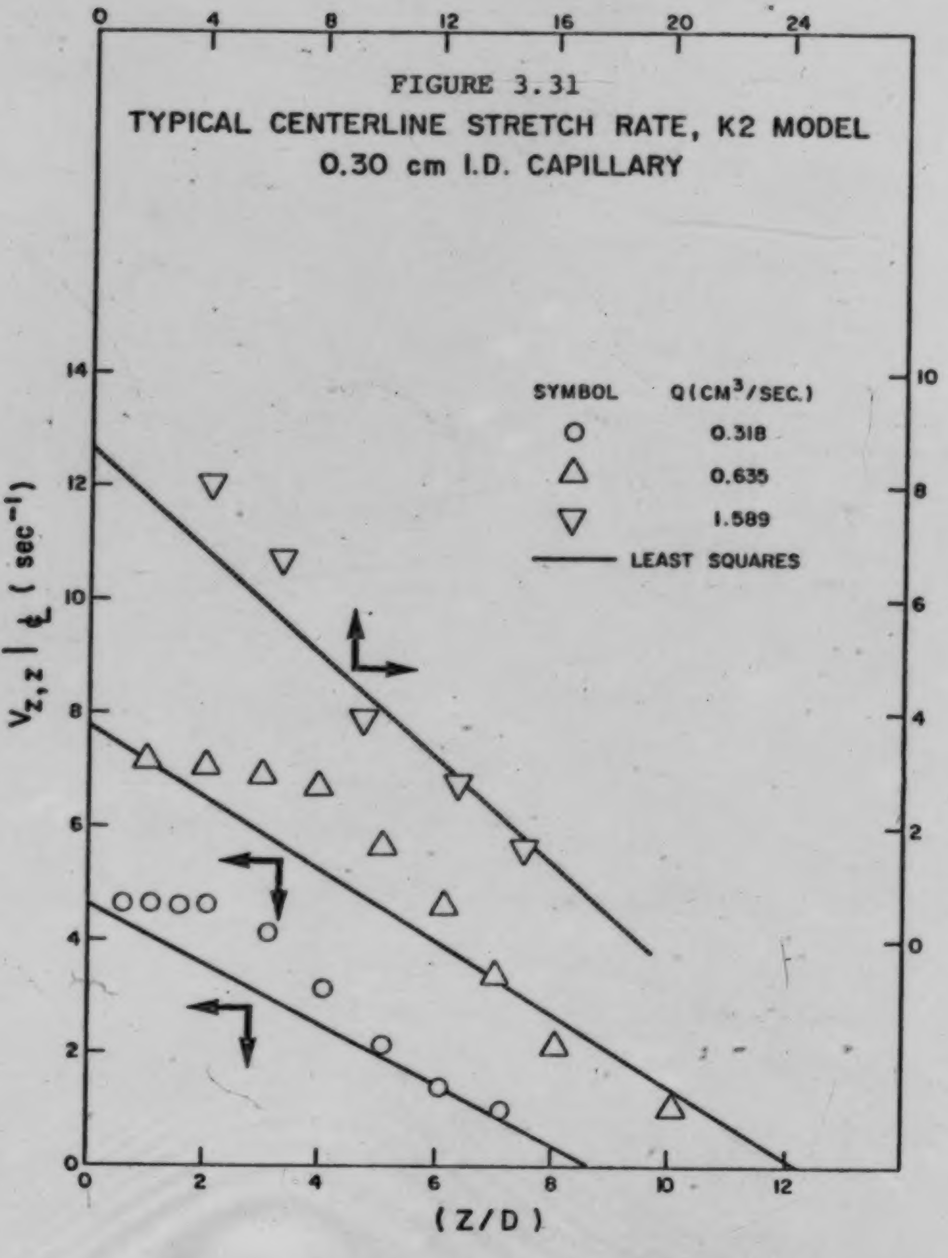

FIGURE 3.31
TYPICAL CENTERLINE STRETCH RATE, K2 MODEL
0.30 cm I.D. CAPILLARY

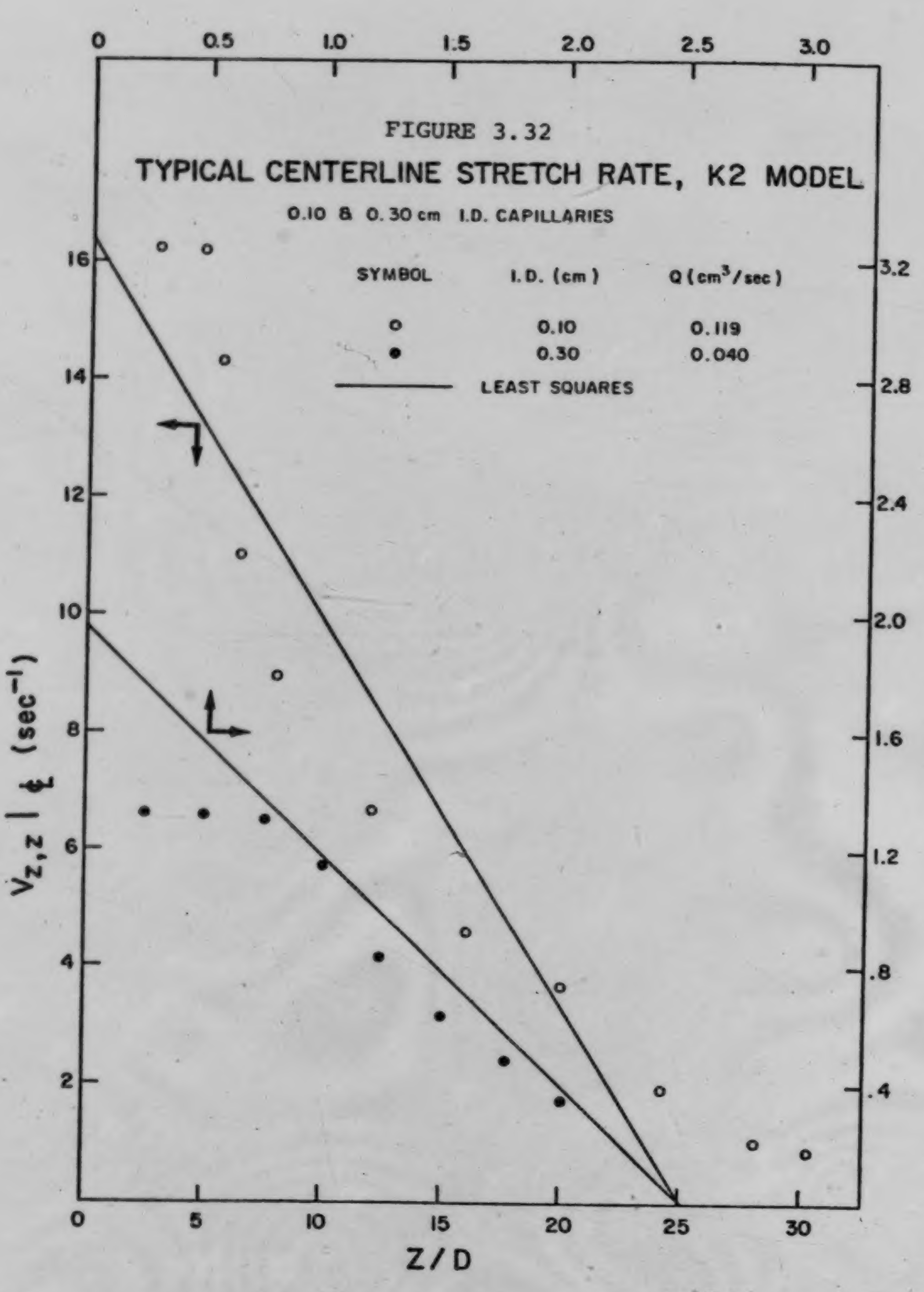

FIGURE 3.32

TYPICAL CENTERLINE STRETCH RATE, K2 MODEL

0.10 & 0.30 cm I.D. CAPILLARIES

experimental velocity are not linear with respect to axial location as given by Equation 3.15. As the contraction was approached, the derivatives of velocity increased exponentially to a value which remained reasonably constant over a range of upstream axial locations. For the data shown, the range over which the derivatives were considered to be constant is given on page 151. As a result of poor agreement between predicted and experimental derivatives of velocity, the K 2 model was considered to be inadequate.

### (iii) Exponential Decay Model

Plots of velocity and derivatives of velocity along the centerline versus upstream axial location obtained in this study suggest an exponential decay model given by Equation 3.16

$$v_z\big|_{\mathbb{C}} = V_0 \exp(-b(z/D)) \qquad 3.16$$

where $V_0$ is the velocity along the centerline at the contraction and z/D is the axial position measured upstream of the contraction. This model predicts the dependence of velocity upon z/D which is in agreement with other experimental evidence (25, 71, 123).

The K 2 model is included in the exponential decay model since Equation 3.14 is a truncated Taylor series expansion of Equation 3.16. A Taylor series expansion of Equation 3.16 is

$$V_z|_{\text{℄}} = V_0(1 - b(\frac{z}{D}) + \frac{b^2}{2!}(\frac{z}{D})^2 - \frac{b^3}{3!}(\frac{z}{D})^3 + \ldots) \qquad 3.17$$

Truncating Equation 3.17 after the third term yields

$$V_z|_{\text{℄}} = V_0(1 - b(\frac{z}{D}) + \frac{b^2}{2!}(\frac{z}{D})^2) \qquad 3.18$$

Equation 3.18 is equivalent to Equation 3.14 when

$$a = V_0$$

$$a_1 = -V_0 b$$

$$a_2 = V_0 b^2/2! \qquad 3.19$$

Equation 3.16 implies that the slope of a plot of $V_z$ versus z/D on semi-log coordinates is a constant equal to -b with the intercept at z/D = 0 being equal to $V_0$. The velocity - z/D data measured in this study showed consistent deviations when plotted on semi-log coordinates in accordance with Equation 3.16. A better, although a more complicated relationship, was

$$V_z|_{\text{℄}} = V_0 \exp(-b(z/D)^c) \qquad 3.20$$

where c is constant. The evaluation of c was obtained in the following manner: For a given reservoir, capillary tube, and flow rate, $V_z$ was plotted against $(z/D)^c$ on semi-log coordinates for various values of c until it was judged by eye that errors between experimental and predicted values over the characteristic flow pattern length were a minimum. This procedure was repeated for the remaining flow rates, capillary tubes and both reservoirs. In the final analysis, c was determined to be equal to 1.4. Typical plots of velocity versus $(z/D)^{1.4}$ are shown in Figure 3.33 for the data obtained with capillary tube 3. The solid lines representing Equation 3.20 are in excellent agreement with experimental data. Plots similar to those in Figure 3.33 can be found in Appendix E and are in excellent agreement with the data. Further support of Equation 3.20 as representative of centerline velocities is evidenced by data reported by Boger and Rama Murthy (25) in a 2 to 1 contraction (5.08 cm I.D. to 2.54 cm I.D.), by Halmos and Boger (71) in a 2 to 1 expansion and by Nakamura et al. (123) in a sudden contraction (7.0 cm I.D. to 2.0 cm I.D.) In all experiments centerline velocities were represented by Equation 3.20 with c = 1.4.

Since the velocities were measured only to within one streak length from the contraction, the velocities at the contraction, $V_0$, were not measured directly. These velocities were estimated by curve fitting the data to Equation 3.21 by the least squares method.

$$\log(V_z|_{\text{℄}}) = \log V_0 - b\left(\frac{z}{D}\right)^{1.4} \qquad 3.21$$

The resulting values of $V_0$ are plotted against flow rate in

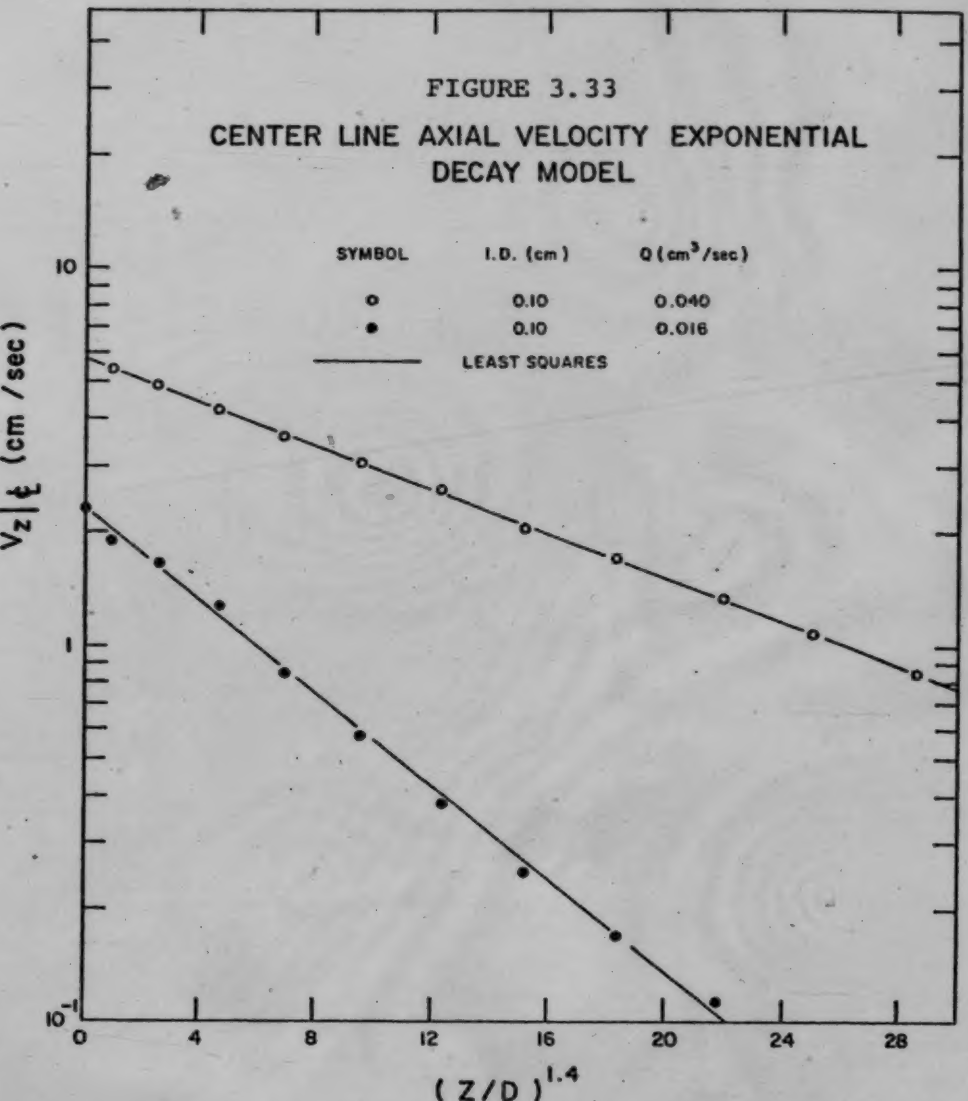

FIGURE 3.33

CENTER LINE AXIAL VELOCITY EXPONENTIAL DECAY MODEL

Figure 3.34. No significant differences in the values of $V_0$ were noted over the range of flow rates in region I where data from both reservoirs overlapped. It was conjectured, therefore, that the values of $V_0$ were independent of reservoir size for all flow rates within region I. From Figure 3.6, the flow rates in question for capillary tubes 1, 2, and 3 are less than 0.119, 0.318, and 0.635 $cm^3$/sec respectively. The data between the two sizes of reservoirs cannot be compared for flow rates greater than these since the flow fields were different; the flow field was "chaotic" in reservoir S while in reservoir L it was stable even to much higher flow rates.

The degree to which the velocity profiles were developed at the contraction was estimated by the ratio of $V_0$ to the centerline velocity for SLSF in the capillary tube. This ratio was equal to 0.75 and remained constant for all experimental runs. Hence, $V_0$ can be expressed as

$$V_0 = 0.75 \left(\frac{3n'+1}{n'+1}\right)\left(\frac{Q}{A}\right) \qquad 3.22$$

Over the range of apparent shear rates where the velocity profiles were measured, the flow behavior index, given in Appendix D, was approximately equal to a constant, 0.50. Substitution of this value n' into Equation 3.22 yields

$$V_0 = 1.25(Q/A) \qquad 3.23$$

FIGURE 3.34

AXIAL CENTERLINE VELOCITY AT CONTRACTION VERSUS FLOW RATE

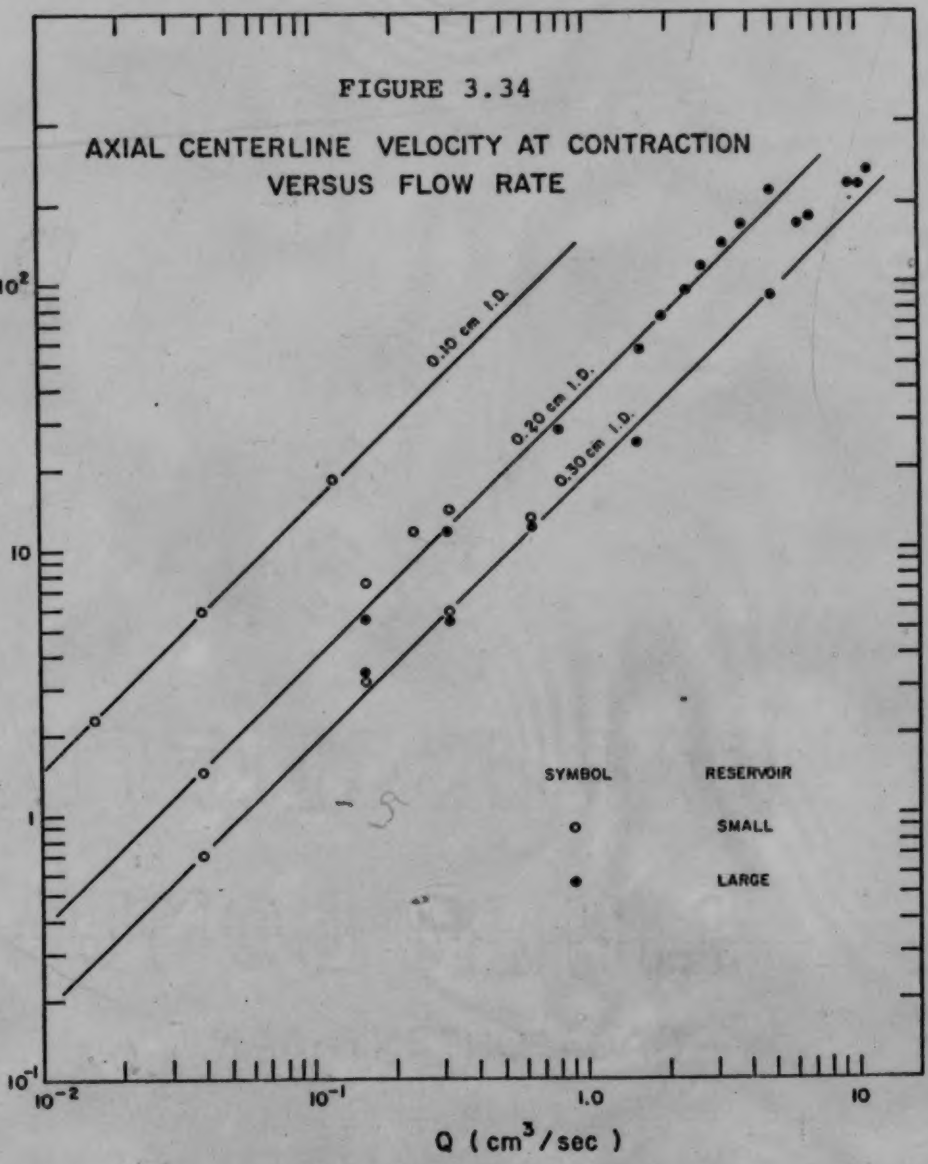

Equation 3.23 is plotted as the solid line in Figure 3.35 and shows that the preceding approximations are in reasonable agreement with the experimental data for capillary tube velocities that ranged from 0.60 to 160 cm/sec. Experimental values of $V_0$ were slightly higher than the predicted values (Equation 3.23) for capillary tube average velocities greater than 70 cm/sec. At first this may not appear to be a major discrepancy but closer examination revealed that these capillary tube average velocities corresponded with flow rates defining the onset of region II in reservoir L. Therefore, Equation 3.23 is valid only for flow rates that are within region I. Values of $V_0$ obtained by replotting the centerline velocities measured and reported by Boger and Rama Murthy (25),Halmos and Boger (71), and Nakamura et al. (123) against $(z/D)^{1.4}$ are given in Figure 3.35. The solutions used by Boger and Rama Murthy (75) and Halmos and Boger (71) were aqueous solutions of Methocel 90HG having (n' = 0.521, 0.550 and 0.580) whereas, the solution used by Nakamura et al. (123) was a 0.40% weight aqueous solution polyacrylite (n' = 0.46). Only the data obtained by Halmos and Boger (25) and Nakamura et al. (71) are somewhat higher; Equation 3.22 represents their data when the constant 0.75 is replaced by 0.89 and 1.26 respectively.

Velocity measurements as far as 60 diameters upstream were necessary to define the major portion of the velocity field at high flow rates. At low flow rates, measurements

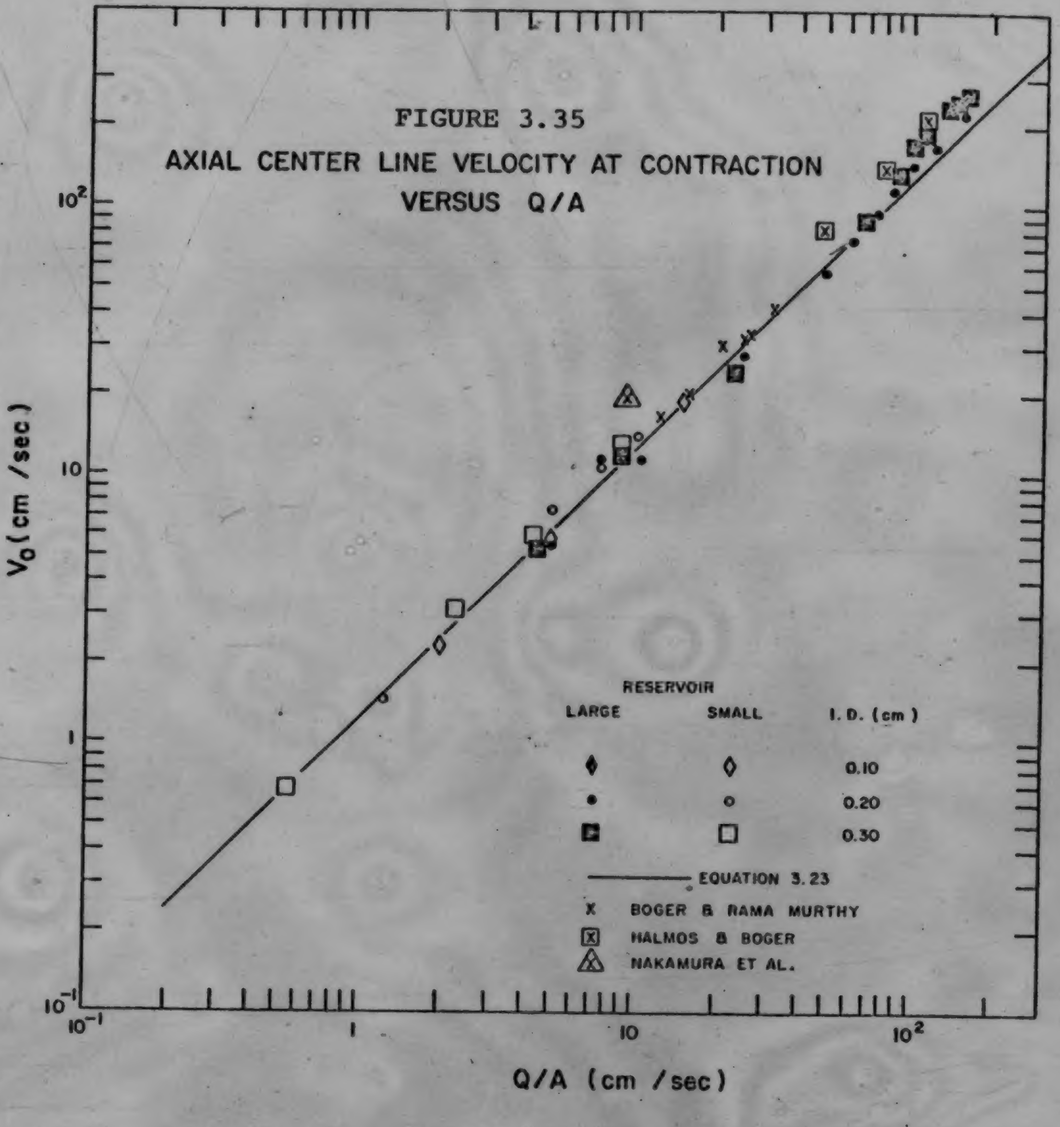

FIGURE 3.35

AXIAL CENTER LINE VELOCITY AT CONTRACTION VERSUS Q/A within two diameters were sufficient to define the major portion of the velocity field. In order to scale the velocity fields with respect to axial location and achieve axial similarity, the velocities were normalized with respect to $V_0$. The normalized axial location variable, Z*, was defined as

$$Z^* = (z/D)/(X/D) \qquad 3.24$$

where (X/D) is a characteristic flow pattern length which defines the major portion of the flow field over which velocities were measured. Normalized velocities range from zero to unity and by a proper choice of the characteristic flow pattern length normalized axial locations should range from zero to values approximately equal to unity. The following outlines the method used to obtain Z*: The velocity along the centerline is a function of the physical properties of the fluid, the geometry, the flow rate, and the upstream axial location. This can be written as

$$V_z|_{\text{℄}} = f(\rho, K_0, \theta, n', D, D_R, Q, z) \qquad 3.25$$

Since dimensional consistency must exist rearrangement of the variables in Equation 3.25 by Rayleigh's method so that each term is dimensionless must give

$$V_z|_{\text{℄}} = f\left(\beta,\ N'_{Re},\ \frac{D^3}{\theta Q},\ \frac{z}{D},\ n'\right) \qquad 3.26$$

By substituting the relationship given by Equation 3.20 into Equation 3.26 we have

$$V^* = \frac{V_z|_{\mathrm{C\!\!L}}}{V_0} = f_1(\beta,\ N'_{Re},\ \frac{D^3}{\theta Q},\ \frac{z}{D},\ n') \qquad 3.27$$

It was mentioned on page 145 that velocities were measured over the major portion of the flow field which corresponded to one and one half times the center of the eddies. This axial location was approximately equal to the axial location where the product $\Gamma\theta_0$ was equal to unity. It is this axial position that is referred to as the characteristic flow pattern length. Qualitatively, as the initial cone semi-angle decreased, the axial location, where $\Gamma\theta_0$ was equal to unity, increased (the central core protruded farther upstream). The sink flow kinematics, although not representative of velocities and derivatives along the centerline, may qualitatively indicate the dependence of the characteristic flow pattern length with D, $\theta_0$ and Q. By equating the integral of the radial velocity component, Equation 3.10, over the flow cross-sectional area to flow rate, yields

$$v_1 = \frac{Q}{2\pi r^2(1-\cos\phi_0)} \qquad 3.28$$

The derivative of Equation 3.28 with respect to radial location r, is

$$v_{1,1} = \frac{-Q}{\pi r^3(1-\cos\phi_0)} \qquad 3.29$$

As an approximation for small cone initial semi-angles we have

$$1 - \cos\phi_0 = x^2/2 \qquad 3.30$$

where x is expressed in radians. The product of the stretch rate times the zero shear relaxation time is therefore given by

$$V_{1,1}\theta_0 = \frac{2\theta_0 Q}{\pi r^3 x^2} \qquad 3.31$$

Hence, the radial location where $V_{1,1}\theta_0$ is equal to unity, $r_1$, is

$$r_1 = \left(\frac{2\theta_0 Q}{\pi x^2}\right)^{1/3}. \qquad 3.32$$

From Equation 3.8 we have

$$x = \left(\frac{19}{180}\right)\left(\frac{D^3}{\theta_0 Q}\right)^{0.60} \qquad 3.33$$

and substitution of Equation 3.33 into Equation 3.32 yields

$$r_1 = 3.9\left(\frac{\theta_0^2 Q^2}{D^3}\right)^{1/3} \qquad 3.34$$

This suggests that the dimensionless axial position, Z*, can be derived from dimensionless groups in Equation 3.27 as

$$Z^* = \frac{(z/D)}{\left(\frac{\theta_0 Q}{D^3}\right)^{2/3}} = \frac{z}{\left(\frac{\theta_0^2 Q^2}{D^3}\right)^{1/3}} \qquad 3.35$$

where $(\theta_0^2 Q^2/D^3)$ has the dimension of length cubed. The combination of Equations 3.20, 3.27, and 3.35 yields

$$V^* = \exp[-b_1(\beta,\ N'_{Re},\ \frac{D^3}{\theta_0 Q},\ n')(Z^*)^{1.4}] \qquad 3.36$$

Equation 3.36 is equivalent to Equation 3.20 and suggests that on semi-log coordinates $V^*$ is linear with respect to $(Z^*)^{1.4}$. The functional form for parameter $b_1$ with $\beta$, $N'_{Re}$, $D^3/\theta_0 Q$ and $n'$ must be evaluated empirically.

Semi-log plots of $V^*$ versus $(Z^*)^{1.4}$ are given in Figures 3.36 to 3.40 with Equation 3.36 being represented as the solid lines. Experimental values of $V^*$ are related linearly to $(Z^*)^{1.4}$ on semi-log coordinates with a slope equal to $-b_1/2.303$. The dimensionless axial locations were condensed to values of $(Z^*)^{1.4}$ less than 2.2. Parameter $b_1$, estimated by the method of least squares, is plotted in Figure 3.41 against $(\theta_0 Q/D^3)$. The data in this figure show clearly that the extrapolation of the relationship between $b_1$ and $(\theta_0 Q/D^3)$ obtained with flow rates within region I is not applicable within region II where the first signs of flow instabilities were observed. Therefore, for flow rates within region I Equation 3.37 is applicable.

$$b_1 = 1.0(\theta_0 Q/D_3)^{0.216} \qquad 3.37$$

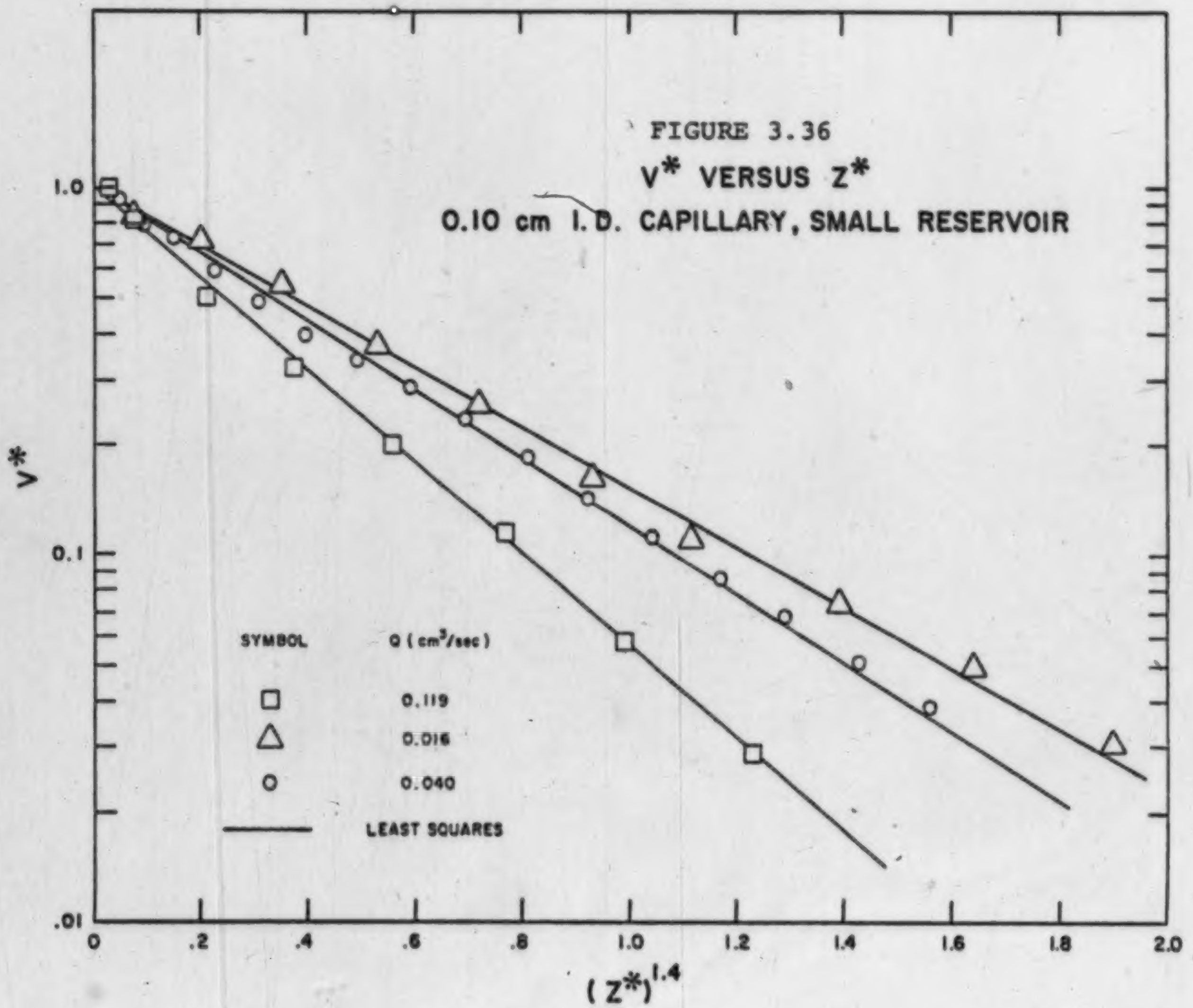

FIGURE 3.36
$V^*$ VERSUS $Z^*$
0.10 cm I.D. CAPILLARY, SMALL RESERVOIR

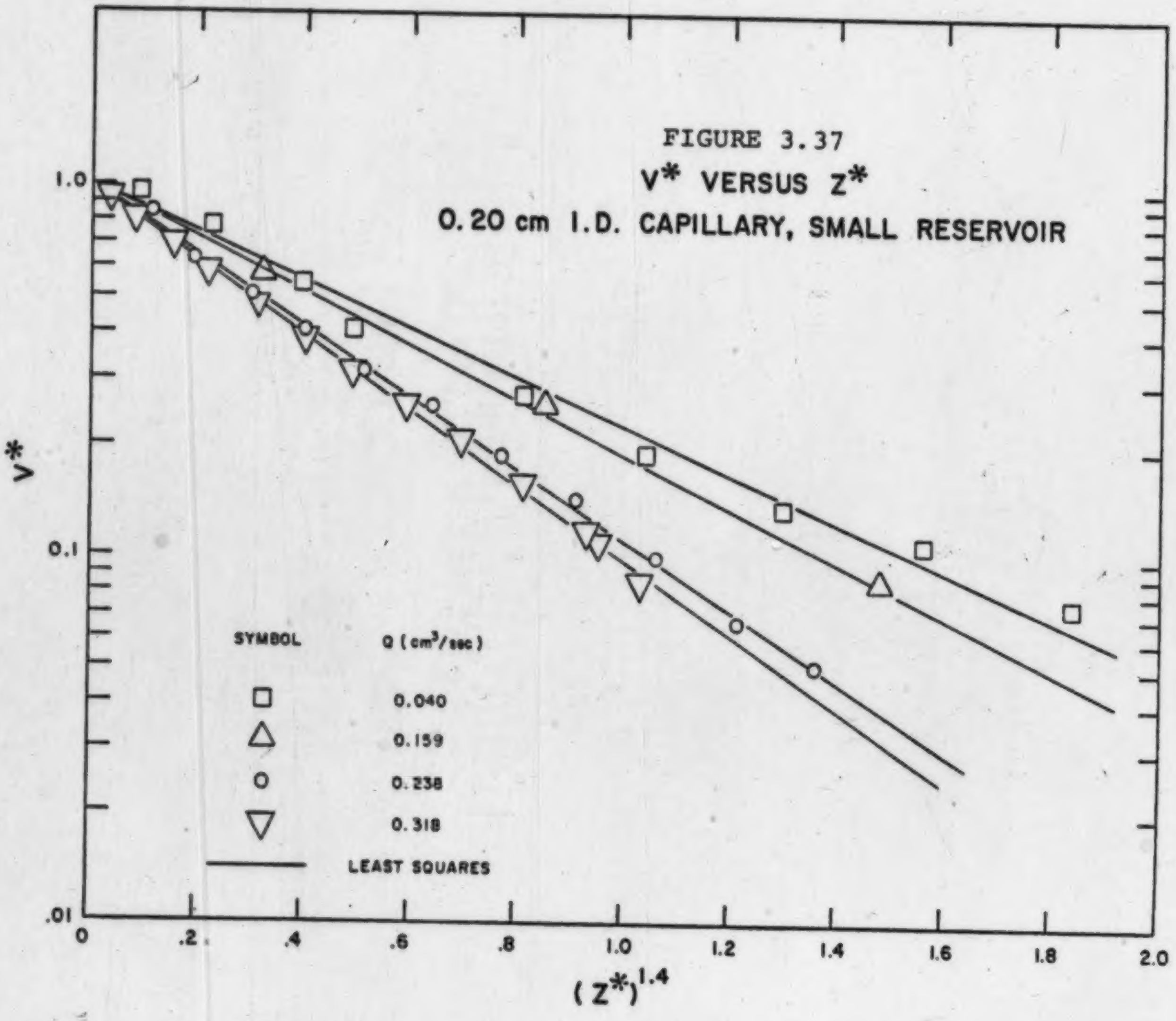

FIGURE 3.37

V* VERSUS Z*

0.20 cm I.D. CAPILLARY, SMALL RESERVOIR

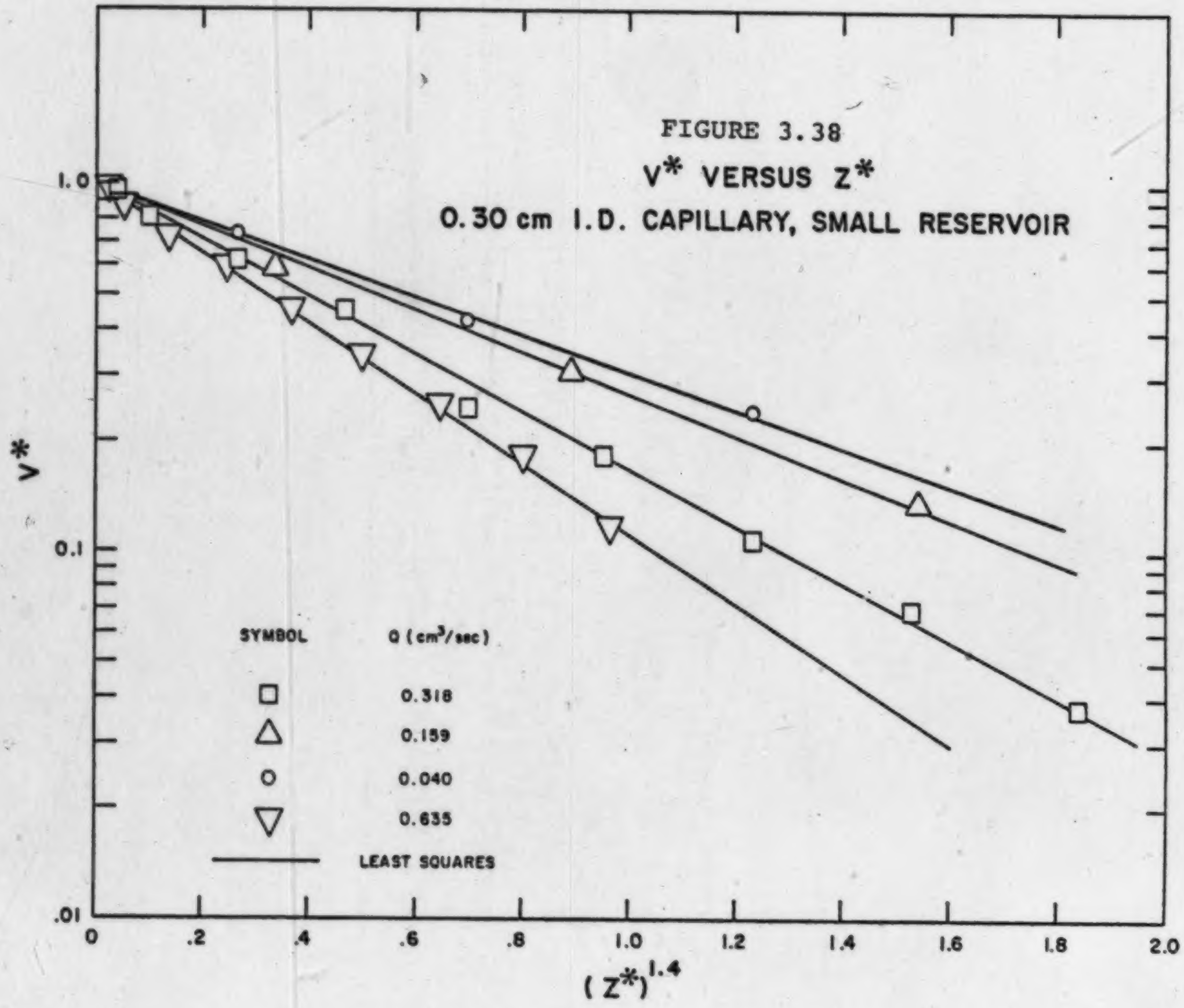

FIGURE 3.38

$V^*$ VERSUS $Z^*$

0.30 cm I.D. CAPILLARY, SMALL RESERVOIR

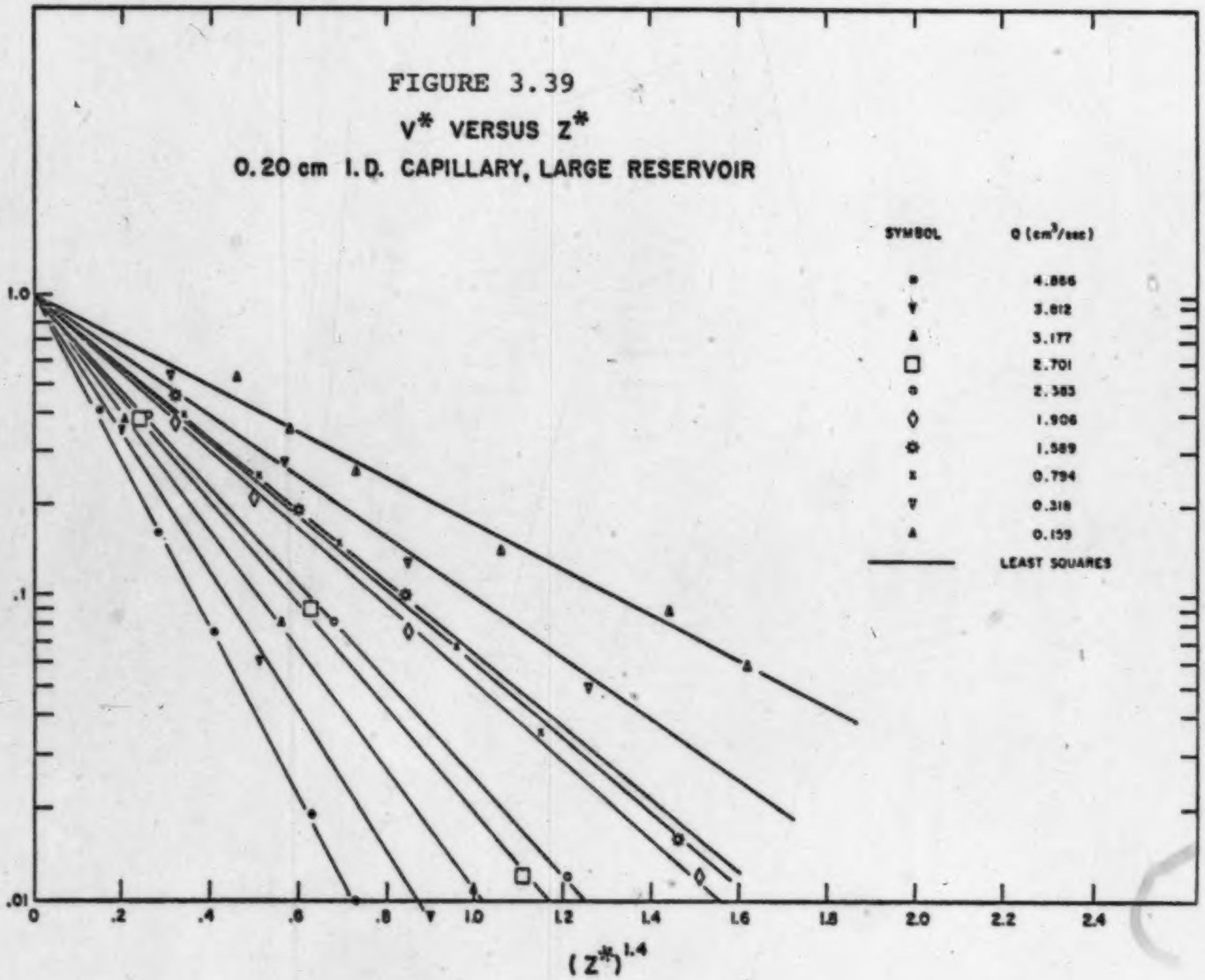

FIGURE 3.39

V* VERSUS Z*

0.20 cm I.D. CAPILLARY, LARGE RESERVOIR

FIGURE 3.40
V* VERSUS Z*
0.30 cm I.D. CAPILLARY, LARGE RESERVOIR

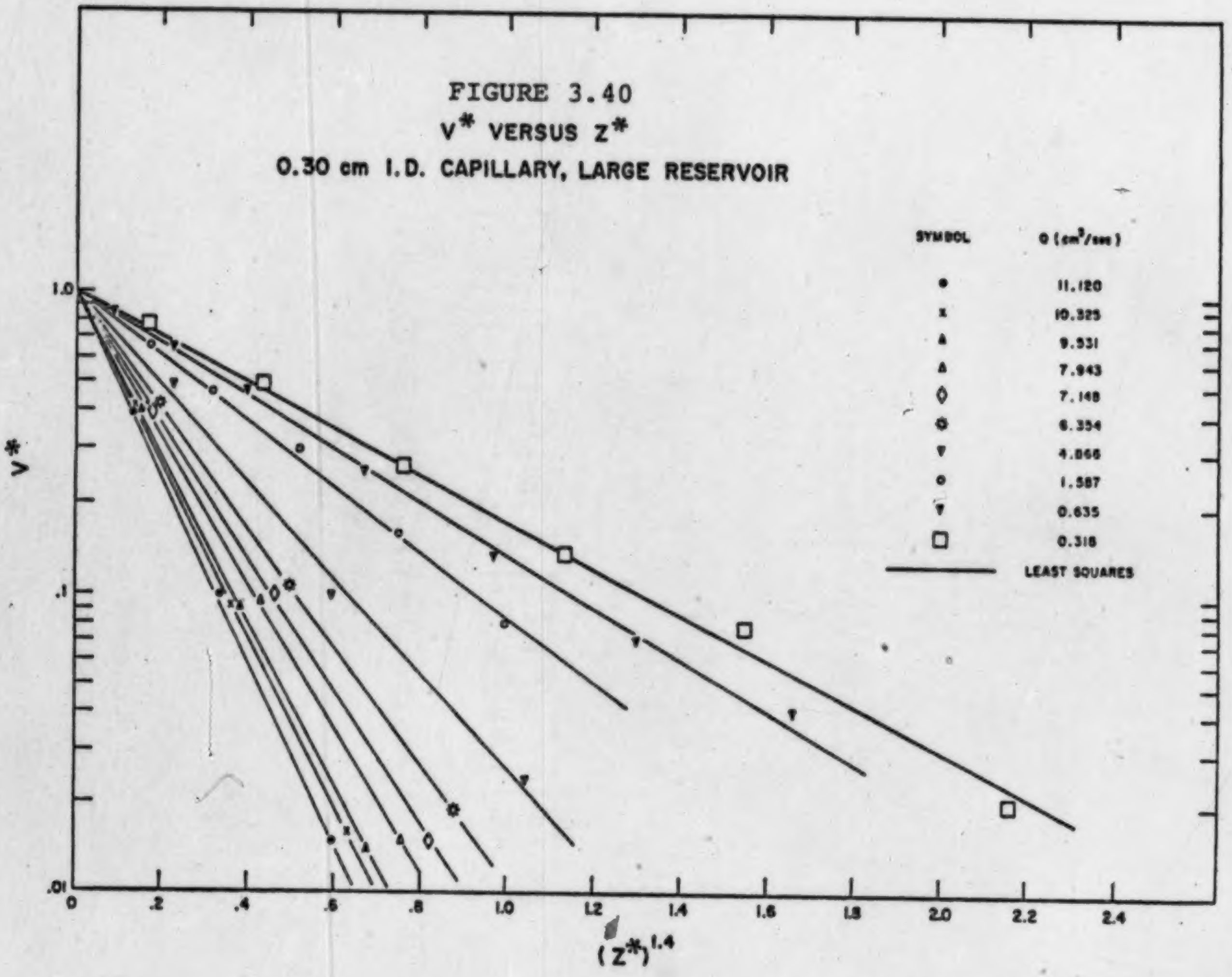

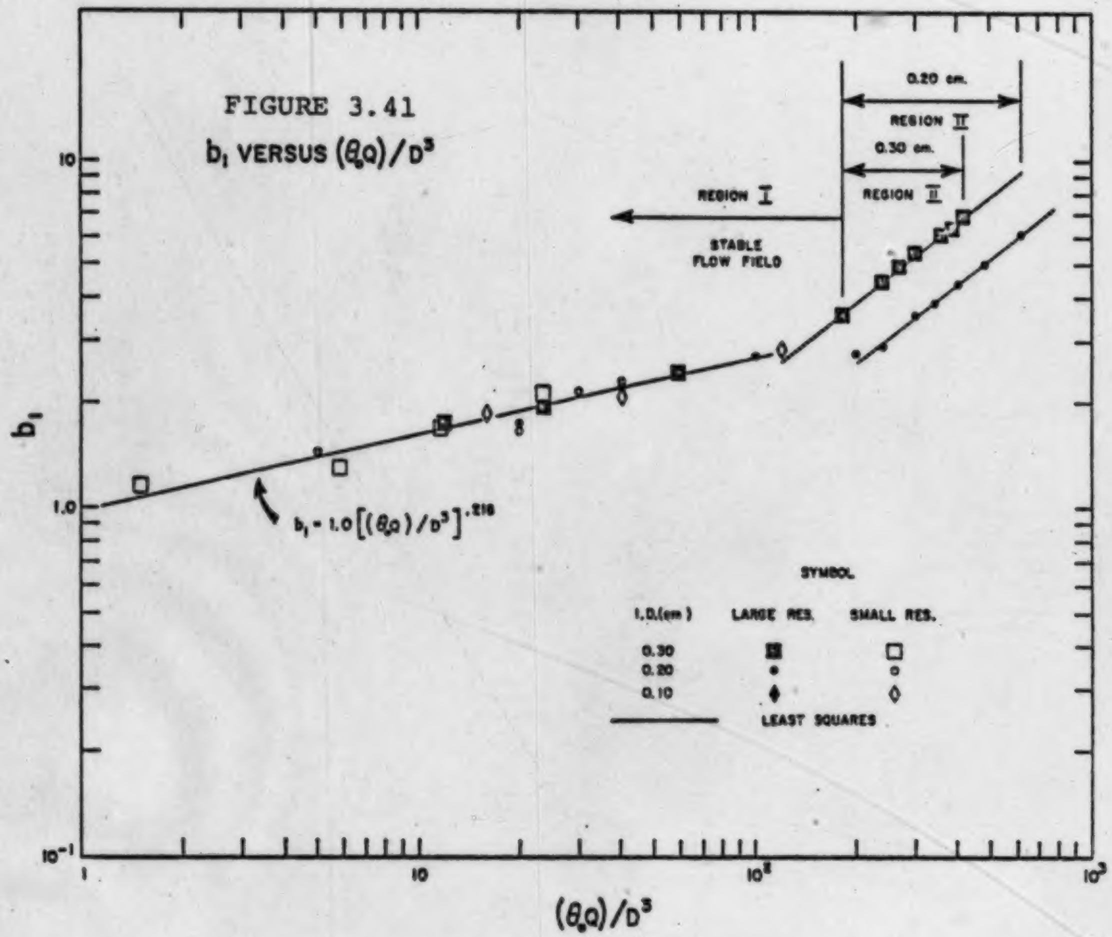

FIGURE 3.41

$b_1$ VERSUS $(\theta_0 Q)/D^3$

Over the range $10 < \theta_0 Q/D^3 < 40$, no significant differences in the values of $b_1$ were noted with reservoir size. This conclusion was also reported for $V_0$ (page 161). It was conjectured, therefore, that the effect of reservoir size on $b_1$ was negligible for all experimental runs. The limited data further suggest that parameter $b_1$ is independent of $N'_{Re}$ and $n'$. Hence, it was assumed that as a first approximation $b_1$ was dependent only on $(\theta_0 Q/D^3)$. By defining

$$(Z^{**})^{1.4} = b_1 (Z^*)^{1.4} \qquad 3.38$$

and using Equation 3.37 and 3.38 we have

$$(Z^{**})^{1.4} = \left(\frac{\theta_0 Q}{D^3}\right)^{0.216} \left[\frac{z}{(\theta_0^2 Q^2/D^3)^{1/3}}\right]^{1.4}$$

$$= \frac{(z/D)^{1.4}}{(\theta_0 Q/D^3)^{.717}}$$

$$\simeq \left[\frac{z/D}{\sqrt{\frac{\theta_0 Q}{D^3}}}\right]^{1.4} \qquad 3.39$$

which eliminates $b_1$. Equivalent plots would be

$$V^* = \exp(-(Z^{**})^{1.4}) \qquad 3.40$$

If valid, all data should be represented by a single line given by Equation 3.40. The velocity data replotted in Figure 3.42 (semi-log coordinates) show that Equation 3.40 is indeed representative of data within region I.

## LENGEND FOR FIGURE 3.42

| Symbol | I.D. (cm) | $Q(cm^3/sec)$ | Reservoir |
|---|---|---|---|
| A | 0.10 | 0.016 | S |
| B | 0.10 | 0.040 | S |
| C | 0.10 | 0.119 | S |
| D | 0.20 | 0.160 | L |
| E | 0.20 | 0.318 | L |
| F | 0.20 | 0.794 | L |
| G | 0.20 | 1.589 | L |
| H | 0.20 | 0.239 | S |
| I | 0.20 | 0.159 | S |
| J | 0.20 | 0.040 | S |
| K | 0.20 | 0.318 | S |
| M | 0.30 | 4.866 | L |
| N | 0.30 | 1.589 | L |
| O | 0.30 | 0.635 | L |
| P | 0.30 | 0.318 | L |
| R | 0.30 | 0.635 | S |
| S | 0.30 | 0.318 | S |
| T | 0.30 | 0.159 | S |
| V | 0.30 | 0.040 | S |

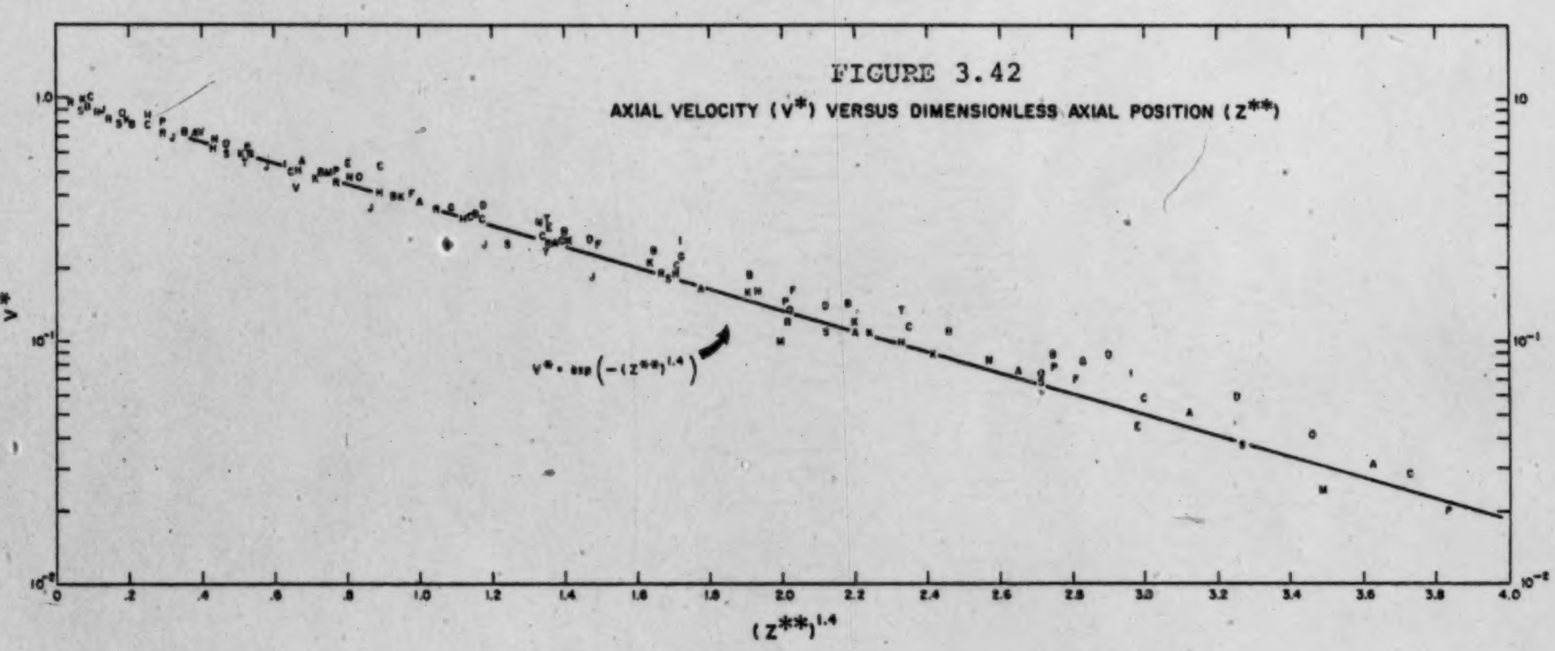

FIGURE 3.42

AXIAL VELOCITY ($V^*$) VERSUS DIMENSIONLESS AXIAL POSITION ($Z^{**}$)

As a further test of the "goodness" of Equation 3.40 comparison is made between the experimental and predicted stretch rates. The predicted stretch rates along the centerline, $V_{z,z}|_{\mathrm{C\!\!\!L}}$ , were obtained by differentiation of Equation 3.40. The result is

$$V_{z,z}|_{\mathrm{C\!\!\!L}} = \frac{1.4V_0(Z^{**})^{0.4}}{D(\frac{\theta_0 Q}{D^3})^{0.5}} \exp(-(Z^{**})^{1.4}) \qquad 3.41$$

The stretch rates given by Equation 3.41 show excellent agreement with the experimental values at several flow rates with capillary tube 3 (Figure 3.43) and at two flow rates with capillary tube 1 (Figure 3.44). In these experimental runs, the smallest value of Z** where axial velocities were measured was 0.10, hence the experimental stretch rates are not shown in Figures 3.43 and 3.44 for Z** less than 0.10. With the remaining data, velocities were also measured as close as Z** ≈ 0.10 and up to these axial locations, the predicted stretch rates are in good agreement with the data. Furthermore, the predicted stretch rates over a range of values of Z** near to the contraction are predicted to be reasonably constant which is consistent with the experimental data. At larger values of Z**, the stretch rates are again in good agreement with the data and in the limit, $Z^{**} \geq 2$, the stretch rates are predicted to asymptotically approach zero. At values of Z** less than 0.10 the stretch rates are predict-

FIGURE 3.43

TYPICAL CENTERLINE STRETCH RATES
EXPONENTIAL DECAY MODEL
0.30 cm I.D. CAPILLARY

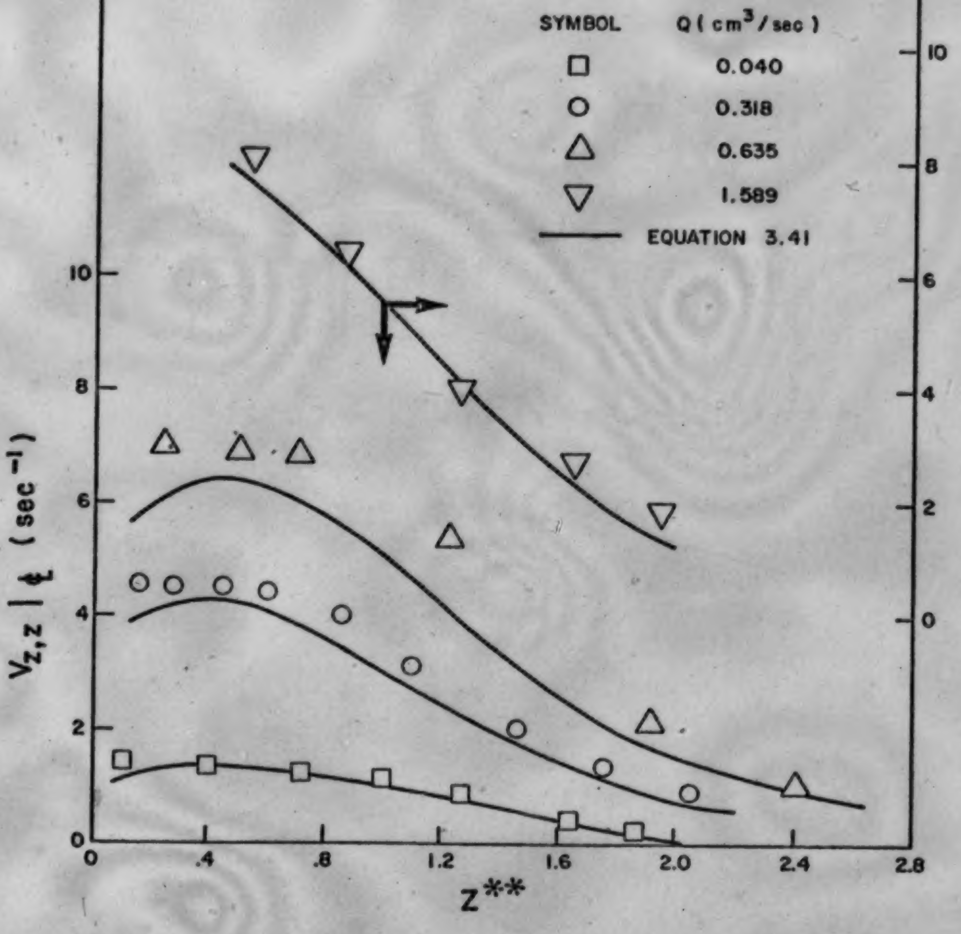

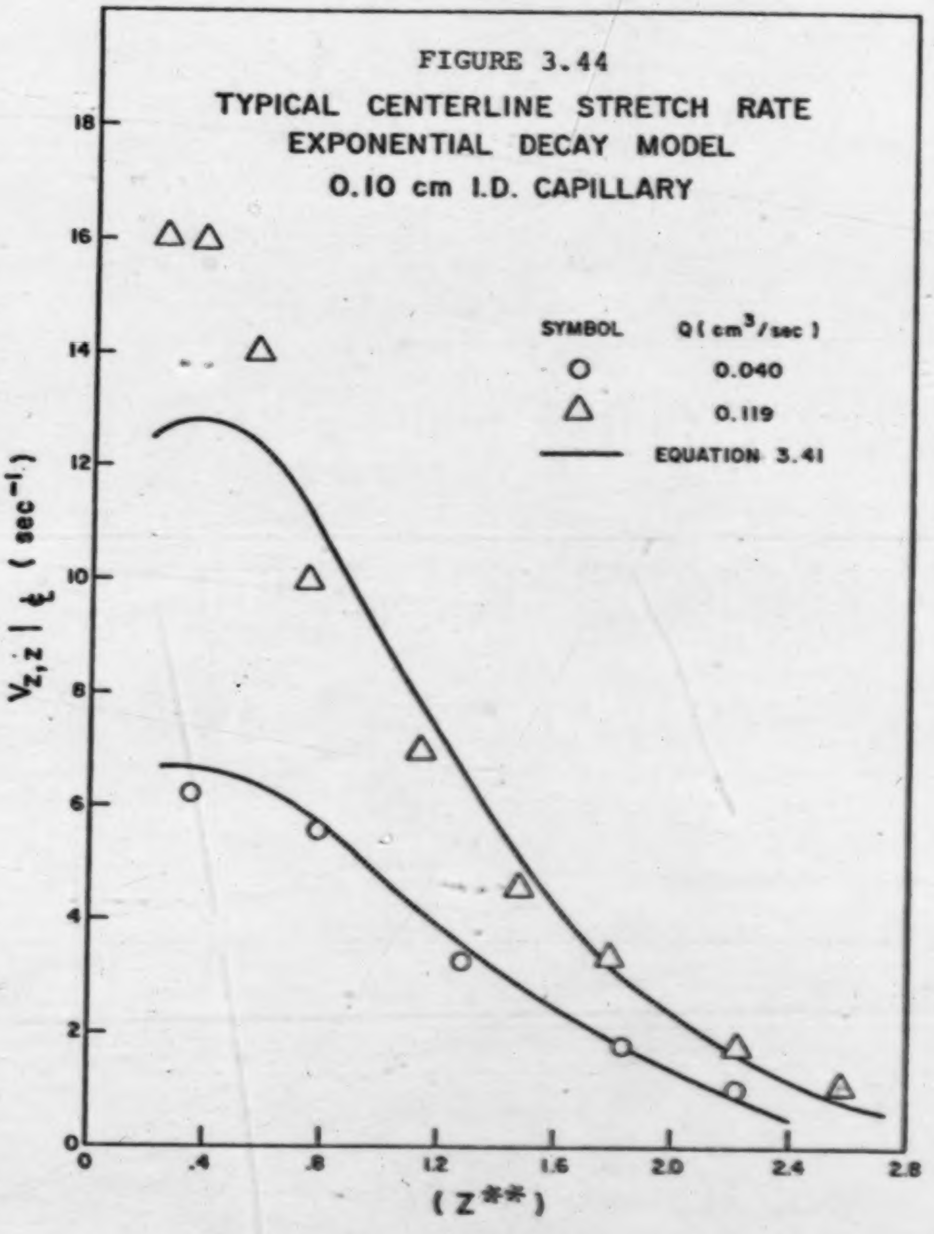

FIGURE 3.44

TYPICAL CENTERLINE STRETCH RATE
EXPONENTIAL DECAY MODEL
0.10 cm I.D. CAPILLARY

ed to decrease to a value equal to zero at the contraction. Since velocities were not measured within this range it was not possible to confirm this experimentally. However, for a few streamlines other than along the centerline, velocities were measured to within one streak length from the contraction. For these streamlines a plot of velocity versus axial location revealed that as the contraction was approached the velocity was independent of axial location, i.e., the stretch rate approached zero. An example of such a plot is given in Figure 3.45. Boger and Rama Murthy (24) did not measure centerline velocities at the contraction but the measured velocities upstream of the capillary entrance reported by them support the observations noted in this research, i.e., the stretch rates tend to a value equal to zero in the immediate vicinity of the contraction. Nakamura et al. (123) show clearly that only along the centerline was the stretch rate at the contraction equal to zero.

### (iv) Radial Dependence

The data in Appendix E and the data plotted in Figures 3.17 to 3.22 clearly indicate a strong dependence of axial velocity upon radial location. Qualitatively, these velocity profiles resemble the velocity profiles for a jet of fluid issuing into a stagnant body of the same fluid (free jet). Therefore, in an attempt to obtain similarity, a dimensionless axial velocity defined as

FIGURE 3.45

## TYPICAL EXAMPLE OF CONSTANT STRETCH RATE

0.30 cm I.D., Q = 0.318 $cm^3/sec$

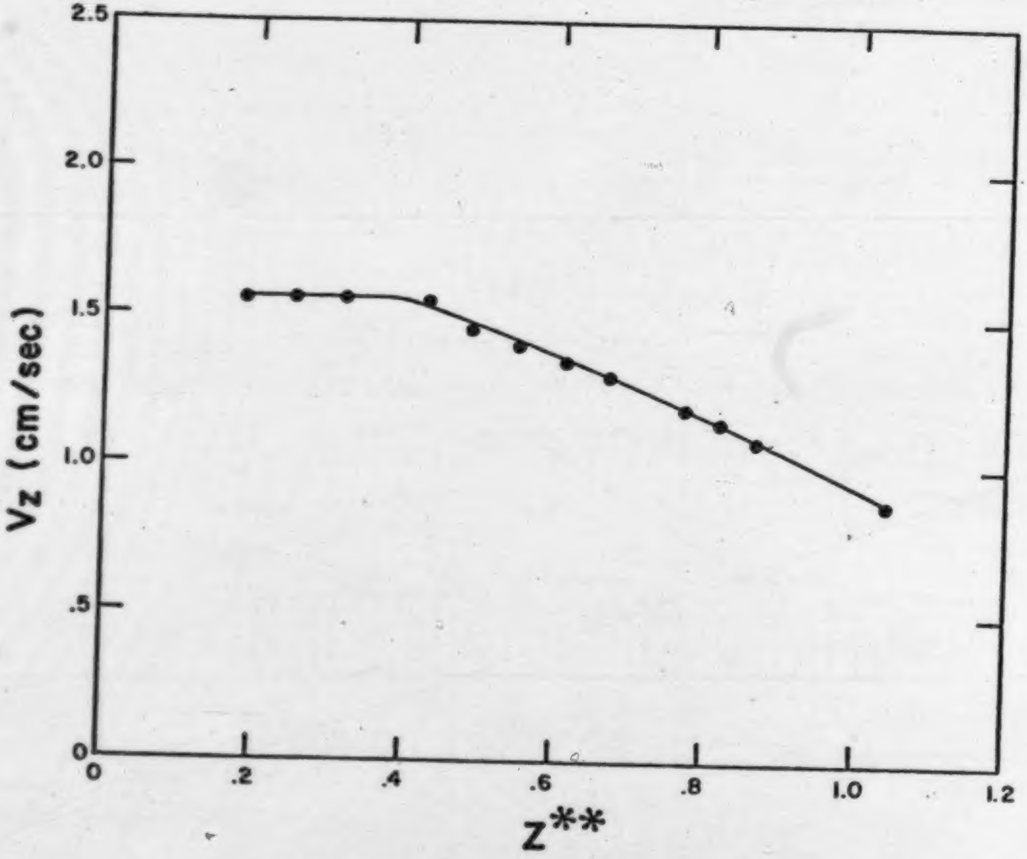

$$f(\eta) = \frac{V_z}{V_z\rceil_{\mathbb{C}}} \qquad 3.42$$

was plotted against a dimensionless radial coordinate, $\eta = r/r_0$. The parameter $r_0$ is defined as the radial location where the axial velocity is equal to one half of the centerline velocity. The values of $r_0$ determined from the plots of velocity profiles similar to those shown in Figures 3.19 to 3.22 are tabulated in Appendix E, Section E.4. Other definitions of $r_0$ such as the distance from the centerline to the outermost streamline were used to define $\eta$. This definition of $r_0$ did not result in the velocity profiles being similar, i.e., when the dimensionless axial velocities, $f(\eta)$, were plotted against the variable $\eta$ all of the data did not superimpose on a single curve.

From the values of $r_0$ tabulated in Appendix E it can be concluded that: (a) for a given capillary tube I.D., $r_0$ approached a constant value at $Z^{**} = 0.0$ independent of flow rate or reservoir size, and (b) over the characteristic flow pattern length, $r_0$ was consistently larger within reservoir L. The effect of decreasing the capillary tube I.D. was a decrease in values of $r_0$. The author was unsuccessful in correlating these data. Typical examples of the variation of $r_0$ with reservoir size and axial location upstream of the contraction are given in Figures 3.46 and 3.47. The data plotted in these figures indicate

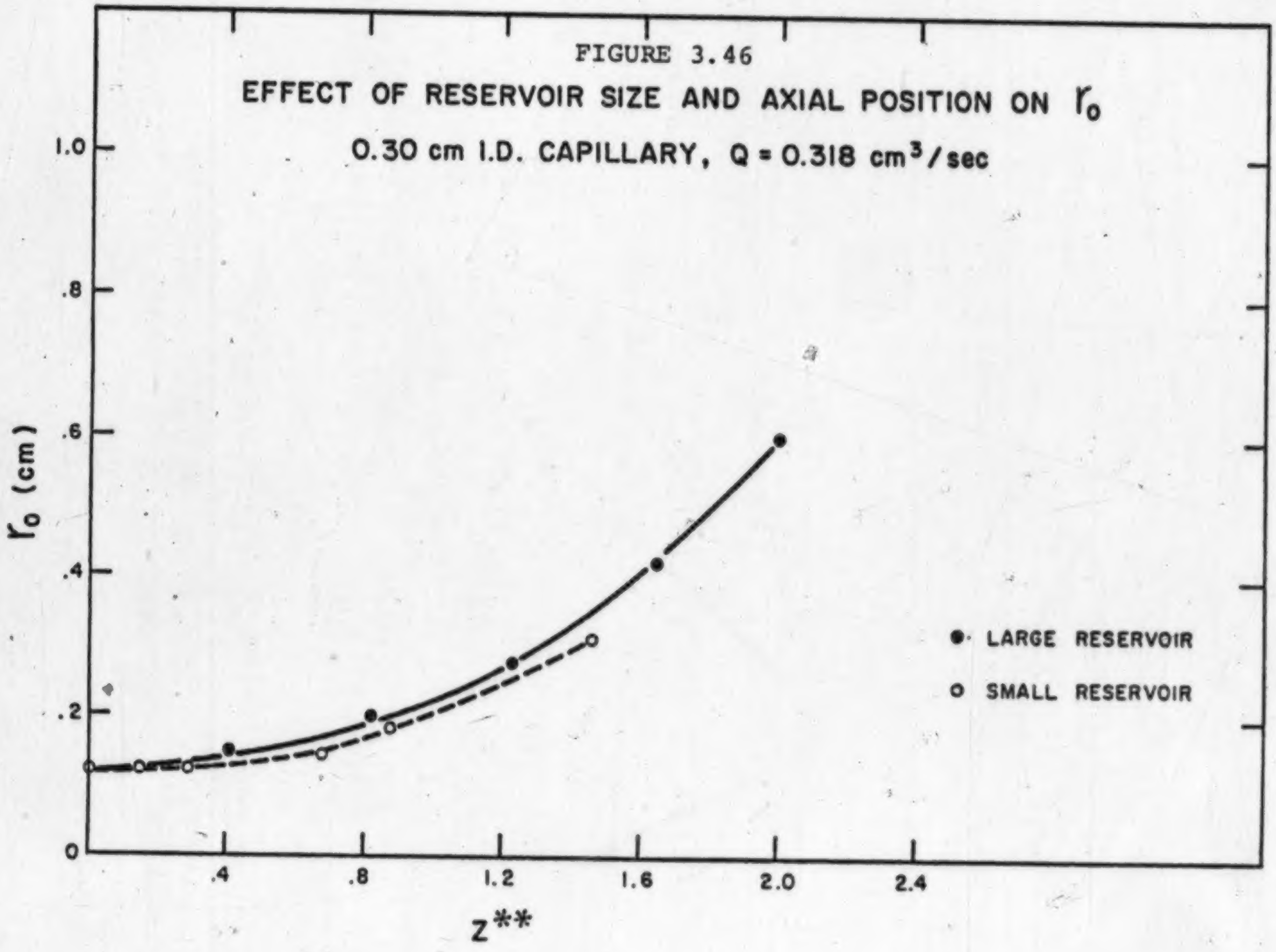

FIGURE 3.46

EFFECT OF RESERVOIR SIZE AND AXIAL POSITION ON $r_o$

0.30 cm I.D. CAPILLARY, $Q = 0.318$ cm$^3$/sec

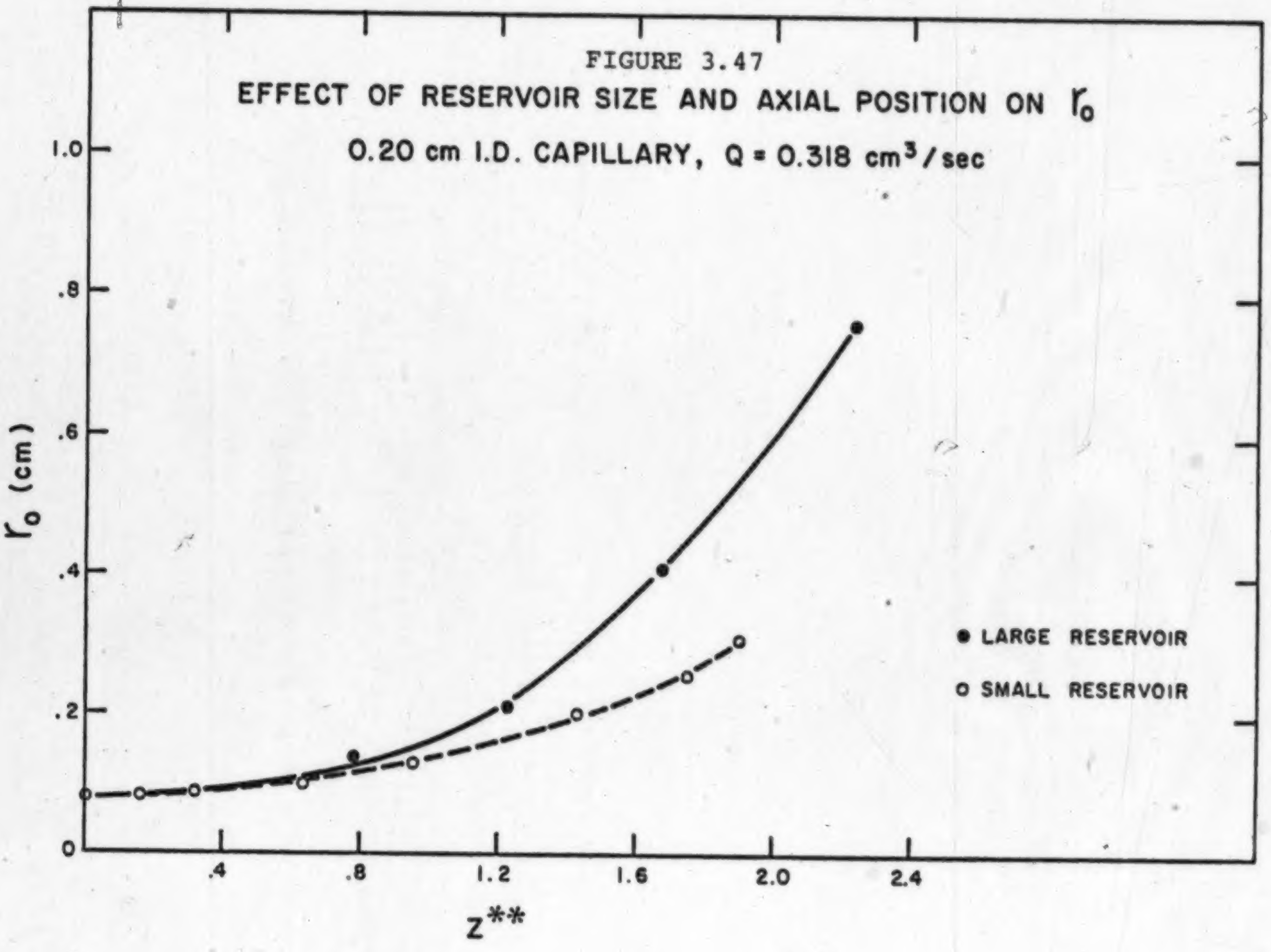

FIGURE 3.47

EFFECT OF RESERVOIR SIZE AND AXIAL POSITION ON $r_o$

0.20 cm I.D. CAPILLARY, $Q = 0.318\ cm^3/sec$

that $r_0$ is independent of reservoir size for values of $Z^{**} \leq 0.40$. At values of $Z^{**} > 0.40$ a strong dependence on reservoir size was observed. At a fixed flow rate, $Q = 0.318\ cm^3/sec$ and at $Z^{**} = 1.4$, $r_0$ was equal to 0.29 and 0.33 in reservoirs S and L respectively with capillary tube 3 (Figure 3.46) and 0.19 and 0.28 in reservoirs S and L respectively with capillary tube 2 (Figure 3.47). The above shows the dependence of $r_0$ on reservoir size at a fixed flow rate and axial position.

The dimensionless axial velocities, $f(\eta)$, are graphically plotted against the dimensionless radial location, $\eta$, in Figures 3.48 to 3.52. Log-log coordinates were chosen in order to discern differences in the values of $f(\eta)$ less than $10^{-1}$. The data in these figures were arbitrarily chosen from the tabulated data in Appendix E. If all the data in the appendix were plotted, it would not be possible to distinguish the individual data points for a given flow rate at various axial and radial locations. At values of $\eta$ less than 1.5 a single curve may be representative of the data with deviations being less than 16 percent. Larger deviations were noted at dimensionless radial locations greater than 1.5. Consider values of $\eta$ equal to 1.5, 2.0, and 2.75. The respective average values of the dimensionless axial velocities for capillary tube 2 were 0.275, 0.175, and 0.100 for the data obtained with reservoir L and 0.250, 0.125, and 0.055 for the data obtained with reservoir S. Similar variations were noted for the other data. However, it must be emphasized that at these values

FIGURE 3.48

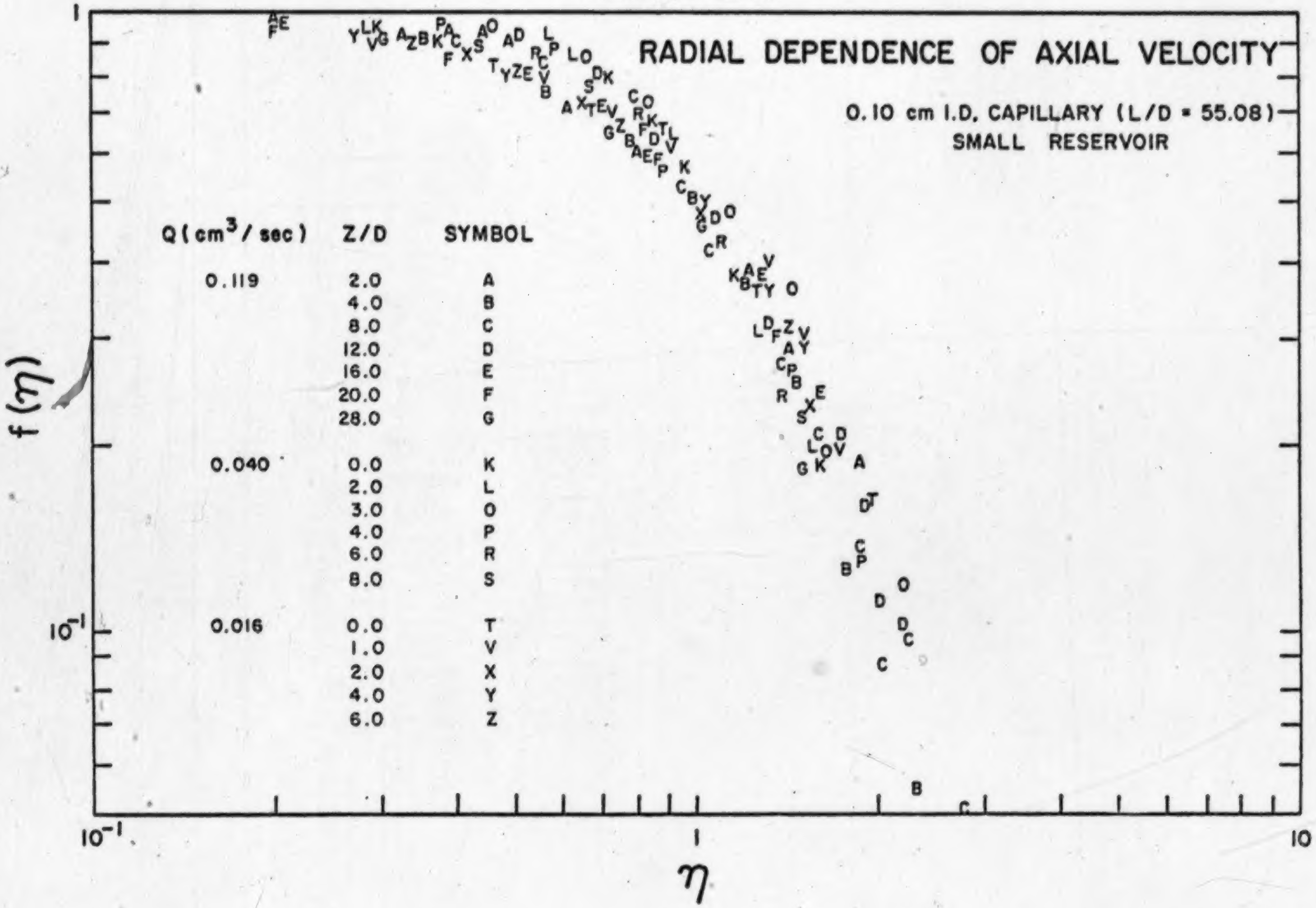
RADIAL DEPENDENCE OF AXIAL VELOCITY
0.10 cm I.D. CAPILLARY (L/D = 55.08)
SMALL RESERVOIR
Q (cm³/sec)
Z/D
SYMBOL
0.119
2.0 A
4.0 B
8.0 C
12.0 D
16.0 E
20.0 F
28.0 G
0.040
0.0 K
2.0 L
3.0 O
4.0 P
6.0 R
8.0 S
0.016
0.0 T
1.0 V
2.0 X
4.0 Y
6.0 Z
f(η)
η
1
10⁻¹
10

FIGURE 3.49

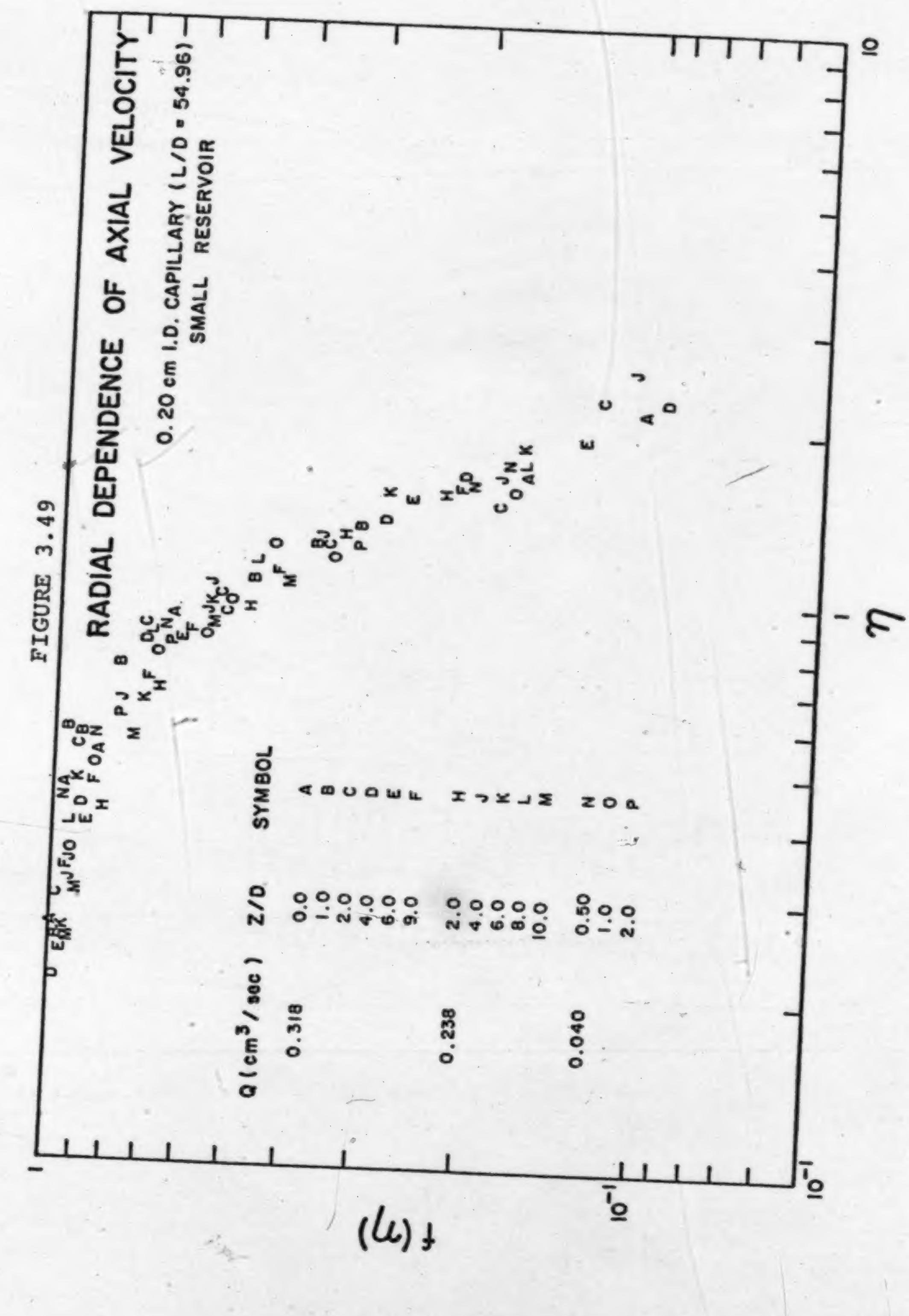
RADIAL DEPENDENCE OF AXIAL VELOCITY
0.20 cm I.D. CAPILLARY (L/D = 54.96)
SMALL RESERVOIR
Q (cm³/sec)
Z/D
SYMBOL
0.318
0.0 A
1.0 B
2.0 C
4.0 D
6.0 E
9.0 F
0.238
2.0 H
4.0 J
6.0 K
8.0 L
10.0 M
0.040
0.50 N
1.0 O
2.0 P
f(η)
η
1
10⁻¹
10⁻¹
1
10

FIGURE 3.50

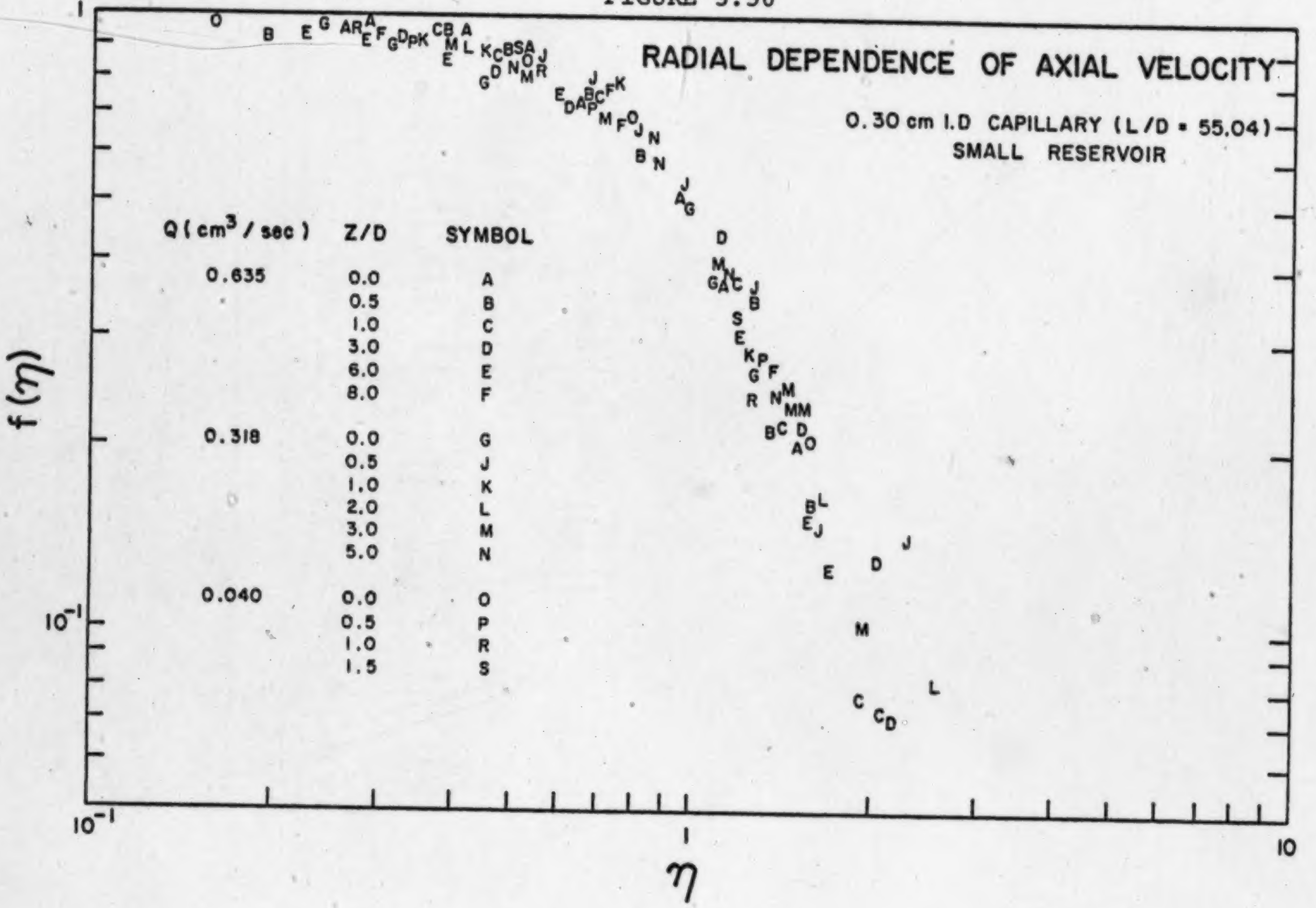
RADIAL DEPENDENCE OF AXIAL VELOCITY
0.30 cm I.D CAPILLARY (L/D = 55.04)
SMALL RESERVOIR
Q (cm³/sec)
Z/D
SYMBOL
0.635
0.0 A
0.5 B
1.0 C
3.0 D
6.0 E
8.0 F
0.318
0.0 G
0.5 J
1.0 K
2.0 L
3.0 M
5.0 N
0.040
0.0 O
0.5 P
1.0 R
1.5 S
f(η)
η
1
10⁻¹
10⁻¹
1
10

FIGURE 3.51

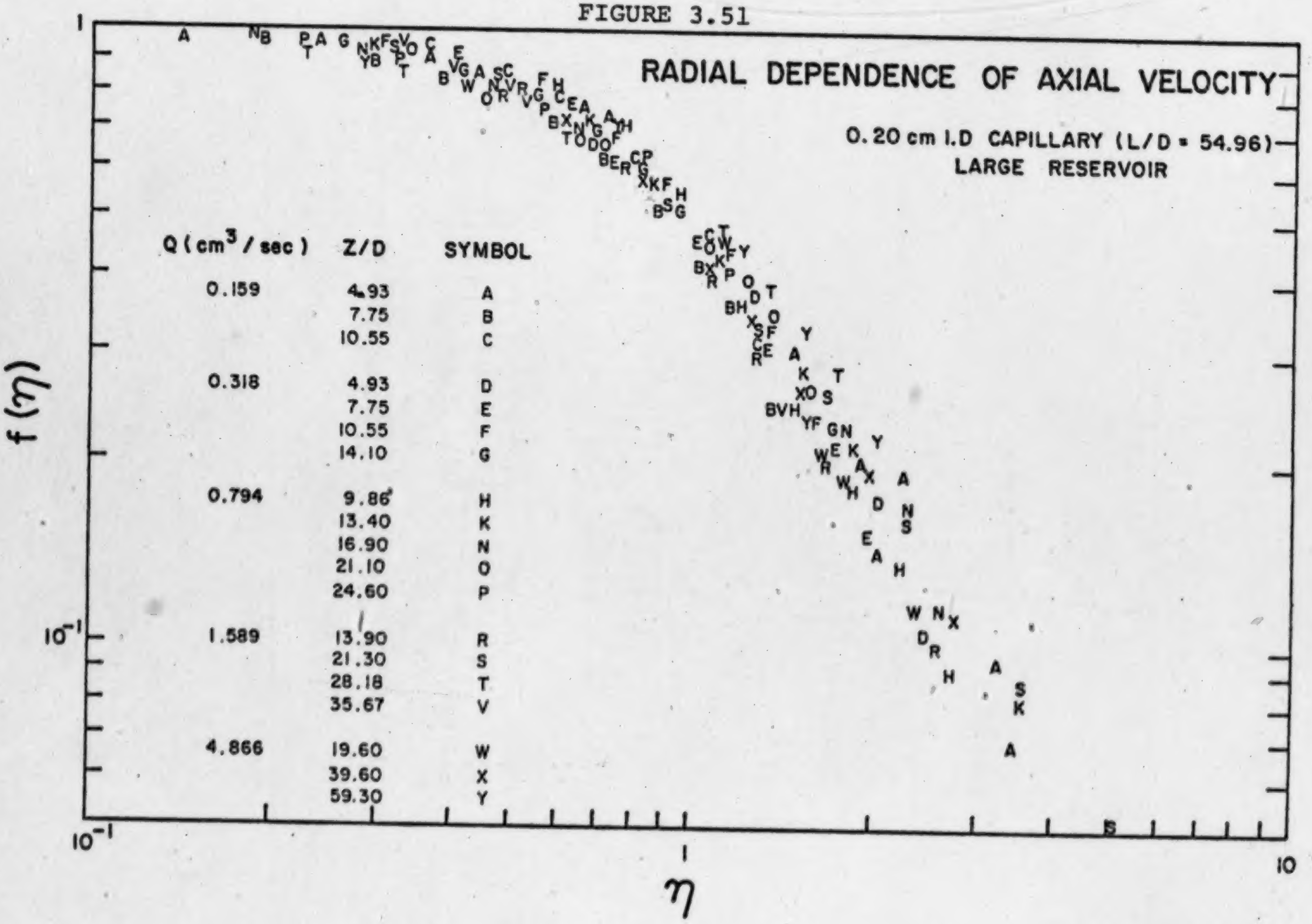
RADIAL DEPENDENCE OF AXIAL VELOCITY
0.20 cm I.D CAPILLARY (L/D = 54.96)
LARGE RESERVOIR
Q (cm³ / sec)
Z/D
SYMBOL
0.159
4.93 A
7.75 B
10.55 C
0.318
4.93 D
7.75 E
10.55 F
14.10 G
0.794
9.86 H
13.40 K
16.90 N
21.10 O
24.60 P
1.589
13.90 R
21.30 S
28.18 T
35.67 V
4.866
19.60 W
39.60 X
59.30 Y
f (η)
1
10⁻¹
η
10⁻¹
1
5
10

FIGURE 3.52

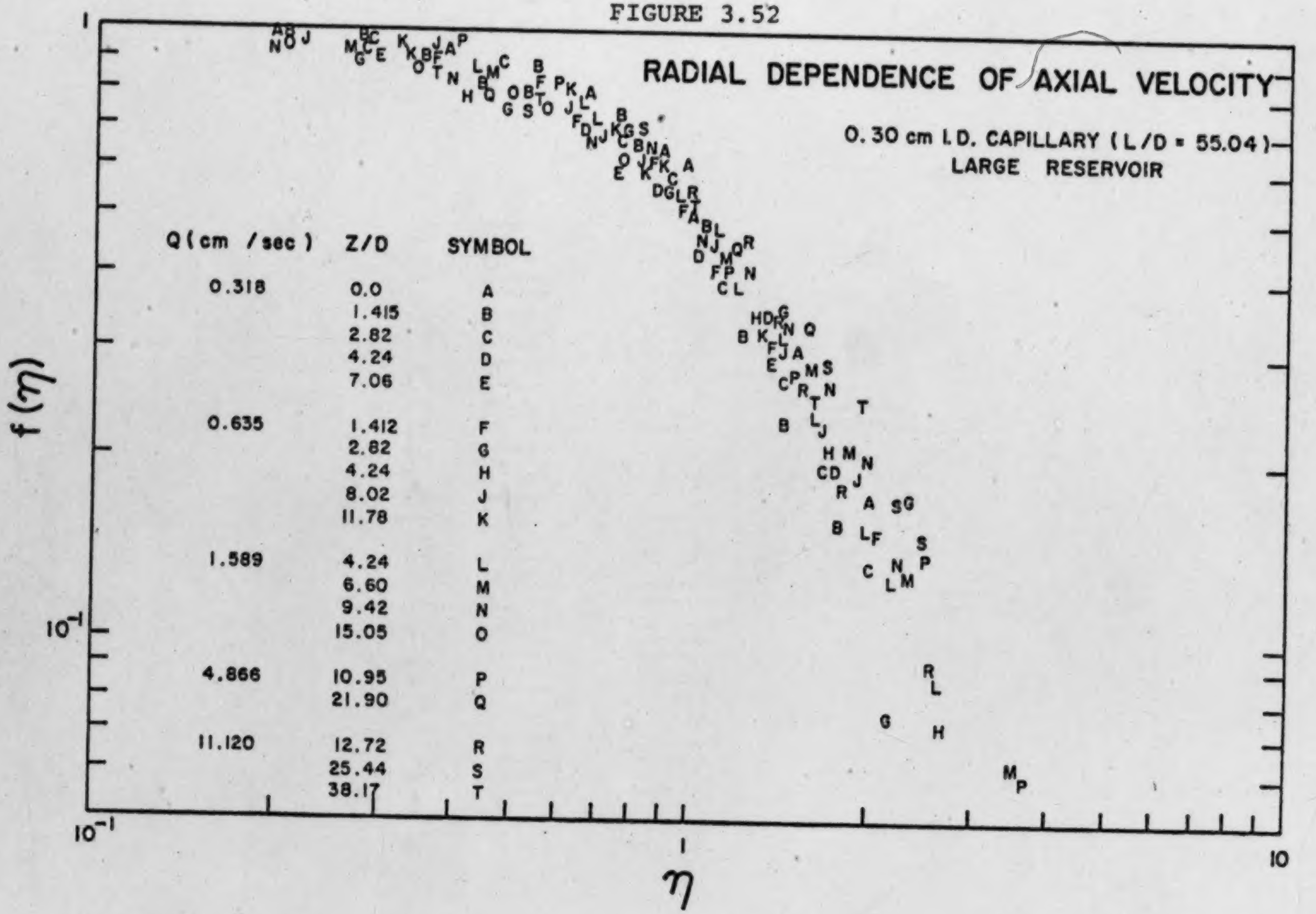
RADIAL DEPENDENCE OF AXIAL VELOCITY
0.30 cm I.D. CAPILLARY (L/D = 55.04)
LARGE RESERVOIR
Q (cm /sec) Z/D SYMBOL
0.318 0.0 A
1.415 B
2.82 C
4.24 D
7.06 E
0.635 1.412 F
2.82 G
4.24 H
8.02 J
11.78 K
1.589 4.24 L
6.60 M
9.42 N
15.05 O
4.866 10.95 P
21.90 Q
11.120 12.72 R
25.44 S
38.17 T
f(η)
η
1
10⁻¹
10⁻¹
1
10

of $\eta$, the axial velocities were measured outside of the central core region. As a result, velocities were small in comparison to the centerline axial velocities and were difficult to measure accurately. Even though the velocities in this region were difficult to measure accurately, the discrepancy was not solely due to the accuracy in measurement. If a single curve is made to pass through the mean of all the data in Figures 3.48 to 3.52 inclusive up to values of $\eta = 2.75$, the maximum discrepancies between the data and this curve at $\eta = 1.5$, 2.0, and 2.75 are 16%, 17% and 42% respectively. The large discrepancies measured for values of $\eta$ greater than 2.0, e.g., 42% at $\eta = 2.75$, are a result of reservoir size. At large radial positions, $r = 2r_0$, the predicted velocities would be approximately 40% larger than measured values in reservoir S or 40% smaller than velocities measured in reservoir L. However, at these large values of $\eta$, axial velocities were measured well outside of the central core region.

A universal curve that is made to pass through data points

$$v_z = v_z|_{\mathrm{¢}} \quad @ \; r=0 \text{ or } f(\eta) = 1.0 \; @ \; \eta=0 \qquad 3.43$$

$$v_z = \frac{1}{2} v_z|_{\mathrm{¢}} \quad @ \; r=r_0 \text{ or } f(\eta) = 0.5 \; @ \; \eta=1.0 \qquad 3.44$$

and subject to the condition

$$v_{z,r} = 0 \; @ \; r=0 \text{ or } f'(\eta) = 0 \; @ \; \eta=0 \qquad 3.45$$

is given by Equation 3.46.

$$f(\eta) = (1 + 0.41\ \eta^2)^{-2.0} \qquad 3.46$$

Equation 3.46 is plotted as the solid line in Figure 3.53 with the vertical bands representing the maximum scatter in the data obtained from Figures 3.48 to 3.52 inclusive. Equation 3.46 passes through the vertical bands up to values of $\eta$ equal to 2.5. A replot of experimental axial velocities ($f(\eta)$ vs $\eta$) measured upstream of an abrupt contraction (123) for $\beta = 8.16 \times 10^{-2}$, $z/D \leq 3.0$ and $r/R \leq 0.550$ are within 10 percent of predicted values, Equation 3.46. Thus, Equation 3.46 predicts velocities which are in reasonable agreement with experimental velocities over a wider range of parameters than studied in this research.

Axial velocities, predicted by combining Equations 3.40 and 3.46, that is

$$V^* = \exp(-(Z^{**})^{1.4})(1+0.41\ \eta^2)^{-2.0} \qquad 3.47$$

are compared to experimental data for two typical runs. The data in Figure 3.54 typify the maximum discrepancy of 17% between experimental and predicted velocities for values of $\eta$ less than 2.0. In this example, $\eta$ less than 2.0 corresponds to values of r less than 0.196 cm at 2.0 diameters upstream of the contraction, whereas at 6.0 diameters upstream of the contraction, $\eta$ less than 2.0

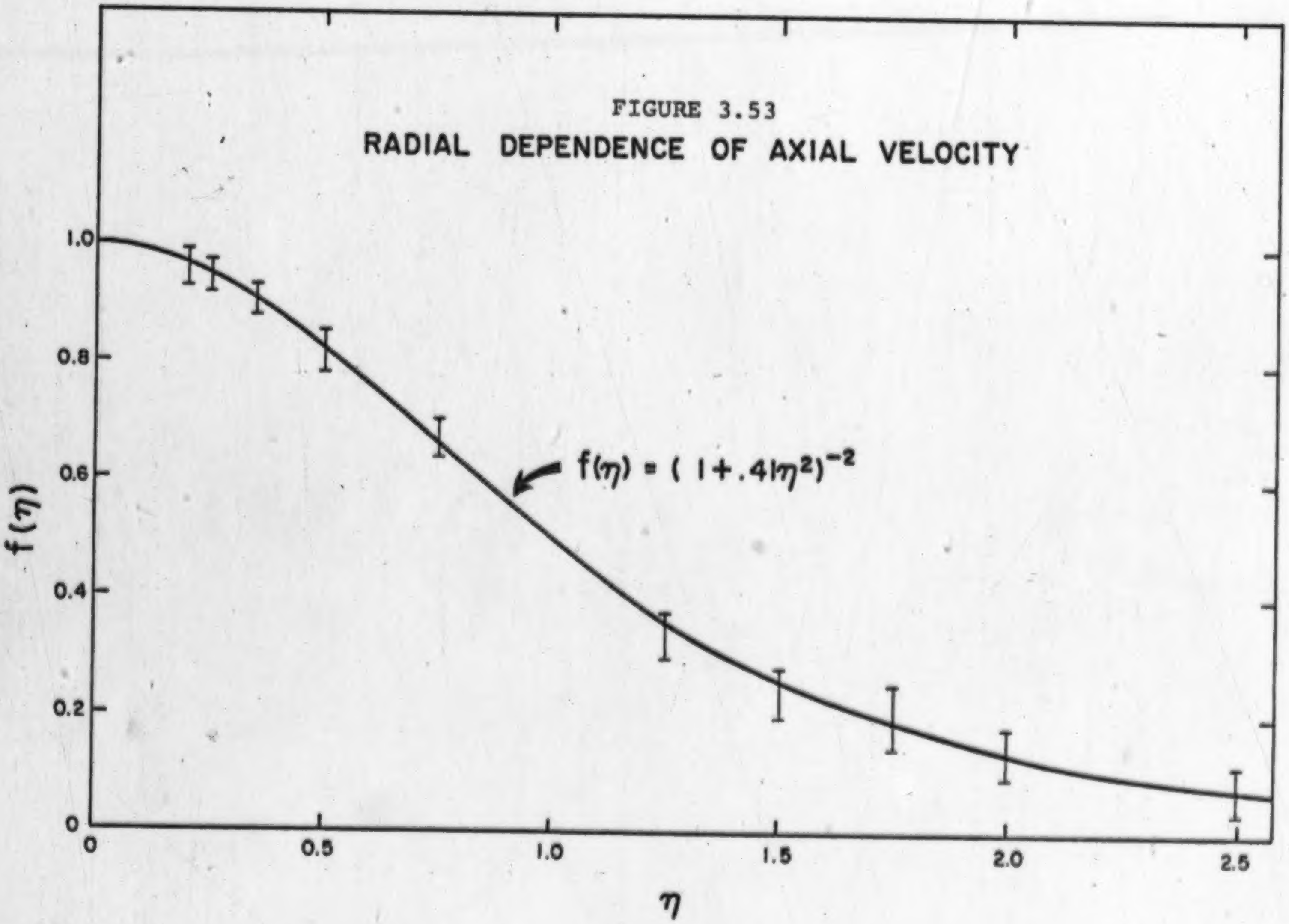

FIGURE 3.53

RADIAL DEPENDENCE OF AXIAL VELOCITY

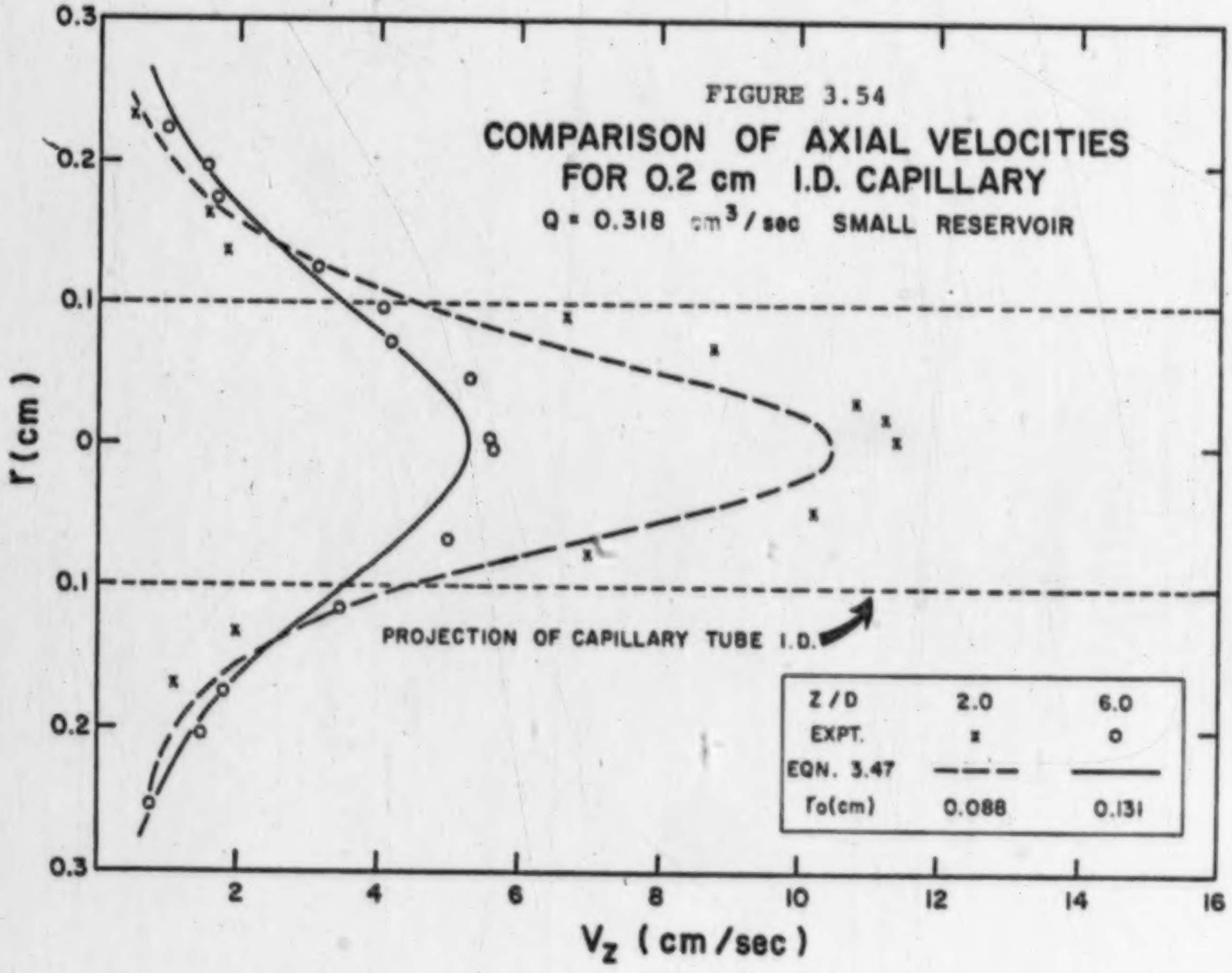

FIGURE 3.54

COMPARISON OF AXIAL VELOCITIES FOR 0.2 cm I.D. CAPILLARY

Q = 0.318 cm$^3$/sec SMALL RESERVOIR

corresponds to values of r less than 0.262 cm. An example of good agreement with experimental data is shown in Figure 3.55. This figure also shows that at 6.60 diameters upstream of the contraction the axial velocities at values of $r = 0.80$ cm or $\eta = 4.0$ are in good agreement with the data. This suggests that for some experimental runs Equation 3.47 is capable of predicting reasonably velocities at values of $\eta$ considerably larger than 2.0.

The features of the flow field (discussed in this section), i.e., cone semi-angles, location of eddy centers, and axial velocities, can be summarized as follows:

(a) The initial cone semi-angles measured within region I are independent of reservoir size and are represented by Equation 3.8, and cone semi-angles measured upstream of the contraction and for $Z^{**} < Z^{**}_{\infty}$ are, within experimental error, independent of reservoir size. The value of $Z^{**}_{\infty}$ varies with capillary tube diameter and flow rate. For example, at 0.318 $cm^3/sec$, $Z^{**}_{\infty}$ was 2.2 and 3.2 for capillary tubes 2 and 3 (Figure 3.24, page 162). Beyond these axial locations, the cone semi-angles, although not measured directly, depend on reservoir size. This can be explained in terms of the qualitative differences in the flow fields in both reservoirs. Since the central core within reservoir S occupied a significant fraction of the reservoir's cross-sectional area at $Z^{**} = Z^{**}_{\infty}$ further cone angle development was restricted. On the other hand, the cross-sectional area in reservoir L was two orders of

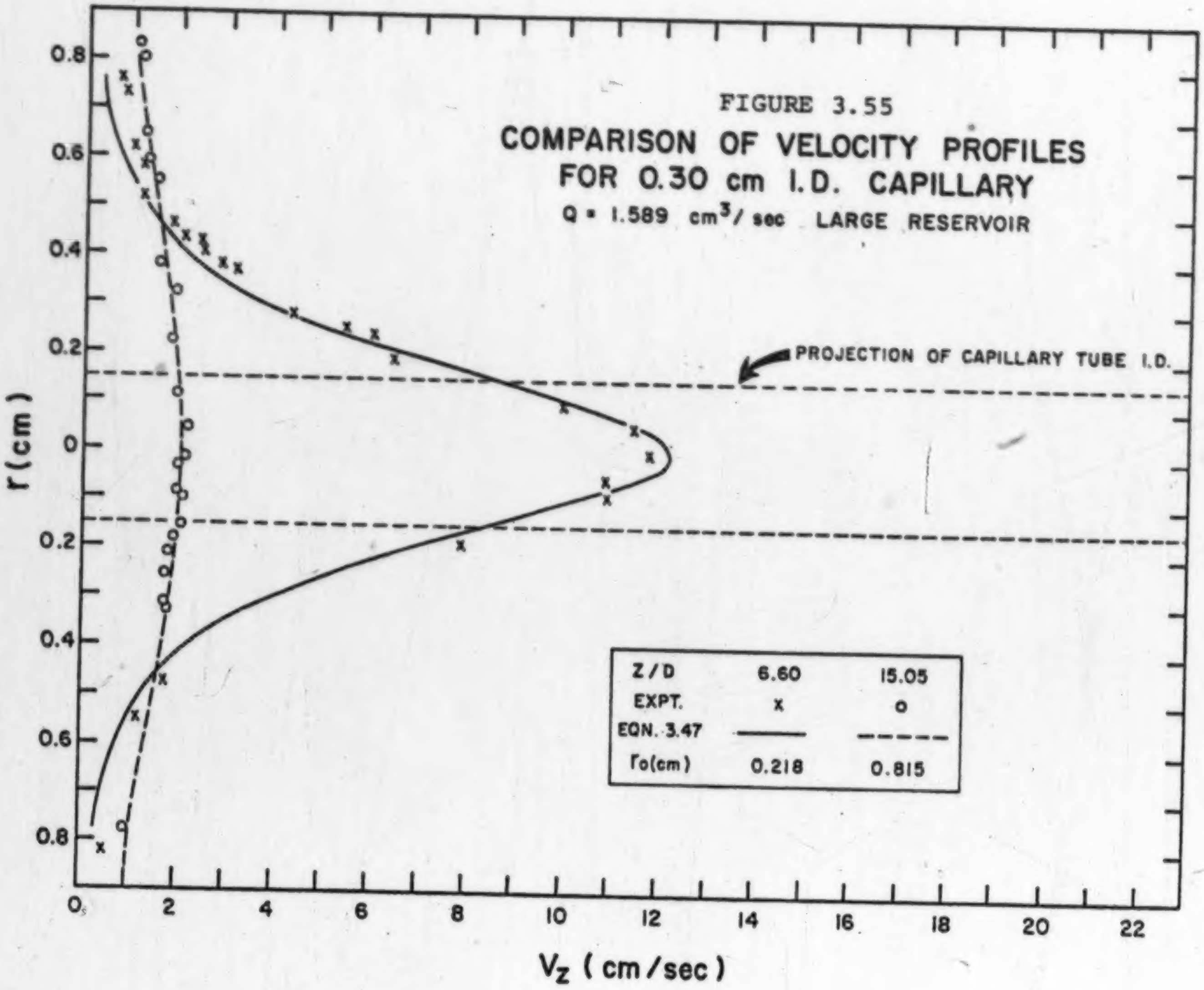

FIGURE 3.55
COMPARISON OF VELOCITY PROFILES FOR 0.30 cm I.D. CAPILLARY
$Q = 1.589\ cm^3/sec$ LARGE RESERVOIR

magnitude larger which allowed cone angle development farther upstream at a given flow rate. The development continued until the central core area approached the reservoir's cross-sectional area. As a result, the center of the eddies were located farther upstream of the contraction and the area occupied by the recirculation region was larger in size in reservoir L.

(b) Within the WGS core the dimensionless centerline axial velocity-axial position plots ($V^*$ vs $(Z^{**})^{1.4}$) are similar, i.e., all of the data superimposed on a single curve given by Equation 3.40. The velocities measured up to values of $Z_0^{**}$, where the product $\Gamma\theta_0$ is equal to unity, are independent of reservoir size. This axial location defined the major portion of the flow field and was approximately equivalent to a distance upstream of the contraction equal to one and one half times the location of the center of the eddies. Axial velocities other than along the centerline, represented by Equation 3.46, are within 17% of experimentally measured velocities for $\eta \leq 2.0$. Parameter $r_0$ used in the definition of $\eta$ was not independent of reservoir size over the full range of upstream axial locations. This parameter was independent of reservoir size only for values of $Z^{**} \leq 0.40$. Farther away from the contraction, $Z^{**} > 0.40$, $r_0$ becomes dependent on reservoir size to the extent that at a fixed $Z^{**}$ and flow rate it increased as reservoir size increased.

(c) The radial velocity component is derived from the use of Equation 3.47, the continuity equation and the boundary condition $V_r = 0$, and $r = 0$. Experimental values are tabulated in Appendix E, Section E.2.

## 3.5 PREDICTION OF INSTABILITY

Empirical criteria presented to date, such as the critical shear stress or recoverable shear strain, attempt to correlate the onset of instabilities with physical properties of the fluid measured under SLSF in the capillary tube. These criteria, although simple to evaluate and require little, if any additional experimentation, do not take into account such variables as reservoir size and the type of instability. More critically, these criteria are inconsistent with experimental observations wherein for many polymer melts and solutions fracture has been observed to occur within the inlet region. Criteria based on inlet conditions have not been tested severely since a detailed quantitative description of the flow field was not known. This led Everage and Ballman (60) to resort to approximating the flow field using the velocity distribution of a Newtonian fluid. Although the onset criteria based on inlet conditions differ significantly, there is a consensus of opinion that instability is a consequence of tensile failure in extensional deformation (46, 60, 88).

Cogswell's (46) expression for a critical extensional stress at the die entry is given by

$$(\tau)_{cr} = \frac{3n'+1}{n'+1} \frac{\tau_w}{\tan\phi_0} \qquad 3.48$$

The practical difficulty in utilizing Equation 3.48 for flows through a sudden contraction is that the initial cone semi-angle, $\phi_0$, must be known or measured in order to predict $(\tau)_{cr}$. In reservoir L and at the onset of region III, $\phi_0$ was too small to be measured accurately ($\phi_0 < 0.5$ degrees) which immediately points to a limitation of Equation 3.48, i.e, not only must $\phi_0$ be known but it must be known accurately. Furthermore, as $\phi_0$ tends to zero, Equation 3.48 predicts infinite extensional stresses. Since $\phi_0$ was too small to be measured accurately at the onset of region III in reservoir L, a conservative estimate of $(\tau)_{cr}$ was obtained by assuming that $\phi_0$ was equal to 0.5 degrees. Critical extensional stresses calculated with Equation 3.48 are given in Table 3.5. These data show that $(\tau)_{cr}$ was not reasonably constant but varied from 1669 dyn/cm$^2$ to values exceeding 100,000 dyn/cm$^2$ (two orders of magnitude variation). If, on the other hand, $(\tau)_{cr}$ was reasonably constant then Equation 3.48 would predict a critical value of the shear stress which is related to inlet conditions by tan $\phi_0$. The initial cone semi-angle for polymer melts exemplified by HDPE is 90 degrees, hence Equation 3.48 would predict, for a constant $(\tau)_{cr}$, a shear stress criterion. Cogswell (46) also showed that the critical extensional stress is related to the pressure losses in the entry region, $P_u$, by

## TABLE 3.5

## CRITICAL EXTENSIONAL STRESSES AT ONSET OF INSTABILITY

|  | I.D. (cm) |  |  |
|---|---|---|---|
|  | Capillary tube 1 | Capillary tube 2 | Capillary tube 3 |
| Reservoir S |  |  |  |
| $(\tau)_{cr}$ (dyn/cm$^2$) | 11,935 | 3,465 | 1,669 |
| Reservoir L |  |  |  |
| $(\tau)_{cr}$ (dyn/cm$^2$) | 67,299** | 23,798 | 26,737 |
| $(\tau)^{*}_{cr}$ (dyn/cm$^2$) | > 120,318 | > 58,249 | > 45,835 |

* Evaluated at the onset of region III

** Flow rate obtained by extrapolation of data plotted in Figure 3.6.

$$(\tau)_{cr} = \frac{3}{8}\,(n'+1)\,P_u \qquad 3.49$$

Predicted values of $P_u$ (obtained by equating Equations 3.48 and 3.49) are compared to the experimentally measured contraction losses, $\Delta P_c$, in Table 3.6. $P_u$ should always be less than $\Delta P_c$ since $\Delta P_c$ includes the pressure losses in the capillary tube entry length as well as within the entry region. With the exception of capillary tubes 2 and 3 in reservoir S, $P_u$ was significantly greater than $\Delta P_c$. Cogswell's own data indicated that for a LDPE melt the predicted value of $P_u$ at the onset of fracture was 0.00 $N/m^2$, and by Equation 3.49 $(\tau)_{cr}$ is equal to 0.00 $N/m^2$. This contradicts the hypothesis that melt fracture is a consequence of tensile failure. We conclude, therefore, that due to: (a) the above contradiction, (b) the predicted values of $P_u$ in the majority of cases being greater than $\Delta P_c$, and (c) the prediction of infinite extensional stresses as $\phi_0$ tends to zero, the generality of Equation 3.48 or 3.49 is seriously limited in predicting parameters at the onset of fracture.

The recoverable extensional strain criterion presented by Everage and Ballman (60) may be quantitatively tested by evaluating the maximum stretch rate at the onset of fracture. If applicable, this stretch rate should be reasonably constant. Experimental maximum stretch rates (along the centerline) varied from 7 to 16 $sec^{-1}$ in reservoir S and in reservoir L they varied from 16.5 to

## TABLE 3.6

## COMPARISON OF $P_u$ WITH $\Delta P_c$ AT ONSET OF FLOW INSTABILITIES

| RESERVOIR | PRESSURE (dyn/cm$^2$) | I.D. (cm) 0.10 | 0.20 | 0.30 |
|---|---|---|---|---|
| S | | | | |
| Region II | $P_u$ | 21238 | 6160 | 2967 |
| | $\Delta P_c$ | 9500 ** | 6947** | 4826** |
| L | | | | |
| Region II | $P_u$ | 119643 | 42308 | 47532 |
| | $\Delta P_c$ | 36500* | 12510 | 12010 |
| Region III | $P_u$ | > 213899 | > 103554 | > 81484 |
| | $\Delta P_c$ | 141700 | 61430 | 53440 |

* interpolation of data in Appendix C

** extrapolation of data in Appendix C

to 28.5 sec$^{-1}$ (region II) or from 32 to 49 sec$^{-1}$ (region III). These data would appear to support the recoverable extensional strain as a criterion for the onset of fracture. However, examination of experimentally measured centerline velocities revealed that over the major portion of the flow field the centerline velocities were independent of reservoir size. Therefore, maximum stretch rates evaluated in reservoir S, which resulted in an unstable flow field, (region II), should have resulted in an unstable flow field in reservoir L. Contrary to this, Figure 3.6 clearly shows that flow fields were stable at significantly higher flow rates in reservoir L. Consequently, although the maximum stretch rates are reasonably constant (7 to 28.5 sec$^{-1}$ at the first signs of an unstable flow field), this is not sufficient evidence to support the recoverable extensional strain criterion.

The hypothesis presented by Everage and Ballman (60), which is an extension of the work of Denn and Marrucci (51), is based upon a time dependent stress growth resulting from the converging flow field. Since this flow field has been shown to be dependent on flow rate and reservoir size, the fluid is subjected to different strain histories. This lends itself to the Hencky's strain measure or total strain as a means of correlating the onset of instability. This measure, which has been used successfully in correlating velocity data (90), i.e., parameter p in Equation 3.9 with the total strain and transient elongational viscosities with the total strain (1), is given as

$$S = \int_{t_i}^{t_f} \Gamma \, dt \tag{3.50}$$

where $t_i$ is the initial time when elongation commences. Acierno et al. (1), using this definition, found that elongation viscosity-total strain curves obtained from spinning and inverse siphon experiments, resulted in a single curve. The data obtained from the inverse siphon experiment covered the initial part of the transient curve while the data from the spinning experiment yielded the upper part of the same transient curve. The basis to their analysis assumes that beyond an axial location, $Z_0^{**}$ , the polymer molecules, represented by elastic dumbbells, are aligned in the direction of stretching without appreciable change in their length, whereas for axial locations less than $Z_0^{**}$ they elongate. Therefore, time, $t_i$, in Equation 3.50 is considered to be equal to zero at $Z^{**} = Z_0^{**}$. The evaluation of $Z_0^{**}$ was determined by a dimensionless stretch rate where the product of the stretch rate times the zero shear relaxation time of the fluid was equal to unity.

Acierno et al. (1) showed that the transient elogational viscosity curve deviates from linear Hookean behavior beyond a value of S. In an attempt to rationalize the effect of reservoir size and capillary tube diameter on the onset of flow instabilities, it is postulated in this dissertation that instabilities may occur whenever the polymer molecules exceed the linear Hookean range. Equivalently, instabilities may occur at a critical value of S, $S_c$. An analytical expression for $S_c$ derived from the empirical equation for the centerline velocity, Equation 3.40, is

$$S_c = \int_0^t \Gamma\, dt = \int_0^t \frac{-1.4V_Z (Z^{**})^{0.4}}{D(\theta_0 Q/D^3)^{0.5}}\, dt$$

$$= \frac{-1.4}{D(\theta_0 Q/D^3)^{0.5}} \int_{Z_0^{**}}^{0} (Z^{**})^{0.4}\, dZ$$

$$= -1.4 \int_{Z_0^{**}}^{0} (Z^{**})^{0.4}\, dZ^{**}$$

$$= (Z_0^{**})^{1.4} \qquad 3.51$$

Therefore, the stretch history is determined uniquely by a dimensionless parameter, $Z_0^{**}$. This dimensionless parameter is not independent of flow rate and other variables since it was obtained from the condition

$$\Gamma\, \theta_0 = 1.0 \qquad 3.52$$

The substitution of Equation 3.40 into Equation 3.52 yields

$$1.0 = \frac{1.4V_0 (Z_0^{**})^{0.4}}{D(\theta_0 Q/D^3)^{0.5}} \exp(-(Z^{**})^{1.4})\, \theta_0 \qquad 3.53$$

From Equation 3.51 we have

$$1.0 = \frac{1.4V_0 S_c^{.286}\theta_0}{D(\theta_0 Q/D^3)^{0.5}} \exp(-S_c) \qquad 3.54$$

For the system considered here, the zero shear relaxation time is equal to 1 sec and with n' equal to 0.50 Equation 3.22 reduces to

$$V_0 = 5.0(\frac{Q}{\pi D^2}) \qquad 3.55$$

Therefore, Equation 3.54 can be rewritten as

$$1 = 2.228(\frac{Q_c}{D^3})^{0.5}(S_c)^{.286}\exp(-S_c) \qquad 3.56$$

where $Q_c$ is the volumetric flow rate evaluated at the onset of region II. Equation 3.56 cannot be used to calculate $S_c$ at the onset of region III (reservoir L) since Equation 3.40 is valid only for flow rates within region I. Given the critical flow rate, $Q_c$, at the onset of region II (Figure 3.6, page 94) and diameter, D, Equation 3.56 yields $S_c$. Following this procedure values of $S_c$ were determined at the onset of region II with the results tabulated in Table 3.7 (next page). The values of $S_c$ are not grossly different, $2.8 \leq S_c \leq 4.2$, and it appears that the difference is largely the result of the insensitivity of $S_c$ to flow rate. On the other hand, if one back calculates a critical flow rate, a small change in $S_c$ results in a large change in critical flow rate. If we accept that $S_c$ is dependent on reservoir size, the question arises whether $S_c$ is a useful ordering parameter for a given system.

TABLE 3.7

CRITICAL VALUES OF S ($S_c$)

| | I.D. (cm) | | |
|---|---|---|---|
| | 0.10 | 0.20 | 0.30 |
| Reservoir L | 4.2 | 3.8 | 3.8 |
| Reservoir S | 3.6 | 3.0 | 2.8 |

From Table 3.7 it is observed that $S_c$ depends moderately on capillary tube diameter. Suppose the criterion for the onset of flow instabilities was $S_c = 3.0$, then by Equation 3.51

$$S_c = 3.0 = (Z_0^{**})^{1.4} \qquad 3.57$$

or

$$Z_0^{**} = 2.19 \qquad 3.58$$

Substitution of Equation 3.57 into 3.56 yields

$$1.0 = 2.228\left(\frac{Q_c}{D^3}\right)^{0.5} (3.0)^{.286} \exp(-3.0) \qquad 3.59$$

which after simplification reduces to

$$Q_c = 43.41\ D^3 \qquad 3.60$$

In general, Equation 3.60 is written as

$$Q_c = 120.54\left(\frac{n'+1}{3n'+1}\right)^2\left(\frac{D^3}{\theta_0}\right) \qquad 3.61$$

The relationships between the critical flow rate and capillary tube diameter were obtained for other values of $S_c$, namely 2.5, 3.5, 4.0, and 4.5 and are plotted in Figure 3.56. Before evaluating the results, the critical flow rate-diameter dependence predicted from the recoverable shear strain criterion is examined. The recoverable shear strain evaluated at the onset of region II was found to vary with reservoir size and capillary tube diameter (Table 3.3, page 106). By Equation 1.42 (page 38) and for an assumed constant value of $S_R$ we have

$$Q_c = \frac{S_R \pi}{32}\left(\frac{D^3}{\theta}\right) \qquad 3.62$$

The data plotted in Figure 3.56 and Equation 3.61 and 3.62 show the following points:

(a) The predicted flow rates at the onset of flow instabilities (region II) are sensitive to the assumed value of $S_c$ or $S_R$.

(b) At constant fluid properties the predicted diameter dependence from both the $S_R$ and $S_c$ criteria ($Q_c \alpha D^3$)

FIGURE 3.56

SENSITIVITY OF FLOW RATE AT ONSET OF INSTABILITY, $S_c$ CRITERION

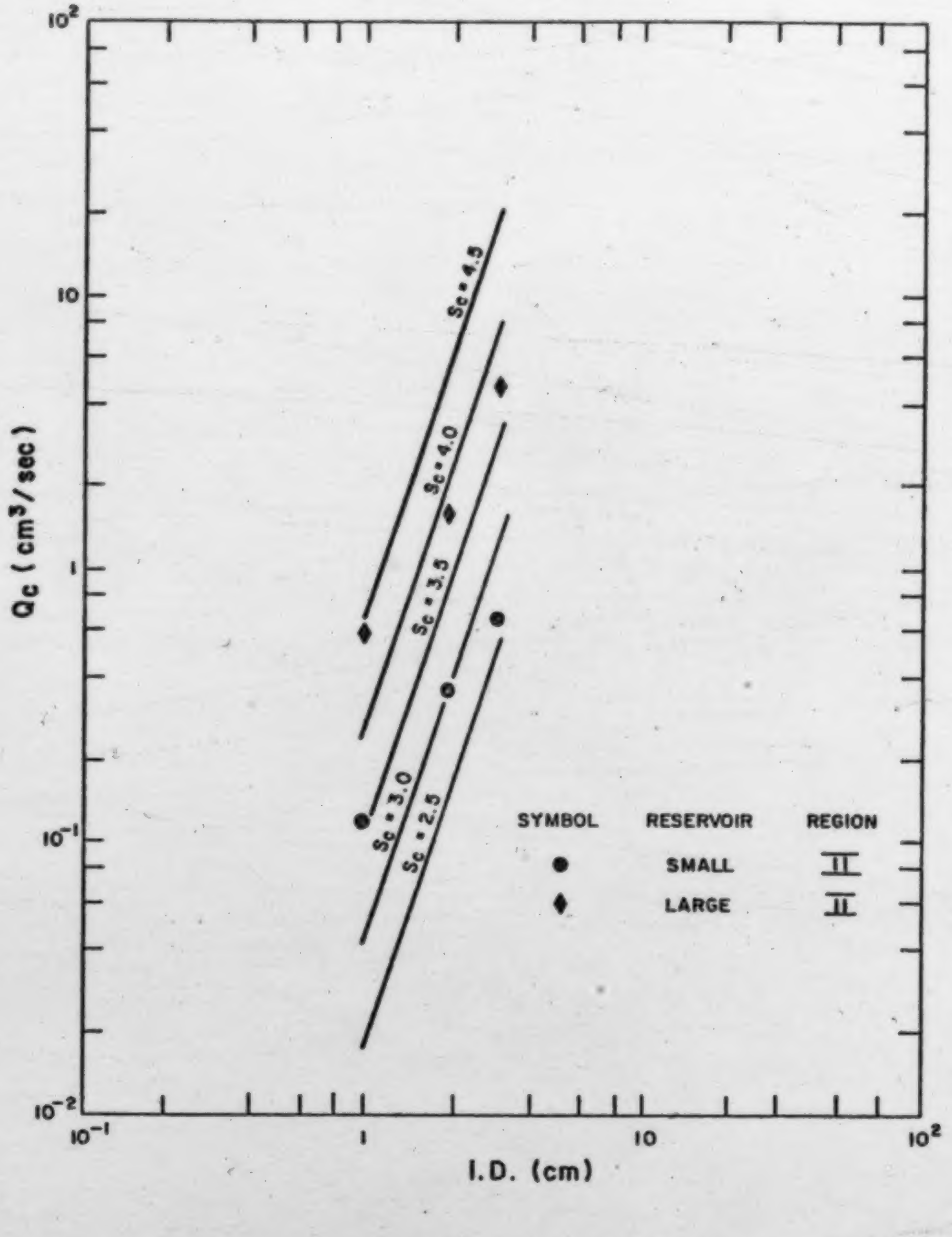

is only qualitatively correct.

(c) The flow rates defining the onset of flow instabilities at region II are inversely proportional to a characteristic relaxation time of the fluid.

(d) Both the $S_c$ and $S_R$ criteria depend upon reservoir size.

Based on the above four points, we conclude that:

(a) The first sign of instability, which is manifested by an observed swirling motion in the inlet region, may occur whenever the polymer molecules exceed the linear Hookean range.

(b) The $S_c$ and $S_R$ criteria do not directly account for the effect of reservoir size on the onset of flow instabilities but they agree qualitatively in predicting the effect of capillary tube diameter on the onset of flow instabilities.

(c) The $S_c$ criterion predicts that the onset of instability depends upon the inelastic nature of the fluid characterized by the flow behavior index, n'. The critical flow rate decreases as the flow behavior index, n', increases. The flow rate at the onset of region II for fixed D, $\theta_0$ and $S_c$ decreases as the flow behavior index increases.

# CHAPTER IV

# CONCLUSIONS AND RECOMMENDATIONS

## 4.1 CONCLUSIONS

1. For capillary tube Reynolds numbers less than 2100, the Newtonian contraction losses for values of $\beta$ approaching zero are represented by

$$\phi = K + \frac{K'}{N_{Re}} \qquad 4.1$$

where, $K \doteq 2.26 \pm 0.26$ 4.2

and $K' = 159 \pm 30$ 4.3

2. Qualitative observations of the upstream velocity field, the pressure traces, and the jet of fluid in the three regions are as follows: Within region I, the velocity field is stable, the pressure traces, (measured at a pressure tap located upstream of the contraction) are smooth, and the jet of fluid issuing from the capillary tube is also smooth. The stable flow field is characterized by a WGS central accelerating core surrounded by large eddies. Within region II the central core of fluid oscillates to and fro; the intensity and frequency of these oscillations increase with flow rate. There are no measurable changes in the pressure traces and in the jet of fluid. At the onset of region III (melt fracture) the flow field is described as "chaotic". Measured pressure fluctuations

coincide reasonably with the visually observed onset of region III. The jet of fluid oscillates with a frequency approximately equal to the frequency of the pressure fluctuations. Since the onset and magnitude of measurable pressure fluctuations are independent of the capillary tube length, the onset of region III (melt fracture) is also independent of the capillary tube L/D ratio. When the velocity field oscillates between stable and "chaotic" flows, the pressure fluctuations are significantly higher than the remaining data and the jet of fluid oscillates between two different trajectories. In one trajectory, corresponding to the stable flow field, the jet of fluid is smooth; in the other, corresponding to the "chaotic" flow field, the jet is distorted. Pressure fluctuations measured only over the interval of time that the flow field was observed to be "chaotic" are consistent with the remaining data.

3. The shear stresses evaluated in the capillary tube under SLSF and at the onset of regions II and III, although four orders of magnitude less than $10^6$ dyn/cm$^2$ for polymer melts, are in reasonable agreement with shear stresses calculated from the analysis presented by Southern and Paul (157). The recoverable shear strain, $S_R$, evaluated at the onset of regions II and III, are within the range reported for polymer melts ($2.2 \leq S_R \leq 67$). However, these criteria are not consistent with experimental observations wherein initiation occurs within the inlet region. A criterion based on inlet conditions, the Hencky's strain measure,

$S_c$, predicts that instability may occur whenever the volumetric flow rate exceeds a critical value given by

$$Q_c = 120.54\left(\frac{n'+1}{3n'+1}\right)^2\left(\frac{D^3}{\theta_0}\right) \qquad 4.4$$

The $S_c$ criterion agrees qualitatively in predicting the effect of capillary tube diameter and degree of elasticity on the onset of instabilities.

4. The onset of flow instabilities does not affect the flow curve. Effects are noted in the total pressure loss - flow rate plots, Bagley plots, and the contraction losses.

4.1 The onset and magnitude of an abrupt increase in the total pressure losses at the onset of region III are independent of the capillary tube L/D ratio. The discontinuity, resulting from the commencement of a "chaotic" flow field within the reservoir, is obtainable only for short capillary tube lengths. As capillary tube length increases, the abrupt increase in pressure cannot be detected and under these conditions the $\Delta P_t$-Q plots are not useful in determining the onset of region III.

4.2 Only when the velocity field oscillates between stable and "chaotic" flows do two Bagley plots exist: one for the stable and one for the "chaotic" velocity field with the only change being with the contraction losses (intercept). The contraction losses are greater whenever a "chaotic" velocity field exists. It is necessary to know the state of the velocity field with each capillary tube L/D ratio; otherwise, erroneous results in the contraction losses and shear stresses are likely to occur.

4.3 The effects of capillary tube diameter and reservoir size on contraction losses can be rationalized in terms of the state of the flow field within the reservoir, i.e., stable, swirling or "chaotic". Furthermore, we conclude that it is not correct to correlate contraction losses with Reynolds number over a wide range of Reynolds numbers when, over the same range of Reynolds numbers, the flow field changes from stable to "chaotic".

5. Within region I the cone semi-angles, eddy center locations and axial velocity profiles are summarized as follows:

5.1 The initial cone semi-angles are represented by

$$\phi_0 = 19\left(\frac{D^3}{\theta_0 Q}\right)^{0.6} \text{ for } 6 \times 10^{-3} \leq \left(\frac{D^3}{\theta_0 Q}\right) \leq 10 \qquad 4.5$$

and are independent of reservoir size for values of $(D^3/\theta_0 Q)$ that overlap. At values of $(D^3/\theta_0 Q) > 10$ the initial cone semi-angles approach 90° and $(D^3/\theta_0 Q)$ less than $6 \times 10^{-3}$ corresponds with the onset of region II. The cone semi-angles, measured at axial locations upstream of the contraction, within the accuracy of measurement and over the range of z/D where they were measured, are independent of reservoir size.

5.2 The location of the eddy centers move farther away from the contraction along a well defined path as flow rates increase. At a given flow rate the center of the eddies are located farther upstream of the contraction in larger size reservoirs.

5.3 The dimensionless axial velocity profiles for values of $\eta \leq 2.0$ can be expressed as

$$f(\eta) = \frac{V_z}{V_z|_{\mathrm{¢}}} = (1.0 + 0.41\ \eta^2)^{-2.0} \qquad 4.6$$

where $\eta = r/r_0$. The maximum error is 17%. For values of $\eta$ greater than 2.0 errors as large as 40% are not uncommon but these large radial locations are well outside of the WGS central core of fluid. The variable $r_0$ is the radial position where the axial velocity is equal to one half of the centerline velocity given by

$$V^* = \frac{V_z|_{\mathrm{¢}}}{V_0} = \exp(-(Z^{**})^{1.4}) \qquad 4.7$$

where

$$Z^{**} = z/D \Bigg/ \sqrt{\frac{\theta_0 Q}{D^3}} \qquad 4.8$$

and $V_0$ is the axial velocity along the centerline at the contraction given by

$$V_0 = 0.75\ \frac{3n'+1}{n'+1}\ (\frac{Q}{A}) \qquad 4.9$$

The derivatives of axial velocity with respect to axial location are in good agreement with experimental data.

The axial velocity profiles within the WGS core, defined by combining Equations 4.6, 4.7 and 4.9 are independent of reservoir size. Parameter $r_0$, however, depends on reservoir size. At a fixed flow rate, and at values of $Z^{**} > 0.40$, $r_0$ increases as reservoir size increases. Therefore, plots of $V_z$ versus r are not independent of reservoir size.

5.4 Mathematical simplifications (discussed in Appendix E. Section E.3), can be employed when predicting the magnitude and growth of normal stresses within the WGS core. These simplifications are:

(a) At flow rates approaching the upper limit of region I $\qquad V_r < V_z$

and $\qquad V_{r,z} + V_{z,r} \simeq V_{z,r}$

where < implies an order of magnitude.

(b) At the lower limit of region I

$$V_r \simeq V_z$$

and $\qquad V_{z,r} + V_{r,z} \simeq V_{z,r}$

Only within the immediate vicinity of the centerline (r<0.2D) can we assume $V_r < V_z$.

## 4.2 RECOMMENDATIONS

This author recommends the following:

1. Contraction losses and visual observations of the flow field be measured over a range of Reynolds numbers which overlap regions I, II, and III.

2. The Hencky strain measure be used as criterion for predicting parameters at the onset of flow instabilities.

3. Velocity profiles for flow rates within region I be measured for other polymer solutions that exhibit a characteristic WGS flow field and be compared with the predictions given by Equation 4.6, 4.7, 4.8, and 4.9.

4. The empirical relationship for axial velocity and the approximations for radial velocity be used to determine the magnitude and rate of growth of normal stresses within the entry region. Furthermore, the empirical relationship for axial velocity should be used with other initiation mechanisms.

5. The axial velocity component, $V_z$, be measured for axial locations less than $Z^{**}$ equal to 0.10 to supplement the limited data that the derivative of velocity with respect to axial position decreases to zero at the contraction.

6. That additional experimental data supplement the limited data in this research which lead to the assumption that parameter $b_1$ is independent of $N'_{Re}$ and n'.

7. That an empirical relationship between $r_0$ and independent parameters be found.

8. That a hydraulic cylinder (rigid plunger system) be used in place of inert gases in future experimental research.

9. That the direct method be used in future research when measuring velocity components.

# REFERENCES

## REFERENCES

1. Acierno, D., Titomanlio, G., and Nicodemo, L., paper presented at the 6th Congress International de Rheologie, Lyon, France, September (1972)
2. Arai, T., Rheol. Acta., 13, 359 (1974)
3. Arai, T., and Aoyama, H., Trans. Soc. Rheol., 7, 333 (1963)
4. Astarita, G., and Greco, G., Jr., Ind. Eng. Chem. Fundam., 7, 27 (1968)
5. Astarita, G., Greco, G., and Peluso, L., Ind. Eng. Chem. Fundam., 7, 595 (1968)
6. Atkinson, B., Brocklebank, M.P., Card, C.C.H., and Smith, J.M., A.I.Ch.E.J., 15, 548 (1969)
7. Atkinson, B., Kemblowski, Z., and Smith, J.M., A.I.Ch.E.J., 13, 17 (1967)
8. Bagley, E.B., Trans. Soc. Rheol., 5, 355 (1961)
9. Bagley, E.B., J. Appl. Phys., 28, 624 (1957)
10. Bagley, E.B., and Birks, A.M., J. Appl. Phys., 31, 556 (1960)
11. Balakrishnan, C., and Gordon, R.J., A.I.Ch.E.J., 21, 1225 (1975)
12. Ballenger, T.F., and White, J.L., J. Appl. Polym. Sci., 15, 1949 (1971)
13. Ballenger, T.F., et al., Trans. Soc. Rheol., 15, 195 (1971)

14. Ballman, R.L., Rademacher, L.E., and Farnham, W.H., Appl. Polym. Symp., 20 63 (1973)

15. Barnett, S.M., Polym. Eng. Sci., 7, 168 (1967)

16. Bartos, O., J. Appl. Phys., 35, 2767 (1964)

17. Bartos, O., and Holomek, J., Polym. Eng. Sci., 11, 324 (1971)

18. Benbow, J.J., and Lamb, P., S.P.E. Trans., 3, 7 (1963)

19. Bialas, G.A., and White, J.L., Rubber Chem. Technol., 42, 683 (1969), 42, 675 (1969); 42, 683 (1969)

20. Bird, R.B., Stewart, W.E., and Lightfoot, E.N., Transport Phenomena, John Wiley and Sons Inc., New York, (1965)

21. Black, J.R., Denn, M.M., and Hsiao, G.C., see Section 1 of Theoretical Rheology, edited by Hutton, J.F., et al., Applied Science Publishers Ltd., London (1975)

22. Blum, D., Private Communication

23. Blyler, L.L., Jr., and Hart, A.C., Jr., Polym. Eng. Sci., 10, 193 (1970)

24. Boger, D.V., and Rama Murthy, A.V., paper presented at the Cancam Conference, Calgary, Alberta, May (1971)

25. Boger, D.V., and Rama Murthy, A.V., Rheol. Acta., 11, 61 (1972)

26. Bogue, D.C., Ind. Eng. Chem., 51, 874 (1959)

27. Bogue, D.C., and White, J.L., AGARD-AG-144-70, July (1970)

28. Boles, R.L., Ph.D. Dissertation, The University of Tennessee, December (1967)

29. Boles, R.L., and Bogue, D.C., paper presented at 27th Annual Technical Conference, Society Plastics Engineers, May (1968)

30. Boles, R.L., Davis, H.L., and Bogue, D.C., Polym. Eng. Sci., 10, 24 (1970)

31. Bond, W.N., Proc. Phys. Soc., 33, 225 (1921)

32. Bond, W.N., ibid, 34, 139 (1922)

33. Boussinesq, J., Compt. Rend., 110, 1160, 1238, (1890)

34. Brenschede, E., and Klein, J., Rheol. Acta., 9, 130 (1970)

35. Campbell, W.D., and Slattery, J.C., Trans. A.S.M.E., J. Basic Eng., 85, Series D, 41 (1963)

36. Carter, T.R., Ph.D. Dissertation, University of Utah (1969)

37. Casey, J.O., Ph.D. Dissertation, University of Tennessee (1969)

38. Catania, P.J., M.Sc. Thesis, The University of Alberta, May (1969)

39. Chen, F.C., J. Appl. Polym. Sci., 16, 2175 (1972)

40. Chong, J.S., Christiansen, E.B., and Baer, A.D., J. Appl. Polym. Sci., 15, 369 (1971)

41. Christiansen, E.B., and Lemmon, H.E., A.I.Ch.E.J., 11, 995 (1965)

42. Christiansen, E.B., and Kelsey, S.J., A.I.Ch.E.J., 18, 713 (1972)

43. Christiansen, E.B., Kelsey, S.J., and Carter, T.R., A.I.Ch.E.J., 18, 372 (1972)

44. Clegg, P.L., The Rheology of Elastomers, edited by Mason P., and Wookey N., p. 174, Pergamon Press, New York, N.Y. (1958)

45. Collins, M., and Schowalter, W.R., A.I.Ch.E.J., 9, 804 (1963)

46. Cogswell, F.N., Polym. Eng. Sci., 12, 64 (1972)

47. Cogswell, F.N., Trans. Soc. Rheol., 16, 383 (1972)

48. Cogswell, F.N., and Lamb, P., Plast. Inst. Trans. J., 35, 809 (1967)

49. Datta, A.B., and Strauss, K., Rheol. Acta., 15, 283 (1976)

50. Day, D.R., M.Sc. Thesis, University of Toronto (1971)

51. Denn, M.M., and Marrucci, G., A.I.Ch.E.J., 14, 329 (1975)

52. Dennison, M.T., Plast. Inst. Trans. J., 35, 803 (1967)

53. den Otter, J.L., Rheol. Acta., 10, 200 (1971)

54. den Otter, J.L., Rheol. Acta., 14, 329 (1975)

55. Dodge, D.W., and Metzner, A.B., A.I.Ch.E.J., 5, 189 (1959)

56. Dorsey, N.E., Phys. Rev., 28, 833 (1926)

57. Duda, J.L., and Vrentas, J.S., Trans. Soc. Rheol., 17, 89 (1973)

58. Duvdenavi, I.J., and Klein, I., S.P.E.J., 23, 41 (1967)

59. Emery, A.F., and Chen, C.S., Trans. A.S.M.E., 35, 134 (1968)

60. Everage, A.E., Jr., and Ballman, R.L., J. Appl. Polym. Sci., 18, 933 (1974)

61. Fehn, G.M., Rheol. Acta., 13, 767 (1974)

62. Ferrari, G.A., Wire and Wire Prod., 39, 1036 (1964)

63. Fields, T.R., Jr., and Bogue, D.C., Trans. Soc. Rheol., 12, 39 (1968)

64. Forsyth, T.H., Polym. Plast. Technol. Eng., 6, 101 (1976)

65. Franklin, R.E., and Wallace, J.M., J. Fluid, Mech., 42, 33 (1970)

66. Giesekus, H., Rheol. Acta., 7, 127 (1968)

67. Giesekus, H., Rheol. Acta., 8, 411 (1969)

68. Haddow, J.B., Personal Communication

69. Hagenbach, see Goldstein, S., Modern Developments in Fluid Dynamics, Vol. 1, p. 300, Dover Publications Inc. (1965)

70. Hagler, G.E., Ph.D. Dissertation, University of Tennessee (1972)

71. Halmos, A.L., and Boger, D.V., Trans. Soc. Rheol., 20, 253 (1976)

72. Han, C.D., A.I.Ch.E.J., 17, 1480 (1971)

73. Han, C.D., A.I.Ch.E.J., 18, 116 (1972)

74. Han, C.D., J. Appl. Polym. Sci., 17, 1403 (1973)

75. Han, C.D., A.I.Ch.E.J., 19, 649 (1973)

76. Han, C.D., Trans. Soc. Rheol., 17, 375 (1973)

77. Han, C.D., Rheol. Acta., 14, 173 (1975)

78. Han, C.D., and Charles, M., A.I.Ch.E.J., 16, 499 (1970)

79. Han, C.D., and Kim, K.U., Trans. Soc. Rheol., 17, 151 (1973)

80. Han, C.D., and Lamonte, R.R., Polym. Eng. Sci., 11, 385 (1971)

81. Han, C.D., and Lamonte, R.R., J. Appl. Polym. Sci., 16, 3307 (1972)

82. Higashitani, K., and Lodge, A.S., Trans. Soc. Rheol., 19, 307 (1975)

83. Hlavacek, B., Personal Communication

84. Holmes, D.B., Ph.D. Dissertation, Delft (1967)

85. Howells, E.R., and Benbow, J.J., Plast. Inst. Trans. J., 30, 240 (1962)

86. Hosking, R., Philos. Mag., 18, 260 (1909)

87. Hudson, N.E., and Ferguson, J., Trans. Soc. Rheol., 20, 265 (1976)

88. Hürlimann, H.P., and Knappe, W., Rheol. Acta., 11, 292 (1972)

89. Huseby, T.W., Trans. Soc. Rheol., 10, 181 (1966)

90. Kanel, F.A., Ph.D. Dissertation, University of Delaware (1972)

91. Kawata, M., Kurase, K., and Yoshida, K., Rheol. Acta., 13, 757 (1974)

92. Kaye, S.E., Ph.D. Dissertation, Carnegie-Mellon University (1973)

93. Kaye, S.E., and Rosen, S.L., A.I.Ch.E.J., 17, 1269 (1971)

94. Kizior, T.E., M.Sc. Thesis, University of Alberta (1973)

95. Klein, J., and Fusser, H., Rheol. Acta., 7, 118 (1968)

96. Knibbs, G.H., Proc. R. Soc. N.S. Wales, 29, 77 (1895)

97. Kreith, F., and Eisenstadt, R., Trans. A.S.M.E., 79, 1070 (1957)

98. Kroesser, F.W., Ph.D. Dissertation, University of Rochester (1968)

99. Kraus, G., and Gruver, J.T., J. Polym. Sci., 2A, 797 (1964)

100. Langhaar, J., Appl. Mech., 9, No. 2A55-9 (1942)

101. La Nieve, H.L., III, M.Sc. Thesis, The University of Tennessee (1963)

102. La Nieve, H.L., III, and Bogue, D.C., J. Appl. Polym. Sci., 12, 353 (1968)

103. Lidorikis, S., and Vlachopoulos, J., paper presented at the 63rd A.I.Ch.E. meeting, Chicago (1970)

104. Lundgren, T.S., Sparrow, E.M., and Starr, J.B., J. Basic Eng., 86, 620 (1964)

105. Lupton, J.M., and Regester, J.W., Polym. Eng. Sci., 5, 235 (1965)

106. Lynch, M.D., and Huntsberger, D.V., Elements of Statistical Inference for Education and Psychology, Allyn and Bacon Inc., Boston (1976)

107. Maxwell, B., and Galt, J.C., J. Polym. Sci., 62, 550 (1962)

108. McHugh, T.W., Harrell, E.R., Powell, J.W., and Chartoff, R.P., Trans. Soc. Rheol., 16, 331 (1972)

109. McIntire, L.V., J. Appl. Poly. Sci., 16, 2901 (1972)

110. Meissner, J., Trans. Soc. Rheol., 16, 405 (1972)

111. Metzger, A.P., and Brodkey, R.S., J. Appl. Polym. Sci., 7, 399 (1963)

112. Metzger, A.P., and Knox, J.R., Trans. Soc. Rheol., 9, 13 (1965)

113. Metzner, A.B., and Reed, J.C., A.I.Ch.E.J., 1, 434 (1955)

114. Metzner, A.B., Carley, E.L., and Park, I.K., Mod. Plast., 38, 133 (1960)

115. Metzner, A.B., and Metzner, A.P., Rheol. Acta., 9, 174 (1970)

116. Metzner, A.B., Uebler, E.A., and Chan Man Fong, C.F., A.I.Ch.E.J., 15, 750 (1969)

117. Michiyoshi, L., Mizuno, K., and Hoshinai, Y., Int. Chem. Eng., 6, 373 (1966)

118. Middleman, S., The Flow of High Polymers; Continuum and Molecular Rheology, Interscience Pub., New York (1968)

119. Murch, R.E., Ph.D. Dissertation, University of Delaware (1970)

120. Myerholtz, R.W., J. Appl. Polym. Sci., 11, 687 (1967)

121. Nason, H.K., J. Appl. Phys., 16, 338 (1945)

122. Nicodemo, L., and Marrucci, G., J. Polym. Sci., 10, 1351 (1972)

123. Nakamura, R., et al., J. Chem. Eng. Japan, 9, 291 (1976)

124. Nikuradse, J., See Goldstein, S., Modern Developments in Fluid Dynamics, Vol. 1, p. 304, Dover Publications Inc. (1965)

125. Nishimura, J., and Oka, S., J. Phys. Soc. Japan, 20, 449 (1965)

126. Novotny, E.J., Jr., and Eckert, R.E., Trans. Soc. Rheol., 17, 227 (1973)

127. Oka, S., J. Phys. Soc. Japan, 19, 1481 (1964)

128. Okeson, J.K., and Emery, A.H., Jr., Trans. Soc. Rheol., 19, 81 (1975)

129. O'Casey, J.O., Jr., Ph.D. Dissertation, University of Tennessee (1969)

130. Oliver, D.R., and Bragg, R., Can. J. Chem. Eng., 51, 287 (1973)

131. Owczarek, J.A., Introduction to Fluid Mechanics, International Textbook Company, Scranton, Pa. (1968)

132. Oyanagi, Y., Appl. Polym. Symp., 20, 123 (1973)

133. Paul, D.R., and Southern, J.H., J. Appl. Polym. Sci., 19, 3375 (1975)

134. Pearson, J.R.A., Plast. Polym., 37, 285 (1969)

135. Pearson, J.R.A., and Petrie, C.J.S., Proc. Fourth Intern. Cong. Rheol., 3, 265 (1965)

136. Petrie, C.J.S., and Denn, M.M., A.I.Ch.E.J., 22, 209 (1976)

137. Philippoff, W., and Gaskins, F.H., Trans. Soc. Rheol., 2, 263 (1958)

138. Porteous, K.C., and Denn, M.M., Trans. Soc. Rheol., 16, 295 (1972)

139. Powell, R.J., Ph.D. Dissertation, University of Rochester (1968)

140. Prados, J.W., and Peebles, F.N., A.I.Ch.E.J., 5, 225 (1959)

141. Ram, A., and Narkis, M., J. Appl. Polym. Sci., 10, 361 (1966)

142. Rama Murthy, A.V., Trans. Soc. Rheol., 18, 431 (1974)

143. Rama Murthy, A.V., Trans. Soc. Rheol., 20, 503 (1976)

144. Rama Murthy, A.V., and Boger, D.V., Trans. Soc. Rheol., 15, 709 (1971)

145. Rivas, M.A., Jr., and Shapiro, A.H., Trans. A.S.M.E., 78, 489 (1956)

146. Roscoe, R., Philos. Mag., 40, 338 (1949)

147. Rothenberger, R., McCoy, D.H., and Denn, M.M., Trans. Soc. Rheol., 17, 259 (1973)

148. Schiller, L., see Goldstein, S., Modern Developments Fluid Dynamics, Vol. 1, p. 303, Dover Publications Inc. (1965)

149. Schmidt, F.W., and Wimmer, K., A.I.Ch.E.J., 17, 1248 (1971)

150. Schmidt, F.W., and Zeldin, B., A.I.Ch.E.J., 15, 612 (1969)

151. Schott, H., J. Polym. Sci., A2, 3791 (1964)

152. Schreiber, H.P., Bagley, E.B., and Birks, A.M., J. Appl. Polym. Sci., 4, 362 (1960)

153. Schulken, R.M., and Boy, R.E., S.P.E.J., 16, 423 (1960)

154. Seyer, F.A., and Catania, P.J., Paper presented at the 21st Canadian Chemical Engineering Conference, Montreal, October (1971)

155. Shaw, R., J. Fluid Mech., 7, 550 (1960)

156. Siegel, R., Sc. D. Thesis, M.I.T. (1953)

157. Southern, J.H., and Paul, D.R., Polym. Eng. Sci., 14, 560 (1974)

158. Spencer, R.S., and Dillon, R.E., J. Colloid Sci., 4, 241 (1949)

159. Sutterby, J.L., Trans. Soc. Rheol., 9, 227 (1965)

160. Swindles, J.F., Coe, J.R., and Godfrey, T.B., J. Res. Nat. Bur. Stand., 48, 1 (1952)

161. Sylvester, N.D., Ph.D. Dissertation, Carnegie-Mellon University, September (1968)

162. Sylvester, N.D., and Rosen, S.L., A.I.Ch.E.J., 16, 964 (1970)

163. Tanner, R.I., and Pipkin, A.C., Trans. Soc. Rheol., 13, 471 (1969)

164. Tomita, Y., Trans. Japan Soc. Mech. Eng., 25, 938 (1959)

165. Tomita, Y., Bull. Japan Soc. Mech. Eng., 4, 77 (1961)

166. Tomita, Y., Bull. Japan Soc. Mech. Eng., 5, 443 (1962)

167. Tomita, Y., J. Chem. Eng. Japan, 23, 525 (1969)

168. Tomita, Y., and Shimbo, T., Appl. Polym. Symp., 20, 137 (1973)

169. Tomita, Y., and Tsuchiya, K., Bull. Japan Soc. Mech. Eng., 6, 709 (1963)

170. Tordella, J.P., J. Appl. Phys., 27, 754 (1956)

171. Tordella, J.P., Rheol. Acta., 1, 216 (1958)

172. Tordella, J.P., J. Appl. Poly. Sci., 7, 215 (1963)

173. Uebler, E.A., Ph.D. Dissertation, University of Delaware (1966)

174. Ultman, J., and Denn, M.M., Paper presented at 40th Meeting, Society of Rheology, St. Paul, Minnesota, October (1969)

175. Vinogradov, G.V., Rheol. Acta., 12, 357 (1973)

176. Vinogradov, G.V., et al., Eur. Polym. J., 9, 1231 (1973)

177. Vlachopoulos, J., and Lidorikis, S., Polym. Eng. Sci., 11, 1 (1971)

178. Vlachopoulos, J., Horie, M., and Lidorikis, S., Trans. Soc. Rheol., 16, 669 (1972)

179. Vlachopoulos, J., and Alam, M., Polym. Eng. Sci., 12, 184 (1972)

180. Vrentas, J.S., and Duda, J.L., Appl. Sci. Res., 28, 241 (1973)

181. Wang, Y.L., and Longwell, P.A., A.I.Ch.E.J., 10, 323 (1964)

182. Westover, R.F., Polym. Eng. Sci., 6, 83 (1966)

183. Westover, R.F., and Maxwell, B., S.P.E.J., 13, 27 (1957)

184. Weinberger, C.B., Ph.D. Dissertation, University of Michigan (1970)

185. Weissberg, H.L., Phys. Fluids, 5, 1033 (1962)

186. Weltmann, R., and Keller, T., Natl. Advis. Comm. Aeronaut., TN 3889 (1957)

187. White, J.A., Appl. Polym. Symp., 20, 155 (1973)

188. White, J.A., and Kondo, A., Polym. Sci. Eng., Report No. 70 (1976)

189. White, J.L., and Metzner, A.B., A.I.Ch.E.J., 11, 324 (1965)

190. Williams, M.C., Ph.D. Dissertation, University of Wisconsin (1964)

# APPENDIX A

# CALIBRATION

## A.1 PRESSURE TRANSDUCERS

Three Pace pressure transducers with diaphragms of 1 p.s.i.g. (transducer 1), 10 p.s.i.g. (transducer 2), and 100 p.s.i.g. (transducer 3) were used in order to obtain more reliable data (pressures varied from $3 \times 10^4$ dyn/cm$^2$ to $6 \times 10^6$ dyn/cm$^2$). Each transducer was connected to a separate Sanborn preamplifier with the output voltage being recorded on a 10 inch Mosely strip chart recorder, Model 7100B. The range selector on the recorder was set at 5 volts full scale, i.e., 2 inch displacement per volt. The recorder's mechanical zero was set at 1 inch displacement. The gain on the preamplifier was adjusted so that a 2 volt signal would displace 4 inches on the recorder chart. With zero load on the transducers each electrical circuit was balanced. This procedure minimized the output voltage when the preamplifier attenuation setting decreased from X200 to X1. At X5 the output voltage for both transducers 1 and 2 was such that the displacement was greater than 9 inches, hence off scale. This resulted in the output voltage varying with preamplifier attenuation settings.

A water manometer was used to calibrate transducer 1, a mercury manometer for transducer 2, and a Ruska Dead Weight Tester, Model 2400 HL for transducer 3. A period of 10 minutes was allowed to elapse between consecutive readings to ensure that the upper and lower meniscuses in both manometers were stationary even after an incremental change in pressure. The calibration data are given in Tables A.1 to A.4.

Transducer 3 (calibration data in Table A.3) was used to obtain pressure data only for the sugar solution #1 and the Primol-355 oil. Due to damage to this transducer another was calibrated (data for transducer 4 given in Table A.4) to obtain pressure data for the remaining Newtonian solutions and the polymer solution.

To assess the presence of a hysteresis loop, the applied pressure was allowed to vary in small incremental steps from a maximum value determined by the transducer being calibrated to a minimum value (10% of the maximum) and then back to the maximum value again. The results showed, however, that the transducers exhibited little or no hysteresis.

## A.2 THRUST CALIBRATION

The thrust apparatus used in this research was described by Kizior (94). The output voltage corresponding to a given thrust, measured in grams, was recorded on a Hewlett Packard recorder (Model number 770213). The Sanborn preamplifier (Model number 8805A) had the gain set to a minimum and the calibration factor set at 200. The data tabulated in Table A.5 resulted in a sensitivity of 293.020 dyn/cm$^2$ per volt.

## A.3 CYLINDER AND INSTRON CALIBRATION

Two stainless steel cylinders, approximately 15.24 cm I.D. (cylinder 1) and 15.60 cm I.D. (cylinder 2) were used in this research. Cylinder 1 was used for all of the Newtonian runs while cylinder 2 was used for the remaining runs. At a synchronous setting of 1 cm/min, cylinders 1 and 2 resulted in measured flow rates of 3.030 and 3.177 $cm^3$/sec respectively. At crosshead speeds greater or less than 1 cm/sec the resultant flow rate was a multiple of the flow rate determined at the crosshead speed of 1 cm/sec. Measured flow rates agreed to within one half of one percent of these values.

The variable speed settings were calibrated by collecting and weighing an amount of water over a period of 15 minutes with the synchronous setting at 1 cm/min. The calibrated variable speed settings tabulated in Table A.6 were used in the calculation of flow rate with cylinder 1. After replacing the faulty tachometer no detectable errors were measured between the crosshead speed of the Instron tester and the variable speed settings.

## A.4 NORMAL FORCE SPRING

The calibration of the normal force spring used in the rheogoniometer to determine the first normal stress difference is given in Figure A.1. The resultant sensitivity is 194.040 dyn/$cm^2$ per volt at a temperature of 68 ± 1°F.

## A.5 ALUMINUM DUST PARTICLES

The thin, irregularly shaped dust particles used as the tracer was a commercial grade Baker aluminum, lot number 2347. The particle size distribution, plotted and shown in Figure A.2, was determined from a sample size of 200 particles using a microscope and a graduated screen.

Thirty-nine divisions of the graduated screen was equivalent to 30 microns at a magnification of 1000. An approximated relationship that seems to hold for a positively skewed distribution (106) is

$$\overline{Y} = \frac{3m-M}{2} \qquad \text{A.1}$$

where m is the median, M is the mode, and $\overline{Y}$ is the mean. Using this equation and the data in Figure A.2

$$\overline{Y} = \frac{3(11)-7.5}{2} \qquad \text{A.2}$$

gives the mean length of 13 microns. The maximum width of the particles was equal to 0.70 times the maximum length with the thickness estimated to be 1 micron. Therefore, the average volume of the aluminum dust particles was $118 \times 10^{-12}$ $cm^3$.

In summary, Appendix A contains the following tables and figures:

| TABLE NO. | DESCRIPTION |
|---|---|
| A.1 | Calibration of Transducer 1 |
| A.2 | Calibration of Transducer 2 |
| A.3 | Calibration of Transducer 3 |
| A.4 | Calibration of Transducer 4 |
| A.5 | Thrust Calibration |
| A.6 | Calibration For Variable Speed Setting |

| FIGURE NO. | |
|---|---|
| A-1 | Normal Force Spring Calibration |
| A-2 | Size Distribution of Aluminum Dust Particles |

## TABLE A.1

## CALIBRATION OF TRANSDUCER 1

$\rho = 0.9896$ gm/cm$^3$

| Pressure (in. water) | Preamp. attenuation | Preamp. Reading Volts @ X 1 |
|---|---|---|
| 29.57 | 200 | 94.00 |
| | 100 | 94.50 |
| | 50 | 92.75 |
| 28.72 | 200 | 88.50 |
| | 100 | 88.75 |
| | 50 | 87.125 |
| 26.64 | 200 | 80.00 |
| | 100 | 81.50 |
| | 50 | 80.50 |
| 24.64 | 200 | 74.50 |
| | 100 | 75.75 |
| | 50 | 74.75 |
| 22.48 | 200 | 68.00 |
| | 100 | 69.00 |
| | 50 | 68.00 |
| 20.64 | 200 | 61.00 |
| | 100 | 63.00 |
| | 50 | 61.375 |
| 18.48 | 200 | 55.00 |
| | 100 | 56.25 |
| | 50 | 55.625 |
| 16.28 | 200 | 48.00 |
| | 100 | 49.50 |
| | 50 | 49.125 |
| 14.44 | 200 | 42.00 |
| | 100 | 44.00 |
| | 50 | 43.50 |
| 12.74 | 100 | 38.50 |
| | 50 | 38.00 |
| 10.95 | 100 | 32.50 |
| | 50 | 32.75 |

TABLE A.1 (continued)

$\rho = 0.9896$ gm/cm$^3$

| Pressure (in. water) | Preamp. attenuation | Preamp. Reading Volts @ x 1 |
|---|---|---|
| 8.66 | 100 | 25.50 |
| | 50 | 26.00 |
| 6.67 | 100 | 19.50 |
| | 50 | 19.75 |
| 4.66 | 50 | 13.75 |
| | 20 | 12.75 |
| 2.89 | 20 | 7.90 |
| 3.66 | 20 | 10.00 |
| 4.91 | 20 | 13.50 |
| 5.55 | 20 | 15.20 |
| 6.69 | 50 | 20.25 |
| | 20 | 18.25 |
| 7.88 | 50 | 23.625 |
| | 20 | 21.30 |
| 9.64 | 100 | 29.25 |
| | 50 | 29.00 |
| 12.55 | 100 | 38.50 |
| | 50 | 37.625 |
| 14.84 | 200 | 44.00 |
| | 100 | 45.00 |
| | 50 | 44.75 |
| 17.20 | 200 | 51.50 |
| | 100 | 53.00 |
| | 50 | 52.00 |
| 18.55 | 200 | 56.00 |
| | 100 | 56.25 |
| | 50 | 56.00 |

TABLE A.1 (continued)

$\rho = 0.9896$ gm/cm$^3$

| Pressure (in. water) | Preamp. attenuation | Preamp. Reading Volts @ x 1 |
|---|---|---|
| 22.63 | 200 | 69.00 |
| | 100 | 69.75 |
| | 50 | 68.00 |
| 26.51 | 200 | 80.00 |
| | 100 | 81.00 |
| | 50 | 80.125 |
| 30.66 | 200 | 93.00 |
| | 100 | 95.00 |
| | 50 | 93.00 |
| 20.76 | 200 | 61.50 |
| | 100 | 62.50 |
| | 50 | 63.25 |

## TABLE A.2

## CALIBRATION OF TRANSDUCER 2

$\rho = 13.5201 \text{ gm/cm}^3$

| Pressure (in. mercury) | Preamp. Attenuation | Preamp. Reading Volts @ X1 |
|---|---|---|
| 1.86 | 100 | 23.25 |
| | 50 | 22.375 |
| 2.95 | 100 | 37.50 |
| | 50 | 36.875 |
| 4.04 | 100 | 50.75 |
| | 50 | 50.00 |
| 5.06 | 100 | 62.50 |
| | 50 | 61.25 |
| 6.21 | 100 | 77.50 |
| | 50 | 75.50 |
| 7.36 | 100 | 92.00 |
| | 50 | 90.00 |
| 8.89 | 100 | 110.50 |
| | 50 | 108.00 |
| 10.31 | 100 | 129.00 |
| | 50 | 125.75 |
| 11.92 | 100 | 149.50 |
| 14.13 | 100 | 177.00 |
| 16.36 | 100 | 205.50 |
| 18.12 | 100 | 229.00 |
| 19.80 | 100 | 250.50 |
| 20.30 | 100 | 257.25 |
| 18.14 | 100 | 230.00 |
| 16.71 | 100 | 211.00 |
| 15.55 | 100 | 196.00 |

TABLE A.2 (continued)

$\rho = 13.5201$ gm/cm$^3$

| Pressure (in. mercury) | Preamp. Attenuation | Preamp. Reading Volts @ X1 |
|---|---|---|
| 13.66 | 100 | 172.25 |
| 12.18 | 100 | 153.75 |
| 10.96 | 100 | 137.50 |
| | 50 | 134.75 |
| 9.89 | 100 | 124.50 |
| | 50 | 121.75 |
| 8.18 | 100 | 103.75 |
| | 50 | 101.50 |
| 6.43 | 100 | 80.75 |
| | 50 | 79.50 |
| 4.99 | 100 | 62.75 |
| | 50 | 61.625 |
| 4.24 | 100 | 53.50 |
| | 50 | 52.00 |
| 3.46 | 100 | 42.50 |
| | 50 | 41.75 |
| 3.00 | 100 | 37.50 |
| | 50 | 35.125 |
| 2.26 | 100 | 28.00 |
| | 50 | 27.50 |

## TABLE A.3

## CALIBRATION OF TRANSDUCER 3

Preamplifier Gain Setting: at X200 and 100 p.s.i.g. displaced 8.49 inches

| Pressure (p.s.i.g.) | Preamp. Attenuation | Preamp. Reading Volts @ X1 |
|---|---|---|
| 6.0 | 200 | 55.00 |
| | 100 | 55.00 |
| | 50 | 55.00 |
| 8.0 | 200 | 68.50 |
| | 100 | 68.00 |
| | 50 | 67.75 |
| 10.0 | 200 | 84.50 |
| | 100 | 85.00 |
| | 50 | 84.75 |
| 12.0 | 200 | 101.00 |
| | 100 | 101.00 |
| | 50 | 101.25 |
| 15.0 | 200 | 128.00 |
| | 100 | 127.25 |
| | 50 | 126.50 |
| 18.0 | 200 | 152.00 |
| | 100 | 153.00 |
| | 50 | 151.50 |
| 20.0 | 200 | 170.00 |
| | 100 | 169.75 |
| | 50 | 168.00 |
| 25.0 | 200 | 211.00 |
| | 100 | 211.50 |
| | 50 | 209.75 |
| 30.0 | 200 | 254.50 |
| | 100 | 254.00 |
| 35.0 | 200 | 297.50 |
| | 100 | 296.00 |
| 40.0 | 200 | 340.00 |
| | 100 | 338.00 |

### TABLE A.3 (continued)

Preamplifier Gain Setting: at X200 and 100 p.s.i.g. displaced 8.49 inches

| Pressure (p.s.i.g.) | Preamp. Attenuation | Preamp. Reading Volts @ X1 |
|---|---|---|
| 45.0 | 200 | 381.50 |
| | 100 | 380.00 |
| 50.0 | 200 | 423.00 |
| | 100 | 421.25 |
| 60.0 | 200 | 509.50 |
| 70.0 | 200 | 594.00 |
| 80.0 | 200 | 679.00 |
| 100.0 | 200 | 849.00 |
| 90.0 | 200 | 766.00 |
| 80.0 | 200 | 680.00 |
| 70.0 | 200 | 595.50 |
| 60.0 | 200 | 510.50 |
| 50.0 | 200 | 426.00 |
| 40.0 | 200 | 340.00 |
| | 100 | 339.75 |
| 30.0 | 200 | 256.00 |
| | 100 | 255.25 |
| 20.0 | 200 | 170.00 |
| | 100 | 170.50 |
| | 50 | 169.50 |
| 10.0 | 200 | 85.00 |
| | 100 | 85.50 |
| | 50 | 85.25 |

## TABLE A.4

## CALIBRATION OF TRANSDUCER 4

| Pressure (p.s.i.g.) | Preamp. Attenuation | Preamp. Reading Volts @ X1 |
|---|---|---|
| 6.0 | 50 | 33.25 |
| 10.0 | 100 | 55.00 |
| | 50 | 53.75 |
| 12.0 | 100 | 65.00 |
| | 50 | 63.75 |
| 14.0 | 100 | 75.00 |
| | 50 | 73.75 |
| 16.0 | 100 | 86.00 |
| | 50 | 84.00 |
| 18.0 | 100 | 96.50 |
| | 50 | 94.75 |
| 20.0 | 100 | 107.00 |
| | 50 | 104.50 |
| 30.0 | 100 | 159.00 |
| | 50 | 156.00 |
| 40.0 | 200 | 214.00 |
| | 100 | 212.00 |
| 50.0 | 200 | 267.00 |
| | 100 | 265.00 |
| 60.0 | 200 | 322.00 |
| 70.0 | 200 | 375.00 |
| 80.0 | 200 | 432.00 |
| 90.0 | 200 | 488.00 |
| 100.00 | 200 | 545.00 |
| 90.00 | 200 | 488.00 |
| 80.00 | 200 | 433.00 |
| 70.00 | 200 | 377.00 |

TABLE A.4 (continued)

| Pressure (p.s.i.g.) | Preamp. Attenuation | Preamp. Reading Volts @ X1 |
|---|---|---|
| 60.0 | 200 | 323.00 |
| 50.0 | 200 | 269.00 |
| 40.0 | 200 | 214.00 |
| | 100 | 213.50 |
| 30.0 | 200 | 160.00 |
| | 100 | 160.50 |
| | 50 | 157.50 |
| 20.0 | 200 | 107.00 |
| | 100 | 107.00 |
| | 50 | 106.00 |
| 10.0 | 100 | 55.00 |
| | 50 | 54.00 |
| 6.0 | 100 | 33.50 |
| | 50 | 33.25 |

## TABLE A.5

## THRUST CALIBRATION

| Thrust (grams) | Volts |
|---|---|
| 2.14 | 7.40 |
| 4.19 | 14.10 |
| 6.23 | 21.00 |
| 8.27 | 28.10 |
| 10.29 | 34.80 |
| 12.33 | 41.20 |
| 14.37 | 48.00 |
| 2.15 | 7.50 |
| 2.15 | 7.20 |
| 10.33 | 35.50 |
| 12.38 | 42.50 |

## TABLE A.6

## CALIBRATION FOR VARIABLE SPEED SETTING

| Setting | Corrected Setting |
|---|---|
| 0.4 | 0.4020 |
| 0.5 | 0.5022 |
| 0.6 | 0.6086 |
| 0.7 | 0.7029 |
| 0.8 | 0.8068 |
| 0.9 | 0.9091 |

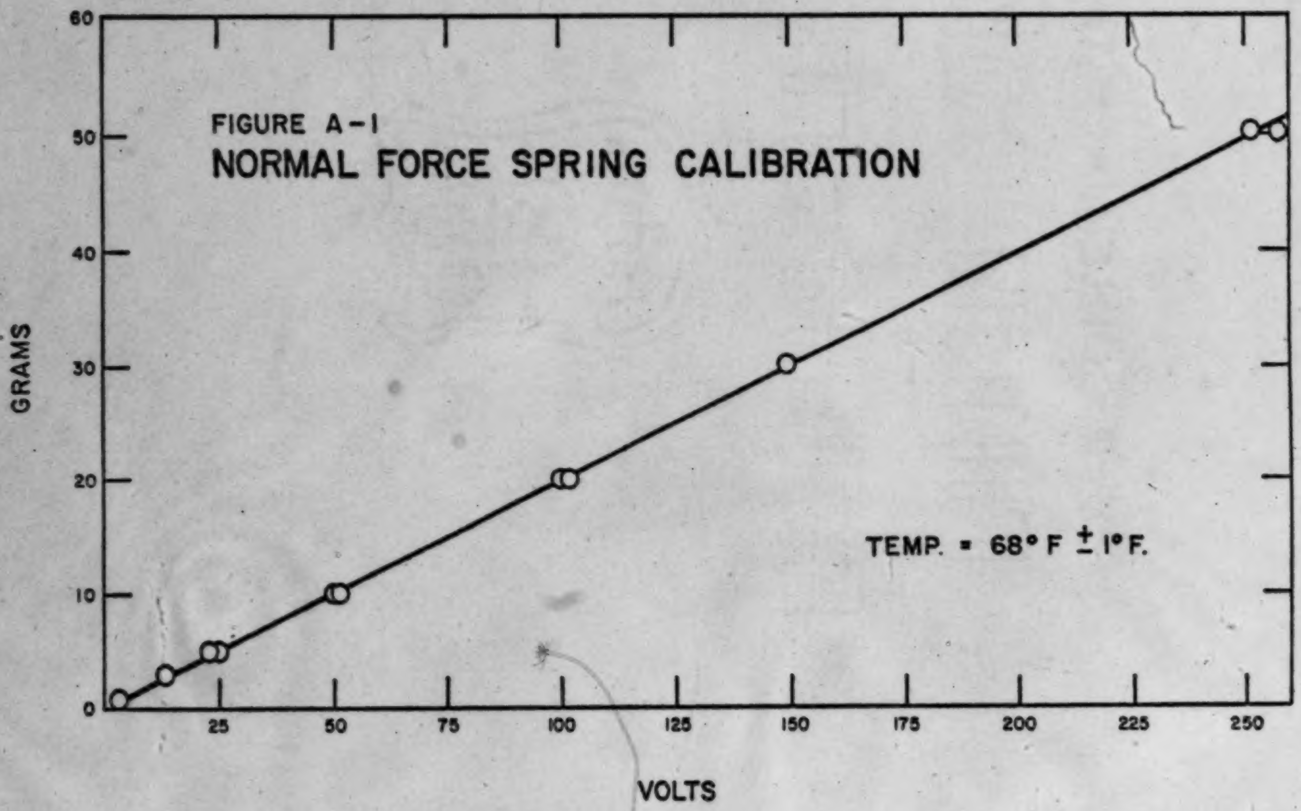

FIGURE A-1
NORMAL FORCE SPRING CALIBRATION

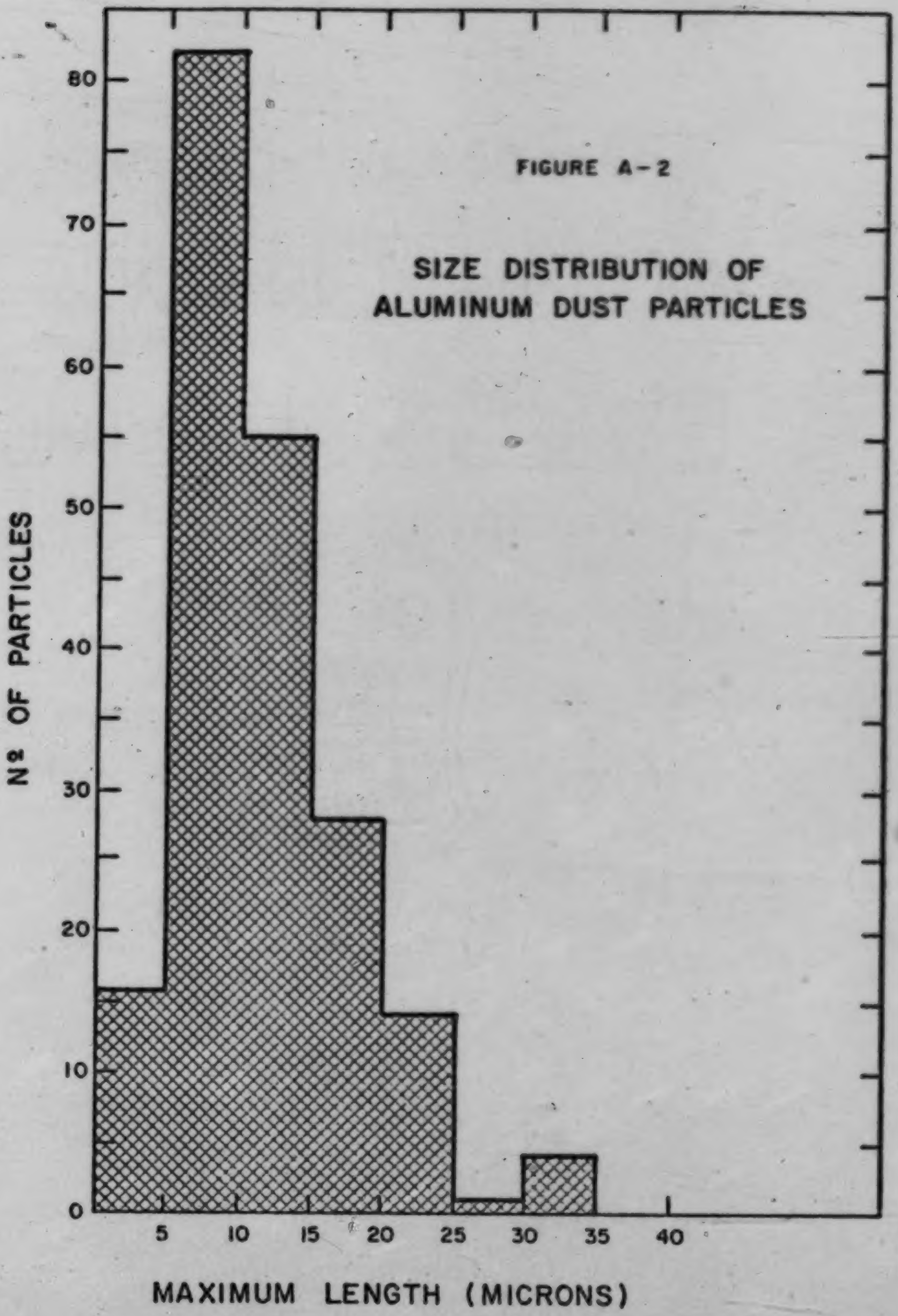

FIGURE A-2

SIZE DISTRIBUTION OF ALUMINUM DUST PARTICLES

# APPENDIX B

# TOTAL PRESSURE LOSS - L/D DATA

This appendix contains the total pressure loss-L/D data for the Newtonian solutions and the 0.20% solution of Separan AP-30. The pressure was measured at pressure taps located 10.2 cm and 27.9 cm upstream of the entrance of the capillary tube in reservoirs S and L respectively. The data were used in the construction of the Bagley plots (discussed in Chapter I, Section 1.1.3 and in Appendix C, Sections C.1 and C.2). The pressure correction value given in each table accounts for the fact that the centers of the capillary tube and the transducer were not in the same plane. Since these correction factors do not affect the slope of the Bagley plots they have to be added only to the intercept in order to obtain the true value for the contraction losses.

The contraction losses and shear stresses obtained from the Bagley plots are given in Appendices C and D respectively. The shear stresses obtained from the Bagley plots and the rheogoniometer were compared at low apparent shear rates. At these shear rates the contraction losses were too small to be measured accurately and were negligible when compared to the total pressure losses measured at large L/D ratios. Therefore, for run numbers 15 to 22 (inclusive) in Table B.9, 14 to 17 (inclusive) in Table B.10, and 17 to 29 (inclusive) in Table B.11 the total pressure losses were measured only at ratios L/D=305.08 in Table B.9, L/D=304.95 in Table B.10, and L/D=304.83 in Table B.11.

Pressure fluctuations were measurable beyond certain flow rates. The pressure fluctuations measured in reservoir

S for several tube lengths of each of the three capillary tubes are reported and discussed in Chapter III, Section 3.2.2. The pressure fluctuations in reservoir L for the same capillary tubes are plotted in Figures B.1 to B.3.

The following lists the order in which the data appear in this appendix:

| TABLE NO. | SOLUTION | CAPILLARY I.D. (cm) | RESERVOIR |
|---|---|---|---|
| B-1 | SUGAR #1 | 0.20 | SMALL |
| B-2 | SUGAR #3 | 0.20 | SMALL |
| B-3 | SUGAR #4 | 0.20 | SMALL |
| B-4 | PRIMOL-355 | 0.20 | SMALL |
| B-5 | SUGAR #1 | 0.20 | LARGE |
| B-6 | SUGAR #3 | 0.20 | LARGE |
| B-7 | SUGAR #4 | 0.20 | LARGE |
| B-8 | PRIMOL-355 | 0.20 | LARGE |
| B-9 | 0.20% SEPARAN AP-30 | 0.10 | SMALL |
| B-10 | | 0.20 | SMALL |
| B-11 | | 0.30 | SMALL |
| B-12 | 0.20% SEPARAN AP-30 | 0.10 | LARGE |
| B-13 | | 0.20 | LARGE |
| B-14 | | 0.30 | LARGE |

## TABLE B-1

## TOTAL PRESSURE LOSS - L/D DATA: SUGAR SOLUTION #1, 0.20 cm I.D. CAPILLARY TUBE, SMALL RESERVOIR

Temp.: 72.5°F

Pressure Correction:
$-.448 \times 10^4$ dyn/cm$^2$

| Run | Trans-ducer | Attenua-tion | Pressure $\times 10^4$ (dyn/cm$^2$) | Flow (cc/sec) | L/D |
|---|---|---|---|---|---|
| 1 | 1 | 50 | 3.089 | 1.515 | 31.60 |
| 2 | 1 | 50 | 4.688 | 2.285 | 31.60 |
| 3 | 2 | 20 | 6.378 | 3.030 | 31.60 |
| 4 | 2 | 50 | 14.203 | 6.080 | 31.60 |
| 5 | 2 | 100 | 24.924 | 9.193 | 31.60 |
| 6 | 2 | 100 | 37.748 | 12.187 | 31.60 |
| 7 | 2 | 100 | 52.227 | 15.090 | 31.60 |
| 8 | 3 | 50 | 70.671 | 18.386 | 31.60 |
| 1 | 2 | 100 | 6.074 | 1.515 | 71.23 |
| 2 | 2 | 20 | 8.791 | 2.285 | 71.23 |
| 3 | 2 | 20 | 11.790 | 3.030 | 71.23 |
| 4 | 2 | 50 | 25.338 | 6.080 | 71.23 |
| 5 | 2 | 100 | 42.265 | 9.193 | 71.23 |
| 6 | 2 | 100 | 61.535 | 12.187 | 71.23 |
| 7 | 3 | 50 | 81.357 | 15.090 | 71.23 |
| 8 | 3 | 50 | 108.592 | 18.386 | 71.23 |
| 1 | 2 | 20 | 7.722 | 1.515 | 96.38 |
| 2 | 2 | 50 | 11.549 | 2.285 | 96.38 |
| 3 | 2 | 50 | 15.272 | 3.030 | 96.38 |
| 4 | 2 | 100 | 32.474 | 6.080 | 96.38 |
| 5 | 2 | 100 | 53.060 | 9.193 | 96.38 |
| 6 | 3 | 50 | 76.531 | 12.187 | 96.38 |
| 7 | 3 | 50 | 100.663 | 15.090 | 96.38 |
| 8 | 3 | 50 | 130.310 | 18.386 | 96.38 |
| 1 | 2 | 50 | 16.375 | 1.515 | 222.36 |
| 2 | 2 | 100 | 24.476 | 2.285 | 222.36 |
| 3 | 2 | 100 | 32.577 | 3.030 | 222.36 |
| 4 | 3 | 50 | 67.568 | 6.080 | 222.36 |
| 5 | 3 | 50 | 108.247 | 9.193 | 222.36 |
| 6 | 3 | 50 | 148.581 | 12.187 | 222.36 |
| 7 | 3 | 100 | 189.604 | 15.090 | 222.36 |
| 8 | 3 | 100 | 237.867 | 18.386 | 222.36 |

## TABLE B-2

## TOTAL PRESSURE LOSS - L/D DATA: SUGAR SOLUTION #3, 0.20 cm I.D. CAPILLARY TUBE, SMALL RESERVOIR

Temp.: 72.10°F

Pressure Correction: $-.462 \times 10^4$ dyn/cm$^2$

| Run | Transducer | Attenuation | Pressure $\times 10^{-4}$ (dyn/cm$^2$) | Flow (cc/sec) | L/D |
|---|---|---|---|---|---|
| 1 | 1 | 100 | 3.999 | 1.060 | 31.60 |
| 2 | 1 | 100 | 5.516 | 1.515 | 31.60 |
| 3 | 2 | 20 | 7.136 | 1.975 | 31.60 |
| 4 | 2 | 50 | 8.963 | 2.440 | 31.60 |
| 5 | 2 | 50 | 14.824 | 3.970 | 31.60 |
| 6 | 2 | 50 | 23.994 | 6.080 | 31.60 |
| 7 | 2 | 100 | 35.680 | 8.425 | 31.60 |
| 8 | 2 | 100 | 48.711 | 10.650 | 31.60 |
| 9 | 4 | 50 | 64.465 | 13.800 | 31.60 |
| 10 | 4 | 50 | 109.488 | 19.750 | 31.60 |
| 1 | 2 | 20 | 7.860 | 1.060 | 71.23 |
| 2 | 2 | 20 | 11.032 | 1.515 | 71.23 |
| 3 | 2 | 50 | 14.286 | 1.975 | 71.23 |
| 4 | 2 | 50 | 18.064 | 2.440 | 71.23 |
| 5 | 2 | 50 | 29.475 | 3.970 | 71.23 |
| 6 | 2 | 100 | 47.056 | 6.080 | 71.23 |
| 7 | 4 | 100 | 66.706 | 8.425 | 71.23 |
| 8 | 4 | 50 | 84.460 | 10.650 | 71.23 |
| 9 | 4 | 50 | 115.486 | 13.800 | 71.23 |
| 10 | 4 | 100 | 185.467 | 19.750 | 71.23 |
| 1 | 2 | 50 | 10.342 | 1.060 | 96.38 |
| 2 | 2 | 50 | 14.617 | 1.515 | 96.38 |
| 3 | 2 | 50 | 18.788 | 1.975 | 96.38 |
| 4 | 2 | 100 | 23.545 | 2.440 | 96.38 |
| 5 | 2 | 100 | 38.266 | 3.970 | 96.38 |
| 6 | 2 | 100 | 60.294 | 6.080 | 96.38 |
| 7 | 4 | 50 | 82.736 | 8.425 | 96.38 |
| 8 | 4 | 50 | 108.592 | 10.650 | 96.38 |
| 9 | 4 | 50 | 146.857 | 13.800 | 96.38 |
| 10 | 4 | 100 | 229.594 | 19.750 | 96.38 |

TABLE B.2 (continued)

| Run | Transducer | Attenuation | Pressure x10$^{-4}$ (dyn/cm$^2$) | Flow (cc/sec) | L/D |
|---|---|---|---|---|---|
| 1 | 2 | 50 | 15.168 | 1.060 | 148.45 |
| 2 | 2 | 50 | 21.511 | 1.515 | 148.45 |
| 3 | 2 | 100 | 27.958 | 1.975 | 148.45 |
| 4 | 2 | 100 | 34.991 | 2.440 | 148.45 |
| 5 | 2 | 100 | 57.571 | 3.970 | 148.45 |
| 6 | 4 | 50 | 86.873 | 6.080 | 148.45 |
| 7 | 4 | 50 | 122.726 | 8.425 | 148.45 |
| 8 | 4 | 50 | 160.647 | 10.650 | 148.45 |
| 9 | 4 | 100 | 213.736 | 13.800 | 148.45 |
| 10 | 4 | 200 | 325.430 | 19.750 | 148.45 |

## TABLE B-3

## TOTAL PRESSURE LOSS - L/D DATA: SUGAR SOLUTION #4, 0.20 cm I.D. CAPILLARY TUBE, SMALL RESERVOIR

Temp.: 71.50°F

Pressure Correction: $-.490 \times 10^4$ dyn/cm$^2$

| Run | Transducer | Attenuation | Pressure x$10^{-4}$ (dyn/cm$^2$) | Flow (cc/sec) | L/D |
|---|---|---|---|---|---|
| 1 | 2 | 100 | 17.409 | 1.515 | 31.60 |
| 2 | 2 | 100 | 22.753 | 1.975 | 31.60 |
| 3 | 2 | 100 | 27.820 | 2.440 | 31.60 |
| 4 | 2 | 100 | 34.645 | 3.030 | 31.60 |
| 5 | 2 | 100 | 43.954 | 3.800 | 31.60 |
| 6 | 2 | 100 | 46.677 | 4.565 | 31.60 |
| 1 | 2 | 100 | 37.231 | 1.515 | 71.23 |
| 2 | 2 | 100 | 47.367 | 1.975 | 71.23 |
| 3 | 2 | 100 | 59.984 | 2.440 | 71.23 |
| 4 | 4 | 50 | 71.705 | 3.030 | 71.23 |
| 5 | 4 | 50 | 90.665 | 3.800 | 71.23 |
| 6 | 4 | 50 | 109.281 | 4.565 | 71.23 |
| 1 | 2 | 100 | 48.952 | 1.515 | 96.38 |
| 2 | 2 | 100 | 63.638 | 1.975 | 96.38 |
| 3 | 4 | 50 | 75.152 | 2.440 | 96.38 |
| 4 | 4 | 50 | 94.802 | 3.030 | 96.38 |
| 5 | 4 | 50 | 118.934 | 3.800 | 96.38 |
| 6 | 4 | 100 | 144.099 | 4.565 | 96.38 |
| 1 | 4 | 50 | 73.773 | 1.515 | 148.45 |
| 2 | 4 | 50 | 94.802 | 1.975 | 148.45 |
| 3 | 4 | 50 | 118.934 | 2.440 | 148.45 |
| 4 | 4 | 100 | 148.581 | 3.030 | 148.45 |
| 5 | 4 | 100 | 179.262 | 3.800 | 148.45 |
| 6 | 4 | 100 | 219.251 | 4.565 | 148.45 |

## TABLE B-4

## TOTAL PRESSURE LOSS - L/D DATA: PRIMOL-355 OIL, 0.20 cm I.D. CAPILLARY TUBE, SMALL RESERVOIR

Temp.: 73.0°F

Pressure Correction:
$-.331 \times 10^4$ dyn/cm$^2$

| Run | Transducer | Attenuation | Pressure x10$^{-4}$ (dyn/cm$^2$) | Flow (cc/sec) | L/D |
|---|---|---|---|---|---|
| 1 | 2 | 50 | 24.407 | 0.758 | 34.99 |
| 2 | 2 | 50 | 33.991 | 1.060 | 34.99 |
| 2 | 2 | 100 | 34.060 | 1.060 | 34.99 |
| 3 | 2 | 100 | 48.125 | 1.515 | 34.99 |
| 3 | 3 | 50 | 47.573 | 1.515 | 34.99 |
| 4 | 3 | 50 | 73.773 | 2.285 | 34.99 |
| 5 | 3 | 100 | 96.526 | 3.030 | 34.99 |
| 6 | 3 | 50 | 116.176 | 3.636 | 34.99 |
| 7 | 3 | 50 | 136.170 | 4.242 | 34.99 |
| 1 | 3 | 50 | 48.952 | 0.758 | 71.23 |
| 2 | 3 | 50 | 67.568 | 1.060 | 71.23 |
| 3 | 3 | 50 | 98.043 | 1.515 | 71.23 |
| 4 | 3 | 50 | 146.857 | 2.285 | 71.23 |
| 5 | 3 | 100 | 195.120 | 3.030 | 71.23 |
| 6 | 3 | 100 | 236.143 | 3.636 | 71.23 |
| 7 | 3 | 100 | 274.064 | 4.242 | 71.23 |
| 1 | 3 | 50 | 65.844 | 0.758 | 96.38 |
| 2 | 3 | 50 | 92.044 | 1.060 | 96.38 |
| 3 | 3 | 50 | 126.518 | 1.515 | 96.38 |
| 4 | 3 | 100 | 191.328 | 2.285 | 96.38 |
| 5 | 3 | 100 | 251.657 | 3.030 | 96.38 |
| 6 | 3 | 100 | 303.367 | 3.636 | 96.38 |
| 7 | 3 | 200 | 351.630 | 4.242 | 96.38 |
| 1 | 3 | 50 | 101.352 | 0.758 | 151.00 |
| 2 | 3 | 50 | 139.962 | 1.060 | 151.00 |
| 3 | 3 | 100 | 198.567 | 1.515 | 151.00 |
| 4 | 3 | 100 | 295.783 | 2.285 | 151.00 |
| 5 | 3 | 200 | 392.998 | 3.030 | 151.00 |
| 6 | 3 | 200 | 467.116 | 3.636 | 151.00 |
| 7 | 3 | 200 | 544.681 | 4.242 | 151.00 |
| 1 | 3 | 50 | 143.410 | 0.758 | 222.36 |
| 2 | 3 | 100 | 203.394 | 1.060 | 222.36 |
| 3 | 3 | 100 | 287.854 | 1.515 | 222.36 |
| 4 | 3 | 200 | 436.090 | 2.285 | 222.36 |

## TABLE B-5

## TOTAL PRESSURE LOSS - L/D DATA: SUGAR SOLUTION #1, 0.20 cm I.D. CAPILLARY TUBE, LARGE RESERVOIR

Temp.: 73.0°F

Pressure Correction:
$-2.427 \times 10^{4}$ dyn/cm$^{2}$

| Run | Transducer | Attenuation | Pressure x10$^{-4}$ (dyn/cm$^{2}$) | Flow (cc/sec) | L/D |
|---|---|---|---|---|---|
| 1 | 1 | 50 | 5.364 | 1.515 | 34.99 |
| 2 | 1 | 100 | 6.998 | 2.285 | 34.99 |
| 3 | 2 | 20 | 8.480 | 3.030 | 34.99 |
| 4 | 2 | 50 | 16.892 | 6.080 | 34.99 |
| 5 | 2 | 50 | 27.579 | 9.193 | 34.99 |
| 6 | 2 | 100 | 40.506 | 12.187 | 34.99 |
| 7 | 2 | 100 | 55.709 | 15.090 | 34.99 |
| 8 | 3 | 50 | 73.084 | 18.386 | 34.99 |
| 1 | 2 | 20 | 7.791 | 1.515 | 71.23 |
| 2 | 2 | 20 | 10.025 | 2.285 | 71.23 |
| 3 | 2 | 20 | 13.514 | 3.030 | 71.23 |
| 4 | 2 | 50 | 26.751 | 6.080 | 71.23 |
| 5 | 2 | 100 | 42.920 | 9.193 | 71.23 |
| 6 | 2 | 100 | 61.225 | 12.187 | 71.23 |
| 7 | 3 | 50 | 81.357 | 15.090 | 71.23 |
| 8 | 3 | 100 | 105.144 | 18.386 | 71.23 |
| 1 | 2 | 20 | 9.308 | 1.515 | 96.38 |
| 2 | 2 | 20 | 12.928 | 2.285 | 96.38 |
| 3 | 2 | 50 | 16.685 | 3.030 | 96.38 |
| 4 | 2 | 100 | 33.267 | 6.080 | 96.38 |
| 5 | 2 | 100 | 52.744 | 9.193 | 96.38 |
| 6 | 3 | 50 | 74.807 | 12.187 | 96.38 |
| 7 | 3 | 50 | 99.973 | 15.090 | 96.38 |
| 8 | 3 | 50 | 126.862 | 18.386 | 96.38 |
| 1 | 2 | 50 | 18.271 | 1.515 | 222.36 |
| 2 | 2 | 50 | 26.338 | 2.285 | 222.36 |
| 3 | 2 | 100 | 34.336 | 3.030 | 222.36 |
| 4 | 2 | 100 | 69.292 | 6.080 | 222.36 |
| 5 | 3 | 50 | 108.592 | 9.193 | 222.36 |
| 6 | 3 | 50 | 148.926 | 12.187 | 222.36 |
| 7 | 3 | 100 | 191.190 | 15.090 | 222.36 |
| 8 | 3 | 100 | 237.178 | 18.386 | 222.36 |

## TABLE B-6

## TOTAL PRESSURE LOSS - L/D DATA: SUGAR SOLUTION #3, 0.20 cm I.D. CAPILLARY TUBE, LARGE RESERVOIR

Temp.: 72.0°F

Pressure Correction:
$-2.517 \times 10^4$ dyn/cm$^2$

| Run | Transducer | Attenuation | Pressure x$10^{-4}$ (dyn/cm$^2$) | Flow (cc/sec) | L/D |
|---|---|---|---|---|---|
| 2 | 2 | 50 | 7.584 | 1.515 | 31.60 |
| 3 | 2 | 50 | 9.135 | 1.975 | 31.60 |
| 4 | 2 | 50 | 10.825 | 2.440 | 31.60 |
| 5 | 2 | 50 | 15.927 | 3.970 | 31.60 |
| 6 | 2 | 50 | 26.131 | 6.080 | 31.60 |
| 7 | 2 | 100 | 37.576 | 8.425 | 31.60 |
| 2 | 2 | 50 | 13.169 | 1.515 | 71.23 |
| 3 | 2 | 50 | 16.409 | 1.975 | 71.23 |
| 4 | 2 | 50 | 19.788 | 2.440 | 71.23 |
| 5 | 2 | 100 | 29.647 | 3.970 | 71.23 |
| 6 | 2 | 100 | 48.504 | 6.080 | 71.23 |
| 7 | 2 | 100 | 68.395 | 8.425 | 71.23 |
| 2 | 2 | 50 | 16.720 | 1.515 | 96.38 |
| 3 | 2 | 50 | 21.029 | 1.975 | 96.38 |
| 4 | 2 | 100 | 25.304 | 2.440 | 96.38 |
| 5 | 2 | 100 | 38.403 | 3.970 | 96.38 |
| 6 | 2 | 100 | 62.363 | 6.080 | 96.38 |
| 7 | 4 | 50 | 84.115 | 8.425 | 96.48 |
| 2 | 2 | 100 | 23.994 | 1.515 | 148.45 |
| 3 | 2 | 100 | 30.337 | 1.975 | 148.45 |
| 4 | 2 | 100 | 36.714 | 2.440 | 148.45 |
| 5 | 2 | 100 | 56.261 | 3.970 | 148.45 |
| 6 | 4 | 50 | 88.252 | 6.080 | 148.45 |
| 7 | 4 | 50 | 124.105 | 8.425 | 148.45 |

# TABLE B-7

## TOTAL PRESSURE LOSS - L/D DATA: SUGAR SOLUTION #4, 0.20 cm I.D. CAPILLARY TUBE, LARGE RESERVOIR

Temp.: 72.0°F

Pressure Correction: $-2.517 \times 10^4$ dyn/cm$^2$

| Run | Transducer | Attenuation | Pressure $\times 10^{-4}$ (dyn/cm$^2$) | Flow (cc/sec) | L/D |
|---|---|---|---|---|---|
| 1 | 2 | 100 | 18.409 | 1.515 | 31.60 |
| 2 | 2 | 100 | 23.270 | 1.975 | 31.60 |
| 3 | 2 | 100 | 28.165 | 2.440 | 31.60 |
| 4 | 2 | 100 | 34.577 | 3.030 | 31.60 |
| 5 | 2 | 100 | 43.264 | 3.800 | 31.60 |
| 6 | 2 | 100 | 52.917 | 4.565 | 31.60 |
| 1 | 2 | 100 | 33.887 | 1.515 | 71.23 |
| 2 | 2 | 100 | 45.643 | 1.975 | 71.23 |
| 3 | 2 | 100 | 55.847 | 2.440 | 71.23 |
| 4 | 2 | 100 | 68.947 | 3.030 | 71.23 |
| 5 | 4 | 50 | 86.184 | 3.800 | 71.23 |
| 6 | 4 | 50 | 105.489 | 4.565 | 71.23 |
| 1 | 2 | 100 | 46.126 | 1.515 | 96.38 |
| 2 | 2 | 100 | 59.639 | 1.975 | 96.38 |
| 3 | 4 | 50 | 70.671 | 2.440 | 96.38 |
| 4 | 4 | 50 | 88.252 | 3.030 | 96.38 |
| 5 | 4 | 50 | 111.349 | 3.800 | 96.38 |
| 6 | 4 | 50 | 134.447 | 4.565 | 96.38 |
| 1 | 4 | 50 | 68.947 | 1.515 | 148.45 |
| 2 | 4 | 50 | 89.631 | 1.975 | 148.45 |
| 3 | 4 | 50 | 110.315 | 2.440 | 148.45 |
| 4 | 4 | 50 | 138.583 | 3.030 | 148.45 |
| 5 | 4 | 100 | 173.746 | 3.800 | 148.45 |
| 6 | 4 | 100 | 208.909 | 4.565 | 148.45 |

## TABLE B-8

## TOTAL PRESSURE LOSS - L/D DATA: PRIMOL-355-OIL, 0.20 cm I.D. CAPILLARY TUBE, LARGE RESERVOIR

Temp.: 73.5°F

Pressure Correction: $-1.779 \times 10^4$ dyn/cm$^2$

| Run | Transducer | Attenuation | Pressure x10$^{-4}$ (dyn/cm$^2$) | Flow (cc/sec) | L/D |
|---|---|---|---|---|---|
| 1 | 2 | 50 | 24.683 | 0.762 | 34.99 |
| 2 | 2 | 50 | 33.819 | 1.066 | 34.99 |
| 3 | 2 | 100 | 47.436 | 1.515 | 34.99 |
| 4 | 3 | 50 | 71.420 | 2.285 | 34.99 |
| 5 | 3 | 50 | 94.457 | 3.030 | 34.99 |
| 6 | 3 | 50 | 113.073 | 3.704 | 34.99 |
| 7 | 3 | 50 | 132.516 | 4.277 | 34.99 |
| 1 | 3 | 50 | 47.229 | 0.762 | 71.23 |
| 2 | 3 | 50 | 66.534 | 1.066 | 71.23 |
| 3 | 3 | 50 | 94.457 | 1.515 | 71.23 |
| 4 | 3 | 50 | 142.376 | 2.285 | 71.23 |
| 5 | 3 | 100 | 186.157 | 3.030 | 71.23 |
| 1 | 2 | 100 | 47.987 | 0.762 | 71.23 |
| 6 | 3 | 100 | 222.699 | 3.704 | 71.23 |
| 7 | 3 | 100 | 258.551 | 4.242 | 71.23 |
| 1 | 3 | 50 | 63.914 | 0.762 | 96.38 |
| 2 | 3 | 50 | 86.873 | 1.066 | 96.38 |
| 3 | 3 | 50 | 122.381 | 1.515 | 96.38 |
| 4 | 3 | 100 | 187.708 | 2.285 | 96.38 |
| 5 | 3 | 100 | 244.762 | 3.030 | 96.38 |
| 1 | 3 | 50 | 102.042 | 0.762 | 160.16 |
| 2 | 3 | 50 | 142.720 | 1.066 | 160.16 |
| 3 | 3 | 100 | 198.223 | 1.515 | 160.16 |

## TABLE B-9

### TOTAL PRESSURE LOSS - L/D DATA: 0.20% SEPARAN AP-30, 0.10 cm I.D. CAPILLARY TUBE, SMALL RESERVOIR

Temp.: 68°F

Pressure Correction
$-1.669 \times 10^4$ dyn/cm$^2$

| Run | Trans-ducer | Attenua-tion | Pressure, $\times 10^{-4}$ (dyn/cm$^2$) | Flow (cc/sec) | L/D |
|---|---|---|---|---|---|
| 1 | 2 | 50 | 21.822 | 0.318 | 222.08 |
| 2 | 2 | 50 | 24.338 | 0.381 | 222.08 |
| 3 | 2 | 50 | 29.372 | 0.508 | 222.08 |
| 4 | 2 | 100 | 34.129 | 0.635 | 222.08 |
| 5 | 2 | 100 | 40.196 | 0.794 | 222.08 |
| 6 | 2 | 100 | 46.022 | 0.953 | 222.08 |
| 7 | 2 | 100 | 51.883 | 1.112 | 222.08 |
| 8 | 2 | 100 | 56.778 | 1.271 | 222.08 |
| 9 | 2 | 100 | 64.569 | 1.430 | 222.08 |
| 9 | 4 | 50 | 70.326 | 1.430 | 222.08 |
| 10 | 4 | 50 | 77.221 | 1.589 | 222.08 |
| 11 | 4 | 50 | 85.839 | 1.747 | 222.08 |
| 12 | 4 | 50 | 93.078 | 1.908 | 222.08 |
| 13 | 4 | 50 | 105.489 | 2.224 | 222.08 |
| 14 | 4 | 50 | 128.241 | 2.701 | 222.08 |
| 1 | 2 | 50 | 15.685 | 0.318 | 148.48 |
| 2 | 2 | 50 | 17.513 | 0.381 | 148.48 |
| 3 | 2 | 50 | 21.029 | 0.508 | 148.48 |
| 4 | 2 | 50 | 24.338 | 0.635 | 148.48 |
| 5 | 2 | 100 | 28.613 | 0.794 | 148.48 |
| 6 | 2 | 100 | 33.267 | 0.953 | 148.48 |
| 7 | 2 | 100 | 37.404 | 1.112 | 148.48 |
| 8 | 2 | 100 | 41.885 | 1.271 | 148.48 |
| 9 | 2 | 100 | 48.814 | 1.430 | 148.48 |
| 9 | 2 | 100 | 53.606 | 1.430 | 148.48 |
| 10 | 2 | 100 | 59.708 | 1.589 | 148.48 |
| 11 | 2 | 100 | 66.534 | 1.747 | 148.48 |
| 12 | 4 | 50 | 72.050 | 1.908 | 148.48 |
| 13 | 4 | 50 | 84.115 | 2.224 | 148.48 |
| 14 | 4 | 50 | 102.731 | 2.701 | 148.48 |
| 1 | 2 | 50 | 11.376 | 0.318 | 96.45 |
| 2 | 2 | 50 | 12.755 | 0.381 | 96.45 |
| 3 | 2 | 50 | 15.306 | 0.508 | 96.45 |
| 4 | 2 | 50 | 17.995 | 0.635 | 96.45 |
| 5 | 2 | 50 | 21.236 | 0.794 | 96.45 |
| 6 | 2 | 50 | 24.752 | 0.953 | 96.45 |

TABLE B-9 (continued)

| Run | Transducer | Attenuation | Pressure x10$^{-4}$ (dyn/cm$^2$) | Flow (cc/sec) | L/D |
|---|---|---|---|---|---|
| 7 | 2 | 50 | 28.096 | 1.112 | 96.45 |
| 8 | 2 | 100 | 31.543 | 1.271 | 96.45 |
| 9 | 2 | 100 | 35.163 | 1.430 | 96.45 |
| 9 | 2 | 100 | 41.575 | 1.430 | 96.45 |
| 10 | 2 | 100 | 46.815 | 1.589 | 96.45 |
| 11 | 2 | 100 | 53.779 | 1.747 | 96.45 |
| 12 | 2 | 100 | 58.088 | 1.908 | 96.45 |
| 13 | 4 | 50 | 67.223 | 2.224 | 96.45 |
| 14 | 4 | 50 | 84.115 | 2.701 | 96.45 |
| 1 | 2 | 50 | 9.515 | 0.318 | 71.32 |
| 2 | 2 | 50 | 10.480 | 0.381 | 71.32 |
| 3 | 2 | 50 | 12.410 | 0.508 | 71.32 |
| 4 | 2 | 50 | 14.755 | 0.635 | 71.32 |
| 5 | 2 | 50 | 17.740 | 0.794 | 71.32 |
| 6 | 2 | 50 | 20.546 | 0.953 | 71.32 |
| 7 | 2 | 50 | 23.408 | 1.112 | 71.32 |
| 8 | 2 | 50 | 27.372 | 1.271 | 71.32 |
| 9 | 2 | 100 | 36.749 | 1.430 | 71.32 |
| 9 | 2 | 100 | 29.854 | 1.430 | 71.32 |
| 10 | 2 | 100 | 41.092 | 1.589 | 71.32 |
| 11 | 2 | 100 | 46.126 | 1.747 | 71.32 |
| 12 | 2 | 100 | 51.538 | 1.908 | 71.32 |
| 13 | 2 | 100 | 59.984 | 2.224 | 71.32 |
| 14 | 4 | 50 | 75.497 | 2.701 | 71.32 |
| 1 | 2 | 50 | 8.101 | 0.318 | 55.08 |
| 2 | 2 | 50 | 9.032 | 0.381 | 55.08 |
| 3 | 2 | 50 | 10.549 | 0.508 | 55.08 |
| 4 | 2 | 50 | 12.617 | 0.635 | 55.08 |
| 5 | 2 | 50 | 15.237 | 0.794 | 55.08 |
| 6 | 2 | 50 | 17.857 | 0.953 | 55.08 |
| 7 | 2 | 50 | 20.581 | 1.112 | 55.08 |
| 8 | 2 | 50 | 23.235 | 1.271 | 55.08 |
| 9 | 2 | 100 | 32.198 | 1.430 | 55.08 |
| 10 | 2 | 100 | 36.887 | 1.589 | 55.08 |
| 11 | 2 | 100 | 42.127 | 1.747 | 55.08 |
| 12 | 2 | 100 | 46.194 | 1.908 | 55.08 |
| 13 | 2 | 100 | 54.882 | 2.224 | 55.08 |
| 14 | 2 | 100 | 69.292 | 2.701 | 55.08 |
| 15* | 1 | 100 | 6.837 | 0.238 | 55.08 |
| 16* | 1 | 100 | 6.155 | 0.159 | 55.08 |
| 17* | 1 | 50 | 4.609 | 0.079 | 55.08 |
| 18* | 1 | 20 | 3.608 | 0.032 | 55.08 |
| 19* | 1 | 20 | 3.298 | 0.023 | 55.08 |

TABLE B-9 (continued)

| Run | Trans-ducer | Attenua-tion | Pressure $\times 10^{-4}$ (dyn/cm$^2$) | Flow (cc/sec) | L/D |
|---|---|---|---|---|---|
| 15* | 2 | 50 | 23.881 | 0.238 | 305.08 |
| 16* | 2 | 50 | 21.978 | 0.159 | 305.08 |
| 17* | 2 | 50 | 15.712 | 0.079 | 305.08 |
| 18* | 2 | 50 | 10.958 | 0.032 | 305.08 |
| 19* | 2 | 50 | 9.600 | 0.023 | 305.08 |
| 20* | 1 | 50 | 5.357 | 0.012 | 305.08 |
| 21* | 1 | 50 | 3.722 | 0.008 | 305.08 |
| 22* | 1 | 50 | 2.343 | 0.004 | 305.08 |

* Data obtained with batch number two

## TABLE B-10

## TOTAL PRESSURE LOSS - L/D DATA; 0.20% SEPARAN AP-30, 0.20 cm I.D. CAPILLARY TUBE, SMALL RESERVOIR

Temp.: 68°F

Pressure Correction:
$-1.669 \times 10^4$ dyn/cm$^2$

| Run | Transducer | Attenuation | Pressure x10$^{-4}$ (dyn/cm$^2$) | Flow (cc/sec) | L/D |
|---|---|---|---|---|---|
| 1 | 2 | 20 | 4.688 | 1.271 | 31.60 |
| 2 | 2 | 20 | 5.171 | 1.589 | 31.60 |
| 3 | 2 | 50 | 6.033 | 1.906 | 31.60 |
| 4 | 2 | 50 | 7.239 | 2.383 | 31.60 |
| 5 | 2 | 50 | 7.984 | 2.701 | 31.60 |
| 6 | 2 | 50 | 8.998 | 3.177 | 31.60 |
| 7 | 2 | 50 | 14.479 | 4.866 | 31.60 |
| 8 | 2 | 50 | 17.237 | 5.401 | 31.60 |
| 9 | 2 | 50 | 18.891 | 5.719 | 31.60 |
| 10 | 2 | 100 | 21.098 | 6.354 | 31.60 |
| 11 | 2 | 100 | 28.337 | 7.943 | 31.60 |
| 12 | 2 | 100 | 37.645 | 9.531 | 31.60 |
| 13 | 2 | 100 | 46.746 | 11.120 | 31.60 |
| 1 | 2 | 50 | 5.792 | 1.271 | 54.96 |
| 2 | 2 | 50 | 6.515 | 1.589 | 54.96 |
| 3 | 2 | 50 | 7.343 | 1.906 | 54.96 |
| 4 | 2 | 50 | 9.032 | 2.383 | 54.96 |
| 5 | 2 | 50 | 9.790 | 2.701 | 54.96 |
| 6 | 2 | 50 | 11.032 | 3.177 | 54.96 |
| 7 | 2 | 100 | 17.513 | 4.866 | 54.96 |
| 8 | 2 | 100 | 20.270 | 5.401 | 54.96 |
| 9 | 2 | 100 | 21.615 | 5.719 | 54.96 |
| 10 | 2 | 100 | 24.200 | 6.354 | 54.96 |
| 11 | 2 | 100 | 32.922 | 7.943 | 54.96 |
| 12 | 2 | 100 | 42.954 | 9.531 | 54.96 |
| 13 | 2 | 100 | 52.262 | 11.120 | 54.96 |
| 1 | 2 | 50 | 6.826 | 1.271 | 71.23 |
| 2 | 2 | 20 | 7.446 | 1.589 | 71.23 |
| 3 | 2 | 50 | 8.515 | 1.906 | 71.23 |
| 4 | 2 | 50 | 10.121 | 2.383 | 71.23 |
| 5 | 2 | 50 | 11.169 | 2.701 | 71.23 |
| 6 | 2 | 50 | 12.617 | 3.177 | 71.23 |
| 7 | 2 | 100 | 19.133 | 4 866 | 71.23 |
| 8 | 2 | 100 | 22.063 | 5.401 | 71.23 |
| 9 | 2 | 100 | 24.545 | 5.719 | 71.23 |

TABLE B-10 (continued)

| Run | Transducer | Attenuation | Pressure $\times 10^{-4}$ (dyn/cm$^2$) | Flow (cc/sec) | L/D |
|---|---|---|---|---|---|
| 10 | 2 | 100 | 26.614 | 6.354 | 71.23 |
| 11 | 2 | 100 | 35.577 | 7.943 | 71.23 |
| 12 | 2 | 100 | 45.298 | 9.531 | 71.23 |
| 13 | 2 | 100 | 55.158 | 11.120 | 71.23 |
| 1 | 2 | 50 | 8.067 | 1.271 | 96.38 |
| 2 | 2 | 50 | 9.135 | 1.589 | 96.38 |
| 3 | 2 | 50 | 10.514 | 1.906 | 96.38 |
| 4 | 2 | 50 | 11.583 | 2.383 | 96.38 |
| 5 | 2 | 50 | 13.720 | 2.701 | 96.38 |
| 6 | 2 | 50 | 14.996 | 3.177 | 96.38 |
| 7 | 2 | 100 | 22.856 | 4.866 | 96.38 |
| 8 | 2 | 100 | 26.027 | 5.401 | 96.38 |
| 9 | 2 | 100 | 27.510 | 5.719 | 96.38 |
| 10 | 2 | 100 | 31.819 | 6.354 | 96.38 |
| 11 | 2 | 100 | 41.575 | 7.943 | 96.38 |
| 12 | 2 | 100 | 51.572 | 9.531 | 96.38 |
| 13 | 2 | 100 | 61.914 | 11.120 | 96.38 |
| 1 | 2 | 50 | 11.032 | 1.271 | 148.45 |
| 2 | 2 | 50 | 12.583 | 1.589 | 148.45 |
| 3 | 2 | 50 | 14.134 | 1.906 | 148.45 |
| 4 | 2 | 100 | 16.444 | 2.383 | 148.45 |
| 5 | 2 | 100 | 17.892 | 2.701 | 148.45 |
| 6 | 2 | 100 | 19.960 | 3.177 | 148.45 |
| 7 | 2 | 100 | 28.268 | 4.866 | 148.45 |
| 8 | 2 | 100 | 32.198 | 5.401 | 148.45 |
| 9 | 2 | 100 | 34.129 | 5.719 | 148.45 |
| 10 | 2 | 100 | 38.817 | 6.354 | 148.45 |
| 11 | 2 | 100 | 49.469 | 7.943 | 148.45 |
| 12 | 2 | 100 | 61.087 | 9.531 | 148.45 |
| 13 | 4 | 50 | 72.394 | 11.120 | 148.45 |
| 14* | 2 | 50 | 15.731 | 0.636 | 304.95 |
| 15* | 2 | 50 | 11.222 | 0.318 | 304.95 |
| 16* | 2 | 50 | 10.073 | 0.239 | 304.95 |
| 17* | 2 | 50 | 8.007 | 0.159 | 304.95 |

* Data obtained with batch number 2

## TABLE B-11

## TOTAL PRESSURE LOSS - L/D DATA: 0.20% SEPARAN AP-30, 0.30 cm I.D. CAPILLARY TUBE, SMALL RESERVOIR

Temp.: 68°F

Pressure Correction: $-1.669 \times 10^4$ dyn/cm$^2$

| Run | Trans-ducer | Attenua-tion | Pressure x10$^{-4}$ (dyn/cm$^2$) | Flow (cc/sec) | L/D |
|---|---|---|---|---|---|
| 1 | 2 | 20 | 3.930 | 2.542 | 34.97 |
| 2 | 2 | 20 | 4.447 | 3.177 | 34.97 |
| 3 | 2 | 50 | 5.757 | 4.866 | 34.96 |
| 4 | 2 | 50 | 7.239 | 6.354 | 34.97 |
| 5 | 2 | 50 | 7.929 | 7.148 | 34.97 |
| 6 | 2 | 50 | 8.791 | 7.943 | 34.97 |
| 7 | 2 | 50 | 9.653 | 8.737 | 34.97 |
| 8 | 2 | 100 | 10.549 | 9.531 | 34.97 |
| 9 | 2 | 100 | 11.790 | 10.325 | 34.97 |
| 10 | 2 | 100 | 12.824 | 11.120 | 34.97 |
| 11 | 2 | 100 | 14.272 | 11.914 | 34.97 |
| 12 | 2 | 100 | 15.616 | 12.708 | 34.97 |
| 13 | 2 | 100 | 17.926 | 14.297 | 34.97 |
| 14 | 2 | 100 | 20.270 | 15.885 | 34.97 |
| 15 | 2 | 100 | 24.131 | 17.474 | 34.97 |
| 16 | 2 | 100 | 26.338 | 19.062 | 34.97 |
| 1 | 2 | 50 | 4.688 | 2.542 | 55.04 |
| 2 | 2 | 50 | 5.205 | 3.177 | 55.04 |
| 3 | 2 | 50 | 6.757 | 4.866 | 55.04 |
| 4 | 2 | 50 | 8.412 | 6.354 | 55.04 |
| 5 | 2 | 50 | 9.377 | 7.148 | 55.04 |
| 6 | 2 | 50 | 10.342 | 7.943 | 55.04 |
| 7 | 2 | 50 | 11.445 | 8.737 | 55.04 |
| 8 | 2 | 100 | 12.583 | 9.531 | 55.04 |
| 9 | 2 | 100 | 14.031 | 10.325 | 55.04 |
| 10 | 2 | 100 | 15.134 | 11.120 | 55.04 |
| 11 | 2 | 100 | 16.478 | 11.914 | 55.04 |
| 12 | 2 | 100 | 18.133 | 12.708 | 55.04 |
| 13 | 2 | 100 | 19.995 | 14.297 | 55.04 |
| 14 | 2 | 100 | 22.890 | 15.885 | 55.04 |
| 15 | 2 | 100 | 26.269 | 17.474 | 55.04 |
| 16 | 2 | 100 | 29.475 | 19.062 | 55.04 |
| 1 | 2 | 20 | 5.378 | 2.542 | 71.13 |
| 2 | 2 | 20 | 6.067 | 3.177 | 71.13 |
| 3 | 2 | 50 | 7.757 | 4.866 | 71.13 |
| 4 | 2 | 50 | 9.584 | 6.354 | 71.13 |

## TABLE B-11 (continued)

| Run | Trans-ducer | Attenua-tion | Pressure $\times 10^{-4}$ (dyn/cm$^2$) | Flow (cc/sec) | L/D |
|---|---|---|---|---|---|
| 5 | 2 | 50 | 10.514 | 7.148 | 71.13 |
| 6 | 2 | 50 | 11.583 | 7.943 | 71.13 |
| 7 | 2 | 100 | 12.928 | 8.737 | 71.13 |
| 8 | 2 | 100 | 13.962 | 9.531 | 71.13 |
| 9 | 2 | 100 | 15.548 | 10.325 | 71.13 |
| 10 | 2 | 100 | 16.754 | 11.120 | 71.13 |
| 11 | 2 | 100 | 18.064 | 11.914 | 71.13 |
| 12 | 2 | 100 | 19.374 | 12.708 | 71.13 |
| 13 | 2 | 100 | 22.235 | 14.297 | 71.13 |
| 14 | 2 | 100 | 24.683 | 15.885 | 71.13 |
| 15 | 2 | 100 | 29.096 | 17.474 | 71.13 |
| 16 | 2 | 100 | 32.198 | 19.062 | 71.13 |
| 1 | 2 | 50 | 6.398 | 2.542 | 96.36 |
| 2 | 2 | 50 | 7.170 | 3.177 | 96.36 |
| 3 | 2 | 50 | 9.239 | 4.866 | 96.36 |
| 4 | 2 | 50 | 11.169 | 6.354 | 96.36 |
| 5 | 2 | 50 | 12.548 | 7.148 | 96.36 |
| 6 | 2 | 100 | 13.789 | 7.943 | 96.36 |
| 7 | 2 | 100 | 14.941 | 8.737 | 96.36 |
| 8 | 2 | 100 | 16.306 | 9.531 | 96.36 |
| 9 | 2 | 100 | 17.685 | 10.325 | 96.36 |
| 10 | 2 | 100 | 18.960 | 11.120 | 96.36 |
| 11 | 2 | 100 | 20.891 | 11.914 | 96.36 |
| 12 | 2 | 100 | 22.235 | 12.708 | 96.36 |
| 13 | 2 | 100 | 25.200 | 14.297 | 96.36 |
| 14 | 2 | 100 | 28.510 | 15.885 | 96.36 |
| 15 | 2 | 100 | 32.405 | 17.474 | 96.36 |
| 16 | 2 | 100 | 36.266 | 19.062 | 96.36 |
| 1 | 2 | 50 | 8.274 | 2.542 | 145.00 |
| 2 | 2 | 50 | 9.549 | 3.177 | 145.00 |
| 3 | 2 | 50 | 12.204 | 4.866 | 145.00 |
| 4 | 2 | 100 | 14.893 | 6.354 | 145.00 |
| 5 | 2 | 100 | 16.203 | 7.148 | 145.00 |
| 6 | 2 | 100 | 17.685 | 7.943 | 145.00 |
| 7 | 2 | 100 | 19.167 | 8.737 | 145.00 |
| 8 | 2 | 100 | 20.753 | 9.531 | 145.00 |
| 9 | 2 | 100 | 22.235 | 10.325 | 145.00 |
| 10 | 2 | 100 | 24.131 | 11.120 | 145.00 |
| 11 | 2 | 100 | 25.683 | 11.914 | 145.00 |
| 12 | 2 | 100 | 27.682 | 12.708 | 145.00 |
| 13 | 2 | 100 | 31.164 | 14.297 | 145.00 |
| 14 | 2 | 100 | 34.336 | 15.885 | 145.00 |
| 15 | 2 | 100 | 39.058 | 17.474 | 145.00 |
| 16 | 2 | 100 | 43.609 | 19.062 | 145.00 |

## TABLE B-11 (continued)

| Run | Trans-ducer | Attenua-tion | Pressure $\times 10^{-4}$ (dyn/cm$^2$) | Flow (cc/sec) | L/D |
|---|---|---|---|---|---|
| 17* | 2 | 50 | 13.423 | 1.589 | 304.83 |
| 18* | 2 | 50 | 12.272 | 1.271 | 304.83 |
| 19* | 2 | 50 | 9.214 | 0.636 | 304.83 |
| 20* | 1 | 50 | 6.764 | 0.318 | 304.83 |
| 21* | 1 | 50 | 6.461 | 0.238 | 304.83 |
| 22* | 1 | 50 | 5.267 | 0.159 | 304.83 |
| 23* | 1 | 10 | 2.399 | 0.012 | 304.83 |
| 24* | 1 | 10 | 2.199 | 0.008 | 304.83 |
| 25* | 1 | 20 | 2.787 | 0.024 | 304.83 |
| 26* | 1 | 20 | 3.014 | 0.032 | 304.83 |
| 27* | 1 | 20 | 4.099 | 0.080 | 304.83 |
| 28* | 1 | 50 | 5.872 | 0.238 | 304.83 |
| 29* | 1 | 50 | 6.293 | 0.318 | 304.83 |

* Data obtained with batch number two.

## TABLE B-12

## TOTAL PRESSURE LOSS - L/D DATA: 0.20% SEPARAN AP-30, 0.10 cm I.D. CAPILLARY TUBE, LARGE RESERVOIR

Temp.: 68°F

Pressure Correction:
$-1.937 \times 10^4$ dyn/cm$^2$

| Run | Transducer | Attenuation | Pressure $\times 10^{-4}$ (dyn/cm$^2$) | Flow (cc/sec) | L/D |
|---|---|---|---|---|---|
| 1 | 2 | 50 | 7.756 | 0.318 | 55.08 |
| 2 | 2 | 50 | 9.135 | 0.381 | 55.08 |
| 3 | 2 | 50 | 10.859 | 0.508 | 55.08 |
| 4 | 2 | 100 | 12.721 | 0.635 | 55.08 |
| 5 | 2 | 100 | 15.341 | 0.794 | 55.08 |
| 6 | 2 | 100 | 18.340 | 0.953 | 55.08 |
| 7 | 2 | 100 | 20.684 | 1.112 | 55.08 |
| 8 | 2 | 100 | 22.753 | 1.271 | 55.08 |
| 9 | 2 | 100 | 25.683 | 1.430 | 55.08 |
| 10 | 2 | 100 | 28.061 | 1.589 | 55.08 |
| 11 | 2 | 100 | 31.200 | 1.748 | 55.08 |
| 11 | 2 | 100 | 33.200 | 1.748 | 55.08 |
| 12 | 2 | 100 | 39.403 | 1.908 | 55.08 |
| 13 | 2 | 100 | 46.746 | 2.224 | 55.08 |
| 14 | 2 | 100 | 57.571 | 2.701 | 55.08 |
| 1 | 2 | 100 | 9.446 | 0.318 | 71.32 |
| 2 | 2 | 100 | 10.514 | 0.381 | 71.32 |
| 3 | 2 | 100 | 12.548 | 0.508 | 71.32 |
| 4 | 2 | 100 | 14.582 | 0.635 | 71.32 |
| 5 | 2 | 100 | 17.340 | 0.794 | 71.32 |
| 6 | 2 | 100 | 20.133 | 0.953 | 71.32 |
| 7 | 2 | 100 | 22.753 | 1.112 | 71.32 |
| 8 | 2 | 100 | 25.683 | 1.271 | 71.32 |
| 9 | 2 | 100 | 29.820 | 1.430 | 71.32 |
| 10 | 2 | 100 | 32.853 | 1.589 | 71.32 |
| 11 | 2 | 100 | 39.782 | 1.748 | 71.32 |
| 12 | 2 | 100 | 44.953 | 1.908 | 71.32 |
| 13 | 2 | 100 | 52.641 | 2.240 | 71.32 |
| 14 | 2 | 100 | 63.604 | 2.701 | 71.32 |
| 1 | 2 | 100 | 10.549 | 0.318 | 96.45 |
| 2 | 2 | 100 | 12.617 | 0.381 | 96.45 |
| 3 | 2 | 100 | 15.237 | 0.508 | 96.45 |
| 4 | 2 | 100 | 17.513 | 0.635 | 96.45 |
| 5 | 2 | 100 | 20.960 | 0.794 | 96.45 |
| 6 | 2 | 100 | 24.304 | 0.953 | 96.45 |
| 7 | 2 | 100 | 27.337 | 1.112 | 96.45 |
| 8 | 2 | 100 | 31.164 | 1.271 | 96.45 |
| 9 | 2 | 100 | 33.991 | 1.430 | 96.45 |

TABLE B-12 (continuous)

| Run | Transducer | Attenuation | Pressure $\times 10^{-4}$ (dyn/cm$^2$) | Flow (cc/sec) | L/D |
|---|---|---|---|---|---|
| 10 | 2 | 100 | 37.231 | 1.589 | 96.45 |
| 11 | 2 | 100 | 42.230 | 1.748 | 96.45 |
| 11 | 2 | 100 | 44.540 | 1.748 | 96.45 |
| 12 | 2 | 100 | 50.400 | 1.908 | 96.45 |
| 13 | 2 | 100 | 58.950 | 2.224 | 96.45 |
| 14 | 4 | 50 | 71.705 | 2.701 | 96.45 |
| 1 | 2 | 100 | 15.548 | 0.318 | 148.48 |
| 2 | 2 | 100 | 17.444 | 0.381 | 148.48 |
| 3 | 2 | 100 | 21.029 | 0.508 | 148.48 |
| 4 | 2 | 100 | 23.959 | 0.635 | 148.48 |
| 5 | 2 | 100 | 28.130 | 0.794 | 148.48 |
| 6 | 2 | 100 | 32.750 | 0.953 | 148.48 |
| 7 | 2 | 100 | 37.300 | 1.112 | 148.48 |
| 8 | 2 | 100 | 41.230 | 1.271 | 148.48 |
| 9 | 2 | 100 | 45.919 | 1.430 | 148.48 |
| 10 | 2 | 100 | 50.400 | 1.589 | 148.48 |
| 11 | 2 | 100 | 55.227 | 1.748 | 148.48 |
| 12 | 2 | 100 | 63.948 | 1.908 | 148.48 |
| 13 | 4 | 50 | 73.084 | 2.224 | 148.48 |
| 14 | 4 | 50 | 88.942 | 2.701 | 148.48 |
| 1 | 2 | 100 | 21.511 | 0.318 | 222.08 |
| 2 | 2 | 100 | 23.890 | 0.381 | 222.08 |
| 3 | 2 | 100 | 27.924 | 0.508 | 222.08 |
| 4 | 2 | 100 | 33.095 | 0.635 | 222.08 |
| 5 | 2 | 100 | 39.024 | 0.794 | 222.08 |
| 6 | 2 | 100 | 44.609 | 0.953 | 222.08 |
| 7 | 2 | 100 | 50.331 | 1.112 | 222.08 |
| 8 | 2 | 100 | 55.847 | 1.271 | 222.08 |
| 9 | 2 | 100 | 61.535 | 1.430 | 222.08 |
| 10 | 2 | 100 | 68.258 | 1.589 | 222.08 |
| 11 | 4 | 50 | 76.186 | 1.748 | 222.08 |
| 12 | 4 | 50 | 84.115 | 1.908 | 222.08 |
| 13 | 4 | 50 | 97.215 | 2.224 | 222.08 |
| 14 | 4 | 50 | 117.899 | 2.701 | 222.08 |
| 1 | 2 | 100 | 27.924 | 0.318 | 305.08 |
| 2 | 2 | 100 | 31.026 | 0.381 | 305.08 |
| 3 | 2 | 100 | 37.231 | 0.508 | 305.08 |
| 4 | 2 | 100 | 43.092 | 0.635 | 305.08 |
| 5 | 2 | 100 | 50.848 | 0.794 | 305.08 |
| 6 | 2 | 100 | 57.743 | 0.953 | 305.08 |
| 7 | 2 | 100 | 65.086 | 1.112 | 305.08 |
| 8 | 4 | 50 | 71.705 | 1.271 | 305.08 |
| 9 | 4 | 50 | 84.460 | 1.430 | 305.08 |

TABLE B-12 (continued)

| Run | Transducer | Attenuation | Pressure x$10^{-4}$ (dyn/cm$^2$) | Flow (cc/sec) | L/D |
|---|---|---|---|---|---|
| 10 | 4 | 100 | 93.768 | 1.589 | 305.08 |
| 11 | 4 | 50 | 104.799 | 1.748 | 305.08 |
| 11 | 4 | 50 | 84.460 | 1.748 | 305.08 |
| 12 | 4 | 50 | 93.906 | 1.908 | 305.08 |
| 13 | 4 | 50 | 122.036 | 2.224 | 305.08 |
| 14 | 4 | 50 | 144.789 | 2.701 | 305.08 |

## TABLE B-13

## TOTAL PRESSURE LOSS - L/D DATA: 0.20% SEPARAN AP-30, 0.20 cm I.D. CAPILLARY TUBE, LARGE RESERVOIR

Temp.: 68°F

Pressure Correction: $-1.937 \times 10^{4}$ dyn/$\text{cm}^2$

| Run | Trans-ducer | Attenua-tion | Pressure $\times 10^{-4}$ (dyn/$\text{cm}^2$) | Flow (cc/sec) | L/D |
|---|---|---|---|---|---|
| 1 | 2 | 50 | 11.859 | 1.271 | 148.45 |
| 2 | 2 | 50 | 10.549 | 1.589 | 148.45 |
| 3 | 2 | 50 | 13.203 | 1.906 | 148.45 |
| 4 | 2 | 50 | 15.203 | 2.383 | 148.45 |
| 5 | 2 | 50 | 16.547 | 2.701 | 148.45 |
| 6 | 2 | 50 | 18.443 | 3.177 | 148.45 |
| 7 | 2 | 50 | 25.304 | 4.866 | 148.45 |
| 9 | 2 | 100 | 29.406 | 5.719 | 148.45 |
| 9 | 2 | 100 | 31.026 | 5.719 | 148.45 |
| 10 | 2 | 100 | 32.267 | 6.354 | 148.45 |
| 10 | 2 | 100 | 33.164 | 6.354 | 148.45 |
| 11 | 2 | 100 | 42.644 | 7.943 | 148.45 |
| 12 | 2 | 100 | 51.745 | 9.531 | 148.45 |
| 13 | 2 | 100 | 62.742 | 11.120 | 148.45 |
| 1 | 2 | 50 | 8.067 | 1.271 | 96.38 |
| 2 | 2 | 50 | 9.101 | 1.589 | 96.38 |
| 3 | 2 | 50 | 10.170 | 1.906 | 96.38 |
| 4 | 2 | 50 | 11.721 | 2.383 | 96.38 |
| 5 | 2 | 50 | 12.686 | 2.701 | 96.38 |
| 6 | 2 | 50 | 14.134 | 3.177 | 96.38 |
| 7 | 2 | 50 | 19.719 | 4.866 | 96.38 |
| 9 | 2 | 50 | 22.925 | 5.719 | 96.38 |
| 9 | 2 | 50 | 24.132 | 5.719 | 96.38 |
| 10 | 2 | 100 | 26.889 | 6.354 | 96.38 |
| 11 | 2 | 100 | 34.922 | 7.943 | 96.38 |
| 12 | 2 | 100 | 43.747 | 9.531 | 96.38 |
| 13 | 2 | 100 | 53.365 | 11.120 | 96.38 |
| 1 | 1 | 50 | 6.881 | 1.271 | 71.23 |
| 2 | 1 | 100 | 7.708 | 1.589 | 71.23 |
| 3 | 2 | 50 | 8.515 | 1.906 | 71.23 |
| 4 | 2 | 50 | 9.722 | 2.383 | 71.23 |
| 5 | 2 | 50 | 10.455 | 2.701 | 71.23 |
| 6 | 2 | 50 | 11.790 | 3.177 | 71.23 |
| 7 | 2 | 50 | 16.616 | 4.866 | 71.23 |
| 8 | 2 | 50 | 18.719 | 5.401 | 71.23 |
| 8 | 2 | 50 | 19.857 | 5.401 | 71.23 |
| 9 | 2 | 50 | 19.995 | 5.719 | 71.23 |

TABLE B-13 (continued)

| Run | Transducer | Attenuation | Pressure x$10^{-4}$ (dyn/cm$^2$) | Flow (cc/sec) | L/D |
|---|---|---|---|---|---|
| 9 | 2 | 50 | 21.236 | 5.719 | 71.23 |
| 10 | 2 | 50 | 21.564 | 6.354 | 71.23 |
| 10 | 2 | 50 | 23.270 | 6.354 | 71.23 |
| 11 | 2 | 100 | 30.337 | 7.943 | 71.23 |
| 12 | 2 | 100 | 38.507 | 9.531 | 71.23 |
| 13 | 2 | 100 | 47.367 | 11.120 | 71.23 |
| 1 | 1 | 100 | 5.750 | 1.271 | 54.96 |
| 2 | 1 | 100 | 6.426 | 1.589 | 54.96 |
| 3 | 2 | 50 | 7.343 | 1.906 | 54.96 |
| 4 | 2 | 50 | 8.343 | 2.383 | 54.96 |
| 5 | 2 | 50 | 9.135 | 2.701 | 54.96 |
| 6 | 2 | 50 | 10.204 | 3.177 | 54.96 |
| 7 | 2 | 50 | 14.582 | 4.866 | 54.96 |
| 8 | 2 | 50 | 15.449 | 5.401 | 54.96 |
| 9 | 2 | 50 | 17.581 | 5.719 | 54.96 |
| 9 | 2 | 50 | 18.754 | 5.719 | 54.96 |
| 10 | 2 | 50 | 19.374 | 6.354 | 54.96 |
| 10 | 2 | 50 | 20.891 | 6.354 | 54.96 |
| 11 | 2 | 50 | 27.062 | 7.943 | 54.96 |
| 12 | 2 | 50 | 35.439 | 9.531 | 54.96 |
| 13 | 2 | 50 | 42.920 | 11.120 | 54.96 |
| 1 | 1 | 100 | 4.671 | 1.271 | 31.60 |
| 2 | 1 | 100 | 5.188 | 1.589 | 31.60 |
| 3 | 1 | 100 | 5.826 | 1.906 | 31.60 |
| 4 | 1 | 100 | 6.688 | 2.384 | 31.60 |
| 5 | 2 | 50 | 7.446 | 2.701 | 31.60 |
| 6 | 2 | 50 | 8.308 | 3.177 | 31.60 |
| 7 | 2 | 50 | 12.066 | 4.866 | 31.60 |
| 8 | 2 | 50 | 14.893 | 5.401 | 31.60 |
| 9 | 2 | 50 | 14.798 | 5.719 | 31.60 |
| 9 | 2 | 50 | 15.823 | 5.719 | 31.60 |
| 10 | 2 | 50 | 17.788 | 6.354 | 31.60 |
| 11 | 2 | 100 | 23.442 | 7.943 | 31.60 |
| 12 | 2 | 100 | 29.820 | 9.531 | 31.60 |
| 13 | 2 | 100 | 38.266 | 11.120 | 31.60 |
| 1 | 2 | 50 | 14.755 | 1.271 | 222.36 |
| 2 | 2 | 50 | 16.616 | 1.589 | 222.36 |
| 3 | 2 | 50 | 18.443 | 1.906 | 222.36 |
| 4 | 2 | 50 | 21.098 | 2.383 | 222.36 |
| 5 | 2 | 100 | 22.753 | 2.701 | 222.36 |
| 6 | 2 | 100 | 25.338 | 3.177 | 222.36 |
| 7 | 2 | 100 | 33.956 | 4.866 | 222.36 |
| 8 | 2 | 100 | 37.576 | 5.401 | 222.36 |
| 9 | 2 | 100 | 39.231 | 5.719 | 222.36 |
| 9 | 2 | 100 | 40.472 | 5.719 | 222.36 |

TABLE B-13 (continued)

| Run | Trans-ducer | Attenua-tion | Pressure $\times 10^{-4}$ (dyn/cm$^2$) | Flow (cc/sec) | L/D |
|---|---|---|---|---|---|
| 10 | 2 | 100 | 44.471 | 6.354 | 222.36 |
| 11 | 2 | 100 | 54.744 | 7.943 | 222.36 |
| 12 | 2 | 100 | 65.844 | 9.531 | 222.36 |
| 13 | 4 | 50 | 76.876 | 11.120 | 222.36 |
| | | | | | |
| 1 | 2 | 50 | 18.960 | 1.271 | 304.95 |
| 2 | 2 | 100 | 21.236 | 1.589 | 304.95 |
| 3 | 2 | 100 | 23.649 | 1.906 | 304.95 |
| 4 | 2 | 100 | 27.027 | 2.383 | 304.95 |
| 6 | 2 | 100 | 29.302 | 2.701 | 304.95 |
| 6 | 2 | 100 | 32.681 | 3.177 | 304.95 |
| 7 | 2 | 100 | 43.816 | 4.866 | 304.95 |
| 8 | 2 | 100 | 48.435 | 5.401 | 304.95 |
| 9 | 2 | 100 | 50.848 | 5.719 | 304.95 |
| 10 | 2 | 100 | 55.227 | 6.354 | 304.95 |
| 11 | 2 | 100 | 69.395 | 7.943 | 304.95 |
| 12 | 4 | 50 | 81.013 | 9.531 | 304.95 |
| 13 | 4 | 50 | 95.147 | 11.120 | 304.95 |
| | | | | | |
| 1 | 2 | 100 | 27.510 | 1.271 | 457.43 |
| 2 | 2 | 100 | 31.026 | 1.589 | 457.43 |
| 7 | 2 | 100 | 63.673 | 4.866 | 457.43 |
| 8 | 4 | 50 | 68.258 | 5.401 | 457.43 |
| 9 | 4 | 50 | 70.671 | 5.719 | 457.43 |
| 10 | 4 | 50 | 76.531 | 6.354 | 457.43 |
| 11 | 4 | 50 | 95.492 | 7.943 | 457.43 |
| 12 | 4 | 50 | 108.247 | 9.531 | 457.43 |
| 13 | 4 | 50 | 129.620 | 11.120 | 457.43 |

# TABLE B-14

## TOTAL PRESSURE LOSS - L/D DATA: 0.20% SEPARAN AP-30, 0.30 cm I.D. CAPILLARY TUBE, LARGE RESERVOIR

Temp.: 68°F

Pressure Correction: $-1.937 \times 10^4$ dyn/cm$^2$

| Run | Trans-ducer | Attenua-tion | Pressure x10$^{-4}$ (dyn/cm$^2$) | Flow (cc/sec) | L/D |
|---|---|---|---|---|---|
| 1 | 2 | 50 | 3.861 | 2.542 | 34.97 |
| 2 | 2 | 50 | 4.275 | 3.177 | 34.97 |
| 3 | 2 | 50 | 5.309 | 4.866 | 34.97 |
| 4 | 2 | 50 | 6.378 | 6.354 | 34.97 |
| 5 | 2 | 50 | 6.998 | 7.148 | 34.97 |
| 6 | 2 | 50 | 7.722 | 7.943 | 34.97 |
| 7 | 2 | 50 | 8.343 | 8.764 | 34.97 |
| 8 | 2 | 50 | 9.135 | 9.531 | 34.97 |
| 9 | 2 | 50 | 9.722 | 10.325 | 34.97 |
| 10 | 2 | 50 | 10.514 | 11.120 | 34.97 |
| 11 | 2 | 100 | 11.962 | 11.914 | 34.97 |
| 12 | 2 | 100 | 12.893 | 12.708 | 34.97 |
| 13 | 2 | 100 | 13.720 | 14.297 | 34.97 |
| 14 | 2 | 100 | 17.064 | 15.885 | 34.97 |
| 15 | 2 | 100 | 19.478 | 17.474 | 34.97 |
| 16 | 2 | 100 | 19.995 | 19.062 | 34.97 |
| 16 | 2 | 100 | 21.925 | 19.062 | 34.97 |
| 1 | 2 | 50 | 4.654 | 2.542 | 55.04 |
| 2 | 2 | 50 | 5.102 | 3.177 | 55.04 |
| 3 | 2 | 50 | 6.343 | 4.866 | 55.04 |
| 4 | 2 | 50 | 7.584 | 6.354 | 55.04 |
| 5 | 2 | 50 | 8.412 | 7.148 | 55.04 |
| 6 | 2 | 50 | 9.135 | 7.943 | 55.04 |
| 7 | 2 | 50 | 9.894 | 8.764 | 55.04 |
| 8 | 2 | 50 | 10.583 | 9.531 | 55.04 |
| 9 | 2 | 50 | 11.514 | 10.325 | 55.04 |
| 10 | 2 | 50 | 12.410 | 11.120 | 55.04 |
| 11 | 2 | 50 | 13.927 | 11.914 | 55.04 |
| 12 | 2 | 50 | 14.686 | 12.708 | 55.04 |
| 13 | 2 | 100 | 16.306 | 14.297 | 55.04 |
| 14 | 2 | 100 | 19.478 | 15.885 | 55.04 |
| 15 | 2 | 100 | 21.718 | 17.474 | 55.04 |
| 16 | 2 | 100 | 24.476 | 19.062 | 55.04 |
| 1 | 2 | 50 | 5.309 | 2.542 | 71.13 |
| 2 | 2 | 50 | 5.895 | 3.177 | 71.13 |
| 3 | 2 | 50 | 7.343 | 4.866 | 71.13 |
| 4 | 2 | 50 | 8.777 | 6.354 | 71.13 |

TABLE B-14 (continued)

| Run | Trans- ducer | Attenua- tion | Pressure $\times 10^{-4}$ (dyn/cm$^2$) | Flow (cc/sec) | L/D |
|---|---|---|---|---|---|
| 5 | 2 | 50 | 9.653 | 7.148 | 71.13 |
| 6 | 2 | 50 | 10.514 | 7.943 | 71.13 |
| 7 | 2 | 50 | 11.307 | 8.764 | 71.13 |
| 8 | 2 | 50 | 12.204 | 9.531 | 71.13 |
| 9 | 2 | 100 | 12.514 | 10.325 | 71.13 |
| 10 | 2 | 100 | 14.307 | 11.120 | 71.13 |
| 10 | 2 | 100 | 14.617 | 11.120 | 71.13 |
| 11 | 2 | 100 | 15.341 | 11.914 | 71.13 |
| 12 | 2 | 100 | 16.168 | 12.708 | 71.13 |
| 12 | 2 | 100 | 16.823 | 12.708 | 71.13 |
| 13 | 2 | 100 | 19.098 | 14.297 | 71.13 |
| 14 | 2 | 100 | 21.374 | 15.885 | 71.13 |
| 15 | 2 | 100 | 23.959 | 17.474 | 71.13 |
| 16 | 2 | 100 | 26.820 | 19.062 | 71.13 |
| 1 | 2 | 100 | 6.412 | 2.542 | 96.36 |
| 2 | 2 | 100 | 7.136 | 3.177 | 96.36 |
| 3 | 2 | 100 | 8.791 | 4.866 | 96.36 |
| 4 | 2 | 100 | 10.584 | 6.354 | 96.36 |
| 5 | 2 | 100 | 11.480 | 7.148 | 96.36 |
| 6 | 2 | 100 | 13.203 | 7.943 | 96.36 |
| 7 | 2 | 100 | 13.514 | 8.764 | 96.36 |
| 8 | 2 | 100 | 14.479 | 9.531 | 96.36 |
| 9 | 2 | 100 | 15.582 | 10.325 | 96.36 |
| 10 | 2 | 100 | 16.547 | 11.120 | 96.36 |
| 11 | 2 | 100 | 18.202 | 11.914 | 96.36 |
| 12 | 2 | 100 | 18.788 | 12.708 | 96.36 |
| 12 | 2 | 100 | 19.374 | 12.708 | 96.36 |
| 13 | 2 | 100 | 21.856 | 14.297 | 96.36 |
| 14 | 2 | 100 | 24.338 | 15.885 | 96.36 |
| 15 | 2 | 100 | 27.131 | 17.474 | 96.36 |
| 16 | 2 | 100 | 30.681 | 19.062 | 96.36 |
| 1 | 2 | 50 | 8.515 | 2.542 | 148.52 |
| 2 | 2 | 50 | 9.515 | 3.177 | 148.52 |
| 3 | 2 | 50 | 11.790 | 4.866 | 148.52 |
| 4 | 2 | 50 | 13.996 | 6.354 | 148.52 |
| 5 | 2 | 50 | 15.237 | 7.148 | 148.52 |
| 6 | 2 | 50 | 16.409 | 7.943 | 148.52 |
| 7 | 2 | 50 | 17.650 | 8.764 | 148.52 |
| 8 | 2 | 50 | 18.754 | 9.531 | 148.52 |
| 9 | 2 | 50 | 20.064 | 10.325 | 148.52 |
| 10 | 2 | 50 | 21.856 | 11.120 | 148.52 |
| 11 | 2 | 50 | 23.304 | 11.914 | 148.52 |
| 12 | 2 | 50 | 24.683 | 12.708 | 148.52 |
| 13 | 2 | 50 | 27.406 | 14.297 | 148.52 |
| 14 | 2 | 100 | 30.681 | 15.885 | 148.52 |

Table B-14 (continued)

| Run | Trans-ducer | Attenua-tion | Pressure x10$^{-4}$ (dyn/cm$^2$) | Flow (cc/sec) | L/D |
|---|---|---|---|---|---|
| 15 | 2 | 100 | 33.887 | 17.474 | 148.52 |
| 16 | 2 | 100 | 37.576 | 19,062 | 148.52 |
| 1 | 2 | 50 | 11.169 | 2.542 | 213.38 |
| 2 | 2 | 50 | 12.583 | 3.177 | 213.38 |
| 3 | 2 | 50 | 15.685 | 4.866 | 213.38 |
| 4 | 2 | 50 | 18.616 | 6.354 | 213.38 |
| 5 | 2 | 50 | 20.133 | 7.148 | 213.38 |
| 6 | 2 | 50 | 21.718 | 7.943 | 213.38 |
| 7 | 2 | 50 | 23.235 | 8.764 | 213.38 |
| 8 | 2 | 50 | 24.717 | 9.531 | 213.38 |
| 9 | 2 | 50 | 26.234 | 10.325 | 213.38 |
| 10 | 2 | 100 | 27.717 | 11.120 | 213.38 |
| 10 | 2 | 100 | 28.958 | 11.120 | 213.38 |
| 11 | 2 | 100 | 29.820 | 11.932 | 213.38 |
| 12 | 2 | 100 | 31.130 | 12.708 | 213.38 |
| 13 | 2 | 100 | 34.474 | 14.297 | 213.38 |
| 14 | 2 | 100 | 38.438 | 15.885 | 213.38 |
| 15 | 2 | 100 | 42.265 | 17.474 | 213.38 |
| 16 | 2 | 100 | 46.953 | 19.062 | 213.38 |
| 1 | 2 | 50 | 15.168 | 2.542 | 304.83 |
| 2 | 2 | 50 | 16.823 | 3.177 | 304.83 |
| 3 | 2 | 50 | 21.167 | 4.866 | 304.83 |
| 4 | 2 | 50 | 24.993 | 6.354 | 304.83 |
| 6 | 2 | 100 | 28.613 | 7.943 | 304.83 |
| 8 | 2 | 100 | 32.543 | 9.531 | 304.83 |
| 10 | 2 | 100 | 36.542 | 11.120 | 304.83 |
| 12 | 2 | 100 | 41.368 | 12.708 | 304.83 |
| 12 | 2 | 100 | 40.610 | 12.708 | 304.83 |
| 13 | 2 | 100 | 45.643 | 14.297 | 304.83 |
| 14 | 2 | 100 | 49.849 | 15.885 | 304.83 |
| 15 | 2 | 100 | 54.330 | 17.474 | 304.83 |
| 16 | 2 | 100 | 58.777 | 19.062 | 304.83 |

FIGURE B.1

PRESSURE FLUCTUATIONS
0.10 cm I.D. CAPILLARY, LARGE RESERVOIR

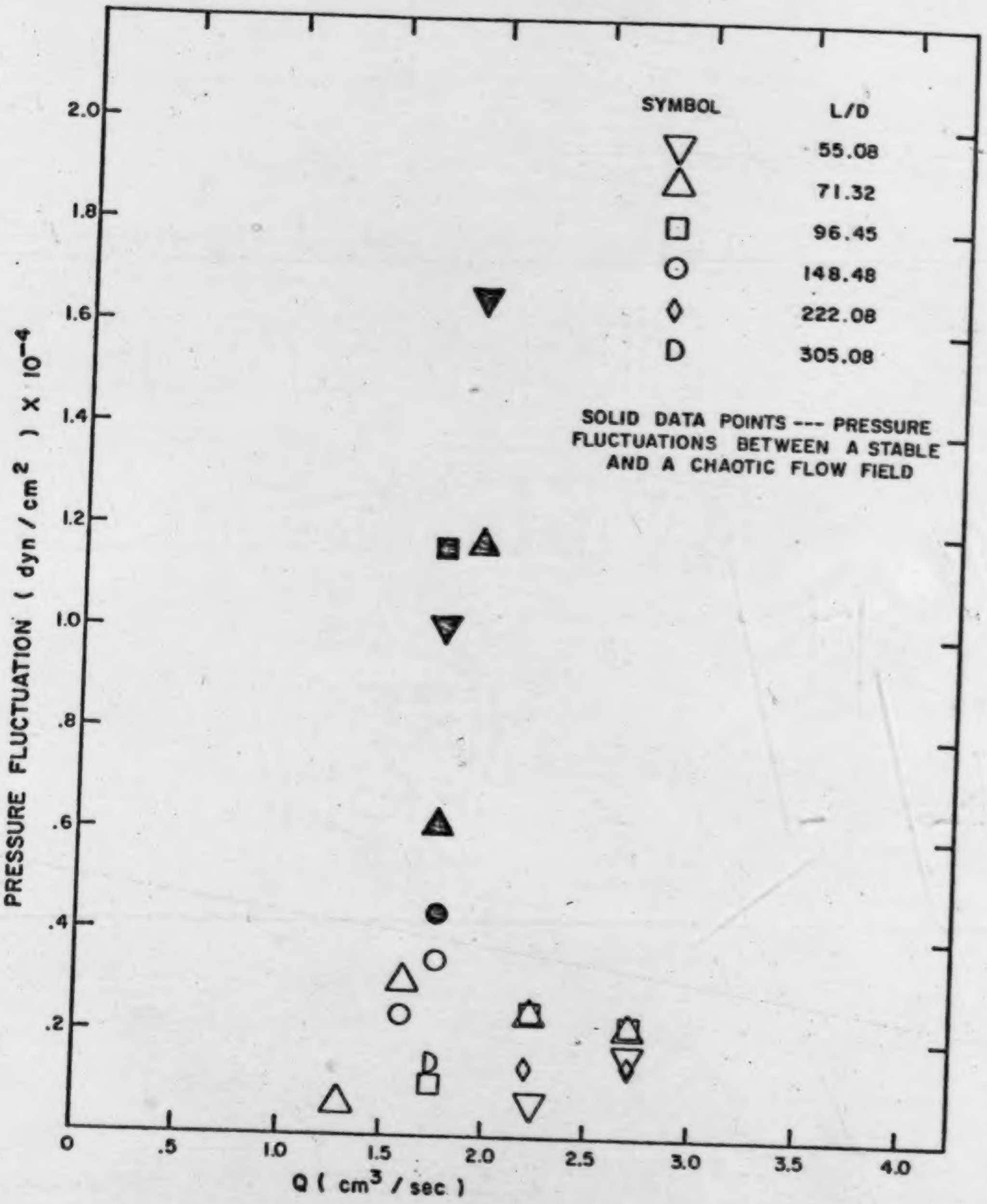

FIGURE B.2

PRESSURE FLUCTUATIONS
0.20 cm I.D. CAPILLARY, LARGE RESERVOIR

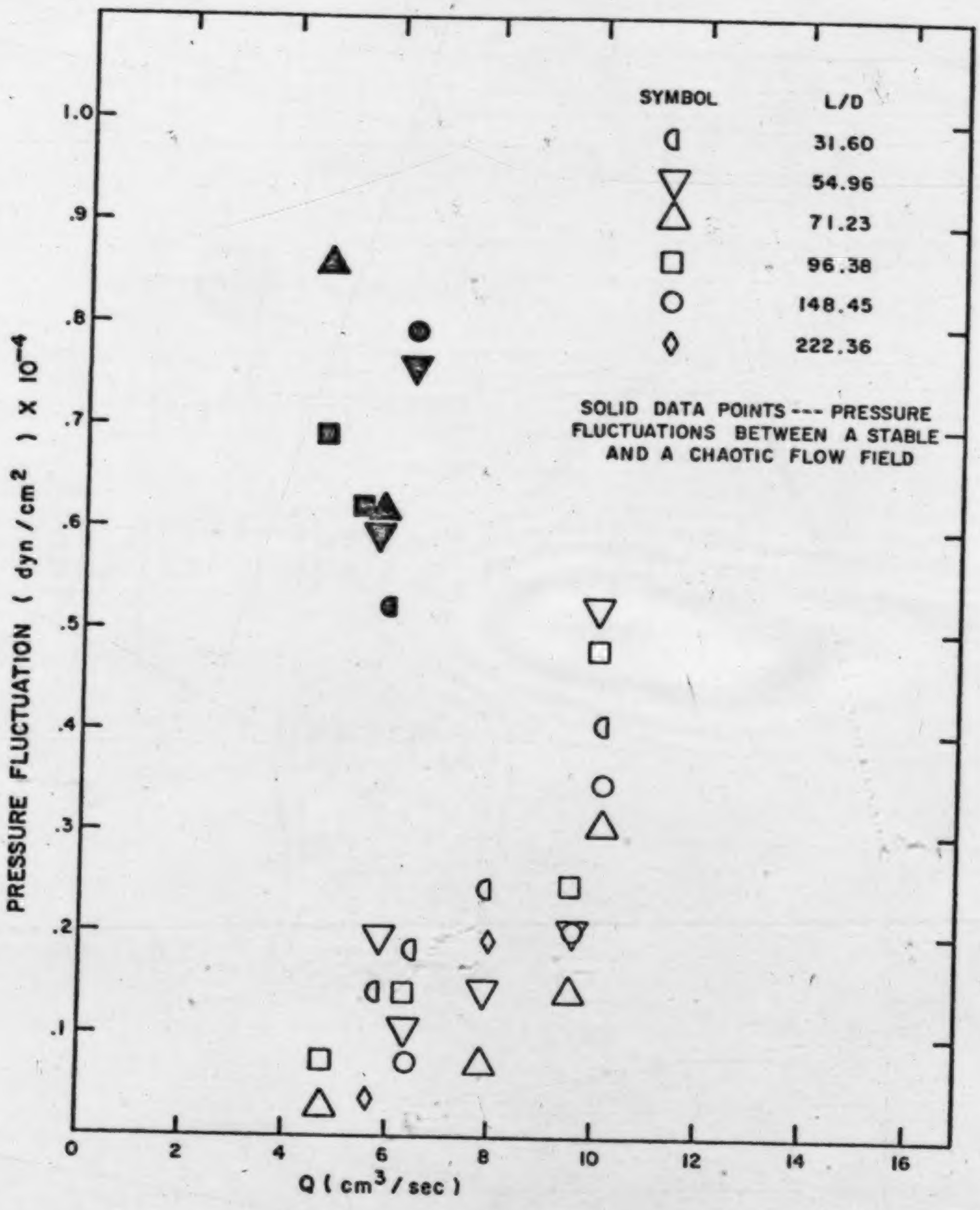

FIGURE B.3
PRESSURE FLUCTUATIONS
0.30 cm I.D. CAPILLARY, LARGE RESERVOIR

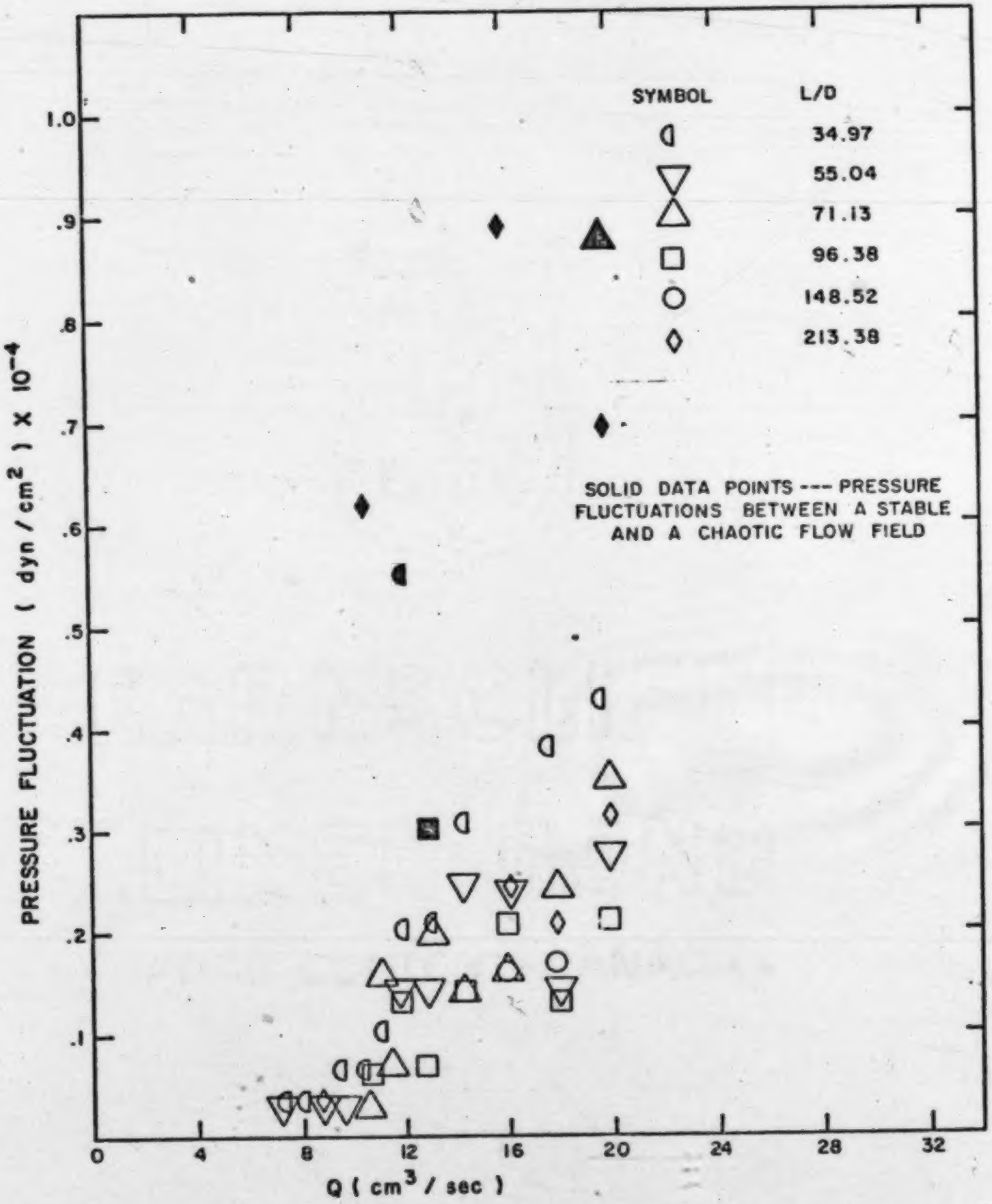

# APPENDIX C

# CONTRACTION LOSSES

## C.1 NEWTONIAN FLUIDS

The Bagley plot was constructed using the total pressure loss-L/D data tabulated in Appendix B. In this analysis the velocity field is assumed to be fully developed prior to the end of the capillary tube. The total pressure loss is comprised, therefore, of the developed pressure losses, $\Delta P_d$, and the contraction losses, $\Delta P_c$, given by

$$\Delta P_t = \Delta P_d + \Delta P_c \tag{C.1}$$

where

$$\Delta P_d = 4\tau_w \; L/D \tag{C.2}$$

Equating the contraction loss to the developed pressure loss measured over an equivalent length of capillary tube, $\varepsilon_v D$, yields

$$\Delta P_t = 4\tau_w (L/D + \varepsilon_v) \tag{C.3}$$

where $\varepsilon_v$ is the Bagley entrance correction (76). The contraction losses and the shear stresses are evaluated from the intercept and slope of Equation C.3. The data in Appendix B was curve fitted to Equation C.3 in the sense of least squares. The resulting values for the contraction losses and the Bagley entrance correction factors are tabulated in Tables C.1 and C.2 for reservoirs S and L respectively. The shear stresses can be found in Appendix D, Table D.1.

Values of the dimensionless contraction loss, $\Phi$, defined by

$$\Phi = \Delta P_c/(\rho\frac{\bar{V}^2}{2}) \qquad \text{C.4}$$

are also tabulated in Tables C.1 and C.2.

## C.2 VISCOELASTIC FLUID

Bagley plots were used also in the evaluation of the contraction losses and shear stresses for the 0.20% aqueous solution of Separan AP-30. The contraction loss - Reynolds number data are tabulated in Tables C.3 and C.4 for reservoirs S and L respectively. To distinguish the difference in the contraction losses, $\varepsilon_t$ was used in place of $\varepsilon_v$ in Equation C.3 where $\varepsilon_t$ includes both the viscous and elastic contributions. The only assumption in estimating the contraction losses with the Bagley plot for the viscoelastic fluid was the assumption of a zero exit pressure.

For capillary tube lengths longer than the entry length, the exit pressures are constant (161). Figure C.1 qualitatively depicts the effect of this exit pressure on the pressure profile and on the Bagley plot. If the exit pressure is not equal to zero then Equation C.3 must be modified to

$$\Delta P_t - \Delta P_{exit} = 4\tau_w(L/D+\varepsilon_t) \qquad \text{C.5}$$

where the equivalent length for the viscoelastic fluid is $\varepsilon_t$. Failure to subtract the exit pressure from the total pressure loss would result in an overestimation of the contraction losses. Although the exit pressure was not measured directly, an estimate of its magnitude can be obtained from the results reported by Sylvester (161). He estimated that the exit pressure was $\pm 6.89 \times 10^2$ dyn/cm$^2$ by using a pressure profile and by extrapolation of the developed pressure gradient, dP/dx, to the end of the capillary tube. Since the solutions used by Sylvester were approximately an order of magnitude greater in concentration than that used in this research and since the exit pressure decreased with increase in concentration, it can be reasonably assumed that the exit pressure for the 0.20% aqueous solutions of Separan AP-30 was less than 70 dyn/cm$^2$. Under the worst condition this exit pressure resulted in a 1.5% error in the contraction losses and was assumed to be negligible for all experimental runs.

The list of tables and a figure contained in this appendix is given below:

| TABLE NO. | DESCRIPTION |
|---|---|
| C.1 | Contraction Losses and Reynolds Numbers for Newtonian Fluids, Small Reservoir |
| C.2 | Contraction Losses and Reynolds Numbers for Newtonian Fluids, Large Reservoir |
| C.3 | Contraction Losses and Reynolds Numbers for 0.20% Separan AP-30 - Small Reservoir |
| C.4 | Contraction Losses and Reynolds Numbers for 0.20% Separan AP-30 - Large Reservoir |
| **FIGURE NO.** | |
| C.1 | Pressure Profile and Bagley Plot |

## TABLE C.1

## CONTRACTION LOSSES AND REYNOLDS NUMBERS FOR NEWTONIAN FLUIDS, SMALL RESERVOIR

| Solution | Run No. | $\Delta P_c \times 10^{-4}$ (dyn/cm$^2$) | $\Phi$ | $\varepsilon_v$ | $N_{Re}$ |
|---|---|---|---|---|---|
| Sugar #1 | 1 | 0.572 | 4.08 | 8.26 | 126.88 |
| | 2 | 0.999 | 3.13 | 9.65 | 191.36 |
| | 3 | 1.575 | 2.81 | 11.47 | 253.75 |
| | 4 | 4.980 | 2.21 | 17.81 | 509.18 |
| | 5 | 10.298 | 2.00 | 23.62 | 769.89 |
| | 6 | 19.605 | 2.16 | 33.85 | 1020.63 |
| | 7 | 29.644 | 2.13 | 41.19 | 1263.75 |
| | 8 | 44.940 | 2.18 | 51.68 | 1539.78 |
| Sugar #3 | 1 | 0.569 | 8.05 | 5.95 | 46.73 |
| | 2 | 0.800 | 5.54 | 5.84 | 66.79 |
| | 3 | 1.096 | 4.47 | 6.15 | 87.07 |
| | 4 | 1.606 | 4.29 | 7.23 | 107.57 |
| | 5 | 2.834 | 2.86 | 7.76 | 175.03 |
| | 6 | 5.757 | 2.48 | 10.02 | 268.05 |
| | 7 | 11.824 | 2.65 | 15.85 | 371.44 |
| | 8 | 16.713 | 2.34 | 17.54 | 469.53 |
| | 9 | 23.759 | 1.98 | 18.62 | 608.41 |
| | 10 | 51.752 | 2.11 | 28.09 | 870.72 |
| Sugar #4 | 1 | 2.324 | 15.42 | 4.88 | 20.63 |
| | 2 | 2.930 | 11.44 | 4.80 | 26.89 |
| | 3 | 3.385 | 8.66 | 4.42 | 33.22 |
| | 4 | 5.171 | 8.58 | 5.58 | 41.25 |
| | 5 | 7.233 | 7.63 | 6.26 | 51.74 |
| | 6 | 7.205 | 5.96 | 5.04 | 62.15 |
| Primol-355 | 1 | 2.772 | 108.71 | 4.36 | 2.60 |
| | 2 | 3.241 | 64.87 | 3.59 | 3.63 |
| | 3 | 4.426 | 43.45 | 3.47 | 5.16 |
| | 4 | 6.722 | 29.01 | 3.49 | 7.79 |
| | 5 | 9.280 | 22.78 | 3.65 | 10.33 |
| | 6 | 11.411 | 19.50 | 3.76 | 12.62 |
| | 7 | 18.629 | 23.33 | 5.36 | 14.58 |

## TABLE C.2

## CONTRACTION LOSSES AND REYNOLDS NUMBERS FOR NEWTONIAN FLUIDS, LARGE RESERVOIR

| Solution | Run No. | $\Delta P_c \times 10^{-4}$ (dyn/cm$^2$) | $\Phi$ | $\varepsilon_v$ | $N_{Re}$ |
|---|---|---|---|---|---|
| Sugar #1 | 1 | 0.439 | 3.13 | 6.39 | 129.28 |
| | 2 | 0.843 | 2.65 | 8.18 | 194.98 |
| | 3 | 1.390 | 2.48 | 10.34 | 258.55 |
| | 4 | 4.985 | 2.21 | 18.40 | 517.11 |
| | 5 | 10.445 | 2.02 | 24.92 | 784.45 |
| | 6 | 17.843 | 1.97 | 31.17 | 1039.93 |
| | 7 | 28.792 | 2.07 | 40.58 | 1287.65 |
| | 8 | 40.686 | 1.97 | 46.76 | 1568.90 |
| Sugar #3 | 2 | 0.448 | 3.10 | 3.19 | 66.98 |
| | 3 | 0.793 | 3.23 | 4.37 | 87.32 |
| | 4 | 1.172 | 3.13 | 5.30 | 107.87 |
| | 5 | 2.379 | 2.40 | 6.70 | 175.52 |
| | 6 | 5.964 | 2.57 | 10.42 | 268.80 |
| | 7 | 11.687 | 2.62 | 15.89 | 372.48 |
| Sugar #4 | 1 | 1.343 | 8.91 | 3.08 | 21.81 |
| | 2 | 1.517 | 5.95 | 2.66 | 28.44 |
| | 3 | 1.862 | 4.77 | 2.62 | 35.13 |
| | 4 | 2.572 | 4.26 | 2.89 | 43.63 |
| | 5 | 3.654 | 3.85 | 3.23 | 54.72 |
| | 6 | 4.454 | 3.69 | 3.25 | 65.73 |
| Primol-355 | 1 | 1.731 | 67.18 | 2.80 | 2.66 |
| | 2 | 2.213 | 43.88 | 2.56 | 3.72 |
| | 3 | 3.434 | 33.71 | 2.79 | 5.29 |
| | 4 | 3.709 | 16.01 | 1.95 | 7.98 |
| | 5 | 7.405 | 18.17 | 3.02 | 10.49 |
| | 6 | 7.474 | 12.28 | 2.50 | 12.93 |
| | 7 | 9.053 | 11.15 | 2.60 | 14.93 |

# TABLE C.3

## CONTRACTION LOSSES AND REYNOLDS NUMBERS FOR 0.20% SEPARAN AP-30, SMALL RESERVOIR

| Capillary I.D. (cm) | Run No. | $\Delta P_c \times 10^{-4}$ (dyn/cm$^2$) | $\Phi_t$ | $\varepsilon_t$ | $N'_{Re}$ |
|---|---|---|---|---|---|
| 0.10 | 1 | 1.904 | 23.28 | 23.23 | 62.59 |
| | 2 | 2.271 | 19.28 | 24.76 | 81.21 |
| | 3 | 2.720 | 13.03 | 24.19 | 121.56 |
| | 4 | 3.891 | 12.00 | 30.37 | 164.92 |
| | 5 | 5.307 | 10.38 | 35.73 | 224.72 |
| | 6 | 6.843 | 9.29 | 40.66 | 286.49 |
| | 7 | 8.391 | 8.37 | 44.83 | 350.53 |
| | 8 | 10.945 | 8.36 | 55.16 | 416.26 |
| | 9 | 12.589 | 7.60 | 55.61 | 483.36 |
| | 9 | 18.358 | 11.08 | 81.10 | 483.36 |
| | 10 | 22.039 | 10.77 | 91.36 | 551.32 |
| | 11 | 26.196 | 10.58 | 100.24 | 619.97 |
| | 12 | 29.553 | 10.01 | 106.39 | 689.96 |
| | 13 | 36.553 | 9.12 | 120.12 | 828.20 |
| | 14 | 48.499 | 8.20 | 137.68 | 1036.98 |
| | 15* | 1.158 | 33.00 | 21.00 | 41.37 |
| | 16* | 1.000 | 49.00 | 17.00 | 22.72 |
| | 17* | 0.525 | 65.00 | 13.50 | 11.34 |
| | 18* | 0.320 | 385.00 | 10.60 | 2.04 |
| | 19* | 0.241 | 525.00 | 9.40 | 1.32 |
| 0.20 | 1 | 1.221 | 14.92 | 22.35 | 90.95 |
| | 2 | 1.359 | 10.63 | 21.29 | 126.36 |
| | 3 | 1.954 | 10.61 | 27.67 | 164.99 |
| | 4 | 2.959 | 10.29 | 38.08 | 228.04 |
| | 5 | 3.515 | 9.51 | 40.86 | 273.00 |
| | 6 | 4.260 | 8.33 | 45.19 | 344.21 |
| | 7 | 9.231 | 8.02 | 77.83 | 607.31 |
| | 8 | 11.489 | 7.77 | 88.94 | 721.05 |
| | 9 | 13.104 | 7.91 | 99.88 | 779.53 |
| | 10 | 13.789 | 6.74 | 83.65 | 908.31 |
| | 11 | 21.201 | 6.63 | 116.09 | 1209.25 |
| | 12 | 29.872 | 6.49 | 148.75 | 1532.84 |
| | 13 | 38.273 | 6.11 | 173.60 | 1865.85 |
| 0.30 | 1 | 0.872 | 13.49 | 21.98 | 93.84 |
| | 2 | 1.054 | 10.43 | 22.52 | 131.00 |
| | 3 | 1.916 | 8.09 | 32.41 | 246.44 |
| | 4 | 2.970 | 7.35 | 42.54 | 364.53 |
| | 5 | 3.561 | 6.96 | 47.10 | 432.63 |
| | 6 | 4.222 | 6.69 | 51.91 | 504.02 |
| | 7 | 5.032 | 6.59 | 58.49 | 578.11 |

* obtained with batch number two

TABLE C.3 (continued)

| Capillary I.D. (cm) | Run No. | $\Delta P_c \times 10^{-4}$ (dyn/cm$^2$) | $\Phi_t$ | $\varepsilon_t$ | $N'_{Re}$ |
|---|---|---|---|---|---|
| 0.30 | 8 | 5.740 | 6.31 | 62.26 | 655.00 |
| | 9 | 7.064 | 6.62 | 75.57 | 734.14 |
| | 10 | 7.743 | 6.26 | 76.48 | 815.51 |
| | 11 | 9.056 | 6.38 | 87.27 | 899.03 |
| | 12 | 10.200 | 6.31 | 93.95 | 984.53 |
| | 13 | 11.868 | 6.80 | 97.81 | 1160.78 |
| | 14 | 14.103 | 5.59 | 109.52 | 1343.36 |
| | 15 | 17.452 | 5.71 | 126.90 | 1531.31 |
| | 16 | 19.237 | 5.29 | 122.20 | 1724.41 |

## TABLE C.4

## CONTRACTION LOSSES AND REYNOLDS NUMBERS FOR 0.20% SEPARAN AP-30, LARGE RESERVOIR

| Capillary I.D. (cm) | Run No. | $\Delta P_c \times 10^{-4}$ (dyn/cm$^2$) | $\Phi_t$ | $\varepsilon_t$ | $N'_{Re}$ |
|---|---|---|---|---|---|
| 0.10 | 1 | 1.377 | 16.83 | 16.98 | 62.59 |
| | 2 | 2.324 | 19.73 | 26.41 | 81.20 |
| | 3 | 3.195 | 15.30 | 30.52 | 121.56 |
| | 4 | 3.943 | 12.05 | 32.31 | 165.92 |
| | 5 | 5.288 | 10.34 | 37.03 | 224.72 |
| | 6 | 7.166 | 9.73 | 44.95 | 286.49 |
| | 7 | 8.398 | 8.39 | 46.73 | 350.53 |
| | 8 | 10.038 | 7.67 | 51.09 | 416.26 |
| | 9 | 12.054 | 7.28 | 56.32 | 483.36 |
| | 10 | 14.171 | 6.93 | 62.23 | 551.32 |
| | 11 | 15.995 | 6.46 | 64.21 | 619.97 |
| | 11 | 17.535 | 7.08 | 68.55 | 619.97 |
| | 12 | 23.612 | 8.00 | 90.54 | 689.96 |
| | 13 | 28.235 | 7.04 | 94.09 | 828.20 |
| | 14 | 36.134 | 6.11 | 102.71 | 1036.99 |
| 0.20 | 1 | 0.938 | 11.46 | 17.55 | 90.95 |
| | 2 | 1.251 | 9.79 | 20.75 | 126.36 |
| | 3 | 1.846 | 10.03 | 28.30 | 164.99 |
| | 4 | 2.413 | 8.39 | 32.35 | 228.04 |
| | 5 | 2.862 | 7.75 | 35.62 | 273.00 |
| | 6 | 3.459 | 6.76 | 38.69 | 344.21 |
| | 7 | 6.143 | 5.34 | 51.26 | 607.31 |
| | 8 | 7.558 | 5.11 | 59.04 | 721.05 |
| | 8 | 8.997 | 6.09 | 71.82 | 721.05 |
| | 9 | 8.741 | 5.28 | 68.41 | 779.53 |
| | 9 | 9.896 | 5.97 | 77.00 | 779.53 |
| | 10 | 9.807 | 4.79 | 70.96 | 898.75 |
| | 10 | 11.523 | 5.63 | 83.59 | 898.75 |
| | 11 | 16.081 | 5.03 | 95.38 | 1209.25 |
| | 12 | 23.269 | 5.06 | 127.74 | 1532.84 |
| | 13 | 29.651 | 4.73 | 140.12 | 1865.85 |
| 0.30 | 1 | 0.416 | 6.43 | 9.95 | 93.84 |
| | 2 | 0.657 | 6.50 | 14.06 | 131.00 |
| | 3 | 1.201 | 5.07 | 20.38 | 246.44 |
| | 4 | 1.918 | 4.75 | 27.72 | 364.53 |
| | 5 | 2.457 | 4.80 | 33.41 | 432.63 |
| | 6 | 3.176 | 5.03 | 41.03 | 504.02 |
| | 7 | 3.437 | 4.50 | 41.19 | 578.11 |
| | 8 | 4.036 | 4.44 | 46.26 | 655.00 |
| | 9 | 4.390 | 4.11 | 47.15 | 734.14 |

TABLE C.4 (continued)

| Capillary I.D. (cm) | Run No. | $\Delta P_c \times 10^{-4}$ (dyn/cm$^2$) | $\Phi_t$ | $\varepsilon_t$ | $N'_{Re}$ |
|---|---|---|---|---|---|
| 0.30 | 10 | 5.344 | 4.32 | 55.55 | 815.51 |
| | 10 | 5.508 | 4.45 | 54.64 | 815.51 |
| | 11 | 6.451 | 4.54 | 64.22 | 873.00 |
| | 12 | 6.933 | 4.29 | 66.57 | 984.53 |
| | 12 | 7.201 | 4.46 | 68.62 | 984.53 |
| | 13 | 8.266 | 4.04 | 71.34 | 1160.78 |
| | 14 | 9.649 | 3.82 | 71.57 | 1343.36 |
| | 15 | 12.780 | 4.18 | 98.64 | 1531.31 |
| | 16 | 14.499 | 3.99 | 102.90 | 1724.41 |
| | 16 | 12.569 | 3.46 | 89.20 | 1724.41 |

FIGURE C.1

PRESSURE PROFILE & BAGLEY PLOT

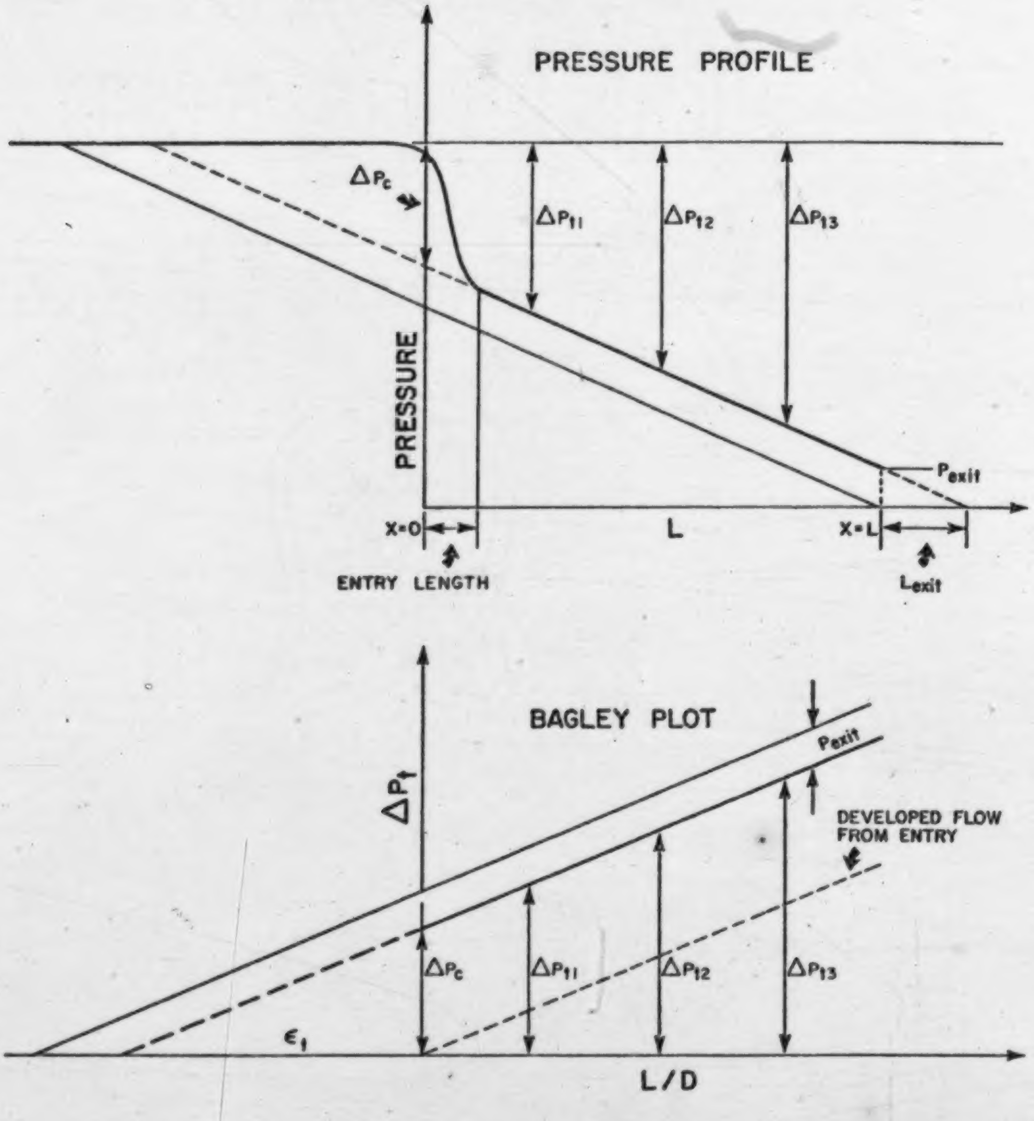
PRESSURE PROFILE
$\Delta P_c$
$\Delta P_{t1}$
$\Delta P_{t2}$
$\Delta P_{t3}$
PRESSURE
$P_{exit}$
X=0
L
X=L
ENTRY LENGTH
$L_{exit}$
BAGLEY PLOT
$\Delta P_t$
$P_{exit}$
DEVELOPED FLOW FROM ENTRY
$\Delta P_c$
$\Delta P_{t1}$
$\Delta P_{t2}$
$\Delta P_{t3}$
$\epsilon_1$
L/D

# APPENDIX D

# PHYSICAL PROPERTIES

## D.1 NEWTONIAN SOLUTIONS

The shear stresses and the corresponding shear rates for each experimental run are tabulated in Table D.1. The shear stresses were obtained from the slope of the Bagley plots as discussed in Appendix C. For the duration of a complete experimental run, i.e., obtaining the total pressure losses for several tube lengths used to construct a Bagley plot, the temperature of each solution fluctuated by as much as ±1°F. This temperature fluctuation is typical of that which occurred between experimental runs. Therefore, for each solution an average viscosity was determined by summing up the viscosities from each experimental run and dividing by the number of experimental runs. The viscosities for each experimental run are plotted in Figure D.1. The average viscosity and mean temperature for each Newtonian solution is given in Table D.2. These average values of viscosity were used in evaluating the Reynolds number. The viscosity of each Newtonian solution was measured with an Ostwald viscometer at the mean temperature and at ±1°F of the mean temperature. The results are also reported in Table D.2. Acceptable agreement was obtained between the measured and experimental values.

The density of each Newtonian fluid was determined to be insensitive to temperature fluctuations of ±1°F of the mean temperature, hence was assumed constant. The densities are reported in Table D.2.

## D.2 VISCOELASTIC SOLUTION

The flow curve for the aqueous 0.20% solution of Separan AP-30 at high apparent shear rates is given in Figure D.2 while that at apparent shear rates less than 2 $\sec^{-1}$ is shown in Figure D.3. The solid line through the data in Figure D.2 was determined by the least squares criterion to be

$$\ell n\tau_w = 0.99765+0.52691[\ell n(\frac{8V}{D})]+0.03464[\ell n(\frac{8V}{D})^2]$$
$$-0.00844[\ell n(\frac{8V}{D})^3]+0.00053[\ell n(\frac{8V}{D})^4] \qquad \text{D.1}$$

where (8V/D) is the apparent shear rate. Equation D.1 adequately represents the data for apparent shear rates greater than unity. Data plotted in Figure D.2 were obtained from both reservoirs (S and L) and the shear stresses were, as expected, independent of reservoir size. The Weissenberg rheogoniometer was used to measure shear stresses at apparent shear rates less than 426 $\sec^{-1}$. These data superimpose upon the data obtained from the Bagley plots. Two batches of 0.20% aqueous polymeric solution of Separan AP-30 were used in this research and as shown in Figure D.2 there were no significant differences in the shear stresses for overlapping apparent shear rates, i.e., apparent shear rates greater than 3 $\sec^{-1}$.

Since the shear stresses were independent of reservoir size, physical properties summarized in Tables D.3 and D.4 were arbitrarily chosen from the data obtained with batch 2 in reservoir S and batch 1 in reservoir L. The flow behaviour index tabulated in Tables D.3 and D.4 is equal to the derivative of Equation D.1 and is given by

$$n' = \frac{d(\ell n \tau_w)}{d\ell n(\frac{8V}{D})} = 0.52691+0.06928[\ell n(\frac{8V}{D})]$$

$$-0.02532[\ell n(\frac{8V}{D})^2]+0.00212[\ell n(\frac{8V}{D})^3] \qquad D.2$$

The apparent viscosities determined by Equation D.3

$$\mu_A = \tau_w/(\frac{8V}{D}) \qquad D.3$$

and plotted in Figure D.4, resulted in the zero shear apparent viscosity being equal to 5.2 poise.

The thrust apparatus and the Weissenberg rheogoniometer were used to measure the first normal stress difference. The calibration curve for the normal force spring used with the Weissenberg rheogoniometer, 5 cm diameter 2° cone, discussed in Appendix A, resulted in a sensitivity of 194.040 dyn/cm$^2$ per volt at 68±1°F. For a given apparent shear rate the inertial contribution to the normal force measurements was subtracted from the total force exerted by the polymer solution. This inertial correction was determined by a Newtonian fluid having a viscosity of 5 poise. The inertial correction factor plotted in Figure D.5 was essentially zero for apparent shear rates less than $10^2$ sec$^{-1}$. For apparent shear rates greater than this, the inertial correction increased to a maximum of 7.840 dyn/cm$^2$ at an apparent shear rate of 850 $\sec^{-1}$. The resulting first normal stress differences, given in Table D.5, are plotted in Figure D.6. The solid lines in Figure D.6 were determined by the least squares criterion, and for batches 1 and 2 were

$$\ell n(P_{11}-P_{22})_w = 0.6178+1.013[\ell n(\frac{8V}{D})] \qquad D.4$$

and

$$\ell n(P_{11}-P_{22})_w = 0.7204+1.024[\ell n(\frac{8V}{D})] \qquad D.5$$

These data indicate no significant differences in the first normal stress difference between batches 1 and 2 and are in agreement with the extrapolation of the data obtained from the rheogoniometer.

In SLSF the relaxation time of the fluid using a Maxwell model (116) is defined as

$$\theta = \frac{(P_{11}-P_{22})_w}{2(\frac{8V}{D})\tau_w} \qquad D.6$$

The relaxation times determined by Equation D.6 and the data in Table D.5 are plotted in Figure D.7. The zero shear relaxation time, $\theta_0$, was somewhat greater than 0.4 sec which was measured at an apparent shear rate approximately equal to 10 $\sec^{-1}$. Hlavacek (83) estimated the zero shear relaxation time to be 1 sec and it was this value that was used in the analysis presented in Chapter III. The zero shear relaxation time calculated by Bueche's analysis (118) was equal to 0.40 sec.

The tables and figures contained in Appendix D are listed below:

| TABLE NO. | DESCRIPTION |
|---|---|
| D.1 | Shear Stress - Shear Rate for Newtonian Solutions |
| D.2 | Viscosity and Density, Newtonian Solutions |
| D.3 | Physical Properties of 0.20% Separan AP-30; Batch 2, Small Reservoir |
| D.4 | Physical Properties of 0.20% Separan AP-30; Batch 1, Large Reservoir |
| D.5 | Normal Force Data |

| FIGURE NO. | DESCRIPTION |
|---|---|
| D-1 | Newtonian Viscosities |
| D-2 | Flow Curve 0.20% Separan AP-30, High Apparent Shear Rates |
| D-3 | Flow Curve 0.20% Separan AP-30, Low Apparent Shear Rates |
| D-4 | Apparent Viscosity, 0.20% Separan AP-30 |
| D-5 | Internal Contribution to Normal Force (Rheogonimeter) |
| D-6 | Normal Stress |
| D-7 | Relaxation Time |

# TABLE D.1

## SHEAR STRESS - SHEAR RATE FOR NEWTONIAN SOLUTIONS

### SHEAR RATE ($sec^{-1}$)

| Run No. | Sugar #1 | Sugar #3 | Sugar #4 | Primol-355 |
|---|---|---|---|---|
| 1 | 1929 | 1350 | 1929 | 971 |
| 2 | 2909 | 1929 | 2515 | 1357 |
| 3 | 3858 | 2515 | 3107 | 1929 |
| 4 | 7741 | 3107 | 3858 | 2909 |
| 5 | 11705 | 5055 | 4838 | 3858 |
| 6 | 15517 | 7741 | 5812 | 4716 |
| 7 | 19213 | 10727 | - | 5446 |
| 8 | 23410 | 13560 | - | - |
| 9 | - | 17571 | - | - |
| 10 | - | 25416 | - | - |

### LARGE RESERVOIR - SHEAR STRESS ($dyn/cm^2$)

| Run No. | Sugar #1 (73.0°F) | Sugar #3 (72.0°F) | Sugar #4 (72.0°F) | Primol-355 (73.5°F) |
|---|---|---|---|---|
| 1 | 172 | - | 1089 | 1544 |
| 2 | 258 | 351 | 1427 | 2165 |
| 3 | 336 | 454 | 1776 | 3075 |
| 4 | 677 | 553 | 2225 | 4753 |
| 5 | 1048 | 888 | 2830 | 6129 |
| 6 | 1431 | 1431 | 3423 | 7467 |
| 7 | 1774 | 1839 | - | 8694 |
| 8 | 2175 | - | - | - |
| 9 | - | - | - | - |
| 10 | - | - | - | - |

## TABLE D.1 (continued)

## SMALL RESERVOIR - SHEAR STRESS (dyn/$cm^2$)

| Run No. | Sugar #1 (72.5°F) | Sugar #3 (72.0°F) | Sugar #4 (73.5°F) | Primol-355 (73.0°F) |
|---|---|---|---|---|
| 1 | 173 | 239 | 1190 | 1588 |
| 2 | 259 | 343 | 1527 | 2254 |
| 3 | 343 | 445 | 1914 | 3189 |
| 4 | 716 | 556 | 2318 | 4812 |
| 5 | 1090 | 913 | 2890 | 6348 |
| 6 | 1448 | 1437 | 3573 | 7581 |
| 7 | 1799 | 1862 | - | 8687 |
| 8 | 2174 | 2400 | - | - |
| 9 | - | 3190 | - | - |
| 10 | - | 4606 | - | - |

## TABLE D.2

## VISCOCITY AND DENSITY

## NEWTONIAN SOLUTIONS

| | SOLUTIONS | | | |
|---|---|---|---|---|
| | Sugar #1 | Sugar #3 | Sugar #4 | Primol-355 |
| **SMALL RESERVOIR** | | | | |
| Mean Temperature (°F) | 72.5 | 72.0 | 71.5 | 73.0 |
| Average Viscosity (cp) | 9.16 | 17.92 | 60.60 | 163.62 |
| *Ostwald Viscometer (cp) | 9.4±.25 | 17.60±.5 | 59.0±2 | 171.75±6.5 |
| Density (gm/cm$^3$) | 1.205 | 1.241 | 1.296 | 0.876 |
| **LARGE RESERVOIR** | | | | |
| Mean Temperature (°F) | 73.0 | 72.0 | 72.0 | 73.5 |
| Average Viscosity (cp) | 8.99 | 17.87 | 57.30 | 159.76 |
| *Ostwald Viscometer (cp) | 9.3±.25 | 17.60±.5 | 58±2 | 168.5±6.5 |
| Density (gm/cm$^3$) | 1.205 | 1.241 | 1.296 | 0.876 |

*Viscosity determined at the mean temperature and at ±1°F of the mean temperature

## TABLE D.3

## PHYSICAL PROPERTIES OF 0.20% SEPARAN AP-30

## BATCH 2 - SMALL RESERVOIR

7

| Capillary I.D. (cm) | Run No. | $\tau_w$ (dyn/cm$^2$) | $\frac{8V}{D}$(sec$^{-1}$) | n' |
|---|---|---|---|---|
| 0.10 | 15 | 182 | 2427 | .542 |
| | 16 | 158 | 1618 | .520 |
| | 17 | 110 | 809 | .498 |
| | 18 | 73.5 | 324 | .494 |
| | 19 | 63.0 | 243 | .497 |
| | 20 | 43.9 | 121 | .511 |
| | 21 | 30.5 | 80.9 | .522 |
| | 22 | 19.2 | 40.5 | .542 |
| 0.20 | 14 | 104 | 810 | .498 |
| | 15 | 72.7 | 405 | .493 |
| | 16 | 65.2 | 304 | .495 |
| | 17 | 50.3 | 202 | .500 |
| 0.30 | 17 | 84.8 | 600 | .494 |
| | 18 | 77.9 | 480 | .493 |
| | 19 | 57.9 | 240 | .497 |
| | 20 | 41.8 | 120 | .511 |
| | 21 | 39.3 | 90 | .519 |
| | 22 | 29.5 | 60 | .530 |
| | 23 | 5.98 | 4.5 | .583 |
| | 24 | 4.35 | 3 | .579 |
| | 25 | 9.17 | 9 | .579 |
| | 26 | 11.0 | 12 | .574 |
| | 27 | 19.9 | 30 | .551 |
| | 28 | 34.4 | 90 | .519 |
| | 29 | 37.9 | 120 | .511 |

## TABLE D.4

## PHYSICAL PROPERTIES OF 0.20% SEPARAN AP-30

## BATCH 1 - LARGE RESERVOIR

| Capillary I.D. (cm) | Run No. | $\tau_w$ (dyn/cm$^2$) | $\frac{8V}{D}$(sec$^{-1}$) | n' |
|---|---|---|---|---|
| 0.10 | 1 | 203 | 3236 | .562 |
| | 2 | 220 | 3883 | .577 |
| | 3 | 262 | 5169 | .604 |
| | 4 | 305 | 6472 | .628 |
| | 5 | 357 | 8091 | .655 |
| | 6 | 399 | 9708 | .680 |
| | 7 | 449 | 11327 | .702 |
| | 8 | 491 | 12944 | .723 |
| | 9 | 535 | 14563 | .742 |
| | 10 | 569 | 16180 | .760 |
| | 11 | 623 | 17799 | .777 |
| | 12 | 652 | 19437 | .793 |
| | 13 | 750 | 22653 | .822 |
| | 14 | 879 | 27507 | .862 |
| 0.20 | 1 | 134 | 1618 | .520 |
| | 2 | 151 | 2023 | .531 |
| | 3 | 163 | 2427 | .542 |
| | 4 | 186 | 3034 | .557 |
| | 5 | 201 | 3438 | .567 |
| | 6 | 223 | 4045 | .580 |
| | 7 | 300 | 6068 | .621 |
| | 8 | 320 | 6877 | .635 |
| | 9 | 319 | 7281 | .642 |
| | 10 | 345 | 8090 | .655 |
| | 11 | 421 | 10113 | .686 |
| | 12 | 455 | 12135 | .713 |
| | 13 | 529 | 14158 | .737 |
| 0.30 | 1 | 104 | 959 | .502 |
| | 2 | 117 | 1199 | .508 |
| | 3 | 147 | 1836 | .523 |
| | 4 | 173 | 2397 | .541 |
| | 5 | 184 | 2697 | .549 |
| | 6 | 193 | 2996 | .556 |

TABLE D.4 (continued)

| Capillary I.D. (cm) | Run No. | $\tau_w$ (dyn/cm$^2$) | $\frac{8V}{D}$(sec$^{-1}$) | n' |
|---|---|---|---|---|
| 0.30 | 7 | 209 | 3296 | .563 |
| | 8 | 218 | 3596 | .570 |
| | 9 | 233 | 3895 | .577 |
| | 10 | 241 | 4195 | .584 |
| | 11 | 251 | 4495 | .585 |
| | 12 | 260 | 4794 | .586 |
| | 13 | 290 | 5394 | .608 |
| | 14 | 337 | 5993 | .620 |
| | 15 | 324 | 6592 | .630 |
| | 16 | 352 | 7191 | .641 |

## TABLE D.5

## NORMAL FORCE DATA

| Capillary I.D. (cm) | L/D | $\frac{8V}{D}$(sec$^{-1}$) | $(P_{11}-P_{22})_w$ (dyn/cm$^2$) |
|---|---|---|---|
| 0.4452* | 196 | 3667 | 11232 |
| | | 3300 | 9901 |
| | | 2933 | 10513 |
| | | 2567 | 6272 |
| | | 2200 | 3952 |
| | | 1833 | 3590 |
| | | 1466 | 3483 |
| | | 1100 | 2566 |
| | | 733 | 2804 |
| | | 2933 | 7120 |
| | | 3300 | 6527 |
| | | 1466 | 2601 |
| 0.2076* | 294 | 10850 | 27354 |
| | | 9042 | 22552 |
| | | 7233 | 18710 |
| | | 6510 | 15009 |
| | | 6148 | 10361 |
| | | 5425 | 6745 |
| | | 5063 | 10089 |
| | | 4701 | 4712 |
| | | 3616 | 4687 |
| | | 7233 | 14971 |
| | | 4340 | 8888 |
| | | 3978 | 11972 |
| | | 3616 | 6231 |
| 0.0861* | 268 | 50664 | 131906 |
| | | 45598 | 103658 |
| | | 40531 | 77835 |
| | | 35465 | 60554 |
| | | 30398 | 43687 |
| | | 25332 | 56133 |
| | | 20265 | 50614 |
| | | 45598 | 103658 |
| | | 50664 | 131906 |

* Data obtained with batch number one

TABLE D.5 (continued)

| Capillary I.D. (cm) | L/D | $\frac{8V}{D}$(sec$^{-1}$) | $(P_{11}-P_{22})_w$ (dyn/cm$^2$) |
|---|---|---|---|
| Rheogonimeter* | | 8.48 | 60 |
| | | 13.5 | 40 |
| | | 26.5 | 128 |
| | | 42.6 | 115 |
| | | 84.8 | 204 |
| | | 135 | 240 |
| | | 265 | 368 |
| | | 426 | 460 |
| 0.4452** | 196 | 3667 | 7962 |
| | | 3300 | 9981 |
| | | 2933 | 10581 |
| | | 2567 | 8037 |
| | | 2200 | 5719 |
| | | 1833 | 4490 |
| | | 1466 | 3499 |
| | | 1100 | 3277 |
| | | 1466 | 2799 |
| 0.2076** | 294 | 10850 | 20009 |
| | | 9042 | 29360 |
| | | 8138 | 17231 |
| | | 7233 | 22564 |
| | | 6510 | 18859 |
| | | 5787 | 8396 |
| | | 5063 | 8610 |
| | | 4701 | 12389 |
| | | 4340 | 11996 |
| | | 9946 | 26032 |
| | | 2531 | 10000 |
| 0.0861** | 268 | 50664 | 142534 |
| | | 45598 | 108029 |
| | | 40531 | 98636 |
| | | 35465 | 114611 |
| | | 30398 | 72953 |
| | | 25332 | 39796 |
| | | 35465 | 81428 |
| | | 50664 | 142534 |

* Data obtained with batch number one

** Data obtained with batch number two

FIGURE D – 1

## NEWTONIAN VISCOSITIES

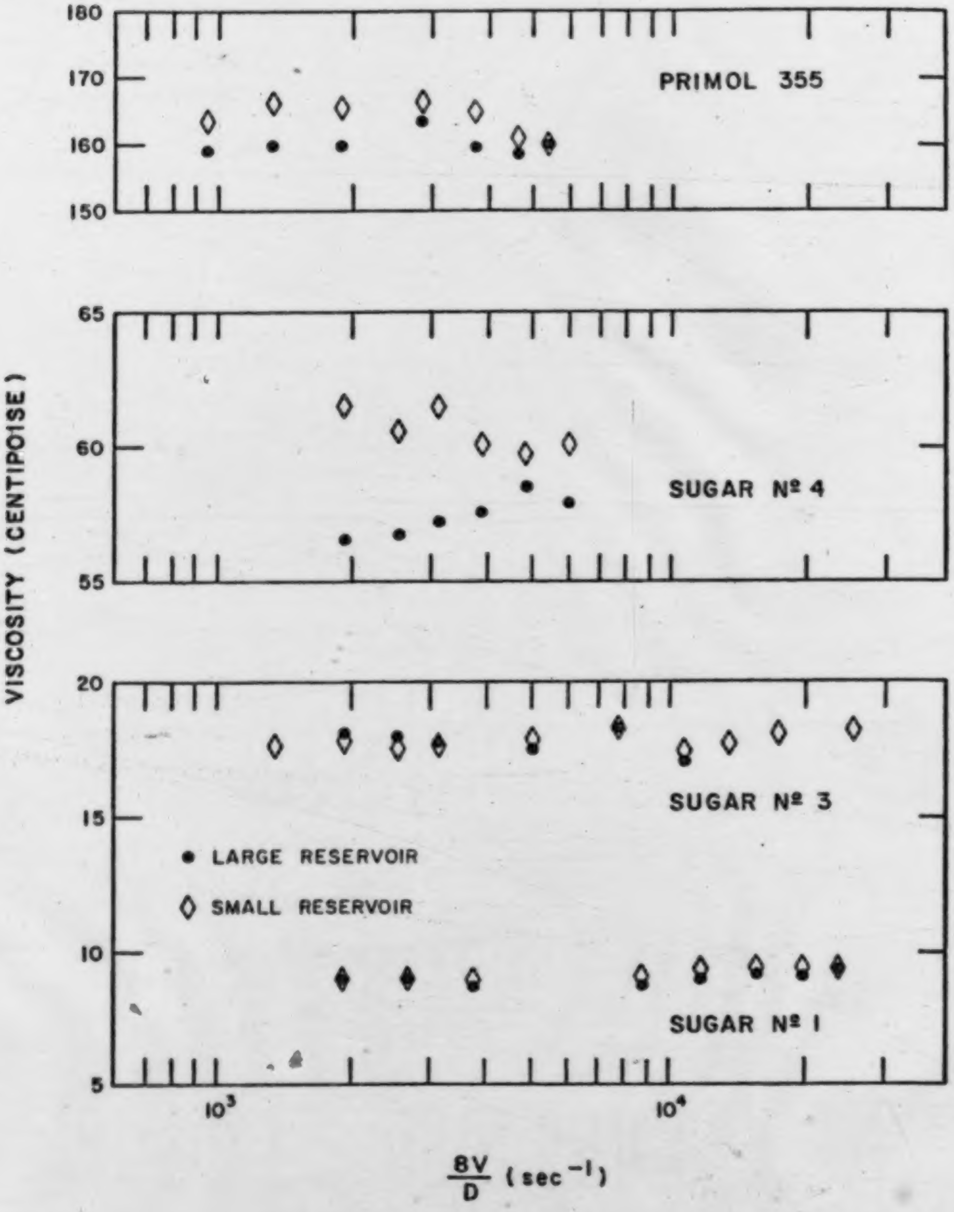

FIGURE D – 2

FLOW CURVE, 0.20 % SEPARAN AP-30
HIGH APPARENT SHEAR RATES

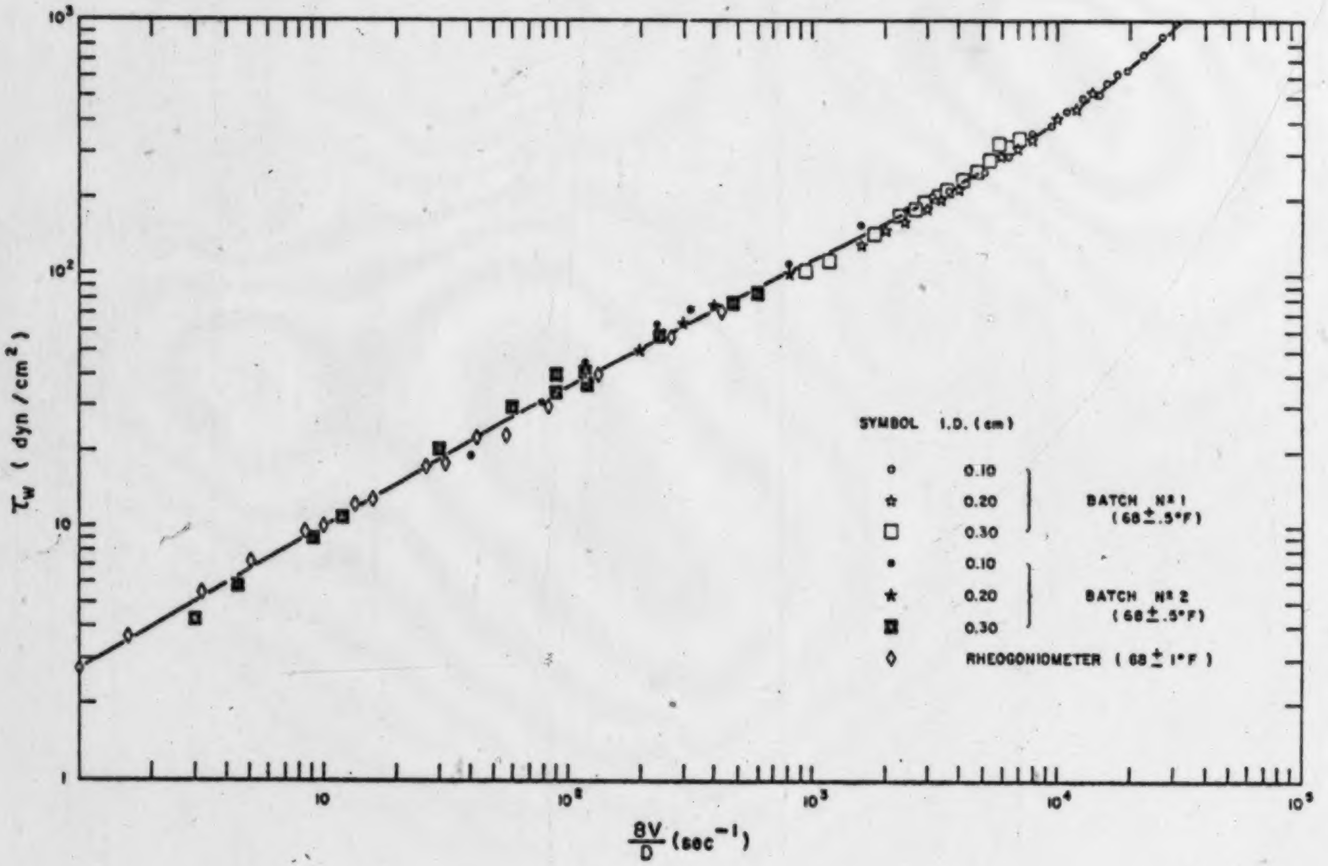

FIGURE D - 3

FLOW CURVE, 0.20% SEPARAN AP-30

LOW APPARENT SHEAR RATES

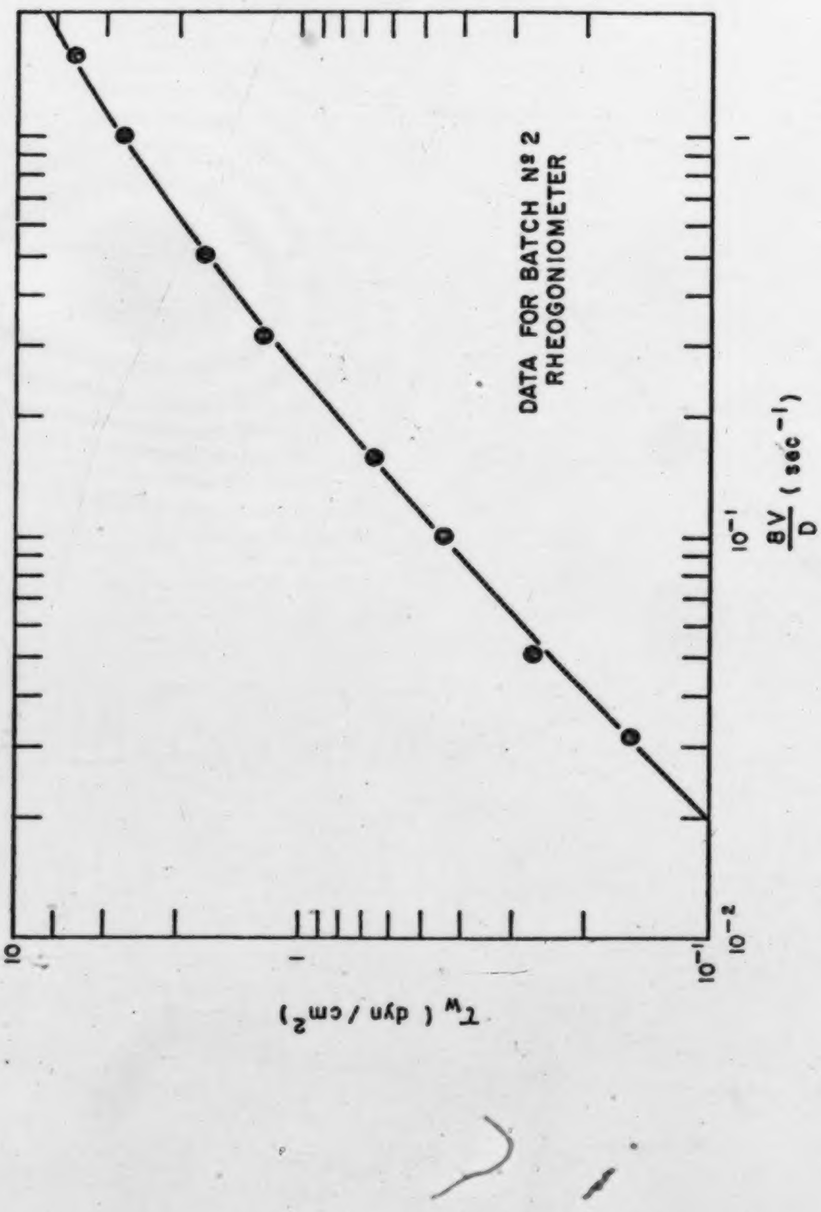

FIGURE D - 4

APPARENT VISCOSITY, 0.20% SEPARAN AP - 30

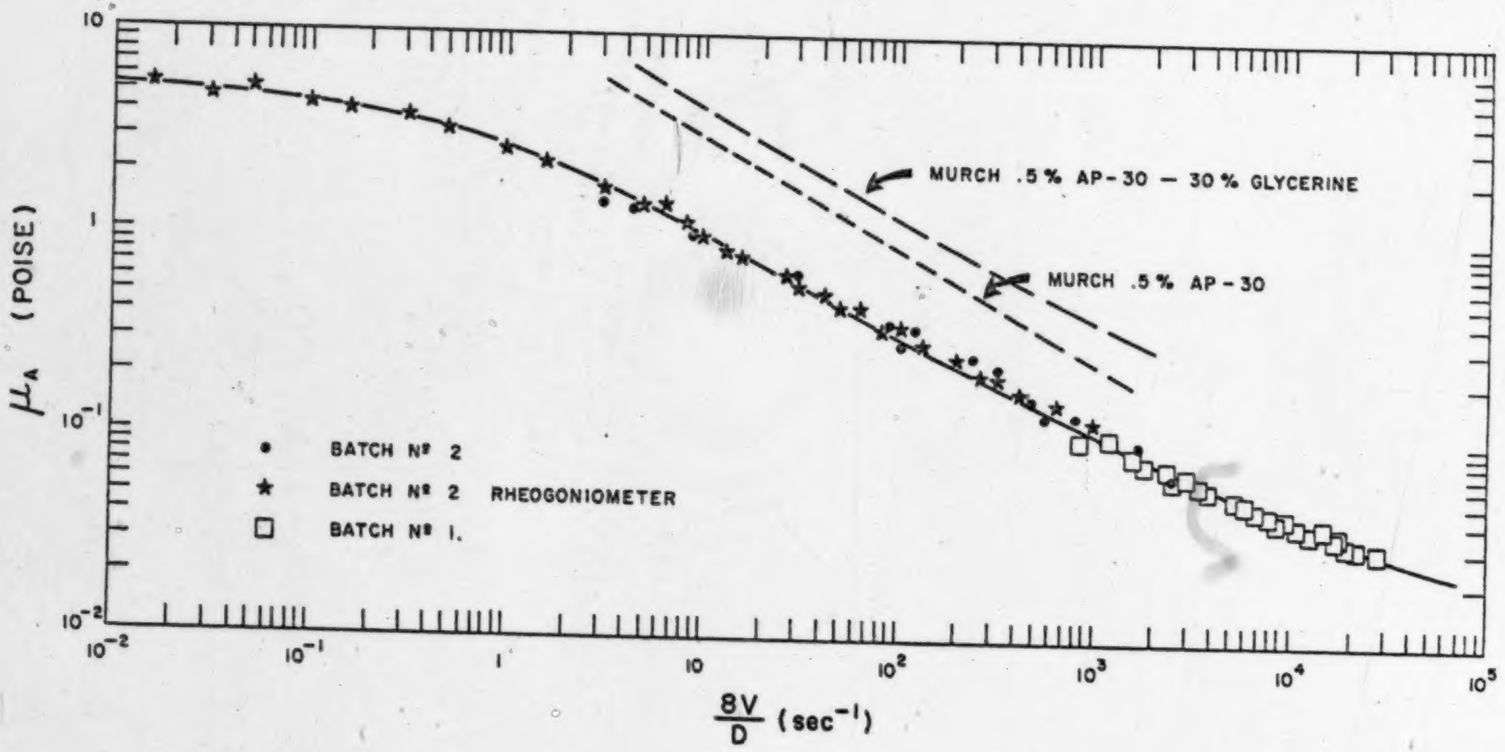

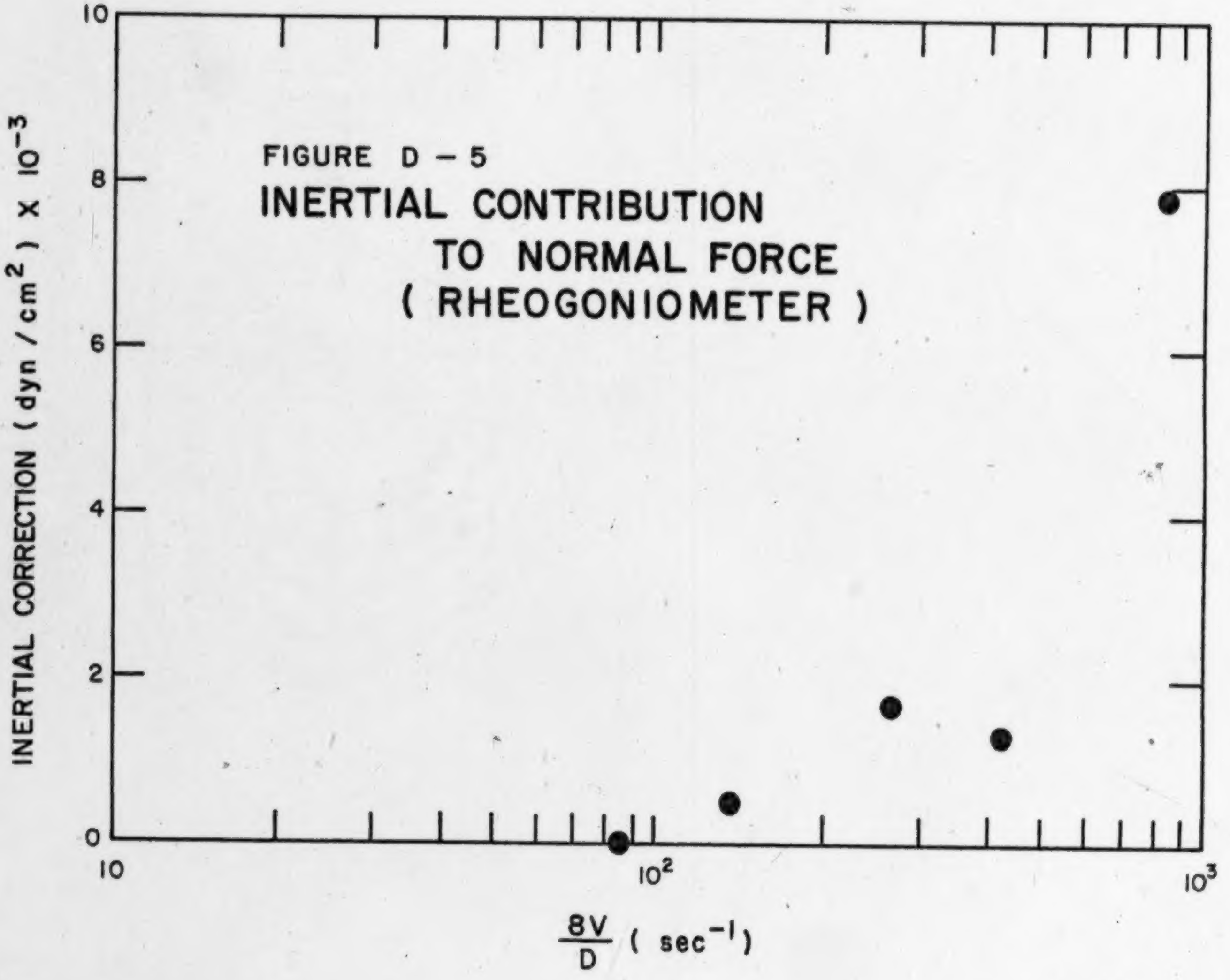

FIGURE D – 5
INERTIAL CONTRIBUTION
TO NORMAL FORCE
( RHEOGONIOMETER )

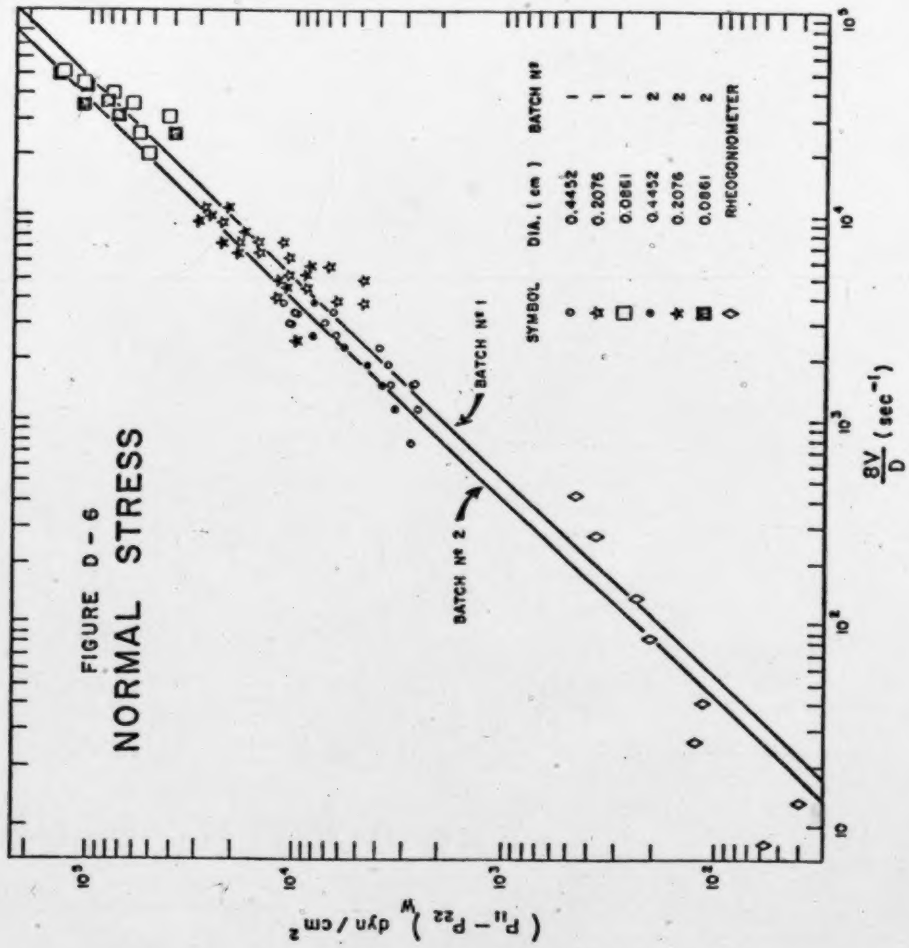

FIGURE D - 6
NORMAL STRESS

FIGURE D-7
RELAXATION TIME

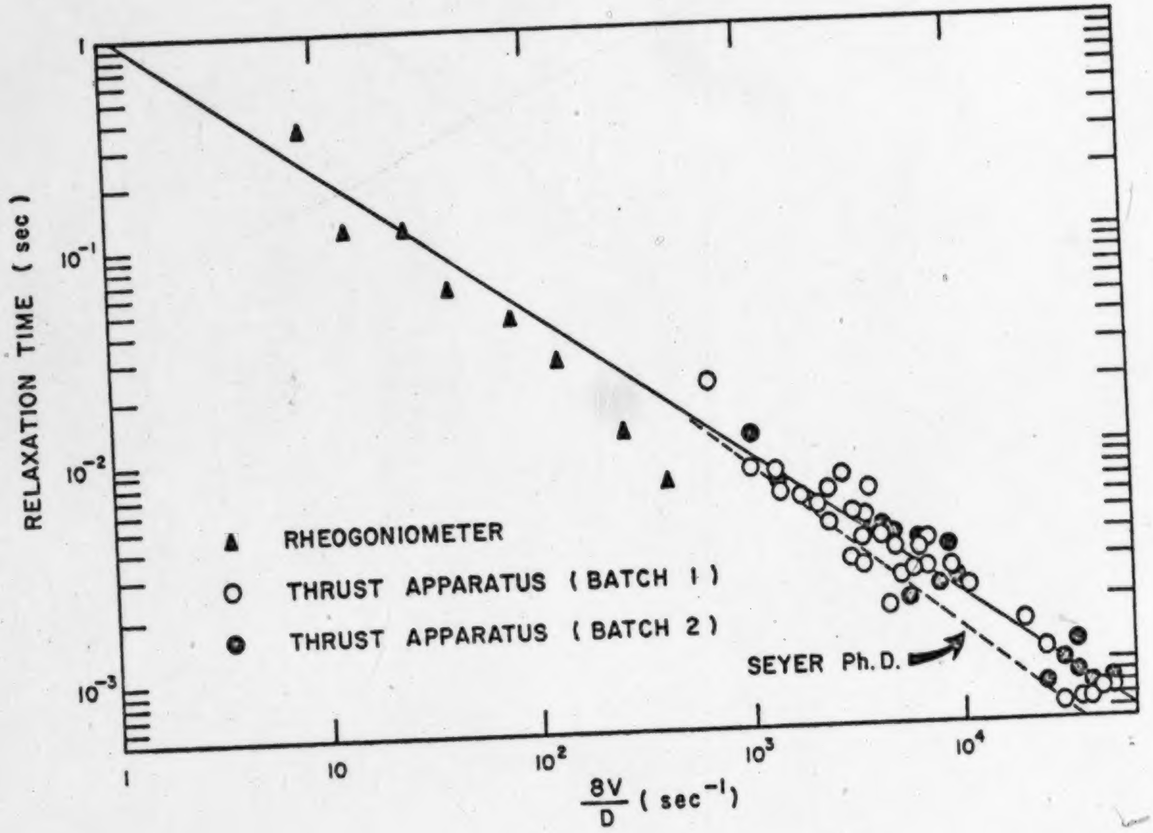

# APPENDIX E

# VELOCITY PROFILES

## E.1 AXIAL VELOCITY PROFILES - DIRECT METHOD

Contained in this section are axial velocities measured at several upstream axial locations for various flow rates and with the three capillary tubes in reservoirs S and L. The method used, the projection of the film directly on to graph paper graduated in 0.10 inches, was discussed in Chapter II. The errors associated with this technique are given in Appendix G.

Since the velocity profiles were axially symmetric, radial locations can be measured relative to an arbitrary reference. The following was used to determine the radial location of a velocity observation: Consider the first two entries in Table E.1 where the centerline corresponds to 12.45 inches. The radial distance between the first two entries under the column labeled "Axial velocity" is

$$\frac{(12.35-12.20)}{24.50} \text{ inches} \times 2.54 \text{ cm/inch} = 0.0155 \text{ cm}$$

where 24.50 is the magnification.

The following lists the tables as they are presented in this section as well as listing the appropriate magnification for each table:

| TABLE NO. | RESERVOIR | MAGNIFICATION | I.D. (cm) | L/D | Q ($cm^3$/sec) |
|---|---|---|---|---|---|
| E.1 | Small | 24.50 | 0.10 | 55.08 | 0.016 |
| E.2 | Small | 24.50 | 0.10 | 55.08 | 0.040 |
| E.3 | Small | 24.50 | 0.10 | 55.08 | 0.119 |
| E.4 | Small | 24.50 | 0.20 | 54.96 | 0.040 |
| E.5 | Small | 24.50 | 0.20 | 54.96 | 0.238 |
| E.6 | Small | 24.50 | 0.20 | 54.96 | 0.318 |
| E.7 | Small | 24.50 | 0.30 | 55.04 | 0.040 |
| E.8 | Small | 24.50 | 0.30 | 55.04 | 0.318 |
| E.9 | Small | 24.50 | 0.30 | 55.04 | 0.635 |
| E.10 | Large | 18.00 | 0.20 | 54.96 | 0.159 |
| E.11 | Large | 18.00 | 0.20 | 54.96 | 0.318 |
| E.12 | Large | 18.00 | 0.20 | 54.96 | 0.794 |
| E.13 | Large | 8.22 | 0.20 | 54.96 | 1.589 |
| E.14 | Large | 18.00 | 0.30 | 55.04 | 0.318 |
| E.15 | Large | 18.00 | 0.30 | 55.04 | 0.635 |
| E.16 | Large | 18.00 | 0.30 | 55.04 | 1.589 |

## TABLE E.1

### AXIAL VELOCITY DATA, 0.10 cm I.D. CAPILLARY
### $Q=0.016\ cm^3/sec$, SMALL RESERVOIR

| Axial Location (No. of Dia.) | Radial Location (in) | Axial Velocity (cm/sec) |
|---|---|---|
| 0.0 | 12.20 | 1.62 |
| (℄ =12.45 in) | 12.35 | 1.90 |
| | 12.45 | 2.30 |
| | 12.60 | 1.90 |
| | 12.70 | 1.62 |
| | 12.75 | 1.48 |
| 1.0 | 11.70 | 0.39 |
| (℄ =12.45 in) | 12.15 | 1.40 |
| | 12.30 | 1.65 |
| | 12.40 | 2.00 |
| | 12.65 | 1.65 |
| | 12.70 | 1.40 |
| | 12.80 | 1.23 |
| | 13.10 | 0.55 |
| | 13.20 | 0.45 |
| 2.0 | 11.70 | 0.43 |
| (℄ =12.45 in) | 11.85 | 0.86 |
| | 12.10 | 1.18 |
| | 12.25 | 1.33 |
| | 12.40 | 1.70 |
| | 12.60 | 1.33 |
| | 12.75 | 1.18 |
| | 12.85 | 0.96 |
| | 13.00 | 0.68 |
| | 13.15 | 0.56 |
| | 13.25 | 0.43 |
| 3.0 | 11.75 | 0.39 |
| (℄ =12.45 in) | 12.05 | 0.90 |
| | 12.25 | 1.05 |
| | 12.35 | 1.25 |
| | 12.60 | 1.05 |
| | 12.65 | 1.05 |
| | 12.80 | 0.90 |
| | 12.90 | 0.73 |
| | 13.05 | 0.58 |
| | 13.25 | 0.47 |
| | 13.30 | 0.38 |

TABLE E.1 (continued)

| Axial Location (No. of Dia.) | Radial Location (in) | Axial Velocity (cm/sec) |
|---|---|---|
| 4.0<br>(℄ =12.45 in) | 11.30 | 0.27 |
| | 11.65 | 0.47 |
| | 12.00 | 0.68 |
| | 12.20 | 0.77 |
| | 12.35 | 0.83 |
| | 12.55 | 0.77 |
| | 12.65 | 0.77 |
| | 12.80 | 0.68 |
| | 13.15 | 0.47 |
| | 13.35 | 0.37 |
| | 13.45 | 0.32 |
| | 13.65 | 0.24 |
| 6.0<br>(℄ =12.45 in) | 10.90 | 0.15 |
| | 11.40 | 0.25 |
| | 11.85 | 0.32 |
| | 12.10 | 0.37 |
| | 12.30 | 0.37 |
| | 12.75 | 0.37 |
| | 13.00 | 0.32 |
| | 13.25 | 0.26 |
| | 13.40 | 0.25 |
| | 13.75 | 0.20 |
| | 13.85 | 0.18 |
| 7.0<br>(℄ =12.45 in) | 10.60 | 0.12 |
| | 11.15 | 0.16 |
| | 11.65 | 0.20 |
| | 12.05 | 0.23 |
| | 12.25 | 0.22 |
| | 12.75 | 0.22 |
| | 12.85 | 0.24 |
| | 13.10 | 0.21 |
| | 13.40 | 0.20 |
| | 13.65 | 0.16 |
| | 14.00 | 0.16 |
| 8.0<br>(℄ =12.45 in) | 10.25 | 0.08 |
| | 10.90 | 0.12 |
| | 11.45 | 0.16 |
| | 12.00 | 0.18 |
| | 12.25 | 0.17 |
| | 12.80 | 0.16 |
| | 13.05 | 0.16 |
| | 13.85 | 0.11 |
| | 14.30 | 0.10 |

## TABLE E.2

### AXIAL VELOCITY DATA, 0.10 cm I.D. CAPILLARY
### Q=0.040 cm$^3$/sec, SMALL RESERVOIR

| Axial Location (No. of Dia.) | Radial Location (in) | Axial Velocity (cm/sec) |
|---|---|---|
| 1.0<br>(℄ =12.55 in) | 11.60 | 0.10 |
| | 12.35 | 4.80 |
| | 12.60 | 5.25 |
| | 12.80 | 4.25 |
| | 12.90 | 2.60 |
| | 13.15 | 0.45 |
| 2.0<br>(℄ =12.55 in) | 11.75 | 0.55 |
| | 12.30 | 4.25 |
| | 12.45 | 4.60 |
| | 12.65 | 4.60 |
| | 12.80 | 4.10 |
| | 13.05 | 2.35 |
| | 13.30 | 0.95 |
| | 13.65 | 0.20 |
| 3.0<br>(℄ =12.55 in) | 11.70 | 0.80 |
| | 12.30 | 3.70 |
| | 12.65 | 4.00 |
| | 12.75 | 4.00 |
| | 12.80 | 3.60 |
| | 12.95 | 2.10 |
| | 13.35 | 1.15 |
| | 13.60 | 0.50 |
| 4.0<br>(℄ =12.55 in) | 11.65 | 0.90 |
| | 12.25 | 3.25 |
| | 12.30 | 3.40 |
| | 12.35 | 3.40 |
| | 12.65 | 3.40 |
| | 12.75 | 3.25 |
| | 12.85 | 2.65 |
| | 13.00 | 1.90 |
| | 13.40 | 1.15 |
| | 13.60 | 0.45 |
| 6.0<br>(℄ =12.55 in) | 10.75 | 0.30 |
| | 11.60 | 1.80 |
| | 12.20 | 2.20 |
| | 12.35 | 2.30 |
| | 12.50 | 2.30 |
| | 12.70 | 2.30 |

TABLE E.2 (continued)

| Axial Location (No. of Dia.) | Radial Location (in) | Axial Velocity (cm/sec) |
|---|---|---|
| | 12.80 | 2.30 |
| | 12.85 | 1.85 |
| | 13.15 | 1.55 |
| | 13.55 | 1.05 |
| | 13.70 | 0.50 |
| 8.0 | 10.10 | 0.18 |
| (℄ =12.55 in) | 10.55 | 0.22 |
| | 11.40 | 0.65 |
| | 11.90 | 1.30 |
| | 12.30 | 1.65 |
| | 12.45 | 1.60 |
| | 12.75 | 1.60 |
| | 12.85 | 1.60 |
| | 13.00 | 1.25 |
| | 13.20 | 1.15 |
| | 13.70 | 0.75 |
| | 13.90 | 0.55 |
| | 14.05 | 0.40 |
| 10.0 | 9.85 | .16 |
| (℄ =12.55 in) | 10.35 | .25 |
| | 11.10 | .47 |
| | 11.75 | .79 |
| | 12.05 | .94 |
| | 12.25 | .94 |
| | 12.35 | 1.09 |
| | 12.40 | 1.08 |
| | 12.45 | 1.04 |
| | 13.35 | .76 |
| | 13.95 | .50 |
| | 14.15 | .42 |
| | 14.30 | .32 |
| 12.0 | 10.85 | .33 |
| (℄ =12.55 in) | 11.55 | .45 |
| | 11.90 | .53 |
| | 12.15 | .56 |
| | 12.25 | .59 |
| | 12.40 | .61 |
| | 12.50 | .62 |
| | 12.65 | .62 |
| | 12.95 | .56 |
| | 13.20 | .52 |
| | 13.55 | .47 |

TABLE E.2 (continued)

| Axial Location (No. of Dia.) | Radial Location (in) | Axial Velocity (cm/sec) |
|---|---|---|
| 14.0 | 10.40 | .20 |
| (℄ =12.55 in) | 11.25 | .28 |
| | 11.70 | .31 |
| | 12.00 | .33 |
| | 12.20 | .34 |
| | 12.35 | .35 |
| | 12.45 | .36 |
| | 12.55 | .36 |
| | 12.95 | .35 |
| | 13.40 | .34 |
| | 13.90 | .33 |
| 16.0 | 10.85 | .17 |
| (℄ =12.55 in) | 11.45 | .20 |
| | 11.85 | .19 |
| | 12.05 | .20 |
| | 12.50 | .19 |
| | 12.60 | .21 |
| | 15.00 | .14 |

## TABLE E.3

## AXIAL VELOCITY DATA, 0.10 cm I.D. CAPILLARY
## $Q=0.119\ cm^3/sec$, SMALL RESERVOIR

| Axial Location (No. of Dia.) | Radial Location (in) | Axial Velocity (cm/sec) |
|---|---|---|
| 2.0 | 12.30 | 12.00 |
| (℄ =12.55 in) | 12.45 | 18.40 |
| | 12.70 | 18.30 |
| | 12.95 | 10.80 |
| | 13.20 | 5.60 |
| 4.0 | 12.25 | 10.00 |
| (℄ =12.55 in) | 12.45 | 14.80 |
| | 12.70 | 14.60 |
| | 12.95 | 9.30 |
| | 13.20 | 4.90 |
| | 13.65 | 0.90 |
| | 13.95 | 0.50 |
| | 13.55 | 0.10 |
| 8.0 | 10.90 | 0.80 |
| (℄ =12.55 in) | 12.10 | 6.90 |
| | 12.35 | 8.80 |
| | 12.65 | 9.20 |
| | 12.75 | 8.70 |
| | 13.05 | 7.70 |
| | 13.00 | 5.90 |
| | 13.25 | 3.80 |
| | 13.75 | 1.30 |
| | 13.95 | 1.00 |
| | 14.10 | 0.80 |
| | 14.35 | 0.50 |
| 12.0 | 10.80 | 1.00 |
| (℄ =12.55 in) | 11.85 | 4.40 |
| | 12.00 | 4.40 |
| | 12.35 | 6.00 |
| | 12.85 | 6.00 |
| | 13.10 | 4.80 |
| | 13.40 | 2.90 |
| | 13.90 | 1.30 |
| | 14.05 | 1.10 |
| | 14.35 | 0.80 |
| | 14.55 | 0.60 |
| 16.0 | 10.00 | 0.60 |
| (℄ =12.55 in) | 10.55 | 0.70 |
| | 11.45 | 2.10 |
| | 11.70 | 2.80 |

TABLE E.3 (continued)

| Axial Location (No. of Dia.) | Radial Location (in) | Axial Velocity (cm/sec) |
|---|---|---|
| | 12.25 | 3.70 |
| | 12.65 | 3.70 |
| | 12.95 | 3.40 |
| | 13.35 | 2.35 |
| | 13.55 | 1.90 |
| | 13.65 | 1.60 |
| | 14.25 | 0.90 |
| | 14.75 | 0.60 |
| 20.0 | 9.60 | 0.40 |
| (℄ =12.55 in) | 10.65 | 1.02 |
| | 11.15 | 1.28 |
| | 11.40 | 1.68 |
| | 11.80 | 1.96 |
| | 12.15 | 2.08 |
| | 12.65 | 2.20 |
| | 13.25 | 1.65 |
| | 13.70 | 1.36 |
| | 14.00 | 1.06 |
| 24.0 | 8.45 | 0.21 |
| (℄ =12.55 in) | 9.90 | 0.65 |
| | 10.45 | 0.75 |
| | 10.60 | 0.80 |
| | 11.50 | 1.04 |
| | 11.75 | 1.17 |
| | 12.00 | 1.04 |
| | 12.75 | 1.08 |
| | 13.55 | 0.96 |
| | 14.05 | 0.80 |
| 28.0 | 9.00 | 0.28 |
| (℄ =12.55 in) | 9.60 | 0.34 |
| | 10.50 | 0.44 |
| | 11.10 | 0.46 |
| | 11.45 | 0.50 |
| | 11.75 | 0.53 |
| | 12.80 | 0.58 |
| | 14.00 | 0.43 |
| | 14.85 | 0.36 |
| | 15.00 | 0.33 |

## TABLE E.4

## AXIAL VELOCITY DATA, 0.20 cm I.D. CAPILLARY
## $Q=0.040\ cm^3/sec$, SMALL RESERVOIR

| Axial Location (No. of Dia.) | Radial Location (in) | Axial Velocity (cm/sec) |
|---|---|---|
| 0.5 | 11.15 | 0.24 |
| (℄ =12.3 in) | 11.55 | 0.93 |
| | 11.72 | 1.40 |
| | 11.90 | 1.34 |
| | 12.10 | 1.42 |
| | 12.35 | 1.36 |
| | 12.50 | 1.40 |
| | 12.70 | 1.20 |
| | 13.10 | 0.64 |
| | 13.25 | 0.72 |
| | 13.55 | 0.30 |
| 1.0 | 10.85 | 0.16 |
| (℄ =12.3 in) | 11.05 | 0.24 |
| | 11.45 | 0.63 |
| | 11.65 | 0.91 |
| | 11.85 | 1.02 |
| | 12.05 | 1.02 |
| | 12.10 | 1.09 |
| | 12.35 | 1.16 |
| | 12.37 | 1.21 |
| | 12.65 | 1.10 |
| | 12.75 | 0.90 |
| | 12.85 | 0.87 |
| | 13.05 | 0.76 |
| | 13.40 | 0.52 |
| | 13.45 | 0.49 |
| | 13.65 | 0.31 |
| | 13.75 | 0.18 |
| 2.0 | 10.65 | 0.18 |
| (℄ =12.3 in) | 11.15 | 0.34 |
| | 11.45 | 0.47 |
| | 11.75 | 0.58 |
| | 11.95 | 0.58 |
| | 12.35 | 0.58 |
| | 12.55 | 0.62 |
| | 12.70 | 0.56 |
| | 12.95 | 0.49 |
| | 13.10 | 0.55 |
| | 13.40 | 0.51 |
| | 13.60 | 0.28 |
| | 13.75 | 0.24 |
| | 14.10 | 0.20 |

TABLE E.4 (continued)

| Axial Location (No. of Dia.) | Radial Location (in) | Axial Velocity (cm/sec) |
|---|---|---|
| 3.0<br>(℄ =12.3 in) | 11.20 | 0.10 |
| | 11.80 | 0.28 |
| | 12.50 | 0.32 |
| | 12.65 | 0.30 |
| | 13.25 | 0.24 |
| | 14.20 | 0.16 |
| | 14.75 | 0.13 |
| 4.0<br>(℄ =12.3 in) | 10.05 | 0.10 |
| | 10.80 | 0.13 |
| | 11.45 | 0.13 |
| | 11.60 | 0.16 |
| | 12.55 | 0.18 |
| | 12.60 | 0.18 |
| | 13.15 | 0.13 |
| | 13.70 | 0.13 |
| | 14.95 | 0.08 |
| | 15.70 | 0.06 |

## TABLE E.5

## AXIAL VELOCITY DATA, 0.20 cm I.D. CAPILLARY
## $Q=0.238\ cm^3/sec$, SMALL RESERVOIR

| Axial Location (No. of Dia.) | Radial Location (in) | Axial Velocity (cm/sec) |
|---|---|---|
| 2.0 | 11.05 | 0.75 |
| (℄ =12.80 in) | 11.55 | 3.10 |
| | 11.85 | 4.40 |
| | 12.20 | 6.20 |
| | 12.45 | 7.80 |
| | 12.70 | 8.90 |
| | 13.05 | 7.80 |
| | 13.65 | 4.40 |
| | 13.80 | 2.35 |
| | 14.00 | 0.70 |
| | 14.80 | 0.25 |
| 4.0 | 10.20 | 0.40 |
| (℄ =12.80 in) | 10.70 | 0.80 |
| | 11.40 | 2.45 |
| | 11.70 | 3.05 |
| | 12.10 | 4.25 |
| | 12.40 | 5.45 |
| | 12.65 | 5.60 |
| | 12.75 | 5.60 |
| | 12.85 | 5.60 |
| | 13.15 | 5.10 |
| | 13.90 | 3.03 |
| | 14.20 | 1.60 |
| | 14.65 | 0.75 |
| | 14.85 | 0.60 |
| 6.0 | 9.95 | 0.55 |
| (℄ =12.80 in) | 11.05 | 1.65 |
| | 11.35 | 1.95 |
| | 11.85 | 2.60 |
| | 12.30 | 3.50 |
| | 12.65 | 3.55 |
| | 12.75 | 3.55 |
| | 12.85 | 3.55 |
| | 13.25 | 3.20 |
| | 14.45 | 1.15 |
| | 14.95 | 0.70 |
| 8.0 | 9.40 | 0.36 |
| (℄ =12.80 in) | 10.15 | 0.74 |
| | 10.65 | 1.05 |
| | 11.65 | 1.60 |

TABLE E.5 (continued)

| Axial Location (No. of Dia.) | Radial Location (in) | Axial Velocity (cm/sec) |
|---|---|---|
| | 12.20 | 2.15 |
| | 12.60 | 2.15 |
| | 12.70 | 2.15 |
| | 12.95 | 2.15 |
| | 13.40 | 1.95 |
| | 14.80 | 0.89 |
| | 15.05 | 0.89 |
| | 15.55 | 0.55 |
| 10.0 | 9.30 | 0.44 |
| (℄ =12.80 in) | 9.95 | 0.60 |
| | 11.05 | 0.80 |
| | 12.05 | 1.10 |
| | 12.50 | 1.10 |
| | 12.60 | 1.10 |
| | 13.00 | 1.10 |
| | 13.70 | 1.00 |
| | 15.86 | 0.46 |
| | 16.55 | 0.25 |

## TABLE E.6

## AXIAL VELOCITY DATA, 0.20 cm I.D. CAPILLARY
## $Q=0.318\ cm^3/sec$, SMALL RESERVOIR

| Axial Location (No. of Dia.) | Radial Location (in) | Axial Velocity (cm/sec) |
|---|---|---|
| 0.0 | 12.10 | 9.30 |
| (℄ =12.70 in) | 12.35 | 13.20 |
| | 12.70 | 14.40 |
| | 12.95 | 14.20 |
| | 13.05 | 13.80 |
| | 13.15 | 11.90 |
| | 13.30 | 11.60 |
| | 13.45 | 8.90 |
| 1.0 | 11.35 | 1.30 |
| (℄ =12.70 in) | 12.05 | 8.25 |
| | 12.15 | 11.80 |
| | 12.70 | 13.10 |
| | 12.90 | 12.80 |
| | 13.05 | 12.40 |
| | 13.20 | 10.60 |
| | 13.35 | 10.20 |
| | 13.50 | 7.90 |
| | 14.00 | 0.70 |
| 2.0 | 11.10 | 1.10 |
| (℄ =12.70 in) | 11.95 | 7.00 |
| | 12.25 | 10.20 |
| | 12.75 | 11.40 |
| | 12.90 | 11.20 |
| | 13.00 | 10.80 |
| | 13.15 | 8.90 |
| | 13.40 | 8.60 |
| | 13.60 | 6.70 |
| | 14.00 | 1.80 |
| | 14.25 | 1.60 |
| | 14.95 | 0.50 |
| 4.0 | 10.45 | 0.80 |
| (℄ =12.70 in) | 11.00 | 1.80 |
| | 11.25 | 1.35 |
| | 11.80 | 5.00 |
| | 12.15 | 7.35 |
| | 12.55 | 8.25 |
| | 12.75 | 8.15 |
| | 12.90 | 7.80 |
| | 13.10 | 6.20 |

TABLE E.6 (continued)

| Axial Location (No. of Dia.) | Radial Location (in) | Axial Velocity (cm/sec) |
|---|---|---|
| | 13.35 | 5.80 |
| | 13.50 | 4.70 |
| | 13.95 | 2.00 |
| | 14.15 | 1.90 |
| | 14.45 | 1.00 |
| 6.0 | 10.25 | 0.80 |
| (℄ =12.70 in) | 10.75 | 1.50 |
| | 11.05 | 1.77 |
| | 11.60 | 3.45 |
| | 12.05 | 4.95 |
| | 12.65 | 5.60 |
| | 12.95 | 5.60 |
| | 13.15 | 5.30 |
| | 13.40 | 4.15 |
| | 13.65 | 4.05 |
| | 13.90 | 3.10 |
| | 14.40 | 1.67 |
| | 14.60 | 1.57 |
| | 14.85 | 0.95 |
| 8.0 | 9.85 | 0.74 |
| (℄ =12.70 in) | 10.40 | 1.12 |
| | 10.70 | 1.35 |
| | 11.35 | 2.40 |
| | 11.85 | 3.35 |
| | 12.60 | 3.90 |
| | 12.95 | 3.80 |
| | 13.25 | 3.70 |
| | 13.55 | 2.90 |
| | 14.10 | 2.20 |
| | 14.75 | 1.30 |
| | 15.15 | 0.85 |
| 9.0 | 9.55 | 0.63 |
| (℄ =12.70 in) | 10.50 | 1.14 |
| | 11.20 | 1.85 |
| | 11.75 | 2.50 |
| | 12.00 | 2.70 |
| | 12.60 | 2.85 |
| | 13.00 | 2.90 |
| | 13.30 | 2.80 |
| | 13.65 | 2.20 |
| | 14.25 | 1.75 |
| | 14.95 | 1.05 |

TABLE E.6 (continued)

| Axial Location (No. of Dia.) | Radial Location (in) | Axial Velocity (cm/sec) |
|---|---|---|
| 11.0 | 9.45 | 0.57 |
| (℄ =12.70 in) | 9.85 | 0.70 |
| | 10.70 | 1.16 |
| | 11.50 | 1.60 |
| | 11.80 | 1.52 |
| | 12.55 | 1.65 |
| | 13.05 | 1.65 |
| | 13.45 | 1.58 |
| | 13.90 | 1.27 |
| | 14.75 | 0.96 |
| | 15.45 | 0.58 |
| 12.0 | 8.95 | 0.42 |
| (℄ =12.70 in) | 10.35 | 0.82 |
| | 11.25 | 1.02 |
| | 12.55 | 1.16 |
| | 12.65 | 1.13 |
| | 13.55 | 1.15 |
| | 14.10 | 0.95 |
| | 15.00 | 0.80 |

## TABLE E.7

## AXIAL VELOCITY DATA, 0.30 cm I.D. CAPILLARY
## $Q=0.040$ cm$^3$/sec, SMALL RESERVOIR

| Axial Location (No. of Dia.) | Radial Location (in) | Axial Velocity (cm/sec) |
|---|---|---|
| 0.0 (℄ =12.50 in) | 11.65 | 0.48 |
| | 11.85 | 0.51 |
| | 12.10 | 0.60 |
| | 12.35 | 0.71 |
| | 12.65 | 0.71 |
| | 13.45 | 0.48 |
| 0.5 (℄ =12.50 in) | 10.85 | 0.127 |
| | 11.25 | 0.255 |
| | 11.50 | 0.332 |
| | 11.95 | 0.410 |
| | 12.25 | 0.50 |
| | 12.70 | 0.50 |
| | 13.45 | 0.385 |
| | 13.80 | 0.385 |
| 1.0 (℄ =12.50 in) | 10.10 | 0.072 |
| | 10.85 | 0.207 |
| | 11.70 | 0.255 |
| | 12.15 | 0.295 |
| | 12.70 | 0.295 |
| | 13.70 | 0.245 |
| | 14.15 | 0.163 |
| 1.5 (℄ =12.50 in) | 10.00 | 0.059 |
| | 11.45 | 0.160 |
| | 12.05 | 0.178 |
| | 12.75 | 0.178 |
| | 14.00 | 0.136 |
| | 14.65 | 0.106 |
| 2.0 (℄ =12.50 in) | 9.20 | 0.035 |
| | 11.15 | 0.092 |
| | 11.95 | 0.105 |
| | 12.80 | 0.105 |
| | 14.45 | 0.080 |
| | 15.30 | 0.060 |

## TABLE E.8

## AXIAL VELOCITY DATA, 0.30 cm I.D. CAPILLARY
## Q=0.318 $cm^3$/sec, SMALL RESERVOIR

| Axial Location (No. of Dia.) | Radial Location (in) | Axial Velocity (cm/sec) |
|---|---|---|
| 0.0 | 11.85 | 5.40 |
| (℄ =12.60 in) | 12.20 | 5.90 |
| | 12.60 | 6.05 |
| | 12.85 | 5.90 |
| | 13.05 | 5.75 |
| | 13.20 | 5.50 |
| | 13.40 | 4.90 |
| | 13.90 | 1.60 |
| 0.5 | 10.75 | 0.45 |
| (℄ =12.60 in) | 11.45 | 3.27 |
| | 11.75 | 4.90 |
| | 12.15 | 5.32 |
| | 12.60 | 5.45 |
| | 12.85 | 5.40 |
| | 13.05 | 5.20 |
| | 13.20 | 4.90 |
| | 13.40 | 4.30 |
| | 14.00 | 1.56 |
| | 14.55 | 0.25 |
| 1.0 | 10.25 | 0.31 |
| (℄ =12.60 in) | 10.70 | 0.75 |
| | 11.35 | 3.00 |
| | 11.65 | 4.25 |
| | 12.15 | 4.75 |
| | 12.70 | 4.90 |
| | 12.85 | 4.85 |
| | 13.10 | 4.65 |
| | 13.25 | 4.35 |
| | 13.50 | 3.70 |
| | 14.05 | 1.50 |
| | 14.50 | 0.95 |
| | 14.75 | 0.35 |
| 2.0 | 10.15 | 0.54 |
| (℄ =12.60 in) | 10.50 | 0.96 |
| | 11.15 | 2.00 |
| | 11.50 | 2.75 |
| | 12.00 | 3.65 |
| | 12.55 | 3.75 |
| | 12.85 | 3.70 |
| | 12.95 | 3.67 |

TABLE E.8 (continued)

| Axial Location (No. of Dia.) | Radial Location (in) | Axial Velocity (cm/sec) |
|---|---|---|
| | 13.15 | 3.45 |
| | 13.35 | 3.20 |
| | 13.60 | 2.70 |
| | 13.65 | 2.35 |
| | 14.25 | 1.36 |
| | 14.55 | 0.92 |
| | 14.80 | 0.62 |
| 3.0 | 9.05 | 0.29 |
| (℄ =12.60 in) | 9.85 | 0.65 |
| | 10.10 | 0.84 |
| | 10.80 | 1.55 |
| | 11.25 | 2.13 |
| | 11.95 | 2.55 |
| | 12.50 | 2.70 |
| | 12.85 | 2.75 |
| | 13.00 | 2.62 |
| | 13.20 | 2.56 |
| | 13.45 | 2.23 |
| | 13.75 | 1.93 |
| | 14.50 | 1.08 |
| | 15.05 | 0.69 |
| 5.0 | 8.50 | 0.30 |
| (℄ =12.60 in) | 8.90 | 0.39 |
| | 9.85 | 0.65 |
| | 10.55 | 0.81 |
| | 11.60 | 1.03 |
| | 12.55 | 1.11 |
| | 13.05 | 1.01 |
| | 13.25 | 1.07 |
| | 13.60 | 1.00 |
| | 13.95 | 0.95 |
| | 14.45 | 0.86 |
| | 15.35 | 0.57 |
| | 15.90 | 0.43 |
| 6.0 | 9.05 | 0.30 |
| (℄ =12.60 in) | 11.30 | 0.57 |
| | 12.55 | 0.65 |
| | 13.50 | 0.63 |
| | 15.05 | 0.45 |
| | 16.30 | 0.32 |

## TABLE E.9

### AXIAL VELOCITY DATA, 0.30 cm I.D. CAPILLARY
### $Q=0.635\ cm^3/sec$, SMALL RESERVOIR

| Axial Location (No. of Dia.) | Radial Location (in) | Axial Velocity (cm/sec) |
|---|---|---|
| 0.0 | 11.50 | 6.90 |
| (℄ =12.60 in) | 12.20 | 12.40 |
| | 12.80 | 13.50 |
| | 12.90 | 13.35 |
| | 13.05 | 12.90 |
| | 13.15 | 12.05 |
| | 13.30 | 10.00 |
| | 13.80 | 5.10 |
| 0.5 | 11.15 | 2.60 |
| (℄ =12.60 in) | 11.45 | 6.90 |
| | 12.15 | 11.55 |
| | 12.80 | 12.40 |
| | 12.90 | 12.30 |
| | 13.05 | 11.80 |
| | 13.15 | 11.10 |
| | 13.35 | 11.35 |
| | 13.85 | 4.85 |
| | 13.95 | 4.65 |
| | 14.20 | 2.00 |
| 1.0 | 11.05 | 2.60 |
| (℄ =12.60 in) | 11.35 | 6.65 |
| | 12.15 | 10.60 |
| | 12.75 | 11.45 |
| | 12.90 | 11.30 |
| | 13.05 | 10.90 |
| | 13.15 | 10.15 |
| | 13.35 | 8.55 |
| | 13.90 | 4.40 |
| | 14.05 | 4.30 |
| | 14.25 | 2.45 |
| | 14.60 | 0.85 |
| | 14.80 | 0.75 |
| 2.0 | 10.05 | 0.85 |
| (℄ =12.60 in) | 10.85 | 2.50 |
| | 11.20 | 4.45 |
| | 12.00 | 8.70 |
| | 12.75 | 9.50 |
| | 12.85 | 9.40 |

TABLE E.9 (continued)

| Axial Location (No. of Dia.) | Radial Location (in) | Axial Velocity (cm/sec) |
|---|---|---|
| | 13.05 | 9.00 |
| | 13.25 | 8.20 |
| | 13.45 | 7.10 |
| | 14.05 | 4.00 |
| | 14.15 | 3.60 |
| | 14.40 | 2.55 |
| | 14.65 | 1.90 |
| | 15.10 | 1.00 |
| | 15.30 | 0.70 |
| | 15.90 | 0.30 |
| 3.0 | 9.90 | 1.05 |
| (℄ =12.60 in) | 10.65 | 1.23 |
| | 11.00 | 3.50 |
| | 11.90 | 6.85 |
| | 12.75 | 7.65 |
| | 12.90 | 7.55 |
| | 13.05 | 7.20 |
| | 13.25 | 6.50 |
| | 13.60 | 5.70 |
| | 14.15 | 3.50 |
| | 14.55 | 2.40 |
| | 14.75 | 1.70 |
| | 15.70 | 0.55 |
| 6.0 | 8.85 | 0.72 |
| (℄ =12.60 in) | 9.65 | 1.15 |
| | 10.15 | 1.60 |
| | 11.50 | 2.95 |
| | 12.35 | 3.20 |
| | 12.75 | 3.35 |
| | 12.95 | 3.15 |
| | 13.15 | 3.15 |
| | 13.50 | 2.75 |
| | 13.85 | 2.50 |
| | 14.90 | 1.65 |
| | 15.20 | 1.40 |
| | 15.60 | 0.95 |
| | 15.95 | 0.70 |
| | 16.50 | 0.50 |
| | 16.75 | 0.40 |

TABLE E.9 (continued)

| Axial Location (No. of Dia.) | Radial Location (in) | Axial Velocity (cm/sec) |
|---|---|---|
| 8.0<br>(℄ =12.60 in) | 7.00 | 0.27 |
| | 8.25 | 0.525 |
| | 8.95 | 0.76 |
| | 10.95 | 1.29 |
| | 11.20 | 1.27 |
| | 12.85 | 1.19 |
| | 13.95 | 1.16 |
| | 13.55 | 1.16 |
| | 15.25 | 0.495 |

## TABLE E.10

## AXIAL VELOCITY DATA, 0.20 cm I.D. CAPILLARY
## Q=0.159 $cm^3$/sec, LARGE RESERVOIR

| Axial Location (No. of Dia.) | Radial Location (in) | Axial Velocity (cm/sec) |
|---|---|---|
| 4.93 | 10.65 | 1.38 |
| (℄ =14.50 in) | 11.35 | 2.06 |
| | 11.85 | 3.06 |
| | 13.30 | 10.60 |
| | 13.53 | 12.50 |
| | 14.05 | 18.10 |
| | 14.45 | 19.30 |
| | 14.65 | 20.00 |
| | 14.80 | 19.30 |
| | 15.25 | 15.00 |
| | 15.85 | 8.96 |
| | 16.20 | 6.44 |
| | 16.75 | 4.84 |
| | 16.85 | 3.80 |
| | 17.10 | 3.54 |
| | 17.35 | 3.06 |
| | 17.80 | 1.75 |
| 7.75 | 10.30 | 1.89 |
| (℄ =14.50 in) | 10.95 | 2.83 |
| | 11.50 | 3.74 |
| | 12.10 | 4.00 |
| | 12.55 | 5.42 |
| | 13.05 | 5.63 |
| | 13.30 | 5.90 |
| | 13.60 | 6.22 |
| | 14.75 | 7.75 |
| | 15.00 | 7.08 |
| | 15.35 | 6.78 |
| | 15.80 | 6.35 |
| | 16.45 | 4.60 |
| | 17.30 | 3.30 |
| | 17.75 | 3.06 |
| | 18.40 | 1.89 |
| 10.55 | 10.85 | 2.00 |
| (℄ =14.50 in) | 11.25 | 2.21 |
| | 11.85 | 2.72 |
| | 12.20 | 3.05 |
| | 12.70 | 3.07 |
| | 13.45 | 3.20 |
| | 14.20 | 3.38 |

TABLE E.10 (continued)

| Axial Location (No. of Dia.) | Radial Location (in) | Axial Velocity (cm/sec) |
|---|---|---|
| | 14.50 | 3.14 |
| | 14.85 | 3.07 |
| | 15.55 | 2.90 |
| | 15.80 | 3.02 |
| | 17.00 | 2.48 |
| | 17.75 | 1.95 |
| | 19.02 | 1.50 |
| 14.10 | 10.15 | 1.02 |
| (℄ =14.50 in) | 11.15 | 1.10 |
| | 13.70 | 1.26 |
| | 13.95 | 1.37 |
| | 15.15 | 1.18 |
| | 15.60 | 1.26 |
| | 16.35 | 1.26 |
| | 16.70 | 1.14 |
| | 17.00 | 1.18 |
| | 18.20 | 1.06 |
| | 19.80 | 1.00 |

## TABLE E.11

## AXIAL VELOCITY DATA, 0.20 cm I.D. CAPILLARY
## Q=0.318 $cm^3$/sec, LARGE RESERVOIR

| Axial Location (No. of Dia.) | Radial Location (in) | Axial Velocity (cm/sec) |
|---|---|---|
| 4.93 | 15.10 | 0.77 |
| (℄ =17.30 in) | 15.55 | 1.10 |
| | 15.85 | 1.54 |
| | 16.15 | 2.36 |
| | 16.45 | 3.28 |
| | 16.85 | 6.20 |
| | 17.05 | 6.40 |
| | 17.70 | 4.25 |
| | 18.65 | 2.48 |
| | 18.95 | 1.32 |
| | 19.45 | 1.09 |
| | 19.90 | 0.58 |
| | 20.60 | 0.36 |
| 7.75 | 13.15 | 0.37 |
| (℄ =17.30 in) | 14.25 | 0.92 |
| | 14.85 | 0.95 |
| | 15.20 | 0.97 |
| | 15.50 | 1.37 |
| | 15.75 | 1.37 |
| | 16.15 | 2.36 |
| | 16.50 | 2.46 |
| | 17.00 | 2.96 |
| | 17.30 | 2.92 |
| | 17.85 | 3.15 |
| | 17.95 | 3.28 |
| | 18.75 | 1.99 |
| | 19.00 | 1.16 |
| | 19.70 | 0.90 |
| | 20.10 | 0.65 |
| | 20.55 | 0.55 |
| | 21.90 | 0.30 |
| | 22.50 | 0.18 |
| 10.55 | 12.35 | 0.35 |
| (℄ =17.30 in) | 14.10 | 0.64 |
| | 14.85 | 0.71 |
| | 15.40 | 1.07 |
| | 15.60 | 1.10 |
| | 16.05 | 1.51 |
| | 16.70 | 1.36 |
| | 17.35 | 1.56 |

TABLE E.11 (continued)

| Axial Location (No. of Dia.) | Radial Location (in) | Axial Velocity (cm/sec) |
|---|---|---|
| | 18.15 | 1.44 |
| | 18.50 | 1.23 |
| | 18.80 | 1.09 |
| | 19.00 | 1.23 |
| | 19.60 | 0.86 |
| | 19.75 | 0.91 |
| | 20.20 | 0.74 |
| | 20.95 | 0.51 |
| | 21.95 | 0.34 |
| 14.10<br>(℄ =17.30 in) | 10.40 | 0.19 |
| | 11.85 | 0.46 |
| | 12.45 | 0.43 |
| | 14.65 | 0.49 |
| | 15.60 | 0.58 |
| | 16.05 | 0.58 |
| | 16.25 | 0.61 |
| | 16.55 | 0.57 |
| | 17.20 | 0.56 |
| | 17.55 | 0.55 |
| | 18.50 | 0.61 |
| | 19.45 | 0.48 |
| | 21.05 | 0.39 |
| | 22.00 | 0.32 |
| | 22.75 | 0.28 |
| | 23.50 | 0.30 |

## TABLE E.12

## AXIAL VELOCITY DATA, 0.20 cm I.D. CAPILLARY $Q=0.794$ cm$^3$/sec, LARGE RESERVOIR

| Axial Location (No. of Dia.) | Radial Location (in) | Axial Velocity (cm/sec) |
|---|---|---|
| 9.86 | 10.50 | 0.96 |
| (℄ =12.50 in) | 11.10 | 2.24 |
| | 11.50 | 4.40 |
| | 11.60 | 4.86 |
| | 12.30 | 9.90 |
| | 12.45 | 10.90 |
| | 12.65 | 10.30 |
| | 13.00 | 7.55 |
| | 13.30 | 2.71 |
| | 13.75 | 1.88 |
| | 14.20 | 1.45 |
| | 14.40 | 1.02 |
| | 14.65 | 0.72 |
| | 15.15 | 0.40 |
| 13.40 | 9.35 | 0.62 |
| (℄ =12.50 in) | 9.65 | 0.75 |
| | 10.50 | 1.32 |
| | 11.45 | 3.60 |
| | 11.65 | 4.46 |
| | 12.30 | 6.63 |
| | 12.45 | 7.30 |
| | 12.75 | 6.13 |
| | 12.90 | 5.92 |
| | 13.15 | 5.15 |
| | 13.40 | 2.88 |
| | 14.20 | 1.49 |
| | 14.30 | 1.50 |
| | 14.50 | 1.24 |
| | 14.60 | 1.20 |
| | 15.15 | 0.76 |
| | 15.50 | 0.60 |
| | 15.80 | 0.44 |
| | 15.85 | 0.48 |
| 16.90 | 9.10 | 0.56 |
| (℄ =12.50 in) | 9.40 | 0.80 |
| | 9.70 | 0.85 |
| | 10.65 | 1.56 |
| | 11.25 | 2.25 |
| | 11.35 | 2.62 |
| | 11.60 | 2.80 |

TABLE E.12 (continued)

| Axial Location (No. of Dia.) | Radial Location (in) | Axial Velocity (cm/sec) |
|---|---|---|
| | 11.80 | 3.16 |
| | 12.05 | 3.90 |
| | 12.25 | 4.22 |
| | 12.50 | 4.32 |
| | 12.60 | 4.30 |
| | 12.85 | 4.00 |
| | 12.90 | 3.82 |
| | 13.35 | 3.00 |
| | 13.45 | 2.71 |
| | 14.35 | 1.51 |
| | 14.60 | 1.07 |
| | 14.95 | 0.96 |
| | 15.25 | 0.96 |
| | 15.35 | 0.83 |
| | 15.50 | 0.72 |
| | 16.00 | 0.50 |
| 21.10 | 9.60 | 0.56 |
| (℄ =12.50 in) | 10.75 | 1.12 |
| | 11.05 | 1.39 |
| | 11.25 | 1.44 |
| | 11.60 | 1.65 |
| | 11.80 | 1.70 |
| | 12.05 | 1.88 |
| | 12.20 | 1.90 |
| | 12.80 | 1.90 |
| | 13.05 | 1.68 |
| | 13.25 | 1.88 |
| | 13.65 | 1.55 |
| | 13.75 | 1.52 |
| | 14.85 | 1.03 |
| | 15.35 | 0.73 |
| | 16.00 | 0.62 |
| | 16.35 | 0.53 |
| 24.60 | 8.60 | 0.48 |
| (℄ =12.50 in) | 9.35 | 0.55 |
| | 10.15 | 0.74 |
| | 11.00 | 0.80 |
| | 11.20 | 0.88 |
| | 11.60 | 0.92 |
| | 11.85 | 0.92 |
| | 12.10 | 0.96 |
| | 12.35 | 0.98 |
| | 12.90 | 0.96 |
| | 13.15 | 0.89 |

TABLE E.12 (continued)

| Axial Location (No. of Dia.) | Radial Location (in) | Axial Velocity (cm/sec) |
|---|---|---|
| | 13.45 | 0.95 |
| | 14.25 | 0.79 |
| | 15.15 | 0.72 |
| | 15.60 | 0.61 |
| | 16.00 | 0.59 |
| | 17.05 | 0.40 |

## TABLE E.13

## AXIAL VELOCITY DATA, 0.20 cm I.D. CAPILLARY
## Q=1.589 $cm^3/sec$, LARGE RESERVOIR

| Axial Location (No. of Dia.) | Radial Location (in) | Axial Velocity (cm/sec) |
|---|---|---|
| 13.90 | 13.95 | 1.35 |
| (℄ =16.60 in) | 14.75 | 2.35 |
| | 15.15 | 3.32 |
| | 15.40 | 4.35 |
| | 15.60 | 6.68 |
| | 15.95 | 11.30 |
| | 16.20 | 15.60 |
| | 16.50 | 23.10 |
| | 16.90 | 20.20 |
| | 17.75 | 3.47 |
| | 18.00 | 2.95 |
| | 18.25 | 2.17 |
| | 18.40 | 2.30 |
| | 18.85 | 1.45 |
| 21.30 | 11.50 | 0.51 |
| (℄ =16.60 in) | 13.25 | 1.10 |
| | 13.35 | 1.15 |
| | 14.25 | 1.45 |
| | 14.45 | 2.32 |
| | 15.00 | 3.04 |
| | 15.25 | 3.76 |
| | 15.55 | 5.50 |
| | 15.80 | 6.06 |
| | 15.95 | 6.80 |
| | 16.10 | 8.40 |
| | 16.15 | 9.70 |
| | 16.25 | 10.10 |
| | 16.40 | 10.80 |
| | 16.60 | 11.55 |
| | 17.00 | 9.20 |
| | 17.10 | 9.70 |
| | 17.50 | 6.36 |
| | 18.35 | 2.60 |
| | 18.55 | 2.31 |
| | 19.00 | 1.58 |
| | 19.40 | 1.44 |
| | 20.25 | 0.87 |
| | 20.55 | 0.89 |
| | 21.25 | 0.53 |
| | 22.05 | 0.36 |

TABLE E.13 (continued)

| Axial Location (No. of Dia.) | Radial Location (in) | Axial Velocity (cm/sec) |
|---|---|---|
| 28.18 | 10.15 | 0.36 |
| (℄ =16.60 in) | 11.35 | 0.61 |
| | 12.75 | 0.94 |
| | 12.90 | 1.15 |
| | 13.40 | 1.25 |
| | 13.55 | 1.37 |
| | 14.35 | 2.04 |
| | 14.65 | 2.54 |
| | 15.15 | 2.90 |
| | 15.30 | 3.20 |
| | 15.45 | 3.67 |
| | 15.65 | 3.76 |
| | 16.20 | 5.65 |
| | 16.40 | 5.50 |
| | 16.85 | 4.90 |
| | 17.20 | 4.30 |
| | 17.35 | 4.34 |
| | 18.40 | 2.68 |
| | 18.70 | 2.30 |
| | 19.25 | 1.74 |
| | 19.55 | 1.56 |
| | 19.95 | 1.23 |
| | 20.45 | 1.04 |
| | 20.75 | 1.04 |
| | 21.15 | 0.55 |
| 35.67 | 12.25 | 0.75 |
| (℄ =16.60 in) | 12.90 | 0.78 |
| | 13.80 | 1.15 |
| | 14.10 | 1.20 |
| | 14.25 | 1.20 |
| | 14.75 | 1.30 |
| | 15.15 | 1.44 |
| | 15.85 | 1.66 |
| | 16.15 | 1.63 |
| | 16.60 | 1.64 |
| | 16.80 | 1.62 |
| | 16.95 | 1.62 |
| | 17.20 | 1.59 |
| | 17.40 | 1.54 |
| | 18.05 | 1.49 |
| | 18.45 | 1.45 |
| | 18.75 | 1.30 |
| | 20.35 | 0.98 |
| | 21.25 | 0.81 |
| | 21.95 | 0.61 |

TABLE E.13 (continued)

| Axial Location (No. of Dia.) | Radial Location (in) | Axial Velocity (cm/sec) |
|---|---|---|
| | 22.45 | 0.54 |
| | 22.85 | 0.50 |
| | 23.45 | 0.39 |
| 42.00 | 10.65 | 0.42 |
| (℄ =16.60 in) | 11.90 | 0.53 |
| | 13.15 | 0.58 |
| | 14.35 | 0.68 |
| | 14.85 | 0.75 |
| | 15.55 | 0.79 |
| | 16.70 | 0.90 |
| | 17.45 | 0.87 |
| | 18.35 | 0.81 |
| | 18.80 | 0.77 |
| | 19.10 | 0.70 |
| | 19.90 | 0.56 |
| | 20.20 | 0.53 |
| | 21.05 | 0.49 |

## TABLE E.14

## AXIAL VELOCITY DATA, 0.30 cm I.D. CAPILLARY Q=0.318 cm$^3$/sec, LARGE RESERVOIR

| Axial Location (No. of Dia.) | Radial Location (in) | Axial Velocity (cm/sec) |
|---|---|---|
| 1.42<br>(℄ =14.50 in) | 13.20 | 0.87 |
| | 13.45 | 2.08 |
| | 14.35 | 4.10 |
| | 14.45 | 4.41 |
| | 14.65 | 4.09 |
| | 14.85 | 3.84 |
| | 15.00 | 3.55 |
| | 15.20 | 3.78 |
| | 15.35 | 2.84 |
| | 15.55 | 2.36 |
| | 15.80 | 1.32 |
| | 15.95 | 0.96 |
| | 16.40 | 0.66 |
| 2.82<br>(℄ =14.50 in) | 12.95 | 0.95 |
| | 13.25 | 1.48 |
| | 14.35 | 2.64 |
| | 14.43 | 2.68 |
| | 14.70 | 2.52 |
| | 14.90 | 2.58 |
| | 15.15 | 2.39 |
| | 15.40 | 2.02 |
| | 15.65 | 1.98 |
| | 15.85 | 1.64 |
| | 16.15 | 1.10 |
| | 16.25 | 0.95 |
| | 16.55 | 0.69 |
| | 16.65 | 0.79 |
| | 16.85 | 0.53 |
| | 17.45 | 0.35 |
| 4.24<br>(℄ =14.50 in) | 12.50 | 0.63 |
| | 13.25 | 1.15 |
| | 14.35 | 1.45 |
| | 14.55 | 1.45 |
| | 14.80 | 1.39 |
| | 15.00 | 1.42 |
| | 15.35 | 1.26 |
| | 15.70 | 1.10 |
| | 16.00 | 0.85 |
| | 16.20 | 0.85 |
| | 16.75 | 0.67 |

TABLE E.14 (continued)

| Axial Location (No. of Dia.) | Radial Location (in) | Axial Velocity (cm/sec) |
|---|---|---|
| | 17.20 | 0.60 |
| | 18.00 | 0.33 |
| | 18.40 | 0.28 |
| 5.65<br>(℄ =14.50 in) | 12.25 | 0.57 |
| | 13.35 | 0.63 |
| | 14.60 | 0.76 |
| | 15.00 | 0.76 |
| | 15.15 | 0.76 |
| | 15.40 | 0.73 |
| | 15.55 | 0.70 |
| | 15.70 | 0.76 |
| | 16.55 | 0.55 |
| | 17.05 | 0.50 |
| | 17.40 | 0.45 |
| | 18.05 | 0.38 |
| 7.06<br>(℄ =14.50 in) | 13.10 | 0.39 |
| | 13.60 | 0.38 |
| | 14.70 | 0.40 |
| | 15.35 | 0.44 |
| | 15.80 | 0.41 |
| | 17.20 | 0.31 |
| | 17.90 | 0.29 |
| | 19.10 | 0.21 |
| 8.95<br>(℄ =14.50 in) | 10.30 | 0.16 |
| | 13.30 | 0.20 |
| | 13.50 | 0.18 |
| | 15.05 | 0.23 |
| | 15.60 | 0.20 |
| | 16.80 | 0.20 |

## TABLE E.15

### AXIAL VELOCITY DATA, 0.30 cm I.D. CAPILLARY $Q=0.635\ cm^3/sec$, LARGE RESERVOIR

| Axial Location (No. of Dia.) | Radial Location (in) | Axial Velocity (cm/sec) |
|---|---|---|
| 1.41 | 14.55 | 2.65 |
| (℄ =16.00 in) | 15.65 | 9.77 |
| | 16.15 | 7.87 |
| | 16.25 | 8.27 |
| | 16.30 | 8.07 |
| | 16.55 | 7.70 |
| | 17.30 | 2.37 |
| 2.83 | 13.65 | 1.49 |
| (℄ =16.00 in) | 14.50 | 3.05 |
| | 15.65 | 7.60 |
| | 16.15 | 6.20 |
| | 16.25 | 6.45 |
| | 16.35 | 6.37 |
| | 16.65 | 5.79 |
| | 17.70 | 1.21 |
| | 19.00 | 0.37 |
| 4.24 | 13.55 | 1.37 |
| (℄ =16.00 in) | 15.60 | 5.55 |
| | 15.95 | 5.75 |
| | 16.20 | 4.47 |
| | 17.20 | 2.24 |
| | 17.40 | 2.18 |
| | 17.95 | 1.57 |
| | 18.05 | 1.24 |
| 6.13 | 13.00 | 1.20 |
| (℄ =16.00 in) | 13.45 | 1.22 |
| | 13.85 | 1.68 |
| | 15.55 | 3.14 |
| | 16.35 | 2.76 |
| | 16.45 | 2.40 |
| | 16.50 | 2.46 |
| | 16.95 | 2.56 |
| | 17.55 | 1.65 |
| | 17.80 | 1.57 |
| | 17.95 | 1.57 |
| | 18.35 | 1.24 |
| | 18.45 | 1.01 |

TABLE E.15 (continued)

| Axial Location (No. of Dia.) | Radial Location (in) | Axial Velocity (cm/sec) |
|---|---|---|
| 8.02<br>(℄ =16.00 in) | 12.05 | 0.63 |
| | 12.20 | 0.80 |
| | 12.25 | 0.76 |
| | 13.10 | 1.04 |
| | 13.20 | 1.08 |
| | 14.85 | 1.57 |
| | 15.50 | 1.61 |
| | 16.55 | 1.66 |
| | 16.70 | 1.49 |
| | 16.80 | 1.53 |
| | 16.95 | 1.53 |
| | 17.20 | 1.36 |
| | 18.05 | 1.11 |
| | 18.15 | 1.02 |
| | 18.40 | 1.00 |
| | 19.20 | 0.73 |
| | 20.95 | 0.39 |
| | 21.75 | 0.31 |
| 9.89<br>(℄ =16.00 in) | 10.75 | 0.44 |
| | 11.00 | 0.46 |
| | 12.20 | 0.60 |
| | 12.30 | 0.61 |
| | 12.95 | 0.70 |
| | 14.00 | 0.77 |
| | 14.50 | 0.83 |
| | 15.45 | 0.87 |
| | 15.75 | 0.87 |
| | 17.15 | 0.80 |
| | 17.40 | 0.77 |
| | 17.70 | 0.76 |
| | 17.95 | 0.72 |
| | 18.45 | 0.66 |
| | 18.80 | 0.64 |
| | 19.05 | 0.62 |
| | 19.70 | 0.53 |
| | 20.35 | 0.44 |
| | 20.60 | 0.46 |
| 11.78<br>(℄ =16.00 in) | 11.10 | 0.36 |
| | 11.25 | 0.38 |
| | 11.85 | 0.41 |
| | 14.40 | 0.50 |
| | 15.75 | 0.50 |
| | 16.35 | 0.50 |
| | 17.25 | 0.50 |

TABLE E.15 (continued)

| Axial Location (No. of Dia.) | Radial Location (in) | Axial Velocity (cm/sec) |
|---|---|---|
| | 17.60 | 0.46 |
| | 18.50 | 0.43 |
| | 19.25 | 0.38 |
| | 19.45 | 0.39 |
| | 19.70 | 0.39 |
| | 20.85 | 0.33 |
| | 21.50 | 0.25 |
| | 21.95 | 0.25 |

## TABLE E.16

### AXIAL VELOCITY DATA, 0.30 cm I.D. CAPILLARY
### Q=1.589 $cm^3$/sec, LARGE RESERVOIR

| Axial Location (No. of Dia.) | Radial Location (in) | Axial Velocity (cm/sec) |
|---|---|---|
| 4.24 | 14.70 | 23.10 |
| (℄ =15.60 in) | 15.00 | 26.80 |
| | 15.20 | 29.00 |
| | 15.30 | 32.80 |
| | 15.60 | 31.80 |
| | 16.00 | 32.80 |
| | 16.20 | 24.80 |
| | 16.75 | 17.10 |
| | 17.10 | 13.50 |
| | 17.85 | 5.64 |
| | 18.30 | 4.05 |
| | 18.80 | 2.42 |
| 6.60 | 11.65 | 2.51 |
| (℄ =15.60 in) | 12.25 | 3.49 |
| | 14.60 | 15.25 |
| | 14.95 | 21.80 |
| | 15.25 | 21.80 |
| | 15.50 | 23.60 |
| | 16.00 | 22.90 |
| | 16.30 | 20.00 |
| | 16.90 | 13.00 |
| | 17.25 | 12.10 |
| | 17.40 | 10.93 |
| | 17.60 | 8.67 |
| | 18.20 | 6.38 |
| | 18.35 | 5.78 |
| | 18.45 | 4.90 |
| | 18.60 | 4.88 |
| | 18.75 | 4.14 |
| | 18.95 | 3.63 |
| | 19.50 | 2.52 |
| | 19.75 | 2.48 |
| | 20.05 | 2.12 |
| | 20.75 | 1.75 |
| | 21.05 | 1.48 |
| 9.42 | 11.90 | 3.72 |
| (℄ =15.60 in) | 12.70 | 5.60 |
| | 13.40 | 6.54 |
| | 14.65 | 11.90 |
| | 14.90 | 12.80 |

TABLE E.16 (continued)

| Axial Location (No. of Dia.) | Radial Location (in) | Axial Velocity (cm/sec) |
|---|---|---|
| | 15.25 | 13.65 |
| | 15.55 | 14.00 |
| | 15.70 | 15.10 |
| | 16.10 | 14.30 |
| | 16.45 | 12.20 |
| | 17.05 | 10.00 |
| | 17.70 | 8.50 |
| | 18.05 | 6.48 |
| | 18.70 | 5.61 |
| | 18.80 | 4.55 |
| | 18.95 | 4.23 |
| | 19.35 | 4.25 |
| | 19.65 | 3.66 |
| | 19.85 | 3.42 |
| | 20.25 | 2.80 |
| | 20.75 | 2.22 |
| | 21.20 | 1.90 |
| | 22.05 | 1.42 |
| | 22.20 | 1.55 |
| 12.25 | 14.70 | 7.30 |
| (℄ =15.60 in) | 15.10 | 8.01 |
| | 15.20 | 7.30 |
| | 15.60 | 7.60 |
| | 15.70 | 8.30 |
| | 15.90 | 7.80 |
| | 16.35 | 8.29 |
| | 16.40 | 7.42 |
| | 17.45 | 6.48 |
| | 18.05 | 4.93 |
| | 18.35 | 5.16 |
| | 18.70 | 4.74 |
| | 18.85 | 4.25 |
| | 18.95 | 3.88 |
| | 19.75 | 3.68 |
| | 20.50 | 2.80 |
| | 21.95 | 2.08 |
| | 22.40 | 1.84 |
| | 23.30 | 1.34 |
| 15.05 | 13.25 | 3.62 |
| (℄ =15.60 in) | 13.40 | 3.48 |
| | 13.80 | 3.52 |
| | 14.10 | 3.60 |
| | 14.20 | 3.67 |
| | 14.30 | 3.81 |

TABLE E.16 (continued)

| Axial Location (No. of Dia.) | Radial Location (in) | Axial Velocity (cm/sec) |
|---|---|---|
| | 14.50 | 4.14 |
| | 14.90 | 4.15 |
| | 15.00 | 3.96 |
| | 15.60 | 3.96 |
| | 15.70 | 4.25 |
| | 16.05 | 4.30 |
| | 16.60 | 3.90 |
| | 17.15 | 3.62 |
| | 17.90 | 3.84 |
| | 18.25 | 3.12 |
| | 19.45 | 3.04 |
| | 19.80 | 2.46 |
| | 20.20 | 2.38 |
| | 20.35 | 2.75 |
| | 21.25 | 2.22 |
| | 21.55 | 2.13 |
| | 22.05 | 1.83 |
| | 22.65 | 2.13 |
| | 23.80 | 1.42 |

## E.2 AXIAL AND RADIAL VELOCITY PROFILES - DIGITIZER METHOD

The digitizer method was used in measuring both axial and radial velocities at three axial locations upstream of the contraction. These axial locations were at distances equal to one and one half times the location of the eddy center, at the eddy center and at a distance equal to one half times the eddy center location. The locations of the eddy centers are tabulated in Appendix F, Section F.1 (page 444). Since the direct method was used to measure the axial velocities for the data in Tables E.17 to E.20, E.22 to E.24, and E.26 to E.27, only radial velocities were measured with the digitizer method.

The radial distance $\Delta r$ (Equation 2.2, page 67), measured by the digitizer method was of the opposite sign for values of r' greater than 1.327 cm in reservoir S and greater than 12.745 in reservoir L. Data given in this manner allows for a clear graphical presentation of $V_r$ versus r'.

The following table lists the order in which the data are presented in this section. In each of the tables the distance measured from the reservoir wall r' was determined by Equation 2.4 (page 68).

| Table No. | Reservoir | I.D.(cm) | $Q(cm^3/sec)$ |
|---|---|---|---|
| 17 | S | 0.10 | 0.016 |
| 18 | S | 0.10 | 0.040 |
| 19 | S | 0.10 | 0.119 |
| 20 | S | 0.20 | 0.040 |
| 21 | S | 0.20 | 0.159 |
| 22 | S | 0.20 | 0.238 |
| 23 | S | 0.20 | 0.318 |
| 24 | S | 0.30 | 0.040 |
| 25 | S | 0.30 | 0.159 |
| 26 | S | 0.30 | 0.318 |
| 27 | S | 0.30 | 0.654 |
| 28 | L | 0.20 | 1.589 |
| 29 | L | 0.20 | 1.906 |
| 30 | L | 0.20 | 2.383 |
| 31 | L | 0.20 | 2.701 |
| 32 | L | 0.20 | 3.177 |
| 33 | L | 0.20 | 3.813 |
| 34 | L | 0.20 | 4.766 |
| 35 | L | 0.30 | 4.766 |
| 36 | L | 0.30 | 6.354 |
| 37 | L | 0.30 | 7.148 |
| 38 | L | 0.30 | 7.943 |
| 39 | L | 0.30 | 8.737 |
| 40 | L | 0.30 | 9.531 |
| 41 | L | 0.30 | 10.325 |
| 42 | L | 0.30 | 11.120 |

## TABLE E.17

## RADIAL VELOCITIES - DIGITIZER METHOD Q=0.016 $cm^3/sec$
## 0.10 cm I.D. CAPILLARY TUBE, SMALL RESERVOIR

(Z/D) = 9.45 (℄ = 1.327 cm)

| r' (cm) | $V_r$ (cm/sec) | r' (cm) | $V_r$ (cm/sec) | r' (cm) | $V_r$ (cm/sec) | r' (cm) | $V_r$ (cm/sec) | r' (cm) | $V_r$ (cm/sec) | r' (cm) | $V_r$ (cm/sec) |
|---|---|---|---|---|---|---|---|---|---|---|---|
| 1.247 | 0.028 | 1.225 | 0.027 | 1.340 | -0.011 | 1.455 | -0.015 | 1.320 | 0.002 | 1.354 | 0.002 |
| 1.463 | -0.015 | 1.409 | -0.011 | 1.442 | -0.023 | 1.524 | -0.022 | 1.449 | -0.016 | 1.528 | -0.044 |
| 1.386 | 0.007 | 1.057 | 0.023 | 1.649 | -0.015 | 1.389 | 0.006 | 1.371 | -0.024 | 1.341 | -0.003 |
| 1.508 | -0.021 | 1.383 | -0.002 | 1.355 | -0.003 | 0.990 | 0.028 | 1.443 | -0.008 | 1.427 | -0.002 |
| 1.220 | 0.035 | 1.088 | 0.028 | 1.451 | -0.018 | 1.274 | 0.004 | 1.160 | 0.029 | 1.504 | -0.028 |
| 1.299 | 0.001 | 1.253 | 0.024 | 1.033 | 0.026 | 1.432 | -0.011 | 1.305 | 0.009 | 1.313 | 0.004 |
| 1.349 | -0.005 | 1.403 | -0.008 | 1.559 | -0.042 | | | | | | |

(Z/D) = 6.30 (℄ = 1.327 cm)

| r' (cm) | $V_r$ (cm/sec) | r' (cm) | $V_r$ (cm/sec) | r' (cm) | $V_r$ (cm/sec) | r' (cm) | $V_r$ (cm/sec) | r' (cm) | $V_r$ (cm/sec) | r' (cm) | $V_r$ (cm/sec) |
|---|---|---|---|---|---|---|---|---|---|---|---|
| 1.180 | 0.038 | 1.417 | -0.044 | 1.214 | 0.048 | 1.327 | 0.008 | 1.489 | -0.060 | 1.243 | 0.039 |
| 1.348 | -0.023 | 1.201 | 0.041 | 1.318 | 0.024 | 1.370 | -0.014 | 1.290 | 0.020 | 1.358 | -0.044 |
| 1.448 | -0.072 | 1.371 | -0.029 | 1.406 | -0.048 | 1.112 | 0.014 | 1.080 | 0.021 | 1.467 | -0.053 |
| 1.380 | -0.003 | 1.198 | 0.039 | 1.392 | -0.026 | 1.433 | -0.021 | 1.258 | 0.060 | 1.404 | -0.012 |
| 1.505 | -0.069 | 1.282 | 0.057 | 1.486 | -0.038 | 1.363 | -0.006 | 1.346 | -0.012 | 1.503 | -0.058 |
| 1.199 | 0.056 | 1.365 | -0.039 | 1.489 | -0.091 | 1.229 | 0.079 | 1.458 | -0.085 | 1.363 | -0.038 |
| 1.351 | -0.016 | 1.303 | 0.036 | 1.350 | -0.030 | 1.401 | -0.020 | 1.369 | -0.007 | 1.405 | -0.011 |
| 1.372 | -0.025 | 1.402 | -0.037 | 1.431 | -0.035 | 1.408 | -0.041 | 1.165 | 0.042 | 1.530 | -0.075 |
| 1.420 | -0.055 | 1.293 | 0.028 | 1.252 | 0.045 | 1.447 | -0.044 | 1.370 | -0.009 | 1.297 | 0.034 |
| 1.638 | -0.025 | 1.180 | 0.040 | 1.394 | -0.002 | 1.262 | 0.070 | 1.432 | -0.043 | 1.442 | -0.049 |
| 1.377 | -0.035 | 1.487 | -0.046 | 1.564 | -0.046 | 1.423 | -0.060 | 1.266 | 0.030 | 1.351 | -0.037 |
| 1.458 | -0.050 | 1.393 | -0.038 | 1.408 | -0.027 | 1.284 | 0.035 | 1.323 | -0.007 | 1.337 | -0.029 |
| 1.420 | -0.058 | 1.197 | 0.037 | 1.361 | -0.011 | 1.369 | -0.030 | 1.398 | -0.025 | 1.238 | 0.048 |
| 1.359 | -0.033 | | | | | | | | | | |

TABLE E.17 (continued)

(Z/D) = 3.15 ( ℄ = 1.327 cm)

| r' (cm) | $V_r$ (cm/sec) | r' (cm) | $V_r$ (cm/sec) | r' (cm) | $V_r$ (cm/sec) | r' (cm) | $V_r$ (cm/sec) | r' (cm) | $V_r$ (cm/sec) | r' (cm) | $V_r$ (cm/sec) |
|---|---|---|---|---|---|---|---|---|---|---|---|
| 1.285 | 0.101 | 1.437 | -0.008 | 1.474 | -0.014 | 1.505 | -0.003 | 1.376 | -0.021 | 1.189 | -0.038 |
| 1.257 | 0.044 | 1.369 | -0.065 | 1.375 | -0.089 | 1.382 | -0.019 | 1.506 | -0.023 | 1.481 | -0.030 |
| 1.166 | -0.027 | 1.386 | -0.026 | 1.414 | 0.029 | 1.435 | -0.015 | 1.446 | -0.028 | 1.207 | 0.003 |
| 1.253 | 0.036 | 1.277 | 0.045 | 1.310 | 0.052 | 1.346 | 0.031 | 1.415 | -0.090 | 1.405 | -0.032 |
| 1.421 | -0.038 | 1.513 | -0.003 | 1.408 | -0.036 | 1.432 | -0.067 | 1.310 | 0.120 | 1.356 | -0.020 |
| 1.400 | -0.029 | 1.194 | -0.012 | 1.230 | 0.015 | 1.313 | 0.052 | 1.347 | -0.023 | 1.371 | -0.061 |
| 1.382 | -0.048 | 1.392 | -0.043 | 1.462 | -0.028 | 1.230 | 0.045 | 1.344 | -0.032 | 1.360 | -0.016 |
| 1.483 | -0.007 | 1.233 | 0.011 | 1.454 | -0.030 | 1.468 | -0.044 | 1.295 | 0.015 | 1.326 | 0.050 |
| 1.435 | -0.007 | 1.448 | -0.067 | 1.501 | -0.017 | 1.371 | -0.044 | 1.395 | -0.033 | 1.430 | -0.033 |
| 1.250 | 0.039 | 1.296 | 0.094 | 1.359 | -0.030 | 1.510 | -0.009 | 1.236 | 0.024 | 1.309 | 0.046 |
| 1.333 | -0.009 | 1.452 | -0.050 | 1.374 | -0.079 | 1.418 | -0.112 | 1.269 | 0.019 | 1.367 | -0.053 |
| 1.412 | -0.036 |  |  |  |  |  |  |  |  |  |  |

## TABLE E.18

## RADIAL VELOCITIES - DIGITIZER METHOD, Q=0.040 cm$^3$/sec
## 0.10 cm I.D. CAPILLARY TUBE, SMALL RESERVOIR

(Z/D) = 16.82          ( ℄ = 1.327 cm)

| r' (cm) | $V_r$ (cm/sec) | r' (cm) | $V_r$ (cm/sec) | r' (cm) | $V_r$ (cm/sec) | r' (cm) | $V_r$ (cm/sec) | r' (cm) | $V_r$ (cm/sec) | r' (cm) | $V_r$ (cm/sec) |
|---|---|---|---|---|---|---|---|---|---|---|---|
| 1.155 | 0.062 | 1.213 | 0.023 | 0.826 | 0.057 | 1.137 | 0.036 | 1.240 | 0.029 | 1.379 | -0.006 |
| 1.417 | -0.024 | 1.541 | -0.044 | 1.589 | -0.059 | 1.219 | 0.036 | 1.242 | 0.051 | 1.256 | 0.056 |
| 1.294 | 0.027 | 1.319 | -0.013 | 1.339 | -0.007 | 1.035 | 0.043 | 1.174 | 0.056 | 1.241 | 0.033 |
| 1.268 | 0.022 | 1.280 | 0.009 | 1.353 | -0.023 | 1.359 | -0.006 | 1.379 | -0.012 | 1.419 | -0.030 |
| 1.467 | -0.041 | 1.524 | -0.060 | 1.583 | -0.056 | 0.980 | 0.052 | 1.155 | 0.046 | 1.261 | 0.056 |
| 1.316 | 0.011 | 1.383 | -0.009 | 1.419 | -0.042 | 1.563 | -0.055 | | | | |

(Z/D) = 11.21          ( ℄ = 1.327 cm)

| r' (cm) | $V_r$ (cm/sec) | r' (cm) | $V_r$ (cm/sec) | r' (cm) | $V_r$ (cm/sec) | r' (cm) | $V_r$ (cm/sec) | r' (cm) | $V_r$ (cm/sec) | r' (cm) | $V_r$ (cm/sec) |
|---|---|---|---|---|---|---|---|---|---|---|---|
| 1.222 | 0.131 | 1.238 | 0.087 | 1.266 | 0.079 | 1.454 | -0.030 | 1.105 | 0.082 | 1.123 | 0.042 |
| 1.261 | 0.082 | 1.318 | -0.058 | 1.376 | -0.060 | 1.400 | -0.075 | 1.528 | -0.074 | 1.218 | 0.120 |
| 1.255 | 0.037 | 1.316 | -0.030 | 1.375 | -0.078 | 1.379 | -0.018 | 1.462 | -0.127 | 1.474 | -0.073 |
| 1.269 | 0.037 | 1.359 | 0.033 | 1.396 | -0.058 | 1.515 | -0.119 | 1.530 | -0.089 | 1.541 | -0.088 |
| 1.593 | -0.005 | 1.343 | -0.046 | 1.382 | -0.064 | 1.421 | -0.066 | 1.444 | -0.090 | 1.289 | 0.119 |
| 1.323 | 0.065 | 1.334 | -0.059 | 1.343 | 0.059 | 1.366 | -0.039 | 1.272 | 0.085 | 1.503 | -0.143 |
| 1.530 | -0.024 | 1.151 | -0.033 | 1.306 | 0.106 | 1.337 | -0.044 | 1.366 | -0.051 | 1.238 | 0.058 |
| 1.263 | 0.047 | 1.358 | 0.060 | 1.385 | -0.045 | 1.492 | -0.024 | 1.514 | -0.110 | 1.554 | -0.077 |
| 1.590 | -0.029 | 1.355 | 0.020 | 1.384 | -0.016 | 1.461 | -0.102 | 1.243 | 0.045 | 1.250 | 0.034 |
| 1.387 | -0.007 | 1.509 | -0.117 | 1.569 | -0.084 | 1.176 | 0.080 | 1.266 | 0.072 | 1.303 | 0.035 |
| 1.388 | -0.047 | 1.396 | -0.063 | 1.457 | -0.094 | 1.489 | -0.040 | 1.334 | 0.001 | 1.413 | -0.043 |
| 1.598 | 0.017 | 1.248 | 0.042 | 1.261 | 0.084 | 1.360 | -0.058 | 1.419 | -0.055 | 1.616 | -0.065 |
| 1.239 | 0.069 | 1.275 | 0.074 | 1.292 | 0.027 | 1.310 | 0.044 | 1.226 | 0.052 | 1.408 | -0.085 |
| 1.520 | -0.101 | 1.555 | -0.074 | 1.569 | -0.008 | 1.117 | 0.049 | | | | |

TABLE E.18 (continued)

(Z/D) = 11.21 ( $\ell$ = 1.327 cm)

| r' (cm) | $V_r$ (cm/sec) | r' (cm) | $V_r$ (cm/sec) | r' (cm) | $V_r$ (cm/sec) | r' (cm) | $V_r$ (cm/sec) | r' (cm) | $V_r$ (cm/sec) | r' (cm) | $V_r$ (cm/sec) |
|---|---|---|---|---|---|---|---|---|---|---|---|
| 1.326 | -0.027 | 1.336 | 0.029 | 1.348 | 0.006 | 1.452 | -0.068 | 1.059 | 0.038 | 1.179 | 0.070 |
| 1.252 | 0.070 | 1.359 | -0.016 | 1.440 | -0.123 | 1.478 | -0.038 | 1.544 | -0.053 | 1.586 | -0.041 |
| 1.184 | 0.090 | 1.223 | 0.053 | 1.244 | 0.098 | 1.297 | 0.016 | 1.383 | -0.045 | 1.405 | -0.017 |
| 1.098 | 0.053 | 1.174 | 0.109 | 1.227 | 0.083 | 1.366 | -0.013 | 1.461 | -0.116 | 1.483 | -0.092 |
| 1.534 | -0.054 | | | | | | | | | | |

(Z/D) = 5.61 ( $\ell$ = 1.327 cm)

| r' (cm) | $V_r$ (cm/sec) | r' (cm) | $V_r$ (cm/sec) | r' (cm) | $V_r$ (cm/sec) | r' (cm) | $V_r$ (cm/sec) | r' (cm) | $V_r$ (cm/sec) | r' (cm) | $V_r$ (cm/sec) |
|---|---|---|---|---|---|---|---|---|---|---|---|
| 1.267 | 0.139 | 1.489 | -0.017 | 1.616 | -0.011 | 1.231 | 0.053 | 1.283 | 0.114 | 1.316 | 0.090 |
| 1.349 | 0.001 | 1.428 | 0.030 | 1.470 | 0.016 | 1.280 | 0.048 | 1.314 | 0.087 | 1.338 | 0.055 |
| 1.404 | -0.028 | 1.496 | -0.012 | 1.237 | 0.024 | 1.450 | 0.002 | 1.549 | -0.014 | 1.576 | -0.008 |
| 1.305 | 0.156 | 1.410 | 0.038 | 1.429 | -0.035 | 1.464 | -0.014 | 1.329 | -0.044 | 1.347 | -0.052 |
| 1.386 | -0.077 | 1.410 | -0.065 | 1.484 | -0.013 | 1.358 | 0.134 | 1.447 | -0.061 | 1.370 | 0.063 |
| 1.411 | -0.081 | 1.458 | -0.047 | 1.476 | -0.063 | 1.299 | 0.075 | 1.372 | -0.100 | 1.360 | -0.129 |
| 1.396 | -0.075 | 1.413 | -0.057 | 1.429 | -0.008 | 1.474 | -0.006 | 1.494 | -0.021 | 1.334 | 0.001 |
| 1.496 | -0.012 | 1.349 | 0.115 | 1.508 | -0.030 | 1.131 | -0.056 | 1.313 | 0.083 | 1.420 | -0.112 |
| 1.464 | -0.018 | 1.496 | -0.030 | 1.485 | -0.021 | 1.525 | -0.027 | 1.142 | -0.038 | 1.479 | -0.026 |
| 1.560 | 0.037 | 1.598 | 0.023 | 1.477 | 0.025 | 1.551 | 0.015 | 1.167 | -0.002 | 1.532 | 0.023 |
| 1.120 | -0.054 | 1.259 | 0.109 | 1.424 | -0.027 | 1.338 | -0.055 | 1.404 | -0.028 | | |

## TABLE E.19

## RADIAL VELOCITIES - DIGITIZER METHOD, Q=0.119 $cm^3$/sec
## 0.10 cm I.D. CAPILLARY TUBE, SMALL RESERVOIR

(Z/D) = 18.22 ( ℄ = 1.327 cm)

| r' (cm) | $V_r$ (cm/sec) | r' (cm) | $V_r$ (cm/sec) | r' (cm) | $V_r$ (cm/sec) | r' (cm) | $V_r$ (cm/sec) | r' (cm) | $V_r$ (cm/sec) | r' (cm) | $V_r$ (cm/sec) |
|---|---|---|---|---|---|---|---|---|---|---|---|
| 1.237 | 0.346 | 1.248 | 0.159 | 1.320 | -0.021 | 1.172 | 0.122 | 1.325 | 0.022 | 1.134 | 0.106 |
| 1.277 | 0.205 | 1.239 | 0.076 | 1.275 | 0.031 | 1.287 | -0.124 | 1.242 | 0.180 | 1.191 | 0.131 |
| 1.231 | -0.095 | 1.272 | 0.081 | 1.288 | 0.298 | 1.326 | -0.270 | 1.286 | 0.198 | 1.304 | -0.103 |
| 1.257 | 0.205 | 1.334 | 0.137 | 1.365 | -0.096 | 1.388 | -0.025 | 1.481 | -0.102 | 1.280 | 0.124 |
| 1.412 | -0.290 | 1.470 | -0.168 | 1.367 | 0.020 | 1.413 | -0.094 | 1.461 | -0.253 | 1.506 | -0.089 |
| 1.538 | -0.031 | 1.572 | -0.003 | 1.298 | -0.011 | 1.322 | -0.023 | 1.383 | -0.150 | 1.432 | -0.168 |
| 1.585 | -0.130 | 1.227 | 0.262 | 1.253 | 0.250 | 1.301 | -0.194 | 1.383 | -0.094 | 1.426 | -0.075 |
| 1.455 | -0.227 | 1.468 | -0.247 | 1.500 | -0.060 | 1.508 | -0.028 | 1.540 | -0.051 | 1.621 | -0.067 |
| 1.211 | 0.102 | 1.527 | -0.130 | 1.537 | -0.187 | 1.561 | -0.025 | 1.291 | 0.135 | 1.313 | -0.036 |
| 1.363 | 0.018 | 1.391 | -0.171 | 1.525 | -0.100 | 1.566 | -0.038 | 1.582 | -0.006 | 1.769 | -0.016 |
| 1.268 | 0.014 | 1.287 | -0.167 | 1.377 | 0.046 | 1.491 | -0.184 | 1.566 | -0.124 | 1.588 | -0.124 |
| 1.281 | -0.113 | 1.452 | -0.204 | 1.490 | -0.167 | 1.511 | -0.114 | 1.531 | -0.009 | 1.194 | 0.081 |
| 1.293 | 0.130 | 1.421 | -0.201 | 1.430 | -0.232 | 1.490 | -0.162 | 1.550 | -0.136 | 1.608 | -0.039 |
| 1.290 | 0.127 | 1.460 | 0.114 | 1.536 | -0.136 | 1.554 | -0.152 | 1.570 | -0.153 | 1.128 | 0.072 |
| 1.261 | 0.196 | 1.391 | -0.120 | 1.462 | -0.105 | 1.506 | -0.209 | 1.525 | -0.148 | 1.550 | -0.029 |
| 1.654 | -0.030 | 1.300 | 0.250 | 1.395 | -0.296 | 1.438 | -0.213 | 1.500 | -0.034 | 1.578 | -0.181 |
| 1.277 | -0.122 | 1.362 | -0.143 | 1.510 | -0.229 | 1.557 | -0.154 | 1.605 | -0.106 | 1.140 | 0.105 |
| 1.284 | 0.034 | 1.500 | -0.156 | 1.533 | -0.157 | 1.543 | -0.142 | 1.636 | -0.083 | 1.071 | 0.022 |
| 1.283 | 0.191 | 1.309 | 0.055 | 1.454 | -0.146 | 1.436 | -0.098 | 1.546 | -0.087 | 1.635 | -0.050 |
| 1.624 | -0.063 | 1.799 | -0.026 | 1.031 | 0.061 | 1.240 | 0.106 | 1.345 | 0.017 | 1.533 | -0.148 |
| 1.553 | -0.169 | 1.569 | -0.100 | 1.586 | -0.058 | 1.755 | -0.020 | 0.951 | 0.021 | 0.970 | 0.049 |
| 1.394 | -0.185 | 1.426 | -0.191 | 1.558 | -0.150 | 1.597 | -0.160 | 1.663 | -0.054 | 1.000 | 0.012 |
| 1.220 | 0.077 | 1.291 | 0.126 | 1.603 | -0.079 | 1.640 | -0.032 | 1.669 | -0.075 | 1.787 | -0.027 |
| 1.055 | 0.025 | 1.132 | 0.045 | 1.259 | 0.107 | 1.493 | -0.204 | 1.593 | -0.026 | 1.714 | -0.017 |
| 1.825 | -0.031 | 0.901 | 0.004 | 0.962 | 0.023 | 1.004 | 0.015 | 1.081 | 0.057 | 1.132 | 0.103 |
| 1.213 | 0.116 | 1.246 | 0.126 | 1.536 | -0.096 | 1.595 | -0.034 | 1.707 | -0.016 | 1.720 | -0.008 |
| 1.867 | 0.000 |  |  |  |  |  |  |  |  |  |  |

## TABLE E.19 (continued)

(Z/D) = 9.11 ( $r_{1/2}$ = 1.327 cm)

| r' (cm) | $V_r$ (cm/sec) | r' (cm) | $V_r$ (cm/sec) | r' (cm) | $V_r$ (cm/sec) | r' (cm) | $V_r$ (cm/sec) | r' (cm) | $V_r$ (cm/sec) | r' (cm) | $V_r$ (cm/sec) |
|---|---|---|---|---|---|---|---|---|---|---|---|
| 1.509 | -0.008 | 1.278 | 0.134 | 1.332 | -0.104 | 1.189 | -0.010 | 1.597 | 0.046 | 1.195 | -0.037 |
| 1.126 | -0.025 | 1.263 | 0.182 | 1.249 | 0.090 | 1.251 | 0.712 | 1.320 | -0.061 | 1.181 | -0.020 |
| 1.278 | 0.243 | 1.312 | -0.386 | 1.151 | 0.020 | 1.352 | -0.372 | 1.366 | -0.372 | 1.403 | -0.593 |
| 1.221 | 0.053 | 1.244 | 0.498 | 1.346 | -0.223 | 1.467 | -0.106 | 1.430 | -0.046 | 1.445 | -0.052 |
| 1.462 | -0.059 | 1.173 | -0.038 | 1.523 | 0.001 | 1.538 | 0.031 | 1.274 | 0.184 | 1.395 | -0.197 |
| 1.483 | -0.017 | 1.511 | -0.032 | 1.477 | -0.052 | 1.497 | -0.021 | 1.538 | 0.093 | 1.510 | -0.083 |
| 1.191 | -0.010 | 1.323 | 0.102 | 1.565 | -0.003 | 1.589 | 0.058 | 1.168 | 0.075 | 1.295 | 0.173 |
| 1.436 | -0.247 | 1.208 | 0.002 | 1.521 | 0.023 | 1.543 | 0.028 | 1.164 | 0.060 | 1.446 | -0.072 |
| 1.457 | -0.126 | 1.514 | 0.047 | 1.302 | 0.109 | 1.461 | -0.114 | 1.535 | -0.050 | 1.553 | 0.026 |
| 1.161 | -0.013 | 1.325 | -0.136 | 1.507 | -0.026 | 1.528 | -0.067 | 1.542 | 0.013 | 1.528 | 0.046 |
| 1.592 | 0.000 | 1.510 | -0.033 | 1.539 | 0.064 | 1.537 | 0.013 | 1.547 | 0.022 | 1.557 | 0.036 |
| 1.147 | -0.022 | 1.523 | 0.080 | 1.536 | -0.009 | 1.556 | 0.047 | 1.162 | -0.016 | 1.180 | 0.054 |
| 1.468 | -0.021 | 1.483 | -0.056 | 1.540 | -0.010 | 1.569 | 0.020 | 1.487 | -0.055 | 1.508 | -0.069 |
| 1.555 | -0.039 | 1.655 | 0.054 | 1.093 | -0.031 | 1.249 | 0.150 | 1.487 | 0.045 | 1.509 | -0.015 |
| 1.509 | -0.014 | 1.522 | 0.046 | 1.562 | 0.006 | 1.596 | 0.009 | 1.488 | -0.029 | 1.561 | 0.038 |
| 1.590 | 0.029 | | | | | | | | | | |

## TABLE E.20

RADIAL VELOCITY - DIGITIZER METHOD, Q=0.040 $cm^3$/sec
0.20 cm I.D. CAPILLARY TUBE, SMALL RESERVOIR

(Z/D) = 5.00 (℄ = 1.327 cm)

| r' (cm) | $V_r$ (cm/sec) | r' (cm) | $V_r$ (cm/sec) | r' (cm) | $V_r$ (cm/sec) | r' (cm) | $V_r$ (cm/sec) | r' (cm) | $V_r$ (cm/sec) | r' (cm) | $V_r$ (cm/sec) |
|---|---|---|---|---|---|---|---|---|---|---|---|
| 1.107 | 0.042 | 1.433 | 0.003 | 0.997 | 0.034 | 1.590 | -0.031 | 1.410 | -0.014 | 1.573 | -0.038 |
| 1.598 | -0.063 | 1.057 | 0.030 | 1.358 | -0.019 | 1.471 | -0.026 | 1.523 | -0.031 | 1.297 | -0.006 |
| 1.342 | -0.017 | 1.395 | -0.040 | 1.153 | 0.024 | 1.306 | 0.011 | 1.346 | -0.012 | 1.404 | -0.014 |
| 1.479 | -0.023 | 1.618 | -0.036 | 1.113 | 0.034 | 1.256 | 0.015 | 1.350 | 0.018 | 1.365 | -0.017 |
| 1.380 | -0.023 | 1.394 | -0.008 | 1.655 | -0.056 | 1.096 | 0.045 | 1.294 | -0.013 | 1.395 | -0.024 |
| 1.294 | 0.032 | 1.350 | 0.000 | 1.441 | -0.034 | 1.045 | 0.022 | 1.253 | -0.008 | 1.546 | -0.053 |
| 1.278 | 0.014 | 1.480 | -0.025 | 1.519 | -0.037 | 1.583 | -0.058 | 1.091 | 0.030 | 1.244 | 0.007 |
| 1.310 | 0.001 | 1.323 | -0.006 | 1.362 | -0.016 | 1.429 | -0.026 | 1.452 | -0.055 | 1.211 | 0.020 |
| 1.261 | 0.005 | 1.226 | 0.030 | 1.735 | -0.036 | 1.411 | 0.003 | 1.531 | -0.021 | 1.662 | -0.027 |
| 1.174 | 0.025 | 1.398 | -0.016 | 1.640 | -0.043 | 1.372 | 0.005 | 1.396 | -0.013 | 1.426 | -0.004 |
| 1.552 | -0.053 | 1.563 | -0.083 | 1.261 | 0.024 | 1.326 | 0.026 | 1.444 | -0.003 | | |

(Z/D) = 3.33 (℄ = 1.327 cm)

| r' (cm) | $V_r$ (cm/sec) | r' (cm) | $V_r$ (cm/sec) | r' (cm) | $V_r$ (cm/sec) | r' (cm) | $V_r$ (cm/sec) | r' (cm) | $V_r$ (cm/sec) | r' (cm) | $V_r$ (cm/sec) |
|---|---|---|---|---|---|---|---|---|---|---|---|
| 1.420 | -0.008 | 1.436 | -0.027 | 1.531 | -0.063 | 1.231 | 0.081 | 1.286 | 0.008 | 1.357 | -0.025 |
| 1.390 | -0.016 | 1.496 | -0.053 | 1.510 | -0.049 | 1.131 | 0.054 | 1.386 | -0.028 | 1.533 | -0.037 |
| 1.549 | -0.014 | 1.182 | 0.030 | 1.437 | -0.075 | 1.453 | -0.085 | 1.094 | 0.063 | 1.412 | -0.057 |
| 1.379 | -0.030 | 1.420 | -0.047 | 1.192 | 0.046 | 1.288 | 0.046 | 1.380 | -0.043 | 1.484 | -0.035 |
| 1.640 | -0.047 | 1.164 | 0.027 | 1.289 | -0.005 | 1.495 | -0.083 | 1.514 | -0.072 | 1.625 | -0.046 |
| 1.137 | 0.084 | 1.277 | 0.054 | 1.376 | -0.111 | 1.582 | -0.064 | 1.602 | -0.050 | 1.208 | 0.012 |
| 1.286 | 0.019 | 1.305 | 0.016 | 1.431 | -0.024 | 1.534 | -0.083 | 1.320 | -0.011 | 1.332 | -0.019 |
| 1.405 | -0.045 | 1.542 | -0.056 | 1.240 | 0.043 | 1.259 | 0.047 | 1.272 | 0.058 | 1.288 | 0.018 |
| 1.491 | -0.065 | 1.538 | -0.057 | 1.195 | 0.063 | 1.357 | 0.000 | 1.476 | -0.020 | 1.561 | -0.038 |
| 1.389 | -0.009 | 1.400 | -0.024 | 1.416 | -0.020 | 1.563 | -0.060 | 1.125 | 0.022 | 1.336 | -0.010 |

TABLE E.20 (continued)

(Z/D) = 3.33 ( ℄ = 1.327 cm)

| r' (cm) | $V_r$ (cm/sec) | r' (cm) | $V_r$ (cm/sec) | r' (cm) | $V_r$ (cm/sec) | r' (cm) | $V_r$ (cm/sec) | r' (cm) | $V_r$ (cm/sec) | r' (cm) | $V_r$ (cm/sec) |
|---|---|---|---|---|---|---|---|---|---|---|---|
| 1.411 | -0.065 | 1.526 | -0.070 | 1.194 | 0.066 | 1.327 | 0.019 | 1.384 | -0.019 | 1.411 | -0.011 |
| 1.498 | -0.104 | 1.591 | -0.049 | 1.114 | 0.064 | 1.301 | 0.031 | 1.343 | 0.009 | 1.421 | -0.047 |
| 1.448 | -0.037 | 1.316 | -0.004 | 1.376 | -0.031 | 1.404 | -0.038 | 1.561 | -0.045 | | |

(Z/D) = 1.67 ( ℄ = 1.327 cm)

| r' (cm) | $V_r$ (cm/sec) | r' (cm) | $V_r$ (cm/sec) | r' (cm) | $V_r$ (cm/sec) | r' (cm) | $V_r$ (cm/sec) | r' (cm) | $V_r$ (cm/sec) | r' (cm) | $V_r$ (cm/sec) |
|---|---|---|---|---|---|---|---|---|---|---|---|
| 1.206 | 0.024 | 1.431 | -0.086 | 1.448 | -0.069 | 1.483 | -0.136 | 1.264 | 0.070 | 1.506 | -0.080 |
| 1.301 | 0.004 | 1.440 | -0.140 | 1.461 | -0.105 | 1.351 | -0.021 | 1.198 | 0.057 | 1.378 | -0.037 |
| 1.443 | -0.116 | 1.474 | -0.045 | 1.543 | -0.024 | 1.229 | 0.091 | 1.273 | 0.065 | 1.359 | -0.022 |
| 1.387 | -0.038 | 1.401 | -0.095 | 1.416 | -0.065 | 1.282 | 0.022 | 1.415 | -0.108 | 1.371 | -0.074 |
| 1.250 | 0.083 | 1.266 | 0.090 | 1.369 | -0.060 | 1.405 | -0.080 | 1.267 | 0.058 | 1.312 | 0.043 |
| 1.370 | -0.005 | 1.384 | -0.059 | 1.399 | -0.056 | 1.447 | -0.105 | 1.559 | -0.030 | 1.324 | 0.038 |
| 1.443 | -0.042 | 1.485 | -0.154 | 1.205 | 0.017 | 1.357 | -0.029 | 1.507 | -0.034 | 1.522 | -0.004 |
| 1.223 | 0.062 | 1.162 | 0.001 | 1.177 | 0.002 | 1.255 | 0.051 | 1.300 | 0.087 | 1.318 | 0.065 |
| 1.422 | 0.000 | 1.190 | -0.005 | 1.346 | -0.014 | 1.354 | -0.060 | 1.470 | -0.088 | 1.274 | 0.077 |
| 1.297 | 0.071 | 1.440 | -0.065 | 1.477 | -0.113 | 1.143 | 0.032 | 1.249 | 0.053 | 1.379 | -0.098 |
| 1.454 | -0.069 | 1.134 | 0.002 | 1.255 | 0.033 | 1.340 | 0.019 | 1.381 | -0.025 | 1.398 | -0.039 |
| 1.447 | -0.097 | 1.147 | 0.028 | 1.222 | 0.060 | 1.319 | 0.057 | 1.351 | 0.022 | 1.507 | -0.012 |

## TABLE E.21

## RADIAL AND AXIAL VELOCITIES - DIGITIZER METHOD, Q=0.159 $cm^3/sec$
0.20 cm I.D. CAPILLARY TUBE, SMALL RESERVOIR

(Z/D) = 9.86 (℄ =1.327 cm)

| r'(cm) | $V_r$ (cm/sec) | $V_z$ (cm/sec) | r'(cm) | $V_r$ (cm/sec) | $V_z$ (cm/sec) | r'(cm) | $V_r$ (cm/sec) | $V_z$ (cm/sec) | r'(cm) | $V_r$ (cm/sec) | $V_z$ (cm/sec) |
|---|---|---|---|---|---|---|---|---|---|---|---|
| 1.415 | 0.040 | 0.652 | 0.758 | 0.050 | 0.100 | 1.126 | 0.102 | 0.444 | 0.811 | 0.068 | 0.129 |
| 1.305 | 0.040 | 0.659 | 0.938 | 0.058 | 0.257 | 1.597 | -0.114 | 0.532 | 1.061 | 0.125 | 0.475 |
| 1.709 | -0.121 | 0.369 | 1.228 | 0.061 | 0.667 | 1.783 | -0.150 | 0.265 | 1.409 | -0.072 | 0.587 |
| 1.505 | -0.121 | 0.509 | 1.586 | -0.147 | 0.456 | 1.657 | -0.138 | 0.375 | 1.148 | 0.137 | 0.607 |
| 1.482 | -0.118 | 0.558 | 1.165 | 0.061 | 0.604 | 1.737 | -0.113 | 0.290 | 1.290 | 0.026 | 0.670 |
| 1.570 | -0.098 | 0.533 | 1.347 | -0.005 | 0.589 | 1.579 | -0.115 | 0.590 | 1.725 | -0.080 | 0.283 |
| 0.959 | 0.077 | 0.232 | 0.747 | 0.059 | 0.076 | 1.704 | -0.106 | 0.304 | 1.122 | 0.080 | 0.448 |
| 1.018 | 0.049 | 0.391 | 1.186 | 0.111 | 0.610 | 1.248 | -0.040 | 0.547 | 1.384 | -0.012 | 0.662 |
| 1.644 | -0.155 | 0.359 | 1.414 | -0.019 | 0.668 | 1.196 | 0.093 | 0.611 | 1.487 | -0.050 | 0.516 |
| 1.364 | -0.008 | 0.617 | 1.498 | -0.142 | 0.591 | 1.558 | -0.115 | 0.534 | 0.883 | 0.079 | 0.147 |
| 1.668 | -0.068 | 0.376 | 1.052 | 0.100 | 0.301 | 1.232 | 0.109 | 0.530 | 1.392 | -0.026 | 0.710 |
| 1.434 | -0.034 | 0.568 | 1.434 | -0.060 | 0.732 | 1.442 | -0.061 | 0.707 | 1.778 | -0.138 | 0.239 |
| 0.923 | 0.049 | 0.159 | 1.160 | 0.102 | 0.486 | 0.930 | 0.070 | 1.191 | 1.179 | 0.116 | 0.553 |
| 1.221 | 0.030 | 0.512 | 1.309 | 0.068 | 0.724 | 1.752 | -0.125 | 0.266 | 1.495 | -0.077 | 0.651 |
| 1.500 | -0.059 | 0.551 | 1.597 | -0.103 | 0.450 | 1.187 | 0.101 | 0.509 | 1.390 | -0.025 | 0.623 |
| 1.294 | 0.047 | 0.669 | 1.413 | -0.034 | 0.710 | 1.435 | -0.093 | 0.628 | 1.453 | -0.051 | 0.615 |
| 1.495 | -0.094 | 0.693 | 1.502 | -0.057 | 0.532 | 1.676 | -0.094 | 0.453 | 1.781 | -0.108 | 0.209 |
| 1.839 | -0.127 | 0.207 | 1.040 | 0.134 | 0.463 | 0.675 | 0.046 | 0.031 | 1.198 | 0.117 | 0.540 |
| 1.037 | 0.111 | 0.410 | 1.256 | 0.100 | 0.662 | 1.143 | 0.093 | 0.571 | 1.054 | 0.064 | 0.268 |
| 1.358 | -0.005 | 0.741 | 1.248 | 0.073 | 0.601 | 1.367 | -0.012 | 0.656 | 1.415 | -0.031 | 0.734 |
| 1.713 | -0.082 | 0.227 | 1.465 | -0.052 | 0.700 | 1.001 | 0.094 | 0.327 | 1.621 | -0.125 | 0.575 |
| 1.691 | -0.090 | 0.329 | | | | | | | | | |

TABLE E.21 (continued)

(Z/D) = 6.57 ($\xi$ = 1.327 cm)

| r'(cm) | $V_r$(cm/sec) | $V_z$(cm/sec) | r'(cm) | $V_r$(cm/sec) | $V_z$(cm/sec) | r'(cm) | $V_r$(cm/sec) | $V_z$(cm/sec) | r'(cm) | $V_r$(cm/sec) | $V_z$(cm/sec) |
|---|---|---|---|---|---|---|---|---|---|---|---|
| 0.997 | 0.018 | 0.177 | 1.274 | 0.022 | 1.937 | 1.320 | 0.082 | 1.873 | 1.297 | 0.025 | 2.282 |
| 1.539 | -0.113 | 1.212 | 1.389 | -0.161 | 1.795 | 1.812 | -0.062 | 0.184 | 1.515 | -0.180 | 0.898 |
| 1.626 | -0.189 | 0.642 | 1.576 | -0.064 | 0.584 | 1.644 | -0.133 | 0.627 | 1.590 | -0.065 | 0.515 |
| 1.662 | -0.100 | 0.471 | 1.800 | -0.031 | 0.108 | 1.169 | 0.027 | 0.703 | 1.342 | -0.046 | 1.822 |
| 1.186 | 0.119 | 1.102 | 1.380 | -0.026 | 1.705 | 1.262 | 0.090 | 1.739 | 1.426 | -0.084 | 1.562 |
| 1.340 | -0.036 | 2.058 | 1.455 | -0.229 | 1.502 | 1.365 | -0.034 | 1.924 | 1.499 | -0.099 | 1.046 |
| 1.384 | -0.073 | 1.720 | 1.559 | -0.130 | 0.647 | 1.413 | -0.089 | 1.594 | 1.742 | -0.053 | 0.148 |
| 1.439 | -0.197 | 1.621 | 1.183 | 0.041 | 0.878 | 1.554 | -0.231 | 0.849 | 1.261 | 0.145 | 1.493 |
| 1.722 | -0.018 | 0.203 | 1.289 | 0.097 | 1.671 | 0.995 | 0.021 | 0.182 | 1.624 | -0.026 | 0.604 |
| 1.426 | -0.023 | 1.591 | 1.659 | -0.078 | 0.502 | 1.668 | -0.106 | 0.477 | 1.074 | 0.065 | 0.484 |
| 1.701 | -0.061 | 0.399 | 1.152 | 0.110 | 0.911 | 1.062 | 0.054 | 0.413 | 1.213 | 0.247 | 1.251 |
| 1.208 | 0.048 | 1.154 | 1.264 | 0.057 | 1.499 | 1.361 | 0.085 | 2.040 | 1.383 | -0.108 | 1.541 |
| 1.387 | 0.000 | 1.551 | 1.414 | -0.058 | 1.652 | 1.400 | -0.137 | 1.897 | 1.591 | -0.084 | 0.640 |
| 1.478 | -0.148 | 1.235 | 1.643 | -0.112 | 0.475 | 1.048 | 0.023 | 0.433 | 1.161 | 0.087 | 0.603 |
| 1.092 | 0.051 | 0.616 | 1.327 | 0.076 | 1.841 | 1.107 | 0.082 | 0.599 | 1.414 | -0.069 | 1.737 |
| 1.237 | 0.109 | 1.355 | 1.446 | -0.038 | 1.664 | 1.379 | -0.105 | 1.801 | 1.563 | -0.278 | 1.063 |
| 1.488 | -0.090 | 0.944 | 1.577 | -0.107 | 0.928 | 1.611 | -0.094 | 0.548 | 1.810 | -0.037 | 0.179 |
| 1.075 | 0.066 | 0.427 | 0.885 | 0.008 | 0.138 | 1.247 | 0.026 | 1.568 | 1.573 | -0.175 | 0.862 |
| 1.281 | 0.032 | 1.936 | 1.648 | -0.103 | 0.456 | 1.476 | -0.211 | 0.889 | 1.663 | -0.044 | 0.435 |
| 1.532 | -0.099 | 0.676 | 1.502 | -0.186 | 1.241 | 1.561 | -0.110 | 0.589 | 1.138 | 0.126 | 0.965 |
| 1.882 | 0.010 | 0.100 | 1.509 | -0.137 | 1.017 | 1.199 | 0.072 | 1.370 | 1.540 | -0.165 | 0.772 |
| 1.228 | 0.108 | 1.602 | 1.549 | -0.103 | 0.830 | 1.299 | 0.056 | 1.832 | 1.587 | -0.091 | 0.503 |
| 1.426 | -0.150 | 1.768 | 1.741 | -0.024 | 0.172 | 1.518 | -0.147 | 1.069 | 0.903 | -0.001 | 0.114 |
| 1.169 | 0.097 | 1.023 | 0.965 | 0.008 | 0.214 | 1.207 | 0.058 | 1.307 | 1.087 | 0.067 | 0.476 |
| 1.236 | 0.134 | 1.593 | 1.124 | 0.075 | 0.702 | 1.365 | -0.075 | 1.880 | 1.259 | 0.079 | 1.829 |
| 1.420 | -0.070 | 1.852 | 1.286 | 0.091 | 1.990 | 1.549 | -0.161 | 0.934 | 1.365 | -0.046 | 2.006 |
| 1.674 | -0.051 | 0.300 | 1.380 | -0.067 | 2.042 | 1.698 | -0.071 | 0.273 | 1.467 | -0.114 | 1.522 |
| 1.067 | 0.059 | 0.324 | 1.635 | -0.093 | 0.537 | 1.175 | 0.102 | 0.680 | 0.908 | 0.015 | 0.097 |
| 1.195 | 0.082 | 0.839 | 1.529 | -0.170 | 1.281 | 1.384 | -0.029 | 1.784 | 1.566 | -0.116 | 0.939 |
| 0.930 | 0.021 | 0.126 | 1.619 | -0.106 | 0.612 | 1.110 | 0.054 | 0.342 | 1.766 | -0.071 | 0.221 |
| 1.337 | 0.096 | 2.142 | 1.093 | 0.087 | 0.507 | 1.659 | -0.066 | 0.511 | 1.218 | 0.109 | 1.331 |

TABLE E.21 (continued)

(Z/D) = 3.29 (℄ = 1.327 cm)

| r'(cm) | $V_r$(cm/sec) | $V_z$(cm/sec) | r'(cm) | $V_r$(cm/sec) | $V_z$(cm/sec) | r'(cm) | $V_r$(cm/sec) | $V_z$(cm/sec) | r'(cm) | $V_r$(cm/sec) | $V_z$(cm/sec) |
|---|---|---|---|---|---|---|---|---|---|---|---|
| 1.219 | 0.002 | 1.186 | 1.282 | 0.108 | 2.909 | 1.340 | 0.169 | 3.946 | 1.373 | -0.082 | 3.633 |
| 1.297 | 0.169 | 3.024 | 1.390 | -0.143 | 3.429 | 1.503 | -0.034 | 1.831 | 1.406 | -0.217 | 3.444 |
| 1.587 | -0.006 | 0.532 | 1.449 | -0.172 | 2.833 | 1.359 | -0.016 | 4.093 | 1.569 | -0.051 | 0.492 |
| 1.486 | -0.118 | 1.297 | 1.121 | -0.042 | 0.251 | 1.148 | -0.010 | 0.384 | 1.308 | 0.112 | 2.800 |
| 1.228 | 0.114 | 1.419 | 1.398 | -0.056 | 3.812 | 1.304 | 0.159 | 3.288 | 1.532 | -0.010 | 1.332 |
| 1.538 | -0.020 | 0.897 | 1.607 | -0.153 | 0.517 | 1.551 | -0.109 | 0.786 | 1.674 | 0.039 | 0.230 |
| 1.646 | 0.029 | 0.237 | 1.201 | 0.075 | 0.899 | 1.105 | -0.020 | 0.312 | 1.506 | -0.214 | 1.827 |
| 1.242 | 0.011 | 2.640 | 1.565 | -0.054 | 0.864 | 1.431 | -0.237 | 2.691 | 1.418 | -0.155 | 2.263 |
| 1.094 | -0.047 | 0.285 | 1.106 | 0.043 | 0.664 | 1.307 | 0.082 | 3.750 | 1.250 | 0.047 | 3.176 |
| 1.359 | -0.126 | 3.766 | 1.305 | -0.124 | 4.107 | 1.408 | -0.336 | 3.306 | 1.391 | -0.199 | 3.383 |
| 1.484 | -0.166 | 1.263 | 1.450 | -0.192 | 1.962 | 1.540 | -0.038 | 0.568 | 1.510 | -0.052 | 0.771 |
| 1.190 | 0.136 | 1.598 | 1.174 | 0.004 | 0.919 | 1.522 | -0.045 | 0.588 | 1.109 | 0.029 | 0.437 |
| 1.321 | -0.014 | 3.882 | 1.206 | 0.106 | 2.420 | 1.337 | -0.078 | 3.840 | 1.491 | -0.095 | 1.070 |
| 1.388 | -0.260 | 3.243 | 1.579 | 0.020 | 0.311 | 1.131 | -0.021 | 0.268 | 1.623 | 0.029 | 0.188 |
| 1.422 | -0.175 | 3.476 | 1.659 | 0.085 | 0.191 | 1.478 | -0.227 | 2.269 | 1.550 | -0.087 | 1.042 |
| 1.525 | -0.150 | 1.312 | 1.592 | -0.037 | 0.049 | 1.558 | -0.193 | 0.901 | 1.178 | 0.005 | 0.529 |
| 1.585 | -0.063 | 0.596 | 1.310 | 0.053 | 3.111 | 1.094 | -0.058 | 0.245 | 1.589 | -0.057 | 0.489 |
| 1.204 | 0.012 | 1.336 | 1.218 | 0.109 | 1.400 | 1.484 | -0.064 | 1.049 | 1.557 | -0.005 | 0.553 |
| 1.138 | 0.003 | 0.561 | 1.598 | -0.012 | 0.290 |  |  |  |  |  |  |

## TABLE E.22

### RADIAL VELOCITIES - DIGITIZER METHOD, Q=0.238 cm$^3$/sec
### 0.20 cm I.D. CAPILLARY TUBE, SMALL RESERVOIR

(Z/D) = 7.27          ( ℄ = 1.327 cm)

| r'(cm) | $V_r$(cm/sec) | r'(cm) | $V_r$(cm/sec) | r'(cm) | $V_r$(cm/sec) | r'(cm) | $V_r$(cm/sec) | r'(cm) | $V_r$(cm/sed) | r'(cm) | $V_r$(cm/sec) |
|---|---|---|---|---|---|---|---|---|---|---|---|
| 0.910 | 0.038 | 1.476 | -0.273 | 1.566 | -0.179 | 1.631 | -0.077 | 1.659 | -0.175 | 1.828 | -0.059 |
| 1.846 | 0.004 | 0.955 | 0.037 | 1.089 | 0.105 | 1.125 | 0.097 | 1.168 | 0.140 | 1.205 | 0.141 |
| 1.228 | 0.132 | 1.706 | -0.058 | 1.857 | 0.036 | 1.225 | 0.105 | 1.260 | 0.140 | 1.355 | -0.078 |
| 1.388 | -0.038 | 1.488 | -0.199 | 1.499 | -0.213 | 1.577 | -0.191 | 0.941 | 0.030 | 1.127 | 0.123 |
| 1.268 | 0.110 | 1.459 | -0.063 | 1.592 | -0.251 | 1.697 | -0.120 | 1.713 | -0.125 | 1.230 | 0.199 |
| 1.258 | 0.048 | 1.382 | -0.102 | 1.577 | -0.259 | 1.588 | -0.147 | 1.652 | -0.112 | 1.119 | 0.112 |
| 1.163 | 0.050 | 1.184 | 0.123 | 1.266 | 0.146 | 1.308 | 0.156 | 1.361 | -0.085 | 1.410 | -0.090 |
| 1.423 | -0.014 | 1.517 | -0.242 | 1.625 | -0.115 | 1.650 | -0.136 | 1.687 | -0.081 | 1.793 | -0.070 |
| 1.128 | 0.042 | 1.194 | 0.105 | 1.335 | -0.056 | 1.377 | -0.094 | 1.597 | -0.176 | 1.606 | -0.229 |
| 1.623 | -0.112 | 1.702 | -0.056 | 1.751 | -0.061 | 1.115 | 0.105 | 1.204 | 0.118 | 1.527 | -0.176 |
| 1.655 | -0.089 | 1.669 | -0.132 | 1.054 | 0.021 | 1.023 | 0.044 | 1.085 | 0.107 | 1.150 | 0.143 |
| 1.235 | 0.086 | 1.246 | 0.243 | 1.308 | 0.056 | 1.323 | 0.075 | 1.350 | -0.082 | 1.356 | -0.026 |
| 1.383 | -0.024 | 1.626 | -0.104 | 1.166 | 0.099 | 1.213 | 0.102 | 1.400 | -0.146 | 1.567 | -0.135 |
| 1.041 | 0.012 | 1.134 | 0.124 | 1.356 | 0.002 | 1.467 | -0.100 | 1.571 | -0.089 | 1.620 | -0.248 |
| 1.634 | -0.212 | 1.251 | 0.118 | 1.348 | -0.023 | 1.516 | -0.218 | 1.172 | 0.062 | 1.270 | 0.174 |
| 1.357 | 0.004 | 1.607 | -0.224 | 1.799 | -0.108 | 1.084 | 0.060 | 1.102 | 0.052 | 1.138 | 0.065 |
| 1.155 | 0.127 | 1.253 | 0.129 | 1.382 | -0.068 | 1.568 | -0.187 | 1.681 | -0.099 | 1.139 | 0.088 |
| 1.362 | -0.074 | 1.380 | -0.097 | 1.396 | -0.046 | 1.478 | -0.251 | 1.578 | -0.131 | 1.661 | -0.125 |
| 1.720 | -0.073 | 1.630 | -0.078 | 1.669 | -0.090 | 1.714 | -0.071 | 1.438 | -0.149 | 1.505 | -0.140 |
| 1.660 | -0.126 | 1.719 | -0.029 | 1.749 | -0.043 | 1.811 | -0.037 | 0.797 | 0.009 | 1.044 | 0.051 |
| 1.141 | 0.069 | 1.505 | -0.140 | 1.776 | -0.078 | 1.050 | 0.065 | 1.080 | 0.067 | 1.139 | 0.098 |
| 1.517 | -0.192 | 1.532 | -0.128 | 1.566 | -0.111 | 1.602 | -0.107 | 1.712 | -0.072 | 1.784 | -0.050 |
| 0.938 | 0.020 | 1.166 | 0.102 | 1.436 | -0.134 | 1.594 | -0.161 | 1.672 | -0.127 | 1.783 | -0.076 |
| 1.085 | 0.067 | 1.199 | 0.117 | 1.307 | 0.022 | 1.397 | -0.094 | 1.640 | -0.110 | 1.779 | -0.051 |

TABLE B.22 (continued)

(Z/D) = 3.62 (℄ = 1.327 cm)

| r' (cm) | $V_r$ (cm/sec) | r' (cm) | $V_r$ (cm/sec) | r' (cm) | $V_r$ (cm/sec) | r' (cm) | $V_r$ (cm/sec) | r' (cm) | $V_r$ (cm/sec) | r' (cm) | $V_r$ (cm/sec) |
|---|---|---|---|---|---|---|---|---|---|---|---|
| 1.430 | -0.195 | 1.489 | -0.191 | 1.549 | -0.136 | 1.576 | -0.090 | 1.083 | -0.041 | 1.194 | 0.117 |
| 1.211 | 0.083 | 1.222 | 0.098 | 1.563 | -0.175 | 1.577 | -0.030 | 0.864 | 0.017 | 1.119 | 0.063 |
| 1.144 | 0.110 | 1.329 | -0.037 | 1.404 | -0.282 | 1.414 | -0.167 | 1.689 | 0.111 | 1.776 | -0.056 |
| 1.282 | 0.064 | 1.345 | -0.071 | 1.391 | -0.114 | 1.434 | -0.283 | 1.503 | -0.171 | 1.285 | 0.167 |
| 1.513 | -0.133 | 1.622 | 0.025 | 1.514 | -0.039 | 1.584 | -0.009 | 1.595 | -0.036 | 1.125 | -0.003 |
| 1.266 | 0.230 | 1.396 | -0.113 | 1.573 | -0.080 | 1.606 | -0.003 | 1.076 | -0.005 | 1.180 | 0.040 |
| 1.207 | 0.092 | 1.339 | -0.084 | 1.408 | -0.234 | 1.521 | -0.118 | 1.546 | -0.070 | 1.627 | 0.040 |
| 1.219 | 0.133 | 1.456 | -0.234 | 1.495 | -0.255 | 1.500 | -0.209 | 1.562 | -0.074 | 1.577 | -0.038 |
| 1.592 | -0.018 | 1.079 | -0.038 | 1.136 | 0.041 | 1.190 | 0.043 | 1.222 | 0.041 | 1.261 | 0.151 |
| 1.341 | -0.065 | 1.378 | -0.116 | 1.470 | -0.229 | 1.546 | -0.067 | 1.180 | 0.060 | 1.245 | 0.180 |
| 1.379 | -0.150 | 1.388 | -0.149 | 1.435 | -0.309 | 1.558 | -0.017 | 1.306 | 0.122 | 1.356 | -0.068 |
| 1.435 | -0.191 | 1.457 | -0.210 | 1.544 | -0.141 | 1.567 | -0.124 | 1.625 | 0.015 | 1.212 | -0.010 |
| 1.269 | 0.132 | 1.384 | -0.280 | 1.435 | -0.281 | 1.448 | -0.230 | 1.132 | -0.012 | 1.149 | 0.054 |
| 1.186 | 0.036 | 1.431 | -0.179 | 1.095 | 0.045 | 1.436 | -0.272 | 1.567 | -0.044 | 1.581 | -0.013 |
| 1.206 | 0.104 | 0.925 | -0.095 | 0.989 | -0.060 | 1.053 | -0.007 | 1.078 | 0.002 | 1.163 | 0.050 |
| 1.189 | 0.132 | 1.506 | -0.126 | 1.545 | -0.051 | 1.131 | -0.044 | 1.219 | 0.159 | 1.491 | -0.164 |
| 1.527 | -0.073 | 1.566 | 0.012 | 1.660 | 0.039 | 1.596 | -0.012 | 1.645 | -0.002 | 1.746 | 0.063 |
| 1.136 | -0.017 | 1.240 | 0.179 | 1.560 | -0.105 | 1.544 | -0.087 | | | | |

## TABLE E.23

### RADIAL VELOCITIES - DIGITIZER METHOD, Q=0.318 cm$^3$/sec
### 0.20 cm I.D. CAPILLARY TUBE, SMALL RESERVOIR

(Z/D) = 7.97 ( ℄ = 1.327 cm)

| r' (cm) | $V_r$ (cm/sec) | r' (cm) | $V_r$ (cm/sec) | r' (cm) | $V_r$ (cm/sec) | r' (cm) | $V_r$ (cm/sec) | r' (cm) | $V_r$ (cm/sec) | r' (cm) | $V_r$ (cm/sec) |
|---|---|---|---|---|---|---|---|---|---|---|---|
| 1.309 | 0.314 | 1.340 | -0.134 | 1.365 | -0.225 | 1.347 | 0.118 | 1.411 | -0.052 | 1.368 | 0.162 |
| 1.306 | -0.096 | 1.300 | -0.063 | 1.291 | 0.121 | 1.169 | 0.157 | 1.352 | -0.132 | 1.328 | -0.096 |
| 1.287 | -0.109 | 1.347 | 0.079 | 1.434 | -0.058 | 1.069 | 0.036 | 1.507 | -0.306 | 1.243 | 0.100 |
| 1.115 | 0.038 | 1.543 | 0.097 | 1.352 | -0.101 | 1.142 | 0.108 | 1.578 | -0.058 | 1.422 | -0.205 |
| 1.339 | -0.063 | 0.917 | -0.001 | 1.650 | -0.137 | 1.457 | -0.261 | 1.140 | 0.084 | 0.955 | 0.019 |
| 1.515 | -0.274 | 1.121 | 0.131 | 1.572 | -0.338 | 1.667 | -0.068 | 1.192 | 0.159 | 1.587 | -0.192 |
| 1.260 | 0.039 | 1.482 | -0.332 | 1.643 | -0.146 | 1.403 | -0.153 | 1.610 | -0.117 | 1.670 | -0.096 |
| 1.569 | -0.086 | 0.953 | 0.026 | 1.149 | 0.170 | 1.671 | -0.108 | 1.378 | -0.045 | 1.276 | 0.087 |
| 1.811 | -0.032 | 1.437 | -0.085 | 1.504 | -0.199 | 0.934 | 0.014 | 1.661 | -0.131 | 1.526 | -0.228 |
| 1.854 | -0.040 | 1.844 | -0.049 | 0.881 | 0.042 | 1.920 | -0.034 | 1.088 | 0.091 | 1.004 | 0.049 |
| 1.033 | 0.033 | 1.145 | 0.137 | 1.116 | 0.138 | 1.394 | 0.044 | 1.248 | 0.084 | 1.136 | 0.124 |
| 1.527 | -0.206 | 1.427 | -0.196 | 1.208 | 0.171 | 1.449 | -0.087 | 1.440 | -0.229 | 0.902 | 0.007 |
| 0.946 | 0.012 | 1.455 | -0.225 | 1.127 | -0.010 | 1.012 | 0.021 | 1.647 | -0.052 | 1.283 | -0.012 |
| 1.124 | 0.075 | 1.043 | 0.055 | 1.353 | -0.116 | 1.243 | 0.111 | 1.139 | 0.132 | 1.418 | -0.123 |
| 0.896 | 0.098 | 1.732 | -0.119 | 1.589 | -0.109 | 1.341 | -0.103 | 1.135 | 0.187 | 1.530 | -0.251 |
| 1.026 | 0.040 | 1.233 | 0.098 | 1.749 | -0.101 | 1.127 | 1.120 | 1.254 | -0.068 | 0.875 | -0.005 |
| 1.173 | 0.149 | 1.397 | -0.199 | 0.921 | 0.035 | 1.356 | 0.036 | 1.572 | -0.140 | 1.683 | -0.102 |
| 1.518 | -0.256 | 1.613 | -0.120 | 1.215 | 0.217 | 1.595 | -0.199 | 1.031 | 0.070 | 1.514 | -0.241 |
| 1.659 | -0.107 | 1.270 | 0.085 | 1.662 | -0.207 | 1.060 | 0.077 | 1.444 | -0.265 | 0.819 | 0.014 |

(Z/D) = 3.99 ( ℄ = 1.327 cm)

| r' (cm) | $V_r$ (cm/sec) | r' (cm) | $V_r$ (cm/sec) | r' (cm) | $V_r$ (cm/sec) | r' (cm) | $V_r$ (cm/sec) | r' (cm) | $V_r$ (cm/sec) | r' (cm) | $V_r$ (cm/sec) |
|---|---|---|---|---|---|---|---|---|---|---|---|
| 1.166 | 0.357 | 1.765 | 0.013 | 1.491 | -0.177 | 1.405 | -0.142 | 1.843 | 0.066 | 1.519 | -0.080 |

TABLE E.23 (continued)

$(Z/D) = 3.99$ $(\xi = 1.327 \text{ cm})$

| r'(cm) | $V_r$ (cm/sec) | r'(cm) | $V_r$ (cm/sec) | r'(cm) | $V_r$ (cm/sec) | r'(cm) | $V_r$ (cm/sec) | r'(cm) | $V_r$ (cm/sec) | r'(cm) | $V_r$ (cm/sec) |
|---|---|---|---|---|---|---|---|---|---|---|---|
| 1.305 | 0.416 | 1.013 | -0.051 | 1.632 | -0.007 | 1.337 | 0.053 | 1.165 | 0.087 | 1.180 | 0.114 |
| 1.155 | -0.214 | 1.499 | -0.166 | 1.237 | 0.171 | 1.301 | 0.097 | 1.502 | -0.124 | 1.620 | -0.028 |
| 1.312 | 0.046 | 1.533 | -0.098 | 1.196 | 0.221 | 1.300 | 0.277 | 1.591 | -0.013 | 1.333 | -0.274 |
| 1.374 | -0.305 | 1.517 | -0.297 | 1.475 | 0.003 | 1.398 | -0.103 | 1.585 | -0.58 | 1.286 | -0.136 |
| 1.159 | 0.331 | 1.629 | -0.030 | 1.561 | -0.124 | 1.309 | -0.263 | 1.651 | -0.061 | 1.170 | -0.038 |
| 1.359 | -0.208 | 1.039 | -0.029 | 1.519 | -0.161 | 1.274 | -0.347 | 1.177 | 0.200 | 1.585 | 0.017 |
| 1.294 | 0.035 | 1.462 | -0.138 | 1.099 | -0.022 | 1.319 | -0.151 | 1.077 | 0.039 | 1.160 | 0.091 |
| 1.340 | -0.208 | 1.179 | 0.099 | 1.247 | 0.292 | 1.359 | 0.190 | 1.481 | -0.115 | 1.265 | -0.037 |
| 1.366 | -0.268 | 1.583 | 0.018 | 1.537 | -0.122 | 1.430 | 0.083 | 1.476 | -0.152 | 1.349 | -0.142 |
| 1.111 | 0.019 | 1.568 | 0.012 | 1.475 | -0.175 | 1.492 | -0.176 | 1.375 | -0.150 | 1.478 | 0.016 |
| 1.562 | -0.022 | 1.019 | -0.026 | 1.366 | -0.256 | 1.596 | -0.009 | 1.136 | 0.138 | 1.440 | -0.114 |
| 1.646 | -0.006 | 1.180 | 0.080 | 1.454 | -0.039 | 1.524 | -0.202 | 1.195 | 0.089 | 1.600 | -0.030 |
| 1.585 | -0.032 | 1.316 | 0.229 | 1.312 | -0.152 | 1.633 | -0.045 | 1.433 | -0.159 | 1.336 | -0.379 |
| 1.353 | -0.331 | 1.506 | -0.070 | 1.577 | -0.104 | 1.404 | -0.300 | 1.532 | -0.022 | 1.588 | -0.070 |
| 1.485 | -0.147 | 1.233 | 0.101 | 1.060 | -0.103 |  |  |  |  |  |  |

## TABLE E.24

### RADIAL VELOCITIES - DIGITZER METHOD, Q=0.040 $cm^3/sec$
### 0.30 cm I.D. CAPILLARY TUBE, SMALL RESERVOIR

(Z/D) = 2.19 ( ℄ = 1.327 cm)

| r'(cm) | $V_r$ (cm/sec) | r'(cm) | $V_r$ (cm/sec) | r'(cm) | $V_r$ (cm/sec) | r'(cm) | $V_r$ (cm/sec) | r'(cm) | $V_r$ (cm/sec) | r'(cm) | $V_r$ (cm/sec) |
|---|---|---|---|---|---|---|---|---|---|---|---|
| 1.489 | -0.040 | 1.567 | -0.025 | 1.346 | -0.005 | 1.577 | -0.045 | 1.034 | 0.022 | 1.445 | -0.013 |
| 1.661 | -0.031 | 1.145 | 0.032 | 1.282 | 0.020 | 1.386 | 0.002 | 1.535 | -0.029 | 1.228 | 0.029 |
| 1.479 | -0.011 | 1.613 | -0.032 | 1.163 | 0.027 | 1.241 | 0.000 | 1.638 | -0.034 | 1.680 | -0.025 |
| 1.365 | -0.040 | 1.047 | 0.033 | 1.431 | -0.020 | 1.229 | -0.019 | 1.254 | 0.003 | 1.349 | 0.001 |
| 1.394 | -0.018 | 1.278 | 0.008 | 1.705 | -0.030 | 1.472 | -0.035 | 1.346 | -0.013 | 1.407 | -0.009 |
| 1.209 | 0.000 | 1.280 | 0.011 | 1.217 | 0.012 | 1.346 | +0.008 | 1.294 | -0.006 | 1.489 | -0.026 |
| 1.445 | -0.021 | 1.556 | -0.030 | 1.661 | -0.020 | 1.246 | 0.006 | 0.908 | 0.018 | 1.241 | 0.000 |
| 1.250 | 0.020 | 1.270 | 0.013 | 1.365 | -0.026 | 1.304 | 0.015 | 1.302 | 0.005 | 1.229 | -0.013 |
| 1.496 | -0.037 | 1.365 | -0.006 | 1.472 | -0.023 | 1.575 | -0.036 | 1.407 | -0.011 | 1.209 | 0.000 |
| 1.241 | 0.032 | 1.632 | -0.025 | | | | | | | | |

(Z/D) = 1.46 ( ℄ = 1.327 cm)

| r'(cm) | $V_r$ (cm/sec) | r'(cm) | $V_r$ (cm/sec) | r'(cm) | $V_r$ (cm/sec) | r'(cm) | $V_r$ (cm/sec) | r'(cm) | $V_r$ (cm/sec) | r'(cm) | $V_r$ (cm/sec) |
|---|---|---|---|---|---|---|---|---|---|---|---|
| 1.364 | 0.028 | 0.954 | 0.017 | 1.225 | -0.031 | 1.405 | -0.017 | 1.224 | 0.030 | 1.293 | 0.000 |
| 1.420 | -0.015 | 1.546 | -0.046 | 1.420 | -0.047 | 1.520 | -0.037 | 1.255 | 0.051 | 1.608 | -0.016 |
| 1.193 | 0.036 | 1.405 | -0.033 | 1.405 | -0.011 | 1.533 | -0.052 | 1.481 | -0.078 | 1.420 | -0.010 |
| 1.251 | -0.007 | 1.275 | 0.077 | 1.520 | -0.024 | 1.333 | -0.027 | 1.535 | -0.060 | 1.193 | 0.023 |
| 1.427 | -0.054 | 1.261 | -0.031 | 1.533 | -0.034 | 0.957 | 0.023 | 1.274 | 0.015 | 1.251 | -0.005 |
| 1.017 | 0.059 | 1.484 | -0.058 | 0.957 | 0.015 | 1.232 | -0.005 | 1.549 | -0.058 | 1.017 | 0.038 |
| 1.344 | -0.050 | 1.561 | -0.052 | 1.126 | 0.035 | 1.140 | 0.049 | 1.136 | 0.011 | 1.232 | -0.003 |
| 1.319 | -0.004 | 1.269 | 0.027 | 1.140 | 0.031 | 1.435 | -0.047 | 1.285 | 0.028 | 1.319 | -0.003 |
| 1.512 | -0.055 | 1.352 | -0.051 | 1.435 | -0.030 | 1.216 | 0.003 | 1.402 | -0.048 | 1.216 | 0.002 |
| 1.342 | -0.032 | 1.307 | 0.000 | 1.342 | -0.021 | 1.348 | 0.006 | 1.365 | -0.004 | 1.348 | 0.004 |

TABLE E.24 (continued)

(Z/D) = 1.46 ($\xi$ = 1.327 cm)

| r'(cm) | $V_r$(cm/sec) | r'(cm) | $V_r$(cm/sec) | r'(cm) | $V_r$(cm/sec) | r'(cm) | $V_r$(cm/sec) | r'(cm) | $V_r$(cm/sec) | r'(cm) | $V_r$(cm/sec) |
|---|---|---|---|---|---|---|---|---|---|---|---|
| 1.412 | -0.069 | 1.380 | -0.008 | 1.412 | -0.044 | 1.481 | -0.060 | 1.352 | -0.001 | 1.481 | -0.039 |
| 1.282 | 0.020 | 1.359 | 0.010 | 1.519 | -0.032 | 1.319 | 0.021 | 1.544 | -0.035 | 1.590 | -0.013 |
| 1.398 | -0.011 | 1.567 | -0.044 | 1.402 | 0.025 | 1.377 | -0.013 | 1.109 | 0.017 | 1.537 | -0.047 |

(Z/D) = 0.73 ($\xi$ = 1.327 cm)

| r'(cm) | $V_r$(cm/sec) | r'(cm) | $V_r$(cm/sec) | r'(cm) | $V_r$(cm/sec) | r'(cm) | $V_r$(cm/sec) | r'(cm) | $V_r$(cm/sec) | r'(cm) | $V_r$(cm/sec) |
|---|---|---|---|---|---|---|---|---|---|---|---|
| 1.437 | -0.080 | 1.560 | -0.057 | 1.495 | -0.036 | 1.366 | -0.003 | 1.102 | 0.035 | 1.513 | -0.075 |
| 1.395 | -0.030 | 1.120 | 0.038 | 1.288 | -0.014 | 1.437 | -0.066 | 1.275 | 0.071 | 1.366 | -0.002 |
| 1.235 | 0.104 | 1.350 | -0.015 | 1.395 | -0.019 | 1.322 | 0.051 | 1.530 | -0.051 | 1.437 | -0.042 |
| 1.477 | -0.060 | 1.688 | -0.006 | 1.470 | -0.042 | 1.499 | -0.063 | 1.281 | 0.041 | 1.374 | -0.006 |
| 1.595 | -0.032 | 1.408 | -0.049 | 1.477 | -0.039 | 1.247 | 0.018 | 1.445 | -0.058 | 1.499 | -0.041 |
| 1.331 | -0.092 | 1.487 | -0.071 | 1.595 | -0.020 | 1.372 | -0.061 | 1.349 | 0.010 | 1.247 | 0.011 |
| 1.040 | -0.012 | 1.369 | 0.004 | 1.227 | 0.028 | 1.148 | 0.084 | 1.086 | 0.018 | 1.441 | -0.048 |
| 1.225 | -0.009 | 1.334 | -0.011 | 1.598 | -0.032 | 1.243 | 0.001 | 1.343 | -0.028 | 1.621 | -0.030 |
| 1.306 | -0.076 | 1.370 | -0.064 | 1.224 | 0.084 | 1.227 | 0.044 | 1.495 | -0.074 | 1.447 | -0.054 |
| 1.350 | -0.017 | 1.313 | 0.032 | 1.358 | -0.006 | 1.441 | -0.075 | 1.368 | -0.016 | 1.471 | -0.072 |
| 1.336 | 0.032 | 1.449 | -0.045 | 1.495 | -0.063 | 1.384 | 0.006 | 1.488 | -0.050 | 1.280 | 0.081 |
| 1.431 | -0.036 | 1.303 | 0.016 | 1.483 | -0.109 | 1.400 | -0.058 | | | | |

## TABLE E.25

### RADIAL AND AXIAL VELOCITIES - DIGITIZER METHOD, Q=0.159 $cm^3$/sec
### 0.30 cm I.D. CAPILLARY TUBE, SMALL RESERVOIR

(Z/D) = 4.38 ( ℄ = 1.327 cm)

| $r'$ (cm) | $V_r$ (cm/sec) | $V_z$ (cm/sec) | $r'$ (cm) | $V_r$ (cm/sec) | $V_z$ (cm/sec) | $r'$ (cm) | $V_r$ (cm/sec) | $V_z$ (cm/sec) | $r'$ (cm) | $V_r$ (cm/sec) | $V_z$ (cm/sec) |
|---|---|---|---|---|---|---|---|---|---|---|---|
| 1.004 | 0.070 | 0.221 | 1.292 | 0.002 | 0.389 | 1.314 | 0.038 | 0.419 | 1.332 | 0.010 | 0.386 |
| 1.388 | -0.003 | 0.462 | 1.351 | -0.009 | 0.413 | 1.598 | -0.077 | 0.365 | 0.973 | 0.088 | 0.209 |
| 1.617 | -0.051 | 0.332 | 1.130 | 0.089 | 0.318 | 1.743 | -0.067 | 0.189 | 1.376 | -0.039 | 0.433 |
| 1.252 | -0.007 | 0.493 | 1.414 | 0.005 | 0.444 | 1.401 | 0.004 | 0.432 | 1.616 | -0.096 | 0.324 |
| 1.460 | -0.039 | 0.395 | 1.833 | -0.076 | 0.141 | 1.773 | -0.068 | 0.153 | 1.101 | 0.079 | 0.275 |
| 1.906 | -0.058 | 0.074 | 1.319 | -0.002 | 0.401 | 1.412 | -0.032 | 0.421 | 1.409 | 0.000 | 0.430 |
| 1.499 | -0.040 | 0.385 | 1.423 | 0.009 | 0.418 | 1.633 | -0.081 | 0.304 | 1.442 | -0.017 | 0.436 |
| 0.858 | 0.078 | 0.118 | 1.683 | -0.093 | 0.297 | 1.403 | -0.014 | 0.372 | 1.378 | 0.027 | 0.461 |
| 1.685 | -0.097 | 0.261 | 1.444 | -0.021 | 0.433 | 1.017 | 0.082 | 0.230 | 1.478 | -0.024 | 0.389 |
| 1.127 | 0.076 | 0.337 | 1.575 | -0.066 | 0.393 | 1.321 | -0.019 | 0.435 | 0.875 | 0.059 | 0.144 |
| 1.327 | -0.010 | 0.464 | 1.325 | -0.009 | 0.382 | 1.334 | -0.017 | 0.431 | 1.784 | -0.072 | 0.129 |
| 1.390 | -0.034 | 0.387 | 0.930 | 0.054 | 0.266 | 1.401 | -0.067 | 0.415 | 1.273 | 0.016 | 0.421 |
| 1.491 | -0.102 | 0.368 | 1.295 | 0.010 | 0.483 | 0.996 | 0.060 | 0.246 | 1.579 | -0.076 | 0.292 |
| 1.302 | 0.030 | 0.460 | 1.718 | -0.067 | 0.174 | 1.337 | -0.046 | 0.455 | 0.892 | 0.089 | 0.135 |
| 1.356 | -0.050 | 0.398 | 0.910 | 0.072 | 0.163 | 1.553 | -0.074 | 0.333 | 1.351 | -0.016 | 0.395 |
| 0.743 | 0.060 | 0.081 | 1.778 | -0.084 | 0.166 | 1.076 | 0.076 | 0.343 | 1.123 | 0.079 | 0.422 |
| 1.131 | 0.063 | 0.343 | 1.345 | -0.009 | 0.429 | 1.430 | -0.058 | 0.361 | 1.372 | -0.043 | 0.408 |
| 1.575 | -0.077 | 0.336 | 0.688 | 0.017 | 0.061 | 1.289 | 0.000 | 0.422 | 0.924 | 0.053 | 0.155 |
| 1.331 | -0.010 | 0.378 | 1.236 | 0.032 | 0.430 | 1.345 | -0.053 | 0.428 | 1.333 | -0.026 | 0.403 |
| 1.437 | -0.059 | 0.380 | 1.350 | -0.013 | 0.418 | 1.519 | -0.068 | 0.382 | 1.375 | -0.062 | 0.432 |
| 1.210 | 0.038 | 0.395 | 1.704 | -0.094 | 0.172 | 1.372 | -0.003 | 0.431 | 1.158 | 0.057 | 0.406 |
| 1.395 | 0.003 | 0.380 | 1.294 | -0.009 | 0.496 | 1.416 | -0.030 | 0.492 | 1.375 | -0.016 | 0.413 |
| 1.439 | -0.022 | 0.415 | 1.408 | -0.060 | 0.373 | 1.454 | -0.062 | 0.447 | 1.575 | -0.075 | 0.343 |
| 1.656 | -0.097 | 0.310 | 1.765 | -0.062 | 0.148 | 1.765 | -0.095 | 0.209 | 1.301 | 0.025 | 0.399 |
| 0.825 | 0.065 | 0.119 | 1.382 | 0.026 | 0.386 | 1.060 | 0.088 | 0.344 | 1.429 | -0.009 | 0.433 |
| 1.324 | -0.012 | 0.448 | 1.444 | -0.002 | 0.425 | 1.479 | -0.024 | 0.375 | 1.520 | -0.040 | 0.363 |
| 1.603 | -0.122 | 0.305 | 1.633 | -0.103 | 0.329 | 1.632 | -0.117 | 0.250 | 1.699 | -0.080 | 0.268 |
| 1.679 | -0.086 | 0.186 | 1.857 | -0.051 | 0.155 | 0.8450 | 0.051 | 0.179 | 1.905 | -0.049 | 0.133 |
| 1.279 | 0.028 | 0.422 | | | | | | | | | |

14

## TABLE E.25 (continued)

(Z/D) = 2.92 (℄ = 1.327 cm)

| r'(cm) | $V_r$ (cm/sec) | $V_z$ (cm/sec) | r'(cm) | $V_r$ (cm/sec) | $V_z$ (cm/sec) | r'(cm) | $V_r$ (cm/sec) | $V_z$ (cm/sec) | r'(cm) | $V_r$ (cm/sec) | $V_z$ (cm/sec) |
|---|---|---|---|---|---|---|---|---|---|---|---|
| 1.123 | 0.136 | 0.421 | 1.752 | -0.055 | 0.100 | 1.324 | 0.088 | 0.944 | 1.140 | 0.171 | 0.813 |
| 1.393 | -0.031 | 0.958 | 1.530 | -0.141 | 0.677 | 1.447 | -0.122 | 0.973 | 1.569 | -0.081 | 0.413 |
| 1.671 | -0.084 | 0.297 | 1.685 | -0.058 | 0.183 | 1.695 | -0.059 | 0.238 | 0.918 | 0.030 | 0.164 |
| 1.069 | 0.100 | 0.385 | 1.081 | 0.042 | 0.405 | 1.283 | 0.073 | 1.025 | 1.301 | 0.014 | 0.999 |
| 1.347 | -0.002 | 0.969 | 1.545 | -0.176 | 0.542 | 1.379 | -0.039 | 0.992 | 1.579 | -0.151 | 0.435 |
| 1.466 | -0.072 | 0.862 | 1.600 | -0.090 | 0.416 | 1.628 | -0.104 | 0.399 | 1.682 | -0.064 | 0.182 |
| 1.717 | -0.060 | 0.193 | 1.142 | 0.117 | 0.589 | 1.771 | -0.056 | 0.125 | 1.203 | 0.112 | 0.832 |
| 1.068 | 0.103 | 0.366 | 1.397 | -0.059 | 0.888 | 1.390 | -0.075 | 0.872 | 1.523 | -0.138 | 0.663 |
| 1.397 | -0.055 | 0.951 | 1.580 | -0.111 | 0.439 | 1.405 | -0.011 | 0.905 | 1.672 | -0.100 | 0.322 |
| 1.423 | -0.089 | 1.021 | 1.743 | -0.034 | 0.158 | 1.453 | -0.036 | 0.886 | 1.339 | 0.069 | 0.987 |
| 1.509 | -0.097 | 0.825 | 1.426 | -0.054 | 0.971 | 1.539 | -0.157 | 0.819 | 1.526 | -0.140 | 0.692 |
| 1.587 | -0.100 | 0.577 | 1.639 | -0.155 | 0.452 | 0.961 | 0.034 | 0.172 | 1.676 | -0.064 | 0.349 |
| 1.172 | 0.190 | 0.708 | 1.382 | 0.007 | 0.932 | 1.352 | -0.035 | 1.029 | 1.423 | -0.018 | 0.883 |
| 1.368 | -0.064 | 1.035 | 1.446 | -0.050 | 0.772 | 1.570 | -0.104 | 0.569 | 1.565 | -0.106 | 0.652 |
| 1.748 | -0.057 | 0.174 | 1.578 | -0.138 | 0.558 | 1.107 | 0.114 | 0.567 | 1.708 | -0.090 | 0.263 |
| 1.314 | 0.052 | 0.803 | 1.313 | -0.023 | 1.016 | 1.436 | -0.089 | 0.853 | 1.531 | -0.122 | 0.519 |
| 0.871 | 0.029 | 0.116 | 1.170 | 0.150 | 0.715 | 1.466 | -0.086 | 0.621 | 1.270 | 0.064 | 0.949 |
| 1.624 | -0.101 | 0.311 | 1.288 | 0.026 | 0.944 | 1.399 | -0.053 | 0.840 | 1.343 | -0.036 | 0.966 |
| 1.030 | 0.096 | 0.250 | 1.437 | -0.100 | 0.789 | 1.047 | 0.078 | 0.298 | 1.507 | -0.100 | 0.621 |
| 1.135 | 0.110 | 0.577 | 1.549 | -0.091 | 0.515 | 1.342 | 0.004 | 0.931 | 1.576 | -0.073 | 0.385 |
| 1.367 | -0.070 | 1.074 | 1.804 | -0.026 | 0.075 | 1.388 | -0.034 | 0.951 | 0.688 | 0.019 | 0.043 |
| 1.557 | -0.134 | 0.605 | 1.261 | 0.103 | 0.856 | 1.600 | -0.102 | 0.338 | 1.288 | 0.034 | 0.925 |
| 1.111 | 0.093 | 0.592 | 1.044 | 0.103 | 0.347 | 1.184 | 0.123 | 0.848 | 1.259 | 0.058 | 0.875 |
| 1.319 | 0.020 | 0.965 | 1.338 | -0.056 | 1.039 | 1.353 | -0.052 | 1.072 | 1.348 | -0.023 | 0.990 |
| 1.702 | -0.033 | 0.167 | 1.573 | -0.095 | 0.466 | 1.364 | 0.010 | 0.942 | 1.284 | 0.029 | 0.979 |
| 1.385 | -0.013 | 1.028 | 1.421 | -0.082 | 0.771 | 1.436 | -0.077 | 0.854 | 1.523 | -0.081 | 0.502 |
| 1.629 | -0.095 | 0.403 | 1.109 | 0.127 | 0.666 | 1.656 | -0.097 | 0.298 | 1.301 | 0.024 | 0.963 |
| 1.678 | -0.061 | 0.234 | 1.431 | -0.069 | 0.900 | 0.852 | 0.041 | 0.103 | 1.731 | -0.078 | 0.257 |

TABLE E.25 (continued)

(Z/D) = 1.46 (℄ = 1.327 cm)

| r'(cm) | $V_r$(cm/sec) | $V_z$(cm/sec) | r'(cm) | $V_r$(cm/sec) | $V_z$(cm/sec) | r'(cm) | $V_r$(cm/sec) | $V_z$(cm/sec) | r'(cm) | $V_r$(cm/sec) | $V_z$(cm/sec) |
|---|---|---|---|---|---|---|---|---|---|---|---|
| 1.383 | -0.061 | 2.321 | 1.499 | -0.108 | 0.657 | 1.402 | -0.054 | 1.688 | 1.589 | 0.001 | 0.192 |
| 1.415 | -0.071 | 1.960 | 1.024 | -0.007 | 0.231 | 1.335 | -0.015 | 2.036 | 1.309 | 0.003 | 2.050 |
| 1.593 | -0.098 | 0.346 | 1.383 | -0.083 | 1.655 | 1.136 | 0.042 | 0.429 | 1.425 | -0.098 | 1.580 |
| 1.298 | -0.011 | 1.553 | 1.453 | -0.078 | 1.096 | 1.344 | 0.040 | 1.690 | 1.490 | -0.044 | 0.557 |
| 1.369 | -0.088 | 1.783 | 1.143 | 0.115 | 1.072 | 1.385 | -0.065 | 2.038 | 1.353 | -0.073 | 2.004 |
| 1.395 | -0.010 | 1.696 | 1.403 | -0.023 | 1.556 | 1.408 | -0.136 | 1.802 | 1.501 | -0.065 | 0.825 |
| 1.415 | -0.038 | 1.811 | 1.201 | 0.110 | 1.060 | 1.455 | -0.072 | 1.529 | 1.243 | 0.040 | 1.293 |
| 1.504 | -0.121 | 1.042 | 1.366 | -0.065 | 1.926 | 1.554 | -0.092 | 0.610 | 1.398 | -0.040 | 1.791 |
| 1.642 | 0.020 | 0.172 | 1.435 | -0.027 | 1.390 | 1.426 | -0.030 | 1.859 | 1.509 | -0.122 | 0.905 |
| 1.462 | -0.070 | 1.489 | 1.351 | 0.051 | 1.963 | 1.524 | -0.066 | 1.086 | 1.404 | -0.111 | 2.064 |
| 1.280 | 0.105 | 1.722 | 1.523 | -0.066 | 1.195 | 1.026 | -0.006 | 0.123 | 1.088 | -0.011 | 0.163 |
| 1.182 | 0.017 | 0.996 | 1.384 | 0.004 | 1.785 | 1.361 | -0.056 | 1.777 | 1.413 | -0.049 | 1.719 |
| 1.390 | -0.066 | 1.882 | 1.440 | -0.129 | 1.078 | 1.427 | -0.108 | 1.701 | 1.456 | -0.090 | 0.915 |
| 1.093 | 0.066 | 0.426 | 1.528 | -0.074 | 0.318 | 1.305 | 0.042 | 2.020 | 1.551 | -0.037 | 0.271 |
| 1.342 | -0.083 | 1.627 | 1.209 | 0.051 | 1.877 | 1.334 | -0.075 | 1.836 | 1.342 | -0.054 | 1.527 |
| 1.390 | -0.113 | 1.680 | 1.521 | -0.040 | 0.265 | 1.491 | -0.108 | 0.776 | 1.543 | -0.034 | 0.244 |
| 1.565 | -0.036 | 0.302 | 1.601 | 0.018 | 0.080 | 1.464 | -0.122 | 0.980 | 1.116 | 0.074 | 0.516 |
| 1.480 | -0.087 | 0.831 | 1.210 | 0.110 | 1.295 | 1.482 | -0.116 | 1.174 | 1.607 | -0.023 | 0.336 |
| 1.530 | -0.124 | 0.751 | 1.742 | 0.032 | 0.055 | 1.551 | -0.081 | 0.594 | 1.183 | 0.119 | 1.428 |
| 1.090 | 0.047 | 0.312 | 1.456 | -0.136 | 1.024 | 1.178 | 0.084 | 1.388 | 0.895 | 0.005 | 0.113 |
| 1.212 | 0.113 | 1.547 | 1.267 | 0.044 | 1.617 | 1.562 | -0.023 | 0.296 | 1.117 | 0.080 | 0.668 |
| 1.066 | 0.058 | 0.471 | 1.271 | 0.042 | 1.546 | 1.138 | 0.116 | 1.271 | 1.502 | -0.121 | 0.666 |
| 1.285 | 0.023 | 1.794 | 1.123 | 0.126 | 1.152 | 1.429 | -0.115 | 1.011 | 1.459 | -0.098 | 0.796 |
| 1.491 | -0.052 | 0.466 | 1.552 | -0.050 | 0.194 | 1.501 | -0.062 | 0.425 | 1.642 | -0.045 | 0.302 |
| 1.541 | -0.038 | 0.400 | 1.691 | -0.006 | 0.164 | 1.564 | -0.057 | 0.510 | | | |

## TABLE E.26

## RADIAL VELOCITIES - DIGITIZER METHOD, $Q=0.318$ cm$^3$/sec
## 0.030 cm I.D. CAPILLARY TUBE, SMALL RESERVOIR

$(Z/D) = 5.96$ (℄ = 1.327 cm)

| r' (cm) | $V_r$ (cm/sec) | r' (cm) | $V_r$ (cm/sec) | r' (cm) | $V_r$ (cm/sec) | r' (cm) | $V_r$ (cm/sec) | r' (cm) | $V_r$ (cm/sec) | r' (cm) | $V_r$ (cm/sec) |
|---|---|---|---|---|---|---|---|---|---|---|---|
| 0.873 | 0.163 | 1.916 | -0.112 | 1.894 | -0.105 | 1.315 | -0.051 | 0.956 | 0.132 | 1.326 | -0.036 |
| 1.389 | -0.081 | 1.068 | 0.160 | 1.345 | -0.060 | 1.403 | -0.092 | 1.432 | -0.060 | 1.414 | -0.074 |
| 1.433 | -0.025 | 1.587 | -0.165 | 1.433 | -0.064 | 1.488 | -0.177 | 1.622 | -0.133 | 1.512 | -0.113 |
| 1.562 | -0.129 | 1.138 | 0.161 | 1.563 | -0.178 | 1.587 | -0.179 | 1.318 | -0.034 | 1.628 | -0.188 |
| 1.707 | -0.152 | 1.338 | -0.052 | 1.728 | -0.184 | 1.753 | -0.152 | 1.501 | -0.086 | 1.812 | -0.126 |
| 1.812 | -0.117 | 1.597 | -0.152 | 1.939 | -0.069 | 1.332 | 0.004 | 1.791 | -0.165 | 0.919 | 0.125 |
| 1.366 | -0.067 | 0.802 | 0.096 | 0.951 | 0.140 | 1.390 | -0.055 | 0.883 | 0.124 | 1.172 | 0.099 |
| 1.381 | -0.024 | 1.402 | -0.056 | 1.384 | -0.068 | 1.491 | -0.071 | 1.381 | -0.024 | 1.419 | -0.078 |
| 1.670 | -0.116 | 1.495 | -0.085 | 1.590 | -0.120 | 1.756 | -0.150 | 1.788 | -0.103 | 1.625 | -0.137 |
| 1.814 | -0.115 | 1.993 | -0.090 | 1.984 | -0.088 | 1.180 | 0.123 | 1.397 | -0.034 | 1.448 | -0.031 |
| 1.388 | -0.019 | 1.405 | -0.032 | 1.521 | -0.106 | 1.399 | -0.103 | 1.501 | -0.071 | 1.581 | -0.119 |
| 1.441 | -0.043 | 1.655 | -0.179 | 1.608 | -0.106 | 1.518 | -0.151 | 1.678 | -0.160 | 1.829 | -0.166 |
| 1.655 | -0.204 | 1.785 | -0.152 | 2.041 | -0.063 | 1.689 | -0.138 | 1.798 | -0.112 | 0.954 | 0.154 |
| 1.739 | -0.133 | 1.824 | -0.115 | 0.994 | 0.141 | 1.042 | 0.135 | 1.806 | -0.130 | 1.473 | -0.021 |
| 1.325 | -0.057 | 1.030 | 0.143 | 1.521 | -0.157 | 1.345 | -0.039 | 1.272 | 0.003 | 1.612 | -0.154 |
| 1.508 | -0.140 | 1.391 | -0.007 | 1.661 | -0.135 | 1.711 | -0.165 | 1.448 | -0.067 | 1.867 | -0.118 |
| 1.812 | -0.151 | 1.657 | -0.163 | 1.933 | -0.089 | 0.743 | 0.067 | 1.709 | -0.181 | 1.427 | -0.086 |
| 1.042 | 0.139 | 1.785 | -0.175 | 1.727 | -0.150 | 1.304 | 0.042 | 1.936 | -0.089 | 1.985 | -0.072 |
| 1.436 | -0.033 | 1.284 | 0.052 | 1.155 | 0.133 | 1.455 | -0.073 | 1.409 | -0.011 | 1.349 | -0.013 |
| 1.547 | -0.101 | 1.588 | -0.099 | 1.362 | -0.052 | 1.961 | -0.085 | 1.811 | -0.171 | 1.378 | -0.023 |
| 0.960 | 0.172 | 1.868 | -0.111 | 1.407 | -0.035 | 0.981 | 0.142 | 1.944 | -0.109 | 1.473 | -0.077 |
| 1.084 | 0.106 | 0.875 | 0.076 | 1.531 | -0.125 | 1.167 | 0.122 | 1.327 | 0.058 | 1.547 | -0.126 |
| 1.390 | -0.018 | 1.340 | -0.006 | 1.446 | -0.097 | 1.398 | 0.003 | 1.346 | -0.055 | 1.674 | -0.153 |
| 1.427 | -0.036 | 1.387 | -0.027 | 1.777 | -0.152 | 1.460 | -0.078 | 1.395 | -0.023 | 0.975 | 0.184 |
| 1.616 | -0.120 | 1.494 | -0.153 | 1.414 | -0.071 | 1.880 | -0.095 | 1.567 | -0.112 | 1.461 | 0.091 |
| 1.965 | -0.106 | 1.381 | -0.024 | 1.532 | -0.104 | 0.713 | 0.074 | 1.367 | -0.031 | 1.867 | -0.102 |
| 0.893 | 0.144 | 1.403 | -0.005 | 1.350 | -0.017 | 1.364 | -0.023 | 1.424 | -0.129 | 1.377 | -0.003 |

TABLE E.26 (continued)

(Z/D) = 3.97 ($\xi$ = 1.327 cm)

| r' (cm) | $V_r$ (cm/sec) | r' (cm) | $V_r$ (cm/sec) | r' (cm) | $V_r$ (cm/sec) | r' (cm) | $V_r$ (cm/sec) | r' (cm) | $V_r$ (cm/sec) | r' (cm) | $V_r$ (cm/sec) |
|---|---|---|---|---|---|---|---|---|---|---|---|
| 1.026 | 0.124 | 1.594 | -0.140 | 1.383 | -0.071 | 1.313 | -0.052 | 1.639 | -0.115 | 1.475 | -0.171 |
| 1.364 | -0.053 | 1.670 | -0.124 | 1.549 | -0.178 | 1.373 | -0.113 | 0.987 | 0.063 | 1.611 | -0.170 |
| 1.383 | -0.013 | 1.244 | 0.117 | 1.671 | -0.116 | 1.483 | -0.137 | 1.433 | -0.027 | 1.760 | -0.076 |
| 1.567 | -0.197 | 1.470 | -0.112 | 1.825 | -0.031 | 1.575 | -0.138 | 1.527 | -0.154 | 0.833 | 0.018 |
| 1.595 | -0.156 | 1.748 | -0.079 | 1.212 | 0.133 | 1.605 | -0.155 | 1.095 | 0.169 | 1.137 | 0.183 |
| 1.634 | -0.117 | 1.158 | 0.169 | 1.367 | -0.053 | 1.660 | -0.114 | 1.404 | -0.045 | 1.541 | -0.187 |
| 1.126 | 0.194 | 1.436 | -0.121 | 1.623 | -0.118 | 1.357 | -0.085 | 1.509 | -0.199 | 1.645 | -0.165 |
| 1.423 | -0.162 | 1.650 | -0.069 | 1.673 | -0.124 | 1.472 | -0.125 | 1.748 | -0.056 | 1.758 | -0.097 |
| 1.435 | -0.023 | 1.164 | 0.174 | 0.907 | 0.085 | 1.552 | -0.116 | 1.204 | -0.134 | 1.040 | 0.138 |
| 1.599 | -0.203 | 1.376 | -0.049 | 1.265 | 0.007 | 1.663 | -0.113 | 1.422 | -0.163 | 1.388 | -0.106 |
| 1.666 | -0.116 | 1.455 | -0.199 | 1.498 | -0.189 | 1.758 | -0.055 | 1.577 | -0.118 | 1.537 | -0.136 |
| 1.116 | 0.178 | 1.613 | -0.122 | 1.599 | -0.173 | 1.236 | 0.156 | 1.668 | -0.092 | 1.608 | -0.134 |
| 1.366 | -0.067 | 0.869 | 0.020 | 1.688 | -0.100 | 1.524 | -0.119 | 0.922 | 0.073 | 1.720 | -0.059 |
| 1.527 | -0.112 | 0.986 | 0.063 | 1.733 | -0.046 | 1.552 | -0.116 | 1.052 | 0.087 | 1.742 | -0.068 |
| 0.911 | 0.069 | 1.052 | 0.115 | 1.354 | -0.089 | 0.924 | 0.066 | 1.126 | 0.141 | 1.365 | -0.033 |
| 1.095 | 0.151 | 1.517 | -0.146 | 1.379 | -0.074 | 1.585 | -0.124 | 1.603 | -0.174 | 1.600 | -0.126 |
| 1.707 | -0.081 | 1.642 | -0.114 | 1.169 | 0.200 | 1.742 | -0.078 | 1.668 | -0.100 | 1.568 | -0.139 |
| 1.761 | -0.084 | 1.699 | -0.089 | 1.771 | -0.031 | 1.384 | -0.014 | 1.798 | -0.050 | 1.872 | -0.038 |
| 1.711 | -0.090 | 0.951 | 0.054 | 1.067 | 0.116 | 1.796 | -0.069 | 1.393 | -0.025 | 1.221 | 0.098 |
| 0.855 | 0.060 | 1.578 | -0.157 | 1.358 | -0.045 | 0.941 | 0.080 | 1.668 | -0.136 | 1.592 | -0.128 |
| 1.072 | 0.174 | 1.711 | -0.133 | 1.661 | -0.083 | 1.107 | 0.178 | 1.816 | -0.032 | 1.699 | -0.074 |
| 1.436 | -0.131 | 1.349 | -0.012 | 1.019 | 0.086 | 1.581 | -0.115 | 1.385 | -0.095 | 1.355 | -0.045 |
| 1.770 | -0.050 | 1.416 | -0.137 | 1.363 | -0.044 | 1.893 | -0.027 | 1.461 | -0.117 | 1.373 | -0.053 |
| 0.809 | 0.023 | 1.479 | -0.125 | 1.382 | -0.026 | 1.421 | -0.019 | 1.590 | -0.129 | 1.412 | -0.080 |
| 1.763 | -0.109 | 1.623 | -0.150 | 1.664 | -0.138 | 1.863 | -0.044 | 1.385 | -0.073 | 1.726 | -0.109 |
| 1.070 | 0.119 | 1.606 | -0.184 | 0.777 | 0.020 | 1.101 | 0.156 | 1.652 | -0.127 | 1.138 | 0.137 |
| 1.776 | -0.065 | 1.668 | -0.159 | 1.215 | 0.086 | 0.736 | 0.020 | 1.709 | -0.053 | 1.232 | 0.072 |
| 1.126 | 0.208 | 1.104 | 0.211 | | | | | | | | |

TABLE E.26 (continued)

(Z/D) = 1.99 (℄ = 1.327 cm)

| r'(cm) | $V_r$(cm/sec) | r'(cm) | $V_r$(cm/sec) | r'(cm) | $V_r$(cm/sec) | r'(cm) | $V_r$(cm/sec) | r'(cm) | $V_r$(cm/sec) | r'(cm) | $V_r$(cm/sec) |
|---|---|---|---|---|---|---|---|---|---|---|---|
| 1.363 | -0.110 | 1.014 | -0.009 | 1.138 | 0.066 | 1.434 | -0.240 | 1.537 | -0.128 | 1.638 | -0.025 |
| 1.493 | -0.162 | 1.572 | -0.110 | 1.691 | 0.006 | 1.502 | -0.162 | 1.590 | -0.108 | 1.723 | 0.018 |
| 1.522 | -0.066 | 1.700 | 0.042 | 1.491 | -0.181 | 1.577 | -0.025 | 1.547 | -0.163 | 1.574 | -0.033 |
| 1.214 | 0.233 | 1.588 | -0.024 | 1.593 | -0.022 | 1.444 | -0.089 | 1.687 | 0.009 | 1.628 | -0.040 |
| 1.523 | -0.138 | 1.715 | 0.032 | 1.645 | 0.005 | 1.584 | -0.003 | 0.928 | -0.047 | 1.649 | 0.053 |
| 1.498 | -0.130 | 1.503 | -0.030 | 0.865 | -0.075 | 1.370 | -0.088 | 1.617 | -0.048 | 1.088 | 0.059 |
| 1.334 | 0.092 | 1.642 | -0.002 | 1.131 | 0.052 | 0.990 | 0.002 | 1.679 | 0.058 | 1.190 | 0.140 |
| 1.181 | 0.080 | 0.982 | -0.043 | 1.560 | -0.073 | 1.463 | -0.140 | 1.548 | -0.154 | 1.632 | -0.023 |
| 1.492 | -0.230 | 1.590 | -0.043 | 1.647 | 0.018 | 1.561 | -0.066 | 1.603 | -0.045 | 1.698 | 0.012 |
| 1.672 | -0.007 | 1.616 | -0.007 | 1.704 | 0.029 | 1.704 | 0.020 | 1.664 | 0.020 | 1.778 | 0.042 |
| 1.213 | 0.232 | 1.697 | 0.042 | 1.327 | 0.075 | 1.378 | -0.019 | 1.682 | -0.001 | 1.511 | -0.079 |
| 1.452 | -0.200 | 1.741 | 0.009 | 1.615 | -0.008 | 1.412 | -0.076 | 1.609 | -0.003 | 1.419 | -0.115 |
| 1.485 | -0.168 | 1.636 | -0.019 | 1.496 | -0.177 | 1.558 | -0.216 | 1.672 | 0.002 | 1.526 | -0.062 |
| 1.593 | -0.184 | 1.769 | 0.022 | 1.573 | -0.116 | 1.341 | -0.086 | 0.945 | -0.071 | 1.359 | -0.082 |
| 1.385 | -0.075 | 1.194 | 0.142 | 1.534 | -0.168 | 1.586 | 0.001 | 0.990 | -0.013 | 1.654 | 0.032 |
| 1.661 | 0.008 | | | | | | | | | | |

## TABLE E.27

## RADIAL VELOCITIES - DIGITZER METHOD, Q=0.635 $cm^3$/sec
## 0.30 cm I.D. CAPILLARY TUBE, SMALL RESERVOIR

(Z/D) = 5.02 (℄ = 1.327 cm)

| r'(cm) | $V_r$(cm/sec) | r'(cm) | $V_r$(cm/sec) | r'(cm) | $V_r$(cm/sec) | r'(cm) | $V_r$(cm/sec) | r'(cm) | $V_r$(cm/sec) | r'(cm) | $V_r$(cm/sec) |
|---|---|---|---|---|---|---|---|---|---|---|---|
| 0.876 | 0.028 | 2.008 | -0.012 | 0.928 | 0.038 | 1.086 | 0.128 | 1.736 | -0.102 | 1.945 | -0.008 |
| 1.043 | 0.147 | 1.871 | -0.014 | 1.605 | -0.189 | 1.100 | 0.154 | 1.927 | -0.017 | 1.686 | -0.070 |
| 1.806 | -0.053 | 0.781 | 0.048 | 1.719 | -0.134 | 1.850 | -0.036 | 0.861 | 0.060 | 1.841 | -0.046 |
| 1.876 | -0.050 | 0.899 | 0.096 | 1.002 | 0.067 | 1.949 | -0.020 | 1.727 | -0.121 | 1.141 | 0.163 |
| 2.013 | 0.001 | 1.800 | -0.040 | 1.244 | 0.073 | 0.780 | 0.008 | 1.842 | -0.050 | 1.527 | -0.192 |
| 0.932 | 0.085 | 0.935 | 0.066 | 1.532 | -0.182 | 1.637 | -0.133 | 1.708 | -0.139 | 1.548 | -0.262 |
| 1.662 | -0.099 | 1.913 | -0.068 | 1.671 | -0.169 | 1.788 | -0.123 | 0.897 | 0.049 | 1.716 | -0.079 |
| 1.868 | -0.022 | 0.939 | 0.062 | 1.722 | -0.133 | 0.715 | 0.021 | 0.962 | 0.052 | 1.743 | -0.085 |
| 0.719 | 0.007 | 1.657 | -0.149 | 1.761 | 0.020 | 0.831 | 0.043 | 1.782 | -0.023 | 1.806 | -0.102 |
| 1.130 | 0.209 | 1.849 | -0.081 | 1.174 | 0.061 | 1.674 | -0.149 | 0.923 | 0.072 | 0.812 | 0.053 |
| 1.843 | -0.053 | 0.966 | 0.052 | 0.871 | 0.064 | 1.942 | -0.012 | 1.675 | -0.135 | 1.036 | 0.179 |
| 0.821 | 0.027 | 1.663 | -0.121 | 1.085 | 0.060 | 0.891 | 0.058 | 1.759 | -0.041 | 1.313 | -0.065 |
| 1.111 | 0.172 | 1.801 | -0.085 | 1.472 | -0.350 | 1.696 | -0.116 | 1.815 | -0.021 | 1.497 | -0.020 |
| 1.766 | -0.092 | 1.914 | -0.048 | 1.513 | -0.229 | 1.967 | -0.014 | 1.022 | 0.094 | 1.563 | -0.175 |
| 1.601 | -0.134 | 1.599 | -0.190 | 1.642 | -0.174 | 1.748 | -0.139 | 1.721 | -0.076 | 1.840 | -0.047 |
| 1.453 | -0.196 | 1.069 | 0.022 | 0.950 | 0.041 | 1.488 | 0.001 | 1.320 | 0.044 | 0.954 | 0.056 |
| 1.505 | -0.314 | 1.501 | -0.162 | 0.977 | 0.022 | 1.661 | -0.108 | 1.541 | -0.252 | 1.150 | 0.206 |
| 1.731 | -0.168 | 1.622 | -0.228 | 1.170 | 0.285 | 1.750 | -0.090 | 1.666 | -0.127 | 1.550 | -0.289 |
| 1.398 | -0.206 | 1.707 | -0.081 | 1.616 | -0.176 | 1.547 | -0.076 | 1.280 | 0.266 | 1.644 | -0.073 |
| 1.605 | -0.419 | 1.431 | -0.156 | 1.667 | -0.076 | 1.721 | -0.070 | 1.475 | -0.136 | 1.701 | -0.153 |
| 1.745 | -0.093 | 1.559 | -0.235 | 1.713 | -0.192 | 1.294 | -0.029 | 1.502 | -0.097 | 0.891 | 0.055 |
| 1.572 | -0.274 | 1.655 | -0.113 | 0.993 | 0.203 | 1.230 | 0.320 | 1.704 | -0.139 | 1.076 | 0.155 |
| 1.457 | -0.235 | 1.733 | -0.136 | 1.238 | 0.154 | 1.738 | -0.160 | 0.950 | 0.039 | 1.363 | -0.034 |
| 0.979 | 0.132 | 1.139 | 0.114 | 1.422 | -0.151 | 1.463 | -0.073 | 1.589 | -0.307 | 1.545 | -0.328 |
| 1.698 | -0.050 | 1.665 | -0.160 | 1.566 | -0.120 | 1.771 | 0.020 | 1.706 | -0.057 | 1.612 | -0.098 |
| 1.150 | 0.189 | 1.723 | -0.075 | 1.626 | -0.084 | 1.201 | 0.202 | 1.080 | 0.136 | 1.644 | -0.113 |
| 1.230 | 0.171 | 1.373 | -0.044 | 1.702 | -0.144 | 1.399 | -0.112 | 1.198 | 0.425 | 1.731 | -0.068 |

TABLE E.27 (continued)

(Z/D) = 5.02 (ξ = 1.327 cm)

| r' (cm) | $V_r$ (cm/sec) | r' (cm) | $V_r$ (cm/sec) | r' (cm) | $V_r$ (cm/sec) | r' (cm) | $V_r$ (cm/sec) | r' (cm) | $V_r$ (cm/sec) | r' (cm) | $V_r$ (cm/sec) |
|---|---|---|---|---|---|---|---|---|---|---|---|
| 1.422 | -0.192 | 1.526 | -0.314 | 1.774 | -0.051 | 1.496 | -0.124 | 1.602 | -0.302 | 1.828 | -0.059 |
| 1.676 | -0.136 | 1.691 | -0.045 | 1.350 | -0.145 | 1.710 | -0.078 | 1.708 | -0.159 | 1.366 | -0.068 |
| 1.722 | -0.037 | 1.714 | -0.073 | 1.375 | 0.032 | 1.810 | -0.073 | 1.731 | -0.178 | 1.907 | -0.068 |
| 0.979 | 0.075 | 1.744 | -0.087 | 0.736 | 0.019 | 1.193 | 0.250 | 1.831 | -0.046 | 0.894 | 0.085 |
| 1.249 | 0.107 | 1.861 | -0.028 | | | | | | | | |

(Z/D) = 2.51 (ξ = 1.327 cm)

| r' (cm) | $V_r$ (cm/sec) | r' (cm) | $V_r$ (cm/sec) | r' (cm) | $V_r$ (cm/sec) | r' (cm) | $V_r$ (cm/sec) | r' (cm) | $V_r$ (cm/sec) | r' (cm) | $V_r$ (cm/sec) |
|---|---|---|---|---|---|---|---|---|---|---|---|
| 0.970 | -0.060 | 1.876 | 0.072 | 1.532 | -0.009 | 1.162 | 0.174 | 1.177 | 0.243 | 1.504 | -0.236 |
| 1.647 | -0.024 | 1.129 | 0.191 | 1.608 | -0.135 | 1.728 | 0.046 | 1.582 | -0.222 | 1.247 | 0.257 |
| 0.835 | -0.102 | 1.629 | -0.076 | 1.492 | -0.127 | 0.981 | -0.059 | 1.649 | -0.060 | 1.521 | -0.079 |
| 1.601 | -0.059 | 1.733 | 0.069 | 1.594 | 0.002 | 1.584 | -0.067 | 1.646 | -0.118 | 1.617 | 0.025 |
| 1.615 | -0.040 | 1.656 | -0.058 | 1.077 | -0.142 | 0.968 | -0.050 | 1.677 | 0.043 | 1.125 | 0.063 |
| 1.010 | -0.008 | 1.780 | 0.069 | 1.162 | 0.158 | 1.624 | -0.003 | 1.579 | -0.160 | 1.594 | -0.156 |
| 1.627 | 0.003 | 1.281 | 0.198 | 1.603 | -0.051 | 1.685 | -0.001 | 1.141 | 0.191 | 1.678 | -0.047 |
| 1.662 | -0.008 | 1.529 | -0.080 | 1.719 | 0.074 | 1.689 | 0.035 | 1.576 | 0.010 | 1.201 | 0.152 |
| 1.707 | 0.070 | 1.602 | -0.053 | 1.239 | 0.332 | 0.864 | -0.075 | 1.701 | 0.044 | 1.264 | 0.092 |
| 0.997 | -0.014 | 1.436 | -0.144 | 1.557 | -0.109 | 1.580 | -0.071 | 1.474 | -0.192 | 1.601 | -0.212 |
| 1.604 | -0.044 | 1.572 | -0.444 | 1.630 | -0.065 | 1.008 | -0.016 | 1.631 | -0.125 | 1.643 | -0.035 |
| 0.903 | -0.066 | 1.654 | -0.133 | 1.733 | 0.067 | 1.022 | -0.006 | 1.710 | -0.037 | 1.122 | 0.113 |
| 1.783 | 0.046 | 1.723 | 0.026 | 1.535 | -0.199 | 1.081 | -0.005 | 1.125 | 0.040 | 1.551 | 0.031 |
| 1.671 | 0.013 | 1.658 | -0.019 | 1.591 | -0.054 | 1.729 | 0.040 | 1.290 | -0.176 | 1.602 | -0.069 |
| 1.661 | 0.010 | 1.033 | 0.039 | 1.649 | -0.084 | 1.607 | 0.010 | 1.257 | -0.163 | 1.817 | 0.034 |

## TABLE E.27 (continued)

(Z/D) = 2.51 (℄ = 1.327 cm)

| r' (cm) | $V_r$ (cm/sec) | r' (cm) | $V_r$ (cm/sec) | r' (cm) | $V_r$ (cm/sec) | r' (cm) | $V_r$ (cm/sec) | r' (cm) | $V_r$ (cm/sec) | r' (cm) | $V_r$ (cm/sec) |
|---|---|---|---|---|---|---|---|---|---|---|---|
| 1.320 | -0.177 | 1.016 | 0.038 | 1.022 | -0.065 | 1.458 | -0.172 | 1.126 | 0.068 | 1.136 | 0.134 |
| 1.475 | -0.397 | 1.480 | -0.320 | 1.594 | -0.038 | 1.390 | -0.014 | 1.623 | -0.050 | 1.644 | -0.113 |
| 1.454 | -0.219 | 1.662 | -0.079 | 1.025 | -0.005 | 1.644 | -0.132 | 1.683 | -0.014 | 1.161 | 0.276 |
| 1.660 | -0.055 | 1.692 | 0.030 | 1.544 | -0.213 | 1.677 | -0.087 | 1.017 | 0.031 | 1.552 | -0.118 |
| 1.756 | 0.036 | 1.504 | -0.088 | 1.612 | -0.096 | 1.068 | -0.047 | 1.568 | -0.031 | 1.698 | -0.039 |
| 1.197 | 0.099 | 1.578 | -0.002 | | | | | | | | |

## TABLE E.28

### RADIAL AND AXIAL VELOCITIES - DIGITIZER METHOD, Q=1.589 $cm^3/sec$
### 0.20 cm I.D. CAPILLARY TUBE, LARGE RESERVOIR

(Z/D) = 30.67 ( ℄ = 12.745 cm)

| r' (cm) | $V_r$ (cm/sec) | $V_z$ (cm/sec) | r' (cm) | $V_r$ (cm/sec) | $V_z$ (cm/sec) | r' (cm) | $V_r$ (cm/sec) | $V_z$ (cm/sec) | r' (cm) | $V_r$ (cm/sec) | $V_z$ (cm/sec) |
|---|---|---|---|---|---|---|---|---|---|---|---|
| 12.940 | 0.562 | 2.827 | 14.111 | -0.207 | 0.786 | 12.479 | 0.312 | 3.318 | 13.806 | -0.308 | 1.415 |
| 11.879 | 0.306 | 1.112 | 13.514 | -0.271 | 1.931 | 11.670 | 0.217 | 1.287 | 12.964 | 0.162 | 2.780 |
| 10.316 | 0.153 | 0.216 | 12.030 | 0.344 | 1.646 | 9.813 | 0.098 | 0.119 | 11.617 | 0.184 | 0.992 |
| 10.761 | 0.185 | 0.478 | 10.737 | 0.218 | 0.530 | 14.650 | -0.268 | 0.553 | 10.198 | 0.106 | 0.236 |
| 14.319 | -0.120 | 0.708 | 14.137 | -0.189 | 0.840 | 14.052 | -0.203 | 0.955 | 13.345 | -0.464 | 2.408 |
| 13.764 | -0.224 | 1.142 | 12.497 | 0.548 | 2.468 | 13.165 | -0.278 | 2.839 | 10.332 | 0.097 | 0.267 |
| 12.763 | 0.235 | 3.885 | 14.754 | -0.113 | 0.464 | 12.624 | 0.089 | 3.027 | 12.865 | -1.276 | 2.962 |
| 12.537 | 1.106 | 2.840 | 12.611 | 0.423 | 4.064 | 11.918 | 0.403 | 1.363 | 11.767 | 0.495 | 1.362 |
| 11.147 | 0.362 | 0.769 | 11.535 | 0.267 | 0.948 | 10.463 | 0.170 | 0.305 | 10.796 | 0.147 | 0.521 |
| 14.624 | -0.202 | 1.152 | 10.318 | 0.114 | 0.313 | 13.739 | -0.478 | 1.251 | 13.903 | -0.350 | 1.273 |
| 13.458 | -0.585 | 1.782 | 13.620 | -0.201 | 1.401 | 12.546 | -0.292 | 3.551 | 13.627 | -0.418 | 1.517 |
| 12.274 | 0.204 | 2.603 | 13.197 | -0.032 | 2.170 | 10.398 | 0.162 | 0.275 | 12.847 | -0.841 | 3.213 |
| 13.822 | -0.335 | 1.299 | 12.556 | 0.044 | 1.767 | 12.671 | 0.919 | 5.288 | 11.591 | 0.191 | 0.949 |
| 11.754 | 0.293 | 1.163 | 10.910 | 0.337 | 0.562 | 9.712 | 0.082 | 0.115 | 10.005 | 0.137 | 0.303 |

(Z/D) = 15.34 ( ℄ = 12.745 cm)

| r' (cm) | $V_r$ (cm/sec) | $V_z$ (cm/sec) | r' (cm) | $V_r$ (cm/sec) | $V_z$ (cm/sec) | r' (cm) | $V_r$ (cm/sec) | $V_z$ (cm/sec) | r' (cm) | $V_r$ (cm/sec) | $V_z$ (cm/sec) |
|---|---|---|---|---|---|---|---|---|---|---|---|
| 13.471 | -0.465 | 0.912 | 13.105 | -0.154 | 5.760 | 13.277 | -0.299 | 3.425 | 12.267 | 0.148 | 2.032 |
| 13.180 | -0.243 | 3.836 | 12.889 | -0.712 | 24.070 | 13.025 | 0.393 | 10.045 | 13.399 | 0.053 | 3.096 |
| 12.682 | 0.850 | 19.025 | 12.522 | 0.324 | 6.729 | 12.289 | 0.220 | 2.995 | 12.642 | 0.640 | 10.068 |
| 11.796 | -0.235 | 0.563 | 12.079 | -0.012 | 1.903 | 11.672 | -0.028 | 0.702 | 13.570 | -0.099 | 1.528 |
| 12.971 | -0.482 | 19.095 | 13.451 | 0.008 | 2.046 | 13.127 | -0.477 | 5.538 | 13.024 | 0.058 | 8.646 |
| 13.009 | 0.364 | 11.003 | 12.625 | 1.712 | 15.191 | 12.708 | 1.768 | 24.915 | 12.217 | -0.189 | 1.810 |
| 12.257 | 0.203 | 2.673 | 12.059 | -0.367 | 1.416 | 13.126 | -0.405 | 4.474 | 11.669 | -0.779 | 0.666 |
| 12.850 | 0.362 | 14.177 | 13.147 | -0.365 | 4.224 | 11.752 | 0.007 | 1.192 | 13.070 | -0.030 | 6.547 |
| 10.719 | -0.196 | 0.114 | 12.277 | 0.086 | 3.276 | 13.443 | 0.005 | 1.192 | 11.975 | -0.099 | 1.296 |
| 12.690 | 0.498 | 17.161 | 13.147 | -0.365 | 4.224 | 13.069 | 0.086 | 3.276 | 12.277 | -0.030 | 6.547 |

### TABLE E.29

### RADIAL AND AXIAL VELOCITIES - DIGITIZER METHOD, Q=1.906 cm$^3$/sec
### 0.20 cm I.D. CAPILLARY TUBE, LARGE RESERVOIR

(Z/D) = 31.20 (℄ = 12.745 cm)

| r' (cm) | $V_r$ (cm/sec) | $V_z$ (cm/sec) | r' (cm) | $V_r$ (cm/sec) | $V_z$ (cm/sec) | r' (cm) | $V_r$ (cm/sec) | $V_z$ (cm/sec) | r' (cm) | $V_r$ (cm/sec) | $V_z$ (cm/sec) |
|---|---|---|---|---|---|---|---|---|---|---|---|
| 14.343 | -0.407 | 0.719 | 13.511 | -0.577 | 1.959 | 13.870 | -0.516 | 1.623 | 13.080 | 0.062 | 2.670 |
| 13.640 | -0.417 | 1.697 | 12.595 | 0.415 | 4.566 | 13.241 | -0.441 | 2.586 | 12.541 | 0.684 | 4.609 |
| 13.075 | 0.094 | 2.778 | 12.252 | 0.739 | 3.828 | 12.071 | 0.627 | 1.796 | 12.043 | 0.380 | 3.391 |
| 11.794 | 0.467 | 1.489 | 10.956 | 0.304 | 0.613 | 11.539 | 0.778 | 1.213 | 14.217 | -0.155 | 1.437 |
| 10.623 | 0.106 | 1.439 | 13.448 | -0.310 | 1.558 | 9.502 | 0.101 | 0.307 | 12.973 | -0.876 | 5.208 |
| 9.914 | 0.032 | 0.289 | 12.792 | -0.709 | 5.283 | 14.314 | -0.204 | 0.697 | 12.176 | 1.068 | 3.123 |
| 14.020 | -0.057 | 0.870 | 11.697 | 0.473 | 1.293 | 13.579 | -0.256 | 1.986 | 10.414 | 0.228 | 0.615 |
| 12.781 | 0.547 | 6.064 | 14.261 | -0.305 | 0.704 | 12.700 | -0.318 | 5.578 | 13.036 | -0.064 | 3.877 |
| 12.562 | 0.702 | 4.039 | 12.991 | -0.189 | 3.482 | 12.329 | 0.780 | 3.027 | 12.825 | -0.252 | 5.971 |
| 12.265 | 0.446 | 2.254 | 12.543 | 0.286 | 4.704 | 11.563 | 0.544 | 1.118 | 12.113 | 0.217 | 2.763 |
| 11.459 | 0.678 | 1.175 | 12.044 | 0.498 | 1.685 | 12.820 | -0.391 | 5.772 | 11.768 | 0.369 | 1.415 |
| 13.792 | -0.239 | 1.417 | 11.585 | 0.324 | 1.218 | 13.585 | -0.206 | 1.898 | 13.851 | -0.396 | 0.933 |
| 12.935 | -0.083 | 4.552 | 13.548 | -0.434 | 2.408 | 12.444 | 1.031 | 3.264 | 13.395 | -0.316 | 2.108 |
| 12.389 | 0.378 | 3.710 | 12.963 | -0.632 | 4.787 | 12.320 | 0.281 | 3.530 | 12.670 | 0.418 | 5.953 |
| 11.840 | 0.456 | 1.969 | 12.330 | 1.242 | 4.160 | 11.615 | 0.358 | 1.183 | 12.234 | 0.939 | 4.116 |
| 11.189 | 0.180 | 0.876 | 12.054 | 0.879 | 2.514 | 10.166 | 0.105 | 0.309 | 12.062 | 0.945 | 2.587 |
| 9.922 | 0.092 | 0.228 | 10.862 | 0.203 | 0.622 | 9.818 | 0.121 | 0.248 | 10.096 | 0.085 | 0.277 |
| 13.190 | 0.353 | 3.354 | 13.643 | -0.479 | 1.150 | 12.851 | 0.177 | 4.915 | 13.360 | -0.295 | 2.412 |
| 12.537 | 0.298 | 5.487 | 12.252 | 0.782 | 3.968 | 10.197 | 0.125 | 0.304 | 11.896 | 0.333 | 1.573 |
| 12.292 | 1.359 | 3.593 | 11.367 | 0.399 | 0.970 | 12.021 | 0.774 | 2.084 | 14.009 | -0.524 | 1.410 |
| 11.907 | 0.435 | 1.470 | 13.357 | -0.531 | 2.371 | 12.660 | 0.194 | 5.271 | 12.972 | -0.312 | 4.440 |
| 12.532 | 0.486 | 5.706 | 12.906 | -0.084 | 4.766 | 12.288 | 0.244 | 2.177 | 12.784 | 0.049 | 6.228 |
| 12.141 | 0.668 | 2.135 | 12.367 | 1.106 | 3.763 | 12.047 | 0.722 | 2.012 | 12.211 | 1.321 | 2.559 |
| 10.493 | 0.137 | 0.338 | 11.137 | 0.299 | 0.897 | 11.127 | 0.352 | 1.006 | 10.168 | 0.157 | 0.247 |
| 14.510 | -0.173 | 0.769 | 13.272 | -0.795 | 2.115 | 14.020 | -0.276 | 0.846 | 13.059 | -0.382 | 4.509 |
| 12.854 | -0.241 | 1.455 | 11.893 | 0.460 | 1.862 | 13.050 | -0.052 | 0.657 | 11.013 | 0.294 | 0.719 |
| 13.332 | -0.257 | 1.986 | 14.053 | -0.183 | 1.223 | 13.261 | -0.516 | 2.832 | 11.978 | 0.692 | 1.992 |
| 12.904 | -0.265 | 6.376 | 12.805 | 0.364 | 5.560 | 12.607 | 0.548 | 4.676 | 12.550 | 0.492 | 5.848 |
| 11.501 | 0.440 | 1.186 | 12.504 | 0.393 | 5.098 | 10.677 | 0.162 | 0.625 | | | |

TABLE E.29 (continued)

(Z/D) = 15.60 ( ℄ = 12.745 cm)

| r' (cm) | $V_r$ (cm/sec) | $V_z$ (cm/sec) | r' (cm) | $V_r$ (cm/sec) | $V_z$ (cm/sec) | r' (cm) | $V_r$ (cm/sec) | $V_z$ (cm/sec) | r' (cm) | $V_r$ (cm/sec) | $V_z$ (cm/sec) |
|---|---|---|---|---|---|---|---|---|---|---|---|
| 13.082 | -0.030 | 6.155 | 13.095 | -0.406 | 9.881 | 12.750 | 0.249 | 26.017 | 12.963 | -1.037 | 15.663 |
| 12.407 | 0.852 | 6.001 | 12.765 | 0.874 | 29.700 | 11.943 | 0.293 | 1.040 | 12.626 | 1.235 | 14.053 |
| 11.680 | -0.243 | 0.883 | 12.602 | 1.178 | 13.696 | 13.283 | 0.012 | 4.804 | 12.373 | 0.272 | 3.764 |
| 13.024 | -0.479 | 13.473 | 12.291 | 0.179 | 2.104 | 12.593 | 0.618 | 11.508 | 12.231 | 0.114 | 2.996 |
| 12.354 | 0.499 | 4.282 | 13.105 | -0.107 | 8.614 | 12.230 | 0.285 | 1.914 | 12.651 | 0.706 | 17.810 |
| 12.155 | 0.102 | 1.350 | 12.616 | 0.707 | 14.669 | 13.440 | -0.008 | 1.637 | 12.464 | 0.572 | 5.078 |
| 13.341 | 0.019 | 1.922 | 12.381 | 0.569 | 3.965 | 12.940 | -0.400 | 17.175 | 11.958 | -0.170 | 1.312 |
| 12.250 | 0.178 | 2.993 | 13.980 | 0.266 | 0.790 | 12.144 | 0.529 | 1.792 | 13.806 | 0.161 | 1.588 |
| 13.139 | -0.189 | 7.396 | 11.836 | -0.228 | 0.955 | 13.097 | -0.003 | 6.725 | 12.058 | -0.005 | 1.494 |
| 12.930 | -0.258 | 19.349 | 13.593 | -0.301 | 1.868 | 12.669 | 1.145 | 19.919 | 13.352 | -0.036 | 2.703 |
| 12.492 | 0.445 | 6.856 | 12.438 | 0.771 | 5.464 | 12.020 | -0.008 | 1.619 | 12.208 | 0.432 | 2.893 |
| 11.955 | 0.001 | 1.281 | 12.132 | 0.249 | 1.808 | 11.845 | 0.079 | 0.856 | 13.277 | -0.152 | 3.483 |
| 11.156 | -0.953 | 0.448 | 12.995 | -0.878 | 14.004 | 13.257 | -0.169 | 5.475 | 12.656 | 0.576 | 15.313 |
| 12.948 | -0.261 | 23.667 | 12.427 | 0.996 | 4.898 | 12.628 | 1.140 | 9.919 | 12.321 | 0.202 | 2.816 |
| 12.325 | 0.215 | 3.487 | 12.101 | 0.128 | 1.675 | 13.190 | -0.309 | 6.396 | 11.978 | -0.172 | 1.544 |
| 12.207 | 0.122 | 1.711 | 11.671 | -0.416 | 0.968 | 12.048 | -0.021 | 1.649 | 13.847 | 0.176 | 0.984 |
| 11.041 | -0.714 | 0.327 | 13.462 | -0.363 | 1.540 | 11.598 | -0.200 | 0.528 | 12.646 | 0.975 | 11.306 |
| 12.909 | 0.040 | 28.253 | 13.424 | -0.573 | 2.683 | 13.532 | 0.049 | 2.100 | 13.300 | 0.369 | 2.749 |
| 13.312 | -0.213 | 2.282 | 13.148 | -0.107 | 6.829 | 13.198 | -0.572 | 4.142 | 13.000 | -0.205 | 13.099 |
| 13.098 | -0.619 | 8.595 | 12.829 | 0.990 | 40.480 | 12.386 | 0.263 | 5.735 | 12.548 | 1.096 | 9.035 |
| 11.739 | -0.216 | 0.493 | 12.157 | 0.213 | 1.733 | 11.703 | -0.172 | 0.520 | 11.879 | -0.192 | 0.902 |
| 11.531 | -0.241 | 0.640 | 12.096 | 0.214 | 1.827 | 12.261 | 0.510 | 2.504 |  |  |  |

## TABLE E.30

RADIAL AND AXIAL VELOCITIES - DIGITIZER METHOD, $Q=2.383\ cm^3/sec$
0.20 cm I.D. CAPILLARY TUBE, LARGE RESERVOIR

(Z/D) = 34.65 (℄ = 12.745 cm)

| r' (cm) | $V_r$ (cm/sec) | $V_z$ (cm/sec) | r' (cm) | $V_r$ (cm/sec) | $V_z$ (cm/sec) | r' (cm) | $V_r$ (cm/sec) | $V_z$ (cm/sec) | r' (cm) | $V_r$ (cm/sec) | $V_z$ (cm/sec) |
|---|---|---|---|---|---|---|---|---|---|---|---|
| 14.535 | -0.349 | 0.589 | 14.617 | -0.108 | 0.495 | 13.266 | -0.368 | 2.410 | 14.257 | -0.376 | 1.288 |
| 12.927 | -0.271 | 6.397 | 13.261 | -0.307 | 2.339 | 12.817 | -0.339 | 6.396 | 12.824 | -0.047 | 8.290 |
| 12.728 | -0.587 | 8.097 | 12.403 | 0.209 | 4.691 | 11.818 | 0.475 | 2.317 | 12.284 | 0.040 | 4.271 |
| 11.165 | 0.848 | 1.108 | 12.167 | 0.707 | 3.437 | 10.056 | 0.127 | 0.401 | 12.086 | 0.727 | 2.762 |
| 9.731 | 0.065 | 0.222 | 11.866 | 0.680 | 2.084 | 14.551 | -0.378 | 0.951 | 9.529 | 0.058 | 0.128 |
| 14.373 | -0.250 | 0.874 | 14.464 | -0.148 | 0.714 | 13.218 | -0.473 | 2.728 | 13.822 | -0.467 | 1.127 |
| 12.886 | -0.213 | 7.217 | 13.629 | -0.246 | 0.550 | 12.844 | 0.440 | 6.736 | 13.328 | -0.264 | 3.730 |
| 12.487 | 0.618 | 6.384 | 13.234 | -0.285 | 3.231 | 12.348 | 0.492 | 4.638 | 13.157 | -0.509 | 4.097 |
| 12.239 | 0.434 | 2.893 | 13.020 | -0.372 | 4.687 | 12.117 | 0.832 | 4.539 | 12.849 | -0.396 | 5.667 |
| 11.907 | 0.418 | 2.216 | 12.270 | 1.520 | 3.952 | 11.760 | 0.699 | 1.761 | 11.623 | 0.323 | 1.912 |
| 10.262 | 0.226 | 0.426 | 10.161 | 0.266 | 0.392 | 14.057 | -0.332 | 1.094 | 9.662 | 0.176 | 0.199 |
| 13.831 | -0.380 | 1.663 | 14.473 | -0.140 | 0.850 | 13.538 | -0.400 | 1.815 | 13.962 | -0.093 | 1.012 |
| 13.195 | -0.147 | 3.092 | 13.179 | -0.204 | 2.735 | 12.351 | 0.581 | 3.680 | 12.765 | 0.067 | 8.043 |
| 12.194 | 0.572 | 4.018 | 12.572 | 0.881 | 7.921 | 11.435 | 0.469 | 1.435 | 12.271 | 1.235 | 4.595 |
| 10.719 | 0.381 | 0.692 | 11.871 | 0.792 | 2.048 | 11.037 | 0.219 | 0.559 | 11.604 | 0.667 | 1.653 |
| 14.736 | -0.081 | 0.507 | 11.429 | 0.454 | 1.446 | 13.895 | -0.229 | 0.990 | 11.237 | 0.338 | 1.307 |
| 12.778 | -0.211 | 6.577 | 11.088 | 0.462 | 1.097 | 12.198 | 1.015 | 3.692 | 11.785 | 0.472 | 1.876 |
| 11.553 | 0.597 | 1.652 | 13.109 | -0.547 | 2.904 | 11.495 | 0.480 | 1.614 | 12.798 | -1.613 | 6.837 |
| 11.064 | 0.518 | 0.815 | 12.582 | 0.296 | 6.255 | 13.207 | -0.604 | 3.684 | 12.162 | 0.391 | 3.177 |
| 13.102 | -0.071 | 3.948 | 13.457 | -0.594 | 1.976 | 12.934 | -0.275 | 6.540 | 13.276 | 0.297 | 2.748 |
| 12.578 | 0.479 | 6.097 | 12.857 | -0.737 | 5.993 | 12.320 | 0.216 | 4.484 | 12.538 | 0.216 | 6.684 |
| 11.797 | 0.551 | 2.096 | 12.458 | 0.133 | 6.117 | 11.442 | 0.538 | 1.366 | 11.855 | 0.153 | 1.819 |
| 9.429 | 0.117 | 0.230 | 11.185 | 0.238 | 1.163 | 14.487 | -0.233 | 0.785 | 14.180 | -0.206 | 0.813 |
| 13.515 | -0.225 | 1.643 | 13.674 | -0.545 | 1.516 | 11.998 | 0.623 | 2.335 | 13.513 | -0.275 | 2.200 |
| 11.083 | 0.332 | 1.130 | 12.980 | -0.116 | 4.551 | 12.868 | 0.088 | 7.794 | 12.423 | 0.067 | 5.339 |
| 12.320 | 0.867 | 4.788 | 12.352 | 1.132 | 5.935 | 12.023 | 0.662 | 2.737 | 11.468 | 0.551 | 1.580 |
| 11.740 | 0.607 | 2.185 | 11.229 | 0.452 | 1.488 | 11.169 | 0.314 | 1.021 | 10.783 | 0.240 | 0.531 |
| 13.061 | -0.936 | 3.319 | 9.856 | 0.082 | 0.290 | 12.647 | 1.098 | 6.684 | 14.141 | -0.156 | 0.779 |

TABLE E.30 (continued)

(Z/D) = 34.65 ( ℄ = 12.745 cm)

| r' (cm) | $V_r$ (cm/sec) | $V_z$ (cm/sec) | r' (cm) | $V_r$ (cm/sec) | $V_z$ (cm/sec) | r' (cm) | $V_r$ (cm/sec) | $V_z$ (cm/sec) | r' (cm) | $V_r$ (cm/sec) | $V_z$ (cm/sec) |
|---|---|---|---|---|---|---|---|---|---|---|---|
| 12.138 | 0.437 | 3.771 | 13.425 | -0.403 | 1.990 | 11.762 | 0.545 | 1.670 | 13.204 | -0.644 | 3.968 |
| 9.827 | 0.159 | 0.451 | 12.918 | -0.097 | 3.698 | 9.518 | 0.141 | 0.324 | 12.318 | 0.789 | 4.646 |
| 11.633 | 0.602 | 1.492 | 12.098 | 0.465 | 2.859 | 11.695 | 0.468 | 1.471 | | | |

(Z/D) = 17.33 ( ℄ = 12.745 cm)

| r' (cm) | $V_r$ (cm/sec) | $V_z$ (cm/sec) | r' (cm) | $V_r$ (cm/sec) | $V_z$ (cm/sec) | r' (cm) | $V_r$ (cm/sec) | $V_z$ (cm/sec) | r' (cm) | $V_r$ (cm/sec) | $V_z$ (cm/sec) |
|---|---|---|---|---|---|---|---|---|---|---|---|
| 13.017 | -0.240 | 8.760 | 13.278 | -0.565 | 3.078 | 12.342 | -0.196 | 6.588 | 13.101 | 0.050 | 5.090 |
| 12.065 | 0.631 | 2.934 | 12.913 | 0.249 | 10.825 | 12.002 | -0.216 | 1.791 | 12.096 | 0.135 | 3.384 |
| 11.379 | 0.009 | 0.943 | 11.825 | -0.050 | 1.671 | 13.770 | 0.255 | 1.269 | 11.432 | -0.013 | 0.996 |
| 13.432 | -0.412 | 2.430 | 13.987 | 0.504 | 0.778 | 13.253 | -0.931 | 4.851 | 13.365 | -0.605 | 2.755 |
| 13.042 | -0.197 | 14.725 | 13.248 | -0.028 | 5.587 | 12.743 | 0.734 | 35.669 | 13.133 | -0.277 | 8.248 |
| 12.596 | 0.737 | 13.823 | 12.295 | 0.109 | 5.020 | 12.350 | 0.163 | 4.274 | 12.190 | 0.657 | 3.361 |
| 12.233 | 0.015 | 3.487 | 12.092 | -0.050 | 2.204 | 11.792 | -0.106 | 1.563 | 11.726 | -0.280 | 1.060 |
| 11.567 | -0.174 | 0.228 | 13.556 | -0.353 | 3.354 | 11.312 | -0.353 | 0.632 | 13.014 | -0.104 | 14.306 |
| 10.928 | -0.135 | 0.065 | 13.047 | -0.144 | 14.762 | 10.441 | -0.154 | 0.079 | 13.078 | 0.090 | 12.242 |
| 13.217 | -0.600 | 6.989 | 12.572 | 1.482 | 13.239 | 13.088 | -0.279 | 9.742 | 12.243 | 0.213 | 3.528 |
| 12.597 | 0.666 | 13.751 | 12.116 | 0.225 | 2.390 | 12.221 | -0.244 | 2.983 | 13.612 | -0.053 | 2.596 |
| 11.628 | -0.001 | 0.712 | 13.286 | 0.113 | 4.558 | 12.747 | 1.603 | 27.508 | 12.577 | 1.213 | 15.119 |
| 13.112 | -0.331 | 9.918 | 12.399 | 0.410 | 4.815 | 12.983 | 0.415 | 17.410 | 12.178 | -0.003 | 2.633 |
| 12.509 | 1.307 | 9.250 | 11.778 | -0.056 | 1.440 | 12.462 | 0.153 | 8.223 | 11.736 | -0.280 | 0.989 |
| 12.319 | 0.189 | 5.591 | 11.426 | -0.171 | 0.716 | 11.996 | -0.006 | 1.512 | 13.722 | -0.034 | 1.333 |
| 11.868 | -0.360 | 1.467 | 13.034 | -0.338 | 7.890 | 11.591 | -0.138 | 0.743 | 12.976 | -0.032 | 10.460 |
| 11.414 | -0.027 | 0.702 | 12.110 | -0.028 | 3.041 | 13.767 | 0.080 | 0.785 | 11.895 | -0.038 | 2.134 |
| 13.560 | -0.110 | 1.533 | 13.365 | -0.066 | 4.196 | 12.022 | 0.019 | 2.402 | 13.045 | -0.137 | 10.892 |
| 11.673 | -0.210 | 0.984 | 12.400 | 0.202 | 4.869 | 11.455 | -0.071 | 0.736 | 12.244 | -0.126 | 3.341 |
| 12.612 | 0.828 | 17.847 | 11.831 | 0.055 | 1.674 | 12.328 | 0.954 | 6.286 | 11.500 | 0.083 | 0.652 |
| 12.105 | -0.080 | 3.129 | 13.574 | -0.442 | 1.555 | 11.661 | -0.045 | 1.084 | 12.861 | -1.118 | 27.244 |
| 10.641 | -0.274 | 0.109 | 12.835 | 0.216 | 32.595 | 13.117 | -0.264 | 7.551 | 12.465 | 1.167 | 6.396 |
| 12.061 | -0.097 | 2.275 | 12.400 | 0.120 | 4.984 | 12.157 | -0.151 | 3.003 | 12.251 | 0.057 | 3.346 |
| 13.285 | -0.202 | 3.837 | 11.780 | -0.094 | 1.136 | 13.151 | -0.356 | 7.019 | 12.270 | -0.172 | 3.987 |
| 13.056 | -0.380 | 10.593 | 12.014 | 0.040 | 2.314 | 12.657 | 1.873 | 25.063 | 11.800 | -0.033 | 1.262 |
| 12.345 | 0.720 | 5.997 | 11.352 | -0.235 | 0.590 | | | | | | |

## TABLE E.31

### RADIAL AND AXIAL VELOCITIES - DIGITIZER METHOD, $Q=2.701\ cm^3/sec$
### 0.20 cm I.D. CAPILLARY TUBE, LARGE RESERVOIR

(Z/D) = 53.13 (℄ = 12.745 cm)

| r' (cm) | $V_r$ (cm/sec) | $V_z$ (cm/sec) | r' (cm) | $V_r$ (cm/sec) | $V_z$ (cm/sec) | r' (cm) | $V_r$ (cm/sec) | $V_z$ (cm/sec) | r' (cm) | $V_r$ (cm/sec) | $V_z$ (cm/sec) |
|---|---|---|---|---|---|---|---|---|---|---|---|
| 13.352 | -0.123 | 0.778 | 13.334 | -0.029 | 0.924 | 12.715 | -0.040 | 1.040 | 12.956 | 0.026 | 0.784 |
| 12.529 | -0.026 | 1.102 | 11.820 | 0.211 | 0.807 | 12.272 | 0.015 | 0.908 | 11.030 | 0.289 | 0.596 |
| 11.965 | 0.163 | 1.021 | 9.194 | 0.279 | 0.583 | 14.330 | -0.251 | 0.585 | 9.346 | 0.261 | 0.582 |
| 14.821 | -0.222 | 0.516 | 10.169 | 0.341 | 1.097 | 13.504 | -0.133 | 0.681 | 14.165 | -0.125 | 0.720 |
| 12.802 | 0.085 | 0.964 | 13.935 | -0.259 | 0.685 | 12.612 | -0.120 | 1.046 | 13.781 | -0.125 | 0.717 |
| 12.197 | 0.230 | 0.905 | 13.458 | -0.055 | 0.915 | 12.214 | 0.114 | 0.849 | 13.308 | -0.083 | 0.994 |
| 9.562 | 0.276 | 0.302 | 12.247 | 0.242 | 0.941 | 9.023 | 0.271 | 0.258 | 11.375 | 0.313 | 0.866 |
| 8.030 | 0.201 | 0.091 | 11.105 | 0.291 | 0.794 | 13.512 | -0.143 | 0.734 | 12.311 | -0.010 | 0.940 |
| 8.833 | 0.193 | 0.238 | 14.169 | -0.232 | 0.687 | 8.425 | 0.221 | 0.207 | 13.631 | -0.223 | 0.852 |
| 10.950 | 0.259 | 0.763 | 12.572 | 0.034 | 0.909 | 9.735 | 0.253 | 0.430 | 12.833 | -0.164 | 1.008 |
| 9.048 | 0.244 | 0.256 | 12.227 | 0.105 | 1.036 | 7.793 | 0.210 | 0.087 | | | |

(Z/D) = 35.42 (℄ = 12.745 cm)

| r' (cm) | $V_r$ (cm/sec) | $V_z$ (cm/sec) | r' (cm) | $V_r$ (cm/sec) | $V_z$ (cm/sec) | r' (cm) | $V_r$ (cm/sec) | $V_z$ (cm/sec) | r' (cm) | $V_r$ (cm/sec) | $V_z$ (cm/sec) |
|---|---|---|---|---|---|---|---|---|---|---|---|
| 14.456 | -0.341 | 2.710 | 14.455 | -0.306 | 0.613 | 14.177 | -0.287 | 1.306 | 13.362 | 0.005 | 3.096 |
| 14.101 | -0.305 | 1.341 | 13.795 | -0.115 | 3.697 | 13.486 | -0.667 | 2.395 | 13.072 | -0.326 | 3.975 |
| 13.130 | -0.665 | 4.958 | 13.013 | -0.382 | 5.789 | 13.033 | -0.088 | 4.019 | 12.835 | -0.111 | 8.366 |
| 12.974 | -0.390 | 4.826 | 12.577 | 0.715 | 8.492 | 12.909 | -0.298 | 5.932 | 12.464 | 0.633 | 6.781 |
| 12.523 | 0.349 | 8.414 | 12.226 | 0.764 | 5.295 | 12.069 | 0.738 | 3.624 | 11.989 | 0.960 | 3.873 |
| 11.993 | 0.736 | 2.805 | 11.634 | 0.664 | 1.978 | 11.355 | 0.541 | 1.302 | 11.559 | 0.504 | 1.692 |
| 11.144 | 0.494 | 1.639 | 11.246 | 0.412 | 1.418 | 10.752 | 0.121 | 0.788 | 11.054 | 0.444 | 1.473 |
| 10.363 | 0.313 | 0.879 | 10.358 | 0.457 | 1.055 | 14.456 | -0.242 | 0.668 | 9.659 | 0.117 | 0.280 |
| 14.396 | -0.152 | 0.991 | 9.574 | 0.114 | 0.291 | 13.727 | -0.189 | 1.577 | 9.026 | 0.079 | 0.171 |
| 13.149 | 0.677 | 3.902 | 14.814 | -0.396 | 0.743 | 13.023 | 0.110 | 5.663 | 14.550 | -0.147 | 0.885 |
| 12.956 | 0.142 | 4.738 | 13.521 | -0.569 | 2.417 | 12.495 | 2.839 | 8.817 | 13.443 | -0.294 | 3.834 |

TABLE E.31 (continued)

(Z/D) = 35.42 ( ℄ = 12.745 cm)

| r' (cm) | $V_r$ (cm/sec) | $V_z$ (cm/sec) | r' (cm) | $V_r$ (cm/sec) | $V_z$ (cm/sec) | r' (cm) | $V_r$ (cm/sec) | $V_z$ (cm/sec) | r' (cm) | $V_r$ (cm/sec) | $V_z$ (cm/sec) |
|---|---|---|---|---|---|---|---|---|---|---|---|
| 12.393 | 0.627 | 7.452 | 13.419 | -0.528 | 3.755 | 12.270 | 1.005 | 5.159 | 13.131 | -0.593 | 5.746 |
| 11.985 | 1.007 | 3.131 | 12.861 | 0.363 | 7.485 | 11.875 | 0.691 | 2.515 | 12.774 | 0.357 | 9.762 |
| 11.552 | 0.427 | 1.331 | 12.301 | 0.578 | 4.005 | 11.520 | 0.507 | 1.957 | 12.210 | 0.844 | 3.088 |
| 11.387 | 0.622 | 1.569 | 12.174 | 0.769 | 3.335 | 11.311 | 0.713 | 1.377 | 11.936 | 0.395 | 2.362 |
| 11.300 | 0.511 | 1.352 | 11.697 | 0.518 | 1.669 | 10.926 | 0.410 | 1.082 | 10.069 | 0.315 | 0.797 |
| 10.477 | 0.182 | 0.843 | 14.704 | -0.202 | 0.828 | 10.337 | 0.340 | 1.073 | 14.586 | 0.019 | 0.783 |
| 14.121 | -0.038 | 1.351 | 13.696 | -0.397 | 2.211 | 13.864 | 0.131 | 1.767 | 13.316 | -0.724 | 3.391 |
| 13.664 | -0.461 | 2.224 | 12.381 | 0.279 | 6.629 | 13.501 | -0.207 | 2.626 | 11.147 | 0.612 | 1.356 |
| 13.167 | -0.710 | 5.026 | 14.314 | -0.357 | 1.056 | 13.115 | 0.206 | 5.775 | 13.755 | -0.164 | 1.827 |
| 12.812 | -0.046 | 9.503 | 13.493 | 0.458 | 2.400 | 12.394 | 0.826 | 5.480 | 13.142 | -0.631 | 3.644 |
| 12.517 | 0.154 | 6.236 | 13.011 | -0.043 | 5.230 | 12.101 | 0.434 | 3.043 | 12.830 | -0.145 | 8.216 |
| 11.755 | 0.792 | 2.132 | 12.417 | 0.603 | 7.067 | 11.033 | 2.935 | 1.347 | 12.357 | 0.705 | 7.035 |
| 10.920 | 1.553 | 1.273 | 12.151 | 0.524 | 3.435 | 10.777 | 0.318 | 0.700 | 11.957 | 0.482 | 2.638 |
| 14.523 | -0.163 | 0.929 | 11.755 | 0.905 | 2.166 | 14.288 | -0.233 | 0.989 | 11.547 | 0.486 | 1.582 |
| 13.101 | -0.750 | 3.536 | 10.194 | 0.193 | 0.562 | 12.929 | -0.384 | 5.931 | 9.759 | 0.157 | 0.449 |
| 12.521 | 0.420 | 8.340 | 9.317 | 0.102 | 0.203 | 12.359 | 0.521 | 8.343 | 14.252 | -0.177 | 1.150 |
| 12.086 | 0.838 | 3.513 | 14.091 | -0.367 | 1.250 | 11.825 | 0.534 | 2.401 | 13.777 | -0.429 | 2.031 |
| 11.570 | 0.284 | 1.752 | 13.096 | -0.414 | 4.825 | 10.530 | 0.219 | 0.696 | 13.030 | -0.239 | 5.579 |
| 9.663 | 0.171 | 0.318 | 12.959 | -1.707 | 6.024 | 12.917 | -0.388 | 5.503 | 12.821 | -0.131 | 8.182 |
| 11.428 | 0.414 | 1.740 | 12.469 | 0.246 | 6.167 | 11.087 | 0.523 | 1.512 | 12.342 | 1.741 | 5.937 |
| 10.867 | 0.502 | 0.800 | 12.156 | 0.510 | 4.131 | 9.790 | 0.121 | 0.338 | 12.998 | 0.414 | 3.432 |
| 12.261 | -0.199 | 1.328 | 11.367 | 0.458 | 1.789 | 12.695 | -0.103 | 3.374 | 10.709 | 0.147 | 0.815 |
| 13.045 | 0.883 | 4.698 | 9.526 | 0.105 | 0.251 | 12.340 | 1.126 | 1.953 | 12.691 | -0.067 | 2.775 |
| 13.140 | -0.681 | 6.027 | 12.779 | -0.073 | 2.333 |  |  |  |  |  |  |

## TABLE E.31 (continued)

(Z/D) = 17.71 ( ℄ = 12.745 cm)

| r' (cm) | $V_r$ (cm/sec) | $V_z$ (cm/sec) | r' (cm) | $V_r$ (cm/sec) | $V_z$ (cm/sec) | r' (cm) | $V_r$ (cm/sec) | $V_z$ (cm/sec) | r' (cm) | $V_r$ (cm/sec) | $V_z$ (cm/sec) |
|---|---|---|---|---|---|---|---|---|---|---|---|
| 13.601 | 0.406 | 1.724 | 13.417 | 0.204 | 3.209 | 13.572 | 0.381 | 2.364 | 13.096 | 0.159 | 7.905 |
| 13.021 | 0.217 | 11.876 | 13.066 | 0.075 | 6.265 | 12.509 | -0.039 | 9.716 | 12.408 | 1.101 | 9.109 |
| 12.071 | 0.111 | 2.354 | 12.169 | 0.017 | 2.705 | 11.948 | 0.027 | 2.777 | 10.659 | -0.640 | 0.316 |
| 11.805 | 0.054 | 1.230 | 13.752 | 1.756 | 0.985 | 11.542 | -0.092 | 0.619 | 13.189 | 0.543 | 3.862 |
| 12.495 | 0.315 | 4.815 | 12.437 | 1.007 | 10.035 | 12.465 | 0.308 | 9.156 | 12.383 | 0.571 | 7.992 |
| 12.293 | -0.009 | 3.381 | 12.320 | 1.175 | 7.123 | 12.131 | 0.167 | 2.105 | 12.176 | 0.173 | 3.814 |
| 11.939 | -0.098 | 1.954 | 12.051 | -0.016 | 3.416 | 11.787 | -0.015 | 0.960 | 11.905 | 0.139 | 2.353 |
| 10.538 | -0.443 | 0.116 | 11.864 | -0.070 | 0.567 | 13.399 | -0.730 | 2.178 | 9.743 | -0.646 | 0.013 |
| 13.467 | -0.009 | 4.414 | 10.838 | -0.584 | 0.391 | 13.168 | -0.702 | 8.195 | 13.220 | 0.461 | 3.290 |
| 13.021 | -0.678 | 20.157 | 13.007 | -0.133 | 7.790 | 12.738 | -0.430 | 26.539 | 12.923 | -0.848 | 11.894 |
| 12.386 | -0.056 | 4.732 | 12.332 | 0.392 | 8.234 | 12.343 | 0.445 | 5.714 | 12.237 | 0.108 | 6.082 |
| 12.051 | 0.086 | 2.887 | 13.475 | -0.069 | 2.026 | 11.814 | -0.074 | 1.421 | 13.073 | -0.479 | 9.095 |
| 11.678 | -0.245 | 1.058 | 12.913 | 0.122 | 20.184 | 10.302 | -0.270 | 0.094 | 12.555 | 0.129 | 18.973 |
| 13.647 | 0.366 | 1.292 | 12.341 | 0.476 | 5.853 | 13.323 | -0.345 | 3.548 | 11.806 | -0.042 | 2.223 |
| 12.909 | 0.234 | 14.419 | 11.775 | -0.580 | 1.172 | 12.968 | -0.234 | 12.056 | 11.611 | -0.189 | 1.097 |
| 12.854 | -1.920 | 26.310 | 13.691 | 0.227 | 1.645 | 12.423 | 0.608 | 17.667 | 13.319 | 0.472 | 3.683 |
| 11.982 | -0.068 | 2.400 | 13.274 | -0.148 | 4.017 | 11.500 | -0.220 | 0.539 | 13.188 | 0.166 | 5.594 |
| 12.372 | 0.013 | 7.902 | 12.963 | -1.095 | 30.157 | 11.988 | 0.045 | 2.458 | 12.788 | 1.764 | 34.915 |
| 11.900 | 0.535 | 2.903 | 13.112 | 0.790 | 10.199 | 11.505 | -0.261 | 0.667 | 12.726 | -1.395 | 27.275 |
| 10.604 | -0.832 | 0.298 | 12.513 | 0.263 | 11.851 | 13.301 | 0.264 | 4.208 | 13.046 | 0.627 | 6.463 |
| 12.683 | 1.189 | 31.963 | 12.378 | 0.304 | 7.021 | 12.789 | -0.385 | 6.633 | 12.145 | 0.464 | 4.286 |
| 12.052 | 0.166 | 2.586 | 11.725 | -0.123 | 1.135 | 11.643 | -0.207 | 1.132 |  |  |  |

## TABLE E.32

### RADIAL AND AXIAL VELOCITIES - DIGITIZER METHOD, Q=3.177 cm$^3$/sec
### 0.20 cm I.D. CAPILLARY TUBE, LARGE RESERVOIR

(Z/D) = 54.78 (℄ = 12.745 cm)

| r' (cm) | $V_r$ (cm/sec) | $V_z$ (cm/sec) | r' (cm) | $V_r$ (cm/sec) | $V_z$ (cm/sec) | r' (cm) | $V_r$ (cm/sec) | $V_z$ (cm/sec) | r' (cm) | $V_r$ (cm/sec) | $V_z$ (cm/sec) |
|---|---|---|---|---|---|---|---|---|---|---|---|
| 14.296 | -0.433 | 0.854 | 11.926 | 0.124 | 1.038 | 13.620 | -0.249 | 1.102 | 9.387 | 0.422 | 0.584 |
| 13.399 | -0.166 | 0.989 | 8.133 | 0.508 | 0.401 | 12.438 | 0.193 | 1.227 | 9.756 | 0.386 | 0.721 |
| 12.309 | 0.245 | 1.381 | 15.011 | -0.547 | 1.103 | 10.077 | 0.508 | 0.798 | 14.072 | -0.220 | 0.769 |
| 14.235 | -0.226 | 0.614 | 13.684 | -0.099 | 1.091 | 13.717 | -0.100 | 0.842 | 9.358 | 0.522 | 0.486 |
| 13.173 | -0.133 | 1.054 | 14.197 | -0.241 | 0.733 | 12.982 | 0.069 | 1.053 | 12.089 | 0.267 | 0.775 |
| 12.452 | -0.029 | 0.987 | 15.514 | -0.500 | 0.644 | 14.428 | -0.303 | 0.837 | 13.948 | -0.250 | 0.890 |
| 13.511 | -0.140 | 1.009 | 13.494 | -0.073 | 0.887 | 12.575 | 0.042 | 1.096 | 13.386 | -0.060 | 0.763 |
| 12.057 | 0.171 | 1.030 | 13.014 | -0.099 | 0.904 | 10.910 | 0.381 | 0.614 | 12.361 | 0.102 | 0.947 |
| 9.824 | 0.663 | 0.912 | 10.199 | 0.522 | 0.963 | 14.219 | -0.321 | 0.725 | 13.057 | 0.034 | 0.856 |
| 13.940 | -0.350 | 0.860 | 12.632 | 0.301 | 1.382 | 13.629 | -0.280 | 0.791 | 14.557 | -0.346 | 0.866 |
| 13.265 | -0.046 | 1.093 | 13.817 | -0.180 | 0.794 | 13.006 | -0.171 | 1.053 | 12.243 | 0.325 | 1.097 |
| 12.537 | -0.022 | 1.120 | 11.281 | 0.212 | 0.719 | | | | | | |

(Z/D) = 36.52 (℄ = 12.745 cm)

| r' (cm) | $V_r$ (cm/sec) | $V_z$ (cm/sec) | r' (cm) | $V_r$ (cm/sec) | $V_z$ (cm/sec) | r' (cm) | $V_r$ (cm/sec) | $V_z$ (cm/sec) | r' (cm) | $V_r$ (cm/sec) | $V_z$ (cm/sec) |
|---|---|---|---|---|---|---|---|---|---|---|---|
| 14.369 | -0.126 | 0.974 | 14.404 | -0.197 | 0.863 | 13.961 | -0.088 | 3.289 | 14.107 | -0.267 | 1.110 |
| 13.915 | -0.345 | 1.374 | 13.739 | -0.227 | 2.144 | 13.844 | -0.181 | 1.897 | 13.487 | -0.059 | 3.161 |
| 13.531 | -0.504 | 2.328 | 13.405 | -1.072 | 4.511 | 13.416 | -0.354 | 3.581 | 13.260 | -0.095 | 3.770 |
| 13.315 | -0.714 | 4.100 | 13.146 | -0.908 | 6.191 | 13.163 | 0.055 | 5.093 | 13.002 | -0.140 | 7.969 |
| 13.158 | -0.775 | 5.557 | 12.653 | 0.051 | 8.227 | 12.933 | -0.079 | 6.654 | 12.384 | 0.546 | 6.930 |
| 12.793 | -0.139 | 9.678 | 12.172 | 0.750 | 4.554 | 12.653 | -0.422 | 8.384 | 12.107 | 0.554 | 4.403 |
| 12.127 | 0.393 | 3.897 | 11.786 | 0.534 | 1.732 | 12.656 | 0.117 | 8.011 | 11.376 | 0.540 | 1.572 |
| 11.340 | 0.689 | 1.685 | 10.583 | 0.141 | 0.789 | 10.929 | 0.249 | 0.901 | 9.519 | 0.155 | 0.497 |
| 10.635 | 0.040 | 0.785 | 9.158 | 0.071 | 0.280 | 10.285 | 0.176 | 0.541 | 14.703 | -0.185 | 0.812 |
| 14.483 | -0.321 | 0.895 | 14.624 | -0.262 | 1.156 | 14.055 | -0.259 | 1.467 | 14.219 | -0.475 | 3.348 |
| 13.976 | -0.206 | 1.861 | 13.884 | -0.346 | 1.607 | 13.960 | -0.223 | 1.861 | 13.611 | -0.733 | 3.390 |

TABLE E.32 (continued)

(Z/D) = 36.52 (℄ = 12.745 cm)

| r'(cm) | $V_r$(cm/sec) | $V_z$(cm/sec) | r'(cm) | $V_r$(cm/sec) | $V_z$(cm/sec) | r'(cm) | $V_r$(cm/sec) | $V_z$(cm/sec) | r'(cm) | $V_r$(cm/sec) | $V_z$(cm/sec) |
|---|---|---|---|---|---|---|---|---|---|---|---|
| 13.892 | -0.323 | 1.821 | 13.149 | -0.702 | 4.388 | 13.673 | -0.323 | 2.266 | 12.734 | 0.518 | 10.662 |
| 13.562 | -0.556 | 3.040 | 12.611 | -0.612 | 7.452 | 13.388 | -0.642 | 3.535 | 12.411 | 0.598 | 5.753 |
| 13.069 | -0.282 | 6.467 | 12.071 | 0.721 | 3.800 | 12.836 | -0.422 | 14.507 | 11.720 | 0.633 | 1.145 |
| 12.335 | 0.788 | 6.312 | 11.396 | 0.483 | 1.548 | 12.049 | 0.528 | 4.274 | 11.144 | 0.459 | 1.298 |
| 11.861 | 0.406 | 2.614 | 10.769 | 0.219 | 0.702 | 11.606 | 0.543 | 0.804 | 9.919 | 0.187 | 0.822 |
| 11.024 | 0.443 | 0.996 | 8.950 | 0.184 | 0.110 | 14.696 | -0.224 | 1.042 | 14.491 | -0.139 | 1.579 |
| 14.042 | -0.001 | 0.907 | 13.932 | -0.353 | 1.910 | 13.878 | -0.150 | 1.311 | 13.567 | -0.251 | 3.372 |
| 13.679 | -0.646 | 1.934 | 13.202 | -0.397 | 3.688 | 13.193 | -1.738 | 4.140 | 12.983 | -0.113 | 6.224 |
| 13.159 | -0.718 | 5.704 | 13.061 | -0.722 | 8.232 | 12.988 | -0.275 | 7.393 | 12.757 | 0.146 | 12.426 |
| 12.120 | 0.617 | 3.401 | 12.333 | 1.041 | 5.089 | 11.589 | 0.352 | 1.437 | 12.066 | 1.095 | 4.486 |
| 11.364 | 0.737 | 1.522 | 11.939 | 0.920 | 4.658 | 11.030 | 0.336 | 0.956 | 11.378 | 0.264 | 1.646 |
| 10.064 | 0.240 | 0.907 | 10.926 | 0.240 | 1.052 | 9.631 | 0.205 | 0.439 | 10.884 | 0.234 | 0.800 |
| 9.165 | 0.102 | 0.255 | 10.283 | 0.154 | 0.579 | 14.104 | -0.594 | 1.828 | 10.048 | 0.104 | 0.407 |
| 13.379 | -0.018 | 0.462 | 9.452 | 0.107 | 0.597 | 13.314 | -0.468 | 5.962 | 14.596 | -0.122 | 0.529 |
| 14.593 | -0.243 | 0.917 | 14.202 | -0.200 | 1.220 | 13.932 | -0.213 | 2.270 | 14.069 | -0.197 | 1.594 |
| 13.684 | -0.068 | 1.991 | 13.917 | -0.448 | 4.079 | 13.633 | -0.479 | 2.155 | 13.618 | -0.450 | 2.316 |
| 13.415 | -0.455 | 3.899 | 13.365 | -0.160 | 4.087 | 13.276 | -0.228 | 3.694 | 13.255 | -0.237 | 4.333 |
| 13.189 | -0.011 | 5.231 | 13.148 | -0.274 | 6.147 | 12.786 | 0.175 | 7.693 | 12.958 | -0.170 | 6.935 |
| 12.327 | 1.095 | 3.525 | 12.534 | 0.499 | 7.103 | 12.170 | 1.588 | 3.898 | 12.652 | -0.039 | 13.098 |
| 12.023 | 0.650 | 3.133 | 12.708 | 0.222 | 8.160 | 11.900 | 0.580 | 2.280 | 12.131 | 0.316 | 3.145 |
| 10.864 | 0.219 | 0.705 | 11.943 | 0.755 | 1.418 | 14.499 | -0.255 | 1.005 | 11.635 | 0.535 | 2.726 |
| 13.684 | -0.231 | 2.697 | 11.227 | 0.410 | 0.746 | 13.433 | -0.382 | 3.154 | 11.036 | 0.250 | 0.674 |
| 13.233 | -0.606 | 5.673 | 10.371 | 0.119 | 0.545 | 13.186 | -0.573 | 5.674 | 12.747 | 0.366 | 11.011 |
| 12.966 | -0.100 | 18.042 | 12.659 | 0.319 | 10.084 | 12.172 | 0.295 | 4.067 | 12.807 | -1.006 | 10.883 |
| 11.706 | 0.322 | 2.343 | 12.639 | 0.629 | 9.701 | 10.927 | 0.485 | 1.067 | 12.397 | 0.406 | 5.897 |
| 10.721 | 0.294 | 0.749 | 13.200 | -0.742 | 4.893 | 10.358 | 0.267 | 0.561 | 12.539 | 0.615 | 6.946 |
| 10.326 | 0.125 | 0.449 | 13.057 | -0.304 | 6.454 | 13.264 | -0.506 | 4.814 | 13.037 | -0.189 | 6.583 |
| 12.124 | 0.522 | 4.355 | | | | | | | | | |

TABLE E.32 (continued)

(Z/D) = 18.26 ( ℄ = 12.745 cm)

| r'(cm) | $V_r$(cm/sec) | $V_z$(cm/sec) | r'(cm) | $V_r$(cm/sec) | $V_z$(cm/sec) | r'(cm) | $V_r$(cm/sec) | $V_z$(cm/sec) | r'(cm) | $V_r$(cm/sec) | $V_z$(cm/sec) |
|---|---|---|---|---|---|---|---|---|---|---|---|
| 13.510 | -2.889 | 2.014 | 13.397 | -0.115 | 2.274 | 13.455 | -0.649 | 6.559 | 13.169 | 0.105 | 4.634 |
| 13.347 | 0.173 | 4.707 | 13.038 | 0.097 | 7.160 | 13.270 | -0.485 | 4.287 | 12.916 | -0.668 | 14.746 |
| 13.163 | 0.834 | 5.732 | 12.007 | -0.151 | 3.281 | 13.016 | -0.632 | 11.330 | 11.848 | -0.209 | 2.501 |
| 12.378 | -0.029 | 8.685 | 11.695 | 0.095 | 1.713 | 12.279 | 0.063 | 4.916 | 11.574 | -0.122 | 1.259 |
| 11.799 | 0.037 | 1.515 | 11.118 | -0.840 | 1.068 | 11.627 | -0.165 | 0.705 | 13.725 | 0.051 | 1.746 |
| 11.559 | 0.068 | 1.195 | 13.474 | 0.459 | 2.118 | 13.821 | 0.234 | 1.432 | 13.425 | -0.203 | 1.772 |
| 13.234 | 0.006 | 4.859 | 13.110 | -0.355 | 6.607 | 12.241 | 0.352 | 6.028 | 12.551 | 0.186 | 18.908 |
| 11.643 | 0.093 | 1.587 | 11.226 | -0.142 | 0.585 | 11.589 | -0.167 | 1.329 | 10.857 | -0.662 | 0.437 |
| 11.494 | -0.093 | 1.005 | 14.033 | 0.328 | 1.257 | 13.308 | -0.205 | 3.425 | 13.757 | 0.096 | 1.623 |
| 13.217 | -0.087 | 7.472 | 11.832 | 0.205 | 1.893 | 12.948 | -0.699 | 24.107 | 13.872 | 0.179 | 1.275 |
| 12.556 | 0.448 | 14.576 | 13.639 | 0.077 | 2.191 | 12.324 | 0.069 | 4.310 | 13.574 | 0.178 | 3.191 |
| 12.932 | -0.157 | 16.935 | 12.399 | 0.336 | 6.952 | 12.346 | 0.158 | 7.443 | 11.9[illegible]5 | -0.206 | 2.057 |
| 12.318 | 0.688 | 7.746 | 11.262 | -0.315 | 0.327 | 12.053 | -0.132 | 3.835 | 12.683 | 1.629 | 28.922 |
| 11.772 | -0.107 | 1.687 | 12.908 | -0.756 | 18.212 | 12.629 | 1.110 | 32.112 | 12.588 | 0.886 | 30.163 |
| 12.620 | 2.014 | 37.604 | 12.379 | 0.189 | 9.402 | | | | | | |

### TABLE E.33

### RADIAL AND AXIAL VELOCITIES - DIGITIZER METHOD, Q=3.812 $cm^3/sec$
### 0.20 cm I.D. CAPILLARY TUBE, LARGE RESERVOIR

(Z/D) = 56.17 ( ℄ = 12.745 cm)

| r' (cm) | $V_r$ (cm/sec) | $V_z$ (cm/sec) | r' (cm) | $V_r$ (cm/sec) | $V_z$ (cm/sec) | r' (cm) | $V_r$ (cm/sec) | $V_z$ (cm/sec) | r' (cm) | $V_r$ (cm/sec) | $V_z$ (cm/sec) |
|---|---|---|---|---|---|---|---|---|---|---|---|
| 13.562 | -0.117 | 1.016 | 13.299 | -0.035 | 1.244 | 11.820 | 0.156 | 0.955 | 12.157 | 0.235 | 0.681 |
| 11.091 | 0.359 | 0.927 | 11.508 | 0.106 | 1.095 | 13.362 | -0.276 | 0.948 | 12.939 | 0.075 | 1.115 |
| 13.097 | -0.166 | 1.055 | 12.445 | -0.042 | 1.289 | 12.365 | 0.223 | 1.184 | 12.404 | 0.079 | 1.166 |
| 11.980 | 0.082 | 0.911 | 11.992 | 0.325 | 1.187 | 11.582 | 0.174 | 1.146 | 13.293 | -0.253 | 1.289 |
| 14.110 | -0.342 | 1.001 | 12.646 | -0.084 | 1.296 | 12.507 | 0.136 | 1.477 | 12.194 | 0.095 | 1.309 |
| 11.431 | 0.372 | 0.869 | 11.337 | 0.259 | 1.140 | 12.368 | 0.161 | 1.108 | 12.889 | -0.012 | 1.121 |
| 11.022 | 0.426 | 0.978 | 12.298 | 0.136 | 1.074 | 11.324 | 0.311 | 1.063 | 11.954 | 0.317 | 1.330 |

(Z/D) = 38.78 ( ℄ = 12.745 cm)

| r' (cm) | $V_r$ (cm/sec) | $V_z$ (cm/sec) | r' (cm) | $V_r$ (cm/sec) | $V_z$ (cm/sec) | r' (cm) | $V_r$ (cm/sec) | $V_z$ (cm/sec) | r' (cm) | $V_r$ (cm/sec) | $V_z$ (cm/sec) |
|---|---|---|---|---|---|---|---|---|---|---|---|
| 13.485 | -0.287 | 2.253 | 14.096 | -0.274 | 1.058 | 12.957 | -0.416 | 4.861 | 13.916 | -0.254 | 1.450 |
| 12.552 | 0.784 | 11.562 | 13.684 | -0.218 | 1.380 | 12.284 | 0.435 | 10.054 | 13.431 | -0.084 | 2.382 |
| 12.220 | 0.669 | 10.134 | 13.326 | -0.022 | 1.566 | 11.611 | 0.702 | 2.909 | 13.083 | -0.498 | 5.464 |
| 11.196 | 0.602 | 1.500 | 12.828 | 0.434 | 7.604 | 10.748 | 0.418 | 1.474 | 11.773 | 0.582 | 2.618 |
| 10.581 | 0.335 | 1.205 | 11.701 | 0.612 | 3.492 | 14.071 | 0.050 | 1.284 | 10.853 | 0.362 | 1.223 |
| 13.666 | -0.467 | 2.384 | 13.530 | -0.203 | 3.053 | 12.491 | 0.742 | 9.286 | 13.229 | -0.250 | 4.688 |
| 11.601 | 0.462 | 2.780 | 12.822 | 0.236 | 8.694 | 10.982 | 0.623 | 1.289 | 12.211 | 1.058 | 7.552 |
| 13.964 | -0.117 | 1.811 | 11.718 | 1.008 | 3.600 | 13.670 | -0.236 | 1.806 | 11.520 | 0.969 | 2.282 |
| 13.539 | -0.282 | 2.586 | 11.436 | 0.582 | 2.181 | 12.916 | -1.100 | 7.788 | 11.187 | 0.630 | 2.036 |
| 12.598 | 0.239 | 8.124 | 10.799 | 0.039 | 1.068 | 12.264 | 1.242 | 7.521 | 14.043 | -0.261 | 0.927 |
| 11.986 | 1.507 | 6.712 | 13.930 | -0.234 | 1.682 | 11.357 | 0.612 | 2.550 | 13.815 | -0.072 | 1.724 |
| 11.096 | 0.606 | 1.446 | 13.598 | -0.142 | 2.426 | 10.880 | 0.416 | 1.200 | 13.236 | -0.100 | 1.242 |
| 10.673 | 0.400 | 0.786 | 12.709 | 0.116 | 10.042 | 10.178 | 0.154 | 0.694 | 12.647 | 0.618 | 11.023 |
| 13.513 | -0.246 | 1.984 | 12.173 | 1.706 | 7.364 | 13.100 | -0.120 | 4.800 | 11.969 | 0.914 | 5.161 |
| 12.980 | 0.120 | 6.447 | 11.767 | 1.149 | 4.316 | 12.660 | 1.986 | 9.651 | 11.683 | 0.700 | 4.583 |
| 12.465 | -0.750 | 11.432 | 11.546 | 0.432 | 2.366 | 12.282 | 0.635 | 10.527 | 11.443 | 0.314 | 2.344 |

TABLE E.33 (continued)

(Z/D) = 38.78 ( ℄ = 12.745 cm)

| r' (cm) | $V_r$ (cm/sec) | $V_z$ (cm/sec) | r' (cm) | $V_r$ (cm/sec) | $V_z$ (cm/sec) | r' (cm) | $V_r$ (cm/sec) | $V_z$ (cm/sec) | r' (cm) | $V_r$ (cm/sec) | $V_z$ (cm/sec) |
|---|---|---|---|---|---|---|---|---|---|---|---|
| 12.206 | 0.999 | 9.828 | 11.172 | 0.412 | 1.992 | 12.056 | 1.287 | 5.959 | 10.516 | 0.433 | 0.818 |
| 11.896 | 0.840 | 3.883 | 11.727 | 0.058 | 4.946 | 14.481 | -0.027 | 1.013 | 11.657 | 0.729 | 3.375 |
| 13.630 | -0.008 | 2.170 | 11.394 | 0.591 | 2.479 | 13.274 | -0.454 | 3.774 | 11.246 | 0.557 | 1.748 |
| 12.507 | 0.380 | 9.844 | 10.447 | 0.349 | 0.856 | 12.339 | 0.812 | 8.532 | 14.091 | -0.175 | 1.453 |
| 12.173 | 0.932 | 8.040 | 13.600 | -0.368 | 2.068 | 11.935 | 1.028 | 4.378 | 13.057 | -0.180 | 5.510 |
| 11.738 | 1.203 | 3.212 | 13.019 | 0.024 | 6.300 | 11.566 | 0.894 | 2.896 | 12.560 | 0.316 | 12.684 |
| 11.474 | 0.460 | 2.258 | 12.267 | 2.248 | 9.912 | 11.270 | 0.434 | 2.026 | 11.905 | 0.874 | 3.916 |
| 10.545 | 0.415 | 0.992 | 11.857 | 0.860 | 4.768 | 10.443 | 0.414 | 0.940 | 11.704 | 0.462 | 3.311 |
| 14.186 | -0.333 | 0.825 | 11.497 | 0.524 | 2.583 | 13.676 | -0.315 | 1.962 | 12.907 | 0.240 | 6.182 |
| 13.340 | -0.264 | 3.157 | 12.826 | -0.626 | 6.065 | 13.131 | -0.252 | 4.476 | 12.618 | 0.133 | 9.014 |
| 13.007 | -0.468 | 4.787 | 13.000 | -0.493 | 5.322 | 12.782 | 0.340 | 10.587 | 12.656 | 0.520 | 8.190 |
| 12.023 | 0.762 | 5.262 | 13.040 | -0.287 | 4.470 | 11.213 | 0.480 | 2.318 | 12.583 | 1.352 | 10.146 |
| 11.009 | 0.278 | 1.453 | 13.104 | -0.051 | 5.837 | 10.109 | 0.204 | 0.661 | 12.640 | -0.146 | 8.503 |
| 12.358 | 0.643 | 10.783 | | | | | | | | | |

(Z/D) = 19.39 ( ℄ = 12.745 cm)

| r' (cm) | $V_r$ (cm/sec) | $V_z$ (cm/sec) | r' (cm) | $V_r$ (cm/sec) | $V_z$ (cm/sec) | r' (cm) | $V_r$ (cm/sec) | $V_z$ (cm/sec) | r' (cm) | $V_r$ (cm/sec) | $V_z$ (cm/sec) |
|---|---|---|---|---|---|---|---|---|---|---|---|
| 12.976 | -0.133 | 6.568 | 13.591 | -0.131 | 3.270 | 13.232 | -0.056 | 2.126 | 13.372 | -0.506 | 3.366 |
| 13.525 | -0.061 | 1.042 | 12.226 | 0.612 | 3.264 | 11.878 | 0.037 | 0.666 | 12.007 | 0.500 | 2.446 |
| 11.806 | 0.127 | 0.823 | 11.587 | 0.054 | 1.604 | 11.496 | -0.001 | 0.617 | 11.256 | -0.527 | 0.922 |
| 11.327 | -0.148 | 0.955 | 13.657 | -0.386 | 1.676 | 13.098 | -0.537 | 7.452 | 13.056 | -0.026 | 5.906 |
| 12.999 | -1.492 | 10.589 | 12.872 | -0.314 | 20.241 | 12.209 | 0.270 | 6.630 | 11.937 | 0.484 | 4.076 |
| 12.157 | 1.183 | 0.591 | 11.602 | 0.014 | 1.816 | 12.004 | 0.031 | 4.806 | 11.502 | -0.041 | 1.066 |
| 11.931 | 0.559 | 3.259 | 11.275 | -0.286 | 0.843 | 11.863 | 0.125 | 2.620 | 13.033 | 0.413 | 8.881 |
| 11.762 | -0.240 | 2.161 | 12.072 | 0.105 | 5.452 | 11.612 | 0.209 | 1.545 | 11.964 | 0.423 | 3.147 |
| 11.378 | -0.216 | 1.309 | 11.890 | 0.003 | 3.097 | 13.035 | 0.576 | 7.320 | 11.450 | -0.738 | 1.076 |
| 12.329 | 1.274 | 12.401 | 13.809 | 0.204 | 1.681 | 12.082 | 0.402 | 5.284 | 13.210 | -0.492 | 3.966 |
| 11.604 | 0.080 | 1.444 | 12.935 | 0.766 | 13.236 | 13.293 | -1.065 | 3.009 | 12.282 | 0.870 | 11.424 |
| 13.218 | -0.288 | 5.600 | 12.069 | 0.586 | 6.530 | 12.368 | 1.266 | 11.725 | 11.772 | 0.054 | 3.811 |

## TABLE E.33 (continued)

(Z/D) = 19.39 (℄ = 12.745 cm)

| r' (cm) | $V_r$ (cm/sec) | $V_z$ (cm/sec) | r' (cm) | $V_r$ (cm/sec) | $V_z$ (cm/sec) | r' (cm) | $V_r$ (cm/sec) | $V_z$ (cm/sec) | r' (cm) | $V_r$ (cm/sec) | $V_z$ (cm/sec) |
|---|---|---|---|---|---|---|---|---|---|---|---|
| 12.229 | 0.384 | 7.247 | 11.578 | -0.011 | 2.011 | 12.077 | 0.080 | 3.136 | 11.401 | -0.198 | 1.185 |
| 11.870 | 0.270 | 2.609 | 12.172 | 0.112 | 5.450 | 11.814 | 0.015 | 2.653 | 11.879 | 0.271 | 2.890 |
| 11.603 | 0.230 | 1.468 | 11.525 | -0.082 | 1.581 | 11.417 | 0.027 | 1.051 | 11.342 | -0.224 | 0.916 |
| 11.216 | -0.253 | 0.703 | 12.911 | -1.302 | 13.464 | 13.052 | 0.312 | 9.685 | 12.843 | 0.711 | 16.738 |
| 12.816 | 1.821 | 35.758 | 12.785 | 3.194 | 32.654 | 12.954 | -0.403 | 12.581 | 12.701 | 4.394 | 46.882 |
| 12.160 | 1.104 | 8.384 | 12.213 | 0.958 | 10.641 | 12.996 | -1.211 | 9.614 | 12.713 | 3.074 | 51.158 |
| 12.941 | -0.635 | 15.158 | 12.278 | 0.132 | 7.179 | | | | | | |

## TABLE E.34

### RADIAL AND AXIAL VELOCITIES - DIGITIZER METHOD, Q=4.866 cm$^3$/sec
### 0.20 cm I.D. CAPILLARY TUBE, LARGE RESERVOIR

(Z/D) = 59.18 ( ℄ = 12.745 cm)

| r'(cm) | $V_r$(cm/sec) | $V_z$(cm/sec) | r'(cm) | $V_r$(cm/sec) | $V_z$(cm/sec) | r'(cm) | $V_r$(cm/sec) | $V_z$(cm/sec) | r'(cm) | $V_r$(cm/sec) | $V_z$(cm/sec) |
|---|---|---|---|---|---|---|---|---|---|---|---|
| 10.913 | 0.600 | 1.445 | 13.880 | -0.344 | 1.891 | 12.194 | 0.298 | 2.040 | 13.021 | -0.246 | 1.539 |
| 11.790 | 0.352 | 1.799 | 12.358 | -0.007 | 1.922 | 12.880 | -0.332 | 2.159 | 12.126 | 0.396 | 1.955 |
| 13.047 | -0.034 | 1.405 | 11.860 | 0.240 | 0.806 | 13.989 | -0.419 | 1.302 | 11.707 | 0.560 | 1.659 |
| 14.236 | -0.291 | 0.891 | 10.998 | 0.565 | 1.090 | 14.131 | -0.362 | 0.996 | 10.810 | 0.299 | 0.991 |
| 13.549 | -0.336 | 1.376 | 13.638 | -0.108 | 1.491 | 13.227 | -0.097 | 2.014 | 13.183 | -0.175 | 1.915 |
| 12.207 | 0.515 | 1.655 | 12.875 | -0.133 | 2.148 | 11.905 | 0.448 | 2.098 | 13.599 | -0.509 | 0.942 |
| 11.214 | 0.309 | 1.275 | 13.028 | -0.437 | 1.500 | 10.623 | 0.492 | 0.890 | 12.416 | 0.154 | 1.961 |
| 10.383 | 0.871 | 1.146 | 11.932 | 0.275 | 1.648 | 13.434 | 0.134 | 1.178 | 10.591 | 0.499 | 1.367 |
| 12.784 | -0.083 | 1.634 | 12.431 | 0.129 | 1.704 | 12.287 | 0.580 | 2.010 | 11.611 | 0.350 | 1.834 |
| 12.212 | 0.236 | 2.234 | 13.979 | -0.497 | 1.493 | 13.880 | -0.353 | 1.304 | 13.421 | -0.502 | 1.277 |
| 13.821 | -0.447 | 1.104 | 12.994 | -0.401 | 1.622 | 13.366 | -0.082 | 0.833 | 11.072 | 0.462 | 1.869 |
| 12.612 | 0.226 | 2.019 | 11.981 | 0.526 | 2.051 | 12.115 | 0.249 | 1.896 | 11.611 | 0.566 | 1.997 |

(Z/D) = 39.45 ( ℄ = 12.745 cm)

| r'(cm) | $V_r$(cm/sec) | $V_z$(cm/sec) | r'(cm) | $V_r$(cm/sec) | $V_z$(cm/sec) | r'(cm) | $V_r$(cm/sec) | $V_z$(cm/sec) | r'(cm) | $V_r$(cm/sec) | $V_z$(cm/sec) |
|---|---|---|---|---|---|---|---|---|---|---|---|
| 14.135 | -0.021 | 1.530 | 10.336 | 0.385 | 0.868 | 13.863 | 0.038 | 1.646 | 14.212 | -0.373 | 1.482 |
| 13.770 | 0.009 | 1.638 | 13.505 | -0.254 | 3.354 | 13.713 | 0.099 | 1.890 | 13.329 | -0.331 | 4.579 |
| 13.639 | -0.240 | 2.910 | 13.100 | -0.701 | 5.492 | 13.262 | -1.272 | 3.996 | 13.013 | -0.154 | 7.978 |
| 13.015 | -1.455 | 4.860 | 12.292 | 0.626 | 9.916 | 13.030 | -0.361 | 7.539 | 12.135 | 1.090 | 9.256 |
| 12.237 | 1.857 | 13.023 | 11.585 | 0.762 | 2.464 | 11.900 | 0.900 | 6.795 | 11.211 | 0.521 | 1.958 |
| 11.618 | 0.710 | 3.129 | 10.852 | 0.089 | 1.284 | 11.540 | 0.378 | 2.611 | 10.716 | 0.224 | 1.307 |
| 13.473 | -0.809 | 4.346 | 13.141 | -0.126 | 5.415 | 13.173 | -0.088 | 3.948 | 13.049 | -0.228 | 5.970 |
| 12.775 | -0.450 | 11.910 | 12.925 | 0.224 | 8.838 | 12.134 | 1.516 | 7.000 | 11.710 | 1.116 | 3.459 |
| 12.095 | 1.380 | 7.956 | 11.457 | 0.408 | 3.468 | 11.694 | 0.848 | 4.196 | 11.184 | 0.488 | 2.279 |
| 11.572 | 1.220 | 3.358 | 10.868 | 0.096 | 1.463 | 11.504 | 0.452 | 3.112 | 10.602 | 0.222 | 0.958 |
| 11.403 | 1.028 | 2.996 | 13.775 | -0.146 | 2.041 | 10.872 | 0.270 | 1.292 | 12.951 | -0.216 | 8.284 |

TABLE E.34 (continued)

$(Z/D) = 39.45$ ( ℄ = 12.745 cm)

| r' (cm) | $V_r$ (cm/sec) | $V_z$ (cm/sec) | r' (cm) | $V_r$ (cm/sec) | $V_z$ (cm/sec) | r' (cm) | $V_r$ (cm/sec) | $V_z$ (cm/sec) | r' (cm) | $V_r$ (cm/sec) | $V_z$ (cm/sec) |
|---|---|---|---|---|---|---|---|---|---|---|---|
| 10.704 | 0.286 | 1.288 | 12.859 | 0.180 | 10.292 | 10.618 | 0.278 | 1.524 | 12.777 | -0.080 | 10.924 |
| 10.597 | 0.141 | 1.126 | 12.422 | 1.624 | 15.832 | 9.831 | 0.249 | 0.979 | 12.059 | 0.740 | 8.928 |
| 14.509 | -0.050 | 0.923 | 11.828 | 0.536 | 4.540 | 13.732 | 0.131 | 2.388 | 11.527 | 0.720 | 2.948 |
| 13.305 | -0.776 | 4.460 | 11.189 | 0.408 | 1.688 | 13.197 | -0.280 | 4.831 | 10.777 | 0.426 | 1.190 |
| 13.056 | -0.227 | 7.053 | 10.082 | 0.105 | 0.778 | 12.990 | -0.280 | 5.275 | 11.860 | 1.008 | 8.210 |
| 12.916 | -0.236 | 7.857 | 11.887 | 1.730 | 4.215 | 12.382 | 1.514 | 12.535 | 11.455 | 0.463 | 2.576 |
| 12.034 | 1.375 | 8.190 | 11.346 | 0.365 | 2.466 | 11.309 | 0.867 | 2.588 | 14.229 | -0.288 | 1.376 |
| 11.097 | 0.605 | 2.331 | 13.625 | -0.296 | 2.444 | 13.380 | -0.197 | 3.060 | 13.487 | -0.010 | 3.276 |
| 13.146 | -0.879 | 6.510 | 12.900 | -1.232 | 8.460 | 13.040 | -0.396 | 5.850 | 12.626 | 0.162 | 18.010 |
| 12.581 | 0.768 | 15.261 | 12.193 | 1.692 | 10.601 | 12.612 | 1.899 | 14.694 | 11.445 | 0.640 | 2.742 |
| 12.449 | 1.504 | 13.173 | 11.246 | 0.620 | 2.427 | 12.233 | 1.206 | 11.466 | 11.046 | 0.573 | 1.819 |
| 12.164 | 1.254 | 10.188 | 14.149 | 0.060 | 1.070 | 12.042 | 0.915 | 7.620 | 13.928 | -0.085 | 2.168 |
| 11.956 | 0.330 | 5.814 | 13.295 | -0.236 | 5.152 | 11.509 | 0.510 | 3.612 | 13.064 | -0.267 | 5.116 |
| 11.298 | 0.231 | 1.983 | 12.999 | -0.427 | 6.604 | 10.464 | 0.140 | 0.788 | 12.885 | -0.304 | 9.492 |
| 13.641 | -0.439 | 1.462 | 12.805 | 0.196 | 7.965 | 13.459 | -0.286 | 3.392 | 12.762 | 0.360 | 9.768 |
| 12.970 | -0.516 | 5.108 | 12.681 | -0.181 | 14.978 | 12.849 | -0.511 | 8.596 | 12.486 | 0.148 | 14.204 |
| 12.128 | 0.910 | 8.712 | 12.345 | 1.712 | 14.092 | 11.101 | 0.538 | 1.514 | 10.983 | 0.376 | 1.617 |
| 10.938 | 0.348 | 1.649 | 11.839 | 1.174 | 4.496 | 10.348 | 0.197 | 1.004 | 11.364 | 0.873 | 2.277 |

$(Z/D) = 19.73$ ( ℄ = 12.745 cm)

| r' (cm) | $V_r$ (cm/sec) | $V_z$ (cm/sec) | r' (cm) | $V_r$ (cm/sec) | $V_z$ (cm/sec) | r' (cm) | $V_r$ (cm/sec) | $V_z$ (cm/sec) | r' (cm) | $V_r$ (cm/sec) | $V_z$ (cm/sec) |
|---|---|---|---|---|---|---|---|---|---|---|---|
| 13.067 | -0.103 | 10.282 | 13.560 | 0.106 | 2.708 | 12.999 | 0.120 | 11.572 | 13.244 | 0.639 | 4.600 |
| 12.323 | 1.452 | 13.008 | 12.987 | -0.146 | 15.548 | 12.212 | 0.997 | 9.753 | 12.013 | 0.260 | 3.470 |
| 11.979 | 0.671 | 3.833 | 11.636 | 0.032 | 1.860 | 12.025 | 0.434 | 3.850 | 11.529 | -0.160 | 2.600 |
| 11.843 | -0.111 | 3.057 | 11.290 | -0.108 | 1.135 | 12.398 | 1.078 | 14.897 | 13.331 | 0.120 | 4.738 |
| 11.437 | -0.157 | 1.525 | 12.964 | -0.528 | 17.640 | 13.462 | 0.208 | 1.644 | 12.818 | 0.754 | 49.010 |
| 13.335 | 0.336 | 3.572 | 12.242 | 0.614 | 9.350 | 13.099 | -0.112 | 9.108 | 12.023 | 0.292 | 3.750 |
| 12.946 | -0.396 | 18.244 | 11.866 | 0.029 | 3.151 | 12.293 | 0.738 | 8.321 | 13.502 | 0.028 | 2.813 |
| 12.073 | 0.374 | 4.321 | 13.109 | -0.343 | 8.103 | 11.664 | 0.474 | 2.652 | 11.751 | -0.033 | 3.620 |

TABLE E.34 (continued)

(Z/D) = 19.73 (℄ = 12.745 cm)

| r' (cm) | $V_r$ (cm/sec) | $V_z$ (cm/sec) | r' (cm) | $V_r$ (cm/sec) | $V_z$ (cm/sec) | r' (cm) | $V_r$ (cm/sec) | $V_z$ (cm/sec) | r' (cm) | $V_r$ (cm/sec) | $V_z$ (cm/sec) |
|---|---|---|---|---|---|---|---|---|---|---|---|
| 11.590 | 0.283 | 2.307 | 11.474 | -0.386 | 2.156 | 13.695 | 0.368 | 1.761 | 12.189 | 1.646 | 8.746 |
| 12.966 | -1.079 | 12.416 | 12.005 | 0.158 | 4.028 | 12.221 | 0.484 | 8.626 | 11.925 | 0.075 | 4.512 |
| 11.998 | 0.149 | 5.164 | 11.639 | 0.188 | 2.267 | 11.588 | 0.080 | 2.956 | 13.909 | 0.358 | 1.686 |
| 11.448 | -0.251 | 1.611 | 13.754 | 0.353 | 1.869 | 11.305 | -0.072 | 1.279 | 13.631 | 0.428 | 2.081 |
| 13.259 | 0.021 | 5.482 | 13.368 | 0.334 | 3.763 | 12.895 | -0.284 | 20.128 | 12.898 | -0.879 | 16.941 |
| 12.370 | 1.064 | 14.010 | 11.850 | 0.461 | 3.862 | 12.163 | 0.214 | 8.070 | 13.179 | -0.121 | 7.154 |
| 11.981 | 0.240 | 5.100 | 12.067 | 0.150 | 5.414 | 12.071 | 0.470 | 4.396 | 11.504 | 0.054 | 1.853 |
| 11.209 | -0.207 | 0.971 | 12.649 | 1.002 | 31.394 | 12.789 | 0.690 | 14.786 | 12.304 | 1.547 | 37.977 |
| 12.746 | 1.293 | 22.730 | | | | | | | | | |

TABLE E.35

RADIAL AND AXIAL VELOCITIES - DIGITIZER METHOD, Q=4.766 $cm^3/sec$
0.30 cm I.D. CAPILLARY TUBE, LARGE RESERVOIR

(Z/D) = 21.90 ( ℄ = 12.745 cm)

| r' (cm) | $V_r$ (cm/sec) | $V_z$ (cm/sec) | r' (cm) | $V_r$ (cm/sec) | $V_z$ (cm/sec) | r' (cm) | $V_r$ (cm/sec) | $V_z$ (cm/sec) | r' (cm) | $V_r$ (cm/sec) | $V_z$ (cm/sec) |
|---|---|---|---|---|---|---|---|---|---|---|---|
| 14.102 | -0.428 | 1.407 | 12.620 | 0.178 | 7.407 | 13.622 | -0.190 | 3.776 | 11.998 | 0.610 | 3.147 |
| 13.011 | 0.236 | 6.631 | 11.175 | 0.314 | 1.474 | 12.827 | 0.251 | 8.437 | 12.817 | 0.501 | 7.617 |
| 12.274 | 0.433 | 5.551 | 12.622 | 0.951 | 6.977 | 12.475 | 0.455 | 6.529 | 12.257 | 0.790 | 3.741 |
| 11.897 | 0.364 | 2.755 | 12.015 | 0.604 | 3.342 | 12.682 | 0.498 | 7.120 | 11.335 | 0.305 | 1.248 |
| 9.434 | 0.042 | 0.166 | 11.069 | 0.470 | 1.084 | 14.629 | -0.305 | 1.072 | 9.566 | 0.087 | 0.217 |
| 13.493 | -0.490 | 3.594 | 13.361 | -0.248 | 4.877 | 13.219 | -0.495 | 6.411 | 13.067 | -0.529 | 7.199 |
| 12.922 | -0.032 | 7.739 | 11.724 | 0.410 | 2.473 | 11.881 | 0.656 | 2.742 | 11.482 | 0.362 | 1.771 |
| 11.823 | 0.876 | 3.180 | 11.080 | 0.377 | 1.339 | 14.877 | -0.262 | 0.772 | 10.868 | 0.250 | 0.900 |
| 13.436 | -0.702 | 3.475 | 13.809 | -0.230 | 1.835 | 13.064 | -0.254 | 6.606 | 13.253 | -0.529 | 6.110 |
| 12.706 | 0.528 | 7.980 | 12.832 | -0.160 | 8.187 | 12.492 | 0.637 | 5.353 | 11.902 | 0.714 | 2.500 |
| 12.056 | 0.799 | 3.986 | 11.144 | 0.608 | 1.201 | 11.258 | 0.523 | 1.386 | 9.560 | 0.386 | 0.233 |
| 10.254 | 0.162 | 0.448 | 13.589 | -0.881 | 3.205 | 14.003 | -0.281 | 2.322 | 12.550 | 0.373 | 6.549 |
| 11.738 | 0.591 | 2.384 | 11.839 | 0.258 | 2.074 | 11.566 | 0.495 | 2.006 | 11.755 | 0.423 | 2.530 |
| 11.298 | 0.720 | 1.308 | 10.787 | 0.280 | 0.769 | 13.902 | -0.211 | 2.042 | 13.790 | -0.410 | 2.947 |
| 13.615 | -0.573 | 2.991 | 13.077 | -0.331 | 7.039 | 13.179 | -0.147 | 5.970 | 12.590 | 0.183 | 5.579 |
| 13.070 | -0.507 | 6.111 | 12.307 | 0.624 | 5.317 | 12.936 | -0.164 | 8.111 | 12.208 | 0.713 | 3.605 |
| 12.524 | 0.437 | 6.867 | 11.341 | 0.283 | 1.267 | 11.954 | 0.392 | 2.903 | 12.840 | -0.433 | 8.329 |
| 14.179 | -0.785 | 1.875 | 14.624 | -0.252 | 0.988 | 13.494 | -0.118 | 4.092 | 13.316 | -0.102 | 4.619 |
| 13.435 | -0.918 | 4.633 | 12.856 | -0.514 | 8.852 | 12.585 | 0.676 | 5.957 | 11.356 | 0.452 | 0.398 |
| 11.934 | 0.446 | 2.982 | 9.800 | 0.102 | 0.339 | 13.630 | -0.580 | 2.726 | 12.548 | 0.108 | 7.100 |
| 13.288 | -0.102 | 5.859 | 13.057 | -0.364 | 6.032 | 12.938 | -0.294 | 8.126 | 13.340 | -0.326 | 4.464 |
| 11.786 | 0.576 | 2.234 | 12.775 | 0.099 | 7.646 | 12.698 | 0.380 | 7.666 | 13.631 | -0.508 | 3.579 |
| 12.446 | 0.793 | 6.146 | 13.240 | -0.529 | 6.300 | 11.815 | 0.505 | 2.381 | 13.112 | -0.651 | 7.059 |
| 11.153 | 0.429 | 1.319 | 12.796 | 0.262 | 7.682 | 10.947 | 0.432 | 1.139 | 11.189 | 0.285 | 1.304 |
| 9.968 | 0.153 | 0.888 | 13.318 | -0.452 | 4.871 | 13.056 | -0.126 | 7.929 | 13.000 | -0.327 | 6.040 |
| 12.941 | 0.083 | 8.983 | 12.818 | -0.404 | 8.555 | 12.882 | -0.331 | 8.520 | 12.562 | 0.684 | 6.785 |
| 12.190 | 0.439 | 3.132 | 11.781 | 0.531 | 2.588 | 11.961 | 0.580 | 3.193 | 11.476 | 0.711 | 1.807 |
| 11.778 | 0.565 | 2.516 | 14.643 | -0.309 | 0.884 | 11.677 | 0.445 | 1.780 | 14.002 | -0.841 | 1.853 |

TABLE E.35 (continued)

(Z/D) = 21.90 ( ℄ = 12.745 cm)

| r'(cm) | $V_r$(cm/sec) | $V_z$(cm/sec) | r'(cm) | $V_r$(cm/sec) | $V_z$(cm/sec) | r'(cm) | $V_r$(cm/sec) | $V_z$(cm/sec) | r'(cm) | $V_r$(cm/sec) | $V_z$(cm/sec) |
|---|---|---|---|---|---|---|---|---|---|---|---|
| 9.375 | 0.355 | 0.138 | 13.493 | -0.568 | 4.605 | 10.060 | 0.109 | 0.469 | 12.506 | 0.744 | 6.035 |
| 12.976 | -0.317 | 7.543 | 12.417 | 0.582 | 4.301 | 12.733 | 0.348 | 7.975 | 12.247 | 0.320 | 3.542 |
| 10.876 | 0.341 | 0.993 | | | | | | | | | |

(Z/D) = 10.95 ( ℄ = 12.745 cm)

| r'(cm) | $V_r$(cm/sec) | $V_z$(cm/sec) | r'(cm) | $V_r$(cm/sec) | $V_z$(cm/sec) | r'(cm) | $V_r$(cm/sec) | $V_z$(cm/sec) | r'(cm) | $V_r$(cm/sec) | $V_z$(cm/sec) |
|---|---|---|---|---|---|---|---|---|---|---|---|
| 13.059 | 2.586 | 10.961 | 11.946 | -0.061 | 2.027 | 12.784 | 0.962 | 37.429 | 11.633 | -0.261 | 1.552 |
| 11.729 | -0.298 | 1.301 | 13.728 | -0.080 | 2.625 | 13.240 | -0.458 | 8.967 | 13.397 | -0.994 | 5.681 |
| 13.054 | -0.960 | 22.179 | 13.239 | -0.099 | 7.888 | 11.689 | 0.058 | 1.786 | 12.645 | 0.743 | 28.303 |
| 13.952 | 0.419 | 1.627 | 12.315 | 0.384 | 6.099 | 13.465 | 0.436 | 4.859 | 12.238 | 0.763 | 5.359 |
| 11.839 | 0.064 | 1.561 | 11.949 | 0.184 | 2.148 | 11.663 | -0.156 | 1.123 | 11.309 | -0.157 | 0.484 |
| 10.844 | -0.262 | 0.189 | 13.183 | -0.007 | 9.769 | 13.728 | 0.045 | 2.763 | 12.527 | 0.832 | 15.093 |
| 13.274 | -0.084 | 9.090 | 12.313 | 0.405 | 6.738 | 12.068 | -0.048 | 2.892 | 12.077 | 0.306 | 3.485 |
| 13.888 | 0.451 | 1.946 | 13.828 | -0.218 | 2.549 | 13.417 | -0.487 | 5.323 | 11.586 | -0.034 | 1.164 |
| 13.010 | 0.032 | 32.085 | 12.326 | 0.061 | 5.525 | 12.193 | -0.187 | 4.692 | 13.471 | 0.148 | 5.678 |
| 11.571 | -0.179 | 1.123 | 12.509 | 0.739 | 13.174 | 13.187 | -0.416 | 13.139 | 12.153 | 0.002 | 3.029 |
| 13.043 | -0.339 | 15.396 | 11.736 | -0.012 | 1.578 | 12.226 | 0.091 | 4.249 | 13.143 | -0.458 | 19.695 |
| 13.620 | -0.081 | 2.816 | 12.905 | 0.539 | 31.449 | 13.365 | 0.219 | 4.741 | 12.946 | -0.649 | 27.148 |
| 12.349 | 0.610 | 7.269 | 12.589 | 0.407 | 28.030 | 11.192 | -0.249 | 0.284 | 11.572 | -0.096 | 0.899 |
| 13.366 | -0.300 | 5.552 | 12.827 | -0.034 | 38.324 | 13.224 | 0.029 | 10.953 | 13.064 | -0.016 | 20.366 |
| 12.481 | 0.077 | 9.015 | 12.298 | 0.421 | 7.227 | 12.246 | 0.167 | 5.452 | 11.993 | 0.466 | 2.269 |
| 12.535 | 0.989 | 12.092 | 11.665 | -0.052 | 1.708 | 11.420 | -0.200 | 0.727 | 13.670 | -0.290 | 2.848 |
| 12.855 | 0.639 | 50.822 | 13.486 | -0.379 | 4.837 | 13.480 | 0.294 | 5.608 | 13.403 | 0.268 | 5.981 |
| 13.206 | -0.615 | 12.118 | 13.212 | -0.725 | 9.824 | 12.555 | 0.893 | 15.320 | 12.357 | 0.549 | 7.491 |
| 12.250 | -0.233 | 4.164 | 12.260 | 1.279 | 5.520 | 13.421 | 0.250 | 5.869 | 13.013 | 2.096 | 25.966 |
| 12.497 | 0.751 | 12.671 | 12.913 | 0.011 | 26.672 | 12.317 | 1.179 | 5.785 | 12.825 | 1.899 | 34.015 |
| 11.786 | -0.208 | 1.553 | 12.773 | 2.464 | 35.773 | 12.696 | 0.839 | 30.412 | 12.537 | -2.489 | 6.413 |
| 12.922 | 3.336 | 38.176 | 12.861 | 2.199 | 37.617 | 12.735 | 3.330 | 30.027 | | | |

TABLE E.36

RADIAL AND AXIAL VELOCITIES - DIGITIZER METHOD, Q=6.354 $cm^3/sec$
0.30 cm I.D. CAPILLARY TUBE, LARGE RESERVOIR

(Z/D) = 23.12 (℄ = 12.745 cm)

| r' (cm) | $V_r$ (cm/sec) | $V_z$ (cm/sec) | r' (cm) | $V_r$ (cm/sec) | $V_z$ (cm/sec) | r' (cm) | $V_r$ (cm/sec) | $V_z$ (cm/sec) | r' (cm) | $V_r$ (cm/sec) | $V_z$ (cm/sec) |
|---|---|---|---|---|---|---|---|---|---|---|---|
| 14.216 | -0.273 | 2.430 | 14.604 | -0.296 | 1.120 | 13.693 | -0.219 | 4.104 | 11.525 | 0.219 | 2.598 |
| 12.735 | 1.783 | 12.884 | 13.826 | -0.360 | 3.580 | 12.630 | 0.897 | 10.905 | 11.798 | 1.185 | 3.416 |
| 11.630 | 0.530 | 1.726 | 11.658 | 0.400 | 2.731 | 12.734 | 1.872 | 11.631 | 11.625 | 0.953 | 2.789 |
| 13.619 | -0.447 | 3.145 | 10.812 | 0.767 | 1.225 | 13.780 | -1.359 | 7.004 | 14.660 | -0.322 | 1.164 |
| 12.851 | 0.409 | 11.551 | 12.200 | 0.046 | 5.300 | 12.452 | 0.780 | 7.837 | 11.638 | 0.500 | 2.551 |
| 12.578 | 1.167 | 10.808 | 11.501 | 0.530 | 2.403 | 11.811 | 0.646 | 2.983 | 11.357 | 0.522 | 2.102 |
| 13.159 | 0.268 | 9.641 | 10.054 | 0.142 | 1.136 | 13.227 | -0.326 | 8.701 | 13.486 | -0.954 | 4.579 |
| 12.437 | 1.540 | 10.436 | 12.546 | 0.673 | 10.920 | 13.745 | -0.685 | 3.575 | 11.246 | 0.733 | 2.091 |
| 13.696 | -0.693 | 3.874 | 10.561 | 0.291 | 0.902 | 13.235 | 0.619 | 6.112 | 13.136 | 0.238 | 9.023 |
| 13.357 | -0.609 | 5.809 | 11.221 | 0.154 | 1.676 | 13.231 | -0.328 | 6.959 | 13.470 | -0.475 | 4.683 |
| 12.360 | 1.263 | 9.448 | 11.970 | 1.007 | 5.285 | 13.562 | -0.728 | 4.677 | 11.797 | 0.791 | 3.965 |
| 11.953 | 0.771 | 3.251 | 13.475 | -0.388 | 4.048 | 11.129 | 0.519 | 1.385 | 13.342 | -0.786 | 5.691 |
| 12.505 | 1.540 | 8.758 | 12.952 | 0.602 | 9.972 | 11.982 | 0.573 | 3.763 | 12.877 | 0.325 | 12.482 |
| 11.526 | 0.369 | 2.152 | 12.620 | 0.600 | 11.474 | 12.119 | 0.238 | 3.875 | 12.067 | 0.903 | 3.742 |
| 11.974 | 0.706 | 3.622 | 11.259 | 0.509 | 1.704 | 11.622 | 0.792 | 2.966 | 14.554 | -0.194 | 1.197 |
| 13.788 | -0.774 | 3.775 | 11.838 | 0.957 | 4.047 | 13.552 | -0.479 | 3.369 | 11.428 | 0.491 | 2.230 |
| 11.420 | 0.508 | 2.436 | 11.989 | 0.150 | 4.476 | 13.559 | -0.548 | 3.967 | 11.798 | 0.722 | 2.051 |
| 13.465 | 1.176 | 3.568 | | | | | | | | | |

(Z/D) = 11.56 (℄ = 12.745 cm)

| r' (cm) | $V_r$ (cm/sec) | $V_z$ (cm/sec) | r' (cm) | $V_r$ (cm/sec) | $V_z$ (cm/sec) | r' (cm) | $V_r$ (cm/sec) | $V_z$ (cm/sec) | r' (cm) | $V_r$ (cm/sec) | $V_z$ (cm/sec) |
|---|---|---|---|---|---|---|---|---|---|---|---|
| 13.344 | 0.112 | 11.378 | 12.175 | 0.426 | 4.785 | 12.892 | 0.153 | 50.968 | 13.313 | -0.171 | 8.618 |
| 13.045 | -2.746 | 35.965 | 13.189 | 0.029 | 11.197 | 12.912 | 1.234 | 46.296 | 12.341 | 0.743 | 8.417 |
| 12.848 | -1.834 | 49.268 | 12.426 | 0.464 | 11.208 | 13.010 | 0.046 | 47.685 | 11.428 | 0.335 | 2.244 |
| 13.581 | 0.655 | 4.644 | 12.275 | 1.406 | 8.119 | 12.423 | 0.078 | 5.937 | 11.661 | -0.163 | 1.949 |
| 13.027 | 1.893 | 42.723 | 12.535 | 1.418 | 18.270 | 13.615 | -0.105 | 4.107 | 12.300 | 0.914 | 7.160 |

TABLE E.36 (continued)

(Z/D) = 11.56 (℄ = 12.745 cm)

| r' (cm) | $V_r$ (cm/sec) | $V_z$ (cm/sec) | r' (cm) | $V_r$ (cm/sec) | $V_z$ (cm/sec) | r' (cm) | $V_r$ (cm/sec) | $V_z$ (cm/sec) | r' (cm) | $V_r$ (cm/sec) | $V_z$ (cm/sec) |
|---|---|---|---|---|---|---|---|---|---|---|---|
| 13.199 | -1.202 | 18.802 | 11.921 | 0.173 | 2.993 | 13.134 | 1.664 | 27.911 | 11.666 | 0.207 | 1.341 |
| 13.406 | 1.848 | 6.686 | 11.389 | -0.223 | 0.838 | 12.081 | 0.309 | 4.199 | 13.834 | 0.171 | 1.847 |
| 13.834 | -0.147 | 3.039 | 13.275 | -0.653 | 7.199 | 13.262 | -0.552 | 12.121 | 12.593 | 1.041 | 22.343 |
| 12.416 | -0.500 | 10.056 | 12.443 | 1.062 | 11.598 | 12.256 | 0.729 | 7.945 | 12.267 | -0.185 | 5.931 |
| 12.024 | -0.125 | 3.566 | 11.992 | 0.086 | 2.256 | 11.158 | -0.227 | 0.511 | 12.401 | 1.168 | 10.778 |
| 13.270 | 1.408 | 9.128 | 11.967 | -0.525 | 2.881 | 13.168 | -0.418 | 20.691 | 11.792 | 0.180 | 2.408 |
| 12.448 | 0.273 | 11.729 | 11.879 | 0.355 | 2.827 | 11.977 | 0.144 | 2.746 | 13.034 | -0.424 | 30.610 |
| 11.511 | -0.385 | 1.136 | 12.481 | 1.024 | 17.011 | 11.385 | -0.432 | 0.653 | 12.352 | 0.512 | 9.802 |
| 11.699 | 0.562 | 1.575 | 12.330 | 0.659 | 10.915 |  |  |  |  |  |  |

## TABLE E.37

## RADIAL AND AXIAL VELOCITIES - DIGITIZER METHOD, Q=7.148 $cm^3$/sec
## 0.30 cm I.D. CAPILLARY TUBE, LARGE RESERVOIR

(Z/D) = 23.12 ( ξ = 12.745 cm)

| r' (cm) | $V_r$ (cm/sec) | $V_z$ (cm/sec) | r' (cm) | $V_r$ (cm/sec) | $V_z$ (cm/sec) | r' (cm) | $V_r$ (cm/sec) | $V_z$ (cm/sec) | r' (cm) | $V_r$ (cm/sec) | $V_z$ (cm/sec) |
|---|---|---|---|---|---|---|---|---|---|---|---|
| 11.905 | 1.403 | 5.631 | 13.461 | -0.135 | 6.308 | 12.933 | 1.597 | 15.225 | 12.274 | 0.693 | 9.975 |
| 11.325 | 1.079 | 3.897 | 11.145 | 0.741 | 2.274 | 10.758 | 0.575 | 1.217 | 13.536 | -0.303 | 4.820 |
| 9.830 | 0.262 | 0.933 | 12.927 | 0.117 | 12.026 | 12.229 | 1.273 | 8.406 | 12.750 | 0.104 | 12.514 |
| 12.204 | 1.308 | 6.829 | 12.226 | 1.801 | 6.805 | 11.346 | 0.604 | 2.474 | 11.822 | 1.185 | 5.178 |
| 11.033 | 0.879 | 1.335 | 11.446 | 1.201 | 3.187 | 12.961 | -0.526 | 12.348 | 8.898 | 0.071 | 0.196 |
| 13.519 | -0.532 | 6.599 | 8.863 | 0.079 | 0.207 | 12.418 | 1.747 | 9.402 | 13.935 | -0.303 | 3.449 |
| 11.898 | 0.489 | 4.409 | 13.618 | -0.605 | 4.117 | 10.852 | 0.425 | 1.110 | 11.173 | 0.219 | 1.884 |
| 10.661 | 0.344 | 1.146 | 14.149 | 0.179 | 2.597 | 13.277 | -0.938 | 8.614 | 12.227 | 0.774 | 5.619 |
| 11.975 | 0.475 | 5.538 | 13.424 | -0.937 | 5.744 | 11.246 | 0.181 | 2.260 | 12.421 | 1.421 | 10.056 |
| 9.225 | 0.062 | 0.299 | 13.108 | -0.661 | 10.053 | 13.399 | 0.019 | 5.661 | 12.370 | 0.936 | 10.690 |
| 12.431 | 2.319 | 10.942 | 12.375 | 1.215 | 9.771 | 12.487 | 1.041 | 13.412 | 12.210 | 0.695 | 7.745 |
| 11.969 | 0.886 | 5.901 | 13.053 | -1.571 | 9.651 | 13.043 | -0.217 | 11.097 | 13.389 | -0.291 | 4.919 |
| 12.959 | -0.386 | 11.411 | 13.095 | 0.036 | 7.621 | 11.694 | 0.843 | 4.344 | 12.411 | 0.955 | 10.363 |

(Z/D) = 11.92 ( ℓ = 12.745 cm)

| r' (cm) | $V_r$ (cm/sec) | $V_z$ (cm/sec) | r' (cm) | $V_r$ (cm/sec) | $V_z$ (cm/sec) | r' (cm) | $V_r$ (cm/sec) | $V_z$ (cm/sec) | r' (cm) | $V_r$ (cm/sec) | $V_z$ (cm/sec) |
|---|---|---|---|---|---|---|---|---|---|---|---|
| 12.241 | 0.053 | 5.638 | 12.214 | 0.139 | 6.016 | 10.967 | -0.208 | 0.407 | 13.386 | -0.839 | 8.544 |
| 11.122 | 9.243 | 1.021 | 13.316 | -0.256 | 9.386 | 11.080 | -0.143 | 0.823 | 12.570 | 1.582 | 20.445 |
| 13.685 | -0.132 | 3.566 | 13.238 | -1.017 | 10.423 | 12.455 | 0.414 | 12.372 | 12.669 | 3.490 | 37.441 |
| 12.211 | 0.209 | 5.454 | 13.013 | -0.297 | 33.086 | 12.154 | 0.539 | 5.124 | 12.688 | 2.577 | 39.685 |
| 12.855 | 1.060 | 40.341 | 12.664 | 2.716 | 33.701 | 12.135 | 0.082 | 5.112 | 12.103 | 0.563 | 4.585 |
| 11.251 | -0.027 | 1.033 | 12.651 | 4.015 | 55.823 | 13.357 | 0.044 | 10.409 | 12.374 | 0.615 | 12.643 |
| 13.309 | -0.561 | 13.060 | 12.809 | 0.963 | 56.740 | 12.212 | 0.538 | 5.237 | 12.371 | 0.168 | 9.548 |
| 11.276 | -0.246 | 1.215 | 12.272 | 0.500 | 6.495 | 13.314 | -0.001 | 12.473 | 12.209 | -0.062 | 6.198 |
| 12.411 | 1.742 | 11.241 | 11.359 | 0.126 | 1.262 | 12.222 | 1.284 | 5.481 | 11.872 | -0.059 | 3.215 |
| 12.412 | 0.967 | 14.007 | 12.876 | 1.079 | 66.834 | 12.309 | 0.935 | 7.994 | | | |

## TABLE E.38

## RADIAL AND AXIAL VELOCITIES - DIGITIZER METHOD, Q=7.943 cm$^3$/sec
0.30 cm I.D. CAPILLARY TUBE, LARGE RESERVOIR

(Z/D) = 24.08 (℄ = 12.745 cm)

| r'(cm) | $V_r$(cm/sec) | $V_z$(cm/sec) | r'(cm) | $V_r$(cm/sec) | $V_z$(cm/sec) | r'(cm) | $V_r$(cm/sec) | $V_z$(cm/sec) | r'(cm) | $V_r$(cm/sec) | $V_z$(cm/sec) |
|---|---|---|---|---|---|---|---|---|---|---|---|
| 14.123 | -0.349 | 2.713 | 12.645 | 0.605 | 13.187 | 13.553 | -0.091 | 6.286 | 12.540 | -0.174 | 15.454 |
| 12.443 | 0.898 | 9.276 | 12.408 | 0.553 | 11.117 | 13.296 | -0.300 | 7.838 | 11.631 | 0.587 | 3.444 |
| 12.797 | -0.090 | 17.741 | 12.638 | 0.380 | 13.672 | 12.591 | 1.525 | 13.102 | 12.162 | 2.005 | 6.528 |
| 12.368 | 2.744 | 13.895 | 13.347 | -0.549 | 8.151 | 12.093 | 1.170 | 6.779 | 12.827 | -0.328 | 14.252 |
| 12.417 | 0.875 | 10.798 | 12.298 | 2.398 | 8.002 | 12.180 | 1.220 | 7.443 | 12.141 | 0.777 | 7.650 |
| 12.151 | 1.590 | 8.131 | 11.929 | 1.288 | 4.772 | 12.020 | 0.732 | 5.999 | 11.902 | 0.416 | 5.348 |
| 11.797 | 0.260 | 2.977 | 11.733 | 1.147 | 3.490 | 11.191 | 0.535 | 2.197 | 11.476 | 0.240 | 2.806 |
| 10.803 | 0.314 | 1.307 | 11.072 | 0.763 | 1.976 | 12.036 | 1.049 | 5.405 | 13.442 | -0.479 | 7.013 |
| 11.350 | 1.228 | 2.422 | 11.858 | 0.837 | 4.532 | 10.788 | 0.527 | 1.444 | 10.946 | 0.065 | 1.505 |
| 10.469 | 0.211 | 0.683 | 12.196 | 0.674 | 8.922 | 14.116 | -0.379 | 2.318 | 11.805 | 1.077 | 5.408 |
| 12.347 | 0.952 | 12.357 | 11.667 | 0.940 | 4.088 | 12.004 | 1.063 | 6.761 | 11.309 | 0.607 | 2.217 |
| 11.809 | 0.754 | 5.323 | 11.147 | 0.728 | 1.789 | 13.085 | -0.650 | 12.456 | 10.948 | 0.587 | 1.728 |
| 12.097 | 0.686 | 7.009 | 10.247 | 0.074 | 0.763 | 11.907 | 0.598 | 5.128 | 12.178 | 1.035 | 9.500 |
| 11.641 | 0.344 | 2.866 | 12.003 | 0.294 | 4.480 | 9.419 | -0.462 | 0.556 | 11.456 | 0.481 | 2.983 |
| 12.798 | -1.399 | 11.457 | 13.360 | -0.679 | 8.171 | 12.374 | 0.929 | 12.313 | 12.944 | -0.191 | 16.678 |
| 12.208 | 0.967 | 10.999 | 11.408 | 0.966 | 2.792 | 11.941 | 2.000 | 6.069 | 12.119 | 1.434 | 5.828 |
| 11.393 | 0.400 | 2.783 | 11.579 | 0.682 | 2.894 | 9.811 | 0.122 | 0.717 | 11.486 | 0.568 | 2.534 |
| 9.947 | -0.227 | 0.476 | 11.010 | 0.388 | 1.402 | 12.827 | -0.259 | 14.384 | 13.946 | -0.683 | 3.473 |
| 11.880 | 0.622 | 4.152 | 12.401 | 1.927 | 10.997 | 11.651 | 1.045 | 3.151 | 11.829 | 0.894 | 5.440 |
| 10.250 | -0.060 | 0.806 | 11.277 | 0.812 | 1.924 |  |  |  |  |  |  |

## TABLE E.38 (continued)

(Z/D) 12.04 (℄ = 12.745 cm)

| r' (cm) | $V_r$ (cm/sec) | $V_z$ (cm/sec) | r' (cm) | $V_r$ (cm/sec) | $V_z$ (cm/sec) | r' (cm) | $V_r$ (cm/sec) | $V_z$ (cm/sec) | r' (cm) | $V_r$ (cm/sec) | $V_z$ (cm/sec) |
|---|---|---|---|---|---|---|---|---|---|---|---|
| 12.715 | 4.019 | 50.719 | 13.030 | 4.649 | 25.141 | 12.355 | 2.858 | 9.759 | 12.659 | 2.504 | 27.822 |
| 12.641 | 0.451 | 25.265 | 13.156 | -1.304 | 27.291 | 12.613 | 1.468 | 50.648 | 13.300 | 0.145 | 11.203 |
| 12.277 | 0.042 | 6.805 | 13.215 | -0.470 | 15.993 | 13.484 | 0.209 | 6.319 | 12.477 | 2.072 | 16.787 |
| 12.417 | -0.307 | 10.550 | 12.237 | 0.127 | 7.256 | 12.142 | -0.028 | 5.673 | 12.055 | 0.354 | 3.468 |
| 11.997 | 0.537 | 4.675 | 11.916 | 0.623 | 3.965 | 13.561 | 0.342 | 5.683 | 13.325 | -0.538 | 6.671 |
| 13.409 | -0.814 | 8.807 | 12.152 | 0.237 | 6.960 | 12.294 | 0.703 | 8.851 | 12.217 | 0.507 | 8.509 |
| 11.940 | -0.112 | 3.829 | 12.416 | 0.682 | 11.781 | 11.715 | 0.045 | 2.105 | 12.053 | 0.146 | 4.532 |
| 12.406 | 1.683 | 15.867 | 13.334 | -0.569 | 9.715 | 12.365 | 0.707 | 11.368 | 12.094 | 0.745 | 5.019 |
| 11.778 | 0.339 | 5.571 | 11.668 | 0.230 | 1.885 | 12.369 | -0.203 | 1.985 | 13.950 | 0.055 | 2.707 |
| 11.803 | -0.205 | 2.060 | 12.226 | 0.870 | 6.191 | 11.679 | -0.229 | 1.684 | 12.111 | 0.049 | 4.022 |
| 10.677 | -0.518 | 0.313 | | | | | | | | | |

### TABLE E.39

### RADIAL AND AXIAL VELOCITIES - DIGITIZER METHOD, Q=8.737 $cm^3/sec$
### 0.30 cm I.D. CAPILLARY TUBE, LARGE RESERVOIR

(Z/D) = 24.90 ( ℄ = 12.745 cm)

| r'(cm) | $V_r$(cm/sec) | $V_z$(cm/sec) | r'(cm) | $V_r$(cm/sec) | $V_z$(cm/sec) | r'(cm) | $V_r$(cm/sec) | $V_z$(cm/sec) | r'(cm) | $V_r$(cm/sec) | $V_z$(cm/sec) |
|---|---|---|---|---|---|---|---|---|---|---|---|
| 13.422 | -0.495 | 7.651 | 13.376 | -0.425 | 6.601 | 13.272 | 0.004 | 7.665 | 12.029 | 1.269 | 7.247 |
| 11.938 | 0.629 | 5.653 | 11.946 | 0.515 | 4.785 | 11.518 | 0.952 | 3.073 | 11.255 | 0.830 | 2.314 |
| 11.531 | 1.118 | 3.450 | 10.002 | 0.433 | 1.286 | 11.353 | 0.666 | 2.367 | 9.122 | 0.109 | 0.307 |
| 11.224 | 0.898 | 2.373 | 8.662 | 0.047 | 0.122 | 13.131 | -1.341 | 7.252 | 12.064 | 0.821 | 6.784 |
| 12.404 | 1.392 | 16.658 | 11.766 | 0.731 | 4.753 | 11.901 | 1.065 | 5.327 | 11.671 | 0.763 | 3.552 |
| 11.167 | 0.663 | 1.822 | 11.569 | 0.956 | 4.346 | 10.833 | 0.442 | 1.440 | 11.058 | 0.588 | 2.063 |
| 9.126 | 0.212 | 1.103 | 12.037 | 1.011 | 5.905 | 13.518 | -0.352 | 4.987 | 11.882 | 0.744 | 4.945 |
| 12.590 | 1.698 | 13.348 | 11.736 | 0.601 | 5.003 | 12.071 | 1.511 | 5.941 | 13.209 | -0.542 | 10.054 |
| 11.730 | 0.399 | 3.618 | 12.191 | 0.768 | 12.835 | 11.411 | 0.543 | 2.908 | 11.593 | 0.707 | 2.651 |
| 11.369 | 0.519 | 2.513 | 11.493 | 0.896 | 2.280 | 11.091 | 0.888 | 1.415 | 10.536 | 0.323 | 1.146 |
| 10.289 | 0.271 | 1.153 | 9.388 | 0.145 | 0.421 | 12.999 | 1.097 | 14.762 | 12.096 | 0.860 | 9.078 |
| 10.974 | 0.349 | 1.467 | 11.637 | 0.427 | 3.934 | 11.881 | 0.857 | 4.872 | 11.258 | 0.756 | 2.350 |
| 11.490 | 0.402 | 3.281 | 10.677 | 0.540 | 1.123 | 11.298 | 0.403 | 2.078 | 12.222 | 1.006 | 10.196 |
| 9.962 | 0.537 | 1.782 | 11.869 | 0.653 | 5.637 | 13.462 | -0.737 | 4.789 | 11.819 | 1.087 | 4.539 |
| 12.465 | 0.986 | 13.553 | 11.635 | 0.697 | 3.759 | 12.136 | 1.663 | 9.626 | 11.550 | 0.883 | 4.157 |
| 12.056 | 1.367 | 8.716 | 11.210 | 0.462 | 1.985 | 11.830 | 0.732 | 4.529 | 13.967 | 0.607 | 2.349 |
| 11.644 | 0.338 | 3.316 | 11.562 | 0.642 | 4.642 | 14.988 | -0.041 | 0.487 | 11.729 | 0.913 | 5.101 |
| 12.112 | 1.056 | 7.883 | 11.371 | 0.710 | 2.427 | 11.575 | 0.998 | 2.471 | 12.655 | 0.461 | 14.819 |
| 10.234 | 0.159 | 0.972 | 11.974 | 0.565 | 5.623 | 12.738 | -0.307 | 14.090 | 12.964 | -0.421 | 15.361 |
| 12.801 | -0.878 | 13.694 | 12.667 | 0.670 | 17.654 | 12.235 | 2.755 | 9.108 | 12.101 | 1.071 | 6.397 |
| 12.027 | 0.714 | 6.051 | | | | | | | | | |

TABLE E.39 (continued)

(Z/D) = 12.45 ( ℄ = 12.745 cm)

| r' (cm) | $V_r$ (cm/sec) | $V_z$ (cm/sec) | r' (cm) | $V_r$ (cm/sec) | $V_z$ (cm/sec) | r' (cm) | $V_r$ (cm/sec) | $V_z$ (cm/sec) | r' (cm) | $V_r$ (cm/sec) | $V_z$ (cm/sec) |
|---|---|---|---|---|---|---|---|---|---|---|---|
| 12.443 | 1.194 | 13.672 | 13.779 | -0.365 | 2.996 | 13.146 | -0.213 | 31.179 | 12.232 | 0.468 | 6.550 |
| 12.145 | 0.479 | 5.950 | 11.812 | -0.165 | 2.851 | 11.692 | 0.120 | 2.126 | 11.670 | -0.170 | 2.362 |
| 12.420 | 1.350 | 11.872 | 11.177 | -0.211 | 0.576 | 12.386 | 1.182 | 19.195 | 12.244 | 0.904 | 7.688 |
| 12.256 | 0.744 | 9.226 | 11.676 | -0.075 | 1.501 | 11.953 | 0.129 | 4.362 | 13.304 | 0.177 | 11.615 |
| 11.630 | -0.316 | 2.396 | 12.389 | 3.716 | 16.410 | 12.128 | 0.487 | 7.605 | 12.420 | 1.368 | 17.547 |
| 12.040 | 0.200 | 4.064 | 11.360 | -0.332 | 1.682 | 12.491 | 1.533 | 18.381 | 14.032 | 0.383 | 2.302 |
| 12.267 | 0.267 | 7.974 | 12.460 | 0.490 | 15.466 | 11.942 | 0.355 | 2.394 | 11.952 | -0.093 | 3.454 |
| 11.675 | -0.078 | 2.666 | 11.199 | -0.072 | 1.279 | 12.498 | 1.210 | 22.279 | 12.296 | 1.450 | 12.213 |
| 10.953 | -0.758 | 2.796 | 11.026 | -0.333 | 0.868 | 13.767 | 0.595 | 2.686 | 13.344 | 0.549 | 10.612 |
| 12.094 | 0.889 | 5.889 | 12.178 | 0.326 | 5.984 | 13.276 | 0.922 | 14.941 | 12.143 | 0.247 | 7.484 |
| 12.519 | 3.171 | 19.468 | 11.876 | 0.571 | 3.699 | 12.990 | -0.786 | 47.199 | 12.620 | 0.176 | 34.883 |
| 13.173 | -0.065 | 19.049 | 12.280 | 1.082 | 7.921 | 12.229 | 1.050 | 7.538 | 12.976 | -2.392 | 46.331 |
| 13.224 | 0.327 | 18.851 | 12.250 | 0.425 | 7.360 | | | | | | |

## TABLE E.40

### AXIAL AND RADIAL VELOCITIES - DIGITIZER METHOD, Q=9.531 $cm^3/sec$
### 0.30 cm I.D. CAPILLARY TUBE, LARGE RESERVOIR

(Z/D) = 37.59 (℄ = 12.745 cm)

| r' (cm) | $V_r$ (cm/sec) | $V_z$ (cm/sec) | r' (cm) | $V_r$ (cm/sec) | $V_z$ (cm/sec) | r' (cm) | $V_r$ (cm/sec) | $V_z$ (cm/sec) | r' (cm) | $V_r$ (cm/sec) | $V_z$ (cm/sec) |
|---|---|---|---|---|---|---|---|---|---|---|---|
| 11.895 | 0.721 | 2.558 | 10.351 | 0.876 | 1.336 | 11.486 | 0.784 | 1.938 | 15.236 | -0.559 | 1.077 |
| 11.118 | 0.625 | 1.859 | 12.655 | -0.217 | 3.339 | 11.027 | 0.876 | 1.612 | 12.278 | 0.337 | 2.487 |
| 11.231 | 0.586 | 1.629 | 8.824 | 0.339 | 0.376 | 10.716 | 0.847 | 1.731 | 11.456 | 0.871 | 2.536 |
| 13.370 | -0.545 | 2.617 | 14.296 | -0.448 | 1.718 | 12.515 | 0.307 | 3.501 | 11.300 | 0.861 | 1.882 |
| 12.471 | 0.740 | 3.286 | 13.611 | -0.216 | 2.381 | 12.069 | 0.561 | 3.320 | 13.130 | -0.074 | 3.192 |
| 9.470 | 0.507 | 0.651 | 12.729 | 0.017 | 2.330 | 11.084 | 0.872 | 2.480 | 11.208 | 0.888 | 1.692 |
| 13.878 | -0.362 | 1.870 | 9.786 | 0.734 | 0.637 | 12.293 | 0.753 | 2.680 | 11.900 | 0.810 | 2.790 |
| 11.831 | 0.442 | 2.564 | 11.590 | 0.874 | 2.274 | 14.006 | -0.256 | 1.647 | 10.225 | 0.846 | 1.166 |
| 12.113 | 0.493 | 3.056 | 12.153 | 0.521 | 3.132 | 11.480 | 0.871 | 2.201 | 11.856 | 0.519 | 3.245 |
| 10.907 | 0.726 | 1.596 | 8.603 | 0.628 | 0.727 | 11.115 | 0.813 | 1.860 | 8.292 | 0.584 | 0.433 |

(Z/D) = 25.06 (℄ = 12.745 cm)

| r' (cm) | $V_r$ (cm/sec) | $V_z$ (cm/sec) | r' (cm) | $V_r$ (cm/sec) | $V_z$ (cm/sec) | r' (cm) | $V_r$ (cm/sec) | $V_z$ (cm/sec) | r' (cm) | $V_r$ (cm/sec) | $V_z$ (cm/sec) |
|---|---|---|---|---|---|---|---|---|---|---|---|
| 12.517 | -0.251 | 15.360 | 14.956 | -0.189 | 1.132 | 12.375 | 1.780 | 12.862 | 13.247 | -0.040 | 12.747 |
| 11.922 | 1.497 | 7.669 | 12.182 | 3.759 | 7.723 | 11.382 | 0.476 | 2.756 | 11.750 | 0.186 | 3.875 |
| 11.286 | 0.315 | 2.770 | 10.997 | 0.470 | 1.834 | 11.209 | 0.522 | 2.363 | 10.947 | 0.417 | 1.795 |
| 10.806 | 0.359 | 1.814 | 12.262 | 0.756 | 9.937 | 10.347 | 0.372 | 1.025 | 12.060 | 1.920 | 7.523 |
| 9.526 | 0.089 | 0.449 | 11.928 | 0.745 | 5.992 | 9.062 | 0.091 | 0.299 | 11.286 | 0.611 | 2.720 |
| 12.191 | 0.580 | 7.601 | 10.106 | 0.188 | 0.709 | 11.676 | 0.704 | 3.622 | 12.597 | 1.683 | 18.713 |
| 11.335 | 0.277 | 1.960 | 12.540 | 1.645 | 17.472 | 9.571 | 0.168 | 0.462 | 12.119 | 0.720 | 10.011 |
| 8.981 | 0.121 | 0.191 | 12.029 | 0.477 | 5.346 | 13.352 | -0.520 | 9.005 | 11.310 | 0.635 | 3.209 |
| 12.268 | 4.602 | 11.109 | 11.253 | 0.588 | 2.121 | 11.895 | 0.053 | 7.026 | 11.086 | 0.567 | 1.592 |

TABLE E.40 (continued)

(Z/D) = 25.06 ( ℄ = 12.745 cm)

| r' (cm) | $V_r$ (cm/sec) | $V_z$ (cm/sec) | r' (cm) | $V_r$ (cm/sec) | $V_z$ (cm/sec) | r' (cm) | $V_r$ (cm/sec) | $V_z$ (cm/sec) | r' (cm) | $V_r$ (cm/sec) | $V_z$ (cm/sec) |
|---|---|---|---|---|---|---|---|---|---|---|---|
| 11.710 | 0.794 | 2.760 | 10.633 | 0.270 | 1.378 | 10.160 | 0.054 | 0.799 | 12.234 | 1.323 | 10.892 |
| 9.563 | 0.126 | 0.486 | 11.857 | 0.681 | 4.000 | 11.991 | 1.225 | 8.669 | 11.527 | 0.198 | 3.386 |
| 11.926 | 0.650 | 4.260 | 11.055 | 0.151 | 2.446 | 11.239 | 0.407 | 2.414 | 13.530 | -0.749 | 6.483 |
| 10.820 | 0.543 | 1.196 | 12.311 | 1.661 | 11.983 | 10.696 | 0.308 | 1.341 | 12.002 | 0.656 | 5.800 |
| 14.572 | -0.553 | 1.641 | 11.755 | 0.551 | 4.107 | 10.459 | 0.066 | 1.053 | 9.661 | 0.226 | 0.543 |
| 9.913 | 0.384 | 0.788 | 14.247 | -0.464 | 2.862 | 11.727 | 0.418 | 3.653 | 12.117 | 1.872 | 9.139 |
| 13.390 | -0.456 | 7.353 | 12.116 | 0.875 | 10.504 | 12.433 | 1.304 | 12.916 | 11.891 | 0.251 | 5.567 |
| 12.209 | 1.156 | 8.517 | 10.501 | 0.428 | 1.382 | 12.257 | 0.314 | 11.015 | 8.506 | 0.084 | 0.663 |
| 11.923 | 1.358 | 6.005 | 8.889 | 0.047 | 0.352 | 10.297 | 0.157 | 0.896 | 14.445 | -0.356 | 1.963 |
| 8.963 | 0.050 | 0.238 | 13.416 | -0.698 | 7.420 | 12.940 | 1.386 | 15.473 | 12.388 | 2.090 | 15.460 |
| 11.841 | 0.788 | 5.954 | 11.749 | 0.502 | 3.883 | 10.811 | 0.379 | 1.324 | 12.224 | 1.190 | 9.205 |
| 13.910 | -0.710 | 3.317 | 13.053 | 1.631 | 15.071 | 13.081 | -1.033 | 14.450 | 13.900 | -0.652 | 3.682 |
| 12.990 | 0.143 | 16.661 | 12.403 | 3.100 | 13.811 | 12.011 | 0.955 | 6.342 | 12.561 | 1.201 | 18.110 |
| 13.753 | -0.358 | 4.563 | 11.949 | 0.691 | 6.118 | 12.618 | 1.519 | 16.154 | 12.646 | -0.425 | 16.319 |
| 12.440 | 1.107 | 12.332 | 12.349 | 1.823 | 11.704 | 13.357 | -0.337 | 7.883 | | | |

(Z/D) = 12.53 ( ℄ = 12.745 cm)

| r' (cm) | $V_r$ (cm/sec) | $V_z$ (cm/sec) | r' (cm) | $V_r$ (cm/sec) | $V_z$ (cm/sec) | r' (cm) | $V_r$ (cm/sec) | $V_z$ (cm/sec) | r' (cm) | $V_r$ (cm/sec) | $V_z$ (cm/sec) |
|---|---|---|---|---|---|---|---|---|---|---|---|
| 13.567 | -0.478 | 8.178 | 12.605 | 0.970 | 17.796 | 12.609 | 2.267 | 33.729 | 11.217 | -0.045 | 1.070 |
| 12.495 | 1.164 | 17.053 | 13.264 | -0.566 | 17.381 | 12.188 | 0.537 | 8.845 | 11.308 | -0.104 | 2.492 |
| 10.996 | -0.255 | 0.838 | 14.073 | 0.484 | 2.116 | 12.551 | 1.987 | 31.306 | 12.263 | 0.646 | 8.657 |
| 12.102 | 0.742 | 6.179 | 11.904 | 0.375 | 5.067 | 11.501 | -0.055 | 1.922 | 12.513 | 1.346 | 21.331 |
| 12.360 | 0.520 | 12.236 | 11.352 | -0.281 | 1.403 | 11.055 | -0.193 | 0.672 | 12.305 | 1.067 | 8.406 |
| 12.250 | 0.558 | 8.768 | 11.507 | -0.121 | 1.913 | 13.207 | -0.840 | 28.495 | 13.374 | -0.002 | 9.768 |
| 13.122 | -0.129 | 33.170 | 12.284 | 0.886 | 8.322 | 11.889 | 0.071 | 3.082 | 11.160 | -0.152 | 0.973 |
| 11.269 | -0.401 | 1.155 | 13.798 | 0.884 | 3.103 | 12.081 | 0.344 | 5.380 | 12.488 | 1.020 | 21.666 |
| 11.899 | -0.057 | 3.106 | 12.122 | 0.462 | 7.113 | 11.540 | -0.007 | 1.916 | 11.634 | 0.080 | 2.463 |

TABLE E.40 (continued)

(Z/D) = 12.53 ( ℄ = 12.745 cm)

| r' (cm) | $V_r$ (cm/sec) | $V_z$ (cm/sec) | r' (cm) | $V_r$ (cm/sec) | $V_z$ (cm/sec) | r' (cm) | $V_r$ (cm/sec) | $V_z$ (cm/sec) | r' (cm) | $V_r$ (cm/sec) | $V_z$ (cm/sec) |
|---|---|---|---|---|---|---|---|---|---|---|---|
| 13.252 | -0.632 | 17.980 | 11.204 | -0.213 | 1.366 | 12.133 | 1.093 | 6.637 | 13.520 | 0.213 | 5.341 |
| 10.521 | -0.386 | 0.242 | 11.441 | 0.167 | 1.733 | 13.209 | -0.510 | 18.810 | 13.011 | -1.637 | 40.220 |
| 13.328 | -0.177 | 12.206 | 12.834 | -6.631 | 85.872 | 12.458 | 2.084 | 17.668 | 12.315 | 0.523 | 10.576 |
| 12.588 | 2.069 | 26.460 | 13.482 | 0.002 | 7.457 | 12.258 | 0.314 | 7.934 | 12.523 | 1.480 | 19.056 |
| 11.650 | -0.022 | 2.461 | 12.395 | 2.206 | 15.574 | 11.172 | -0.150 | 1.105 | 12.006 | 0.234 | 4.633 |
| 13.762 | 0.334 | 4.039 | 12.689 | 2.182 | 78.445 | 12.752 | 2.067 | 89.243 | 12.685 | 4.439 | 60.683 |
| 12.748 | 6.222 | 72.609 | 12.267 | 0.786 | 9.226 | | | | | | |

## TABLE E.41

### AXIAL AND RADIAL VELOCITIES - DIGITIZER METHOD, Q=10.325 $cm^3/sec$
### 0.30 cm I.D. CAPILLARY TUBE, LARGE RESERVOIR

(Z/D) = 38.16 ( ℄ = 12.745 cm)

| r' (cm) | $V_r$ (cm/sec) | $V_z$ (cm/sec) | r' (cm) | $V_r$ (cm/sec) | $V_z$ (cm/sec) | r' (cm) | $V_r$ (cm/sec) | $V_z$ (cm/sec) | r' (cm) | $V_r$ (cm/sec) | $V_z$ (cm/sec) |
|---|---|---|---|---|---|---|---|---|---|---|---|
| 14.225 | -0.695 | 2.011 | 13.114 | -0.672 | 2.953 | 12.382 | 0.210 | 2.861 | 12.210 | 0.720 | 2.871 |
| 12.399 | 0.121 | 2.834 | 7.614 | 0.274 | 0.324 | 11.882 | 0.776 | 3.026 | 8.642 | 0.209 | 1.016 |
| 11.103 | 0.827 | 1.769 | 14.173 | -0.706 | 2.050 | 14.636 | -0.418 | 1.174 | 12.580 | 0.534 | 4.608 |
| 13.969 | -0.691 | 2.201 | 12.272 | 0.606 | 3.057 | 12.678 | -0.301 | 3.900 | 12.000 | 0.654 | 2.532 |
| 12.396 | 0.172 | 3.498 | 11.578 | 0.636 | 2.532 | 11.474 | 0.789 | 2.178 | 11.436 | 0.771 | 2.103 |
| 11.546 | 0.959 | 2.576 | 12.776 | -0.115 | 3.322 | 11.515 | 0.665 | 1.339 | 12.194 | 0.734 | 2.835 |
| 10.136 | 0.641 | 0.850 | 11.731 | 0.769 | 2.122 | 10.072 | 0.729 | 1.247 | 13.764 | -0.585 | 1.976 |
| 8.084 | 0.480 | 0.213 | 11.648 | 0.734 | 1.954 | 13.399 | -0.673 | 2.877 | 14.890 | -0.812 | 1.088 |
| 12.037 | 0.720 | 2.759 | 14.021 | -0.659 | 2.087 | 11.920 | 0.983 | 2.953 | 9.468 | 0.555 | 0.596 |
| 14.743 | -0.610 | 1.374 | 13.976 | -0.815 | 2.123 | 12.249 | 0.833 | 3.927 | 14.265 | -0.622 | 1.678 |
| 10.335 | 0.956 | 1.037 | 13.960 | -0.561 | 2.186 | 11.979 | 0.511 | 2.940 | 11.036 | 0.724 | 1.217 |
| 8.242 | 0.314 | 0.267 | | | | | | | | | |

(Z/D) = 25.44 ( ℄ = 12.745 cm)

| r' (cm) | $V_r$ (cm/sec) | $V_z$ (cm/sec) | r' (cm) | $V_r$ (cm/sec) | $V_z$ (cm/sec) | r' (cm) | $V_r$ (cm/sec) | $V_z$ (cm/sec) | r' (cm) | $V_r$ (cm/sec) | $V_z$ (cm/sec) |
|---|---|---|---|---|---|---|---|---|---|---|---|
| 13.723 | -0.450 | 4.910 | 12.261 | 1.438 | 12.242 | 12.903 | 0.027 | 16.570 | 12.168 | 1.073 | 9.416 |
| 12.404 | 1.736 | 13.947 | 12.064 | 0.091 | 5.524 | 11.685 | 0.522 | 4.550 | 11.539 | 0.609 | 3.057 |
| 11.576 | 0.429 | 2.641 | 9.740 | 0.113 | 0.542 | 11.485 | 0.499 | 3.376 | 9.538 | 0.098 | 0.469 |
| 11.362 | 0.416 | 3.148 | 13.416 | -0.192 | 9.777 | 10.649 | 0.483 | 1.619 | 12.662 | 1.232 | 17.423 |
| 13.521 | -1.093 | 7.451 | 12.781 | 0.312 | 20.144 | 12.036 | 0.751 | 7.482 | 12.829 | 0.243 | 15.602 |
| 11.795 | 0.783 | 4.864 | 12.105 | 1.241 | 10.924 | 11.049 | 0.368 | 1.849 | 11.983 | 1.235 | 6.641 |
| 9.440 | 0.192 | 0.553 | 11.478 | 0.165 | 2.108 | 8.430 | 0.127 | 0.627 | 9.067 | 0.139 | 0.593 |
| 13.991 | -0.445 | 3.709 | 12.858 | 0.143 | 20.893 | 12.566 | 1.657 | 21.567 | 12.150 | 0.729 | 7.721 |
| 12.460 | 0.815 | 16.550 | 9.751 | 0.175 | 1.373 | 12.109 | 0.753 | 7.269 | 12.814 | -0.500 | 21.515 |

TABLE E.41 (continued)

(Z/D) = 25.44 ( ℄ = 12.745 cm)

| r'(cm) | $V_r$(cm/sec) | $V_z$(cm/sec) | r'(cm) | $V_r$(cm/sec) | $V_z$(cm/sec) | r'(cm) | $V_r$(cm/sec) | $V_z$(cm/sec) | r'(cm) | $V_r$(cm/sec) | $V_z$(cm/sec) |
|---|---|---|---|---|---|---|---|---|---|---|---|
| 11.992 | 0.774 | 6.368 | 12.592 | 1.157 | 20.765 | 11.469 | 0.221 | 2.673 | 12.082 | 1.152 | 7.202 |
| 10.598 | 0.771 | 1.296 | 11.704 | 0.389 | 3.202 | 9.289 | 0.126 | 0.413 | 11.483 | 0.343 | 2.112 |
| 13.220 | -0.603 | 10.110 | 8.624 | 0.034 | 0.157 | 13.510 | -0.541 | 7.313 | 9.106 | 0.058 | 0.262 |
| 12.235 | 2.408 | 11.933 | 14.815 | -0.140 | 1.368 | 12.132 | 0.866 | 9.452 | 11.989 | 1.076 | 7.201 |
| 11.836 | 0.881 | 4.643 | 11.862 | 0.970 | 4.156 | 11.824 | 0.919 | 5.960 | 11.572 | 0.544 | 2.605 |
| 11.735 | 0.531 | 4.423 | 11.516 | 0.698 | 3.623 | 11.534 | 0.291 | 3.990 | 11.076 | 0.339 | 2.225 |
| 11.358 | 0.349 | 3.040 | 10.695 | 0.230 | 1.583 | 10.022 | 0.206 | 1.020 | 9.952 | 0.125 | 0.974 |
| 9.872 | 0.196 | 0.700 | 13.122 | -0.031 | 14.277 | 11.493 | 0.534 | 2.729 | 12.110 | 1.117 | 10.432 |
| 10.670 | 0.297 | 1.572 | 13.069 | -0.029 | 13.572 | 10.152 | 0.156 | 0.990 | 12.729 | 0.154 | 18.075 |
| 13.718 | -0.351 | 5.027 | 12.184 | 0.605 | 10.575 | 12.454 | 1.123 | 16.702 | 13.456 | -0.094 | 7.836 |
| 12.243 | 1.221 | 10.130 | 13.359 | -0.086 | 7.509 | 11.475 | 0.642 | 3.469 | 13.192 | -0.758 | 9.888 |
| 8.680 | 0.159 | 0.389 | 12.613 | 1.081 | 19.186 | 11.600 | 0.788 | 2.995 | 12.599 | 1.067 | 19.512 |
| 13.578 | -0.420 | 7.120 | 12.080 | 0.611 | 8.724 | 13.264 | -0.276 | 9.899 | 12.015 | 0.685 | 7.219 |
| 12.121 | 1.014 | 9.929 | 13.861 | -0.489 | 3.879 | 11.942 | 1.021 | 7.371 | 13.135 | -0.321 | 12.184 |
| 13.321 | -0.335 | 9.190 | 12.819 | 1.724 | 20.839 | 13.114 | -0.101 | 12.190 | 12.695 | 0.265 | 21.344 |
| 11.758 | 1.099 | 5.580 | 12.296 | 1.383 | 14.189 | 12.110 | 0.866 | 8.755 | 11.843 | 1.041 | 5.579 |

(Z/D) = 12.72 ( ℄ = 12.745 cm)

| r'(cm) | $V_r$(cm/sec) | $V_z$(cm/sec) | r'(cm) | $V_r$(cm/sec) | $V_z$(cm/sec) | r'(cm) | $V_r$(cm/sec) | $V_z$(cm/sec) | r'(cm) | $V_r$(cm/sec) | $V_z$(cm/sec) |
|---|---|---|---|---|---|---|---|---|---|---|---|
| 12.414 | 1.579 | 13.116 | 14.086 | 0.563 | 3.681 | 12.200 | 0.817 | 9.565 | 13.243 | -0.060 | 10.668 |
| 14.037 | 0.244 | 3.274 | 12.564 | 2.335 | 24.809 | 13.803 | 0.716 | 4.450 | 12.309 | 1.027 | 9.903 |
| 12.473 | 1.590 | 14.276 | 12.418 | 1.224 | 12.092 | 12.440 | 0.780 | 14.127 | 11.740 | -0.354 | 2.696 |
| 12.354 | 0.924 | 12.944 | 11.485 | -0.438 | 1.817 | 12.255 | 0.681 | 9.444 | 11.172 | -0.088 | 1.350 |
| 12.149 | 0.167 | 5.301 | 12.504 | 1.779 | 24.686 | 12.272 | 1.116 | 9.458 | 12.195 | 0.933 | 8.925 |
| 12.184 | 0.456 | 5.948 | 11.978 | 0.779 | 4.827 | 11.900 | 0.242 | 3.037 | 11.245 | -0.731 | 1.330 |
| 14.025 | 0.593 | 3.695 | 13.306 | -0.220 | 10.260 | 12.311 | 0.711 | 9.483 | 12.797 | 2.662 | 41.039 |
| 12.236 | 0.411 | 6.997 | 12.178 | 0.254 | 6.805 | 12.441 | 1.210 | 16.471 | 11.857 | -0.397 | 3.749 |
| 13.782 | 0.065 | 3.404 | 12.639 | 3.082 | 50.251 | 12.506 | 3.001 | 20.140 | 12.621 | 3.506 | 60.984 |

## TABLE E.41 (continued)

(Z/D) = 12.72 (℄ = 12.745 cm)

| r' (cm) | $V_r$ (cm/sec) | $V_z$ (cm/sec) | r' (cm) | $V_r$ (cm/sec) | $V_z$ (cm/sec) | r' (cm) | $V_r$ (cm/sec) | $V_z$ (cm/sec) | r' (cm) | $V_r$ (cm/sec) | $V_z$ (cm/sec) |
|---|---|---|---|---|---|---|---|---|---|---|---|
| 12.223 | 1.168 | 8.794 | 12.265 | 0.236 | 9.356 | 11.895 | 0.310 | 3.982 | 12.512 | 2.852 | 38.500 |
| 13.666 | 0.583 | 5.729 | 13.161 | -0.320 | 22.322 | 13.346 | -0.724 | 12.719 | 12.277 | 1.026 | 9.385 |
| 13.125 | -1.016 | 30.288 | 12.011 | -0.470 | 4.779 | 12.488 | -1.426 | 16.076 | 12.486 | 1.383 | 23.439 |
| 12.588 | 2.657 | 54.857 | 12.439 | 1.025 | 12.871 | 13.604 | 0.033 | 5.635 | 12.324 | 0.660 | 10.237 |
| 13.216 | -1.506 | 14.658 | 13.174 | -0.727 | 16.529 | 11.871 | -0.068 | 4.734 | | | |

## TABLE E.42

## AXIAL AND RADIAL VELOCITIES - DIGITIZER METHOD, Q=11.120 $cm^3/sec$
## 0.30 cm I.D. CAPILLARY TUBE, LARGE RESERVOIR

(Z/D) = 38.16 (℄ = 12.745 cm)

| r'(cm) | $V_r$(cm/sec) | $V_z$(cm/sec) | r'(cm) | $V_r$(cm/sec) | $V_z$(cm/sec) | r'(cm) | $V_r$(cm/sec) | $V_z$(cm/sec) | r'(cm) | $V_r$(cm/sec) | $V_z$(cm/sec) |
|---|---|---|---|---|---|---|---|---|---|---|---|
| 13.638 | -0.173 | 4.350 | 13.237 | -0.361 | 22.852 | 13.790 | -0.515 | 3.742 | 12.617 | 2.648 | 34.792 |
| 13.304 | -0.764 | 16.636 | 12.386 | 1.956 | 16.922 | 13.243 | 1.306 | 20.285 | 11.731 | 0.162 | 2.834 |
| 12.261 | 0.375 | 8.992 | 12.766 | 4.223 | 73.497 | 12.237 | 0.459 | 10.462 | 12.299 | 1.135 | 11.028 |
| 12.752 | 0.867 | 84.389 | 12.021 | 1.027 | 5.690 | 11.935 | 0.750 | 5.081 | 12.758 | 4.394 | 71.741 |
| 12.328 | 1.163 | 14.293 | 12.141 | 0.432 | 7.467 | 12.052 | 1.022 | 6.124 | 12.611 | 2.311 | 39.432 |
| 12.329 | 0.943 | 10.581 | 12.642 | 4.079 | 73.630 | 12.274 | 1.404 | 9.278 | 11.427 | 0.095 | 1.975 |
| 12.013 | 0.838 | 6.296 | 13.261 | -0.337 | 21.293 | 11.613 | 0.078 | 2.557 | 13.200 | 0.632 | 15.473 |
| 14.132 | 0.181 | 2.183 | 11.990 | 0.242 | 5.002 | 13.791 | -0.086 | 3.717 | 11.911 | 0.035 | 3.157 |
| 13.471 | -0.451 | 10.208 | 11.677 | -0.157 | 2.213 | 12.337 | 0.451 | 14.362 | 11.519 | -0.208 | 2.081 |
| 11.972 | 0.382 | 6.583 | 12.425 | 0.882 | 16.437 | 11.697 | 0.037 | 4.547 | 12.410 | -0.051 | 23.554 |
| 13.943 | 0.118 | 4.135 | 12.241 | 0.736 | 11.213 | 10.878 | -0.626 | 0.493 | 12.471 | 1.820 | 22.663 |
| 10.697 | -0.331 | 0.434 | 11.968 | 1.111 | 5.438 | 13.287 | -0.671 | 22.864 | 11.936 | -0.076 | 2.891 |
| 12.487 | 0.927 | 15.353 | 12.568 | 1.763 | 25.778 | 12.306 | 0.622 | 9.146 | 12.225 | 0.314 | 7.634 |
| 10.659 | -0.421 | 0.431 | 12.422 | 0.727 | 18.054 | 12.595 | 2.443 | 53.413 | 11.823 | -0.271 | 3.600 |
| 12.036 | -0.389 | 5.438 | | | | | | | | | |

(Z/D) = 25.44 (℄ = 12.745 cm)

| r'(cm) | $V_r$(cm/sec) | $V_z$(cm/sec) | r'(cm) | $V_r$(cm/sec) | $V_z$(cm/sec) | r'(cm) | $V_r$(cm/sec) | $V_z$(cm/sec) | r'(cm) | $V_r$(cm/sec) | $V_z$(cm/sec) |
|---|---|---|---|---|---|---|---|---|---|---|---|
| 13.206 | -0.892 | 9.773 | 12.903 | 0.679 | 18.387 | 13.130 | 0.757 | 9.928 | 12.632 | 1.529 | 20.172 |
| 12.551 | -0.332 | 23.071 | 11.903 | 0.782 | 7.795 | 12.434 | 1.869 | 21.935 | 11.451 | 0.103 | 3.233 |
| 13.391 | -0.697 | 8.527 | 11.103 | 0.605 | 2.343 | 12.676 | -0.140 | 24.056 | 8.958 | 0.070 | 0.281 |
| 12.286 | 2.366 | 11.714 | 12.639 | 0.509 | 24.620 | 13.354 | -0.710 | 9.889 | 11.818 | 0.065 | 4.660 |
| 12.681 | 0.416 | 20.694 | 10.350 | 0.282 | 1.218 | 12.328 | -0.006 | 12.737 | 9.122 | 0.102 | 0.306 |
| 12.002 | 0.907 | 7.153 | 8.562 | 0.030 | 0.121 | 13.041 | -1.478 | 15.744 | 13.477 | -0.731 | 8.699 |

TABLE E.42 (continued)

(Z/D) = 25.44 (℄ = 12.745)

| r' (cm) | $V_r$ (cm/sec) | $V_z$ (cm/sec) | r' (cm) | $V_r$ (cm/sec) | $V_z$ (cm/sec) | r' (cm) | $V_r$ (cm/sec) | $V_z$ (cm/sec) | r' (cm) | $V_r$ (cm/sec) | $V_z$ (cm/sec) |
|---|---|---|---|---|---|---|---|---|---|---|---|
| 13.484 | -0.435 | 6.248 | 11.710 | 0.795 | 4.263 | 12.635 | 2.110 | 24.011 | 11.016 | 0.529 | 1.815 |
| 11.898 | 1.505 | 7.065 | 12.397 | 0.908 | 15.048 | 11.634 | 1.366 | 4.666 | 12.810 | 0.172 | 23.747 |
| 12.545 | -0.109 | 24.817 | 12.259 | 0.803 | 11.702 | 12.668 | 0.964 | 23.212 | 10.264 | 0.740 | 1.362 |
| 12.581 | 0.299 | 20.909 | 12.473 | 1.531 | 17.728 | 12.047 | -0.298 | 7.722 | 12.422 | 1.000 | 19.144 |
| 12.014 | 1.036 | 8.082 | 12.287 | 1.122 | 13.662 | 12.328 | 1.163 | 14.293 | 12.128 | 1.196 | 10.320 |
| 12.052 | 1.022 | 6.124 | 11.667 | -0.029 | 2.929 | 12.929 | 1.694 | 23.012 | 11.582 | 0.496 | 4.933 |
| 12.661 | 1.654 | 20.507 | 10.653 | 0.395 | 1.455 | 12.567 | 2.363 | 21.070 | 10.444 | 0.222 | 1.254 |
| 13.573 | -0.763 | 8.960 | 13.757 | -0.233 | 6.982 | 12.631 | 0.555 | 20.227 | 14.321 | -0.959 | 4.486 |
| 12.622 | 0.283 | 29.500 | 12.931 | -0.939 | 26.727 | 12.539 | 0.967 | 20.839 | 12.912 | -0.089 | 25.432 |
| 12.212 | 0.233 | 9.060 | 8.606 | 0.020 | 0.177 | 12.042 | 1.637 | 9.923 | 14.129 | -0.791 | 4.526 |
| 11.487 | 0.807 | 4.717 | 13.814 | 0.178 | 4.287 | 11.338 | 0.480 | 2.886 | 12.311 | 1.493 | 14.389 |
| 10.124 | 0.268 | 1.060 | 12.063 | 0.893 | 8.438 | 12.826 | 0.949 | 20.800 | 12.854 | 0.969 | 26.964 |
| 12.366 | 2.669 | 18.963 | 12.481 | 4.320 | 18.824 | 12.577 | 1.594 | 19.200 | 12.333 | 1.612 | 13.305 |
| 11.802 | 1.127 | 5.626 | 11.958 | 1.323 | 6.647 | 11.484 | 0.812 | 3.213 | 11.857 | 1.088 | 6.115 |
| 11.311 | 1.739 | 3.199 | 11.492 | 0.269 | 3.351 | 10.128 | 0.267 | 0.927 | 10.387 | 0.193 | 1.142 |
| 14.102 | -0.431 | 4.310 | 12.183 | 1.849 | 8.986 | 12.971 | -0.053 | 22.992 | 10.648 | 0.374 | 1.465 |
| 12.727 | 2.024 | 24.059 | 10.466 | 0.313 | 1.060 | 12.682 | 0.631 | 19.966 | 13.938 | -0.172 | 3.753 |
| 14.310 | -0.647 | 2.989 | 11.830 | 0.777 | 4.266 | 12.345 | 0.968 | 15.053 | 11.440 | 1.248 | 2.664 |
| 12.240 | 1.445 | 13.149 | 10.457 | 0.478 | 1.441 | 9.474 | 0.109 | 0.508 | 10.347 | 0.223 | 1.002 |
| 9.301 | 0.021 | 0.429 | 9.906 | 0.077 | 0.672 | | | | | | |

(Z/D) = 12.72 (℄ = 12.745)

| r' (cm) | $V_r$ (cm/sec) | $V_z$ (cm/sec) | r' (cm) | $V_r$ (cm/sec) | $V_z$ (cm/sec) | r' (cm) | $V_r$ (cm/sec) | $V_z$ (cm/sec) | r' (cm) | $V_r$ (cm/sec) | $V_z$ (cm/sec) |
|---|---|---|---|---|---|---|---|---|---|---|---|
| 12.895 | 0.100 | 3.083 | 13.339 | -0.753 | 3.138 | 12.739 | 0.622 | 3.585 | 12.656 | -0.067 | 4.244 |
| 8.313 | 0.359 | 0.310 | 11.737 | 1.154 | 2.395 | 7.826 | 0.304 | 0.203 | 11.191 | 1.069 | 2.224 |
| 13.572 | 0.297 | 2.562 | 10.596 | 0.841 | 1.354 | 12.982 | -0.248 | 4.540 | 12.578 | -0.211 | 4.616 |
| 12.438 | 0.685 | 4.299 | 9.783 | 0.608 | 0.892 | 11.548 | 0.799 | 2.423 | 14.270 | -0.763 | 2.275 |

TABLE E.42 (continued)

$(Z/D) = 12.72$ (℄ = 12.745)

| r' (cm) | $V_r$ (cm/sec) | $V_z$ (cm/sec) | r' (cm) | $V_r$ (cm/sec) | $V_z$ (cm/sec) | r' (cm) | $V_r$ (cm/sec) | $V_z$ (cm/sec) | r' (cm) | $V_r$ (cm/sec) | $V_z$ (cm/sec) |
|---|---|---|---|---|---|---|---|---|---|---|---|
| 11.263 | 0.911 | 2.219 | 13.158 | 0.221 | 4.475 | 10.678 | 0.288 | 1.397 | 12.962 | 0.106 | 3.271 |
| 12.832 | 0.049 | 4.096 | 8.511 | 0.358 | 0.380 | 12.375 | 0.963 | 3.028 | 14.251 | -0.576 | 1.790 |
| 12.218 | 0.986 | 3.592 | 12.913 | -0.035 | 4.583 | 11.544 | 0.835 | 2.386 | 11.986 | 0.786 | 3.024 |
| 7.646 | 0.299 | 0.159 | 8.206 | 0.378 | 0.294 | 8.331 | 0.399 | 0.359 | 14.391 | -0.678 | 2.200 |
| 8.334 | 0.375 | 0.327 | 13.908 | -0.565 | 2.691 | 12.210 | 0.341 | 3.315 | 12.827 | 0.015 | 3.720 |
| 11.847 | 0.646 | 3.248 | 11.898 | 0.636 | 3.134 | 13.766 | -0.758 | 3.174 | 11.412 | 0.716 | 2.046 |
| 13.022 | -0.012 | 4.658 | 10.198 | 0.997 | 0.776 | 12.660 | 0.253 | 4.064 | 14.794 | -0.702 | 1.597 |
| 11.840 | 0.654 | 3.004 | 14.421 | -0.811 | 2.308 | 13.765 | -0.579 | 3.292 | 12.932 | -0.165 | 4.805 |
| 12.751 | -0.201 | 3.865 | 13.213 | -0.365 | 3.090 | 12.271 | 0.325 | 2.789 | 13.002 | -0.211 | 4.052 |
| 10.521 | 0.843 | 1.260 | 12.948 | -0.087 | 3.379 | 11.121 | 1.100 | 1.606 | 12.624 | -0.021 | 3.344 |
| 11.249 | 0.868 | 2.295 | | | | | | | | | |

## E.3 MATHEMATICAL SIMPLIFICATIONS

The use of Equation 3.47 and a tractable constitutive equation allows for the prediction of normal forces in the converging flow field. The magnitude and/or rate of growth of these normal forces have been suggested as an explanation for the onset of fracture. To predict the growth of the normal forces this analysis requires a prior knowledge of the magnitude of the velocity components which are then used to evaluate the components of the deformation rate tensor.

Assuming axial symmetry, the deformation rate tensor in a cylindrical coordinate system is given by

$$d_{<ij>} = \begin{bmatrix} V_{z,z} & \frac{1}{2}(V_{z,r}+V_{r,z}) & 0 \\ \frac{1}{2}(V_{z,r}+V_{r,z}) & V_{r,r} & 0 \\ 0 & 0 & \frac{V_r}{r} \end{bmatrix} \quad \text{E.1}$$

The magnitude of the shear component of the deformation rate tensor was obtained from plots of axial and radial velocities. Using the raw data tabulated in the preceding sections of this appendix, maximum values of $V_{z,r}$ and $V_{r,z}$ were estimated at several radial positions for the smallest and largest flow rates within region I and in reservoir S. The radial positions were arbitrarily chosen to 0.2D, 0.4D, 0.6D, 0.8D, and D where D is the internal diameter of the capillary tube. The results are tabulated in Table E.43. The data show that the shear component of the deformation rate tensor can be evaluated as a first approximation by $V_{z,r}$ alone. The errors are less than 15%. Therefore, as a first approximation, the deformation rate tensor can be simplified as

$$d_{<ij>} = \begin{bmatrix} V_{z,z} & \frac{1}{2}V_{z,r} & 0 \\ \frac{1}{2}V_{z,r} & V_{r,r} & 0 \\ 0 & 0 & \frac{V_r}{r} \end{bmatrix} \qquad \text{E.2}$$

The mathematical analysis may be simplified further by comparison of the magnitudes of the radial velocity and axial velocity components. This was determined by estimating the maximum values of the ratio, $(V_r/V_z)_M$ at the same radial positions where the shear component was evaluated. These ratios are plotted in Figures E.1 to E.3. In addition to indicating that $(V_r/V_z)_M$ increases as we move away from the centerline, the data in Figures E.1 to E.3 also show that at the largest flow rate within region I the ratio $(V_r/V_z)_M$ is approximately equal to 0.10, even under worst condition, i.e., at a radial distance equal to one tube diameter. At radial positions greater than this, the ratio tends to be equal to zero. In reservoir L, region I extended to even higher flow rates. Although not shown in Figures E.1 to E.3 the ratio, $(V_r/V_z)_M$, for these higher flow rates was in all cases less than 0.10. At the lowest flow rate where velocities were measured in reservoir S the radial velocity component is approximately equal to one half the magnitude of the axial velocity component. As an example, the data in Figure E.2 show that at a flow rate of 0.040 $cm^3$/sec $V_r$ approaches 0.60 $V_z$ at r equal to 0.8D. A photograph of this flow field is given in Figure 2.5. Within the vicinity of the centerline (r<0.2D) the simplification $V_r < V_z$ holds to within 10% error.

In summary, for flow rates at the upper limit of region I, mathematical analyses can be simplified by assuming that

$$V_r < V_z \qquad \text{E.3}$$

where < implies an order of magnitude, and

$$V_{r,z} + V_{z,r} \simeq V_{z,r} \qquad \text{E.4}$$

At the lower limit of region I where velocities were measured

$$V_r \simeq V_z \qquad \text{E.5}$$

and

$$V_{r,z} + V_{z,r} \simeq V_{z,r} \qquad \text{E.6}$$

Only within the vicinity of the contraction (r<0.2D) can we assume $V_r < V_z$.

# TABLE E.43

## SHEAR COMPONENT OF DEFORMATION RATE TENSOR

| I.D. (cm) | Q ($cm^3$/ sec) | Shear Component ($sec^{-1}$) | RADIAL COORDINATE | | | | |
|---|---|---|---|---|---|---|---|
| | | | .2D | .4D | .6D | .8D | D |
| 0.30 | 0.040 | $V_{r,z}$ | 0.005 | 0.011 | 0.011 | 0.005 | 0.005 |
| | | $V_{z,r}$ | 0.800 | 0.292 | 0.208 | 0.017 | - |
| | 0.635 | $V_{r,z}$ | 0.042 | 0.069 | 0.042 | 0.111 | 0.138 |
| | | $V_{z,r}$ | - | 4.200 | 3.300 | 2.500 | - |
| 0.20 | 0.040 | $V_{r,z}$ | 0.060 | 0.105 | 0.105 | 0.075 | 0.180 |
| | | $V_{z,r}$ | 3.130 | 5.000 | 3.750 | 3.750 | - |
| | 0.318 | $V_{r,z}$ | 0.088 | 0.163 | 0.150 | 0.066 | 0.012 |
| | | $V_{z,r}$ | 3.750 | 2.500 | 6.250 | 16.300 | - |
| 0.10 | 0.016 | $V_{r,z}$ | 0.063 | 0.140 | 0.156 | 0.125 | 0.100 |
| | | $V_{z,r}$ | 0.500 | 1.000 | 1.250 | 1.250 | - |
| | 0.119 | $V_{r,z}$ | 0.150 | 0.150 | 0.280 | 0.160 | 0.050 |
| | | $V_{z,r}$ | - | 0.750 | 1.250 | 1.500 | - |

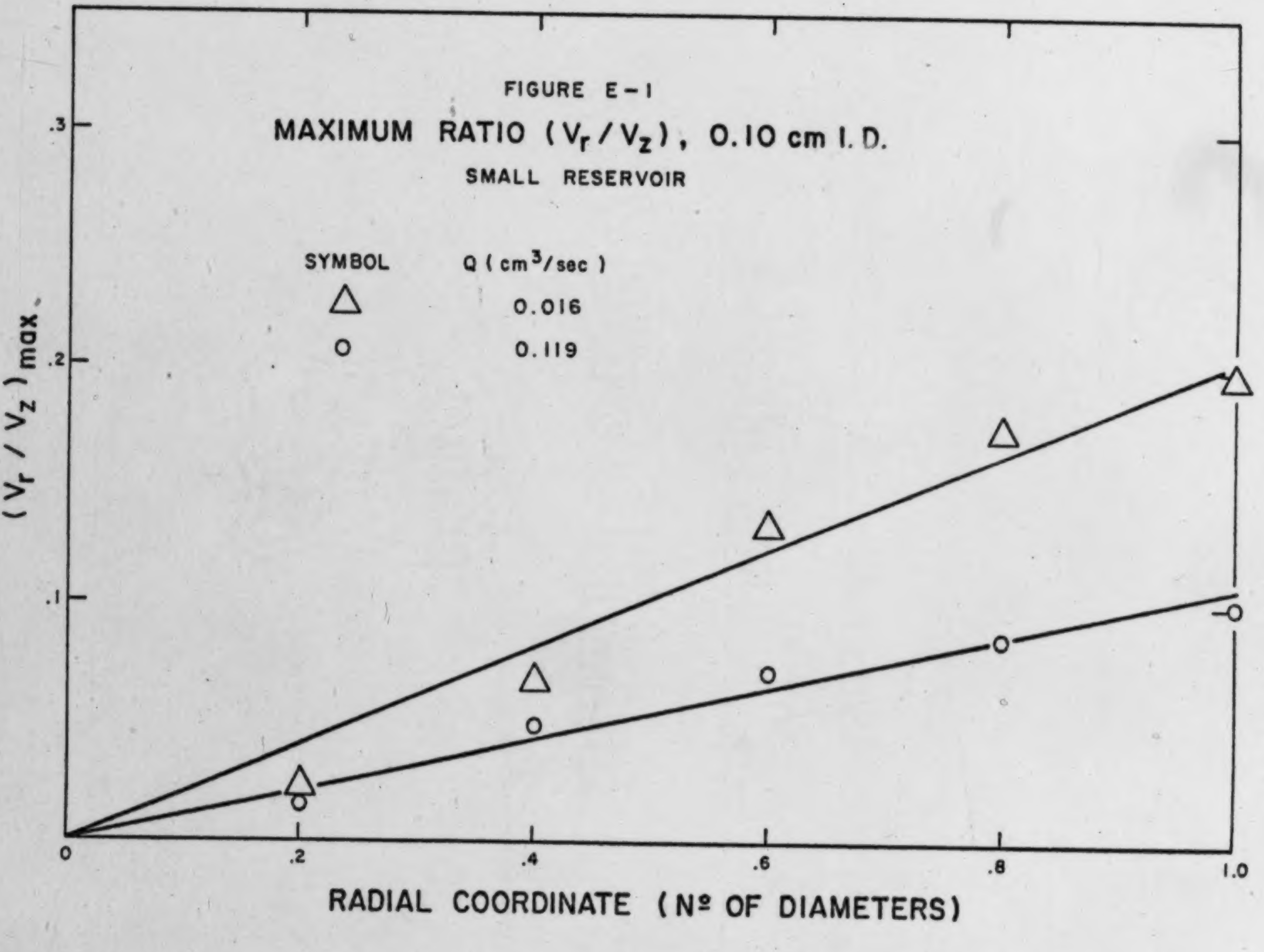

FIGURE E-1

MAXIMUM RATIO $(V_r / V_z)$, 0.10 cm I.D.

SMALL RESERVOIR

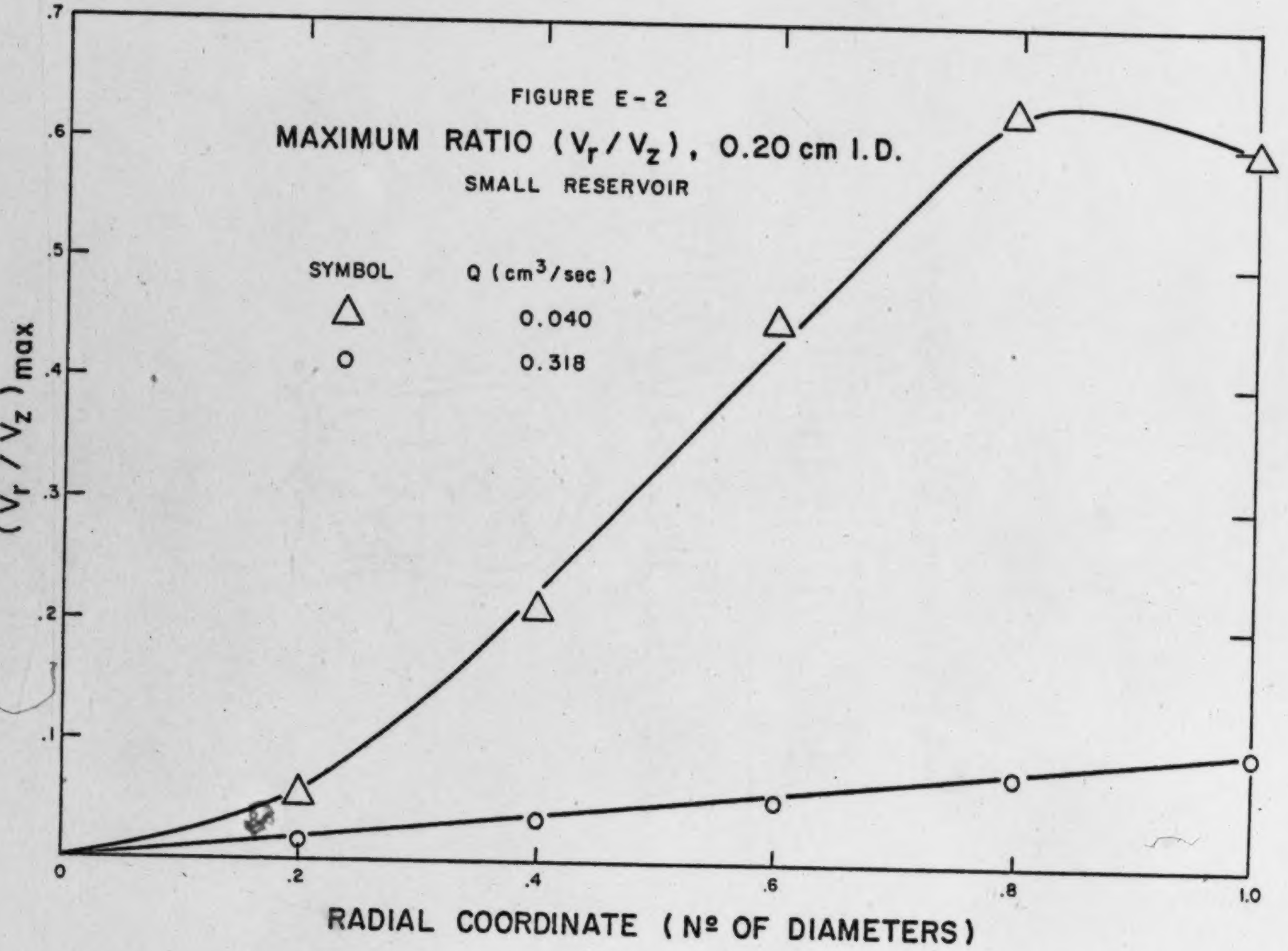

FIGURE E-2

MAXIMUM RATIO $(V_r / V_z)$, 0.20 cm I.D.

SMALL RESERVOIR

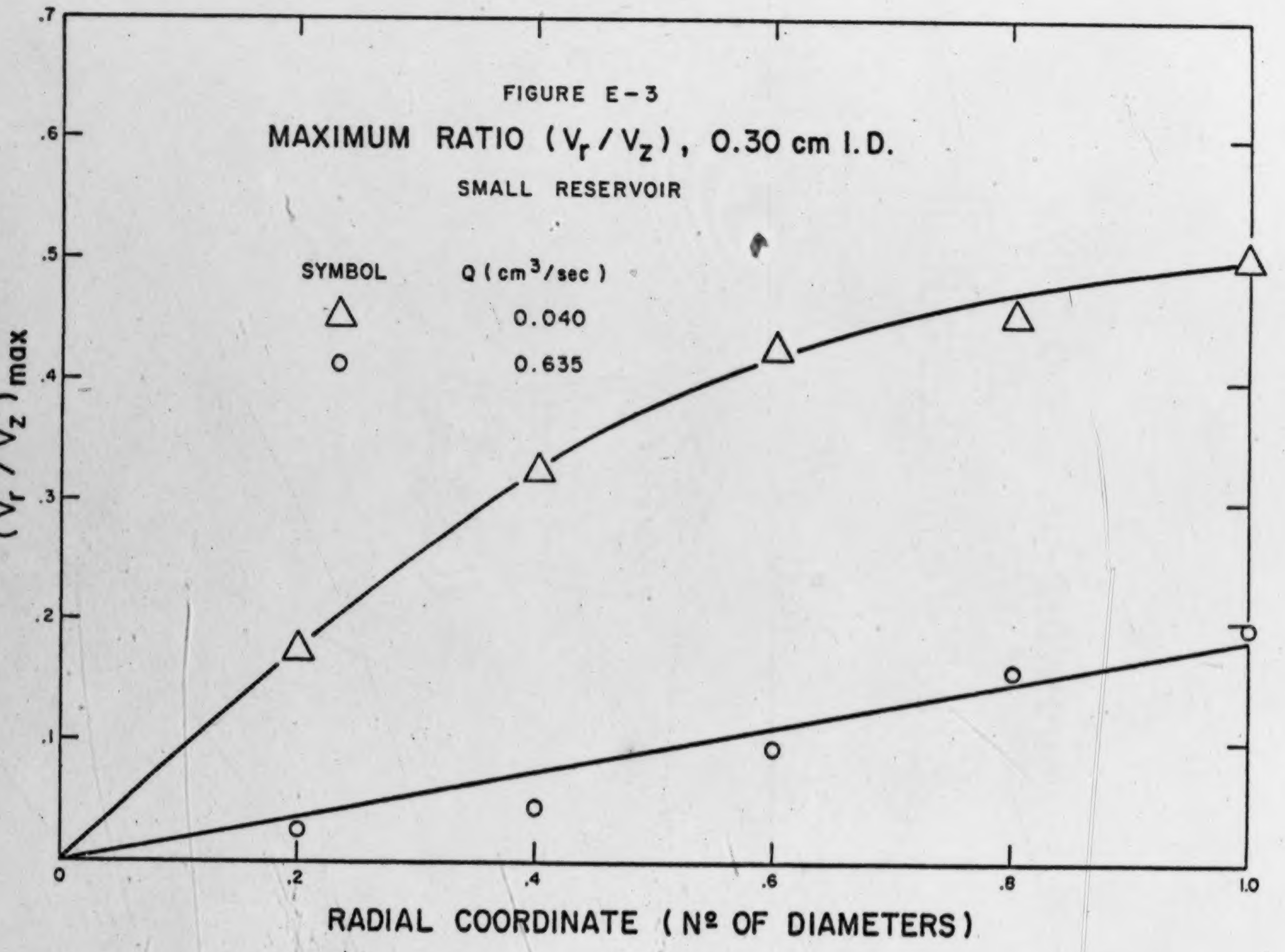

FIGURE E-3

MAXIMUM RATIO $(V_r / V_z)$, 0.30 cm I.D.

SMALL RESERVOIR

## E.4 CENTERLINE AXIAL VELOCITIES

The centerline axial velocities for the three capillary tubes in each reservoir are plotted in Figures E.4 to E.10. As discussed in Chapter III the centerline axial velocities can be represented by Equation 3.20 with c = 1.4. On log-log coorinates Equation 3.20 yields

$$\log(V_z|_{\mathrm{¢}}) = \log V_0 - \frac{b}{2.303}\left(\frac{z}{D}\right)^{1.4} \qquad \text{E.7}$$

Equation E.7 is plotted as solid lines in Figures E.4 to E.10. The least squares estimators of $V_0$, the centerline axial velocity at the contraction, are given in Table E.44. The values of $V_0$ are used in the derivation of an empirical expression for local axial velocities the discussion of which is found in Chapter III.

## TABLE E.44

## CENTERLINE AXIAL VELOCITY AT CONTRACTION

### RESERVOIR S

| I.D. (cm) | $Q(cm^3/sec)$ | $V_0$(cm/sec) |
|---|---|---|
| 0.10<br>(L/D=55.08) | 0.016 | 2.30 |
| | 0.040 | 5.80 |
| | 0.119 | 18.99 |
| 0.20<br>(L/D=54.96) | 0.040 | 1.46 |
| | 0.159 | 7.50 |
| | 0.238 | 10.90 |
| | 0.318 | 14.00 |
| 0.30<br>(L/D=55.04) | 0.040 | 0.70 |
| | 0.159 | 3.20 |
| | 0.318 | 5.97 |
| | 0.635 | 12.96 |

### RESERVOIR L

| I.D. (cm) | $Q(cm^3/sec)$ | $V_0$(cm/sec) |
|---|---|---|
| 0.20<br>(L/D=54.96) | 0.159 | 5.40 |
| | 0.318 | 11.61 |
| | 0.794 | 27.82 |
| | 1.589 | 62.00 |
| | 1.906 | 75.00 |
| | 2.383 | 95.00 |
| | 2.701 | 115.00 |
| | 3.177 | 140.00 |
| | 3.812 | 165.00 |
| | 4.866 | 220.00 |
| 0.30<br>(L/D=55.04) | 0.318 | 5.36 |
| | 0.635 | 12.21 |
| | 1.589 | 24.87 |
| | 4.866 | 90.80 |
| | 6.354 | 130.15 |
| | 7.148 | 170.77 |
| | 7.943 | 187.44 |
| | 9.531 | 239.00 |
| | 10.325 | 239.00 |
| | 11.120 | 267.00 |

FIGURE E-4
AXIAL CENTERLINE VELOCITY

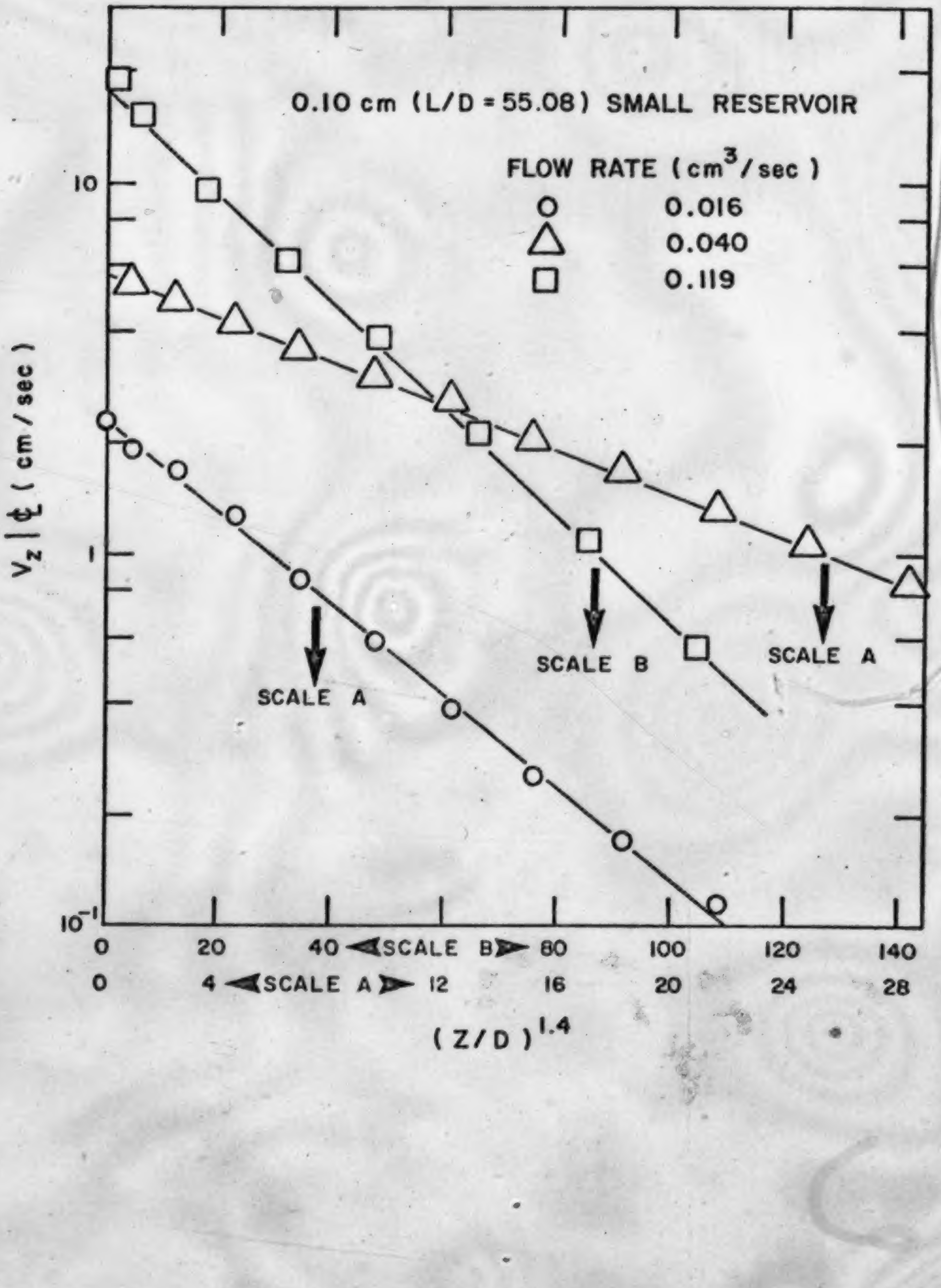

FIGURE E — 5

## AXIAL CENTERLINE VELOCITY

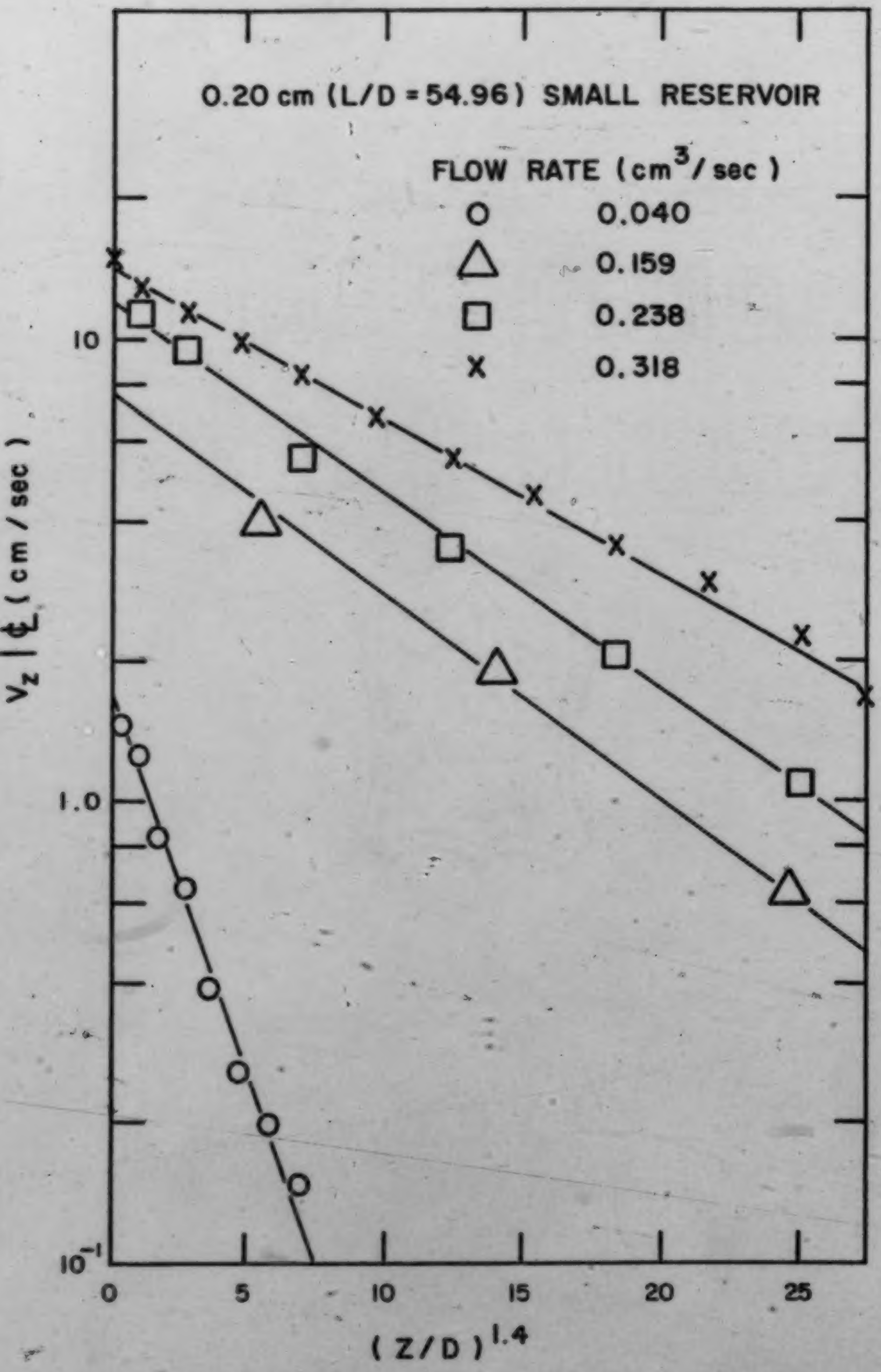

FIGURE E-6

AXIAL CENTERLINE VELOCITY

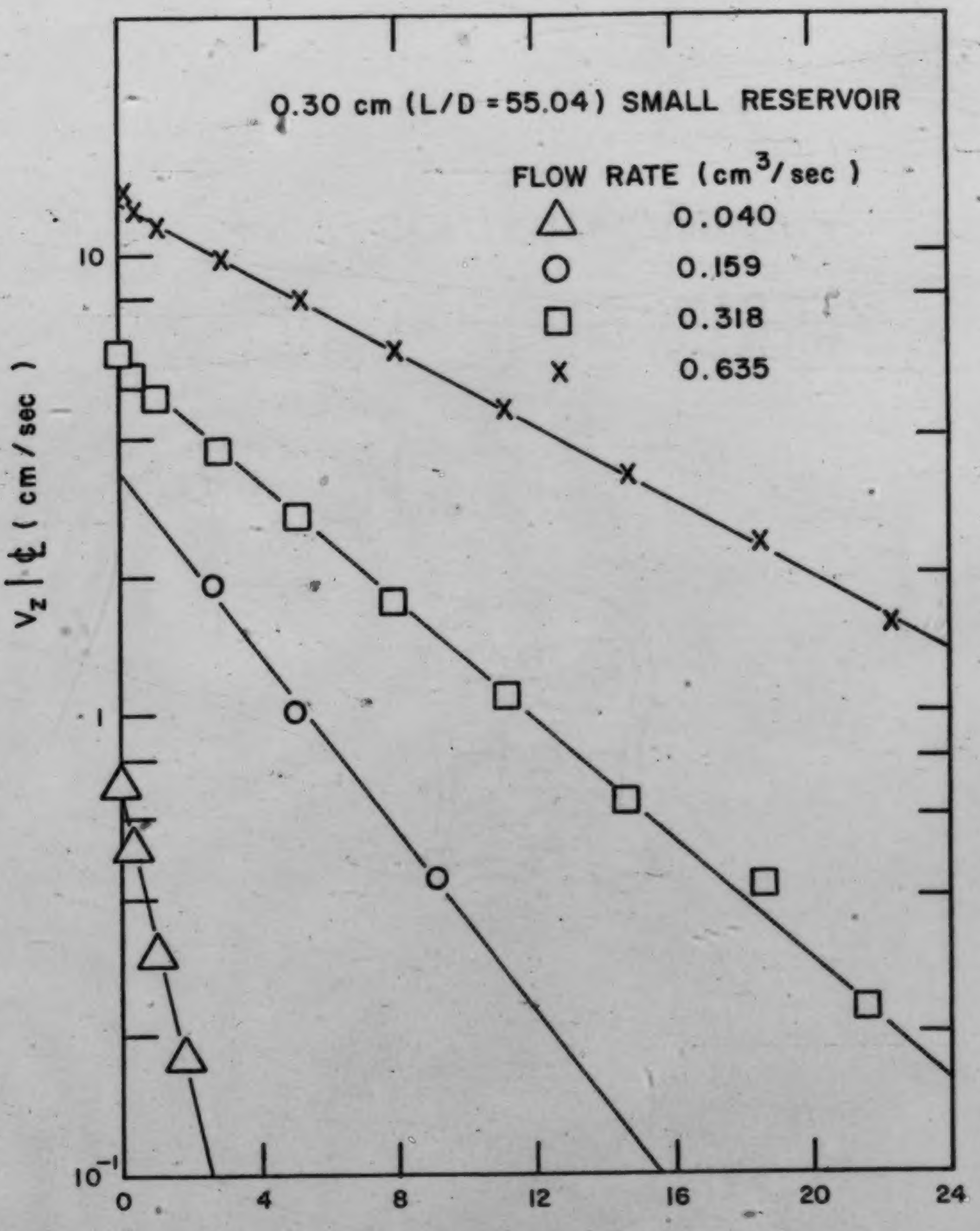

FIGURE E – 7

## AXIAL CENTERLINE VELOCITY

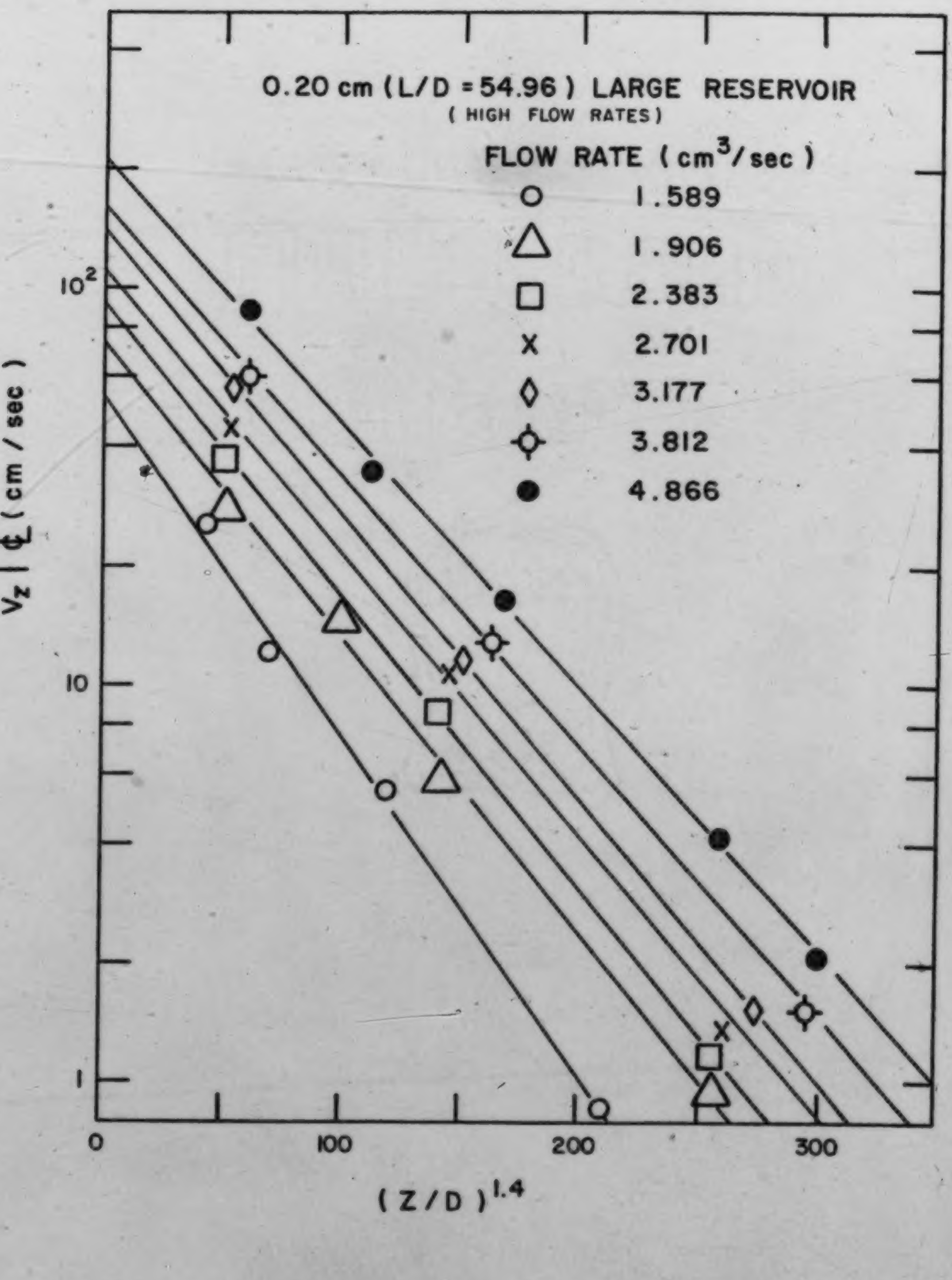

FIGURE E—8

## AXIAL CENTERLINE VELOCITY

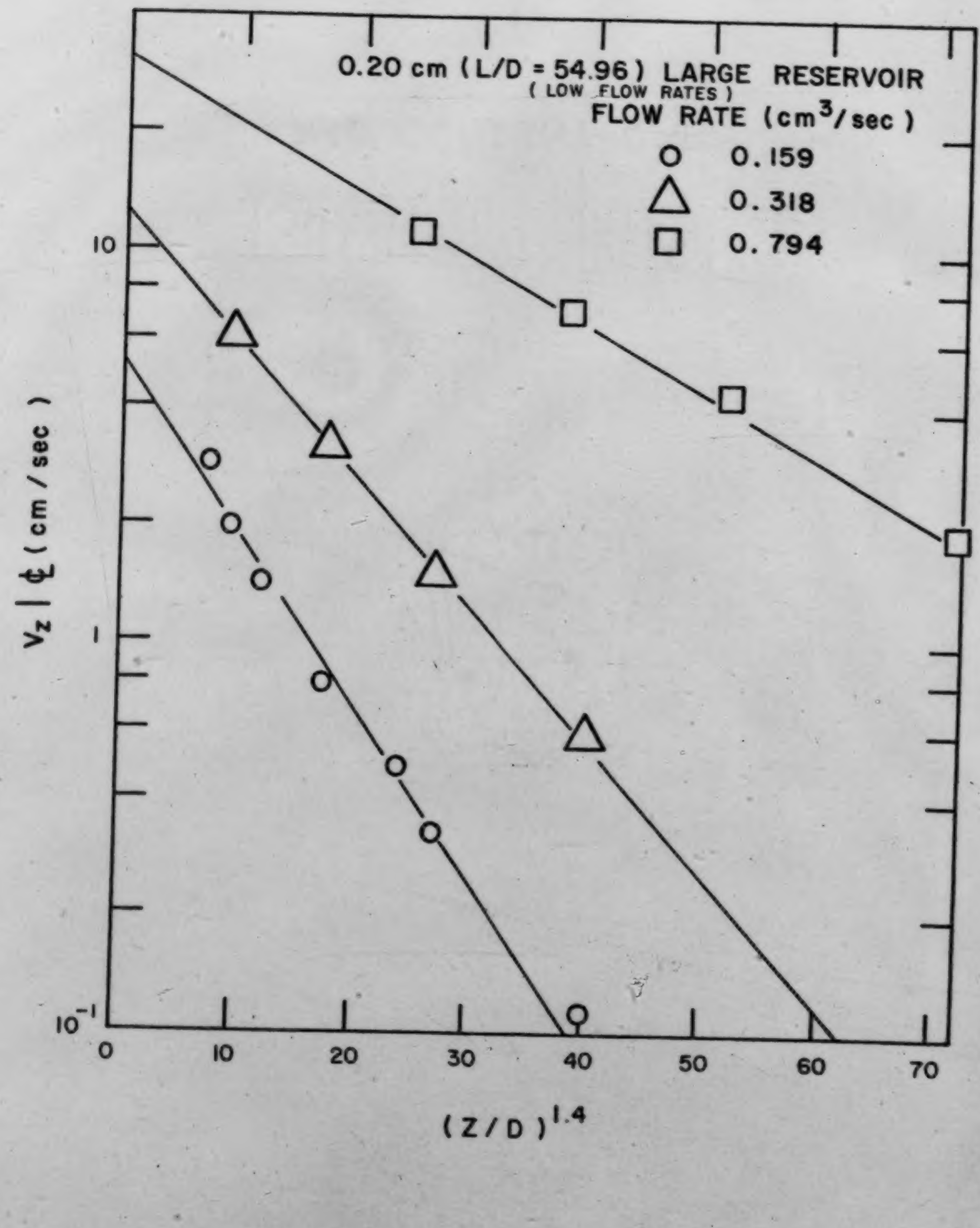

FIGURE E - 9

AXIAL CENTERLINE VELOCITY

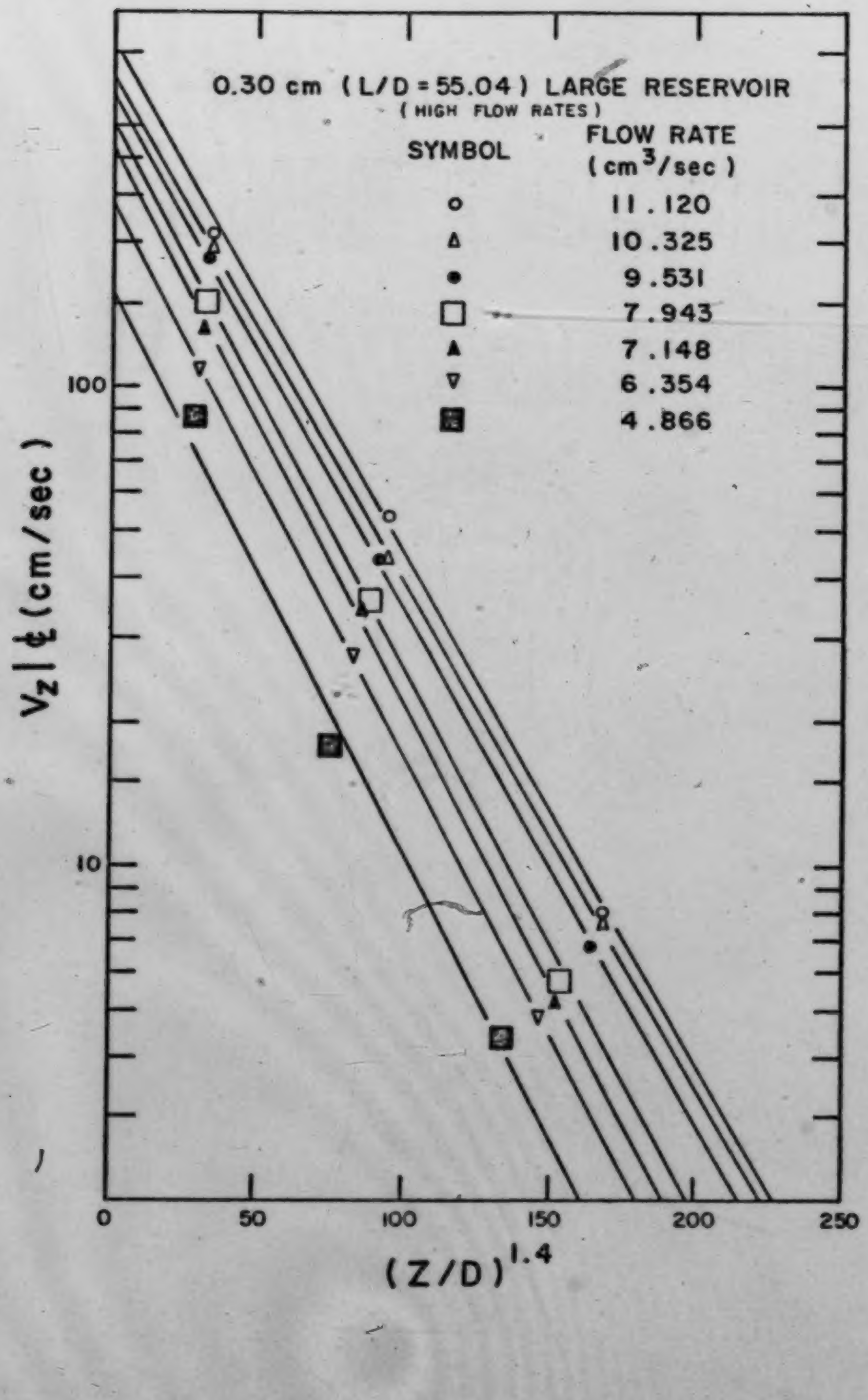

FIGURE E – 10

## AXIAL CENTERLINE VELOCITY

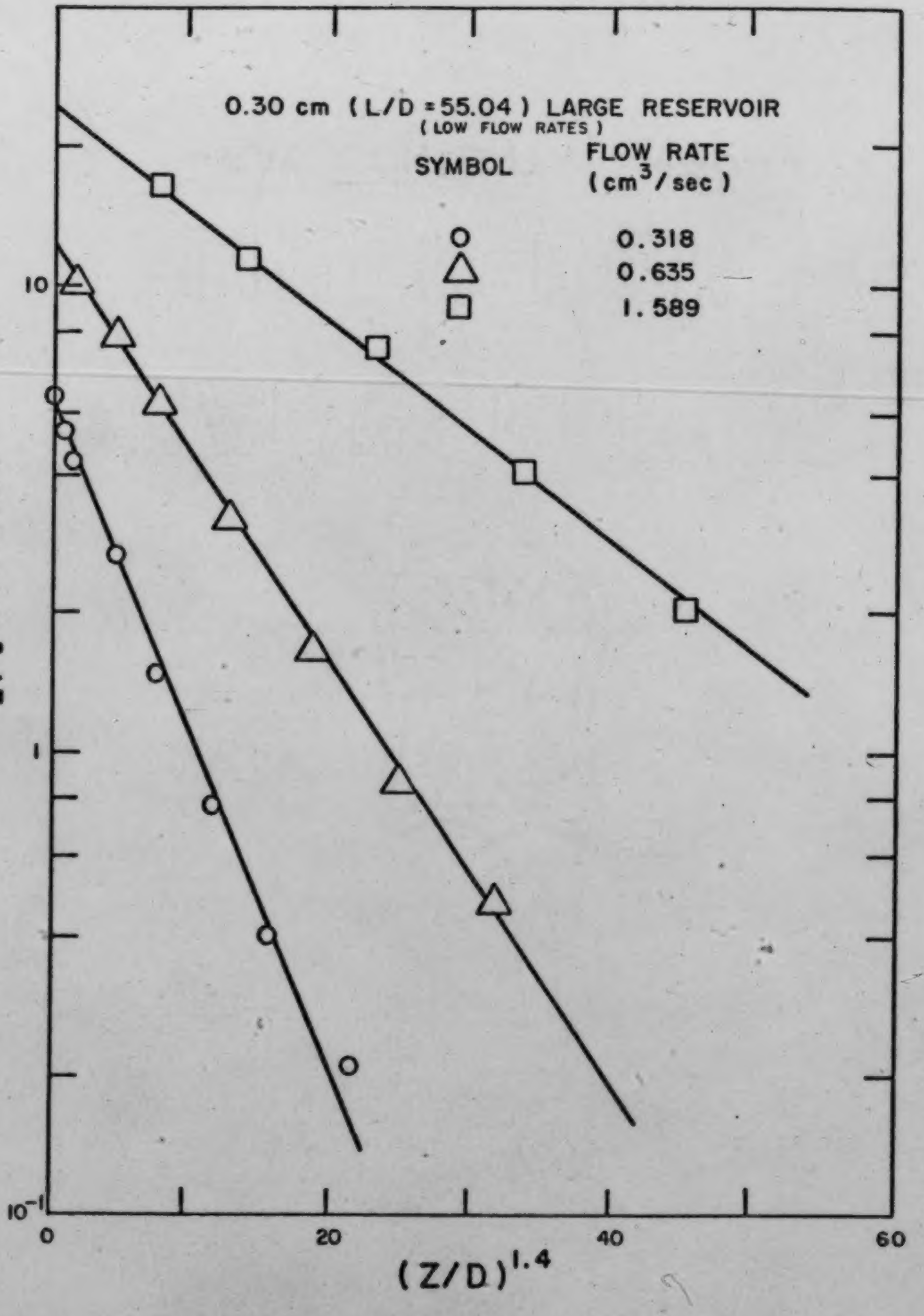

## E.5 PARAMETER $r_0$

Parameter $r_0$ was defined in Chapter III as the radial distance where the axial velocity was equal to one half of the centerline axial velocity. Using this definition, the radial dependence of axial velocities was shown to be represented by

$$f(\eta) = \frac{V_z|_{\mathrm{¢}}}{V_z} = (1+0.41\ \eta^2)^{-2} \qquad \text{E.8}$$

where $\eta$ is a dimensionless radial coordinate equal to $(r/r_0)$. The values $r_0$ are tabulated in Table E.45.

## TABLE E.45

## VARIATION OF PARAMETER $r_0$ WITH RESERVOIR SIZE, CAPILLARY TUBE I.D., FLOW RATE AND DIMENSIONLESS AXIAL POSITION Z**

Reservoir S

| I.D. (cm) | Flow Rate ($cm^3$/sec) | Z** | $r_0$ (cm) |
|---|---|---|---|
| 0.10 | .016 | 0.000 | .037 |
| | | 0.251 | .043 |
| | | 0.502 | .053 |
| | | 1.004 | .084 |
| | | 1.505 | .141 |
| | | 1.756 | .202 |
| | | 2.007 | .220 |
| | .040 | 0.158 | .043 |
| | | 0.316 | .054 |
| | | 0.474 | .051 |
| | | 0.632 | .060 |
| | | 0.949 | .083 |
| | | 1.265 | .104 |
| | | 1.581 | .135 |
| | | 1.897 | .187 |
| | | 2.214 | .259 |
| | .119 | 0.183 | .043 |
| | | 0.367 | .047 |
| | | 0.733 | .064 |
| | | 1.100 | .077 |
| | | 1.467 | .113 |
| | | 1.833 | .185 |
| | | 2.567 | .360 |
| 0.20 | .040 | 0.224 | .082 |
| | | 0.447 | .092 |
| | | 0.742 | .120 |
| | | 0.894 | .133 |
| | | 1.485 | .190 |
| | | 1.795 | .249 |
| | .159 | 0.736 | .120 |
| | | 1.472 | .190 |
| | | 2.207 | .380 |

TABLE E.45 (continued)

Reservoir S

| I.D. (cm) | Flow Rate ($cm^3$/sec) | Z** | $r_0$ (cm) |
|---|---|---|---|
| 0.20 | .238 | 0.367 | .087 |
| | | 0.733 | .110 |
| | | 1.100 | .144 |
| | | 1.467 | .185 |
| | | 1.833 | .293 |
| | .318 | 0.000 | .079 |
| | | 0.159 | .083 |
| | | 0.317 | .095 |
| | | 0.635 | .097 |
| | | 0.952 | .131 |
| | | 1.428 | .206 |
| | | 1.745 | .254 |
| | | 1.903 | .310 |
| 0.30 | .040 | 0.000 | .098 |
| | | 0.411 | .129 |
| | | 0.822 | .197 |
| | | 1.232 | .218 |
| | | 1.649 | .290 |
| | .159 | 0.581 | .165 |
| | | 1.199 | .235 |
| | | 1.780 | .370 |
| | .318 | 0.000 | .122 |
| | | 0.145 | .124 |
| | | 0.291 | .124 |
| | | 0.583 | .145 |
| | | 0.875 | .186 |
| | | 1.457 | .311 |
| | | 1.749 | .373 |
| | .635 | 0.000 | .114 |
| | | 0.103 | .114 |
| | | 0.206 | .119 |
| | | 0.412 | .134 |
| | | 0.619 | .145 |
| | | 1.237 | .260 |
| | | 1.649 | .388 |

TABLE E.45 (continued)

Reservoir L

| I.D. (cm) | Flow Rate ($cm^3$/sec) | Z** | $r_0$ (cm) |
|---|---|---|---|
| 0.20 | .159 | 1.106 | .179 |
| | | 1.738 | .423 |
| | | 2.366 | .613 |
| | | 3.163 | .785 |
| | .318 | 0.782 | .134 |
| | | 1.229 | .211 |
| | | 1.674 | .408 |
| | | 2.237 | .761 |
| | .794 | 0.990 | .204 |
| | | 1.345 | .274 |
| | | 1.696 | .380 |
| | | 2.118 | .654 |
| | | 2.469 | 1.071 |
| | 1.589 | 0.993 | .200 |
| | | 1.064 | .215 |
| | | 1.511 | .295 |
| | | 2.000 | .480 |
| | | 2.531 | 1.335 |
| | | 2.980 | 1.575 |
| | 4.866 | 0.795 | .165 |
| | | 1.606 | .400 |
| | | 2.404 | 1.500 |
| 0.30 | .318 | 0.000 | .127 |
| | | 0.414 | .148 |
| | | 0.822 | .200 |
| | | 1.236 | .274 |
| | | 1.647 | .423 |
| | | 2.058 | .600 |
| | .635 | 0.293 | .135 |
| | | 0.584 | .145 |
| | | 0.874 | .204 |
| | | 1.264 | .290 |
| | | 1.654 | .444 |
| | | 2.039 | .719 |
| | | 2.429 | .846 |

## TABLE E.45 (continued)

Reservoir L

| I.D. (cm) | Flow Rate ($cm^3$/sec) | Z** | $r_0$ (cm) |
|---|---|---|---|
| 0.30 | 1.589 | 0.553 | .177 |
| | | 0.860 | .218 |
| | | 1.228 | .310 |
| | | 1.597 | .493 |
| | | 1.962 | .817 |
| | 4.866 | 0.816 | .250 |
| | | 1.631 | .500 |
| | 11.120 | 0.627 | .225 |
| | | 1.254 | .420 |
| | | 1.881 | 1.500 |

# APPENDIX F

# EDDY CENTERS AND CONE SEMI-ANGLES

## F.1 EDDY CENTERS

This section contains the tabulated location of the centers of the eddies that surrounded the core of fluid in the inlet region. A summary of the tabulated data is given below.

EDDY CENTERS

| TABLE NO. | DIA. (cm) | RESERVOIR | L/D |
|---|---|---|---|
| F.1 | 0.10 | S | 55.08 |
| F.2 | 0.20 | S | 54.96 |
| F.3 | 0.30 | S | 55.04 |
| F.4 | 0.10 | L | 55.08 |
| F.5 | 0.20 | L | 54.96 |
| F.6 | 0.30 | L | 55.04 |

The location of the eddy centers was determined by four measurements, A, B, C, and D. Consider as a typical example the first entry in Table F.4. Since the magnification was 2.175 the actual distances A, B, C, and D are found by dividing by 2.175. This results in the location of the eddy centers as shown schematically in Figure F.1.A. However, for the data where the magnification was 24.437, e.g., the data in Table F.1 indicated by an asterisk, the actual distances A, B, C, and D are obtained by dividing by 24.437, with the distance D being measured from the opposite wall. Shown schematically in Figure F.1.B is the location of the eddy center for the first entry in Table F.1. The accuracy in the measurements was ±0.32 cm at magnifications of 2.175, 9.063 or 24.437.

## TABLE F.1

## EDDY CENTER LOCATION

## 0.10 cm I.D. CAPILLARY, L/D=55.08, SMALL RESERVOIR

Magnification: 9.063

| Flow Rate (cc/sec) | A cm | B cm | C cm | D cm |
|---|---|---|---|---|
| 0.004* | 7.620 | 7.303 | 23.495 | 23.813 |
| 0.012* | 13.018 | 13.335 | 20.003 | 20.912 |
| 0.016* | 15.558 | 15.240 | 19.050 | 19.845 |
| 0.024* | 19.368 | 19.368 | 18.495 | 18.733 |
| 0.032* | 22.543 | 22.860 | 18.098 | 18.258 |
| 0.040 | 10.160 | 10.160 | 6.350 | 17.780 |
| 0.079 | 13.970 | 14.288 | 6.510 | 17.305 |
| 0.119 | 16.510 | 16.510 | 6.668 | 17.463 |

* The magnification for these data was 24.437.

## TABLE F.2

## EDDY CENTER LOCATION

### 0.20 cm I.D. CAPILLARY, L/D=54.96, SMALL RESERVOIR

Magnification: 9.063

| Flow Rate (cc/sec) | A cm | B cm | C cm | D cm |
|---|---|---|---|---|
| 0.004* | 3.175 | 3.175 | - | 25.083 |
| 0.012* | 6.033 | 6.033 | 21.590 | 23.495 |
| 0.016* | 7.620 | 8.890 | 18.098 | 21.273 |
| 0.024* | 10.160 | 11.113 | 18.098 | 20.320 |
| 0.032* | 11.905 | 12.700 | 17.780 | 19.050 |
| 0.040 | 6.033 | 6.033 | 6.668 | 17.620 |
| 0.059 | 7.460 | 7.460 | 6.350 | 17.620 |
| 0.079 | 8.890 | 8.573 | 6.190 | 17.780 |
| 0.103 | 10.317 | 10.638 | 6.190 | 17.780 |
| 0.159 | 12.065 | 11.748 | 6.190 | 17.780 |
| 0.318 | 14.288 | 14.605 | 6.590 | 17.940 |

* The magnification for these data was 24.437.

## TABLE F.3

## EDDY CENTER LOCATION

0.30 cm I.D. CAPILLARY, L/D=55.04, SMALL RESERVOIR

Magnification: 9.063

| Flow Rate (cc/sec) | A cm | B cm | C cm | D cm |
|---|---|---|---|---|
| 0.004* | 1.588 | 1.588 | 24.295 | 24.448 |
| 0.012* | 2.223 | 2.223 | 22.860 | 21.908 |
| 0.016* | 3.810 | 3.810 | 20.955 | 20.701 |
| 0.024* | 6.033 | 6.033 | 18.098 | 18.415 |
| 0.032* | 7.938 | 7.938 | 17.145 | 17.145 |
| 0.040 | 3.970 | 3.970 | 6.350 | 17.940 |
| 0.079 | 5.398 | 5.398 | 6.033 | 18.098 |
| 0.119 | 6.668 | 6.668 | 5.875 | 18.098 |
| 0.159 | 7.938 | 7.938 | 6.350 | 18.258 |
| 0.238 | 9.365 | 9.365 | 6.350 | 18.415 |
| 0.318 | 10.795 | 10.795 | 6.350 | 18.258 |
| 0.394 | 11.590 | 11.590 | 6.350 | 18.098 |
| 0.477 | 12.383 | 12.383 | 6.350 | 18.258 |
| 0.635 | 13.653 | 13.653 | 5.875 | 18.098 |

* The magnification for these data was 24.437.

## TABLE F.4

## EDDY CENTER LOCATION

0.10 cm I.D. CAPILLARY, L/D=55.08, LARGE RESERVOIR

Magnification: 2.175

| Flow Rate (cc/sec) | A cm | B cm | C cm | D cm |
|---|---|---|---|---|
| 0.159 | 7.938 | 7.938 | 21.115 | 32.703 |
| 0.318 | 10.478 | 10.478 | 19.050 | 34.762 |
| 0.381 | 11.125 | 11.430 | 18.733 | 35.243 |
| 0.508 | 12.700 | 12.700 | 18.098 | 35.720 |
| 0.635* | 13.970 | 13.495 | 17.305 | 35.878 |
| 0.794* | 15.240 | 14.765 | 16.828 | 36.513 |
| 0.953* | 16.353 | 15.240 | 16.510 | 36.673 |
| 1.120* | 16.828 | 16.193 | 16.340 | 36.990 |
| 1.271* | 17.145 | 16.670 | 16.510 | 36.990 |

* Measured only when the flow field was observed to be stable.

## TABLE F.5

### EDDY CENTER LOCATION

### 0.20 cm I.D. CAPILLARY, L/D=54.96, LARGE RESERVOIR

Magnification: 2.175

| Flow Rate (cc/sec) | A cm | B cm | C cm | D cm |
|---|---|---|---|---|
| 0.159 | 3.912 | 3.912 | 23.020 | 30.798 |
| 0.238 | 5.240 | 5.240 | 22.225 | 31.593 |
| 0.318 | 6.452 | 6.452 | 21.463 | 32.385 |
| 0.477 | 7.938 | 7.938 | 20.638 | 33.338 |
| 0.794 | 10.320 | 10.160 | 19.210 | 34.768 |
| 1.271 | 12.065 | 12.383 | 18.098 | 35.878 |
| 1.589 | 13.178 | 13.335 | 17.780 | 36.513 |
| 1.906* | 13.970 | 12.860 | 17.297 | 36.673 |
| 2.383* | 15.083 | 15.083 | 16.988 | 36.990 |
| 2.701* | 15.718 | 15.400 | 16.828 | 36.830 |
| 3.177* | 16.193 | 15.875 | 16.670 | 37.069 |
| 3.812* | 16.993 | 16.828 | 16.353 | 37.313 |
| 4.766* | 18.098 | 17.145 | 15.718 | 37.160 |

* Measured only when the flow field was observed to be stable.

## TABLE F.6

### EDDY CENTER LOCATION

### 0.30 cm I.D. CAPILLARY, L/D=55.04, LARGE RESERVOIR

Magnification: 2.175

| Flow Rate (cc/sec) | A cm | B cm | C cm | D cm |
|---|---|---|---|---|
| 0.318 | 3.988 | 3.988 | 23.622 | 31.496 |
| 0.635 | 5.969 | 5.969 | 22.225 | 32.690 |
| 0.794 | 6.985 | 6.985 | 21.273 | 33.338 |
| 1.589 | 9.843 | 9.843 | 19.342 | 35.230 |
| 2.383 | 11.748 | 11.430 | 18.415 | 36.038 |
| 3.177 | 12.860 | 12.700 | 17.780 | 36.673 |
| 4.766 | 14.765 | 14.288 | 17.145 | 37.148 |
| 6.354* | 15.558 | 17.623 | 16.828 | 37.226 |
| 7.148* | 15.875 | 15.558 | 16.683 | 37.148 |
| 7.943* | 16.193 | 15.718 | 16.683 | 37.465 |
| 8.737* | 16.828 | 16.193 | 16.510 | 37.465 |
| 9.531* | 17.145 | 16.353 | 16.353 | 37.625 |
| 10.325* | 17.305 | 16.670 | 16.271 | 37.625 |
| 11.120* | 17.145 | 16.670 | 16.510 | 36.990 |

* Measured only when the flow field was observed to be stable.

FIGURE F-1

## EDDY CENTER LOCATION

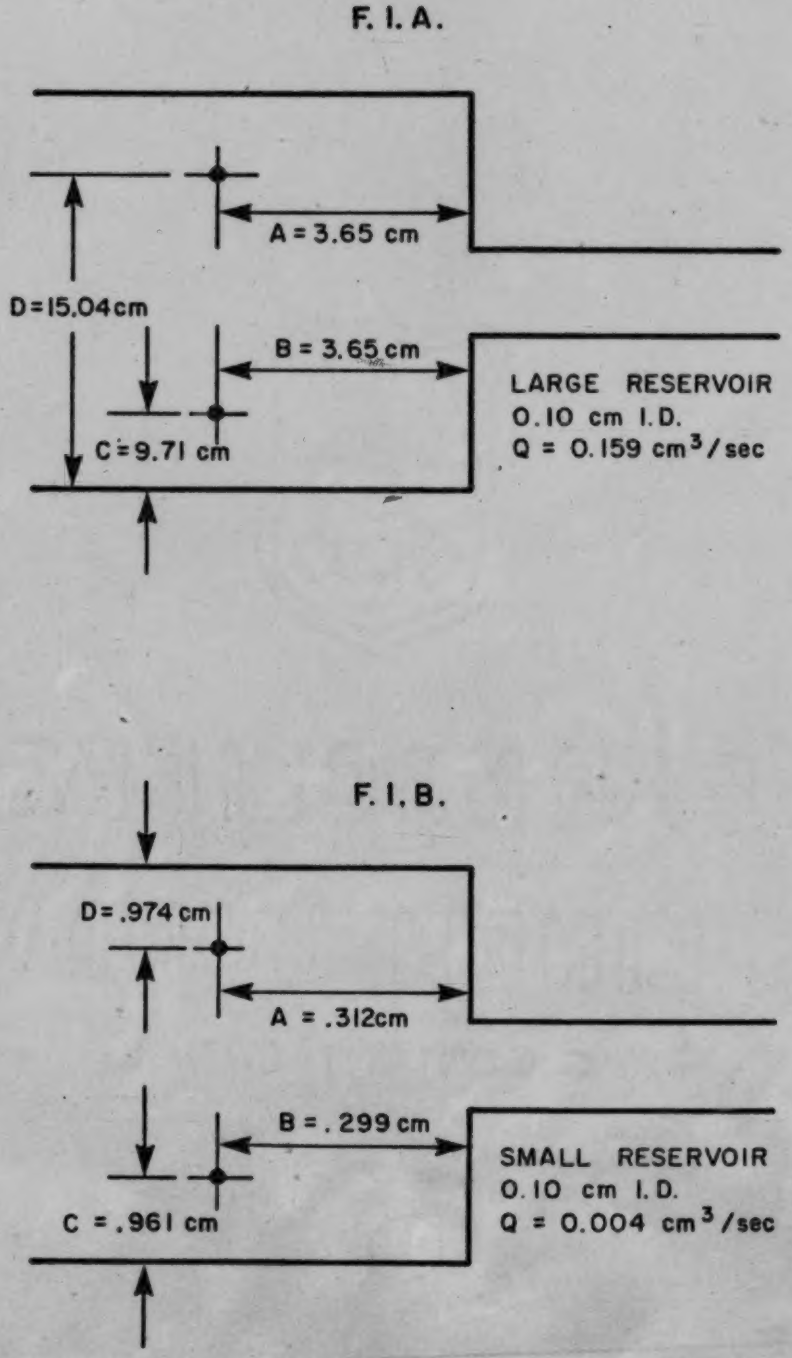
F. I. A.
A = 3.65 cm
D = 15.04 cm
B = 3.65 cm
C = 9.71 cm
LARGE RESERVOIR
0.10 cm I.D.
Q = 0.159 cm³/sec
F. I. B.
D = .974 cm
A = .312cm
B = . 299 cm
C = .961 cm
SMALL RESERVOIR
0.10 cm I.D.
Q = 0.004 cm³/sec

## F.2 CONE SEMI-ANGLES

The cone semi-angle, measured in degrees, was defined in Chapter II, Section 2.3.4, as the angle tangent to the outermost streamline that entered into the capillary tube. The cone semi-angles in Tables F.7 and F.8 were measured at L/D ratios equal to 55.08, 54.96, and 55.04 for capillary tubes 1, 2, and 3 respectively.

## TABLE F.7

## CONE SEMI-ANGLES - SMALL RESERVOIR

| I.D. (cm) | Flow Rate ($cm^3$/sec) | z/D | Cone Semi-angle (degrees) |
|---|---|---|---|
| 0.10 | .016 | 0.00 | 3.5 |
| | | 2.00 | 5.5 |
| | | 4.00 | 8.0 |
| | | 6.00 | 12.5 |
| | | 8.00 | 22.5 |
| | | 10.00 | 38.0 |
| 0.10 | .040 | 0.00 | 2.0 |
| | | 3.00 | 2.5 |
| | | 6.00 | 2.8 |
| | | 8.00 | 3.3 |
| | | 11.00 | 6.7 |
| | | 14.00 | 11.0 |
| 0.10 | .119 | 0.00 | 1.0 |
| | | 4.00 | 1.1 |
| | | 8.00 | 1.5 |
| | | 12.00 | 2.5 |
| | | 16.00 | 3.3 |
| | | 20.00 | 5.0 |
| | | 24.00 | 8.0 |
| | | 28.00 | 13.5 |
| 0.20 | .040 | 0.00 | 8.0 |
| | | 1.00 | 11.5 |
| | | 2.00 | 16.0 |
| | | 3.00 | 25.0 |
| | | 4.00 | 32.0 |
| 0.20 | .159 | 0.00 | 3.7 |
| | | 1.57 | 4.5 |
| | | 3.14 | 5.4 |
| | | 4.72 | 7.6 |
| | | 6.29 | 10.8 |
| | | 7.86 | 17.8 |
| | | 9.43 | 32.7 |

TABLE F.7 (continued)

| I.D. (cm) | Flow Rate ($cm^3$/sec) | z/D | Cone Semi-angle (degrees) |
|---|---|---|---|
| 0.20 | .238 | 0.00 | 2.7 |
| | | 2.00 | 3.0 |
| | | 4.00 | 4.1 |
| | | 6.00 | 5.0 |
| | | 8.00 | 10.0 |
| | | 12.00 | 14.0 |
| | | 16.00 | 15.0 |
| 0.20 | .318 | 0.00 | 2.0 |
| | | 3.00 | 3.0 |
| | | 6.00 | 4.2 |
| | | 8.00 | 7.0 |
| | | 11.00 | 11.0 |
| 0.30 | .040 | 0.00 | 18.0 |
| | | 0.50 | 21.0 |
| | | 1.00 | 28.0 |
| | | 1.50 | 32.0 |
| | | 2.00 | 39.0 |
| | | 2.50 | 46.0 |
| 0.30 | .159 | 0.00 | 6.5 |
| | | 1.50 | 8.0 |
| | | 2.09 | 9.7 |
| | | 2.62 | 13.6 |
| | | 3.14 | 18.8 |
| | | 3.67 | 25.3 |
| | | 4.19 | 33.1 |
| 0.30 | .318 | 0.00 | 4.4 |
| | | 1.00 | 4.7 |
| | | 3.00 | 6.0 |
| | | 4.00 | 9.5 |
| | | 5.00 | 14.0 |
| | | 6.00 | 19.0 |
| | | 8.00 | 21.0 |
| 0.30 | .635 | 0.00 | 3.2 |
| | | 2.00 | 4.0 |
| | | 4.00 | 5.0 |
| | | 6.00 | 8.5 |
| | | 8.00 | 11.0 |
| | | 10.00 | 17.0 |
| | | 11.00 | 21.0 |

## TABLE F.8

## CONE SEMI-ANGLES - LARGE RESERVOIR

| I.D. (cm) | Flow Rate ($cm^3$/sec) | z/D | Cone Semi-angle (degrees) |
|---|---|---|---|
| 0.20 | .159 | 0.00 | 3.5 |
| | | 5.00 | 8.0 |
| | | 10.00 | 14.5 |
| | | 15.00 | 18.0 |
| | | 20.00 | 21.0 |
| | | 30.00 | 30.0 |
| | | 40.00 | 40.0 |
| 0.20 | .238 | 0.00 | 3.0 |
| | | 4.54 | 5.5 |
| | | 9.08 | 12.0 |
| | | 13.62 | 13.0 |
| | | 18.16 | 16.0 |
| | | 22.70 | 17.0 |
| 0.20 | .318 | 0.00 | 2.0 |
| | | 3.01 | 3.0 |
| | | 7.50 | 6.0 |
| | | 10.50 | 8.5 |
| | | 14.00 | 13.0 |
| 0.20 | .794 | 0.00 | 1.0 |
| | | 7.60 | 2.5 |
| | | 10.00 | 4.0 |
| | | 13.60 | 5.5 |
| | | 20.00 | 11.0 |
| | | 24.80 | 12.0 |
| | | 30.00 | 13.5 |
| | | 38.00 | 15.0 |
| | | 40.00 | 16.5 |
| | | 44.00 | 18.0 |
| | | 50.00 | 21.0 |
| 0.20 | 1.589 | 0.00 | .65 |
| | | 6.50 | 1.0 |
| | | 10.00 | 1.35 |
| | | 12.60 | 1.7 |
| | | 18.80 | 2.5 |
| | | 20.00 | 2.8 |
| | | 25.00 | 4.0 |
| | | 30.00 | 6.0 |
| | | 31.50 | 6.5 |
| | | 35.60 | 8.5 |
| | | 40.00 | 12.0 |

TABLE F.8 (continued)

| I.D. (cm) | Flow Rate (cm$^3$/sec) | z/D | Cone Semi-angle (degrees) |
|---|---|---|---|
| 0.30 | .318 | 0.00 | 4.2 |
| | | 1.40 | 4.5 |
| | | 2.80 | 6.0 |
| | | 4.20 | 9.0 |
| | | 5.60 | 13.0 |
| | | 6.00 | 16.0 |
| | | 9.00 | 20.0 |
| | | 11.00 | 22.0 |
| 0.30 | .635 | 0.00 | 3.5 |
| | | 3.00 | 5.2 |
| | | 4.20 | 6.6 |
| | | 5.00 | 7.5 |
| | | 6.00 | 8.5 |
| | | 8.00 | 15.0 |
| | | 10.00 | 17.0 |
| | | 12.00 | 19.0 |
| | | 15.00 | 21.0 |
| 0.30 | .794 | 0.00 | 2.5 |
| | | 3.00 | 4.5 |
| | | 6.00 | 9.0 |
| | | 9.00 | 12.0 |
| | | 12.00 | 15.0 |
| | | 15.00 | 17.0 |
| | | 18.00 | 20.0 |
| | | 21.00 | 24.0 |
| 0.30 | 1.589 | 0.00 | 0.85 |
| | | 2.24 | 1.0 |
| | | 5.25 | 2.0 |
| | | 9.18 | 4.0 |
| | | 10.00 | 4.5 |
| | | 13.20 | 6.0 |
| | | 15.00 | 8.0 |
| | | 17.10 | 8.5 |
| | | 20.00 | 9.5 |
| | | 21.10 | 9.0 |
| | | 25.00 | 11.5 |
| | | 30.00 | 15.0 |
| | | 33.00 | 16.5 |
| | | 40.00 | 20.0 |

TABLE F.8 (continued)

| I.D. (cm) | Flow Rate ($cm^3$/sec) | z/D | Cone Semi-angle (degrees) |
|---|---|---|---|
| 0.30 | 3.177 | 0.00 | 0.8 |
| | | 5.96 | 1.5 |
| | | 9.95 | 4.0 |
| | | 13.90 | 6.0 |
| | | 17.90 | 10.5 |
| | | 21.80 | 15.0 |
| | | 25.80 | 18.0 |
| | | 29.80 | 21.0 |
| | | 33.80 | 26.0 |
| | | 37.70 | 29.0 |
| 0.30 | 4.866 | 0.00 | 0.55 |
| | | 3.00 | 1.0 |
| | | 10.00 | 2.3 |
| | | 20.00 | 7.0 |
| | | 30.00 | 12.0 |
| | | 40.00 | 19.0 |

# APPENDIX G

# ERROR ANALYSIS

The digitizer and direct methods used to measure velocity components were discussed in detail in Chapter II, Section 2.3. The sources of error in measuring axial and radial velocity components with these methods are:

a. digitizer calibration,

b. measuring the slope of the reservoir wall relative to the digitizer's X axis,

c. measuring velocities over a band width rather than at a fixed upstream axial location,

d. centering of the capillary tube, and

e. depth of field of the camera.

Since the sources of error are assumed independent, the error in measuring velocity components is the sum of errors. Hence, for the digitizer method, the sources of error were "a" through "e" of the above whereas, for the direct method sources of error were "d" and "e".

## G.1 DIGITIZER METHOD ERROR

The sources of error were calibration, slope of reservoir wall, measurement over a band width, centering of capillary tube, and depth of the camera field.

### G.1.1 CALIBRATION

The full scale movement of the digitizer's cross hair for the X and Y axes were 33,000 counts and 32,000 counts respectively. The digitizer cross hair was moved 2.54 cm along the X and then along the Y axis in order to convert these readings into distances. Repeated measurements, tabulated in Table G.1, resulted in a sample mean equal to 1414 counts and 1490 counts for the X and Y respectively. The standard deviation of the mean, arising from digitizer electronic error and error in positioning the cross hair, for the X and Y axes were 55.63 and 52.72 respectively. The calibration procedure was repeated at the upper and lower limits of the digitizer's X and Y axes in order to detect nonlinearity over the full range of the digitizer's X and Y axes. No nonlinearity was detected.

The relative errors in measuring axial and radial velocities can be evaluated by considering an example where the axial distance traversed by an aluminum dust particle was equal to 400 counts and another of 1000 counts. Expressed as percentages, the relative errors, within one standard deviation, for the axial velocity component are

$$\frac{55.63}{400} \times 100 \quad \text{or} \quad \frac{55.63}{1000} \times 100$$

or 18.9 percent and 5.6 percent. These errors are representative errors for axial velocities measured outside ($\eta>1.5$) and within the WGS core respectively. In addition, blurry ends of the streaks resulted in a judgement error in positioning the cross hair. This error, determined by the time involved for the splitter to cut the beam of light, was less than 2 percent. Therefore, the sums of errors obtained by the propagation of error through addition, arising from digitizer electronic error, human factor, and the blurry ends of the streaks, were 20.9 percent and 7.6 percent out-

## TABLE G.1

## CALIBRATION OF DIGITIZER

| X axis No. of counts measured over 2.54 cm | Y axis No. of counts measured over 2.54 cm |
|---|---|
| 1402 | 1430 |
| 1416 | 1498 |
| 1366 | 1496 |
| 1418 | 1462 |
| 1440 | 1554 |
| 1418 | 1414 |
| 1388 | 1514 |
| 1410 | 1472 |
| 1408 | 1524 |
| 1428 | 1500 |
| 1388 | 1512 |
| 1408 | 1436 |
| 1464 | 1536 |
| 1402 | 1450 |
| 1454 | 1514 |
| 1390 | 1526 |
| 1364 | 1468 |
| 1470 | 1436 |
| 1416 | 1532 |
| 1426 | 1530 |
| 1390 | 1486 |
| 1423 | 1436 |
| 1419 | 1546 |
| 1410 | 1434 |
| 1412 | 1495 |
| 1415 | 1491 |
|  | 1486 |
|  | 1500 |
|  | 1496 |

side and within the WGS core respectively.

The magnitude of the velocities were shown in the previous section of this appendix to be less than the axial velocities. The error was therefore larger than the error in measuring the axial velocity component. Qualitatively, this error was found to be, in the worst case, as large as 100 percent and under the best circumstances (largest number of counts) as small as 25 percent.

### G.1.2 SLOPE OF THE RESERVOIR WALL

The axial and radial distances traversed by a single streak or by a number of streaks were measured relative to the wall of the reservoir. As shown in Figure 2.8 (page 66) the wall of the reservoir was not parallel to the X axis of the digitizer. It was therefore necessary to measure the slope of the wall of the reservoir relative to the digitizer's X axis, $m_1$, to determine the axial distance, $\Delta x$, and radial distance, $\Delta r$, given by Equations G.1 and G.2.

$$\Delta x = \frac{(Y_4-Y_3)m_1}{(m_1^2+1)^{1/2}} + \frac{(X_4-X_3)}{(m_1^2+1)^{1/2}} \qquad \text{G.1}$$

$$\Delta r = \frac{(Y_4-Y_3)}{(m_1^2+1)^{1/2}} + \frac{(X_3-X_4)m_1}{(m_1^2+1)^{1/2}} \qquad \text{G.2}$$

Coordinates $(X_3,Y_3)$ and $(X_4,Y_4)$ were defined in Figure 2.7 (page 64). Due to mechanical error, error in positioning the cross hair, and the resolution of the wall of the reservoir projected on to the digitizer screen, the error in measuring the slope $m_1$ was as large as 15 percent. The resulting error in measuring $\Delta x$ or $\Delta r$ was estimated by considering two streaks as typical examples; streak 1 was located near the outer edge of the WGS core and streak 2 was located near the centerline. The coordinates of these two steaks and the slope $m_1$ were

Streak 1

$X_3 = 32.201$ cm $\quad Y_3 = 45.889$ cm

$X_4 = 33.427$ cm $\quad Y_4 = 46.070$ cm

Streak 2

$X_3 = 32.571$ cm $\quad Y_3 = 48.822$ cm

$X_4 = 33.006$ cm $\quad Y_4 = 48.829$ cm

$m_1 = 0.0279$

By using the above data, Equation G.1, and an error of 15% in the value of $m_1$, the error in measuring the axial distance $\Delta x$ was found to be less than one tenth of one percent; hence, was considered to be negligible. A 15 percent error in $m_1$ resulted in a maximum 3.6 percent error in the evaluation of $\Delta r$, hence, a 3.6 percent error in the radial velocity component. The error in measuring $\Delta r$ near the centerline was less than 1 percent.

### G.1.3 UPSTREAM AXIAL LOCATION OF STREAKS

Streaks used in calculating velocities with the digitizer method were taken over a band width rather than at a fixed upstream axial location. This resulted in scatter in the measured velocities which depends upon the width of the band and the velocity gradient. The velocity gradient, in turn, is dependent upon both axial and radial positions. Taking these factors into account it was estimated that scatter in local axial and radial velocities ranged from 1 to 8 percent with the smallest scatter occurring along the centerline.

### G.1.4 CENTERING OF CAPILLARY TUBE AND DEPTH OF FIELD OF CAMERA

Since the wall thickness of each length of capillary tube was not uniform it was necessary to center each capillary tube so that the center of the capillary tube and the center of the beam of light were in the same horizontal plane. The following procedure was used in centering the capillary tubes: With a level, the empty reservoir was adjusted so that it was in a horizontal plane. The capillary tube was then inserted into the holding device which was attached to the end plate. The light source was turned on and except for this source of light the room was in total darkness. The beam of light was clearly visible against the aluminum end wall of the reservoir and the side of the reservoir opposite the side where the adjustment slit was attached. By adjusting the level of the light source, a plane passing through the center of the light beam was coincident with a plane passing through etched marks located on both sides of the reservoir. These etched marks represented a plane which was parallel to the viewing surface of the reservoir and passed through the center of the hole in the aluminum end plate. An eyepiece was focused on the area where the capillary tube was fitted flush with the aluminum end plate. The capillary tube was rotated by hand until the center of the beam of light and the center of the capillary tube was judged, by eye, to be in the same plane. A conservative estimate was that the capillary tube could be centered to within 1/5 of the thickness of the beam of light.

Since the depth of field of the camera was always greater than the beam of light it was not possible to distinguish between aluminum dust particles that were at the top of the beam of light (nearest to the camera), at the bottom of the beam of light (farthest away from the camera), or at any intermediate plane lying within these limits. In fact, there was a distribution of positions which peaked at the center of the band. In the illustration below, the position r + ½sw and r - ½sw, where sw is the slit width, represent the limits of the band at a radial position r.

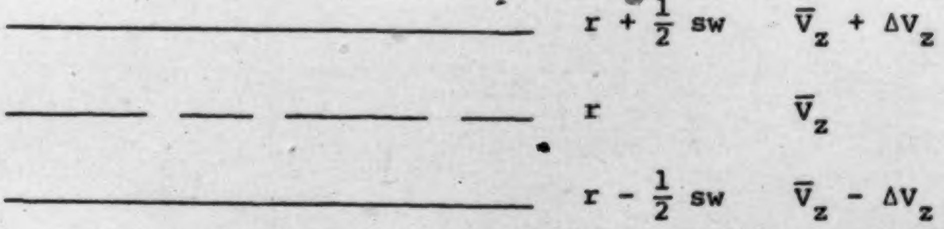

3

If n streaks are observed within the band, roughly n/2 streaks would have velocity characteristic of position r while n/4 streaks would have velocities reflecting the top position (r+½sw) and n/4 reflecting (r−½sw). The variance, resulting from the velocity gradient, is

$$
\begin{aligned}
s^2 &= \frac{1}{n-1}\sum_{i=1}^{n}(\overline{V}_z-V_z)_i^2 \\
&= \frac{1}{n-1}\left[\sum_{i=1}^{n/2}(\overline{V}_z-\overline{V}_z)_i^2 + \sum_{i=n/2}^{3n/4}(\overline{V}_z-(\overline{V}_z+\Delta V_z))_i^2 \right. \\
&\qquad \left. + \sum_{i=3n/4}^{n}(\overline{V}_z+(\overline{V}_z-\Delta V_z))_i^2\right] \qquad \text{G.3} \\
&\simeq \tfrac{1}{2}(\Delta V_z)^2
\end{aligned}
$$

The error within one standard deviation is

$$\text{error} = V_z \pm 0.7\Delta V_z \qquad \text{G.4}$$

Taking these two sources of error into account, i.e., centering of the capillary tube and the depth of field of the camera, the error in measuring axial velocities at any radial position r was estimated from

$$\text{error} = V_z(r,z) \pm V_z(r\pm 0.55sw,z) \qquad \text{G.5}$$

Equation G.5 implies that the larger the velocity gradient the larger the error. The worst estimate of this error was obtained therefore by considering the velocity data measured in reservoir L for capillary tube 2 at a flow rate of 4.866 $cm^3$/sec and at Z/D = 19.73. With the beam of light being 0.508 mm, the errors at several radial positions, i.e., r = 0.0 cm, r = 0.20 cm, r = 0.40 cm, r = 0.80 cm, r = 1.2 cm, and r = 1.6 cm, were 10%, 18%, 17%, 12%, 8%, and 6% respectively. Therefore, as radial distance increased the error passed through maximum; this is consistent with the velocity gradients passing through a maximum. The errors estimated at the same radial positions but at larger values of Z/D (farther upstream) were reduced substantially since the velocity gradients became smaller as Z/D increased. With capillary tube 3, the thickness of the beam of light was a smaller fraction of the diameter and the velocity gradients were not as large as those which occurred with capillary tube 2. Hence, the errors at the same flow rates and axial locations were less than those determined with capillary tube 2. In reservoir S, the maximum error at several radial and axial positions was determined with capillary tube 2 at a flow rate of 0.159 $cm^3$/sec. The magnitude of this error was comparable to the error determined in reservoir L.

In summary, the total error in measuring axial velocities is equal to the sum of the individual errors. Therefore, the error along the centerline was a maximum of 19 percent whereas, for radial locations other than along the centerline, the error was a maximum of 47 percent. The velocities measured with the digitizer method and tabulated in Section E.2 of Appendix E were within the maximum 19 and 47 percents in reservoir L. In reservoir S, the velocities along the centerline and at radial locations other than along the centerline were within a maximum error of 15 and 25 percent respectively. The magnitude of the error in measuring the radial velocity component varied from 0.02 to 1.0 cm/sec.

## G.2 DIRECT METHOD ERROR

The direct method was discussed in Chapter II, Section 2.3. Since axial velocities were measured as a continuous function of axial location along several streamlines, the main sources of error were due to (a) depth of field of camera, (b) centering of the capillary tube, and (c) the blurry ends of the streaks. The sum of these sources of error resulted in a maximum error of 12 percent along the centerline whereas, for values of r other than along the centerline but within the central core region, the maximum error was 20%.

## G.3 PRESSURE TRANSDUCERS AND PRESSURE TAP ERROR

The calibration data for the four transducers are given in Appendix A, Section A.1. The resulting error was less than 1/2 of one percent of the maximum tested pressure. No significant hysteresis was found over the full range for each diaphragm.

The presence of a pressure tap, as shown schematically in Figure G.1, causes a deflection of the streamline into the pressure tap and an eddy or a system of eddies are set up in the pressure tap (155). The curvature of the streamline is such that the measured pressure are greater than the true values (pressures measured flush with the tube wall). The preceeding two factors combine to give a net pressure error. For a fixed flow rate, as the pressure tap size decreases ($d \to 0$) the net pressure error tends to zero (155). The pressure tap error for a finite hole size can be influenced by the hole diameter d, the fluid density $\rho$, the viscosity $\mu$, and the local flow conditions at the surface. Within the boundary layer thickness the local axial velocity at a distance y away from the wall is given by

$$\frac{V_z}{\sqrt{\frac{\tau_w}{\rho}}} = f\left(\frac{y}{\nu}\sqrt{\frac{\tau_w}{\rho}}\right) \qquad \text{G.6}$$

It is apparent that $V_z$, at a distance y, depends on $\tau_w$, $\rho$, and $\mu$. It is therefore the velocity gradient at the tube wall, described by the shear stress $\tau_w$ which defines the local flow conditions at the surface. Thus, the pressure error, $\Delta P_{er}$, for a finite hole size can be written as

$$\Delta P_{er} = f(\tau_w, \rho, \mu, d) \qquad \text{G.7}$$

or

$$\frac{\Delta P_{er}}{\tau_w} = f\left(\frac{d}{\nu}\sqrt{\frac{\tau_w}{\rho}}\right) \qquad \text{G.8}$$

The dimensionless pressure error, $\Delta P_{er}/\tau_w$, was measured experimentally and plotted as a function of the Reynolds number (65, 155) based on the hole diameter (d) and frictional velocity $(\sqrt{\tau_w/\rho})$. By using these results the maximum pressure tap error was determined to be 13 dyn/cm$^2$. This was considered to be negligible since the smallest measured total pressure loss, $\Delta P_t$, was $3.089 \times 10^4$ dyn/cm$^2$.

Tanner and Pipkin (163) concluded that the pressure tap error for viscoelastic solutions was proportional to the magnitude of the first normal stress difference. More recently, Novotny and Eckert (126) measured pressure tap errors for several concentrations (0.9%, 2.0% and 3.0%) of Polyox and found experimentally that the pressure tap error may be positive or negative. Based on these experimental data, the pressure tap errors are estimated to be as large as 40 percent of the magnitude of the first normal stress difference. The presence of a converging flow field within the reservoir augments the magnitude of the first normal stress difference from a value determined under SLSF conditions within the reservoir (90, 119). Therefore, evaluation of the first normal stress difference under SLSF yields a conservative estimate of this error. The apparent shear rate under SLSF in the reservoir, $\gamma_R$, in terms of the apparent shear rate in the capillary tube, is given by

$$\gamma_R = \gamma\left(\frac{D}{D_R}\right)^3 \qquad \text{G.9}$$

The maximum reservoir shear rate of 0.07 $sec^{-1}$ occurred with capillary tube 1 at $Q=0.119$ $cm^3/sec$ and from Figure D.6 (page 313) the normal stress was determined to be less than 10 $dyn/cm^2$. The smallest measurement of $\Delta P_t$, $2.2 \times 10^4$ $dyn/cm^2$, was for run number 24, Table B.11 (page 268). Hence, the pressure tap error was estimated to be less than 0.05 percent. This was considered to be negligible.

FIGURE G-1

## FLOW BEHAVIOUR AT PRESSURE TAP

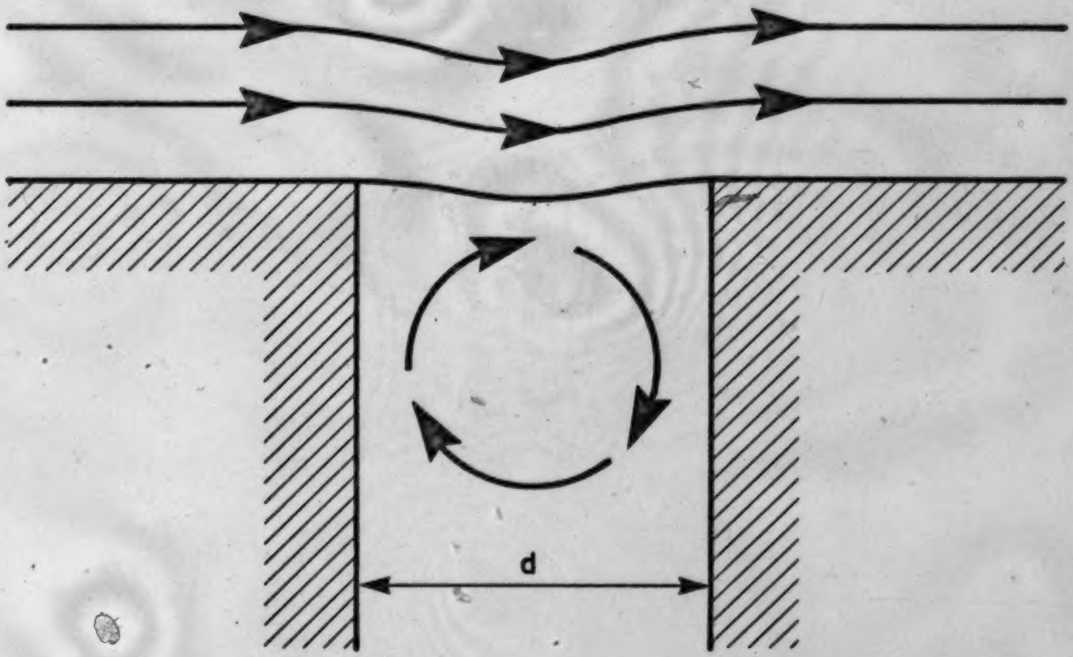

# APPENDIX H

# NOMENCLATURE

| | |
|---|---|
| $a, a_1, a_2$ | parameters defined by Equation 3.14 |
| A | cross sectional area of capillary tube |
| b | parameter defined by Equation 3.16 |
| $b_1$ | parameter defined by Equation 3.36 |
| c | constant defined in Equation 3.20 |
| C | concentration |
| $C_1, C_2$ | constants in Equation 3.9 |
| d | pressure tap diameter |
| D | I.D. of capillary tube |
| $D_R$ | internal diameter of reservoir |
| EL | elasticity number, Equation 2.11 |
| f | Fanning friction factor |
| f(n') | function defined by Equation 1.22 |
| $f(\eta)$ | dimensionless axial velocity defined by Equation 3.42 |
| $f(\phi_0)$ | function defined by Equation 3.10 |
| G | elastic modulus, Equation 1.30 |
| $G_E$ | elastic modulus evaluated under extensional deformation |
| K | Couette correction factor |
| K' | Hagenbach correction factor |
| $K_0$ | consistency index defined by Equation 1.15 |
| $K_1$ | proportionality constant defined by Equation 1.35 |
| L | length of capillary tube |
| m | exponent in Equation 1.35 |
| $m_1$ | slope of reservoir wall relative to digitizer's X axis |
| M | number of streaks |

| | |
|---|---|
| MW | molecular weight |
| $n$ | number of observations |
| $n'$ | flow behavior index defined by Equation 1.14 |
| $N$ | number of slit and spokes on the chopping disc |
| $N_{Re}$ | Reynolds number |
| $N'_{Re}$ | generalized Reynolds number, defined by Equation 1.18 |
| $p$ | dimensionless parameter defined by Equation 3.9 |
| $P$ | pressure fluctuation |
| $P_0$ | pressure measured in reservoir (Figure 1.1) |
| $P_1$ | pressure measured at the contraction |
| $P'_1$ | pressure defined in Figure 1.1 |
| $P^*_1$ | pressure defined in Figure 1.1 |
| $P_2$ | pressure measured in SLSF in capillary tube |
| $\overline{P}$ | average pressure measured in reservoir, Equation 3.6 |
| $(P_{11}-P_{22})_w$ | primary normal stress in SLSF in capillary tube |
| $P_{MAX}$ | maximum recorded pressure in reservoir |
| $P_{MIN}$ | minimum recorded pressure in reservoir |
| $P_u$ | pressure losses in upstream entry region, Equation 1.47 |
| $Q$ | volumetric flow rate |
| $Q_c$ | volumetric flow rate evaluated at onset of instability |
| $r$ | radial coordinate in a spherical or cylindrical coordinate system |

| | |
|---|---|
| $r'$ | distance from reservoir wall to streak, Equation 2.4 |
| $r_0$ | radial location where axial velocity is equal to one half of centerline velocity |
| $r_1$ | radial coordinate in spherical coordinate system where $\Gamma\theta_0$ is equal to unity |
| $r_\infty$ | radial location in spherical coordinate system where primary normal stress is equal to zero |
| $R$ | capillary tube internal radius |
| $R_0$ | universal gas constant |
| $s$ | sample variance, Equation 3.3 |
| $sw$ | slit width |
| $S$ | Hencky's strain measure, Equation 1.56 |
| $S_c$ | critical value of S given by Equation 3.51 |
| $S_R$ | recoverable shear strain |
| $(S_R)_M$ | recoverable shear strain evaluated at fracture for polymer melts |
| $(S_R)_S$ | recoverable shear strain evaluated at fracture for polymer solutions |
| $t$ | time |
| $t_\infty$ | time for centerline velocity to attain 99% of fully developed centerline velocity under SLSF |
| $(t_\infty)_e$ | experimental value of $t_\infty$ |
| $T$ | absolute temperature |
| $V$ | average velocity in capillary tube |
| $v_1, v_2, v_3$ | velocity components in spherical coordinate system |
| $v_{1,1}\big\|_{℄}$ | stretch rate in spherical coordinates along the centerline measured upstream of the contraction |

6

| | |
|---|---|
| $V_r$ | radial velocity, Equation 2.6 |
| $V_z$ | axial velocity in cylindrical coordinate system |
| $V_z\|_{\text{℄}}$ | axial velocity along the centerline |
| $V_{z,z}\|_{\text{℄}}$ | stretch rate in cylindrical coordinates along the centerline measured upstream of the contraction |
| $V^*$ | dimensionless axial velocity, $V_z\|_{\text{℄}}/V_0$ |
| $V_0$ | axial velocity along the centerline at the contraction |
| W | number of revolutions per minute |
| X/D | characteristic flow pattern length |
| $X_1, X_2, X_3, X_4, X_5$<br>$X_6, X_7$ | coordinates defined in Figure 2.8 |
| y | distance measured from capillary tube wall |
| $Y_1, Y_2, Y_3, Y_4, Y_5$<br>$Y_6, Y_7$ | coordinates defined in Figure 2.8 |
| z | axial distance upstream of contraction |
| $Z^*$ | dimensionless axial position variable, Equation 3.24 |
| $Z^{**}$ | dimensionless axial position variable, Equation 3.39 |
| $Z_0^{**}$ | dimensionless axial position variable where $\Gamma\ \theta_0 = 1.0$ |

Greek Symbols

| | |
|---|---|
| $\alpha_1$ | proportionality constant defined by Equation 1.38 |
| $\alpha_2$ | proportionality constant defined by Equation 1.34 |

| | |
|---|---|
| $\beta$ | contraction ratio, ratio of the area of the capillary tube to area of the reservoir |
| $\beta_1, \beta_2, \beta_3$ | parameters defined in Equation 1.39 |
| $\gamma$ | apparent shear rate under SLSF in capillary tube |
| $\gamma_R$ | apparent shear rate under SLSF in reservoir |
| $\dot{\gamma}_w$ | shear rate at capillary tube wall under SLSF, Equation 1.16 |
| $\Gamma$ | stretch rate |
| $\Gamma_c$ | stretch rate evaluated at onset of fracture |
| $\Gamma_{max}$ | maximum extensional stretch rate |
| $\Delta P$ | developed pressure loss over capillary tube length, L |
| $\Delta P_c$ | contraction loss |
| $(\Delta P_c)_{cr}$ | contraction loss evaluated at onset of fracture |
| $\Delta P_d$ | pressure loss due to developed flow in capillary tube, Equation 1.26 |
| $\Delta P_e$ | fraction of contraction loss due to elastic nature of fluid, Equation 1.25 |
| $\Delta P_{er}$ | pressure tap error |
| $\Delta P_{exit}$ | exit pressure loss |
| $\Delta P_t$ | total pressure loss, Equation 1.24 |
| $\Delta P_v$ | fraction of contraction loss due to viscous dissipation, Equation 1.27 |
| $\Delta r$ | radial distance defined by Equation 2.2 |
| $\Delta x$ | axial distance defined by Equation 2.1 |
| $\varepsilon_R$ | recoverable extensional strain |
| $\varepsilon_t$ | end correction factor for viscoelastic fluids |

| | |
|---|---|
| $\varepsilon_v$ | end correction factor for Newtonian fluids |
| $\eta$ | dimensionless radial coordinate, $r/r_0$ |
| $\theta$ | relaxation time |
| $\theta_0$ | zero shear relaxation time |
| $\mu$ | viscosity |
| $\mu_A$ | apparent viscosity |
| $\mu_E$ | elongational viscosity |
| $\mu_0$ | zero shear apparent viscosity |
| $\rho$ | density |
| $\tau$ | extensional stress |
| $(\tau)_{cr}$ | extensional stress evaluated at fracture |
| $\tau_w$ | shear stress at capillary tube wall under SLSF |
| $(\tau_w)_c$ | shear stress evaluated at onset of fracture |
| $(\tau_w)_M$ | shear stress evaluated at fracture for polymer melts |
| $(\tau_w)_S$ | shear stress evaluated at fracture for polymer solutions |
| $\phi_0$ | initial cone semi-angle |
| $\phi_R$ | cone semi-angles upstream of contraction |
| $\Phi$ | dimensionless contraction loss (the sum of the viscous and inertial contributions) |
| $\Phi_c$ | dimensionless contraction loss, viscous contribution |
| $\Phi_H$ | dimensionless contraction loss, inertial contribution |
| $\Phi_t$ | dimensionless contraction loss for viscoelastic fluid |
| $\chi$ | initial cone semi-angle measured in radians |